NASA CR-165502
D180-25956-4

NASA-CR-165502-VOL-2
19820003238

Study of Electrical and Chemical Propulsion Systems for Auxiliary Propulsion of Large Space Systems

Volume 2 Final Report

Boeing Aerospace Company

prepared for

NATIONAL AERONAUTICS AND SPACE ADMINISTRATION

NASA Lewis Research Center
Contract NAS 3-21952

ENTER:
9 1 1 RN/NASA-CR-165502-VOL-2
DISPLAY 09/2/1
82N11111** ISSUE 2 PAGE 157 CATEGORY 20 RPT#: NASA-CR-165502-VOL-2
D180-2595-4-VOL-2 CNT#: NAS3-21952 81/11/00 2 VOLS 540 PAGES
UNCLASSIFIED DOCUMENT
UTTL: Study of electrical and chemical propulsion systems for auxiliary propulsion of large space systems, volume 2 TLSP: Final Report
AUTH: A/SMITH, W. W.
CORP: Boeing Aerospace Co., Seattle, Wash. AVAIL.NTIS SAP: HC A23/MF A01
MAJS: /*AUXILIARY PROPULSION/*CHEMICAL PROPULSION/*ELECTRIC PROPULSION/*LARGE SPACE STRUCTURES
MINS: / AEROSPACE ENGINEERING/ ATTITUDE CONTROL/ SPACECRAFT CONTROL/ STATIONKEEPING
ABA: T.M.
ABS: The five major tasks of the program are reported. Task 1 is a literature search followed by selection and definition of seven generic spacecraft classes. Task 2 covers the determination and description of important disturbance effects. Task 3 applies the disturbances to the generic spacecraft and adds maneuver and stationkeeping functions to define total

1. Report No.	2. Government Accession No.	3. Recipient's Catalog No.

4. Title and Subtitle	5. Report Date
STUDY OF ELECTRICAL AND CHEMICAL PROPULSION SYSTEMS FOR AUXILIARY PROPULSION OF LARGE SPACE SYSTEMS - VOLUME 2 FINAL REPORT	November 1981
	6. Performing Organization Code: 6140
7. Author(s): W. W. Smith and J. P. Clark	8. Performing Organization Report No.: D180-25956-4
	10. Work Unit No.
9. Performing Organization Name and Address: Boeing Aerospace Company, Seattle, Washington	11. Contract or Grant No.: NAS3-21952
	13. Type of Report and Period Covered: Contractor Report
12. Sponsoring Agency Name and Address: National Aeronautics and Space Administration, Lewis Research Center	14. Sponsoring Agency Code

15. Supplementary Notes

Project Manager, Joseph E. Maloy, NASA Lewis Research Center, Cleveland, Ohio

16. Abstract

This document is the final report which has been prepared under Contract NAS3-21952 "Study of Electrical and Chemical Propulsion Systems for Auxiliary Propulsion of Large Space Systems" and covers five analytical tasks. Task 1 includes a literature search followed by selection and definition of seven generic spacecraft classes. Task 2 covers the determination and description of important disturbance effects. Task 3 applies the disturbances to the generic spacecraft and adds maneuver and stationkeeping functions to define total auxiliary propulsion systems requirements for control. The important auxiliary propulsion system characteristics are identified and sensitivities to control functions and large space system characteristics determined. In Task 4, these sensitivities are quantified and the optimum auxiliary propulsion system characteristics determined. Task 5 compares the desired characteristics with those available for both electrical and chemical auxiliary propulsion systems to identify the directions technology advances should take.

17. Key Words (Suggested by Author(s))	18. Distribution Statement
Attitude Control, Auxiliary Propulsion Generic Classes, Large Space Systems Shape Control, Stationkeeping	Unclassified - unlimited

19. Security Classif. (of this report)	20. Security Classif. (of this page)	21. No. of Pages	22. Price*
Unclassified	Unclassified	*	

* For sale by the National Technical Information Service, Springfield, Virginia 22161

N82-11111#

NASA-C-168 (Rev. 10-75)

TABLE OF CONTENTS

LIST OF FIGURES

LIST OF TABLES

ABSTRACT

This document is the final report prepared under Contract NAS3-21952 "Study of Electrical and Chemical Propulsion Systems for Auxiliary Propulsion of Large Space Systems" and covers five analytical tasks. Task 1 includes a literature search followed by selection and definition of seven generic spacecraft classes. Task 2 covers the determination and description of important disturbance effects. Task 3 applies the disturbances to the generic spacecraft and adds maneuver and stationkeeping functions to define total auxiliary propulsion system requirements for control. The important auxiliary propulsion system characteristics are identified and sensitivities to control, functions and large space system characteristics determined. In Task 4, these sensitivities are quantified and the optimum auxiliary propulsion system characteristics determined. Task 5 compares the desired characteristics with those available for both electrical and chemical auxiliary propulsion systems to identify the directions technology advances should take.

KEY WORDS

Attitude control
Auxiliary propulsion
Generic classes
Large space structures
Shape control
Stationkeeping

SUMMARY

This document is the Final Report and describes work performed under Contract NAS3-21952 "Study of Electrical and Chemical Propulsion Systems for Auxiliary Propulsion of Large Space Systems".

The complete study consists of five analytical tasks:

1. Characterization of Large Space Structures
2. Establishment of Disturbance Characteristics
3. Establishment of Auxiliary Propulsion System Characteristics and Requirements
4. Interaction Between Auxiliary Propulsion System Characteristics and Large Space System Characteristics
5. Determination of Electrical and Chemical Propulsion Technology Advances Required

Task 1 was accomplished by first conducting a literature search to identify future spacecraft characteristics. These were then grouped into seven generic classes. Each class was idealized and described in terms of a single scaling parameter. Simple empirical relations were derived to define the mass properties, sizes, areas, etc. in terms of the scaling parameter. This set of classes were then used as a basis for all subsequent work.

Task 2 consisted of a literature search to identify the important disturbance effects. The force and torque generating mechanisms were determined and the significant parameters and dependencies defined.

In Task 3 the disturbances were applied to the generic spacecraft classes. This determined the forces and torques needed to counter the disturbances. To these were added the forces and torques needed for maneuver and stationkeeping to define the total auxiliary propulsion needed for control.

Four flight conditions were used to cover the range of requirements. A minimum number of thrusters, logically placed, were then assumed and the thrust levels determined. Three classes appeared to be candidates for the use of distributed thrusters to achieve shape control. Thrusts per unit area or volume were found for these vehicles.

As part of Task 3, the important characteristics required by auxiliary propulsion systems were determined to satisfy the varied demands of attitude and shape control and stationkeeping. Finally a sensitivity analysis was carried out to identify which auxiliary propulsion system characteristics were significantly impacted by various control requirements.

Task 4 consists of four relatively independent studies: Thrust Level, Thrust Modulation and Transient Effects, Number and Distribution of Thrusts and Allowable Mass. These, in sum, cover the interlocking sensitivities and interrelationships identified in Task 3. Task 4 concludes with a definition of optimum APS characteristics chosen from the results of the four studies.

Task 5 consists of a review of both electric and chemical auxiliary propulsion system present day technology. Comparisons are made between existing capability and desired capability, as defined in Task 4, to identify the directions technology should take to best meet the future demands of large space systems.

The report is organized to follow very closely the contract task sequence. Thus, Sections 1-5 document the work performed in Tasks 1-5. Sections 6 and 7 follow to discuss the results and summarize the conclusions.

INTRODUCTION

Planned spacecraft and the projections of probable future vehicles in the future by government and industry show an unmistakable trend towards larger structures. Many of these vehicles will require construction in orbit. Most probably the construction will take place in low earth orbit to be followed, where necessary, by transfer to geosynchronous orbit. Once on station, the general requirement is for a very long operational life.

This study is part of an ongoing process to determine the propulsion requirements needed to support future space activities. Although there may be some overlapping functions, propulsion divides into the two groupings of prime and auxiliary propulsion. Prime propulsion is used to perform orbit transfer while auxiliary propulsion takes on the attitude control, shape control and stationkeeping tasks.

This study considers auxiliary propulsion only and will supplement other work in progress that is examining prime propulsion needs. The objective is to determine the direction auxiliary propulsion research and development should take to best meet upcoming needs. The approach is to define the important electrical and chemical auxiliary propulsion characteristics in terms of the demands that will be imposed by future spacecraft. Comparison of these desired characteristics and capabilities with those presently available is used to identify deficiencies.

1.0 CHARACTERIZATION OF LARGE SPACE STRUCTURES

There are a large number of diverse structures either planned or proposed for future space missions. The purpose of Task 1 was to reduce these concepts to a manageable set by defining a relatively small number of unique generic classes of structures which would be associated with as many of the concepts identified as possible. This set of idealized structures would then form the foundation for the analysis of disturbance torques and subsequent determination of auxiliary propulsion system requirements for large space systems (LSS).

A literature search was first conducted to collect examples of proposed large space systems. The time frame was not restricted but no systems were found which addressed times beyond 2020. The various concepts were screened, independent of mission, and grouped into generic classes of structures. It was found that the great majority of the vehicles fell naturally into three classes - plate structures, single antenna systems and multiple antenna systems. Several subdivisions appeared appropriate to represent particular control system characteristics. In all, seven generic classes were defined.

The seven generic classes were then idealized by breaking each class down to its basic elements, such as structure, avionics and solar arrays. The intent was to characterize each element in terms of a small number of scaling factors. It was found that a single parameter would suffice although the parameter was not the same in each class. Length was used for the plate structures, antenna diameter for the single antennas and number of antennas for the multiple antenna class. Simple expressions were then developed which defined the size, weight and inertia characteristics of each vehicle in terms of the single describing parameter.

To gain insight into shorter term (1990-2000) auxiliary propulsion requirements, the generic classes were reviewed assuming the vehicles were limited to a single shuttle payload. This process lead to some revision of the describing relations.

1.1 Literature Search

Some ninety sources were collected and are listed alphabetically in the bibliography of Appendix A. After redundant and irrelevant material was weeded out, about half of the sources were found to be useful in contributing to the determination of LSS characteristics. Prime sources of the contributing group are listed in Table 1-1.

The literature study, in general, led to identification of separate missions and their associated structures. In a few cases, such as the Solar Power Satellite and the Soil Moisture Radiometer concepts, detailed analysis of the proposed structures had been completed. The majority of the identified missions, however, were characterized by user needs and a few basic parameters such as total mass, antenna or structure size, orbit, power requirements, and in some cases lifetime and pointing accuracy. A list of the missions examined to determine generic classes is shown in Table 1-2.

1.2 Determination of Large Space Structures Characteristics

Previous studies identifying technology requirements for LSS proceeded with a screening process to reduce the mission sets to a few focus missions. This screening process, based on economic benefit, technical risk, or other factors would result in identification of particular mission needs and could not effectively show the trends desired as an output of this study. It seemed preferable that the goal of this exercise be limited to defining generic classes of structures without regard to any particular mission goals. It should be noted that mission characteristics such as orbit, pointing and slewing requirements, etc. can be associated with a given structure and form an input to the range of characteristic parameters for the associated generic class. The individual mission, however, would lose its identity in the formulation of an idealized structure representative of a generic class. Each generic class would be represented by an associated structure and range of characteristic parameters from which a general non-mission oriented study of auxiliary propulsion could originate.

1.2.1 Generic Classes

As a result of the analysis of mission concepts, three main generic classes were identified. Figure 1-1 shows the structures initially selected for

A REVIEW OF LARGE AREA SPACE SYSTEMS TOWARD IDENTIFICATION OF CRITICAL OR LIMITING TECHNOLOGY, M.A.Dienman et.al., General Electric Co., May 1978, X78-10214 (NASA CR 145339)

ADVANCED SPACE SYSTEM CONCEPTS AND THEIR ORBITAL SUPPORT NEEDS(1980-2000). VOL.1:EXECUTIVE SUMMARY, N76-30244 (NASA CR 148704)

ADVANCED SPACE SYSTEM CONCEPTS AND THEIR ORBITAL SUPPORT NEEDS(1980-2000) VOL.2:FINAL REPORT, N76-30245 (NASA CR 148703)

ADVANCED SPACE SYSTEM CONCEPTS AND THEIR ORBITAL SUPPORT NEEDS(1980-2000) VOL.3:DETAILED DATA, N76-30246 (NASA CR 148710)

DEPLOYABLE ORBITAL SERVICE PLATFORM CONCEPTUAL SYSTEMS STUDY, Mac. Doug., Mar 1979, Report no. MDC G7832 (NASA CR 159091)

DESIGN CONCEPTS OF GEOSTATIONARY PLATFORMS, E.C.Hamilton and W.T.Carey Jr, NASA Marshall Space Flight Center,Ala., Sep 1978, AIAA paper 78-1642.

DESIGN CONSIDERATIONS FOR LARGE SPACE ANTENNAS, R.Johnson Jr., McDonnel-Douglas Corp.,ST. Louis,Mo., 1978, N79-10085 , NTIS HC A23/MF A01, CSCL 22B.

LARGE ANTENNA STRUCTURE TECHNOLOGIES REQUIRED FOR 1985-2000, R.R. Wanlund, TRW Defense and Space Systems Group,Redondo Beach,Calif., 1978, NASA Vol.1 1978,p221-241

LARGE SPACE ERECTABLE ANTENNA STIFFNESS REQUIREMENTS, J.A. Fager, General Dynamics Corp., San Diego Calif., April 1978. 78A322929, AIAA 78-590.

LARGE SPACE SYSTEMS TECHNOLOGY, VOLUME 1, E.C. Naumann and A. Butterfield, NASA, Langley Research Center, Hampton, Va., Jan. 1978. N79-10078 (NASA-CP-2035-Vol-1).

LARGE SPACE SYSTEMS TECHNOLOGY, VOLUME 2, E.C. Naumann and A. Butterfield, NASA, Langley Research Center, Hampton, Va., Jan. 1978. N79-10097 (NASA-CP-2035-Vol-2).

NASA FORECAST OF SPACE TECHNOLOGY (1980-2000), Jan. 1976. NASA-SP-387.

PLATFORM DESIGNED FOR NUMEROUS USES, C. Covault, June 1978. A78-42509.

POINTING AND CONTROL TECHNOLOGY NEEDS FOR FUTURE AUTOMATED SPACE SYSTEMS, J.B. Dahlgren and S.M. Gunter, Jet Propulsion Laboratory, Pasadena, Calif., Sept. 1978. A78-52748 (NASA CNT # NAS7-100).

SERVING THE PUBLIC VIA PLATFORMS IN SPACE, R. Fleisig and J.L. Bernstein, Grumman Aerospace Corp. Bethpage, N.Y., March 1978. A79-11557, AAS 78-015.

STRUCTURES FOR SOLAR POWER SATELLITES, R.H. Nansen and H. di Ramio, Boeing Aerospace Co., Seattle, Wash., A79-10513.

SURVEY OF FUTURE REQUIREMENTS FOR LARGE SPACE STRUCTURES, FINAL REPORT, John M. Hedgepeth, NASA, Washington, D.C., Jan. 1976. N76-15500, NASA-CR-2621, NASA CNT #NAS1-13178.

THE OAF CONCEPT EXTENDED, W.L. Morgan and B.I. Edelson, COMSAT Laboratories, Clarksburg, Md., April 1978. A78-32891, AIAA 78-546.

TABLE 1-1 LISTING OF PRIME SOURCES

	Mission	Comments
1.	Personal Communications Satellite	200 ft antenna
2.	Large Space Telescope	Extreme pointing accuracy to .001 arc sec
3.	Voting/Polling Satellite	150 ft antenna
4.	Multinational Air Traffic Control Radar	Planer array 250 ft x 250 ft
5.	Border Surveillance	Planer array 9000 ft x 9 ft
6.	Night Illuminator	12 mirrors 1000 ft diameter
7.	Pinhole Satellite	Free flying mask 20 m in diameter
8.	Electronic Mail	Two concepts - 1 antenna farm and 1 large antenna
9.	Space Power Relay Satellite	Large 200 m erectible structure
10.	OAF America	Modular antenna farm (8 antennas)
11.	NASA GCP	Geosync platform 32 antennas
12.	NASA/GSFC PSCS	Geosync platform 8 antennas
13.	Grumman PSP	3 large antennas with connecting structure
14.	MOBLOMSAT	75 m antenna
15.	Coastal Waters Surveillance Radar	30 m Cassegrain antenna 6-10 kw RTG
16.	Aircraft Laser Beam	169 mirrors 15 ft in diameter
17.	Coastal Waters Passive Radar	1000 ft x 10000 ft array
18.	High Resolution Earth Mapping Radar	200 nmi polar orbit
19.	Disaster Communications	200 ft antenna
20.	Police Communications Satellite	200 ft antenna
21.	Energy Monitor	150 ft antenna
22.	Parabolic Torous Radiometer (Soil Moisture)	9 km x 3 km Torous
23.	Solar Power Satellite	21.3 km x 5.3 km solar array
24.	High Efficiency Solar Energy Generator	5.3 km x 2.3 km solar array
25.	Burglar Alarm Relay Satellite	200 ft antenna
26.	Advanced Resources/Pollution Observatory	Side looking radar 10 x 60 ft and multi-spectral telescope
27.	Personal Navigation Wrist Set	2 nmi cross
28.	Near Term Navigation Concept	160 ft cross
29.	Train Anti-Collision	42 ft deployable antenna
30.	Vehicle Traffic Control	200 ft antenna (430 kw Nuclear Generator)
31.	Multinational Energy Distribution	750 ft x 750 ft planer array
32.	Space Based Radio Telescope	Very large erectible antennas (up to 3000 m)
33.	Astronomical Super Telescope	800 ft cross w/seperate reflectors
34.	Multi Channel TV Broadcast	56 ft antenna
35.	Holographic Teleconferencing	56 ft antenna
36.	Nuclear Fuel locator	42 ft deployable antenna
37.	National Information Services	200 ft erectible antenna

TABLE 1-2 MISSION SPACECRAFT LISTINGS

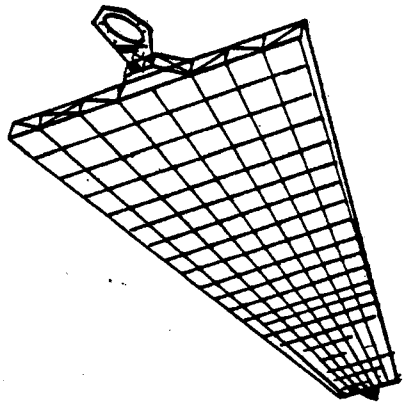

I PLANAR ARRAY

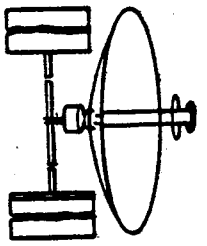

II SINGLE ANTENNA

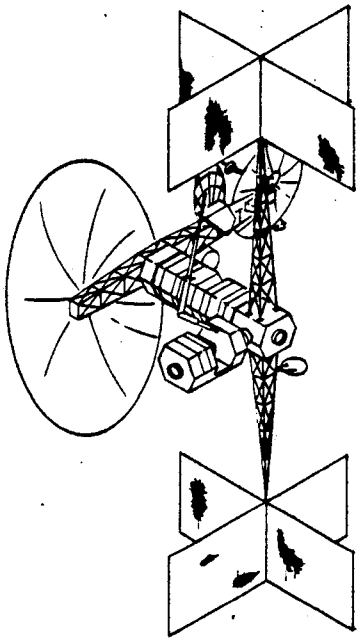

III ANTENNA PLATFORM

FIGURE 1-1 SELECTED GENERIC CLASSES

the primary divisions. The planar array was indicative of missions involving large Solar Array structures (the Solar Power Satellite shown is clearly an upper limit to the mass and dimension of this class) and various radar imaging concepts. The single antenna was by far the most common of the mission concepts. The antennas ranged from relatively small (16m diameter) deployable antennas to very large (9 km x 3 km) parabolics. This large range necessitated further generic subdivision as will be discussed. Multiple antenna platforms were also numerous and widely divergent in their structural approach. The OAF America (Orbital Antenna Farm) shown was felt not to be representative of a broad enough range of platforms, hence this generic class benefited from further subdivision.

The subdivision of the three initially selected classes was conducted to better identify particular aspects of attitude control system requirements. The results are shown in Figure 1-2. Contained in the planar array concept set were three structures which were very long, very thin cross-like structures controlled by a separate stationkept unit orbiting below the cross. Control of the small unit orbiting below the cross structure was not addressed in this study. Due to the extreme aspect ratio (one structure is a 3700m x 0.5m cross), some reservations existed about treating these crosses in the same group as the large planar arrays. Hence the crosses were segregated and the planar arrays separated into flat plate and cross structure subdivisions, Figures 1-3 and 1-4.

The single antenna class contained a large collection of deployable and erectable concepts covering a wide range of configurations. Three natural groupings emerged: (a) a type in which the antenna had extensive structural support, Figure 1-5, (the three soil moisture radiometer concepts were typical of this subdivision), (b) modular configurations consisting basically of a relatively rigid central core with the antenna and solar arrays as controlled appendages, Figure 1-6, and (c) the "maypole" antenna, which consists of a circumferential loop supporting the antenna mesh and is in turn attached to a central column by tension cables.

While few specific missions presently utilizing this concept could be identified, it became clear that many of the single antenna missions requiring relatively low surface accuracies could be served by such a concept. Further, because of the design's potential for compacting very

I PLANAR ARRAY

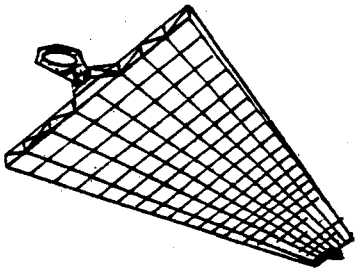

I-A FLAT PLATE

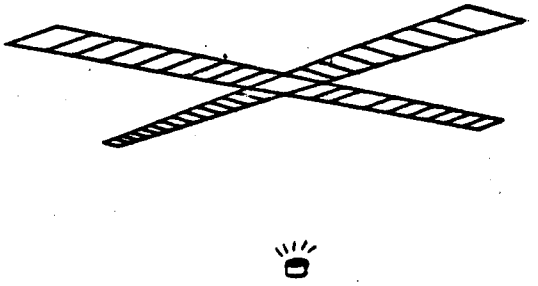

I-B CROSS STRUCTURE

II SINGLE ANTENNAS

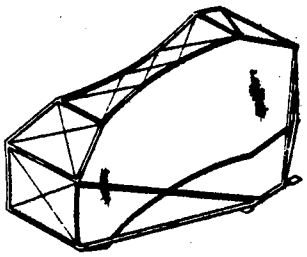

II-A LARGE ERECTABLE STRUCTURE

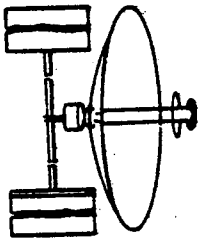

II-B MODULAR SYSTEM

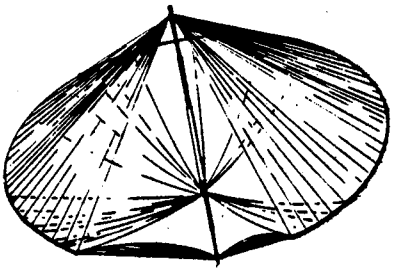

II-C MAYPOLE ANTENNA

III ANTENNA PLATFORMS

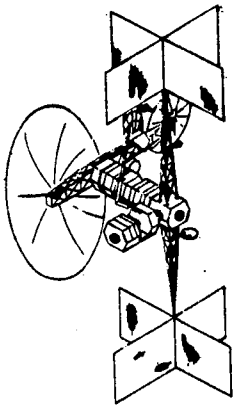

III-A MODULAR ANTENNA FARM

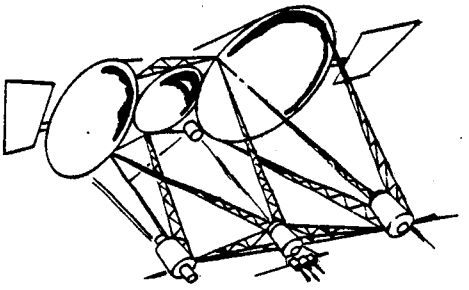

III-B MULTIPLE ANTENNA FARM

FIGURE 1-2 GENERIC CLASS SUBDIVISIONS

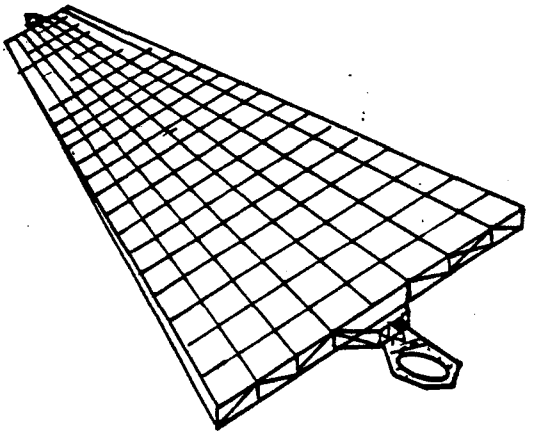

FIGURE 1-3 PLANAR ARRAY

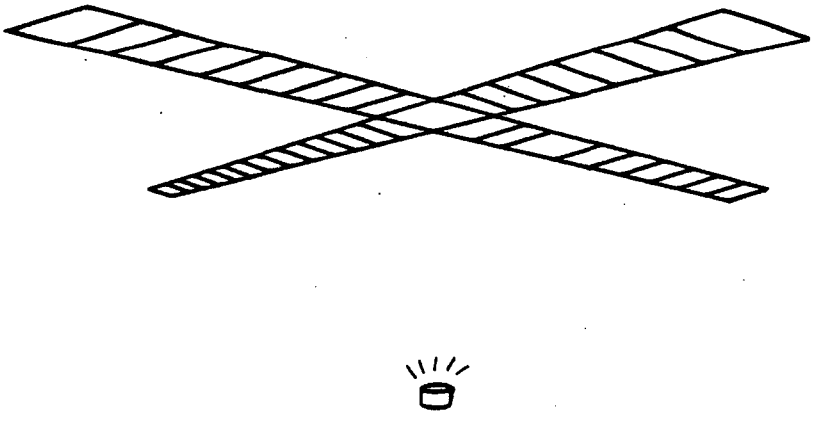

FIGURE 1-4 PLANAR CROSS STRUCTURE

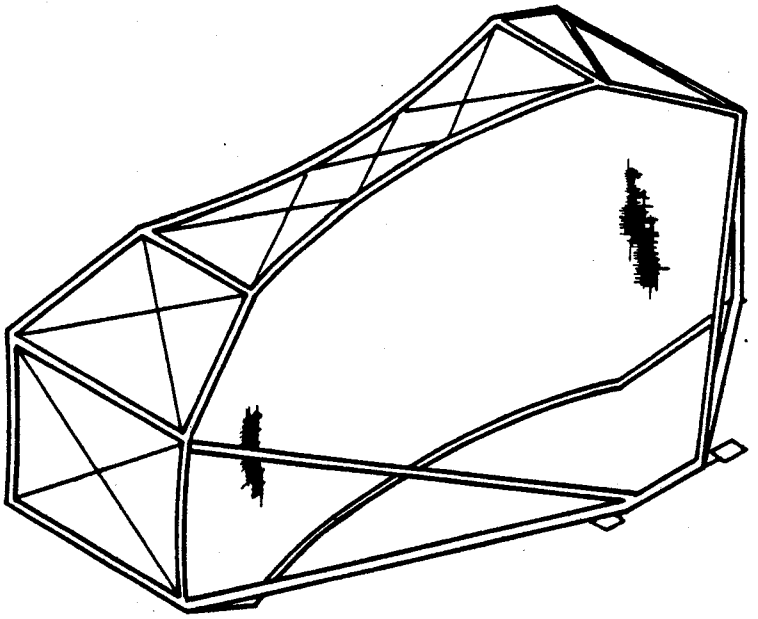

FIGURE 1-5 BOX STRUCTURE ANTENNA

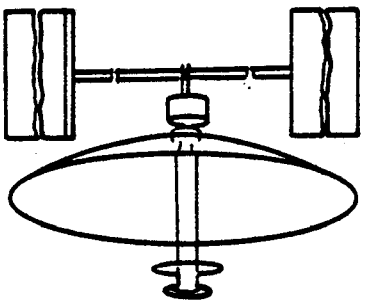

FIGURE 1-6 MODULAR ANTENNA

large antennas into the shuttle bay, work had been previously done which identified the parameters relevant to this study. A representative design is shown in Figure 1-7.

Some of the deployable maypole antennas rotate to maintain structural tension; however, the majority of concepts identified did not rotate after deployment and the generic class will be represented by a non-rotating structure. The range of antenna diameters for this type of antenna is from 30 to 1500 meters in diameter with a corresponding weight range of 100 kg to 2640 kg. This mass range is for the structure only. No avionics or other mission components are included.

The orbital antenna farms were separated into two subdivisions. One class was maintained for the OAF America as a modular structure with solar array power supply, Figure 1-8. This structure has most of its mass concentrated toward the center of the antenna farm and can be joined with another identical unit to form a composite structure. The Grumman Public Service Platform is dominated by large antennas connected with a skeletal structure to each other and the focal point avionics and power modules. This type of structure with a small number of large antennas forms the final class, Figure 1-9.

Sample concepts of the seven generic classes showing the range of major parameters are listed in Table 1-3.

1.2.2 Ideal Structures

Having identified representative concepts for each of the seven generic classes, ideal structures represented by simple generic shapes were developed. The objective in this process was to construct a set of ideal structures which could be characterized by a small number of parameters. These few parameter would determine the dimensional proportions and mass properties of a given structure. The structures would then be subjected to a range of mision oriented requirements.

It is at this point that the "real" missions lose their identity in becoming an ideal structure. Clearly, it is desirable to have as close a correspondence as possible between the idealized structure and the variety

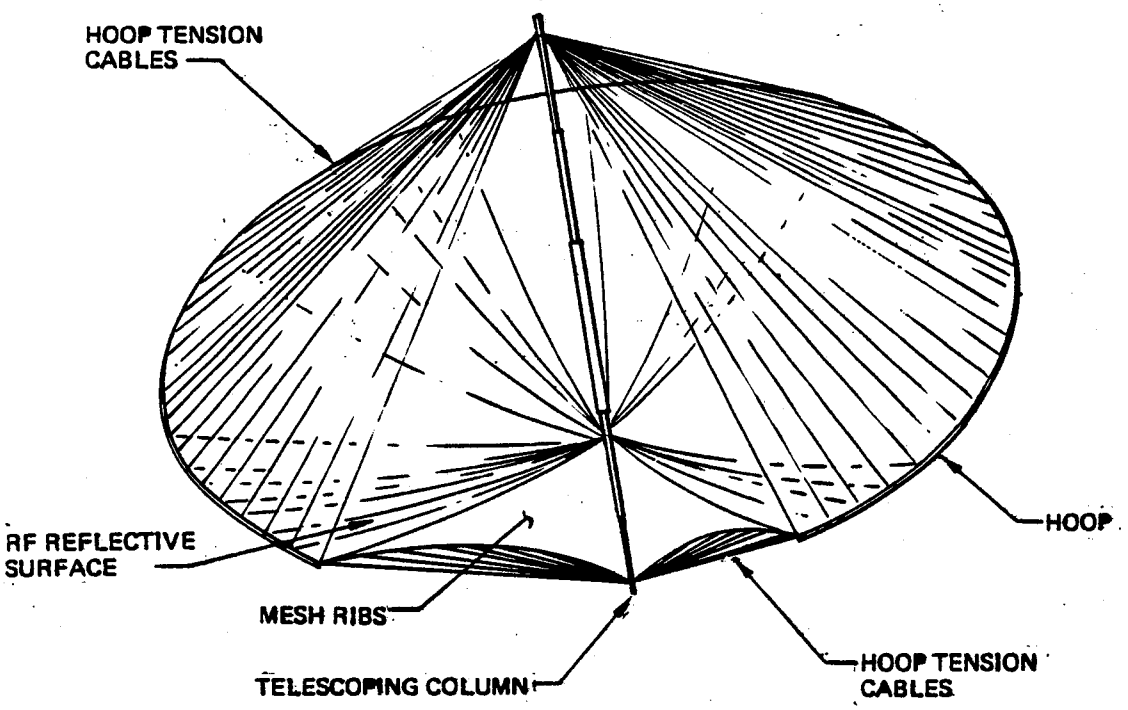

FIGURE 1-7 MAYPOLE ANTENNA

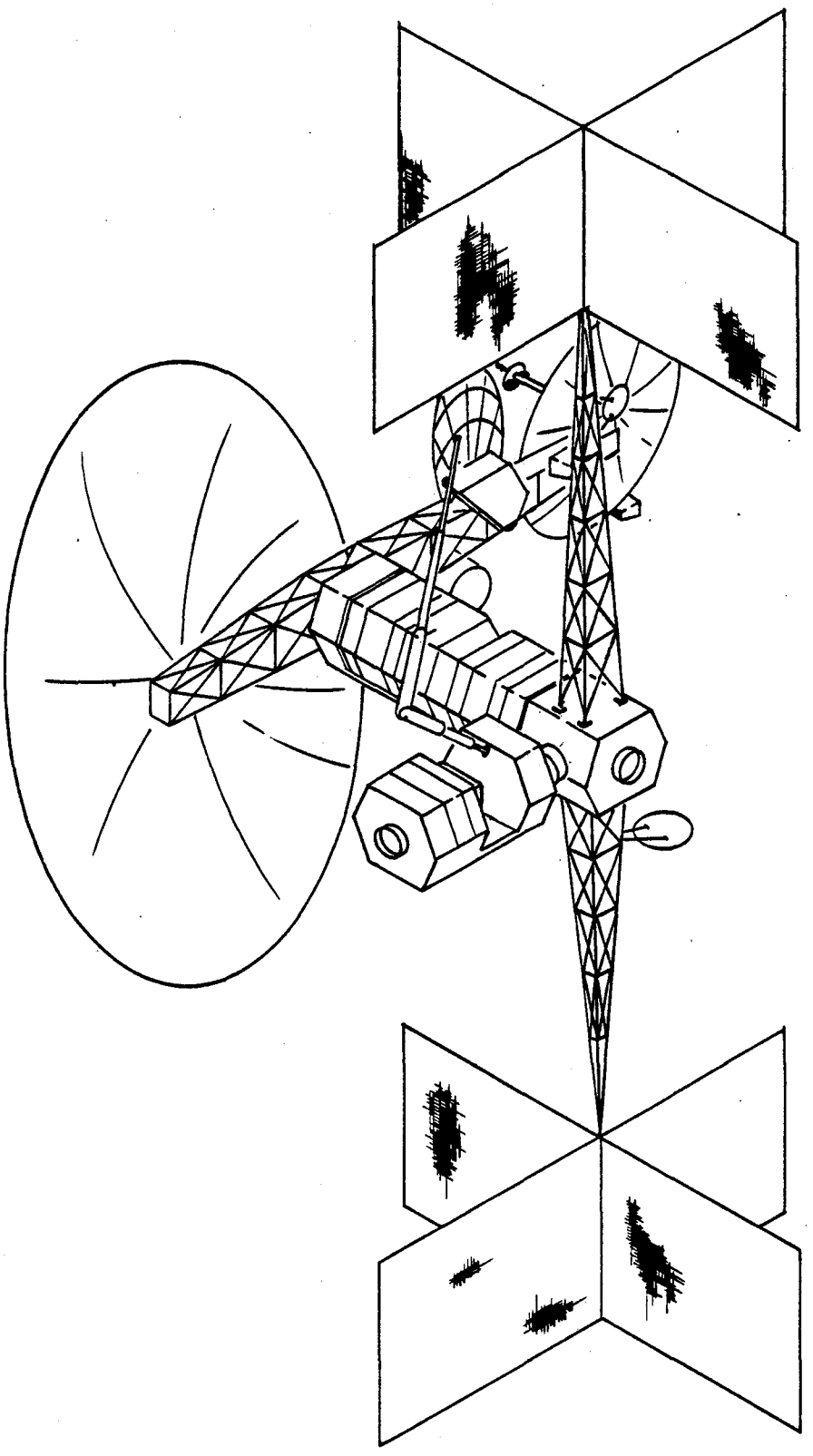

FIGURE 1-8 MODULAR ANTENNA FARM (OAF AMERICA)

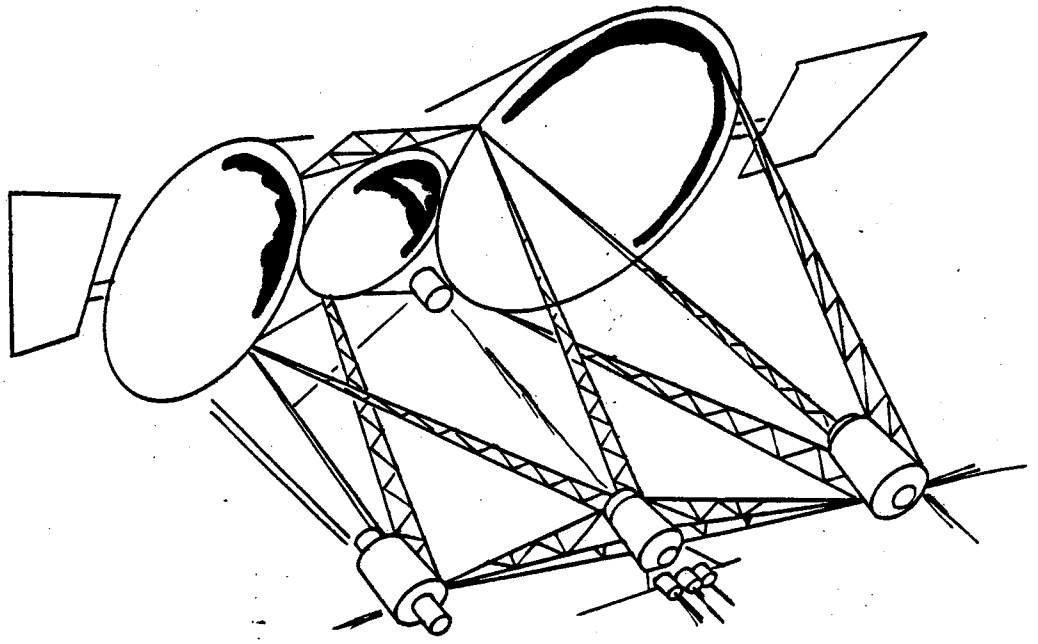

FIGURE 1-9 MULTIPLE ANTENNA FARM (PSP)

TABLE 1-3

GENERIC CLASSES SAMPLE CONCEPTS

I A PLANAR ARRAY - SAMPLE CONCEPTS									
MISSION TITLE	TOTAL MASS (kg)	SIZE	I_{xx} (kg-m^2)	I_{yy} (kg-m^2)	I_{zz} (kg-m^2)	ORBIT	ORIENTATION	POWER (kw)	LIFETIME (YEARS)
Multinational Air Traffic Control Radar	1600	77m x 77m	7.905×10^5	7.905×10^5	1.581×10^6	Geosync	Pointing Accuracy <20 ARCSEC	1	≥ 10
Border Surveillance	3628.7	2743m x 2.74m	2270	2.275×10^9	2.276×10^9	Geosync	TBD	20	≥ 10
Coastal Anti-Collision	9.072×10^5	3048m x 304m	7.923×10^9	7.023×10^{11}	7.0935×10^{11}	Geosync	Pointing Accuracy 20 ARCSEC High Slewing Rates ~2°/Sec	3MW (Beamed to Satellite)	≥ 10
Multinational Energy Distribution	15422	228m x 228m	6.716×10^7	6.716×10^7	1.348×10^8	556km	Pointing Accuracy .001 µrad Trucking Rate 1°/Sec	20	~10
Solar Power Satellite	8.18×10^7	21.3km x 5.3km	4.552×10^{15}	1.554×10^{14}	4.707×10^{15}	Geosync	Pointing Accuracy 1 Arc Minute	10000MW (Generated)	30 Years
I B CROSS STRUCTURE - SAMPLE CONCEPTS									
Near Term Navigation Concept	1600	48m x .5m	1.586×10^5	1.586×10^5	3.172×10^5	Geosync	Pointing Accuracy <20 ARCSEC	1	≥ 5
Personal Navigation Wrist Set	1361	3706m x .5m	7.79×10^8	7.79×10^8	1.56×10^9	Geosync	Pointing Accuracy <20 ARCSEC	2	≥ 10

TABLE 1-3 (Cont'd)

MISSION TITLE	TOTAL MASS (kg)	SIZE	I_{xx} (kg-m^2)	I_{yy} (kg-m^2)	I_{zz} (kg-m^2)	ORBIT	ORIENTATION	POWER (kw)	LIFETIME (YEARS)
II A LARGE ERECTIBLE PARABOLIC ANTENNA - SAMPLE CONCEPTS									
SOIL MOISTURE RADIOMETER									
(Tetrahedral Truss)	2.9×10^5	1294m x 575m x 678m	1.3×10^{10}	2.7×10^{10}	3.1×10^{10}	1000 km Polar Sun Sync.	Pointing to 10 μrad	2	≥10
(Dual Rim Webmesh)	1.3×10^5	1294m x 575m x 678m	$.45 \times 10^{10}$	2.0×10^{10}	2.1×10^{10}	1000 km Polar Sun Sync.	11	2	≥10
II B SMALL (<200M) ANTENNA - SAMPLE CONCEPTS		(Antenna)							
Voting/Polling	5900	45.7m	2.749×10^6	1.022×10^6	2.897×10^6	Sync.	10 ARCSEC Pointing 1 ARCSEC Stability	90	≥5
Electronic Mail	9070	61m	3.269×10^6	3.17×10^6	3.33×10^6	Sync.	10 ARCSEC Pointing 1 ARCSEC Stability	15	≥10
Disaster Communicators	8165	61m	4.41×10^6	2.99×10^6	4.3×10^6	Sync.	10 ARCSEC Pointing 1 ARCSEC Stability	M5	>5
Nuclear Fuel Locator	1360	12.8m				Sync.	10 ARCSEC Pointing 1 ARCSEC Stability	.3	>5

TABLE 1-3 (CONCL.)

III A ORBITING ANTENNA FORM - SAMPLE CONCEPT									
MISSION TITLE	TOTAL MASS (kg)	SIZE	I_{xx} (kg-m^2)	I_{yy} (kg-m^2)	I_{zz} (kg-m^2)	ORBIT	ORIENTATION	POWER (kw)	LIFETIME (YEARS)
OAF AMERICA	6060	68m x 46m x 25m	TBD	TBD	TBD	Geosync.	Pointing Accuracy $\leq$20 ARCSEC	20	$\geq$20
III B GEOSTATIONARY PLATFORMS - SAMPLE CONCEPT									
GRUMMEN PSP	50700	140m x 70m x 70m	TBD	TBD	TBD	Geosync.	Pointing Accuracy $\leq$10 ARCSEC	TBD	$\geq$20

of missions used to make up the generic class. To fully accommodate each individual structure in the composite would require a complete parameterization involving a multitude of parameters. Because of the large number of classes, the large number of mission oriented parameters (orbit, pointing accuracy, etc.), and the desire to identify broad general trends in auxiliary propulsion needs, the identification of a single structural characteristic which could scale the dimensions and mass distributions would be of great value.

Some of the classes yielded readily to a single ideal component while others require some modular construction of ideal components. Where more than one component is necessary, relations linking the scaling parameter with the size and mass of each component were derived. In each class, however, it has been found possible to characterize the dimensions, areas and mass properties in terms of a single parameter. In the following paragraphs a description is given of the ideal structures and the scaling laws which govern them.

Planar Arrays

Flat Plate (IA) - As the name would imply, the simple structure element is a two dimensional flat plate. Three parameters which define the structure can be identified, the length, width, and surface density and these are obvious scaling parameter candidates. Length was chosen as the basic parameter and the other values are either fixed or are mathematically related to length. Figure 1-10 shows the ideal structure chosen for this generic class. Coordinates are defined as shown with y along the major axis and x along the minor axis. This structure is characterized by a constant aspect ratio of $l/w = 4$. A second constant is surface density, set at 0.75 kg/m^2. These factors are based on the individual mission concepts studied.

Cross Structure (IB) - Once again a single ideal structure will be sufficient and a simple two dimensional cross structure is proposed. The scaling parameter chosen is length of the arms and each arm is equal in length and 90^o apart. The surface density will be fixed at 14 kg/m^2 and the width will be set at 0.5 m. The aspect ratio will, therefore, vary as the length varies. Figure 1-11 shows the ideal structure, coordinates and structure parameter ranges.

STRUCTURE VARIABLE: LENGTH (ℓ) RANGE ℓ = 30 TO 21000m

MASS RANGE: 170kg TO 8.27 x 10^7kg

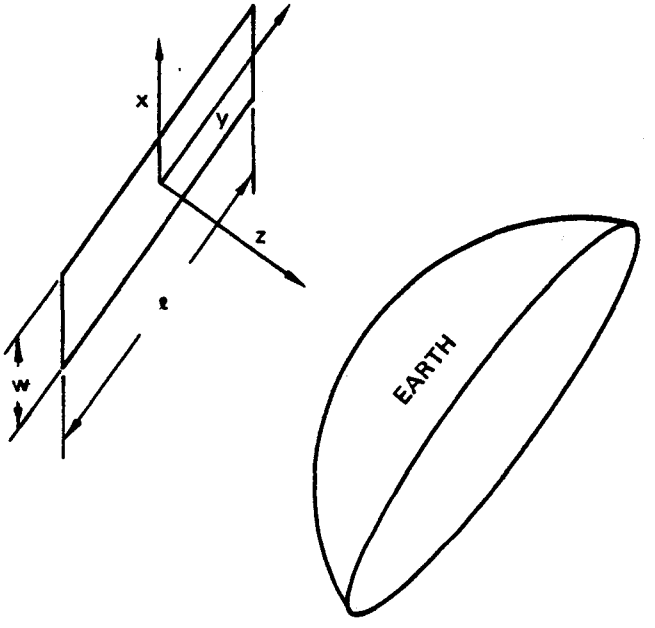

FIGURE 1-10 Flat Plate Ideal Structure (IA)

STRUCTURE VARIABLE: LENGTH (ℓ) RANGE ℓ = 40 TO 4000m

MASS RANGE: 560kg TO 56000kg

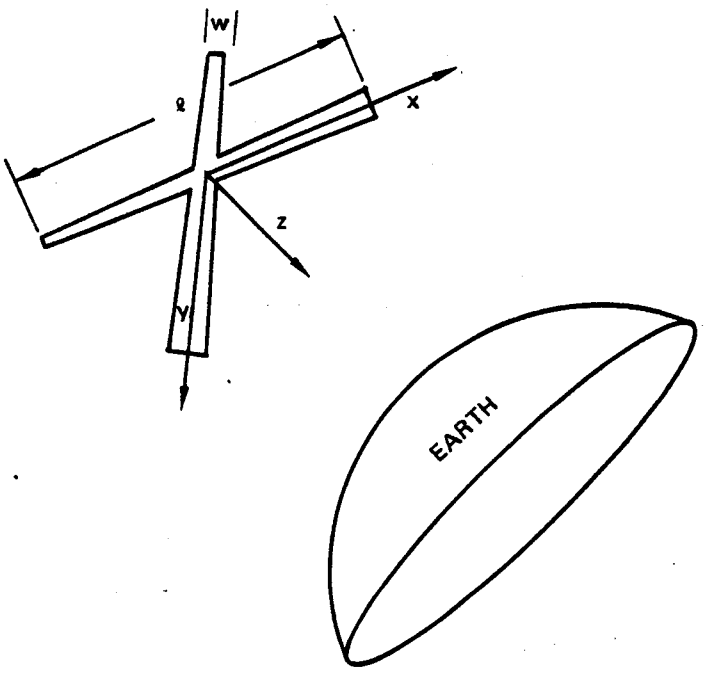

FIGURE 1-11 Cross Ideal Structure (IB)

Single Antenna

Large Erectible Structure (IIA) - This structure would be best idealized by a simple box structure. The solar paddles in the front of the actual structures studied are very small in weight and area because the mean power requirement is only 2 kw. Furthermore, the structure mass dominates the front appendage and in the interest of simplicity the appendage was discarded. The dimensions of the box were defined with box length, l, being the primary variable and w = h = 1/2 l. A specific mass of 150 kg/m (of length) was derived from the mission set. Figure 1-12 shows the ideal structure, coordinants and structure parameter ranges.

Smaller Modular System (IIB) - In this class, it is apparent that no single ideal structure will be adequate. An additional complication is the occurrence of two missions with nuclear power sources instead of solar array power sources. To comply with the one parameter classification goal, it becomes necessary to relate two components, solar array size and avionics size to the scaling parameter, antenna diameter. A relation can be derived relating antenna diameter to power requirements for solar arrays, however, there is no such satisfactory relation between the RTG missions and antenna diameter. It was felt that the inclusion of a single RTG mission would be unproductive. It was therefore eliminated and a single modular structure retained which scales as the antenna diameter. The diameter can be related to the power requirement by a factor of 1.5 kw/m. The antenna mass has been curve fitted to information from the literature sources for erectable and deployable antennas as shown in Figure 1-13. From the relationship shown, antenna mass is determined from the antenna diameter. The power required is also determined from the antenna diameter and can then be used to calculate the solar array (S/A) area and weight.

The total system mass can be determined from antenna diameter scaling based on a relation derived from the mission set. This approximation yields 135 kg/m of antenna diameter. Having now determined total system mass, antenna mass, and S/A mass, the avionics and miscellaneous mass can be found. This mass can be translated into a volume by estimating package densities. A value of 19 kg/m^3 has been assigned for avionics scaling. The resulting volume is used to scale a cube which fits between the antenna and solar arrays. This composite ideal structure is shown in Figure 1-14.

STRUCTURE VARIABLE: LENGTH (ℓ) RANGE ℓ = 82 TO 1300m

MASS RANGE: 1.23×10^5kg TO 1.95×10^5kg

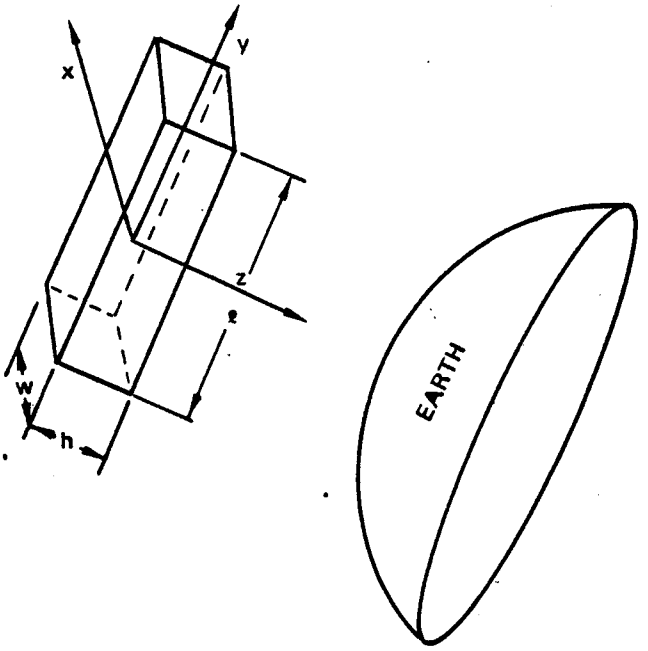

FIGURE 1-12 Box Ideal Structure (IIA)

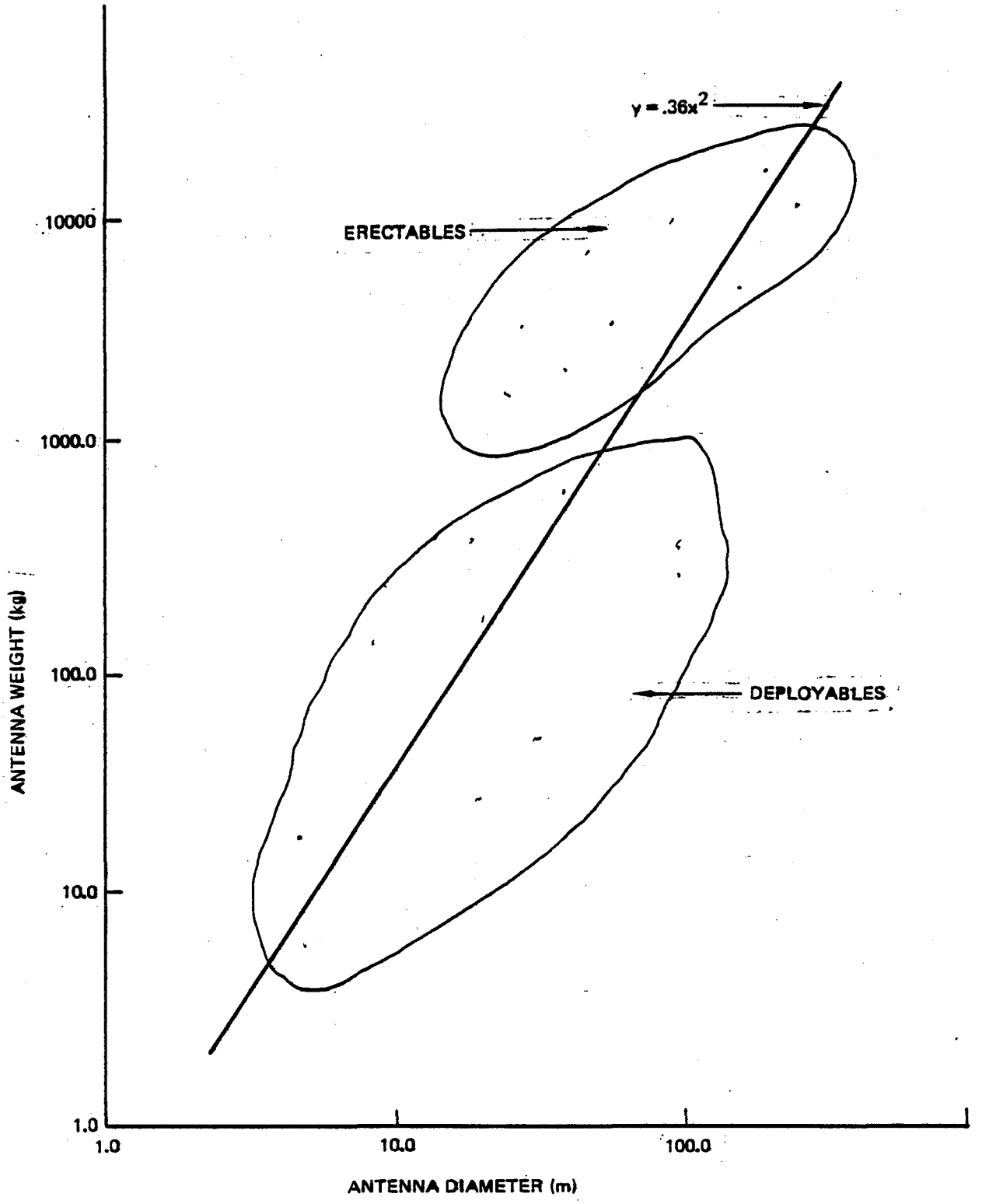

FIGURE 1-13 Antenna Scaling Law

STRUCTURE VARIABLE: ANTENNA DIAMETER D = 15m TO 200m

MASS RANGE: 2025kg TO 27000kg

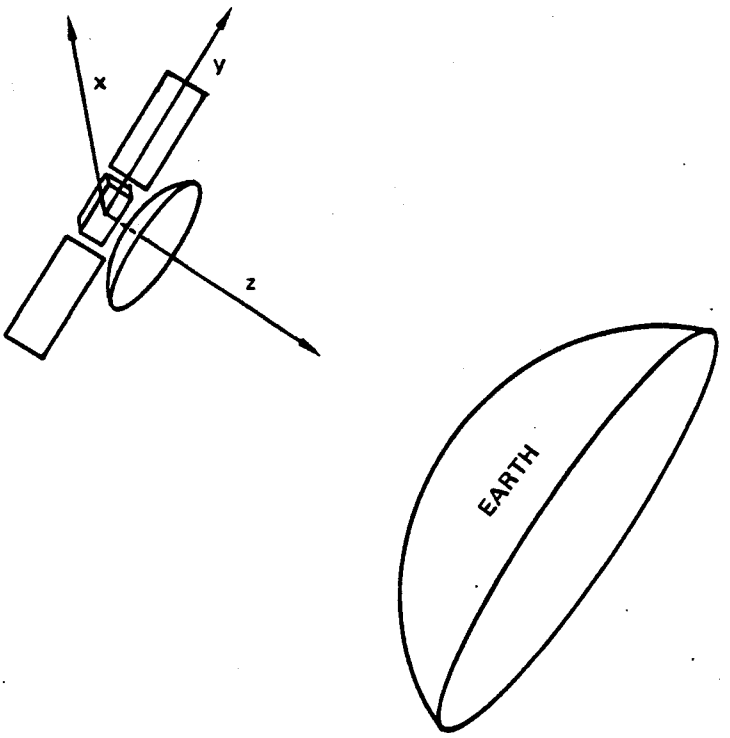

FIGURE 1-14 Modular Single Antenna (IIB)

The parabolic surface will be modelled as a paraboloid with a focus to diameter ratio of 0.5. The solar array will be modelled based on the Lockheed S/A aspect ratio of 8.85 and power density of 13.5 kg/kw.

Maypole or Hoop and Boom Antennas (IIC) - This class of structure is almost idealized without any simplification. The ideal structure consists of a parabolic surface with focus to diameter ratio of 0.5 and a central shaft which has a total length of 70 percent of the antenna diameter. The range of diameters which will characterize this structure are from 30 m to 1500 m. Figure 1-15 shows the ideal structure used for this class. The total mass of the structure is based only on relationships based on mass data available. The relationship used states: mass (kg) = 1.73 (D) + 48.1. The area to mass ratio of the maypole antenna is very high because of the exclusion of avionics or other mission components from the total mass. The exclusion of avionics mass was justified because most of the missions examined had the antenna itself as the dominant factor in determining mass properties.

Multiple Antenna Platform

Centrally Concentrated Mass With Appendages (IIIA) - The Orbital Antenna Farm (OAF) America is the mission model from which an ideal structure will be extracted. A true range of missions is not present in this category and a reasonable range of size variations was determined from analogy to other generic classes. This structure has a modular design which is reflected in the ideal structure. The antenna "rack" is assumed to have two antennas of equal diameter and the antenna diameter will be used to scale the ideal structure. Two square solar arrays will be scaled based on the power needs of the platform. For the baseline model, this power requirement is given by two 30 m antennas needing 20 kw. Power requirements will be assumed to scale linearly with antenna diameter.

The central mass of the platform is modelled as a cylinder of 4 m in diameter and 14.3 m long for a 30 m antenna model. Once again a value of 19 kg/m^3 is used for avionics packaging. Total mass is assumed to scale linearly with antenna diameter, hence avionics mass and volume are determined by substracting antenna and S/A mass from total mass. Figure 1-16 shows the ideal structure used for this class.

Series of Large Antennas (IIIB) - This multiple antenna platform illustrated by the Grumman Public Service Platform (PSP) can be best

STRUCTURE VARIABLE: DIAMETER (d) RANGE 30m TO 1500m

MASS RANGE: 100kg TO 2640kg

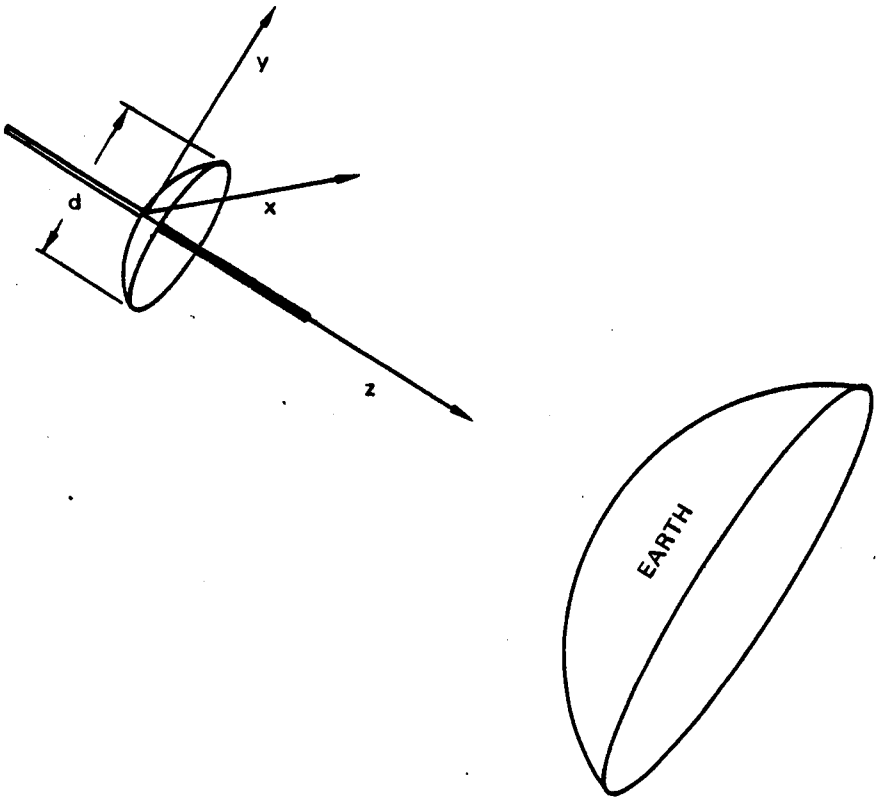

FIGURE 1-15 Maypole Antenna (IIC)

STRUCTURE VARIABLE: DIAMETER (d) RANGE d = 15 TO 60m

MASS RANGE: 3000kg TO 12000kg

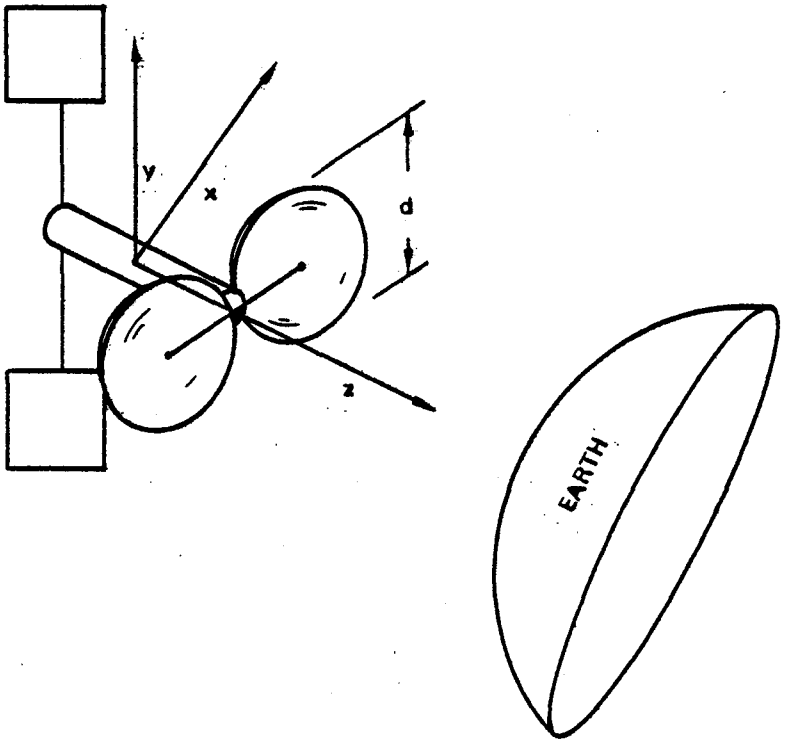

FIGURE 1-16 Multiple Antenna Farm - Centrally Concentrated Mass (IIIA)

parameterized by the number of antennas on the platform. It will be assumed that each antenna will be of equal 60 m diameter. The mass ratios between the antenna row and the avionics row will be fixed at 0.5. The solar arrays will be scaled on the basis of a 10 kw/antenna. The ideal structure chosen for this class is shown in Figure 1-17. Total mass figures are based on antenna mass of 10,000 kg/antenna, and power scaling will be the same as previously discussed. The avionics masses will be assumed to be point masses.

For each of the seven ideal structures, the relations that have been developed have been coded to calculate individual component mass properties and dimensions. This program combines these components into the ideal composite structure with corresponding total mass, dimensions, and inertias. The computer code takes each relevant scaling parameter and, for a full range of this parameter, generates a range of masses, dimensions, and inertias. Mass values for the seven idealized structures have been generated using this code. Examples of the mass and moment of inertia figures are shown in Figures 1-18 and 1-19. The complete mass and inertia data package is shown in Appendix B, Figures B-1 through B-14. These curves characterize the generic space structure classes in terms of a single scaling parameter and lay the groundwork for the work that follows. The rangles of the scaling parameter, mass and moments of inertia are summarized in Table 1-4.

1.3 Single Shuttle Launch Impact on Generic Classes

To better understand the short term auxiliary propulsion requirements of Large Space Structures, a limitation of the generic classes to those which can be launched using a single shuttle flight was examined. The limitation of a single shuttle launch capability will force the study to concentrate on a smaller parameter range and a different antenna type. Consideration of a smaller parameter range allows a more in depth look at the misisons currently planned for the short term (1990-2000).

Figure 1-20 illustrates the shuttle payload envelope. As a general rule for deployable structures, the shuttle is volume limited rather than weight limited. This indicates the need to utilize packaging studies as well as mission concept and system studies in modifying generic classes. The

STRUCTURE VARIABLE: NUMBER OF ANTENNAS RANGE n = 2 TO 10

MASS RANGE: 44000kg TO 216500kg

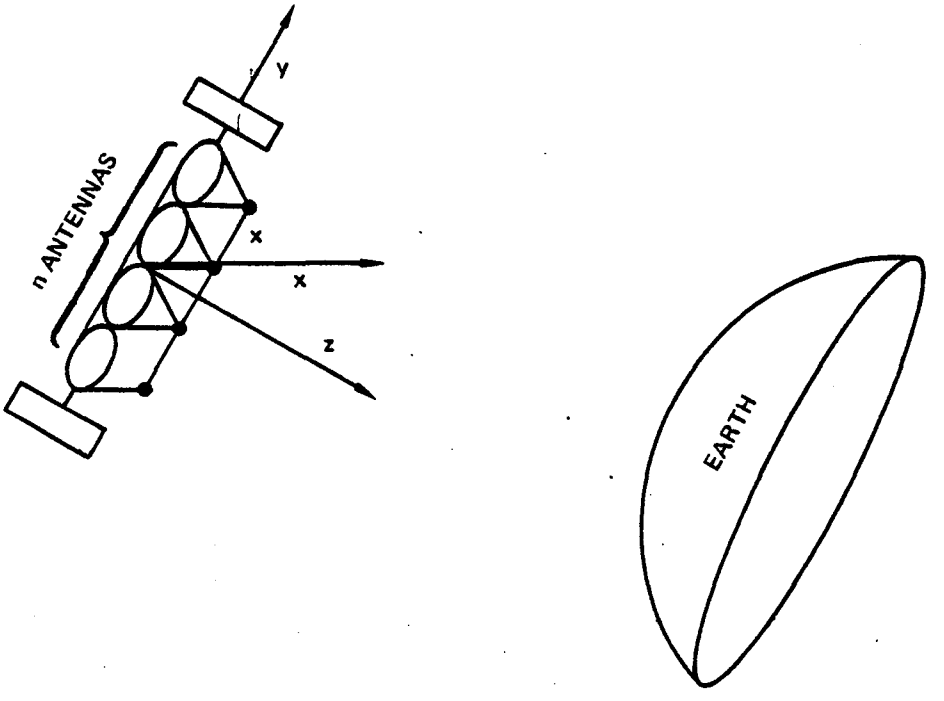

FIGURE 1-17 Multiple Antenna Farm: Series of Large Antennas (IIIB)

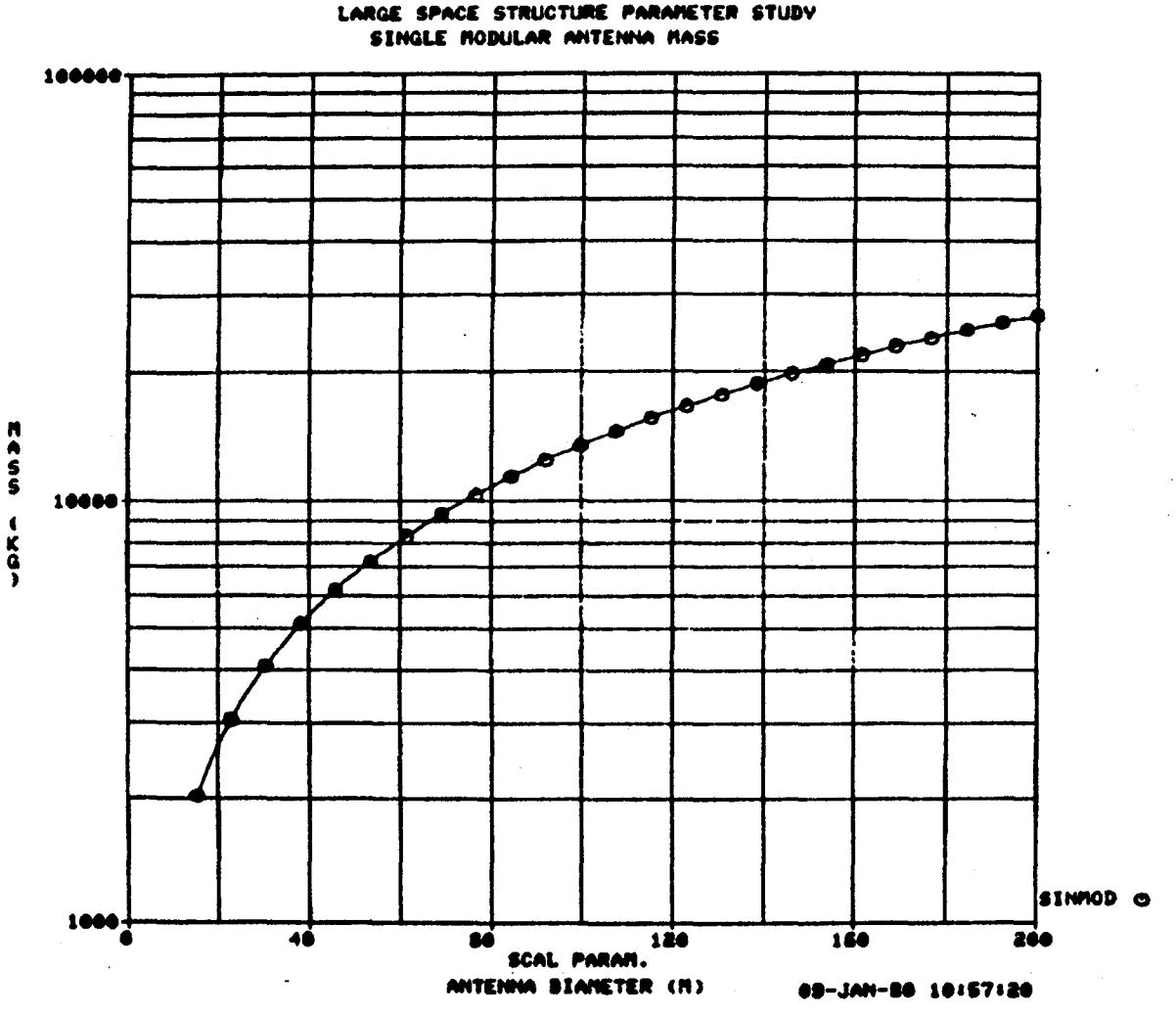

FIGURE 1-18 LARGE SPACE STRUCTURE PARAMETER STUDY
SINGLE MODULAR ANTENNA STRUCTURE MASS

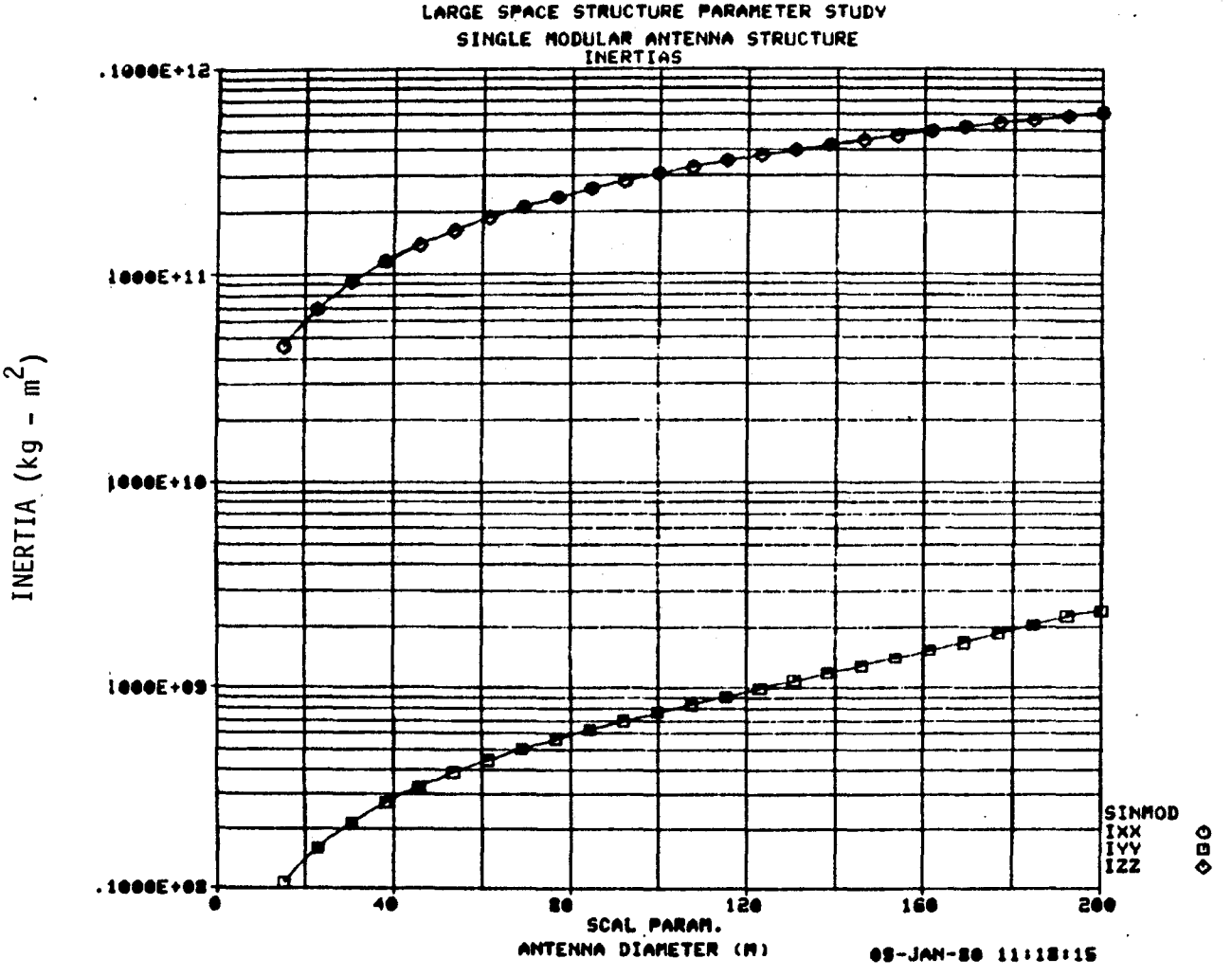

FIGURE 1-19 LARGE SPACE STRUCTURE PARAMETER STUDY
SINGLE MODULAR ANTENNA STRUCTURE INERTIAS

TABLE 1-4

IDEAL STRUCTURE SUMMARY

CLASS	SCALING PARAMETER	PARAMETER RANGE	MASS RANGE	I_{xx} ($kg-m^2$)	I_{yy} ($kg-m^2$)	I_{zz} ($kg-m^2$)
I. PLANAR ARRAY						
A. Flat Plate	Length	30m to 21km	170kg to 8.27×10^7kg	797 to 2.28×10^{15}	12750 to 3.04×10^{15}	13547 to 3.23×10^{15}
B. Cross Structure	Length	40m to 4000m	560kg to 56000kg	7.47×10^4 to 7.47×10^{10}	7.47×10^7 to 7.47×10^{10}	1.49×10^5 to 1.49×10^{11}
II. SINGLE ANTENNA						
A. Large Erectable Structure	Length	82m to 1300m	1.23×10^4kg to 1.95×10^5kg	3.446×10^7 to 1.373×10^{11}	1.378×10^7 to 5.493×10^{10}	3.446×10^7 to 1.373×10^{11}
B. Smaller Modular System	Antenna Diameter	15m to 200m	2025kg to 2.7×10^4kg	1.35×10^5 to 1.0839×10^8	1.171×10^4 to 8.788×10^7	1.35×10^5 to 1.658×10^8
C. Maypole Antennas	Antenna Diameter	30m to 1500m	100kg to 2645kg	4860 to 4.823×10^7	4860 to 4.823×10^7	13425 to 7.83×10^8
III. MULTIPLE ANTENNA PLATFORM						
A. Centrally Concentrated Mass W/Appendages	Antenna Diameter	15m to 60m	3000kg to 1.2×10^4kg	71126 to 3.66×10^5	79349 to 3.12×10^5	30143 to 1.03×10^6
B. Series of Large Antennas	No. of Antennas	2 to 10	4.40×10^4kg to 2.165×10^5kg	2.97×10^7 to 5.31×10^9	9.9×10^6 to 4.87×10^7	1.98×10^7 to 5.26×10^9

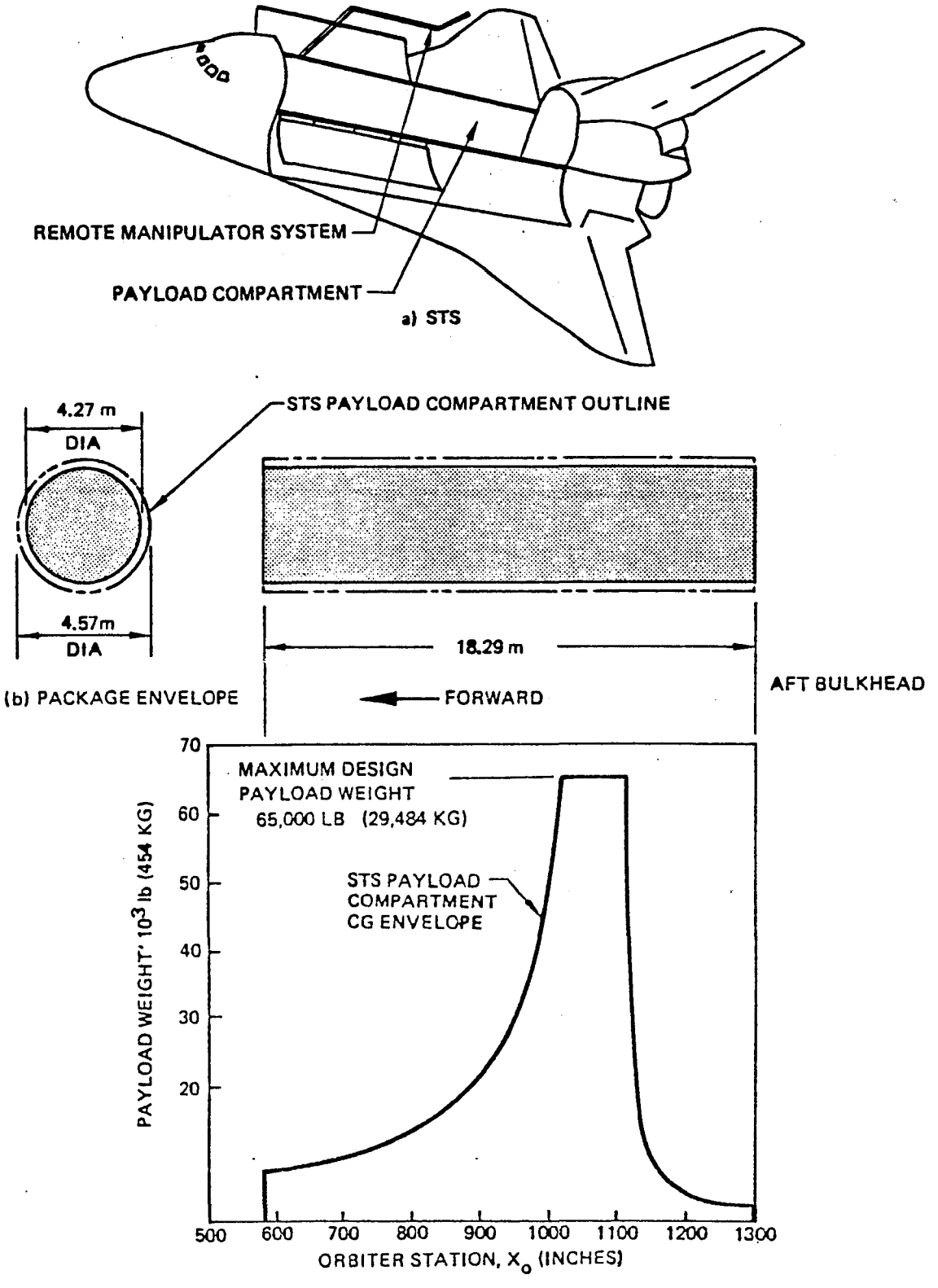

FIGURE 1-20 SHUTTLE IMPOSES MASS AND VOLUME CONSTRAINTS ON PAYLOADS

necessity of using deployable structures rather than erectible structures with a single shuttle launch stems from the characteristics of the building mechanism and its support needs. These characteristics and support needs are outlined below.

It is very unlikely that erectable structures will be built using a single shuttle launch. A need exists not only for the beam builder and raw materials but also for a support platform to serve manufacturing and support crew habitat needs. The need for these platforms breaks down further into two areas - mechanisms and operating time. The primary mechanism to build these structures is the beam builder. From conversations with Boeing Aerospace structures technologists, as well as Tom Dunn (NASA Marshall), and Eric Egler (NASA JSC), it was concluded that there are two main reasons for elimination of the beam builder from single shuttle missions. These are shown below.

1. Beam builder itself may weigh 10's of tons and take up 30-50 percent of shuttle mass capacity. Mass left over for raw materials would not be sufficient to build a significantly large structure.

2. Shuttle on-orbit time capability will not be sufficient to enable the completion of a structure with a single shuttle crew.

Each generic class was modified to be launched in a single shuttle flight. The primary generic classes - the plate, the single antenna, and the multiple antenna were treated by forming four classes of deployable structures. The rectangular plate structure which is an erectible type of LSS was replaced by a deployable tetrahedral truss concept. This truss when deployed forms an eight-sided plate structure and may be used for similar, although smaller scale, missions as the original plate structure. A second deployable class was formed by extending a solar array blanket across the face of the tetrahedral truss. This class is in reality a subclass or modification of the first class (I).

The single antenna class, (II), was restricted to the modular antenna category because this class contained the majority of missions which could be filled with a deployable antenna type. The multiple antenna class requirements were best met with the series of antennas concept using deployable antennas. A series of antennas structure was also chosen to represent the multiple antennas because its configuration poses unique control requirements due to the large differences in inertias. The modifications to each class are discussed in more detail in the following paragraphs.

Plate Structure

A recent study conducted for NASA Langley Research Center by Boeing Aerospace Company (Reference 1) found a tetrahedral truss to be the leading candidate for missions involving large deployable planar trusses. The tetrahedral truss was found to be the least complex (minimum number of different elements), have the highest natural frequency, and the lowest mass for a given area. Figure 1-21 illustrates the tetrahedral truss concept.

This structure can be used alone as a base of operations for multiple antennas, solar power generation, or it may be curved to form a parabolic antenna. Multiple antennas are covered in the third primary generic class and hence will be omitted from the plate class study. We will concentrate instead on two alternatives. First, the structure without any attachments, and second, the structure with a solar array blanket covering one face of the structure.

The shuttle is volume limited by most deployable antennas. For the structure without an attached S/A blanket, the structure sizes that will fit into a single shuttle include a maximum B dimension of 300 meters. If the size and mass of the auxiliary propulsion system is included, the maximum size of the antenna will decrease. To avoid an iterative process to converge on the maximum antenna size, the maximum size considered without a solar array blanket was set at 250 meters. Inertias and mass properties formulae of the tetrahedral truss structure are listed in Figure 1-22.

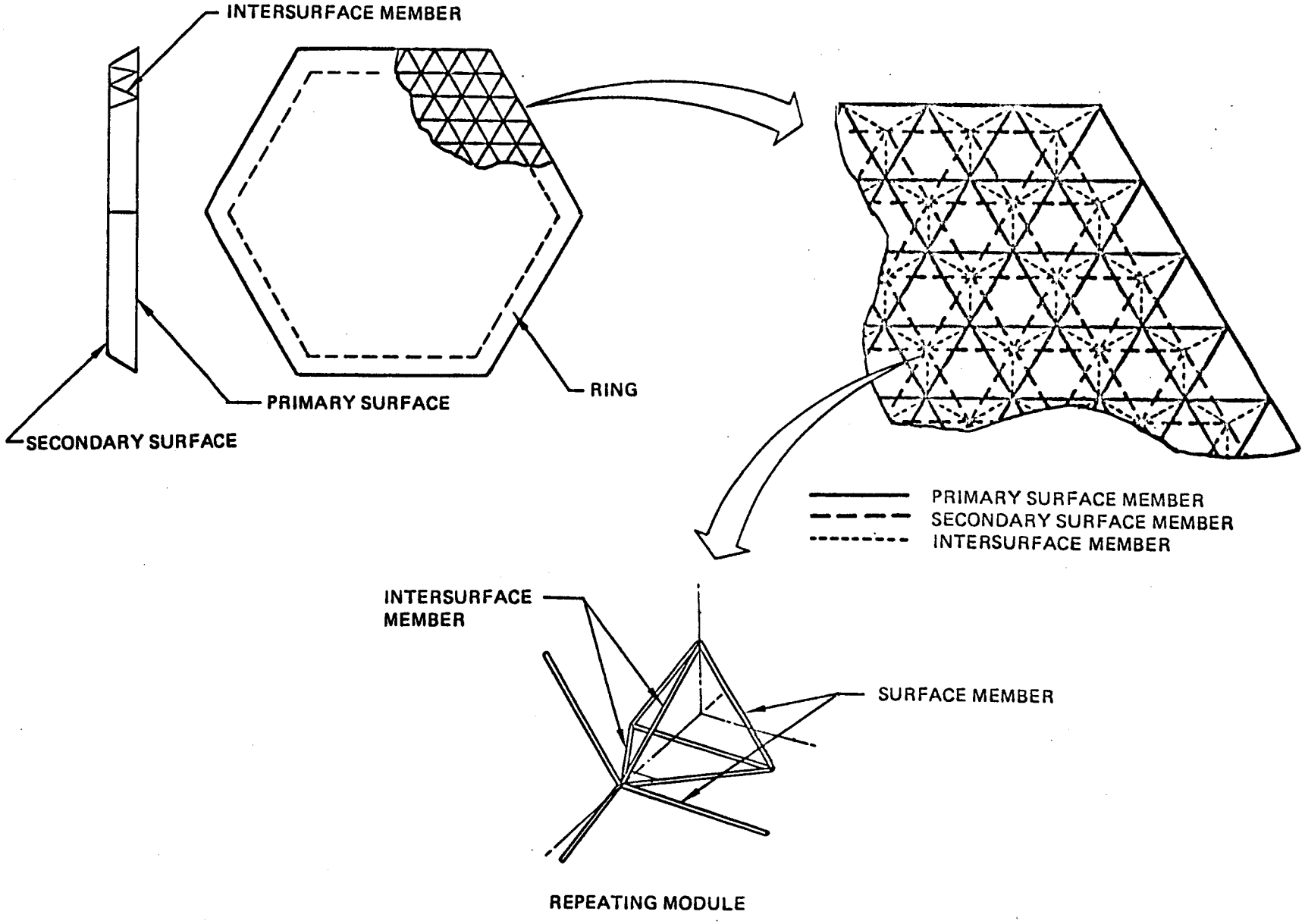

FIGURE 1-21 TETRAHEDRAL TRUSS

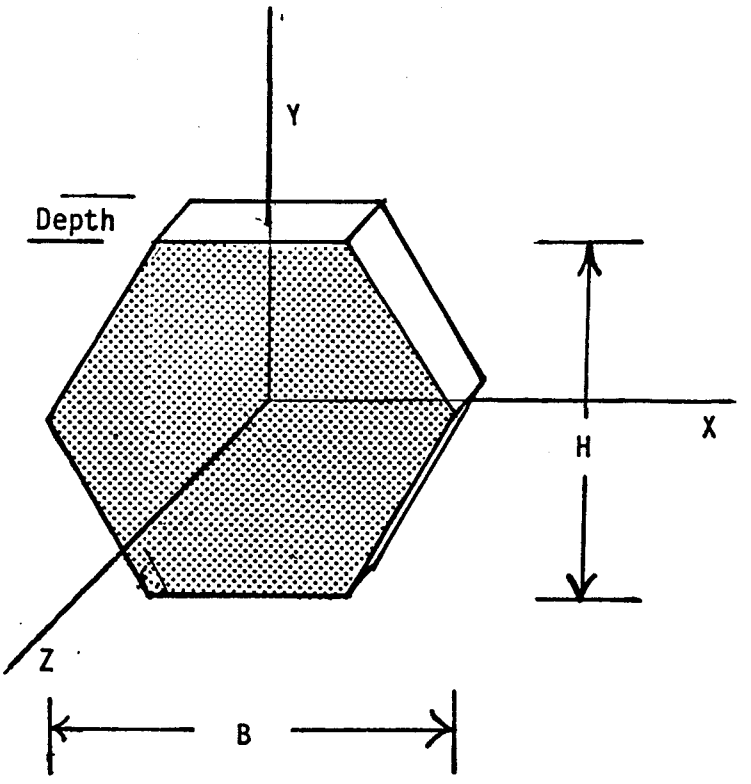

$$M_{Tot} = 19.84\ H - .0133H^2$$

where H = 3 B/2

Area = $.866\ H^2$

Depth = $.0715\ H$

Package Length = $.073 \times H$

I_z = $.1388\ H^2\ M_{Tot}$

$I_x = I_y$ = $1/2\ I_z$

FIGURE 1-22 TETRAHEDRAL TRUSS CONVENTIONS

The plate structure with a solar array blanket is weight limited in a single shuttle because of the solar array mass. Using SOA solar array technology, the solar blanket will weigh 13.5 kg/kw^2 including the storage canisters. Elimination of the canister mass brings the specific mass number to 12 kg/kw^2. Because of the uncertainties in technology development and shuttle requirements, a value of 13.5 kg/kw^2 will be used.

A tetrahedral truss structure with a solar array blanket is limited to a maximum dimension of 150 meters. The resultant mass is 24420 kg or 83 percent of shuttle capacity without the APS. It is intuitively obvious that this type of structure would greatly benefit from electric propulsion if part of the power generated could be used when necessary for the APS. For this study, however, we will charge the mass of the S/A to the vehicle. Table 1-5 illustrates the complete mass properties of the plate structures.

Modular Antenna

The restriction to deployable antennas changes the antenna scaling law to allow only for mesh deployable antenna types. An estimate using the upper limit of mass for mesh deployable antennas has been made from Reference 2. There is a variation in the estimates of antenna mass for mesh deployables of a factor of about three. The variation is due to the variety of configurations for a given antenna diameter. The equation shown below models the mesh deployable antenna mass. This equation includes an allowance for the feed support and represents the upper limit of mass estimates.

$$M_{ANT}(kg) = -1.8345 \times 10^{-3} \times D_{ANT}^{2} + 15.112\, D_{ANT} - 49.11$$

with D_{ANT} in meters

Modelling the system with a mesh deployable antenna rather than a precision deployable antenna lowers the system mass considerably. The 200 meter antenna system with avionics and solar array have a total mass of 18000 kg. The mass properties for the mesh deployable modular antenna are shown in Table 1-6.

TABLE 1-5 PLATE STRUCTURE MASS PROPERTIES

W/O Solar Blanket Parameter			
B(m)	30	100	250
Area(m^2)	584.6	6495	40594
Depth(m)	1.86	6.19	15.48
Package Length(m)	1.90	6.32	15.8
Mass(kg)	506	1618	3672
I_x, I_y(kg-m^2)	23700	8.42×10^5	1.1945×10^7
I_z(kg-m^2)	47400	1.684×10^6	2.389×10^7

W/ Solar Blanket			
B(m)	30	100	150
Area(m^2)	584.6	6495	14612
Depth(m)	1.86	6.19	9.29
Package Length(m)	1.9	6.32	9.48
Mass(kg)	1334	11350	24420
$I_x I_y$(kg-m^2)	52390	5.995×10^6	3.78×10^7
I_z(kg-m^2)	130020	1.1883×10^7	7.549×10^7

TABLE 1-6 MODULAR ANTENNA MASS PROPERTIES

Parameter	Small	Medium	Large
Antenna Diam.(m)	15	60	200
Mass(kg)	2300	8375	18017
I_x(kg-m^2)	26810	7.367×10^5	6.663×10^6
I_y(kg-m^2)	18483	4.707×10^5	5.161×10^6
I_z(km-m^2)	21821	1.059×10^6	7.376×10^6

TABLE 1-7 MULTIPLE ANTENNA MASS PROPERTIES

Parameter	Small	Medium	Large
# Antennas	2	3	4
Mass(kg)	7500	11250	15000
I_x(kg-m^2)	5.6575×10^6	3.271×10^7	8.96×10^7
I_y(kg-m^2)	1.498×10^6	2.278×10^6	3.041×10^6
I_z(kg-m^2)	7.0812×10^6	3.35×10^7	9.966×10^7

Multiple Antenna Systems

For this type of structure, dramatic reductions in mass result from using deployable rather than erectable antennas. It is also necessary to treat the support structure as deployable. The deployable multiple antenna system is volume rather than mass limited. The maximum number of antennas with structural support and avionics included is five. Because of packaging uncertainties and additional APS volume, the maximum number of antennas is taken to be four. The mass properties for the multiple antenna system are shown below in Table 1-7.

2.0 ESTABLISHMENT OF DISTURBANCE CHARACTERISTICS

The objective of Task 2 was to determine the forces and torques which affect the orientation, orbital position and shape of the generic classes defined in Task 1. These disturbances include those due to environmental effects and any that may be generated on board. In short, all forces and torques except those generated specifically for control were considered.

A literature search was first conducted to identify disturbance sources and to separate them into important and insignificant groups. The disturbance literature is extensive and a considerable degree of selectivity was found necessary. Important sources were determined to be: radiation, gravity gradient, aerodynamic and orbit perturbations. Magnetic and thermal effects were examined but eliminated from further consideration. Magnetic torques were found to be too dependent on specific vehicle payloads to be easily characterized. In addition, they were relatively small in low earth orbit and insignificant at geosynchronous altitudes. Thermal effects have many important consequences but were not found to be significant as regards auxiliary propulsion.

Each of the disturbance sources were examined in some detail to describe how each disturbance is generated. Also to define the distribution in magnitude and direction, the variation with time and the functional dependence on configuration, mass properties and mission parameters such as altitude, orbit inclination and eccentricity. The results of this task provided the information necessary to estimate the disturbance effects on each generic class or a function of the scaling factor in Task 3.

2.1 Literature Search

Existing bibliographies dealing with disturbances and passive attitude control were brought up to date and reviewed. Some of these compilations were extensive. The objective of the review was to extract entries which described the environmental field, defined the force and torque generating mechanism and identified the important parameters. Applictions and insignificant effects were screened out. The reduced set of references appears in Appendix B and covers the following:

- o General Surveys
- o Radiation
- o Gravity Gradient
- o Aerodynamic
- o Thermal
- o Orbit Drift
- o Miscellaneous

2.2 Analysis of Disturbances

The important disturbance effects are described individually in the subsections below:

2.2.1 Radiation Disturbances

In the analysis of radiation disturbances for earth orbital missions, three sources of radiation require consideration. The primary disturbance is from direct solar radiation which contributes both electromagnetic forces from photons and a plasma force from the solar wind. A secondary disturbance is earth illumination which can be reflected sunlight or infrared emission. Finally, small effects can result from spacecraft asymmetrical radiation emission in the form of thermal hot spots or radio transmissions. Each of these disturbances is examined below.

There are also three factors to be considered in the determination of forces from any radiation source. The quality of incident radiation determined by the intensity, spectrum, and direction is the first determinant. Second, is the geometry of the spacecraft including the shape of the surface and the location of the sun with respect to the spacecraft mass center. Finally, the optical properties of the surface upon which the radiation is incident or from which it is emitted must be considered. Table 2-1 summarizes the radiation sources and force determination factors to be used during this study.

Direct Solar Radiation

The two sources of direct solar radiation, photon pressure and the solar wind plasma force, are separated by four orders of magnitude. The solar wind is so much weaker than the photon radiation forces that its effect can safely be ignored.

TABLE 2-1

RADIATION DISTURBANCE FACTORS

SOURCES OF RADIATION	FORCE DETERMINATION FACTORS
I Direct Solar Radiation	I Incident Radiation Properties
A. Photons	A. Intensity
B. Solar Wind	B. Spectrum
	C. Direction
II Earth Illumination	II Spacecraft Geometry
A. Reflected Sunlight	A. Surface Shape
B. Infra-red Emission	B. Location of Sun
III Spacecraft Emission	III Surface Optical Properties
A. Thermal Hot Spots	A. Reflection
B. Radio or Power Transmission	B. Emission
	C. Absorbtion

The sun provides essentially collimated radiation with a reasonably well defined intensity and spectrum. The solar photon radiation may be characterized by the solar constant I_o which is the rate of which energy at all wavelengths is received per unit area. The best estimate of this value is 1353 $\pm$ 20 W/m^2 which when converted to force yields 4.513×10^{-6} N/m^2. Because this constant has units of force per unit area, it is often called a pressure. This terminology can be misleading as the pressure here is in reality a vector quantity not a scalar.

The solar constant follows an inverse square law which is important for interplanetary flight, however for earth orbit missions the only source of distance variation is the eccentricity of the earth's orbit. The variation due to eccentricity changes the value by 3.5 percent and can, for the purposes of this investigation, be ignored. Solar radiation, therefore, is taken to be a constant of 1353 W/m^2 from a collimated source.

Earth Illumination (Albedo)

In addition to the direct solar radiation falling on a spacecraft, reflected radiation from the earth also exerts a pressure. The effect is a maximum at noon and tends to partially cancel the direct radiation forces. The earth and its atmosphere act as a diffuse reflector with the result that the albedo radiation is not collimated. This considerably complicates the determination of the resulting forces. Often these forces are ignored on the grounds that their omission will lead to conservative estimates of the total direct and reflected radiation effects. While this approach is often justified, large vehicles in relatively low orbits can experience significant relief from the albedo radiation and it may be important to include the effect.

Assuming the earth to be a perfectly diffuse reflector obeying Lambert's cosine law, the radiation emitted from an element of area dA_1 is $kU\cos\theta\, dA_1$ N/m^2 per unit solid angle in a direction inclined θ to the surface normal. k can be identified as the albedo coefficient and U is the incident radiation. The radiation pressure at a distance r is

$$V = \frac{kU\cos\theta\, dA_1}{\pi r^2} \qquad (2.1)$$

directed along $\vec{r}$.

The normal and tangential components of radiation on an area dA_2, as shown in Figure 2-1 can be expressed

$$V_N = \frac{U}{\pi}\int \frac{k\cos\theta\cos\alpha}{\rho^2}\, dA_1$$

$$= -\frac{U}{\pi}\int \frac{k\cos\theta\,\vec{\rho}\cdot\hat{n}}{\rho^3}\, dA_1 \qquad (2.2)$$

and

$$V_T = \frac{U}{\pi}\int \frac{k\cos\theta\sin\alpha}{\rho^2}\, dA_1$$

$$= \frac{U}{\pi}\int \frac{k\cos\theta\,\hat{n}\times(\vec{\rho}\times\hat{n})}{\rho^3}\, dA_1 \qquad (2.3)$$

where n is a unit vector from surface element dA_2.

As a relatively simple application of the above expressions, the normal component of radiation pressure from the earth albedo will be found for a flat plate oriented paralled to the Earth's surface. The geometry is shown in Figure 2-2. Using equation (2.2)

$$V_N = \frac{U}{\pi}\int k\,dA_1 \int \frac{\cos\lambda\cos\delta}{\sigma^2}\, dA_2 \qquad (2.4)$$

directed along $\vec{\rho}$. Lacking better information, k may be taken as constant over the earth surface at the annual average value of approximately 0.34. Taking

$$dA_1 = r R\, d\theta\, d\eta = R^2\sin\theta\, d\theta\, d\eta$$

$$V_N = \frac{2kUR^2}{\pi}\int_0^{\pi/2}\sin\theta\, d\theta \int_0^{\eta(\theta)} \frac{\cos\lambda\cos\delta}{\sigma^2}\, d\eta \qquad (2.5)$$

and $\eta(\theta)$ is determined by the condition $\delta = \pi/2$

Using axes $\hat{i}\ \hat{j}\ \hat{k}$ as indicated in the figure

$$\vec{R} = \hat{i}R\cos\theta + \hat{j}R\sin\theta\cos\eta + \hat{k}R\sin\theta\sin\eta$$

$$\vec{\rho} = \hat{i}\rho\cos\eta + \hat{j}\rho\sin\eta$$

$$\vec{\sigma} = \vec{\rho} - \vec{R}$$

$$\cos\delta = \vec{R}\cdot\vec{\sigma}/R\rho\,,\quad \cos\lambda = \vec{\sigma}\cdot\vec{\sigma}/\sigma\rho$$

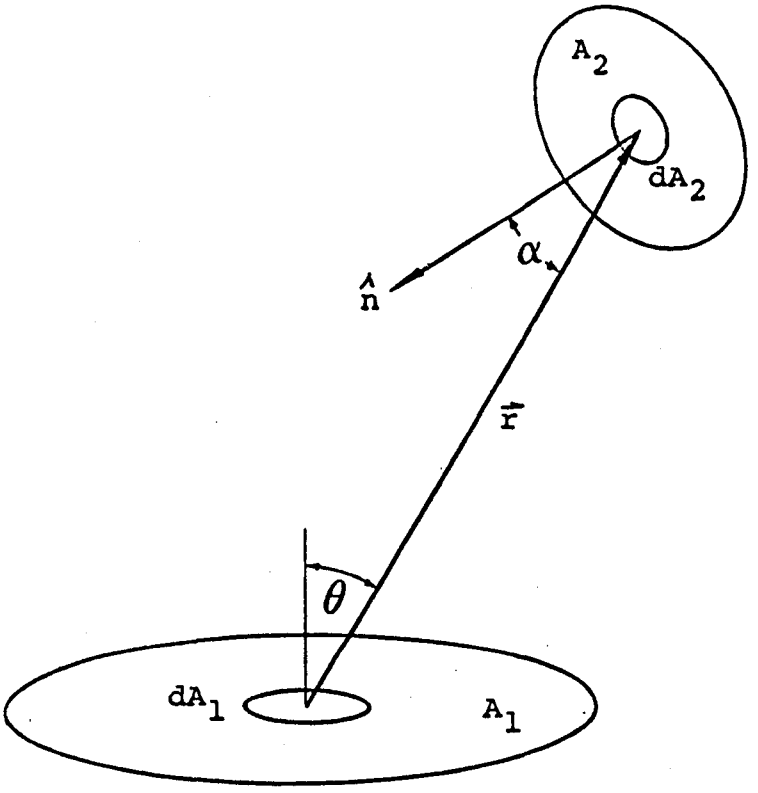

FIGURE 2-1 RADIATION GEOMETRY

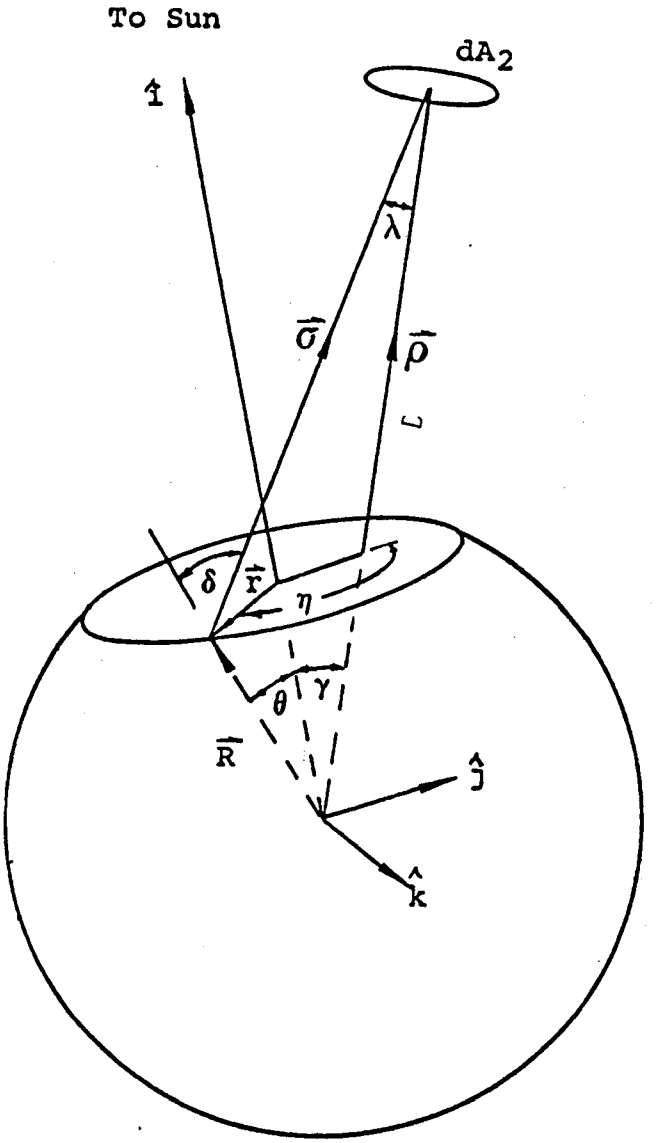

FIGURE 2-2 GEOMETRY FOR EVALUATING NORMAL RADIATION FORCES

When $\delta = \pi/2$, $\vec{R}\cdot\vec{\delta} = 0$, $\sin\theta\cos\eta\sin\gamma' = \frac{R}{\rho} - \cos\theta\cos\gamma'$ (2.6)

Defining $\eta' = \eta - \pi/2$, $\cos\eta = \sin\eta'$ and substituting into (2.6) leads to

$$\eta' = \sin^{-1}\left(\frac{\cos\theta\cos\gamma' - R/\rho}{\sin\theta\sin\gamma'}\right) \quad (2.7)$$

The limit $\eta(\theta)$ can thus be expressed $\eta(\theta) = \pi/2 + \eta'$ (2.8)

Curves of V/kU vs. aspect angle γ are shown in Figure 2-3 with altitude as a parameter.

Earth Radiation

The other source of disturbance from the earth and its atmosphere is a diffuse radiation with a spectrum approximated by the spectrum of a 288^{o} K black body. This temperature varies with the transparency of the atmosphere from 218^{o} K to 288^{o} K with about 95 percent of the emitted radiation originating from the earth or the lower atmosphere. The radiation is not collimated and may be treated in the same was as the earth reflectance problem with the following result

$$I_e = \frac{I_e^o}{\pi}\int_{Esss}\cos\psi\, dS/d^2 \quad (2.9)$$

where I_e^o = global average emmission constant (243 W/m^2)

dS = element of differential area on the surface of the Earth

d = distance from satellite to dS

ψ = angle between the normal to dS and d

Esss = earth surface as seen by satellite

Figure 2-4 shows the relative values of solar radiation, earth reflectance and earth radiation for a spherical satellite for a range or orbit radii.

Spacecraft Radiation

Two sources of disturbance stem from the spacecraft itself. Thermal hotspots resulting from an uneven temperature distribution and radio or power transmissions from onboard antennas. The following expression gives the thermal radiation emitted by the spacecraft at any point (y, θ) and emissivity $\varepsilon(T)$:

$$E(y,\theta) = \varepsilon[T(y,\theta)]\sigma T^4(y,\theta) \text{ in } W/m^2 \quad (2.10)$$

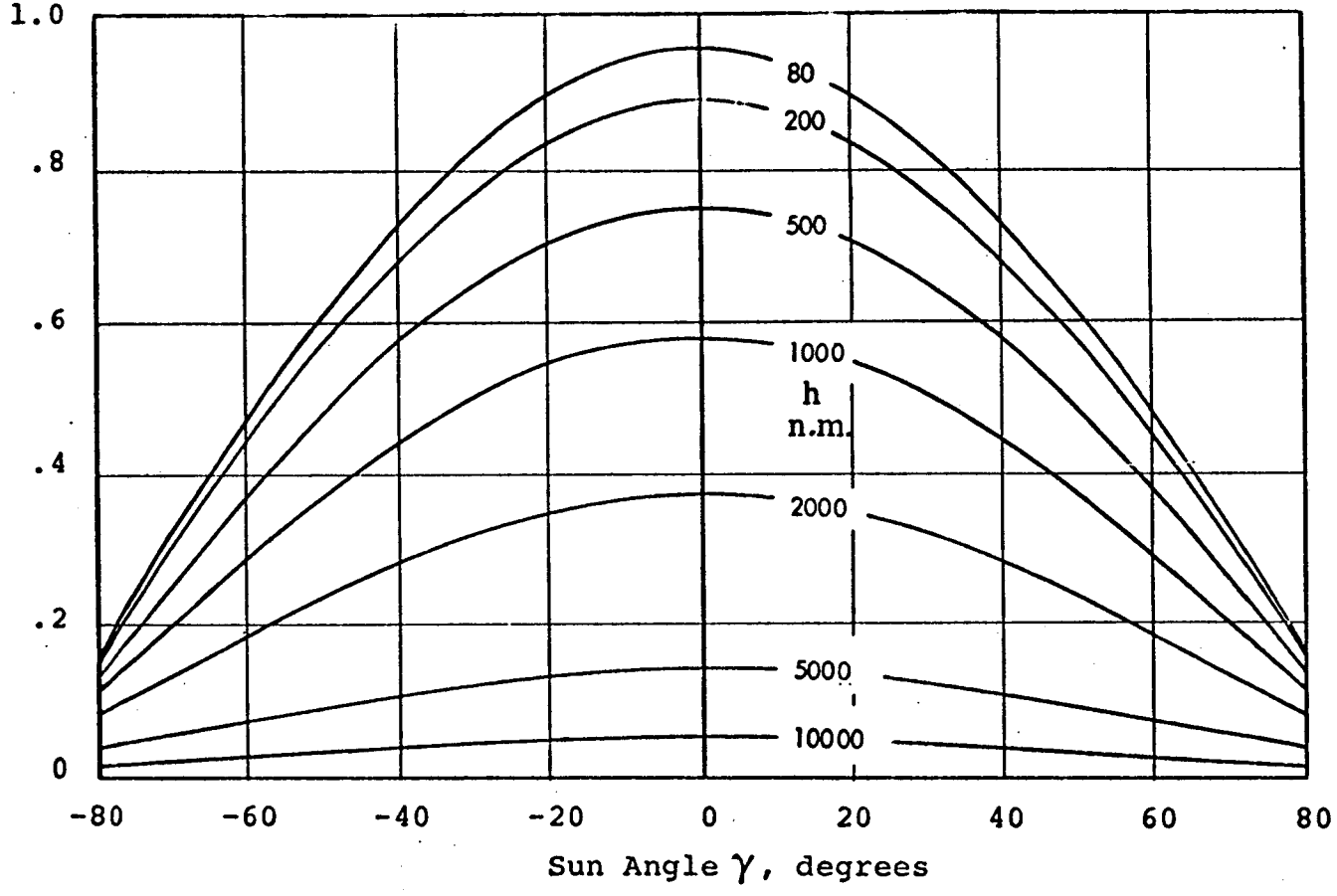

FIGURE 2-3 NORMAL RADIATION FORCE ON A FLAT PLATE

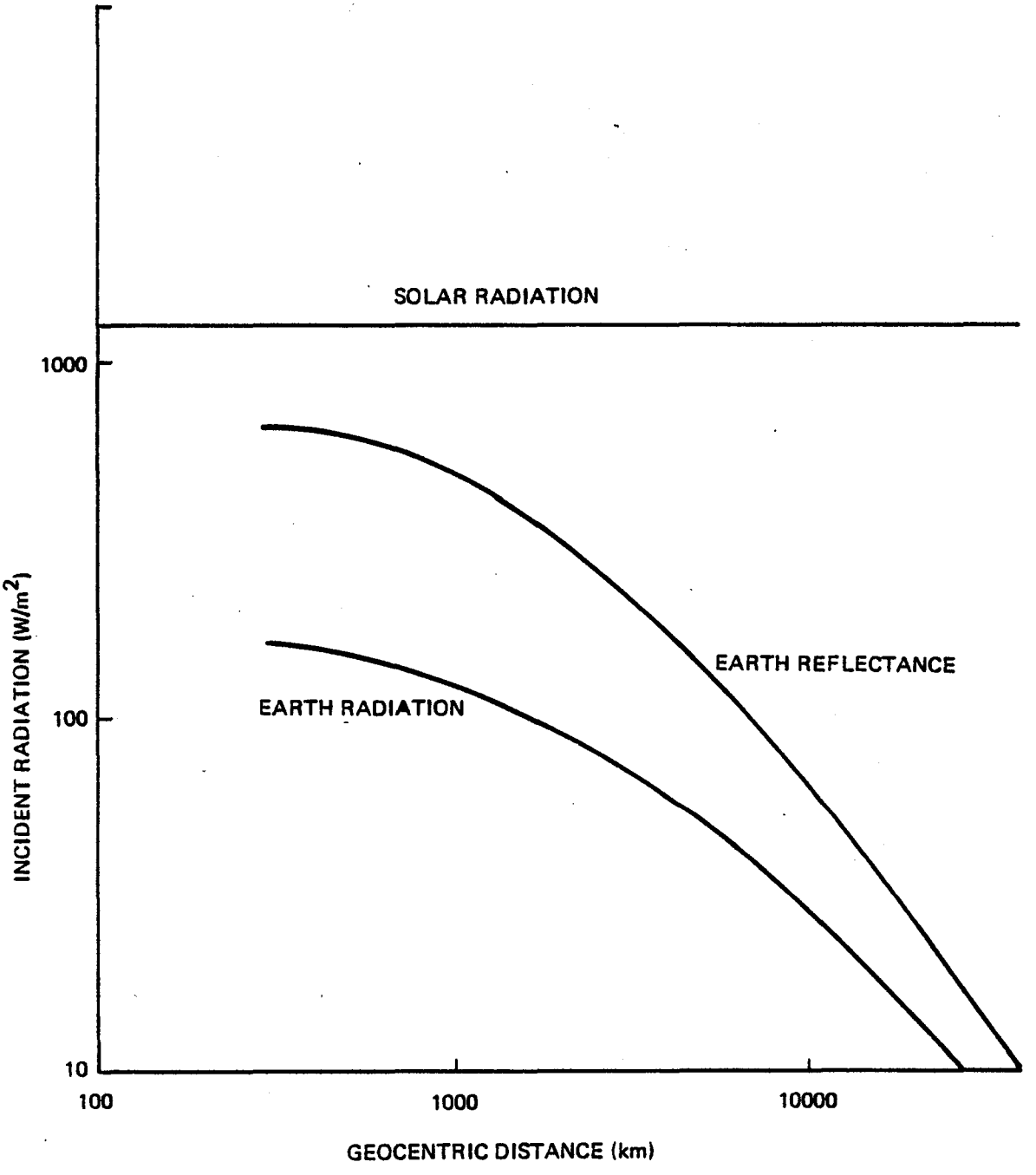

FIGURE 2-4 RADIATION DISTURBANCE FORCES COMPARED

For diffuse emission, the effective flux is normal to the surface and of magnitude 2/3 E (y, θ). Radio and power source disturbances can be calculated from the power densities and beam efficiencies of the transmitter.

Spacecraft Radiation Torques

From the previous sections, the amount of incident radiation on a spacecraft from solar, terrestial, and spacecraft sources may be determined. The resultant force on the spacecraft is dependent on the properties of incident radiation, geometry and surface optical properties.

When radiation falls on any surface, some of the incoming radiation is absorbed and some is reflected. The character of the reflected radiation depends on the surface properties and is rarely well defined. Generally, it is resolved into specularly and diffusely reflected components. In specular reflection, illustrated in Figure 2-5, the incoming and reflected radiation make equal angles with the surface normal. Diffuse reflection is independent of the angle of incidence and the outgoing radiation follows a cosine law, Figure 2-6.

The radiation forces are easily derived for absorbing, specularly reflecting and diffusely reflecting surfaces. With incoming radiation I in W/m^2, the velocity of light c in m/s and angle of incidence θ, the forces are in N and can be broken down into normal $(\hat{n})$ and tangential $(\hat{s})$ components. These forces are given below

Radiation from a completely absorbing surface

$$d\vec{F} = \left(\frac{I}{c}\right)\left(-\hat{n}\cos\theta + \hat{s}\sin\theta\right)\cos\theta\, dA \qquad (2.11)$$

Radiation from a completely specular reflecting surface

$$d\vec{F} = \left(\frac{I}{c}\right)\left(-2\hat{n}\cos\theta\right)\cos\theta\, dA \qquad (2.12)$$

Radiation from a complete diffuse reflecting surface

$$d\vec{F} = \left(\frac{I}{c}\right)\left(-\hat{n}\left(\cos\theta + \frac{2}{3}\right) + \hat{s}\sin\theta\right)\cos\theta\, dA \qquad (2.13)$$

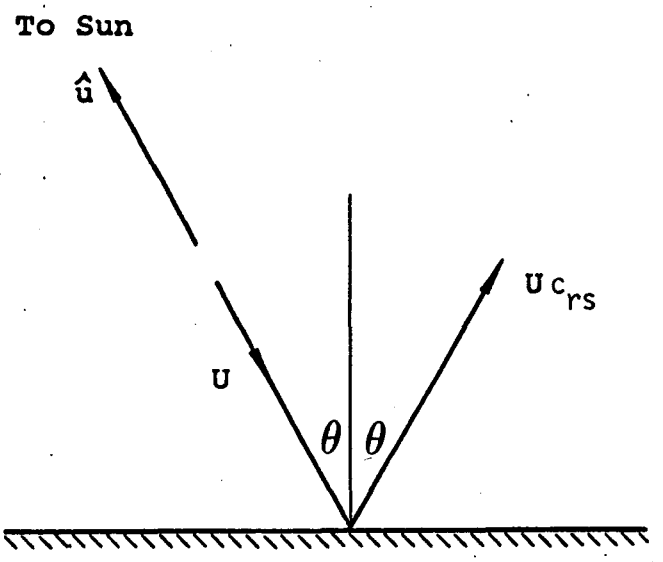

FIGURE 2-5 SPECULAR REFLECTION

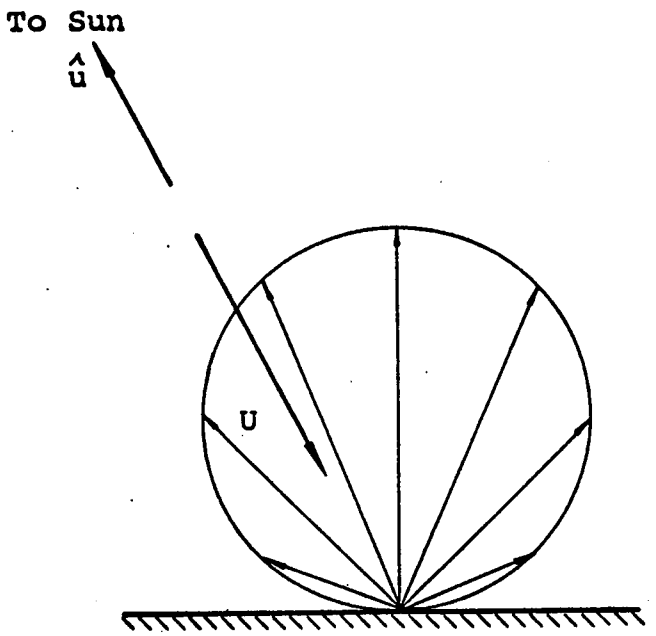

FIGURE 2-6 DIFFUSE REFLECTION

One can combine these expressions for a total incremental force given c_a = absorbtion coefficient, c_{rs} = specular reflection coefficient, and c_{rm} = diffuse reflection coefficient.

$$d\vec{F} = \left(\frac{I}{c}\right)\left[-\hat{n}\left\{\frac{2}{3}c_{rd} + (1+c_{rs})\cos\theta\right\} + \hat{s}(1-c_{rs})\sin\theta\right]\cos\theta\, dA \qquad (2.14)$$

The general expression for the radiation torque acting on a spacecraft is

$$L_r = \int_{ses} \vec{V} \times d\vec{F} \qquad (2.15)$$

where L_r = radiation torque
$\vec{V}$ = vector directed from the spacecraft mass center to element of area dA
$d\vec{F}$ = radiation force on element of area dA
ses = spacecraft exposed surfaces

The practical application of this expression involves a number of approximations in the determination of df and in the integration over all spacecraft surfaces. The usual procedure is to approximate these surfaces by means of simple geometric shapes (planes, cylinders, cones, spheres, etc.). Torque on these surfaces may be calculated separately and summed over the individual components.

2.2.2 Gravity Gradient

Although the generation of gravitational forces is imperfectly understood, the empirical relations are well established. Two homogeneous spherical masses will attract one another by a force

$$F = \frac{G_r M m}{L^2} \qquad (2.16)$$

where G is the gravitational constant; M and m are the two masses, and L is the distance between them.

The earth is neither spherical nor homogeneous in mass, thus, its field is not uniform. A more precise description of the field is given by

$$\vec{F} = m\nabla U$$

where U is the gravitational potential. The potential function has been accurately determined from a study of satellite orbit perturbations. Although the field anomalies are important for orbit determination, their effect on gravity gradient torques is minor. For all practical purposes, the perfect inverse square field described by equation (2.16) will be found adequate for disturbance analysis. Generally, the product GM is given as a constant for a particular primary and is designated μ. In MKS units, for earth

$$\mu = GM = 3.98604 \times 10^5 \ km^3/sec^2$$

If m is defined in kilograms and L in meters, the force is in Newtons. The force is directed along the line joining the two masses. In orbit the force on the satellite is towards the center of the primary body. (The satellite also attracts the primary, but the effect is negligible except when considering large natural satellites such as moons and planets). In vector form equation (2.16) can be written

$$\vec{F} = \frac{\mu m \vec{L}}{L^3}$$

The force of gravity falls off with the square of the distance and theoretically extends to infinity. However, when several bodies are present, as in the solar system, a point is reached where opposing gravitational attractions become equal. It turns out that the region in which the attraction of one body predominates is a sphere. This has been named the gravisphere, and its center is normally displaced from the center of the body. It is only within a gravisphere that orbits can take place. For earth the radius of the sphere is about 1.5×10^6 km.

The torques that stem from the gravity field are often called "gravity gradient" torques because it is the gradient of the field that generates the torque. The mecahnism can probably best be understood by considering a dumbbell consisting of two equal masses separated by a rod. Because the force of gravity varies inversely with the square of the distance, it follows that the mass nearest the center of the earth is attracted a little more strongly than the mass farther away. A torque is thus produced tending to align the dumbbell with the local vertical. It seems reasonable to expect a horizontal orientation of the dumbbell to be a position of

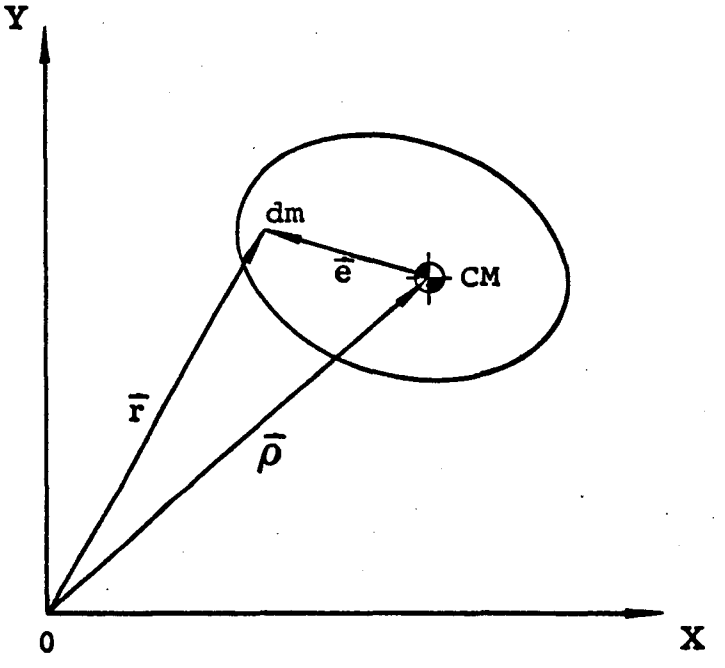

FIGURE 2-7 GEOMETRY

unstable equilibrium. The forces are nominally equal, but any slight rotation immediately increases the attraction of the lower mass at the expense of the upper. At the other extreme, a vertical orientation would be expected to represent a stable equilibrium in which the difference in attraction reaches a maximum. Both these expectations turn out to be correct.

Another way of looking at gravity gradient torques is to consider the center of gravity (CG) and center of mass (CM) of a body. Rotations take place about the CM, but the CG (the point where gravitational forces are effectively concentrated) will be displaced from the CM in an inverse square field. The CG is always closer (or as close) as the CM to the center of the earth. The moment of the force about the CM is the gravity gradient torque. It is very small because the CM-CG displacement is very small.

The gravity gradient torque on an arbitrary body can be found by calculating the force on a mass element and summing the torque elements over the whole body.

The gravitational force on an element of mass is

$$d\vec{F} = -\frac{\mu}{\rho^3}\vec{r}\,dm$$

If vectors $\vec{e}$, $\vec{r}$, and $\vec{\rho}$ are defined as shown in Figure 2-7, the element of torque is

$$d\vec{T} = \vec{e} \times d\vec{F}$$

Since $\vec{r} = \vec{\rho} + \vec{e}$, the torque can be expressed

$$d\vec{T} = -\frac{\mu}{\rho^3}\vec{e}\times\vec{\rho}\,dm \qquad (2.17)$$

By using a binomial expansion, a first order approximation of $1/\rho^3$ can be written

$$\frac{1}{\rho^3} \sim \frac{1}{\rho^3}\left(1 - \frac{3\vec{\rho}\cdot\vec{e}}{\rho^2}\right) \qquad (2.18)$$

Substitution of (2.18) in (1.7) leads to

$$\vec{T} = \frac{3\mu}{\rho^5}\int \vec{\rho}\cdot\vec{e}\,(\vec{e}\times\vec{\rho})\,dm \qquad (2.19)$$

If $\vec{\rho}$ and $\vec{e}$ are defined

$$\vec{\rho} = \begin{bmatrix} a \\ b \\ c \end{bmatrix}, \quad \vec{e} \begin{bmatrix} x \\ y \\ z \end{bmatrix}$$

evaluation of (2.19) yields

$$\vec{T} = \frac{3\mu}{\rho^5}\left[\hat{i}\{acF - abE - D(b^2-c^2) + bc(C-B)\} + \hat{j}\{abD - bcF - F(c^2-a^2) + ac(A-C)\} + \hat{k}\{bcE - acD - F(a^2-b^2) + ab(B-A)\}\right] \quad (2.20)$$

The quantities A through F are elements of the moment of inertia matrix, defined

$$[I] = \begin{bmatrix} A & -F & -E \\ -F & B & -D \\ -E & -D & C \end{bmatrix}$$

This is the general expression for the gravity gradient torque in body axes on an arbitrary vehicle, arbitrarily oriented. In any given application the components of $\vec{\rho}$, i.e., a, b, and c, can be substituted for once the transformation defining the body axis orientation is established. Suppose body and orbit reference axes are related by the conventional ZYX sequence

$$\begin{bmatrix} x \\ y \\ z \end{bmatrix} = [T_1(\phi)][T_2(\theta)][T_3(\psi)]\begin{bmatrix} X_0 \\ Y_0 \\ Z_0 \end{bmatrix}$$

where ϕ, θ, and ψ are the roll, pitch and yaw Euler angles.

Now $\vec{\rho}$ in orbit axes is simply $-k\rho$; thus $\vec{\rho}$ in body axes is

$$\vec{\rho} = \rho[T_1(\phi)][T_2(\theta)][T_3(\psi)]\begin{bmatrix} 0 \\ 0 \\ -1 \end{bmatrix}$$

Evaluation leads to

$$a = -\rho\sin\theta$$
$$b = \rho\sin\phi\cos\theta$$
$$c = \rho\cos\phi\cos\theta$$

and these values, substituted into (2.20) lead to

$$T_x = \frac{3\mu}{2\rho^3}\left[-F\cos\phi\sin 2\theta + E\sin\phi\sin 2\theta + 2D\cos^2\theta\cos 2\phi + (C-B)\cos^2\theta\sin 2\phi\right]$$

$$T_y = \frac{3\mu}{2\rho^3}\left[-D\sin\phi\sin 2\theta - F\cos^2\theta\sin 2\phi - 2E(\cos^2\theta\cos^2\phi - \sin^2\theta) + (C-A)\sin 2\theta\cos\phi\right]$$

$$T_z = \frac{3\mu}{2\rho^3}\left[E\cos^2\theta\sin 2\phi - F\cos^2\theta\sin 2\phi - 2E(\cos^2\theta\sin^2\phi - \sin^2\theta) + (A-B)\sin 2\theta\sin\phi\right] \qquad (2.21)$$

If the body axes are chosen as principle axes of inertia, then D, E, and F are zero, and the body axis torque expressions simplify to

$$T_x = 3\mu(C-B)\cos^2\theta\sin 2\phi/2\rho^3$$

$$T_y = 3\mu(C-A)\sin 2\theta\cos\phi/2\rho^3$$

$$T_z = 3\mu(A-B)\sin 2\theta\sin\phi/2\rho^3 \qquad (2.22)$$

If the orbit is circular, μ/ρ^3 can be replaced Ω^2. If, in addition, the angles are small enough to justify small angle approximation

$$T_x \sim 3\Omega^2(C-B)\phi$$

$$T_y \sim 3\Omega^2(C-A)\theta$$

$$T_z \sim 3\Omega^2(A-B)\phi\theta \sim 0 \qquad (2.23)$$

It should be noted that the yaw angle, ψ, nowhere appears in the torque expressions and that the yaw torque is of second order compared to the roll and pitch torques. For small angles, the roll and pitch torques are proportional to the roll and pitch angles.

2.2.3 Aerodynamic Disturbances

Aerodynamic effects on spacecraft are significant for orbital altitudes up to approximately 1000 km. The forces due to radiation pressure and aerodynamic drag and lift are of similar magnitude for altitudes between 600 and 1000 km, beyond 1000 km the radiation-related forces are typically much greater than those arising aerodynamically. This analysis will, therefore, treat only those altitudes ranging from 300 km (corresponding to low earth orbit, the LSS construction and assembly environment) to 1000 km.

Knowledge of the characteristics of the atmospheric medium is essential for analysis of the aerodynamic forces acting upon the structure. The Knudsen number, defined as the ratio of the molecular mean free path to a characteristic dimension of the spacecraft, serves as a convenient means for dividing the flow into various regimes. The flow is classified as continuum flow if the Knudsen number (K) is less than 10^{-2}, as slip flow for $10^{-2} < K < 10^{-1}$, as transition flow for $10^{-1} < K < 10$, and, for $K > 10$, as free-molecular flow.

Using the above criteria, LSS configurations of classes IIB, IIIA, and IIIB are found to encounter only free-molecular flow. Several members of classes IA, IB, IIA, and IIC have dimensions large enough to place them within the transition flow regime. However, due to the approximate nature of the estimated spacecraft dimensions and the absence of any well-established theoretical or empirical understanding of transition flow effects, it will be assumed for the purposes of this study that free-molecular flow is encountered by all of the LSS configurations. By definition, the term "free-molecular" implies that each particle interacts with the structure on an individual basis and that no inter-molecular effects occur.

Given the assumption of free-molecular flow, there are three analytic methods for the characterization of aerodynamic effects whose complexities are low enough to render them sufficiently tractable and adequately general to suit the applications of this study.

An expression of the form $F = 1/2 C_D \rho V^2 A$ (where C_D is the drag coefficient, ρ the atmospheric density, V the velocity of the vehicle through the medium, and A the projected area normal to the flow direction) may be utilized to estimate the gross value of the aerodynamic force.

Another technique makes use of the equation:

$$d\vec{F} = -\rho V^2 \left[(2 - \sigma_n - \sigma_t)(\hat{e}_n \cdot \hat{e}_V)^2 \hat{e}_n + \sigma_t (\hat{e}_V \cdot \hat{e}_n) \hat{e}_V \right] dA \qquad (2.24)$$

where ρ, V, and A are as defined previously
σ_n, σ_t are the normal and tangential momentum exchange coefficients, respectively (properties of the surface material)
$\hat{e}_V$ is the spacecraft velocity unit vector
$\hat{e}_n$ is the unit vector outward from and normal to dA

The final approach to the problem of analyzing the aerodynamic forces acting upon the vehicle involves the assumption of hyperthermal flow conditions, i.e., that the spacecraft speed is large relative to the thermal motion of the atmospheric particles. The $F = 1/2 C_D \rho V^2 A$ equation is utilized to determine the forces acting upon each of the major components of the vehicle. The drag coefficient is characterized in the literature as a function of the ratio of the reflected and incident particle speeds for various general structural shapes.

Certain assumptions must be involved with the utilization of any of these techniques. However, the second analytic method outlined above appears to be most appropriate for this study and will be described in more detail below. The first approach was eliminated largely because of the degree of approximation involved in the estimation of some characteristic value for the drag coefficient ($C_D = 2.6$ is commonly used). The hyperthermal flow analysis was abandoned because of the unacceptably large errors which can be incurred for surfaces parallel to the flow.

When equation (2.24) is used to calculate the aerodynamic loads on the various LSS configurations, it is seen that atmospheric density, vehicle velocity and the normal and tangential momentum exchange coefficients are the critical parameters.

Density is primarily a function of altitude but significant variations are introduced by geomagnetic activity and a number of cylic effects. These include a diurnal cycle, a semi annual cycle and 27 day and 11 year solar cycles. Models of the density field have been constructed but these are all empirical and correlation with measured values is only fair. The U.S. Standard Atmosphere can be used for mean values but actual densities can vary considerably as shown by the comparison in Table 2-2. If orbit, time, date and solar activity data are available, reasonably good estimates can be obtained from the model described in Reference A15 of Appendix B.

The orbits travelled by the LSS vehicles under consideration will be either circular (assembly and operation environments) or elliptical (encountered primarily during transfer from initial point to final destination). As such, the velocity of the spacecraft may be expressed as a function of the vehicle's angular momentum. Maximum and minimum values will be found at the periapsis and apoapsis, respectively. Table 2-3 summarizes the range of velocity values which will characterize LSS spacecraft in the regions where aerodynamic disturbances will be of significant concern.

Particles impacting on these space structures will adhere momentarily to the surface and then be re-emitted at some velocity which describes the degree of equilibrium attained between the particle and the structure. The normal and tangential momentum exchange coefficients, in addition to the thermal accommmodation coefficient, describe this process in detail and are given in equation form below

$$\alpha = \frac{E_i - E_r}{E_i - E_s} \tag{2.25}$$

where E_i = the energy carried to the surface by an incident particle
E_r = the energy carried away from the surface by a re-emitted particle
E_s = the energy possessed by a particle emitted with a temperature equal to that of the surface.

$$\sigma_t = \frac{\tau_i - \tau_r}{\tau_i - \tau_s} \tag{2.26}$$

TABLE 2-2

ATMOSPHERIC DENSITY VARIATION
(SUNSPOT AND DIURNAL EFFECTS)

Altitude*	1976* US Std. Atm	Low Density Atm ** (Nighttime Near Sunspot Min.)	High Density Atm ** (Daytime Near Sunspot Max)
300	1.92×10^{-11}	4.02×10^{-12}	9.70×10^{-11}
400	2.80×10^{-12}	3.19×10^{-13}	2.38×10^{-11}
500	5.22×10^{-13}	3.26×10^{-14}	7.22×10^{-12}
600	1.14×10^{-13}	5.07×10^{-15}	2.51×10^{-12}
700	3.07×10^{-14}	1.67×10^{-15}	9.65×10^{-13}
800	1.14×10^{-14}	9.37×10^{-16}	3.97×10^{-13}
900	5.75×10^{-15}	6.36×10^{-16}	1.72×10^{-13}
1000	3.56×10^{-15}	4.64×10^{-16}	7.73×10^{-14}

*Altitude, km

**Density, kcg/m^3

TABLE 2-3

ORBITALLY-DETERMINED VEHICLE VELOCITIES

Comment	Perigee Altitude (km)	Apogee Altitude (km)	Perigee Radius (km)	Apogee Radius (km)	Perigee Velocity (km/s)	Apogee Velocity (km/s)
Circular	--	--	LEO*	LEO*	7.726	7.726
Circular	--	--	GEO**	GEO**	3.075	3.075
Circular	1000	1000	--	--	7.350	7.350
Elliptical***	--	--	LEO	GEO	10.152	1.608
Elliptical****	300	1000	--	--	7.916	7.165

* Low Earth Orbit, Altitude = 300 km, Earth Radius ≈ 6378 km
** Geosynchronous Orbit, $R_{GEO} \approx 42164$ km
*** Maximum Velocity Condition at Perigee
**** Minimum Velocity Condition at Apogee (Largest orbit with continual aerodyanmic effect)

$$h^2 = \mu a (1-e^2)$$

$$2a = r_a + r_p$$

$$e = \frac{r_a - r_p}{r_a + r_p}$$

$$h^2 = 2\mu \frac{r_a r_p}{r_a + r_p}$$

$$h = r_a v_a = r_p v_p$$

Where: μ = gravitational parameter, $3.986012 \times 10^5 \frac{km^3}{s^2}$

a = semi-major axis of orbit

e = eccentricity of orbit

r_a, r_p = radius of orbit at apogee and perigee, respectively.

v_a, v_p = velocity at apogee and perigee, respectively.

where τ_i = the tangential momentum carried to the surface by an incident particle

τ_r = the tangential momentum carried away from the surface by a re-emitted particle

τ_s = the tangential momentum carried away from the surface by a re-emitted particle in thermal equilibrium with the surface ($\alpha = 1$).

$$\sigma_n = \frac{P_i - P_r}{P_i - P_s} \tag{2.27}$$

where P_i, P_r and P_s refer to the particle normal momentum values and are defined similarly to τ_i, τ_r, and τ_s.

Particles may be re-emitted, or reflected, either specularly or diffusely. For completely diffuse reflection, $\tau_r = \tau_s = 0$ and $\sigma_t = 1$, independent of thermal accommodation. For completely diffuse reflection and 100 percent thermal accommodation ($\alpha = 1$), $P_r = P_s$ and $\sigma_n = 1$. The thermal accommodation coefficients of materials commonly used in space structures have values which lie primarily between 0.87 and 0.97. Past analyses have shown the reflection of particles to be predominantly diffuse. Recommended average values for σ_n and σ_t range between 0.80 and 1.0.

An exercise using this technique for several bounding cases has been conducted, the results of which are presented in Table 2-4 on a force per unit area basis. These values represent the aerodynamic forces which correspond to the maximum and minimum loading conditions (maximum and minimum velocity and density, respectively) for surfaces oriented 90^o and 45^o to the direction of flow. The values used for the atmospheric density and vehicle velocity were drawn from Tables 2-2 and 2-3; the tangential and normal momentum exchange coefficients were each assumed to have a value of 0.90.

It is important to note that the aerodynamic loading predicted through application of the technique presented herein corresponds to forces acting on solid surfaces. Much of the material involved in the various LSS configurations will consist of truss assemblies, RF mesh, etc. Reasonable

TABLE 2-4

APPLICATIONS FOR EXTREME CONDITIONS

Comment	Perigee	Apogee	Velocity-Surface Unit Vector Angle	Force Per Unit Area (N/m^2) Perigee	Apogee
Max. Velocity & Density	(Radius) LEO	(Radius) GEO	$0.^o$	$-(0.0004\hat{e}_n+0.0018\hat{e}_v)$	(Not Applicable) (No Aerodynamic Effect)
Max. Velocity & Density	(Radius) LEO	(Radius) GEO	45^o	$-(0.0002\hat{e}_n+0.0013\hat{e}_v)$	(Not Applicable) (No Aerodynamic Effect)
Min. Velocity & Density	(Altitude) 300 km	(Altitude) 1000 km	$0.^o$	$-(0.0002\hat{e}_n+0.0011\hat{e}_v)$	$-(3.66\times10^{-8}\ \hat{e}_n + 1.645\times10^{-7}\ \hat{e}_v)$
Min. Velocity & Density	(Altitude) 300 km	(Altitude) 1000 km	45^o	$-(0.0001\hat{e}_n+0.0008\hat{e}_v)$	$-(1.83\times10^{-8}\ \hat{e}_n + 1.16\times10^{-7}\hat{e}_v)$

estimation of the loads which will actually be experienced may be achieved by applying factors to account for the transmissivity of these elements to the forces predicted for identically-sized solid structures.

2.2.4 Magnetic Disturbances

The interaction of a satellite with the earth magnetosphere is represented by the simple equation:

$$\vec{T} = \vec{M} \times \vec{B} \tag{2.28}$$

where $\vec{M}$ = the equivalent magnetic dipole of the spacecraft

$\vec{B}$ = the vector describing the ambient magnetic field

$\vec{T}$ = the resultant torque acting upon the vehicle.

Analysis of these disturbances requires characterization of the earth's magnetic field, estimation of a given configuration's magnetic dipole and determination of the orientation of the spacecraft dipole within the local magnetic field.

Earth Magnetic Field Model

The geomagnetic field is both complex and dynamic in its distribution, magnitude and direction. Near the surface there are local variations in the field caused by ore deposits. Beyond about five earth radii, the field becomes increasingly distorted due to interaction of the field with the solar plasma. Empirical models have been developed and the spherical harmonic expansion can provide accuracies of about 0.1 percent below five earth radii. Simpler models, which are actually truncations of the spherical harmonic expansion, offer simplicity at the expense of accuracy. Common models are

- o Offset tilted dipole (quadrupole model)
- o Centered tilted dipole
- o Centered, spin axis aligned dipole.

The centered tilted dipole (first three terms of the expansion) provides accuracies of about three percent between two and five earth radii and will be used below. At 300 km, errors can reach 60 percent in magnitude and 33^{o}

in direction. At synchronous altitude (about 6.6 earth radii) the errors drop to four percent and two degrees, except during periods of geomagnetic storm activity.

Because of the length of the equations describing the field they are not included in the text but are presented in Table 2-5. The associated coordinate reference frames are given in Figures 2-8 and 2-9. Figures 2-10 and 2-11 provide a graphical representation of the field's spatial distribution and magnitude.

The dynamic behavior of the magnetosphere is composed of both secular (small scale, continuous changes due to variations of field sources within the earth) and temporal (short term but severe in magnitude, usually arising from geomagnetic storms or fluctuations in solar activity) elements. In general, only the temporal variations may be assumed to be of significance. However, it is difficult to characterize the specific nature of these variations; severe changes in magnitude and complete reversals of field direction can occur particularly at high altitude. In order to accommodate the distortions and uncertainties associated with these effects, variations of $\pm$ 50 percent and $\pm 20^{o}$ in the magnitude and direction of the magnetic field is included in the analysis.

Spacecraft Magnetic Dipole

The elements with the most potential of establishing a significant magnetic dipole within a spacecraft are current loops and materials subject to permanent or induced magnetism. Contributions from these components may be altered through interaction with the magnetic environment; for example, eddy currents may be produced within current loops and hysteresis effects may be generated within permeable materials. Certain functional spacecraft components also possess magnetic properties of some significance (batteries, tape recorders, transistors, capacitors, etc.).

The magnitude of the resultant magnetic dipole may be limited to those caused by permeable materials used within the spacecraft structure if appropriate design techniques are utilized. The backwiring of solar arrays (significant sources of current loops effects) and the mounting of batteries in pairs with opposing dipoles are two such procedures. Eddy

TABLE 2-5

GEOMAGNETIC FIELD CENTERED TILTED DIPOLE MODEL

$$B_x = \left(\frac{R_E}{R}\right)^3 \left[-g_1^0 \sin\theta + g_1' \cos\theta \cos\lambda + h_1' \cos\theta \sin\lambda\right]$$

$$B_y = \left(\frac{R_E}{R}\right)^3 \left[g_1' \sin\lambda - h_1' \cos\lambda\right]$$

$$B_z = -2\left(\frac{R_E}{R}\right)^3 \left[g_1^0 \cos\theta + g_1' \sin\theta \cos\lambda + h_1' \sin\theta \sin\lambda\right]$$

$$|\vec{B}| = \left(B_x^2 + B_y^2 + B_z^2\right)^{1/2}$$

where R_E = earth radius = 6371.2 km

R = geocentric radial position of satellite

g_1^0 = -30401.2 nT

g_1' = -2163.8 nT

h_1' = 5778.2 nT

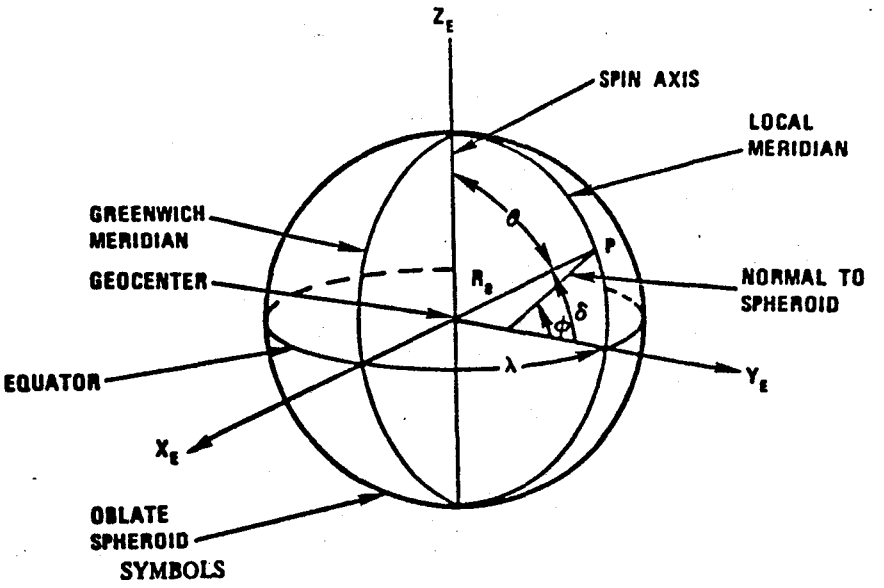

SYMBOLS

X_E	Positively directed along intersection of Greenwich Meridian and Equatorial planes
Z_E	Positively directed north along Earth's mean spin axis
Y_E	$Z_E \times X_E$
λ	Geocentric longitude, measured positive eastward from Greenwich meridian to local meridian
δ	Geocentric latitude, declination measured positive north (geocentric and geodetic latitude differs by 11.6 minutes maximum at 45° latitude.)
θ	Geocentric colatitude = $90° - \delta$
R_e	Mean Earth radius, 6371.2 km
λ	Geodetic longitude = geocentric longitude
ϕ	Geodetic latitude, measured positive north from Equatorial plane to normal to Spheroid

DEFINITIONS

Dipole North Pole.–Defined by axis of calculated central dipole whose magnetic field is best fit to main geomagnetic field over Earth's surface and whose axis passes through geocenter. Defined to be at 78.5°N, 69.0°W in northwestern Greenland.

Dipole Equator.–Defined as great circle of spherical Earth which is normal to central dipole axis.

Dip North Pole.–Shifting point on Earth's surface where geomagnetic field lines are vertical. Location changes by a few kilometers during any day in response to transient magnetic fields. Located northwest of Hudson Bay at about 73°N, 98°W.

Geodetic to Dipole Transformation.–This is defined by the following equations (ref. 11):

$$\sin \Lambda = \frac{\cos \phi \sin (\lambda - 291°)}{\cos \Phi}$$

$$\sin \Phi = \sin \phi \cos 11.7° + \cos \phi \sin 11.7° \cos (\lambda - 291°)$$

FIGURE 2-8 GEOCENTRIC COORDINATE SYSTEM (FROM NASA SP 8017)

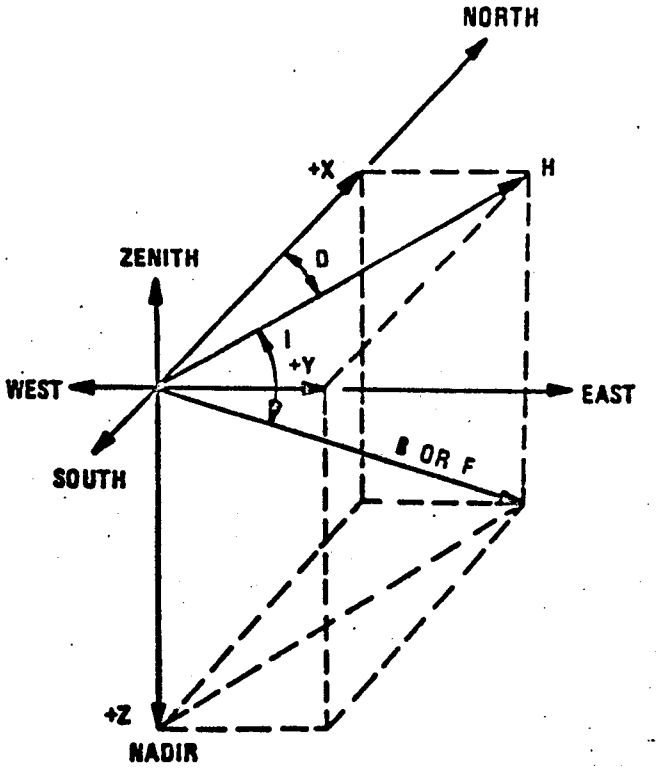

Local geomagnetic coordinate system

SYMBOLS

B	Total computed magnetic field intensity (total magnetic flux density - SI nomenclature)
F	Total measured field intensity
X(B_X)	North component of B
Z(B_Z,V)	Vertical component of B
Y(B_Y)	East component of B (Z × X)
I	Inclination or dip angle
H	Horizontal field intensity (B cos I)
D	Declination angle

FIGURE 2-9 LOCAL GEOMAGNETIC COORDINATE SYSTEM (FROM NASA SP 8017)

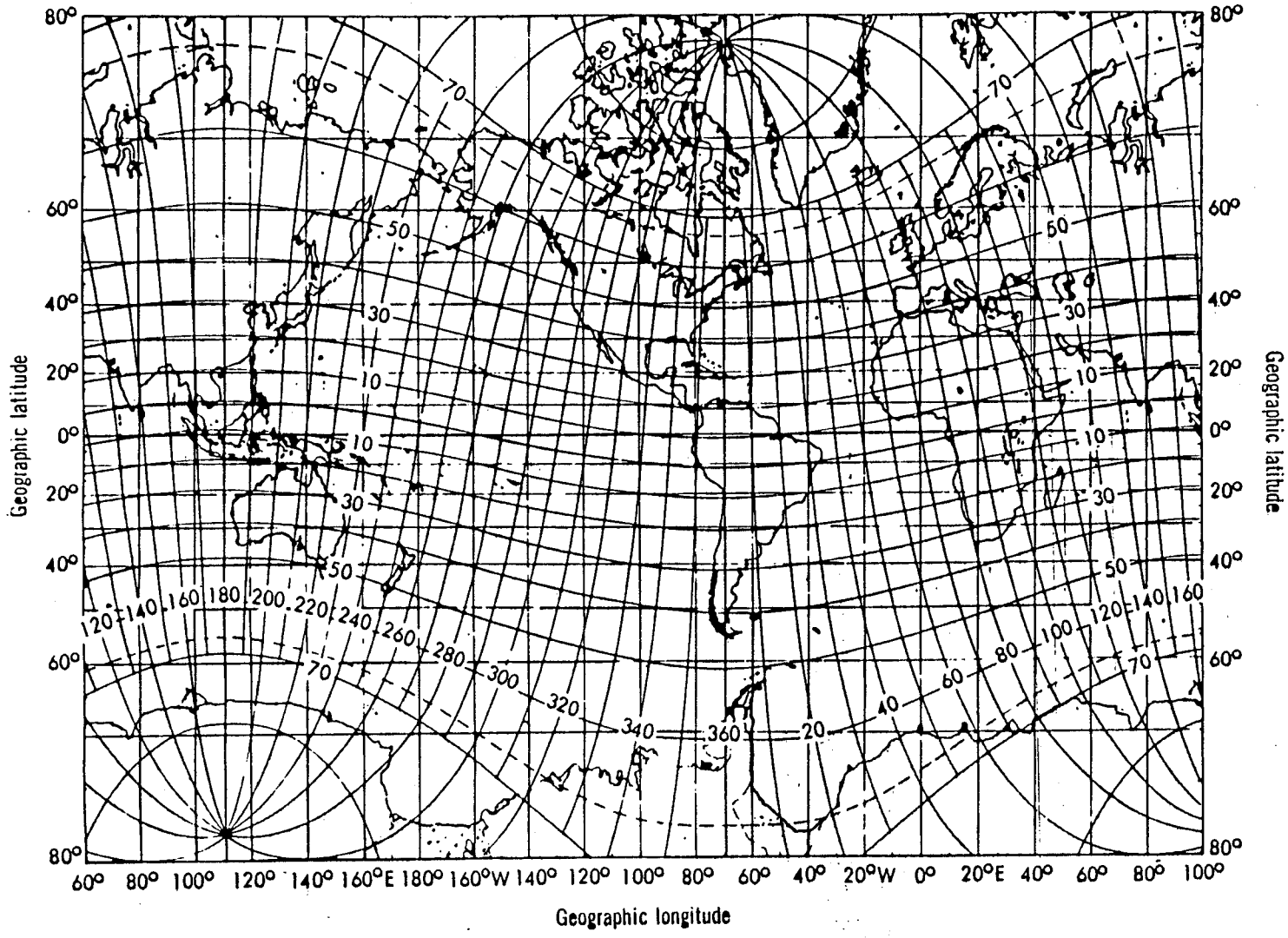

FIGURE 2-10 COMPARISON OF GEOGRAPHICAL AND GEOMAGNETIC COORDINATE SYSTEM (CURVED LINES ARE GEOMAGNETIC COORDINATES SUPERPOSED ON A GEOGRAPHIC MERCATOR PROJECTION) (FROM NASA SP 8018)

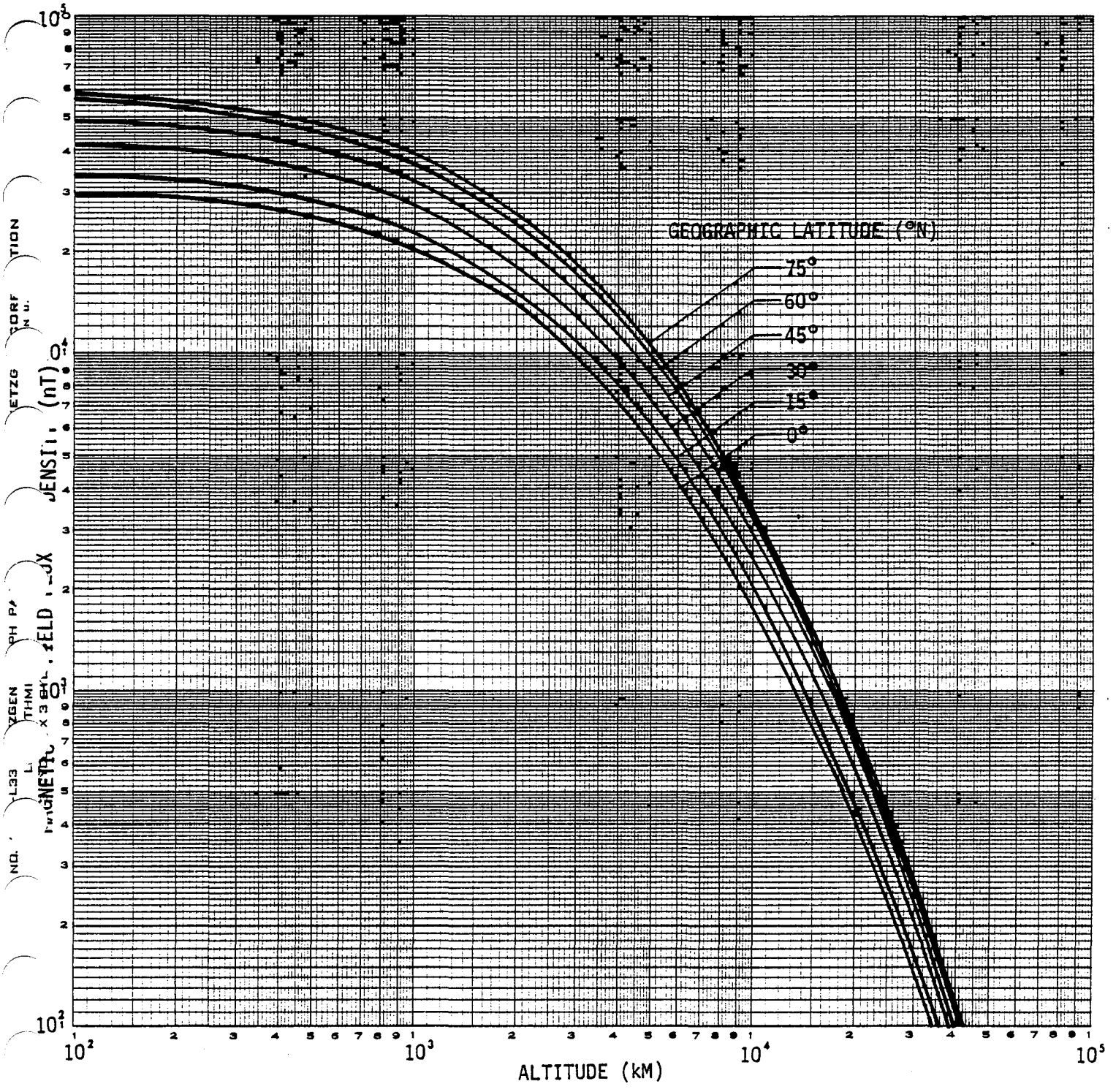

FIGURE 2-11 THE GEOMAGNETIC FIELD

SHEET

current and hysteresis effects, are generally of second order and fall off with the inverse of the sixth power of the geocentric radius. Thus, at geosynchronous altitudes, these may be assumed negligible.

It will be assumed that the only contribution to the spacecraft magnetic dipole arises from the permanently magnetized structural elements within the assembly. A reasonable guideline for estimating the dipole moment of spacecraft flown in the late 1960's and early 1970's is 10^{-2} A-m^2/kg (drawn from NASA SP 8018, March 1969). Application of these scaling factor to LSS vehicles should yield very conservative results since these configurations will be composed almost exclusively of non-magnetic materials (aluminum and graphite epoxy).

Torque Calculation

As mentioned previously, the equation $\vec{T} = \vec{M} \times \vec{B}$ may be utilized to provide a reliable estimate of the magnetic disturbance experienced by a given configuration. The maximum magnitude of this disturbance is established by assuming the vehicle to be fabricated completely of magnetically permeable material, the ambient magnetic field to be at its worst case value and these two vectors to be mutually perpendicular. Sample calculations for the Solar Power Satellite (SPS) are shown below:

$$(\vec{M} \times \vec{B})_{max} = /\vec{M}//\vec{B}/$$

$$/\vec{M}/ = 8.18 \times 10^{-5} \text{ A-m}^2$$

$$/\vec{B}/ = 180 \text{ nT}$$

$$(\vec{M} \times \vec{B})_{max} = 0.15 \text{ Nm}$$

Thus, the magnetic disturbance torque experienced by any of the geosynchronous spacecraft will be 0.15 N-m or less. Corresponding values for vehicles in non-synchronous orbits are typified by the Multinational Energy Distribution satellite (556 km orbital altitude) and the tetrahedral truss version of the Soil Moisture Radiometer configuration (1000 km orbital altitude): 0.006 N-m and -.087 N-m, respectively.

The significance of the magnetic disturbance effects may be determined by comparison with the other disturbances experienced by a given spacecraft. For the SPS, the net force due to solar pressure disturbances is 505 N and that required to counteract the gravity gradient influences is 1525 N.

Allowing a nominal length of ten meters for the moment arm the corresponding torques are 5050 N-m and 15250 N-m.

The level of the disturbance due to interaction of the spacecraft with the magnetic field is seen to be several orders of magnitude less than those arising from other sources.

2.2.5 Thermal Disturbances

The temperatures and thermal disturbances, characterizing the various LSS configurations must be determined principally on an individual mission basis. Parameters of key importance are orbital and orientation requirements, geometric configuration, structural component characteristics and construction materials. The general nature of this study precludes the performance of the detailed analyses necessary to accurately predict the respective temperature history and thermal response traits of the various spacecraft. However, several relevant qualitative conclusions and guidelines may be drawn from other recent studies involving LSS vehicles.

Low orbital altitudes are characterized by direct and reflected solar fluxes, earth-emitted radiation and frequent occultation. In geosynchronous orbit only directed solar radiation is of significance and, for non-ecliptic orbit planes, occultation is infrequent and brief. Figures 2-12, 2-13 and 2-14 summarize the general magnitudes and variations which characterize these elements of the natural thermal load environment.

Figure 2-12 shows the simple cosine relationship between ambient solar flux intensity at 1.0 AU ($\dot{q}_s$) and the intensity incident upon a plane surface ($\dot{q}_n$), i.e.,

$$\dot{q}_n = \dot{q}_s \cos\lambda \tag{2.29}$$

Seasonal variations in q_s, effects of the divergence of the flux, and basic uncertainty yield a $\pm$ 4.2 percent tolerance on the curve.

In Figure 2-13, the incident earth reflected flux is shown as a function of geometry. The reflected thermal radiation is based on an earth albedo (reflectivity) of 0.36 and assumes diffuse reflection from the earth surface. The local value of the albedo can vary significantly from the

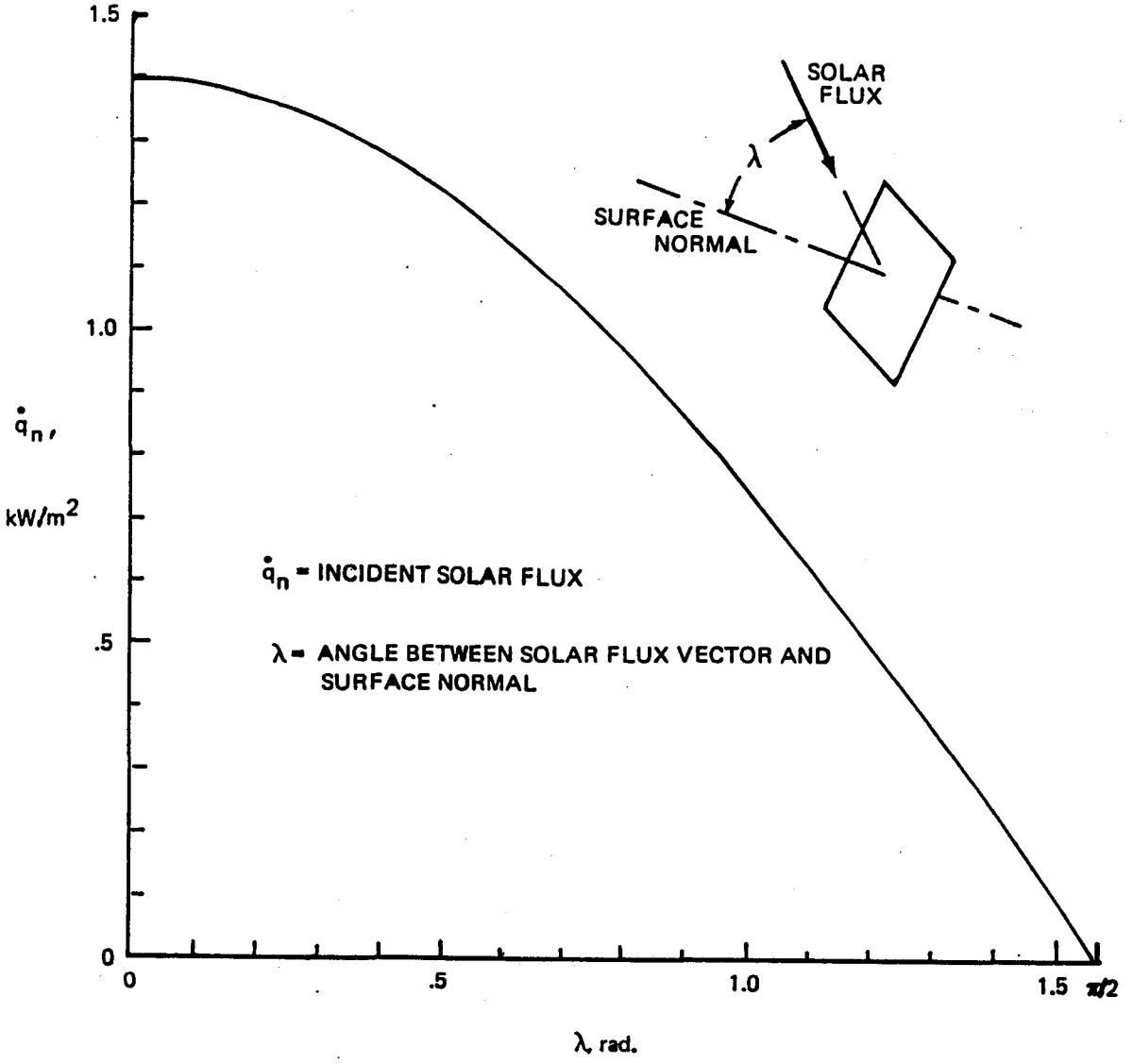

FIGURE 2-12 DIRECT SOLAR RADIATION

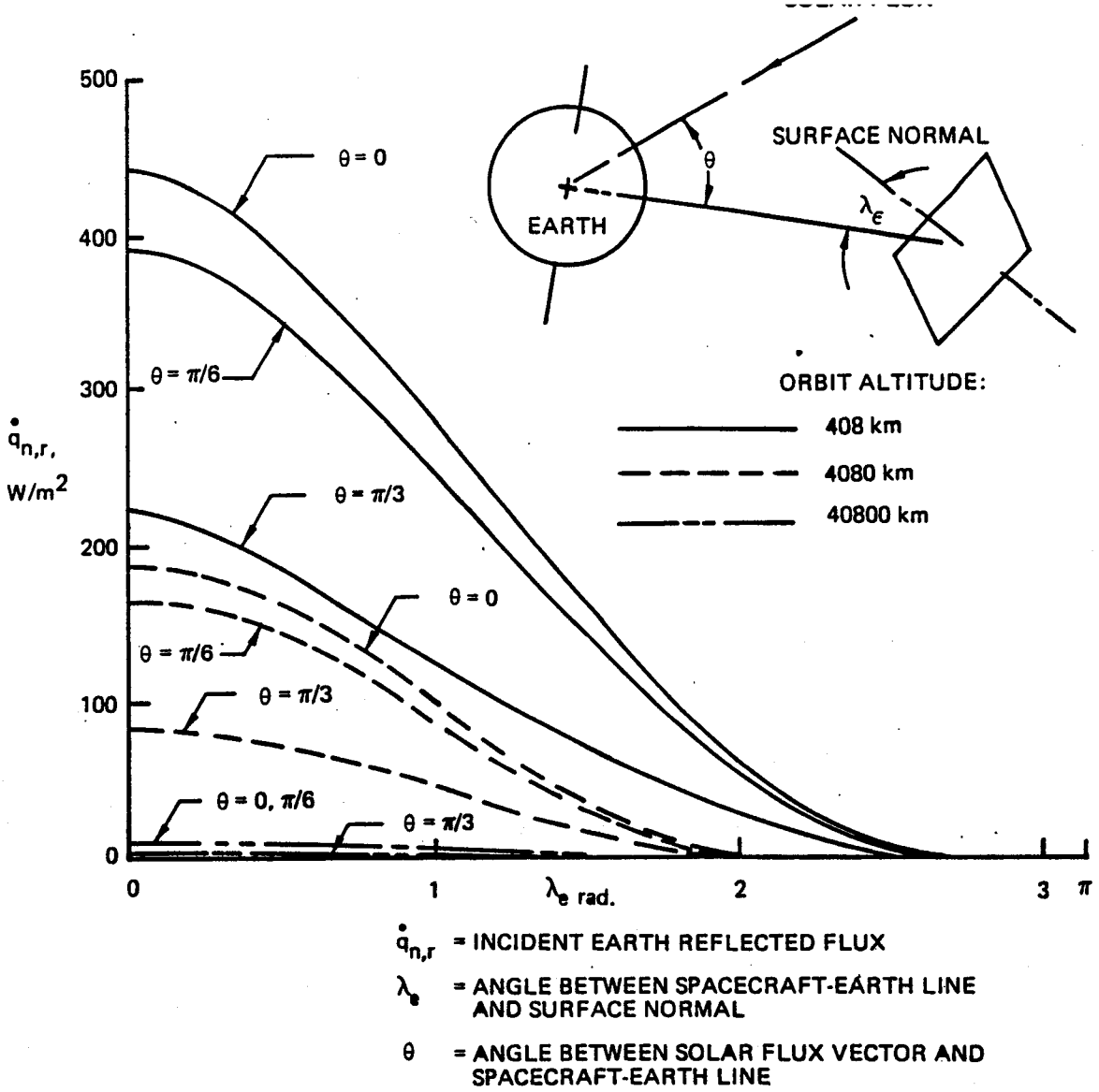

FIGURE 2-13 EARTH-REFLECTED (ALBEDO) SOLAR RADIATION

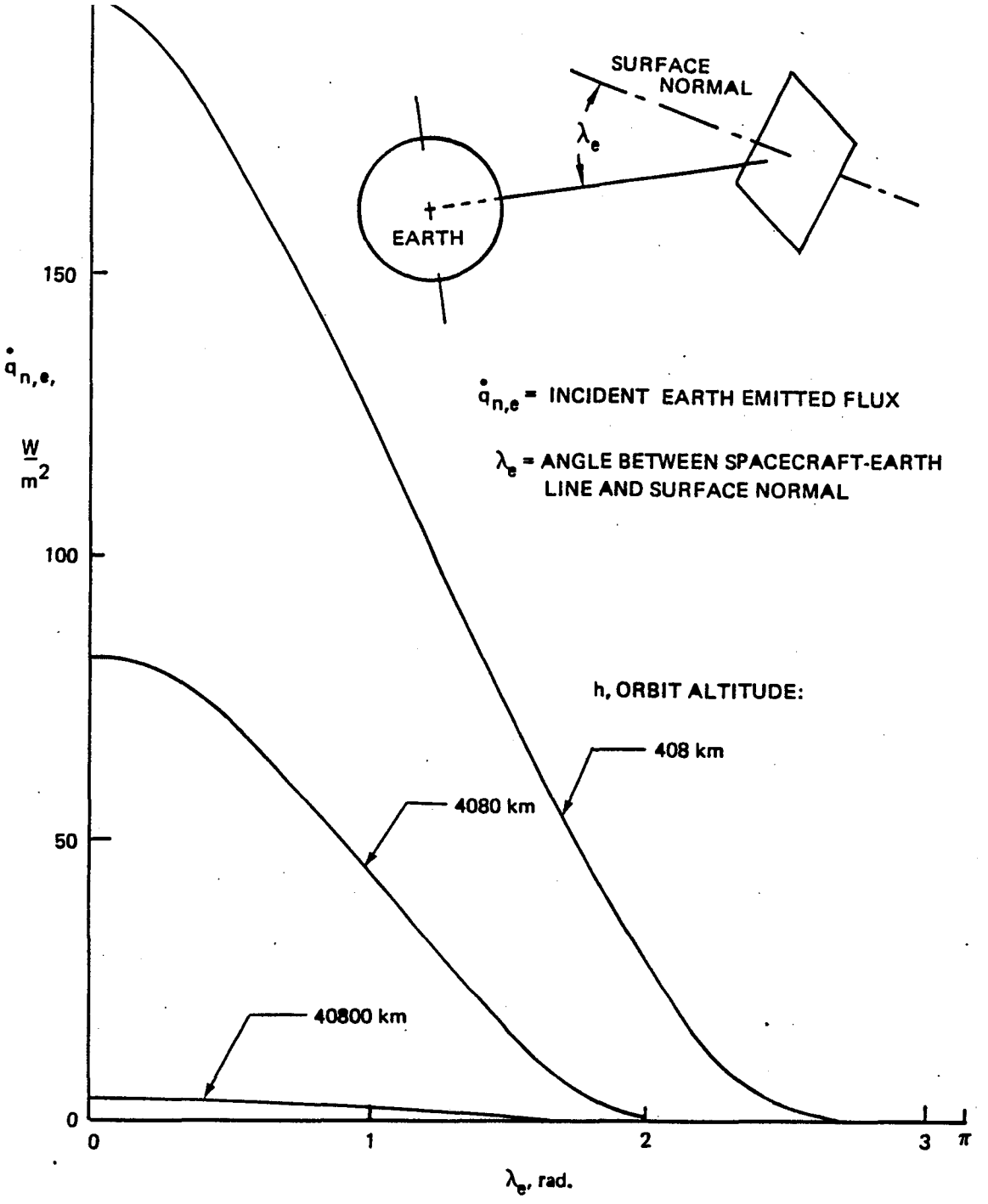

FIGURE 2-14 EARTH-EMITTED RADIATION

average caused by earth surface character and cloud cover. Reflection may also deviate significantly from the diffuse condition.

Earth emitted flux is shown in Figure 2-14. The heat received at the satellite surface is

$$q_{n,e} = F\dot{q}_e \tag{2.30}$$

where $\dot{q}_e$ = flux emitted at the effective earth surface

F = radiation view factor - isothermal sphere to planar element

F = function of h and λ_e

$\dot{q}_e$ varies diurnally, seasonally, and locally, but not by large amounts.

In general, for both high and low earth orbits, the periods of occultation result in a progression toward a uniform structural temperature distribution. Thus, there is only a very small probability that critical thermal deformations will occur during times of shadowing. It is important to note that this observation is valid for the symmetric, repeating truss module type assemblies characterizing the majority of the LSS vehicles. However, very different effects may be encountered in specific appendages of a given configuration; for example, long, slender flexible arms constructed of materials with widely varying thermal expansion characteristics have been found to exhibit behavior very similar to that of a bimetallic strip when passing from solar illumination to occultation conditions.

Satellites in low earth orbit are characterized by relatively high overall temperature levels with the potential for pronounced cyclical temperature variations. Orientation is of prime importance for geosynchronous vehicles as illustrated in Figure 2-15. Sun-facing configurations encounter an essentially constant solar flux while the solar environment of earth-facing vehicles varies continually. Due to the absence of energy loads induced via earth albedo and emission, the temperatures characterizing geosynchronous structures are typically lower than those of low altitude satellites.

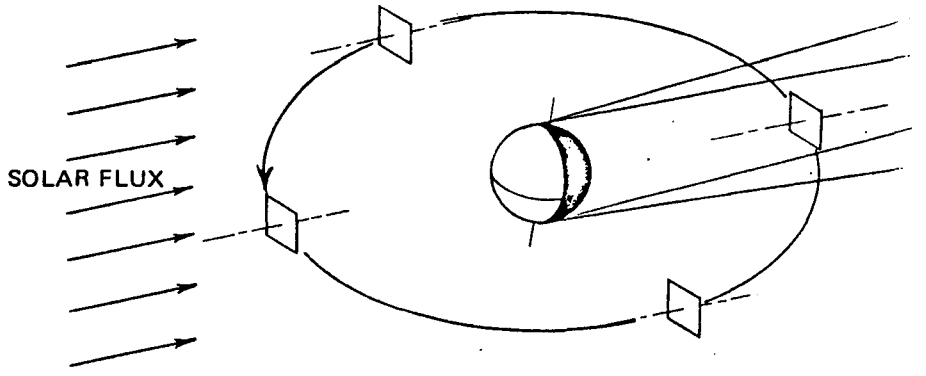

(A) SPACED-FIXED

CONSTANT SOLAR FLUX INCIDENCE
(EXCEPT DURING PERIODS OF ECLIPSE)

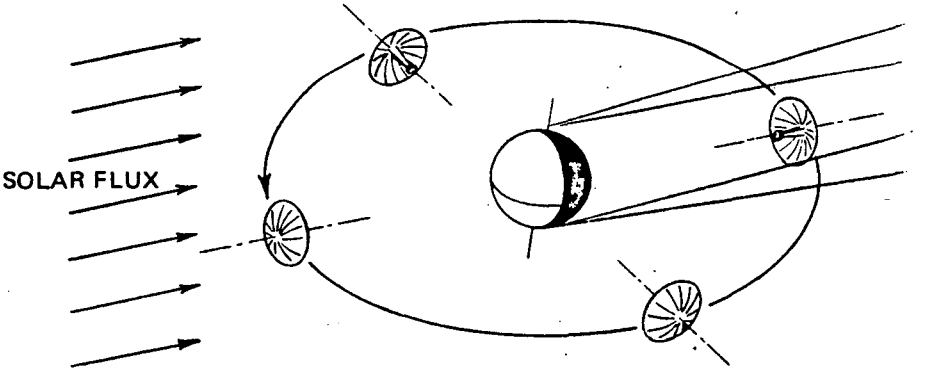

(B) NON-SPACE-FIXED

CONSTANTLY CHANGING SOLAR FLUX INCIDENCE

FIGURE 2-15 SATELLITE ORIENTATIONS IN GEOSYNCHRONOUS ORBIT

Recent studies have shown that no significant overall structural curvature is exhibited in a natural radiation environment (direct solar or direct solar together with earth-reflected and emitted radiation) by configurations composed of repeating truss moduli. Truss assemblies experience little member-to-member shadowing and are therefore chaacterized by little thermal distortion in this environment.

The presence of non-uniformly distributed onboard heat sources (RTG's, PPU's, radiators, etc.) and large scale shielding and/or reflecting surfaces, such as solar cell banks and antenna arrays, can give rise to significant structural disturbances.The distortions produced by non-uniform onboard heating are approximately proportional to the source power levels. The chief impact of shielding and reflecting surfaces lies in their influence upon both the level and distribution of temperatures within the structure. These effects are particularly noticeable for earth-facing satellites in geosynchronous orbit where there is no potential for modulation of the shadowed members' environment by earth-based radiation.

Joint conduction effects are rendered effectively negligible by the long slender nature of the individual structural elements for all but the most detailed thermal analyses. In general, these components are characterized as being isothermal. However, if the member cross-section is not sufficiently small or the length/diameter ratio not adequately large, then significant temperature distributions may be established and produce non-trivial bending moments within the element. At this juncture, the member end conditions become of critical importance - rotating joints will permit the distribution of these bending loads throughout the structural assembly whereas rigid junctions will result in the deformation of the stressed element.

Thermal disturbances in LSS vehicles may be minimized through the utilization of construction materials possessing low thermal expansion characteristics and high rigidity. In general, high values of thermal conductivity will promote the establishment of uniform temperature distributions within the individual members. High thermal capacitance minimizes the time rate of element temperature variation:

$$\Delta L/L \sim \alpha_T \Delta T$$
$$kA\Delta T/\Delta x \sim Q$$
$$C\Delta T/\Delta t \sim \dot{Q}$$

where k = material thermal conductivity

A = member cross-section normal to heat transfer direction

ΔX = distance within member across which temperature difference ΔT exists

Q = quantity of energy being transferred across member

Graphite epoxy composites and structural aluminum (e.g., 6061-T6) typify the property extremes of candidate LSS materials, possessing respectively low and high values of thermal conductivity and coefficient of thermal expansion.

The most pronounced mission-related impacts of LSS thermal environments lie in the possibility of shape change in contour-sensitive components such as antennas. These influences may be most easily controlled via conventional linear actuator type mechanisms. Thus, the damping of thermal disturbances will probably not play a significant role in the determination of first order characteristics and requirements of LSS auxiliary propulsion systems.

2.2.6 Orbit Perturbations

The orbit of an earth satellite deviates from that described by a pure conic section by an amount proportional to the perturbing influences acting upon it. Consequently, in-flight course adjustment may be necessary in order to facilitate satisfactory mission performance. This can be accomplished by on-board auxiliary propulsion systems operating in either a continuous or periodic mode.

Of the various LSS vehicles considered within this study, the stationkeeping requirements of those in geosynchronous orbits are most significant. There are three primary long-term perturbations on the orbit of a 24-hour stationary (equatorial and circular) satellite: the longitude drift due to the triaxiality of the earth, the long term increase in inclination of the satellite's orbital plane due to lunar and solar perturbations, and the change in eccentricity caused by solar radiation effects. These three perturbations are essentially independent of each other.

The analysis is restricted to geosynchronous orbits and involves the determination of the velocity increments required for orbit maintenance in the presence of these major disturbances. The corresponding acceleration levels are calculated for both continuous and periodic correction.

Triaxiality (East-West Stationkeeping)

Triaxiality (earth's oblateness and equatorial ellipticity) gives rise to orbital perturbations due to the longitudinal variation of the earth's gravitational field. In effect, a satellite is found to oscillate, or librate, about some localized well within the gravitational potential field. There are four points at which the satellite could theoretically remain stationary, symmetrically located as extensions of the principal axes of the equatorial ellipse. The two points of the minor axis correspond to positions of stable equilibrium while those of the major axis are positions of unstable equilibrium. The libration induced by only the first order effects of the gravitational field leads to the location of the points of stable equilibrium at 75^{o} E and 105^{o} W longitude. It is about one of these two sites that a satellite will oscillate.

Inclusion of higher order harmonics in the analysis results in the displacement of the actual physical location of the points of stable and unstable equilibrium by 2^{o} or 3^{o}. The net increase in longitudinal acceleration experienced by the satellite due to these higher order effects is approximately 10 percent. Thus, the consideration of only first level quantities will yield acceptably accurate results.

The average annual ΔV requirements for longitudinal stationkeeping are given by the equation:

$$\Delta V = 5.64 \sin 2(\lambda+15) \text{ (ft/s)} \qquad (2.31)$$

where λ = longitude in degrees east of Greenwich

The longitudinal variation of this quantity is described in Figure 2-16 along with the location of the points of stable and unstable equilibrium. The ΔV requirement is found to be maximum for those longitudes midway between these points.

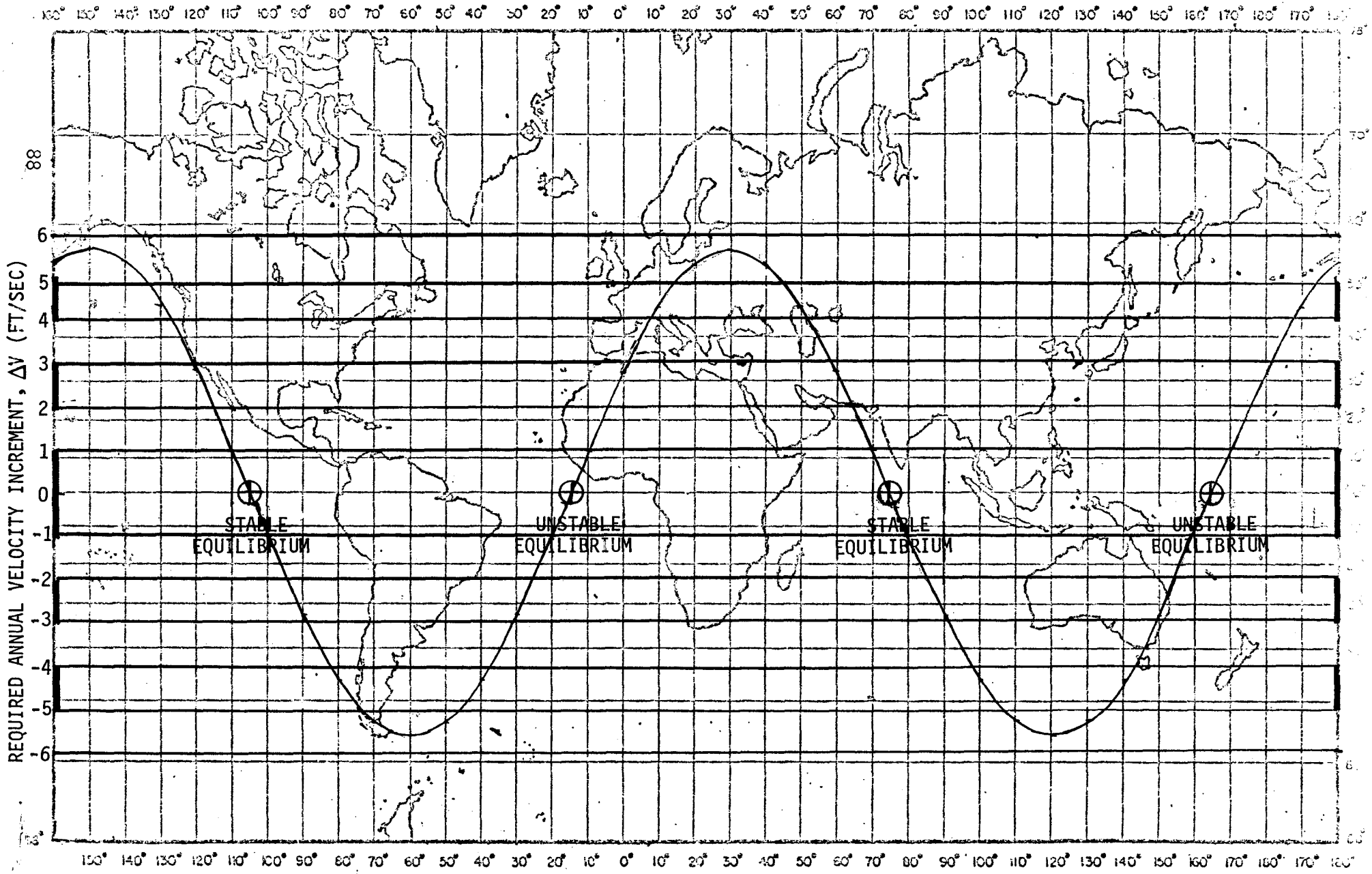

FIGURE 2-16 LONGITUDE (EAST-WEST) STATIONKEEPING REQUIREMENTS

Orbit Inclination (North-South Stationkeeping)

The orbital plane rotation due to the gravitational attraction of the satellite by the sun and moon may be characterized with an equation of the form:

$$i = A \sin\theta \cos\theta \ (^{o}/yr) \tag{2.32}$$

where i = average annual orbital inclination change

A = a quantity whose value depends on the body creating the effect

θ = the inclination of the equatorial plane with respect to the ecliptic or lunar orbital planes

the quantity A is actually the slope of a curve describing the periodic variation of the satellite's latitude. For approximately the first ten years of this cycle (corresponding to low cumulative values of inclination), the slope of the curve is approximately constant. Stationkeeping acts to confine a satellite to this region of essentially nonvariant slope. Thus, constant values may be reasonably ascribed to the variable A in the equation given above.

For the sun, the value of A is 0.74^{o}/yr and the earth's declination (θ) is approximately 23.5^{o} and constant. Thus, the solar-induced out-of-plane orbital perturbation is found to have an average value of 0.270^{o}/yr. The magnitude of the lunar effect varies, due to the periodic change of the moon's inclination relative to the earth. Figure 2-17 summarizes the charactristic variation of the angle between the lunar orbital and earth equatorial planes. A worst case analysis may be made by assuming a relative inclination of 28.7^{o}. The lunar-related value of A is 1.61^{o}/yr. Thus, the corresponding satellite orbital inclination change, due solely to the action of the moon, can be as severe as 0.678^{o}/yr. The combined lunar and solar effects are shown in Figure 2-18.

For the small angles involved in these latitude correction maneuvers, the required annual velocity increments may be approximated as:

$$\Delta V = \Delta\phi \Delta V_{GEO} \ (ft/s\text{-}yr) \tag{2.33}$$

where $\Delta\phi$ = required satellite orbital plane inclination change, rad/yr

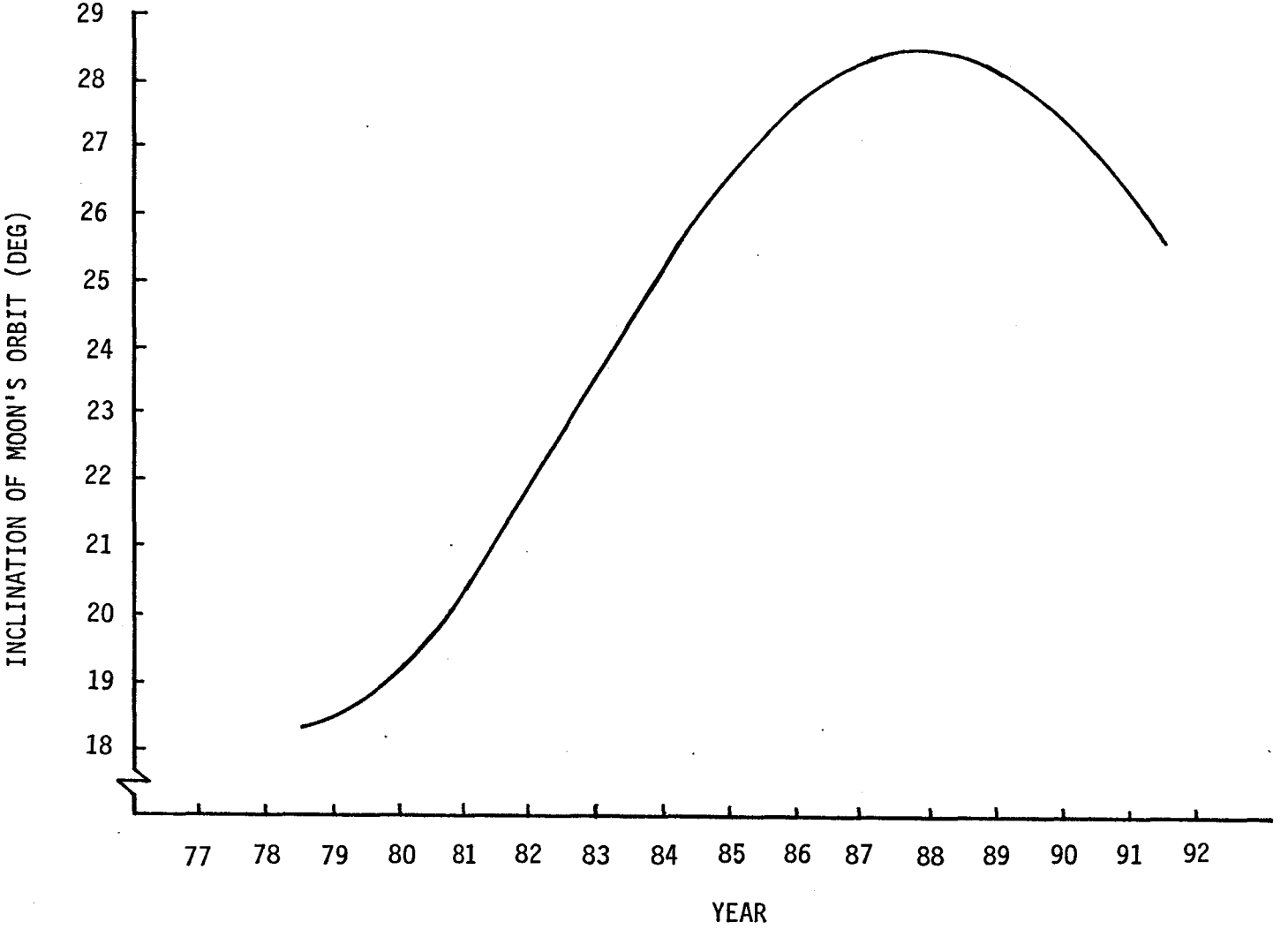

FIGURE 2-17 RELATIVE INCLINATION OF LUNAR ORBITAL AND EARTH EQUATORIAL PLANES

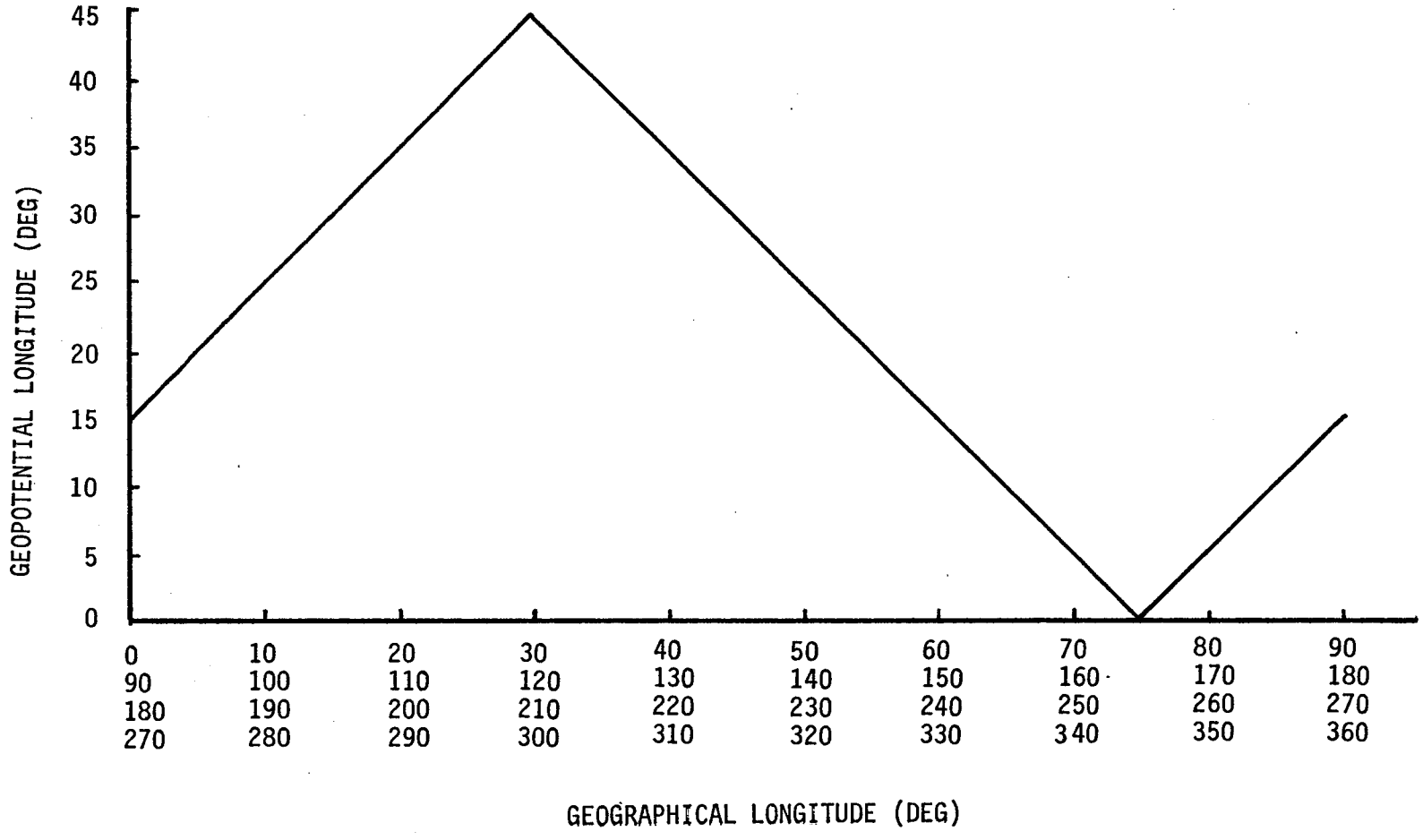

FIGURE 2-18 OUT-OF-PLANE ANGULAR VARIATION DUE TO LUNI-SOLAR PERTURBATIONS

ΔV_{GEO} = tangential velocity of geosynchronous satellite, approx. 1.0085×10^4 ft/s

Thus, the annual north-south stationkeeping requirements due to luni-solar induced orbit perturbations are summarized by the equation

$$\Delta V = \left[(0.74 \sin\theta\cos\theta)_{SOLAR} + (1.61 \sin\theta\cos\theta)_{LUNAR} \right] \frac{1.0085 \times 10^4}{360/2\pi} \text{ ft/sec} \qquad (2.34)$$

This equation is plotted in Figure 2-19 and reflects the variation of the inclination of the lunar orbital plane.

Orbit Eccentricity (East-West Stationkeeping)

Solar radiation pressure acting over a period of time will change orbit eccentricity. An originally circular geosynchronous orbit will gradually become eccentric and cause satellite oscillations in an east-west direction, thus adding to the earth's triaxiality effect.

To minimize propellant consumption, two pulses could be delivered for station correction, each 12 hours apart. These pulses would control the line of apsides such that the projection of the earth-sun line into the orbit plane is coincident with the earth-perigee line. In the case of rigid satellites, the two pulses/orbit solution poses no problems; however, for flexible bodies, it is desirable to have more than two pulses/orbit and continuous thrust may be required for very flexible structures or extremely tight stationkeeping requirements.

The results of a study entitled "Stationkeeping of High Power Communications Satellites" (NASA TMX-2136) are pertinent. The assumptions used are compatible with this analysis; namely, geostationary orbit, flat plate or projected areas and area to mass ratios greater than 0.05 square meters per kilogram.

The effect of solar pressure is to change eccentricity (e) and orientation of the apsidal line. There are, therefore, daily longitudinal oscillations with an amplitude equal to 2e radians. This induced eccentricity also causes a daily oscillation in orbit radius equal to er_0. With the assumptions stated, the perturbing acceleration of the satellite due to solar pressure is

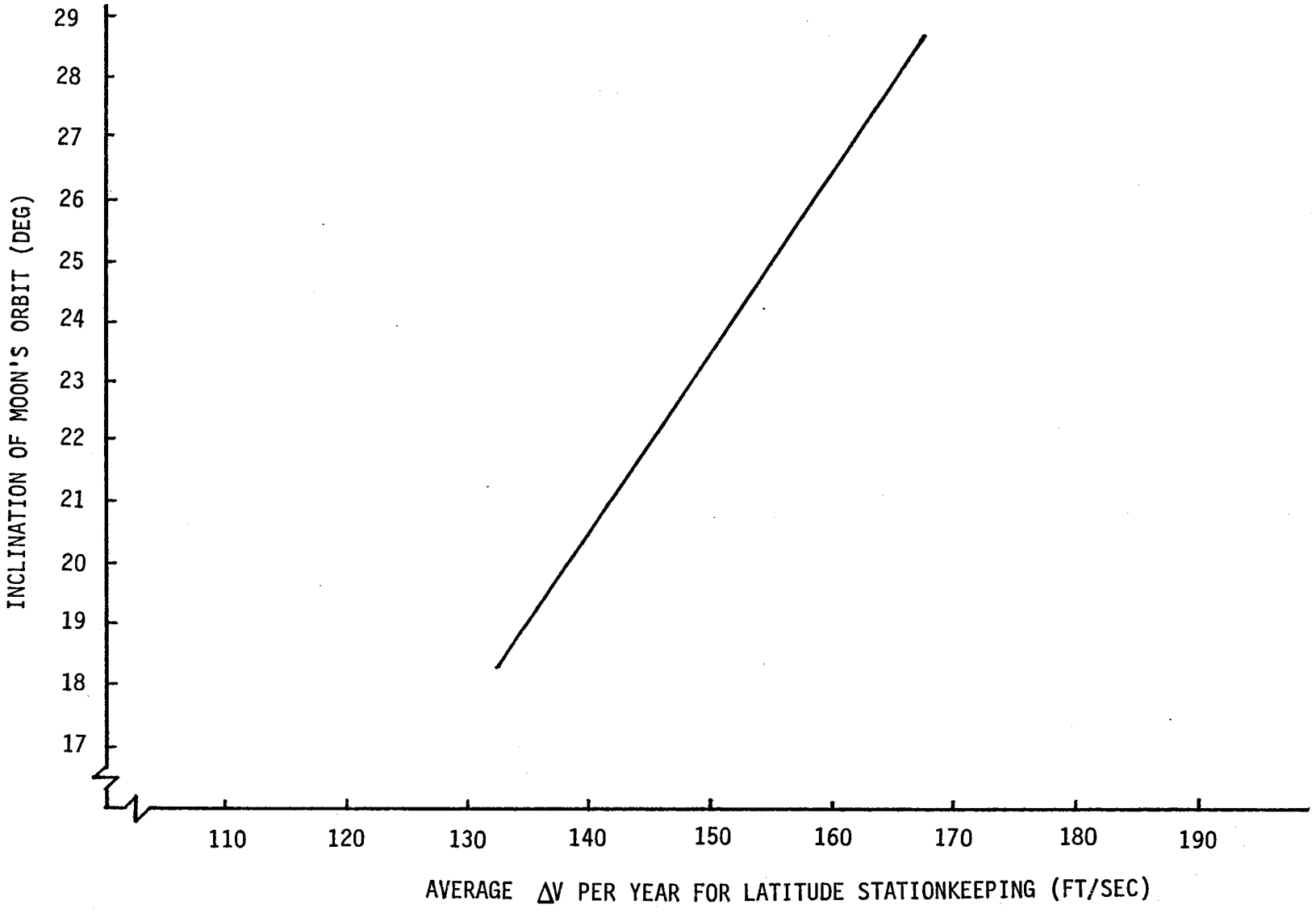

FIGURE 2-19 AVERAGE YEARLY LATITUDE STATIONKEEPING REQUIREMENT

$$\vec{a} = - Sk\vec{U} \tag{2.35}$$

where $\vec{U}$ is a unit vector from the center of the earth to the sun,

S is the solar constant at 1AU

k defined below

$$k = (1 + \sigma) \frac{A}{m}$$

σ is reflectivity

A/m is area to mass ratio

In TMX-2136, four methods of correcting the rise in eccentricity are identified. The first two methods yield a high specific impulse low acceleration thruster system. These methods are most applicable to a large flexible structure and will be used to define ΔV requirements.

Method 1 Continuous thrusting toward the sun.

The ΔV per year is $\Delta V = \frac{2\pi Sk}{\dot{\lambda}}$ (2.36)

where $\dot{\lambda}$ is the mean angular velocity of the earth's orbit about the sun (2 rad/year)

and acceleration level is

$a = Sk$

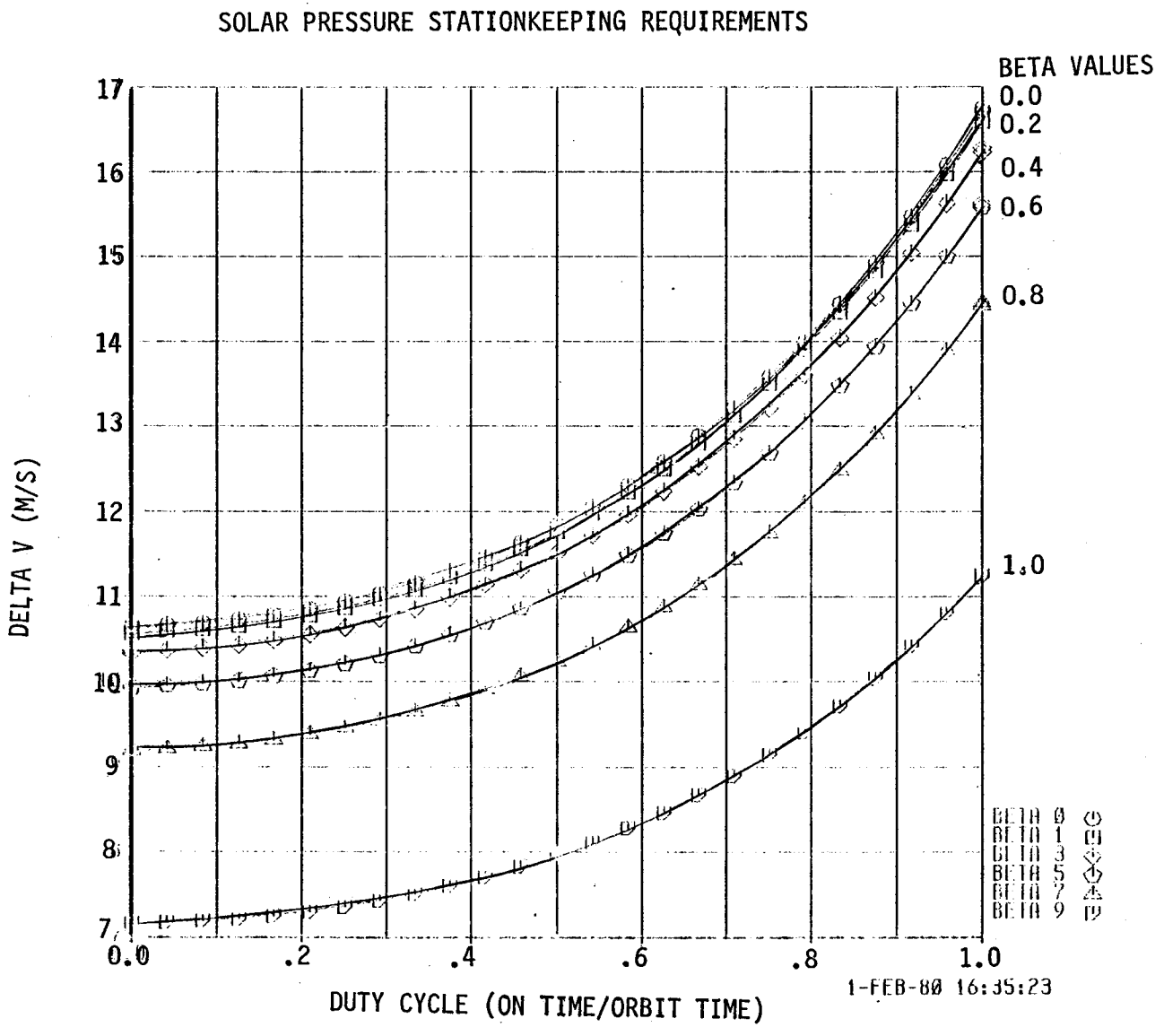

FIGURE 2-20 SOLAR PRESSURE STATIONKEEPING REQUIREMENTS

Method 2 Circularize the orbit when e = e*

Here tangential thrusting is used to circularize the orbit when a certain tolerance is reached. Let ΔL_s denote the maximum allowable longitude excursion in radians, then $e^* = 1/2\,\Delta L_s$. The parameter β is defined as the ratio of maximum allowable eccentricity to the maximum eccentricity that would result from an initially circular orbit (assuming no stationkeeping).

$$\beta = \frac{e^*}{e_p} = 0.4\,\frac{\Delta L_s}{k} \qquad \text{with } L_s \text{ in degrees.}$$

Using this method, ΔV per year is

$$\Delta V = \frac{35k\pi}{2i}\left(\frac{p\pi}{2\sin p\pi/2}\right)\left(\frac{\beta}{\sin^{-1}\beta}\right) \tag{2.37}$$

and acceleration

$$a = \frac{5k}{m}\left(\frac{3\dot{\theta}_E}{8i}\right)\left(\frac{\beta}{\sin p\pi/2}\right) \tag{2.38}$$

with p = duty cycle thruster on time/orbit divided by orbit period

$\dot{\theta}_E$ = angular velocity of Earth's rotation about its axis (7.29×10^{-5} rad/sec)

For purposes of illustration, a graph showing required ΔV versus duty cycle for values of β ranging from 0 (no tolerance) to 1 has been generated in Figure 2-20 for an area to mass ratio of 0.1 m^2/kg.

The value of ΔV obtained by using continuous thrusting to directly counteract solar pressure is a factor of 1.18 less than that obtained by using the tangential thrusting with β =0 and p=1. For purposes of generating the forces and torques required, continuous thrusting will be assumed and it will directly counteract solar pressure.

To illustrate the actual ΔV requirements for east-west stationkeeping due to solar pressure, Table 2-6 was generated. This table shows the area to mass ratio of each of the structures considered as well as yearly ΔV requirements using method 2 with approaching 0. The sizes of each class were reduced to three discrete categories representing a small, medium and large size. The effective area/mass ratio differs from the total area to mass ratio for the RF mesh antennas and truss structures without a solid surface covering. The effective area for solar pressure calculations is taken to be 5 percent of the actual area for RF and truss structures.

	GENERIC CLASS	SIZE	A/M (M2/kg)[1]	EFFECTIVE A/M (M2/kg)[1]	ΔV/YEAR (M/S)
I A	PLATE	SMALL (30 M)	1.33	1.33	151.9
		MEDIUM (700 M)	1.33	1.33	151.9
		LARGE (21,000 M)	1.33	1.33	151.9
I B	CROSS	SMALL (40 M)	.071	.004	.457
		MEDIUM (500 M)	.071	.004	.457
		LARGE (4000 M)	.071	.004	.457
II A	BOX	SMALL (82 M)	.027	.002	.229
		MEDIUM (600 M)	.027	.002	.229
		LARGE (1300 M)	.027	.002	.229
II B	MODULAR ANTENNA	SMALL (15 M)	.186	.104	11.88
		MEDIUM (60 M)	.449	.117	13.37
		LARGE (200 M)	1.085	.135	15.42
II C	MAYPOLE ANTENNA	SMALL (30 M)	7.03	.350	39.98
		MEDIUM (250 M)	101.08	5.05	576.91
		LARGE (1500 M)	661.08	33.00	3770.0
III A	OAF	SMALL (15 M)	.147	.036	4.11
		MEDIUM (35 M)	.305	.044	5.03
		LARGE (60 M)	.501	.053	6.05
III B	SERIES OF ANTENNAS	SMALL (2)	.145	.012	1.37
		MEDIUM (6)	.145	.012	1.37
		LARGE (10)	.145	.012	1.37
	*SINGLE SHUTTLE LAUNCH				
I	PLATE STRUCTURE W/O BLANKET	SMALL (30 M)	.865	.043	4.91
		MEDIUM (100 M)	4.014	.201	22.96
		LARGE (250 M)	11.055	.553	63.17
II	PLATE STRUCTURE W/BLANKET	SMALL (30 M)	.438	.438	50.04
		MEDIUM (100 M)	.572	.572	65.35
		LARGE (150 M)	.598	.598	68.31
III	MODULAR ANTENNA	SMALL (15 M)	.165	.091	10.39
		MEDIUM (60 M)	.433	.113	12.91
		LARGE (200 M)	1.980	.236	26.96
IV	SERIES OF ANTENNAS	SMALL (2)	.826	.085	9.71
		MEDIUM (3)	.802	.085	9.71
		LARGE (4)	.764	.084	9.71

1 INCLUDING SOLAR ARRAYS WHERE APPLICABLE

TABLE 2-6 DELTA-V REQUIREMENTS FROM SOLAR PRESSURE

3.0 ESTABLISHMENT OF AUXILIARY PROPULSION SYSTEM CHARACTERISTICS AND REQUIREMENTS

Perfect spacecraft control will be achieved when the control forces and torques are continuously equal and opposite to the disturbance forces and torques plus the necessary stationkeeping and maneuver forces and torques. This ideal, distributed, method of control can rarely, if ever, be met. In most cases, the control actuators will be localized in a small number of discrete positions. Practical considerations dictate that thrusters be located on relatively rigid portions of a structure avoiding, for the most part, such things as deployable antennas and solar arrays. The plate, cross and box structures, however, are more homogeneous than the other classes and are candidates for a distributed control system.

The purpose in Task 3 was to evaluate the disturbance forces and torques acting on each generic class and from these to define the thrust levels required to provide control. Additional objectives were to determine the important APS characteristics that affect control performance, define areas of interaction and examine the impact of restricting the vehicles to those launchable by a single shuttle.

Before evaluating the disturbance forces and torques, it was necessary to establish some groundrules in order to isolate the maximums and establish a basis for comparison. Four conditions were selected which covered the entire range to be expected. These were: (1) maximum forces and torques in LEO, (2) maximums in LEO-GEO transfer, (3) nominals at GEO and (4) maximums in GEO. In addition, it was necessary to define the vehicle orientations in each of the four conditions. Once the control forces and torques were found it became possible to determine the thrust levels that generate them. This process required assumptions to be made on thruster locations in each of the classes.

Auxiliary propulsion system characteristics and characteristics sensitivities were addressed in the next two subsections. First the various control tasks that are needed to implement attitude control, shape control and stationkeeping were examined to determine the important APS characteristics. A matrix was then developed of control task vs. APS characteristic to define the areas of interaction.

The last task in this section is an assessment of the impact on disturbance effects, thrusts required and APS/LSS interactions as a result of restricting vehicles to those launchable by a single shuttle flight.

The results of Task 3 define quantitatively, the range of thrusts needed for control in each generic class and also identify in a qualitative way other important APS characteristics and sensitivities.

3.1 Analysis of Control Forces

Radiation and aerodynamic forces, gravity gradient torques and orbit perturbations are significant effects that require control forces to overcome. The force and torque generating mechanisms have been discussed in Section 2.2 and expressions developed for estimating the direction and magnitude of the effects. The two other disturbances examined - magnetic and thermal - have a lesser impact.

Magnetic disturbance torques are caused by the interaction of a local satellite field with the earth's magnetic field. The torque is given by the vector cross product of the ambient magnetic field and the magnetic dipole of the spacecraft. The inherent uncertainty in determining the magnetic dipole makes the determination of quantitative values difficult. Some estimates have been made based on previous studies and the results indicate that magnetic disturbances are at least an order of magnitude below the torques imposed by gravity gradient and radiation effects. For these reasons magnetic disturbances will not be evaluated.

Thermal disturbances arise from an uneven temperature distribution across a given structure and are caused by factors such as orbit, orientation, geometric configurations and individual component material characteristics. The sources of heat for the structure are both external and internal. External sources are direct and reflected solar fluxes and earth-emitted radiation. Internal sources may result from PPU's, radiators, RTG's, or onboard experiments. Generally, it has been determined, based on previous work, that thermal disturbances will not play a significant role in the determination of LSS/APS characteristics and these effects too can be ignored.

3.1.1 Analysis Conditions

Before proceding with the evaluation of disturbance effects on the seven generic classes it was necessary to set some groundrules. The operating condition can range from low earth orbit (LEO) through transfer to geosynchronous earth orbit (GEO) to operating on station at GEO. Factors that needed consideration were the vehicle attitude at LEO, during transfer and at GEO. In most cases, the disturbances in the nominal attitude would be much lower than in a worst case attitude. Designs would have to consider contingency situations and provide for recovery from an undesirable attitude, particularly in cases where the nominal attitude is a position of unstable equilibrium. The definition of both maximum and nominal disturbance effects is therefore necessary. It was assumed that all attitude control functions would be provided by APS with no reliance on thrust vector control of the prime propulsion units. Based on the need to establish higher and lower bounds on the disturbance effects, the following four conditions were selected:

1) LEO maximum disturbance, 2) LEO-GEO transfer, 3) Nominal GEO on orbit requirements, 4) Maximum disturbances encountered at GEO. The first set of disturbances are those encountered in a worst case orientation of each LSS in LEO (300 km). Disturbance forces from aerodynamic, gravity gradient, earth radiation, and solar pressure will form a composite requirement for the worst case orientation. The second set of conditions arise from a nominal low earth orbit to geostationary orbit transfer in which the auxiliary propulsion system provides the thrust vector control as a well as countering all disturbance forces and torques. The disturbance factors are those encountered during the transfer given a nominal transfer orientation. This orientation can be chosen to minimize disturbance torques, structural stress, and/or to keep antennas pointed toward the earth. The selection of the orientation will be described below.

The second set of conditions came from the LEO-GEO transfer. For this set a selection of thrust axis and transfer orientation for each was made. The second set of data is actually time dependent because it is a function of the LEO to GEO transfer. Further, since each generic class of structure is also characterized by a scaling parameter, a three dimensional graph relating transfer time and scaling parameter to the level of disturbance would be needed. While this approach may be feasible an alternative has been followed which is simpler and loses none of the value.

value. The nominal transfer torques (category 2) are represented by the maximum nominal torques during an orbit at LEO assuming a time optimal continuous thrust transfer.

The third set of requirements is generated by the geosynchronous operational requirements. Here the vehicle is on station and is subject to mission maneuver requirements, orbital stationkeeping , and the environmental disturbance forces and torques. This set constitutes the nominal on-orbit operation requirements and may dictate a separate auxiliary propulsion system from that dictated by the other more demanding sets of requirements.

Finally, a set of data is generated identifying the forces and torques required by a worst case orientation of the vehicle at geosynchronous altitudes. This data set is similar to the first set of data which was taken at LEO. Not all disturbances need to be considered in each of the four conditions. Aerodynamic effects, for example are non-existent at GEO. The following table summarizes the forces and torques to be analyzed in the calculations for each requirement category.

I	LEO Max Disturbance	a. Gravity Gradient Torque
	b. Radiation Pressure Forces	
	c. Aerodynamic Forces	
II	LEO Transfer Requirement	a. Gravity Gradient Torque
	b. Maneuvering Torque	
	c. Radiation Pressure Forces	
	d. Aerodynamic Forces	
III	GEO Max Disturbance	a. Gravity Gradient Torque
	b. Radiation Pressure Forces	
IV	GEO Max on Orbit	a. Gravity Gradient Torque
	b. Radiation Pressure Forces	
	c. Stationkeeping Forces	

For the transfer condition, maneuvering torque must be combined with the disturbance effects to define the total control requirements. To find the maneuver torques, determination must first be made of the axis for prime propulsion application. The requirement that will come out of the orientation chosen will be a maneuvering torque for out of plane thrusting and disturbance torques at the worst orientation during an orbit. The maneuvering torque requirement arises from the need to change inclination from LEO (300 km at $28\text{-}1/2^{o}$ inclination) to GEO (35869 km at 0^{o} inclination). To change inclination and at the same time to change orbit radius, one must have the thrust vector slew some angle greater than 0 and less than 90 degrees out of the orbit plane in one orbit. The maximum out of plane thrusting angle gets progressively larger as the orbit radius is increased.

The maximum out of plane angle is not of prime concern for maneuver torque estimation, but rather the second derivative or acceleration rate of this angle. Figure 3-1 shows the out of plane angle as a function of time for a typical LEO to GEO transfer. The curve has been fitted with a 7th order fit and a maximum acceleration of 7.838×10^{-7} rad/sec^2 has been calculated. While it is true that the maximum out of plane thrusting angle increases with increasing radius, Figure 3-2, the acceleration levels decrease. These statements hold true for a time optimal trajectory. Since transfer time has been shown to be of prime importance for future space missions, a time optimal trajectory is proposed as the baseline transfer profile. The requirement of 7.838×10^{-7} rad/sec^2 acceleration will be taken as the maneuver requirement for LEO to GEO transfer.

The determination of a prime propulsion axis begins by chosing an axis which will minimize disturbance torques. It must also be kept in mind that there will be a maneuver requirement about the axis pointing at the earth. Finally, in the case of antennas, one would like to keep them pointed at the earth and solar arrays free to seek the sun. Table 3-1 shows the axis selected for each generic class.

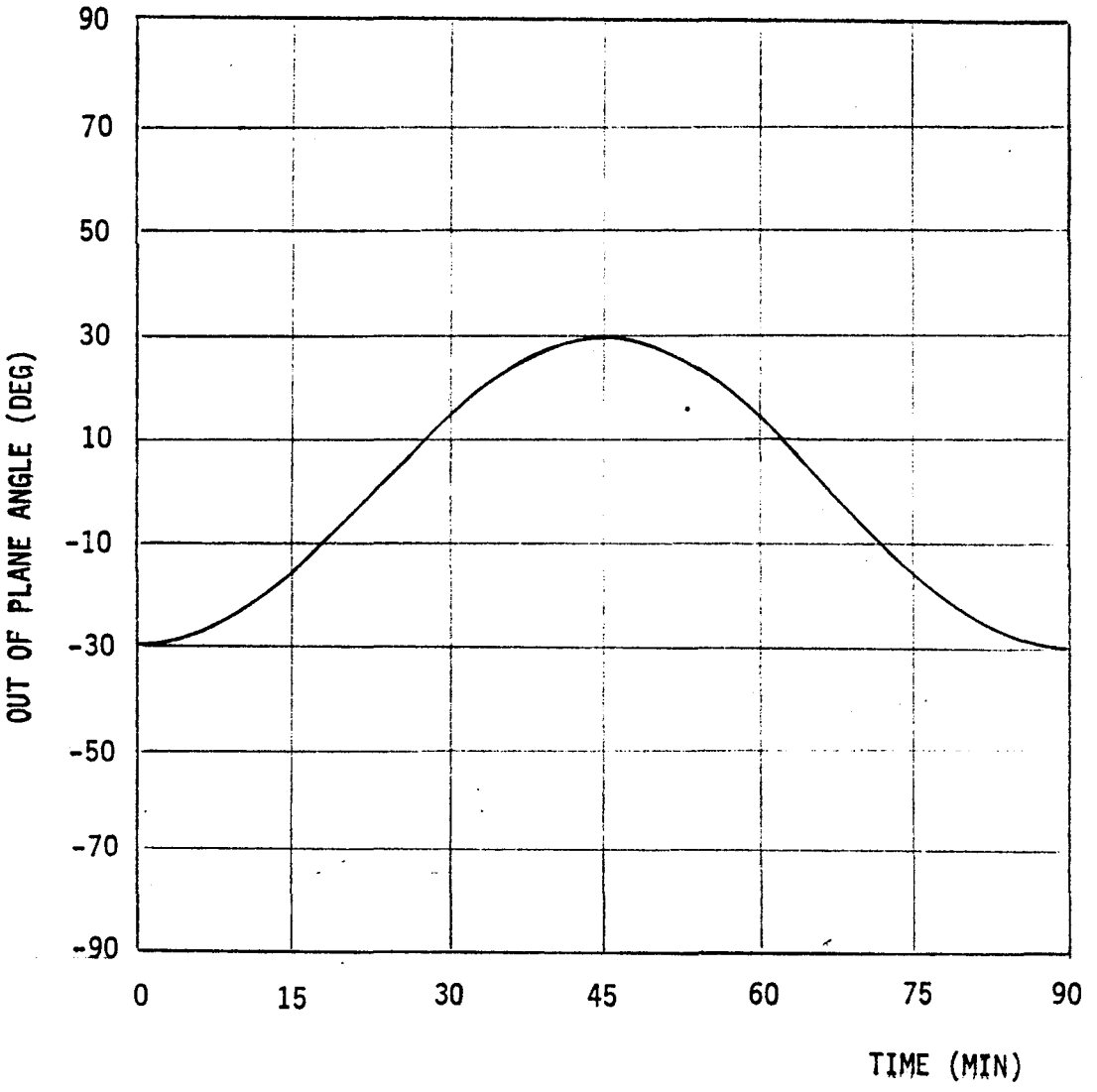

FIGURE 3-1 LEO-GEO TRANSFER DATA FOR ONE ORBIT AT LEO

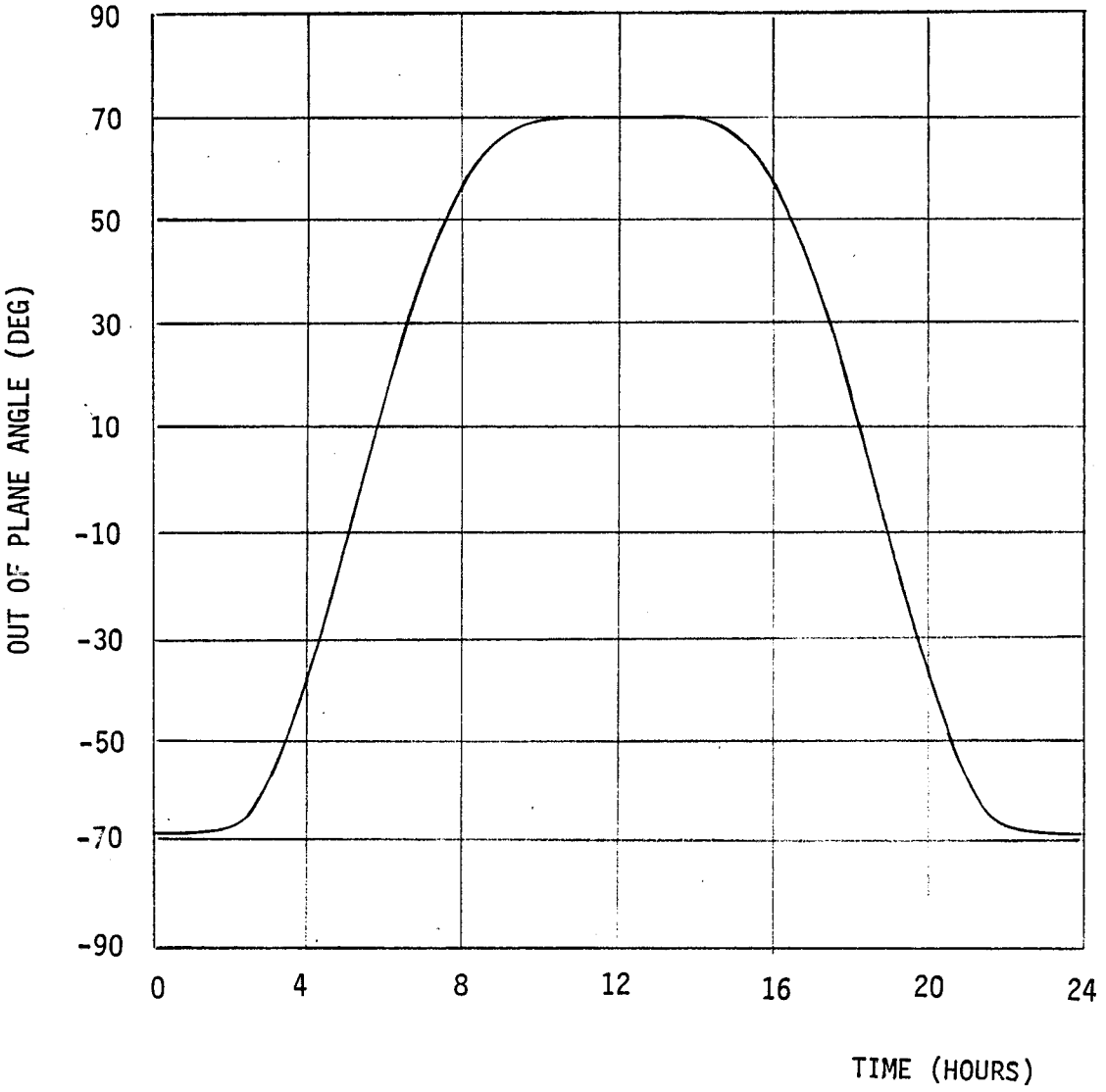

FIGURE 3-2 LEO-GEO TRANSFER DATA FOR FINAL ORBIT

IA Plate X with Y pointing at Earth	o In gravity gradient stable position o Minimal radiation and aerodynamic drag o Minimun inertia about Y axis
IB Cross X with Y pointing at Earth	o Gravity gradient stable o Minimal radiation and aerodynamic drag
IIA Box X with Y pointing at Earth	o Gravity gradient stable o Minimal radiation and aerodynamic drag o Minimum inertia about Y axis
IIB Modular Antenna X with Z pointing at Earth	o Keeps antenna Earth oriented o Allows solar array sun tracking
IIC Maypole Antenna X with Z pointing at Earth	o Gravity gradient stable o Keeps antenna Earth pointed
IIIA Multiple Antenna Farm X with Z pointing at Earth	o Antennas pointed at Earth o Minimal prime exhaust plume interaction with solar arrays
IIIB Series of Antennas X with Z pointing at Earth	o Antennas pointed at Earth o Allows solar array sun tracking

TABLE 3-1 PRIME THRUST AXIS SELECTION

3.1.2 Determination of Total Control Forces and Torques

In this section estimates are made of the total control torques and forces necessary for each structure at the four operating conditions: LEO maximum disturbance, LEO-GEO transfer, GEO maximum disturbance, and GEO maximum on orbit disturbance.

The plate, cross and box structures are nominally symmetrical and have zero aerodynamic and solar torques. Practically, however, a CG-CP offset will exist. To assess the importance of an offset, aerodynamic torques were calculated at three different angles of attack. The values for the plate structure using a CG-CP offset of one percent of the scaling parameter are shown in Figure 3-3.

Figures 3-4 through 3-9 use the 60^{o} angle of attack and show the effect of aerodynamic drag at lower earth orbit for the plate (IA), cross (IB) and box (IIA) structures. These are calculated with a CP-CG offset of 0.1, 1.0 and 10 percent of the scaling parameter.

Comparison of the offset torques (at 10 percent offset) with the maximum torque expected from gravity gradient shows the following:

Plate: Aerodynamic Torque at 300 km = 1% of maximum torque
1000 km = 10^{-4}% of maximum torque

Cross: Aerodynamic Torque at 300 km = 1% of maximum torque
1000 km = 10^{-4}% of maximum torque

Box: Aerodynamic Torque at 300 km = 1% of maximum torque
1000 km = 10^{-2}% of maximum torque

It can be concluded that the torques due to CG-CP offset are negligible compared to the maximum torques from gravity gradient for the multiple shuttle launched LSS.

Plate Structure (IA) - In this case the maximum disturbance at LEO will be due to aerodynamic, radiation, and gravity gradient. The maximum

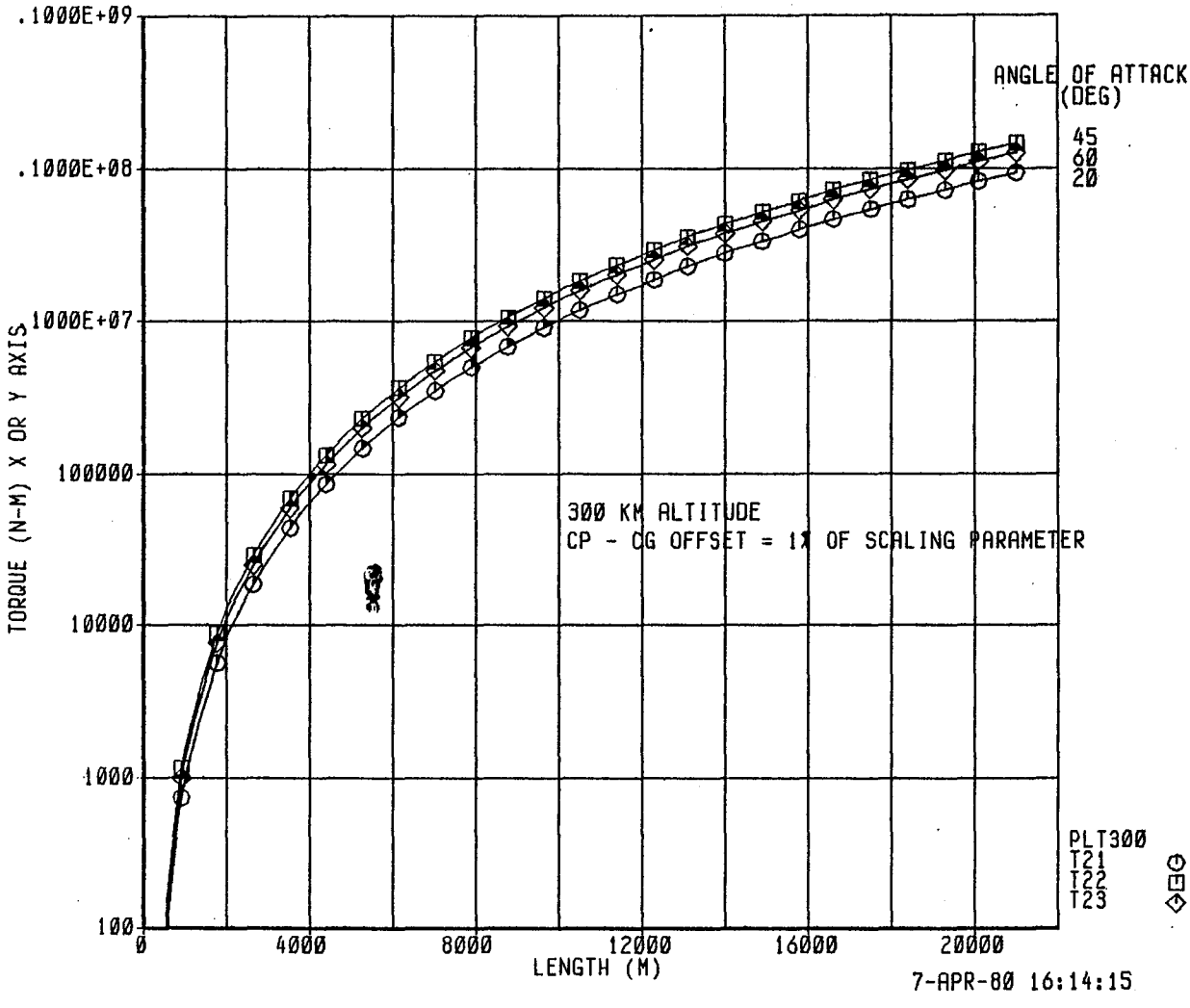

FIGURE 3-3 CP - CG VARIATION EFFECT ON LEO AERODYNAMIC TORQUES PLATE STRUCTURE

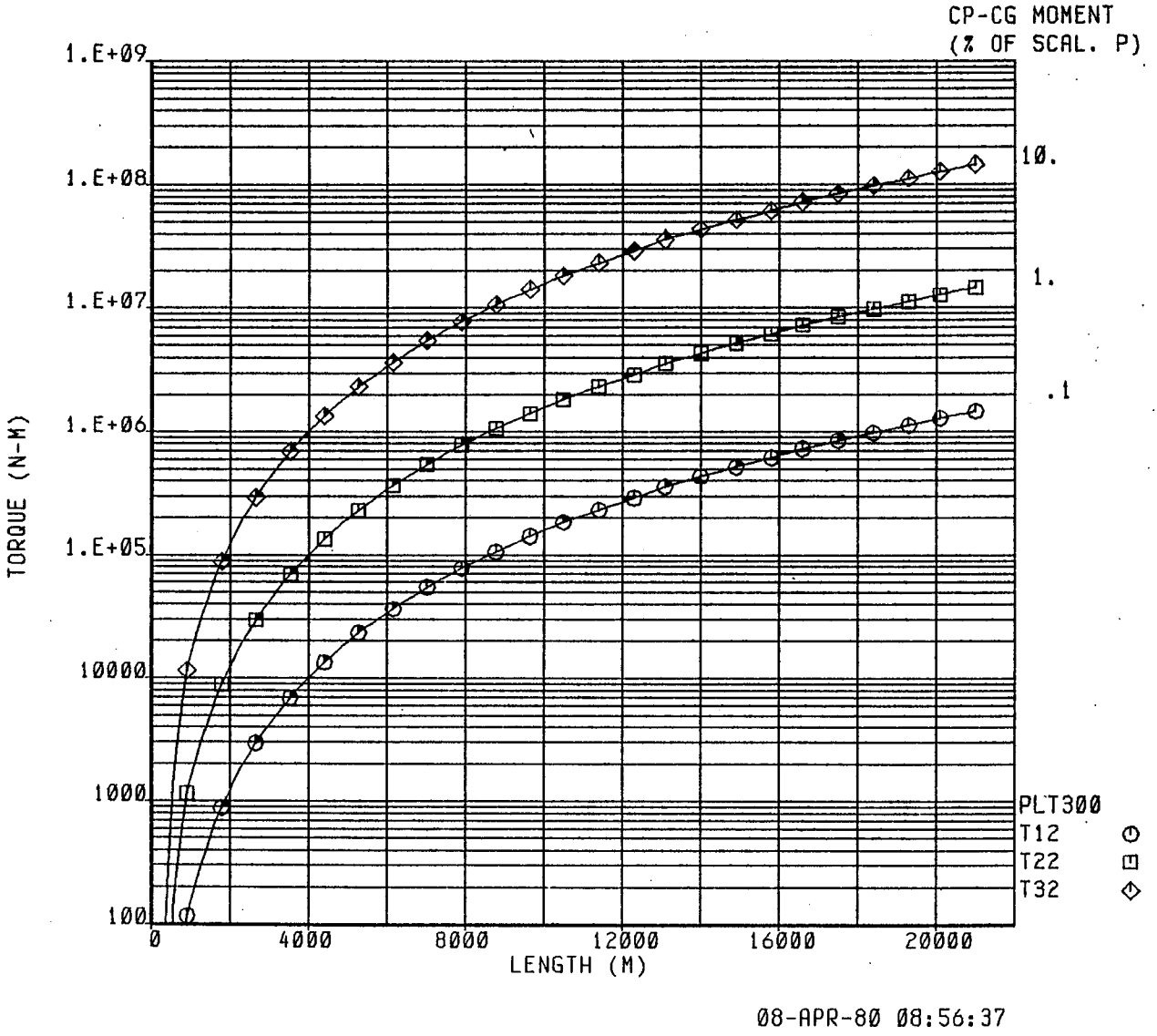

FIGURE 3-4 CP - CG VARIATION EFFECT ON LEO AERODYNAMIC TORQUES
PLATE STRUCTURE AT 300 KM 60 deg ANGLE OF ATTACK

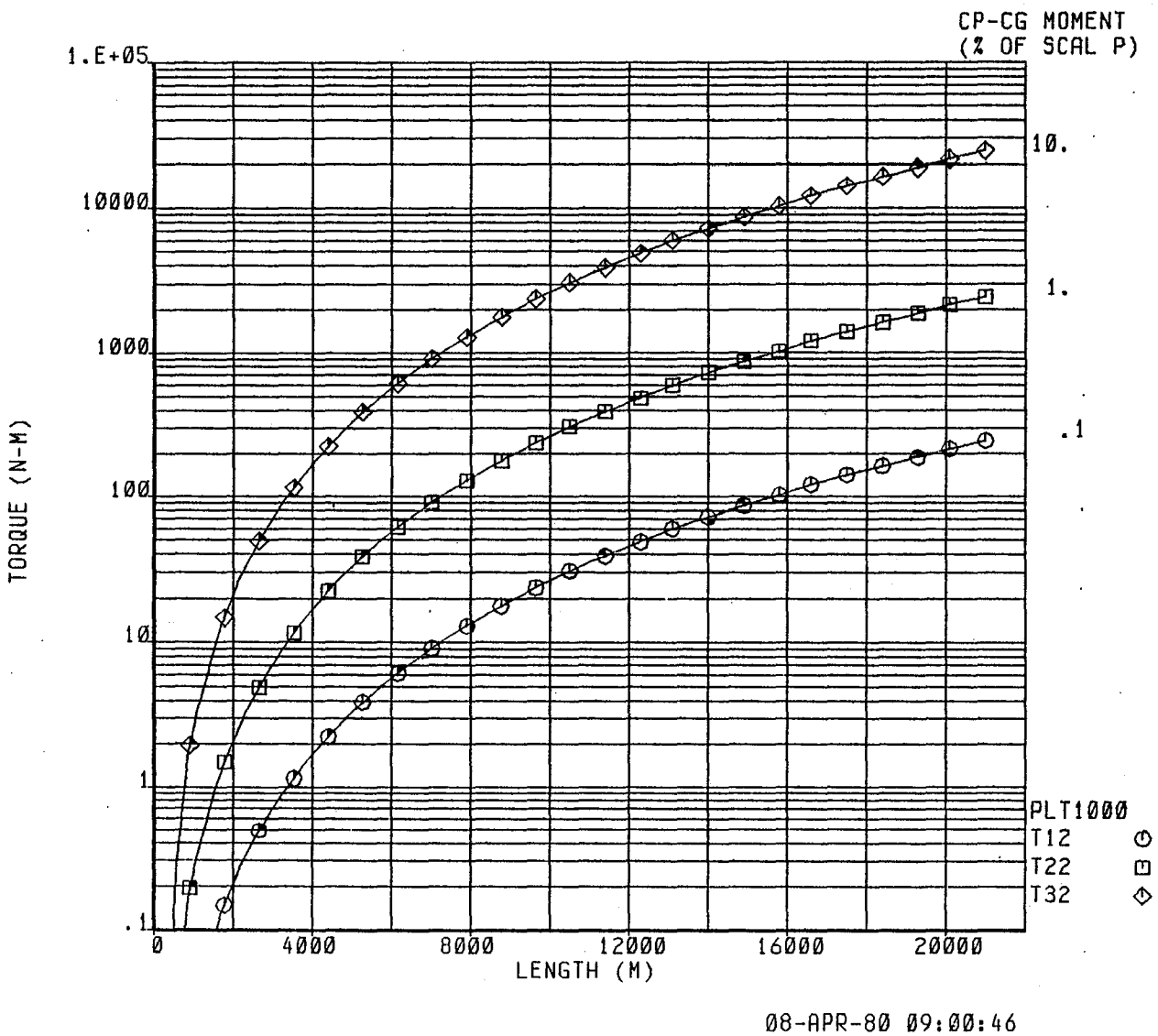

FIGURE 3-5 CP - CG VARIATION EFFECT ON LEO AERODYNAMIC TORQUES
PLATE STRUCTURE AT 1000 KM 60 deg ANGLE OF ATTACK

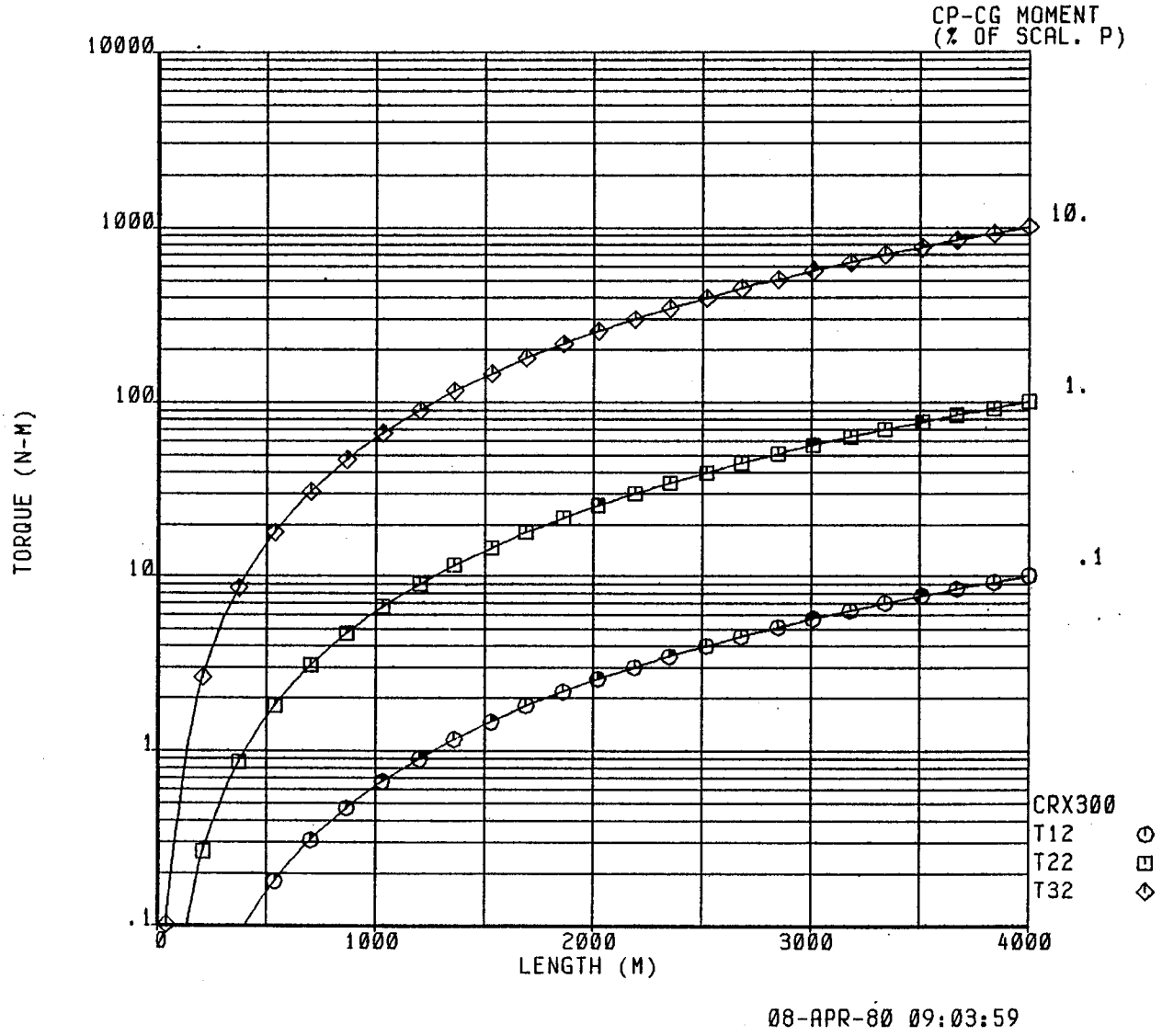

FIGURE 3-6 CP - CG VARIATION EFFECT ON LEO AERODYNAMIC TORQUES
CROSS STRUCTURE AT 300 KM 60 deg ANGLE OF ATTACK

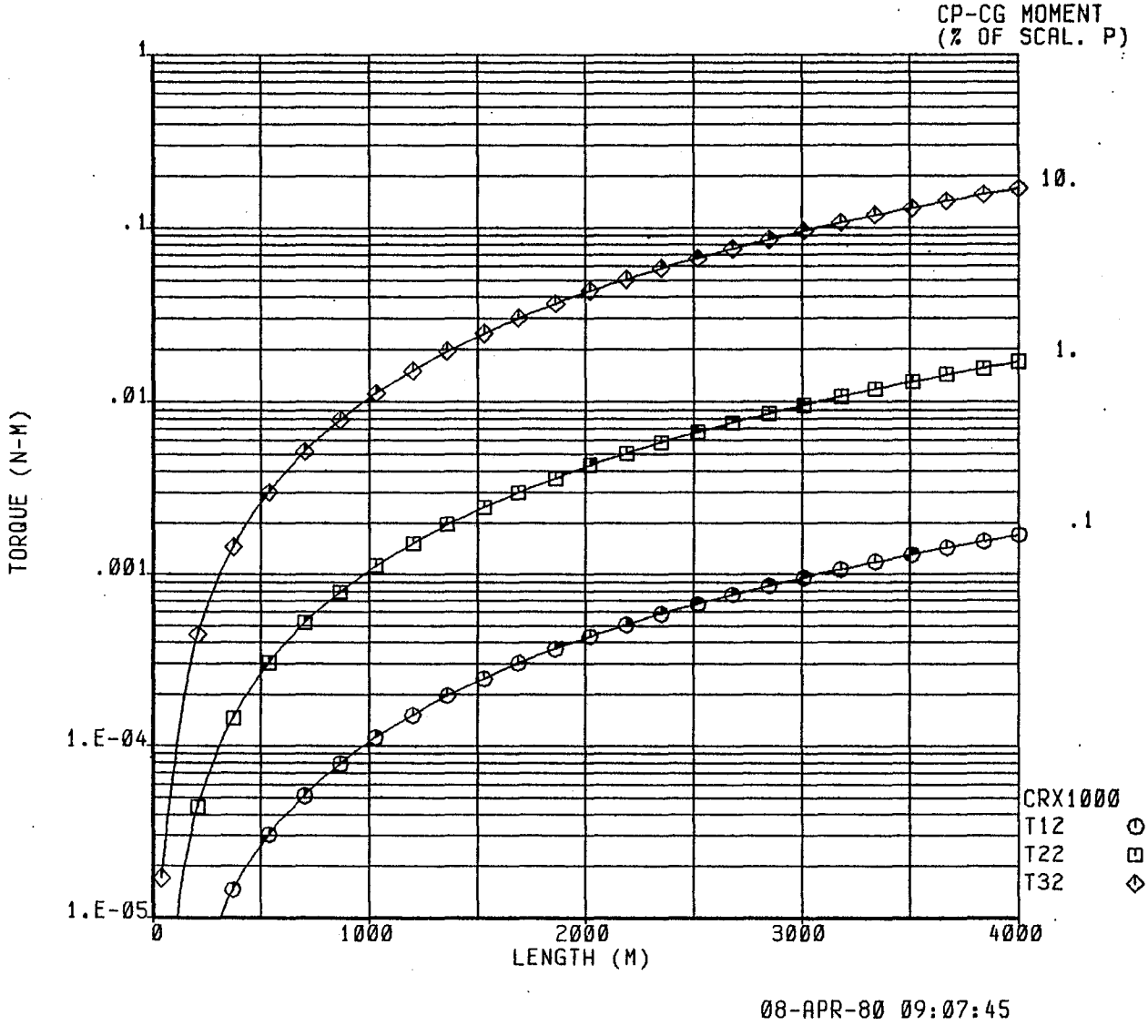

FIGURE 3-7 CP - CG VARIATION EFFECT ON LEO AERODYNAMIC TORQUES
CROSS STRUCTURE AT 1000 KM 60 deg ANGLE OF ATTACK

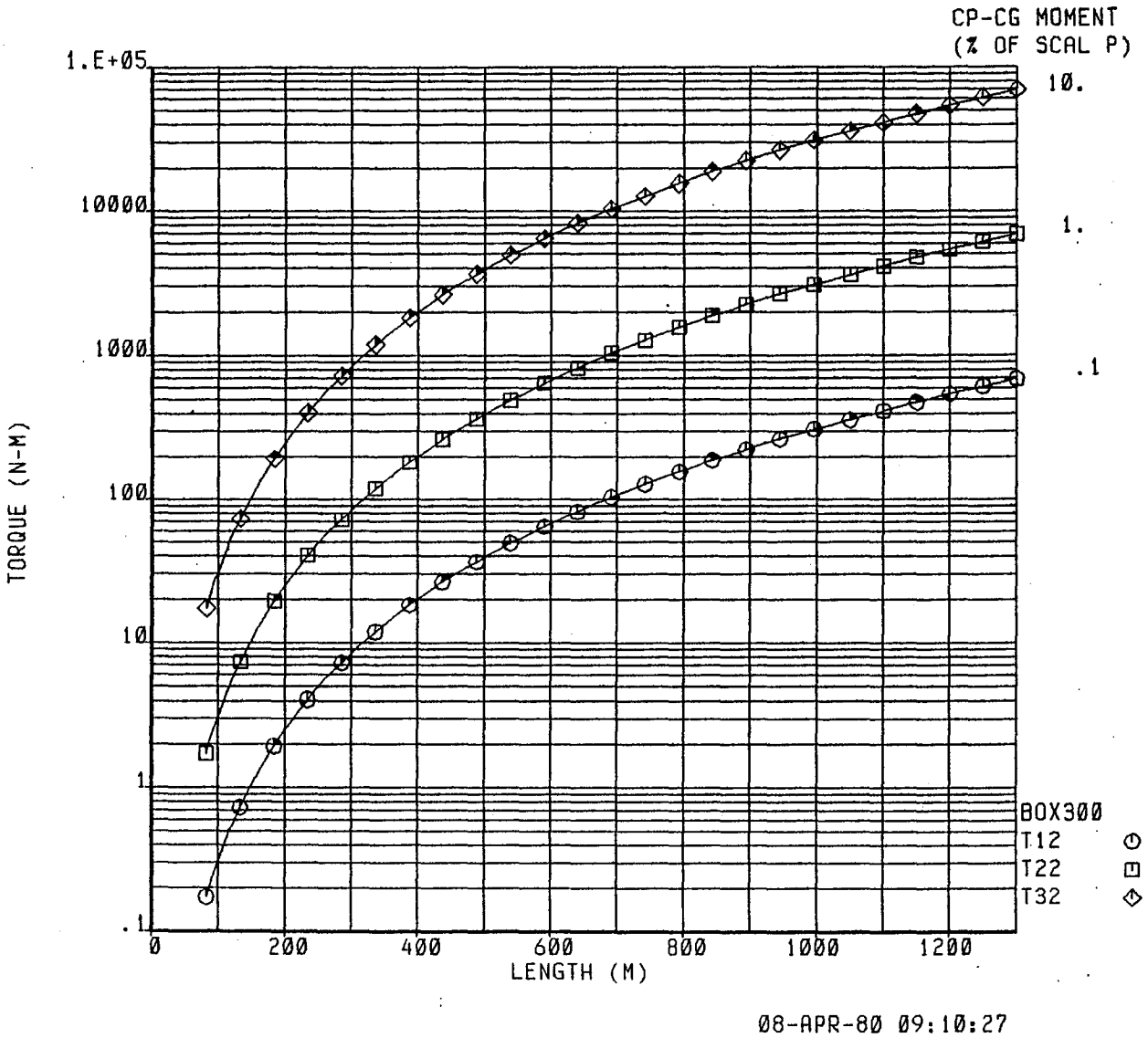

FIGURE 3-8 CP - CG VARIATION EFFECT ON LEO AERODYNAMIC TORQUES
BOX STRUCTURE AT 300 KM 60 deg ANGLE OF ATTACK

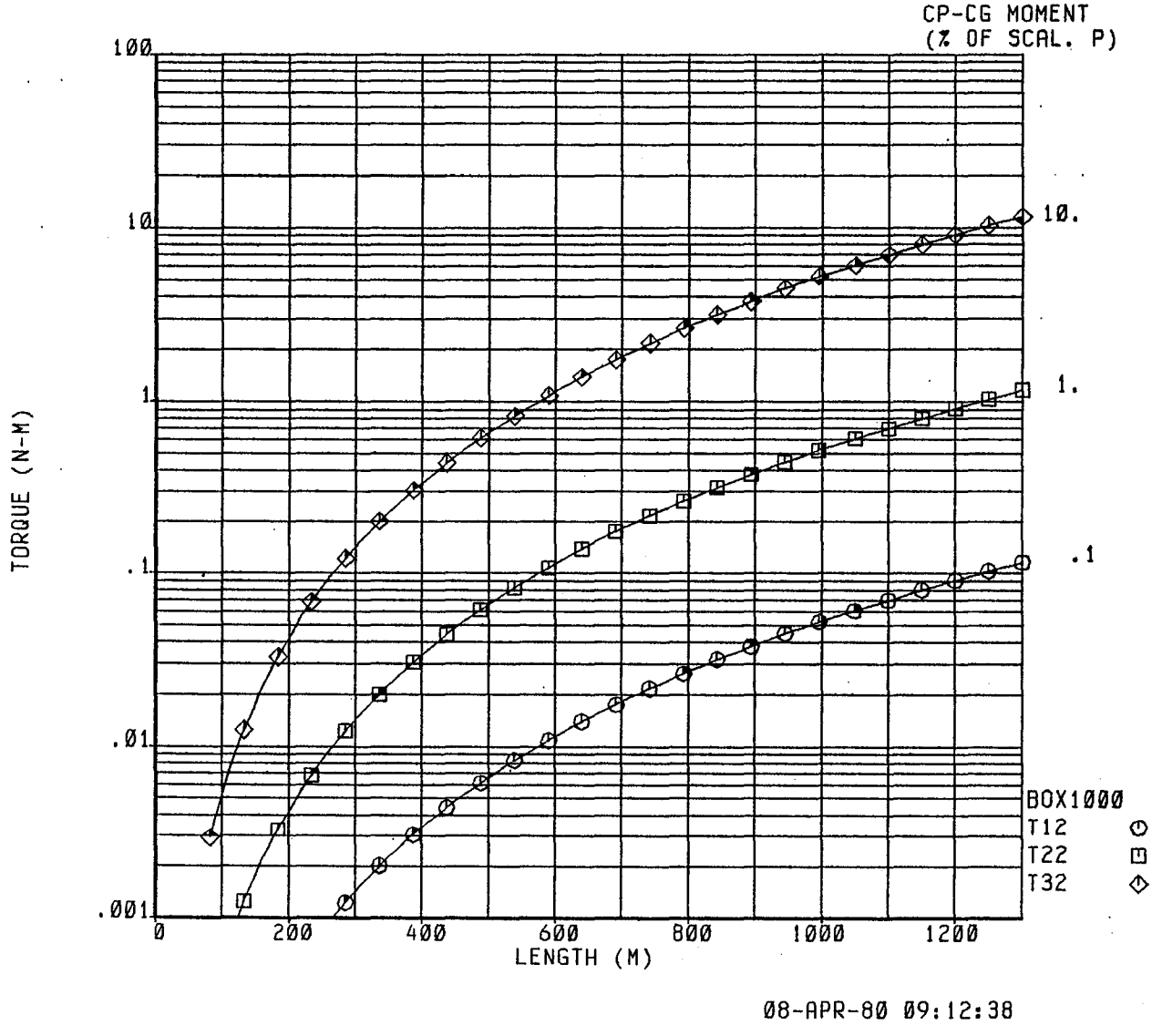

FIGURE 3-9 CP - CG VARIATION EFFECT ON LEO AERODYNAMIC TORQUES
BOX STRUCTURE AT 1000 KM 60 deg ANGLE OF ATTACK

disturbances will occur in different orientations, however, the maximum forces and torques needed for each disturbance type will be used in the maximum disturbance graphs to follow. The maximum nominal torque during transfer will be determined using the equation:

$$T = I_{yy} \ddot{\alpha} \qquad \text{where } \ddot{\alpha} = 7.838 \times 10^{-7} \text{ rad/sec}^2$$

The maximum nominal disturbance force occurs from aerodynamic effects as the plate turns to meet the thrust pointing requirement of 30 degrees. The GEO maximum disturbances will be gravity gradient and solar pressure and the nominal on-orbit disturbances are composed of radiation pressure and stationkeeping loads. The orientation chosen for GEO orbit will be with the y axis parallel to the orbit and z down for each class. Figure 3-10 gives an example of the graphs generated for the Plate Structure. The full set of force and torque data for the Plate is given in Appendix B, Figures B-15 through B-20.

Cross Structure (IB) - Here the same conditions and orientations apply as in the plate structure. Figure 3-11 shows an example of the cross structure. The complete set of data for the cross structue is in Appendix B, Figues B-21 through B-25.

Box Structure (IIA) - At LEO the nominal disturbances also include solar radiation on one end of the box. The y axis is once again assumed to lie in the orbit plane with the z axis toward the earth. Figure 3-12 is an example output for the box structure and complete information is found in Figures B-26 through B-31.

Modular Antenna (IIB) - The LEO nominal torques include aerodynamic, solar pressure and manuever requirements. Figures 3-13 and B-32 through B-37 give the force and torque requirements.

Maypole Antenna (IIC) - The aerodynamic drag and radiation pressure on a mesh antenna has been estimated at 1 percent of that of an equivalent area solid flat plate. The forces and torques given in Figures 3-14 and B-38 through B-43 are, therefore, significantly lower than for the other structures.

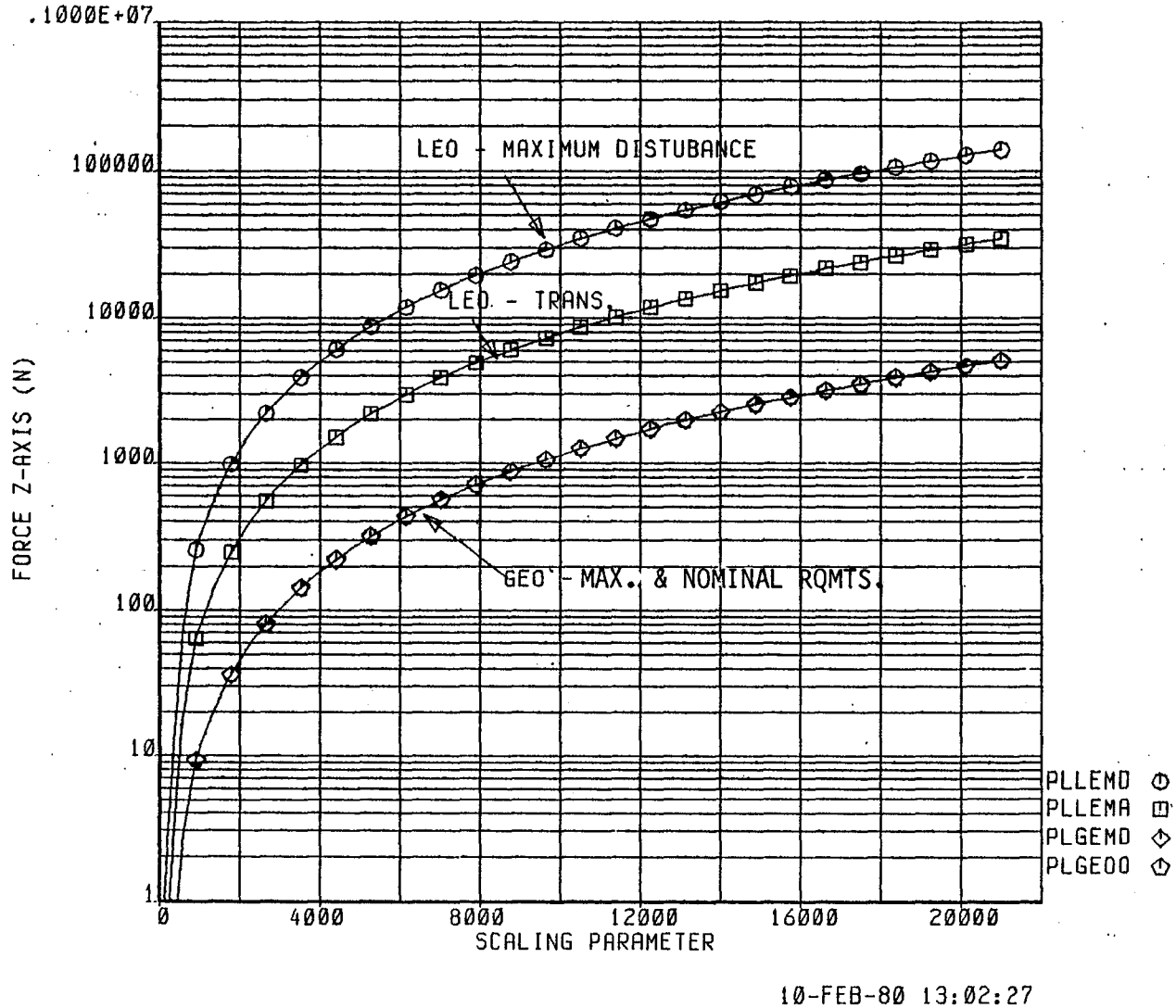

FIGURE 3-10 LSS PARAMETER STUDY PLATE STRUCTURE FORCES - Z AXIS

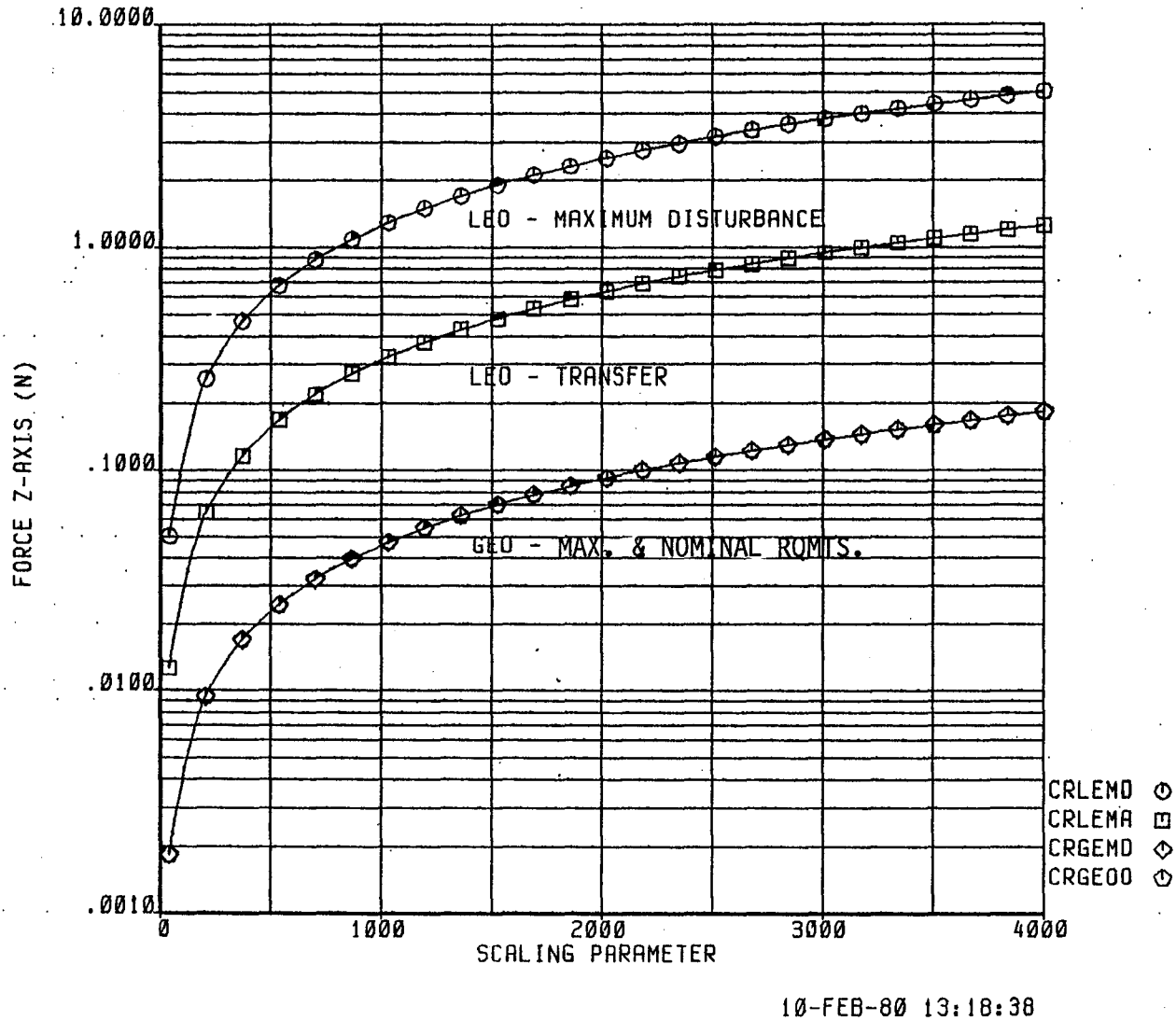

FIGURE 3-11 LSS PARAMETER STUDY CROSS STRUCTURE FORCES - Z AXIS

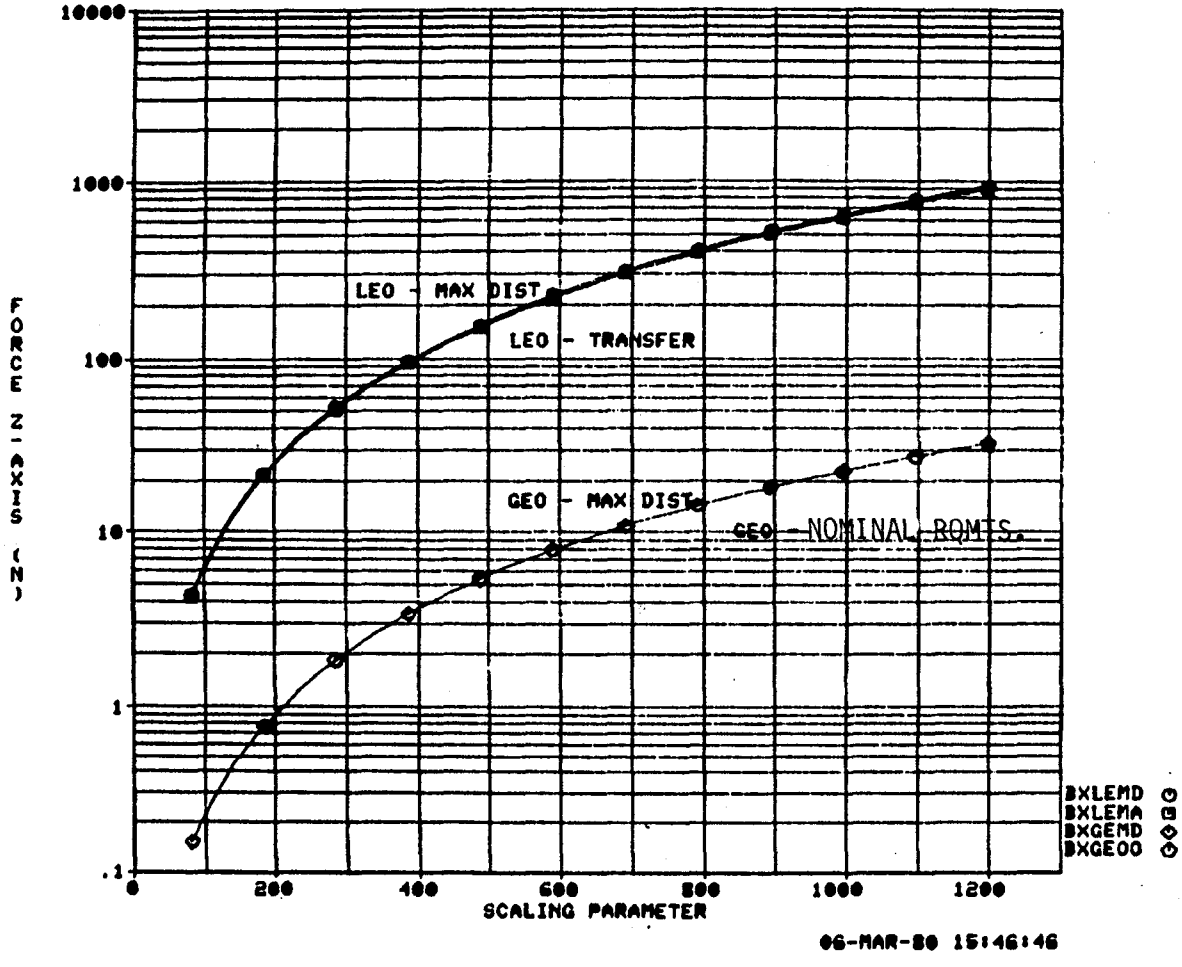

FIGURE 3-12 LSS PARAMETER STUDY BOX STRUCTURE FORCES - Z AXIS

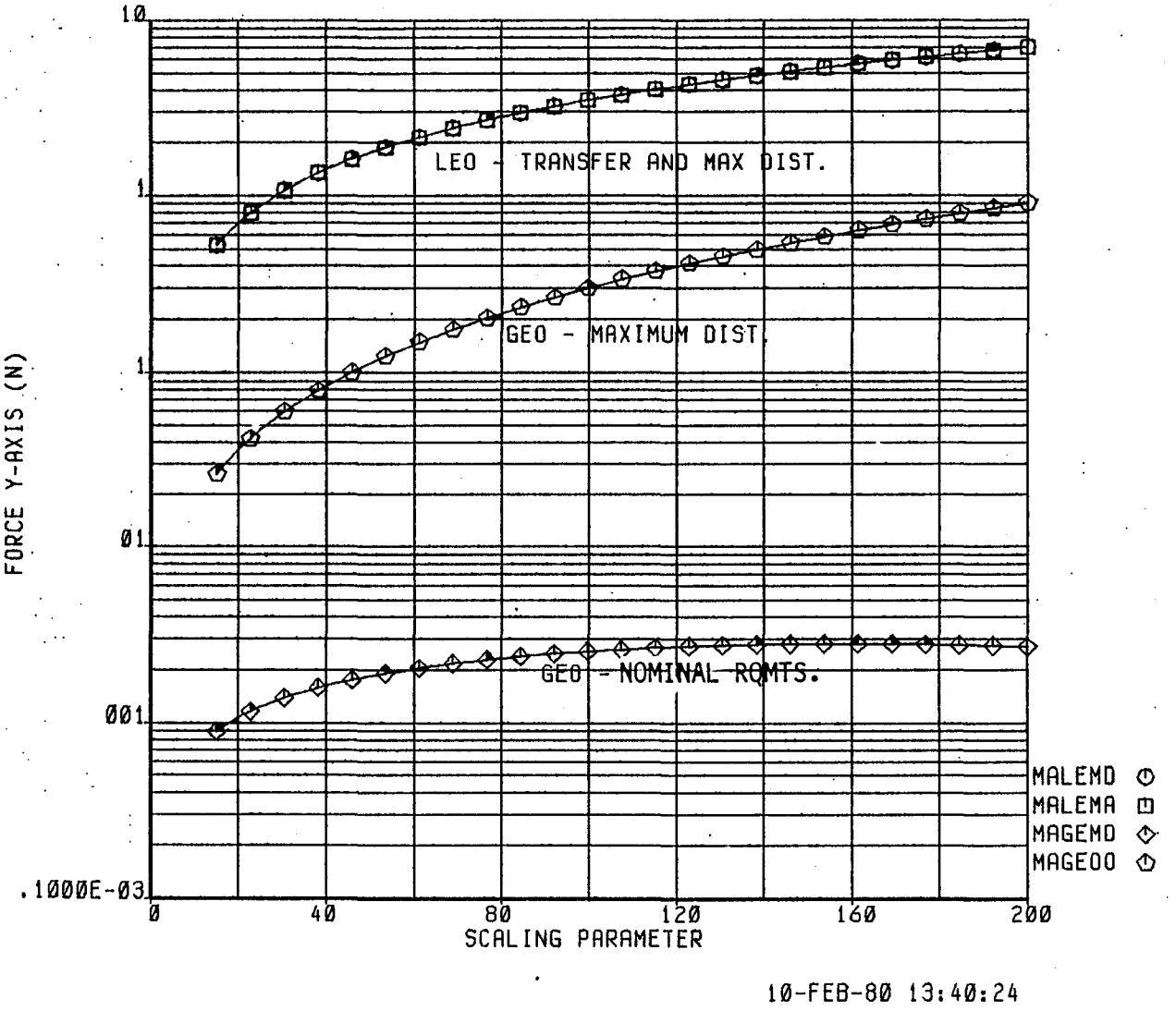

FIGURE 3-13 LSS PARAMETER STUDY MODULAR SINGLE ANTENNA FORCES - Y AXIS

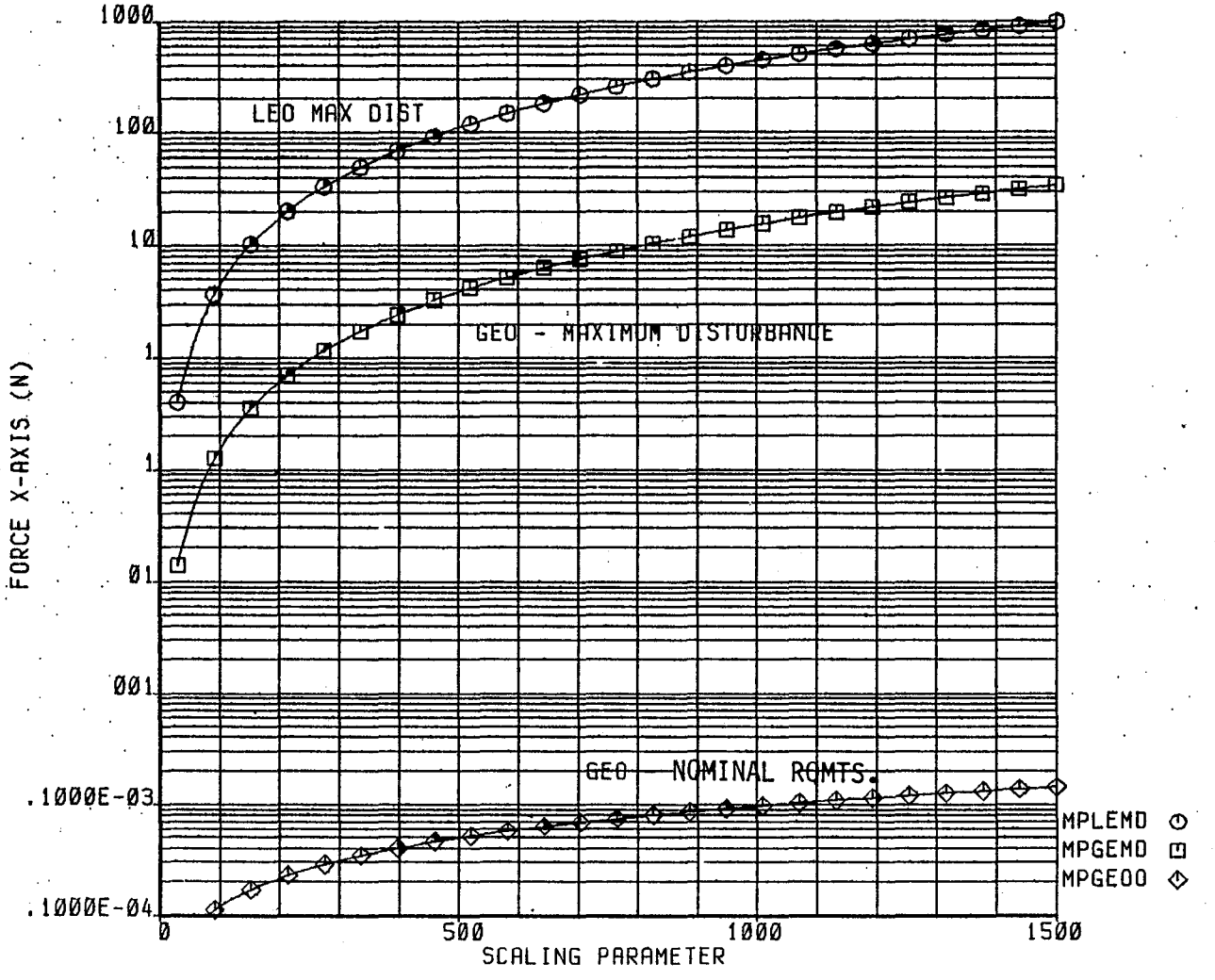

FIGURE 3-14 LSS PARAMETER STUDY MAYPOLE ANTENNA FORCES - X AXIS

Multiple Antenna Farms (IIIA and B) - Disturbances in nominal LEO include aerodynamic, radiation, and manuevering. The disturbance levels are shown in Figures 3-15 and 3-16 and B-44 through B-55.

3.2 Establishment of Auxiliary Propulsion System Characteristics

In order to establish the important APS characteristics the requirements imposed by APS control functions can be examined in turn. There are three basic control tasks: attitude control, shape control and stationkeeping.

Attitude control can be accomplished with APS directly or in conjunction with momentum exchange devices. In the direct mode a chemical APS typically maintains the required orientation by limit cycling back and forth across a small deadband by turning alternate jets on and off. This bang-bang operation is made necessary because of the lack of thrust amplitude modulation capability in small chemical APS. Electrical APS can be amplitude modulated and proportional control is more feasible. Attitude control requires the cancellation of disturbance torques plus, when necessary, the additional expenditure of energy to maintain limit cycle operation.

When momentum exchange devices such as wheels or control moment gyros CMG's are used as prime attitude control torquers cyclic disturbances can be absorbed, provided the momentum capacity is sufficiently large. The secular or accumulating torque impulse must however be removed. Although this secular impulse can be taken out continuously it is typically stored in the momentum exchange system and dumped periodically. This desaturation process requires an external torque which is conveniently provided by APS although gravity gradient and magnetic methods can be used in particular circumstances.

Direct attitude control by APS requires, ideally, the delivery of precise torques to counter disturbances. The ideal can be closely approximated by delivering periodic torque impulse bits. In either case it is clear that thrust level and modulation (amplitude in the continuous case and pulse width in the discrete) are important characteristics. Transient effects such as the rise and decay profiles are also significant particularly in limit cycle operations where they may impact accuracy and propellant

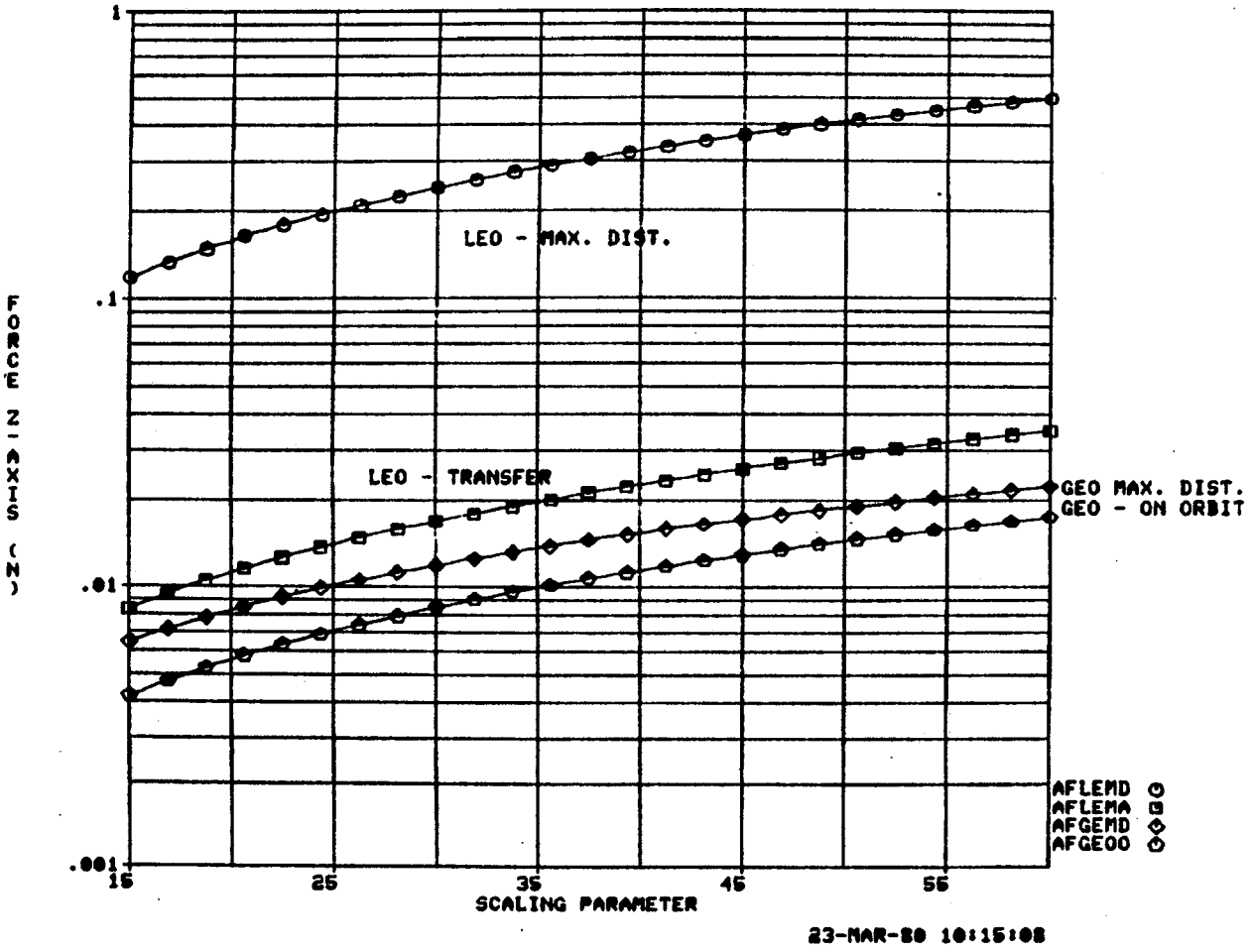

FIGURE 3-15 LSS PARAMETER STUDY ANTENNA FARM FORCES - Z AXIS

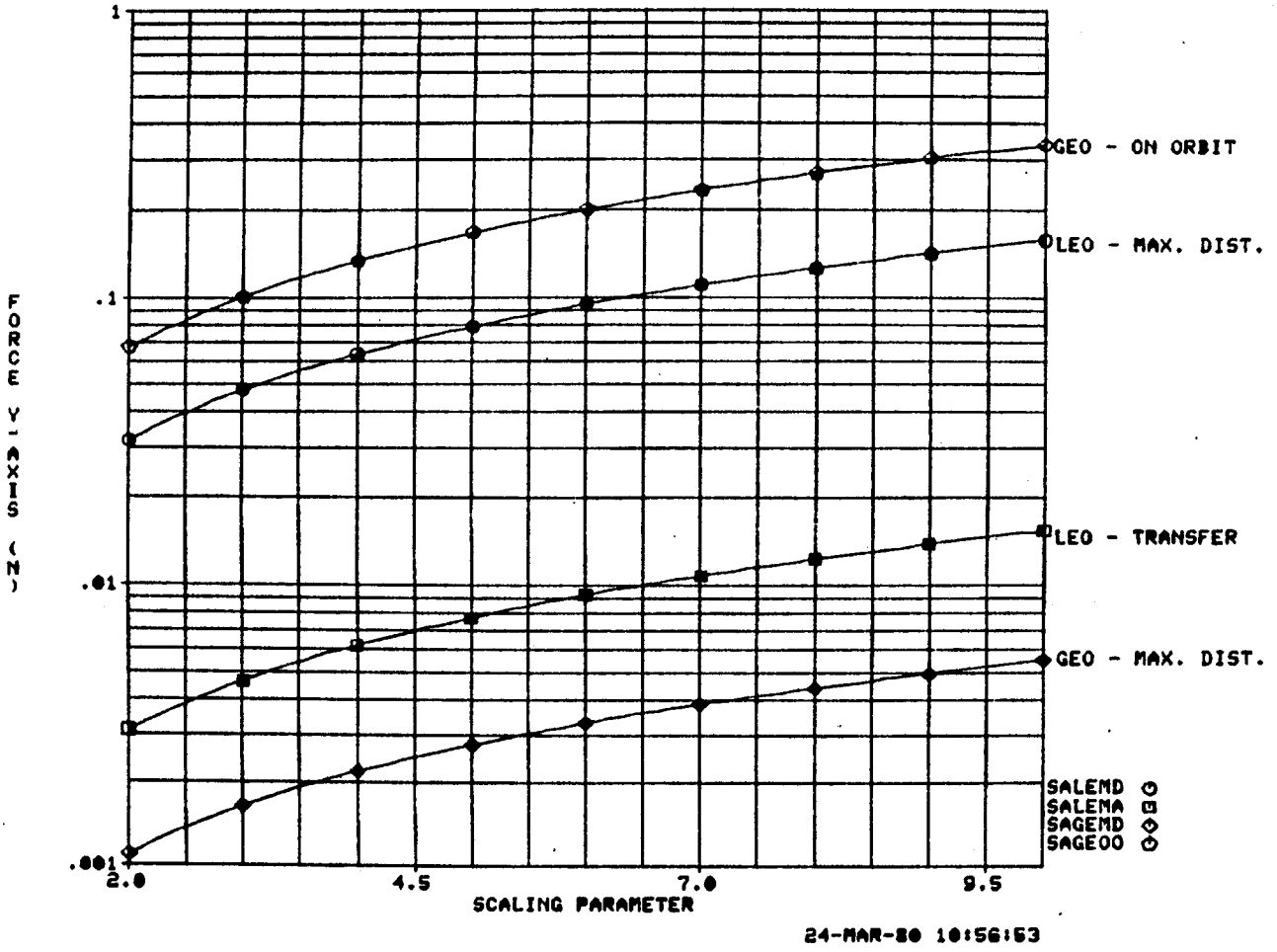

FIGURE 3-16 LSS PARAMETER STUDY SERIES OF ANTENNAS FORCES - Y AXIS

consumption. In summary the important APS characteristics for direct attitude control are:

- o Thrust level
- o Modulation
- o Transient effects

When used in an indirect mode to desaturate a momentum exchange system the APS requirements are considerably relaxed. Torque impulse must be delivered periodically but the desaturation events are often well spaced (days or even weeks apart) and the timing is rarely critical. The thrust levels must be large enough so that the wheel or CMG control torques can contain the transients caused by turning the desaturation jets on and off. The only important identifiable APS characteristics for indirect attitude control is

- o Thrust level

Shape control implies a distributed system in which APS units are spread over or through the vehicle structure. The number and distribution of thrusters is therefore a key characteristic. The control of shape requires the damping of structural oscillations to avoid surface distortions which may affect the mission objective. This means that timing becomes important. Continuous thrusts must be time varying or, when discrete pulses are used, these must be applied at precise times. Modulation and transient effects are thus significant. For shape control APS characteristics are:

- o Number and distribution of thrusters
- o Thrust level
- o Modulation
- o Transient effects

Stationkeeping is in many respects similar to desaturation in that accumulated impulse is removed. In stationkeeping it is linear momentum that is unloaded while in desaturation it is angular momentum. Again the process can be either continuous or discrete and again the APS requirements are not demanding. The only important APS characteristic is

- o Thrust level

Consideration of the three basic control functions has uncovered four important APS characteristics: (1) thrust level, (2) number and distribution of thrusters, (3) modulation and (4) transient effects. These are operating characteristics. From a systems viewpoint, the allowable APS

weight, while not directly affecting system operation, must be considered. It is no good having an ideal operating APS if the weight is excessive. A fifth important characteristic is then allowable mass. APS mass has a number of components, for example the type of propellant, I_{sp}, supporting equipment (such as tanks, plumbing, power processor units, heat exchangers, etc.) and the redundancy necessary to meet lifetime requirements.

Another APS characteristic may be important in specific applications. This is the exhaust plume. There may be contamination effects due to the chemical properties of the exhaust products, space charging effects due to the electrical characteristics or temperature problems if the plume is hot and impinges on the structure. These effects are not of general significance however and although they should be borne in mind for specific applications, the inclusion of plume effects does not appear warranted as an important APS characteristic in a general study of the control of large space structures.

3.2.1 Thrust Levels

The goal of this study is to identify the required thrust level/thruster or more generally the required total thrust level/thrust location. The seven classes of large space structures identified in Task I contain three classes of stuctures which yield themselves to a distributed thruster system. The plate structure was used as an example of a distributed thruster class. For the distributed thruster system used on the plate, various thrust locations were assigned and the number of thrust locations was treated as a parameter. For each location, the required thrust level per location was identified. The remaining classes are considered to have a set number of thrust locations and the number of thrusters at that location was treated as a parameter. The method of distribution for the distributed thruster classes and thruster location selection for non-distributed classes will be discussed later.

Four categories of disturbance requirements were identified in an earlier task and will be reviewed in the thust level study. Stationkeeping requirements will also be discussed as a disturbance requirement. Selected thrust level and impulse sizing philosophy will be covered in this section.

Finally, throttling level requirements will be examined as they relate to the four disturbance categories.

To facilitate coverage of the full range of scaling parameters, each class was assigned a small, medium, and large value. Disturbance analysis was conducted on these three sizes of LSS. One further simplification of the large number of classes and sizes examined was made where appropriate. This step reduced the number of classes to be considered from seven down to three. These three primary classes are class IA, Plate Structure (Distributed Thrusters); class IIB, Modular Antenna (Non-Distributed); and class IIIB, Series of Antennas (Non-Distributed). These three classes cover the range of LSS types and sizes and it is felt that conclusions drawn from these classes will be valid for the broader range of Large Space Structures.

Table 3-2 shows the size selections for each class.

For distributed thruster classes, a method of placing thrusters was determined based on the Number and Distribution of Thrusters study (4.3). Figures 4-28 and 34 show the "N + 1" distribution method produces a smaller deflection than the "N - 1" method for small numbers of thrusters. For a large number of thrust locations N>10, the method of distribution does not significantly affect the surface deflection of the structure.

The plate structure was assumed to have two "lines" of thrusters along the major axis as shown in Figure 3-17. These lines disected the structure into three equal portions hence preserving the "N + 1" philosophy. Figure 3-17 shows the arrangement for four thrusters; however, thruster locations can be added in multiples of two and still preserve the two lateral lines of N + 1 distributed thrusters. Thrusters were assumed to have full gimbal freedom for each class at each of the thruster locations. This assumption allows three axis torque to be applied for all thruster combinations.

For class IIB (modular antenna) thruster locations were set on the rigid portions of the structure. Figure 3-18 shows the eight thruster locations, one on each corner of the cube. Class IIIA (the series of antennas) was given thruster locations on the outer avionics modules and just inboard of the solar arrays along the antenna axis. Figure 3-19 illustrates this arrangement. Thrusters were added in groups of four to maintain symmetry.

	Class	Scaling Parameter	Small	Medium	Large
IA	Plate	Length (m)	30	700	21000
IB	Cross	Length (m)	40	500	4000
IIA	Box	Length (m)	82	600	1300
IIB	Modular Antenna	Antenna Diameter (m)	15	60	200
IIC	Maypole	Antenna Diameter (m)	30	250	1500
IIIA	Antenna Farm	Antenna Diameter (m)	16	35	60
IIIB	Series of Antennas	Number of Antennas	2	6	10

TABLE 3-2 SMALL, MEDIUM AND LARGE PARAMETERS

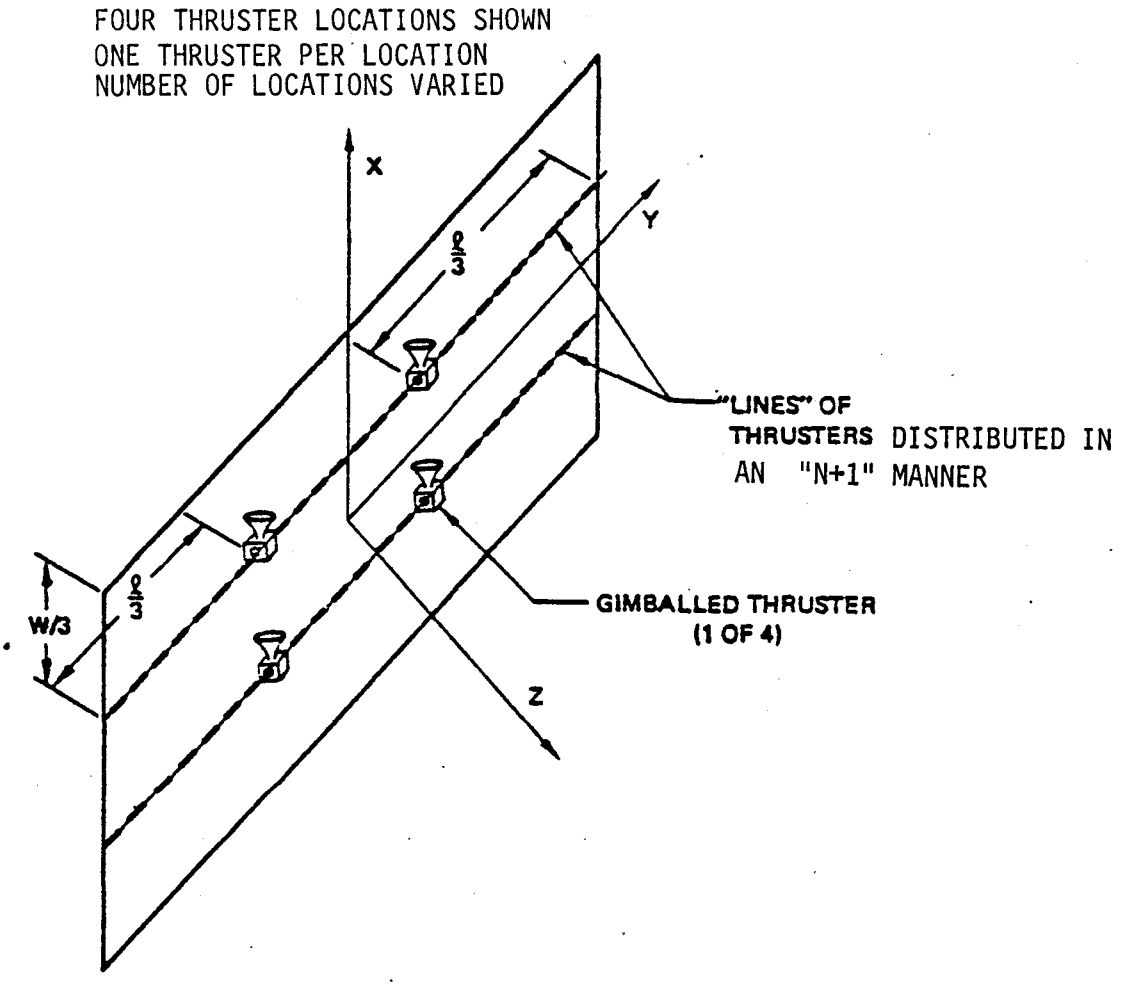

FIGURE 3-17 PLATE STRUCTURE THRUSTER LOCATIONS

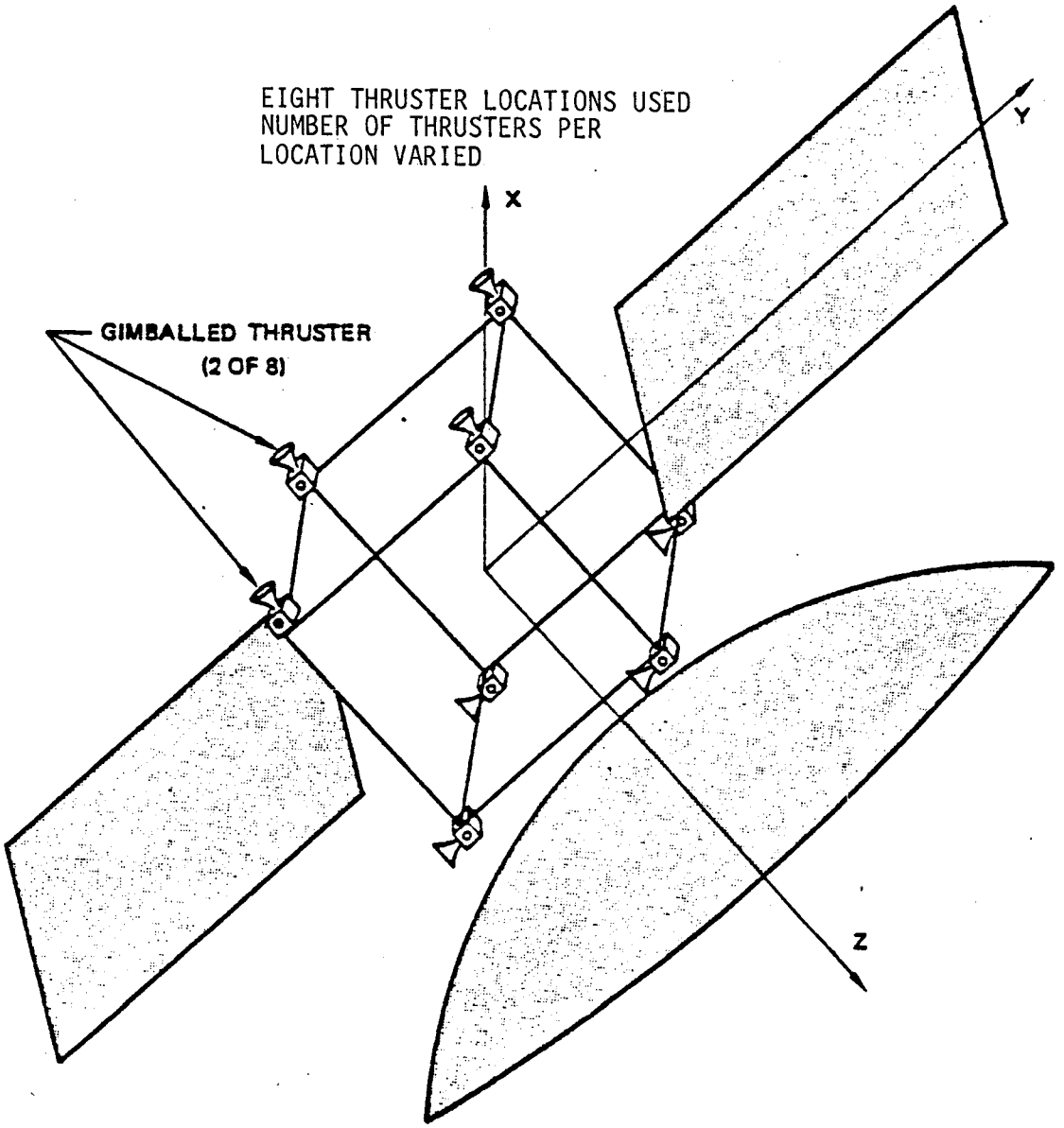

FIGURE 3-18 MODULAR ANTENNA THRUSTER LOCATIONS

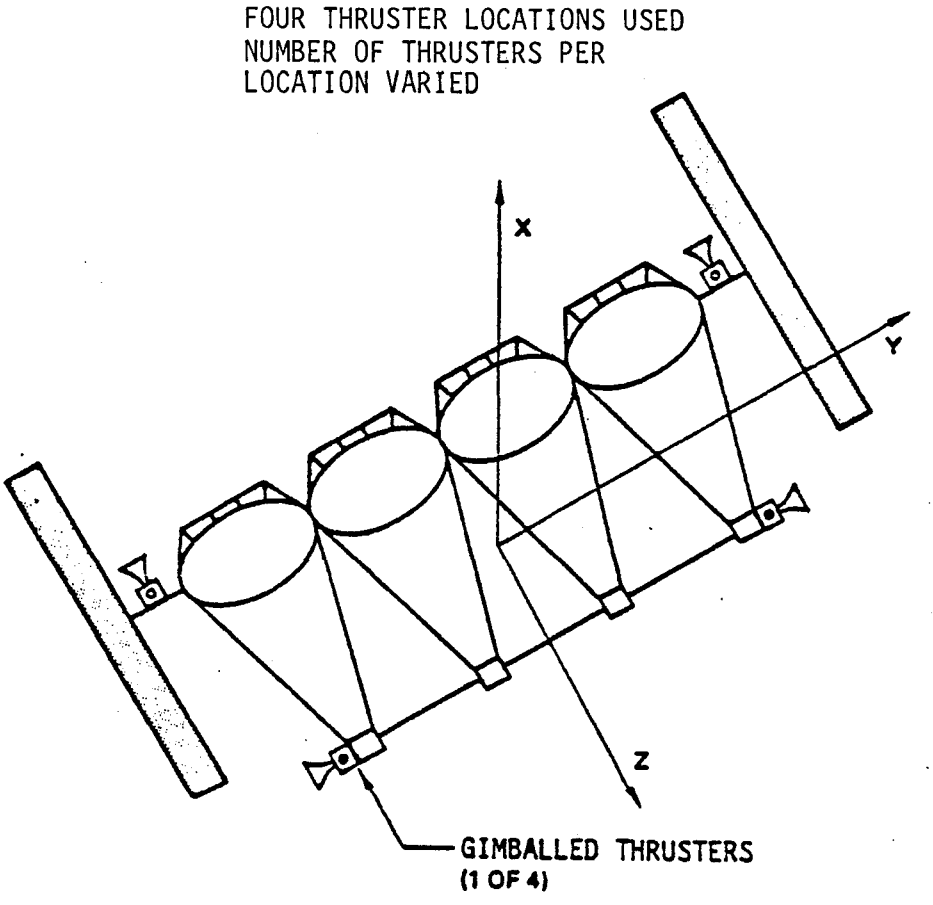

FIGURE 3-19 SERIES OF ANTENNAS THRUSTER LOCATIONS

There are three requirements placed on any auxiliary propulsion system that demand significant amounts of propellant. These are; disturbance torque cancellation, stationkeeping and maneuvering. Due to the non-mission specific nature of this study, the maneuvering requirements on each LSS could not be uniquely identified. Maneuvering requirements were, however, treated in a parametric fashion in a later paragraph in this study. Disturbance torques are classically the largest acceleration requirement on the APS. Stationkeeping requirements are then met by judicious choice of disturbance cancellation thrusting. If, however, the stationkeeping accelerations pose a greater acceleration requirement than disturbance torques, it is disturbance torques that will be made up by judicious choice of stationkeeping accelerations. Unequal stationkeeping pulses from a pair of thrusters result in stationkeeping and disturbance cancellation being performed simultaneously. It is, therefore, appropriate to size thrusters based on the maximum of either the disturbance torque cancellation or stationkeeping requirements.

The following paragraphs review the four disturbance categories that were used in the disturbance torque analysis.

LEO TRANSFER - The vehicle is being transferred from LEO to GEO on a time optimal continuous thrust trajectory with a selected axis as the prime thrust axis. It is assumed that the APS will provide all maneuvering torques to meet the required thrust profile as well as countering the radiation, gravity gradient, and aerodynamic torques found in the first orbit of the transfer. LEO altitude is assumed to be 500 km.

LEO MAXIMUM - Here the vehicle is assumed to be in the worst orientation possible with regard to gravity gradient, radiation torques, and aerodynamic disturbances at 500 km altitude. This requirement may differ only slightly from the LEO transfer requirement. Similarity results from the choice of prime thrust axis in the transfer analysis forcing the vehicle into a worst case or near worst case attitude during the transfer.

GEO MAXIMUM - The structure is in geosynchronous orbit and has a worst case orientation with regard to gravity gradient and radiation torques.

GEO ON-ORBIT - The nominal on-orbit orientation was assumed and inherent gravity gradient or radiation torques calculated. For those structures having no CP-CG offset, an offset equal to five percent of the scaling parameter was assumed.

For maximum disturbance categories it was assumed that disturbance torques could occur from all relevant sources simultaneously. This assumption means that thrust levels required on each axis could be root sum squared to form a composite thrust level/thruster requirement.

Because of the large number of graphs concerning the thrust requirements, a separate appendix for these graphs has been created. Appendix D contains all disturbance cancellation thrust levels and stationkeeping acceleration requirements. Figures D-1 through D-18 show the disturbance torque requirements on the APS system. For each LSS class the small, medium and large scaling parameters are used to generate disturbance torque requirements for each of the four disturbance categories. Number of thrusters was treated as a parameter and the thrust/thruster necessary to counter the disturbance torque was the dependent variable. For the distributed classes, these parameters are replaced by number of thruster locations and thrust/thruster locations.

Before comparing the disturbance torque requirements with the stationkeeping requirements, it is necessary to briefly review stationkeeping disturbances. The three independent variables relevant when counteracting stationkeeping disturbances are the time between successive corrections, the time of the correction and the duty cycle during the corrective period. In addition, there are three sources of stationkeeping disturbance: solar pressure, sun/moon gravity perturbations and earth triaxiality. It is the greatest of these sources that will set a thrust sizing criterion to be compared with disturbance torques since the effects can be countered at different times during the orbit.

One simplification has been made to eliminate one of the independent variables involved in stationkeeping. It has been groundruled that the period of correction be one day, or equivalently, one orbit. The time between the start of successive corrections (N) will be set at three

values: one day, one week and one month. The duty cycle (p) will be the other independent variable and will be allowed to vary from 0 to 1.0. These groundrules mean that stationkeeping requirements can be analyzed from continuous (N = 1, p = 1) to intermittant (N = 30, $p \leq 1$).

Figures 4-23 through 4-30 illustrate the comparison between disturbance torque acceleration requirements and stationkeeping acceleration requirements. Each graph contains information pertaining to a single class and one or more sizes of that class. The disturbance torque acceleration lines are for geosynchronous acceleration only. They are for on-orbit nominal operation and for maximum geosynchronous disturbances. All LEO disturbances were excluded in these graphs.

A summary of the results of this comparison are shown in Table 3-3. This chart shows the category of disturbance which will be used to size the thusters and the propellant needed for 10 year operation.

Based on the thruster sizing criterion of Table 3-3, the following graphs, Figures 3-20, 3-21 and 3-22, illustrate the total APS thrust level required. If stationkeeping is the dominant disturbance, this thrust level when applied in one direction will meet the acceleration levels required by stationkeeping. If geo-maximum disturbances dominate, this value represents the thrust level that 1/2 of the thrusters must produce in one direction and the other thrusters in the opposite direction. In the case of the plate structure (distributed thruster system), the center of thrust is approximated at 1/4 of the major axis from the center. For example, a small plate structure of approximately 800m by 200m must be capable of producing approximately 0.1 Newtons of total thrust. A 10000m by 2500m plate with 12 thrust locations is sized by the counteracting torque it must produce, hence six thruster locations on one side must produce 1000 N of thrust which results in each location producing 170 N of thrust.

A simplifying figure which takes into account the difference between force and torque generation is given in Figures 3-23, -24 and -25. Here one may find the thrust/thruster necessary for a given number of thusters for a wide range of scaling parameters. The graph for the plate structure is not truly accurate for small numbers of thrusters N < 10. This is due to the

THRUSTER SIZING, IMPULSE SIZING

STRUCTURE	SMALL	MEDIUM	LARGE
Plate (IA)	SS,S	SS,S	GM,S
Cross (IB)	N/S,S	GM,S	GM,S
Box (IIA)	N/S,S	GM,S	SS,S
Modular Antenna (IIB)	N/S,S	GM,S	GM,S
Series of Antennas (IIIB)	N/S,S	GM,S	GM,S

SS = Solar Station
S = Solar Station + N/S Station + E/W Station
N/S = North/South Stationkeeping
GM = Geosynchronous Maximum Disturbance Torque

Table 3-3 Thruster and Impulse Sizing Criterion

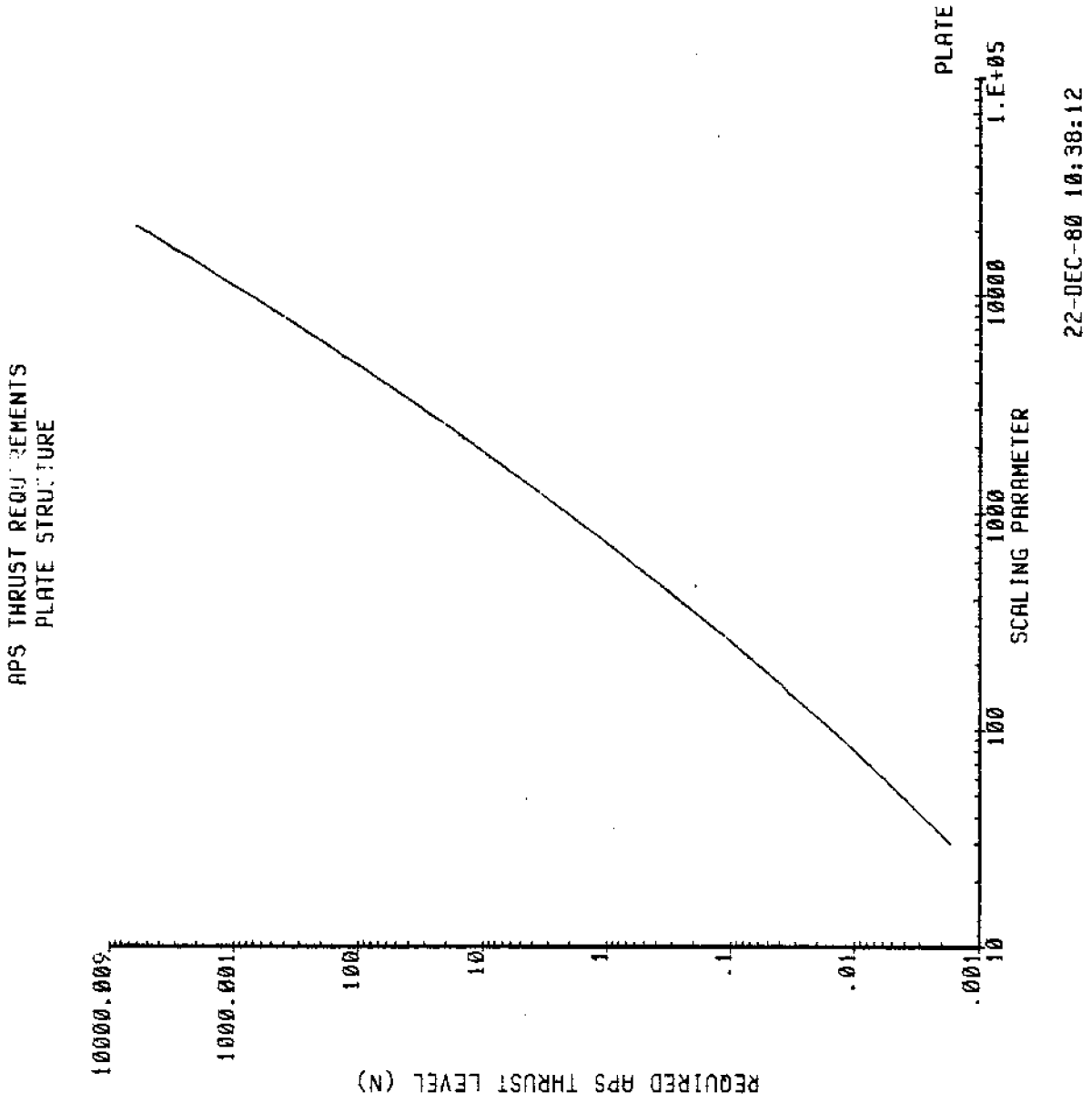

FIGURE 3-20 PLATE STRUCTURE APS THRUST REQUIREMENTS

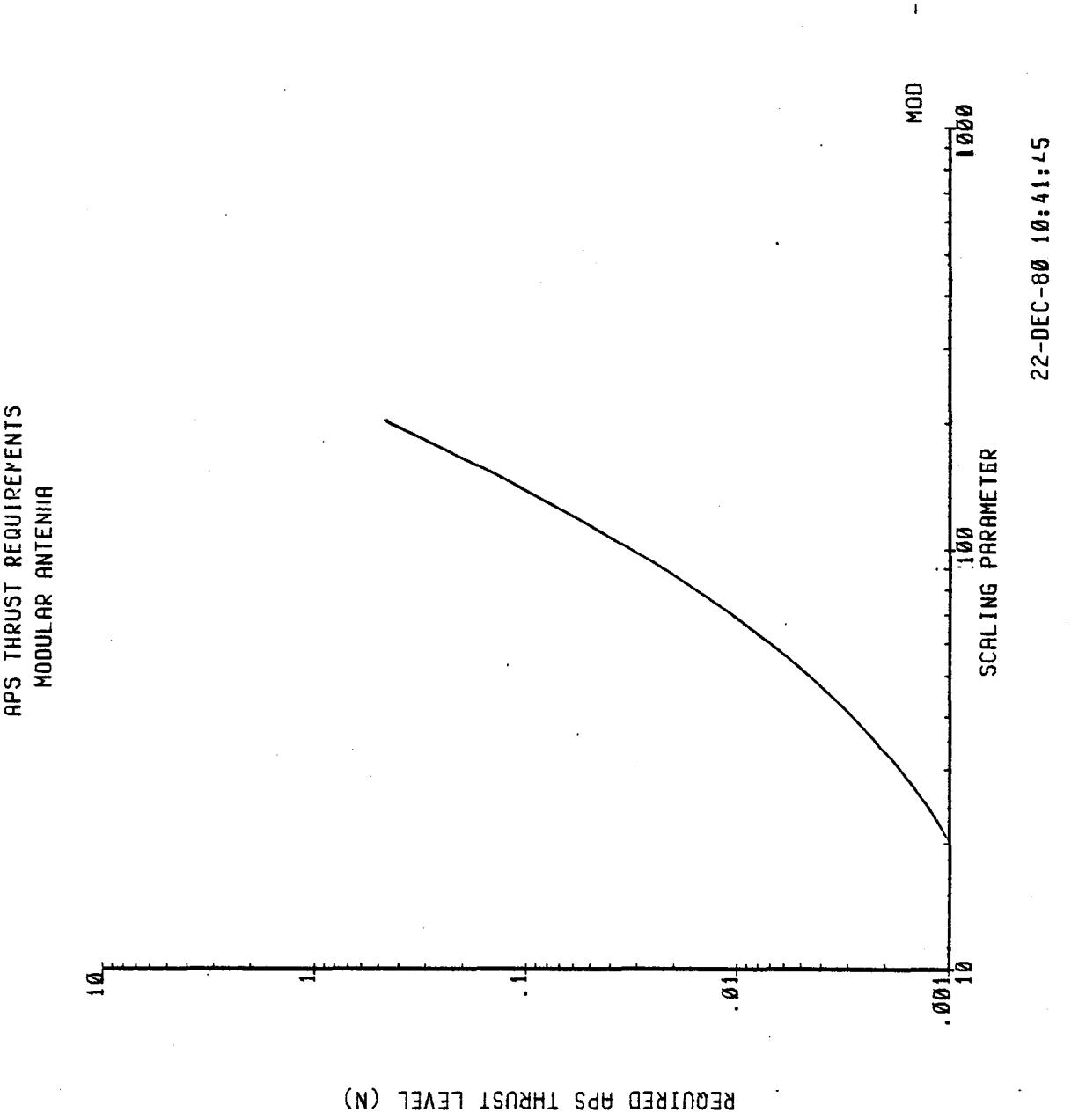

FIGURE 3-21 MODULAR ANTENNA APS THRUST REQUIREMENTS

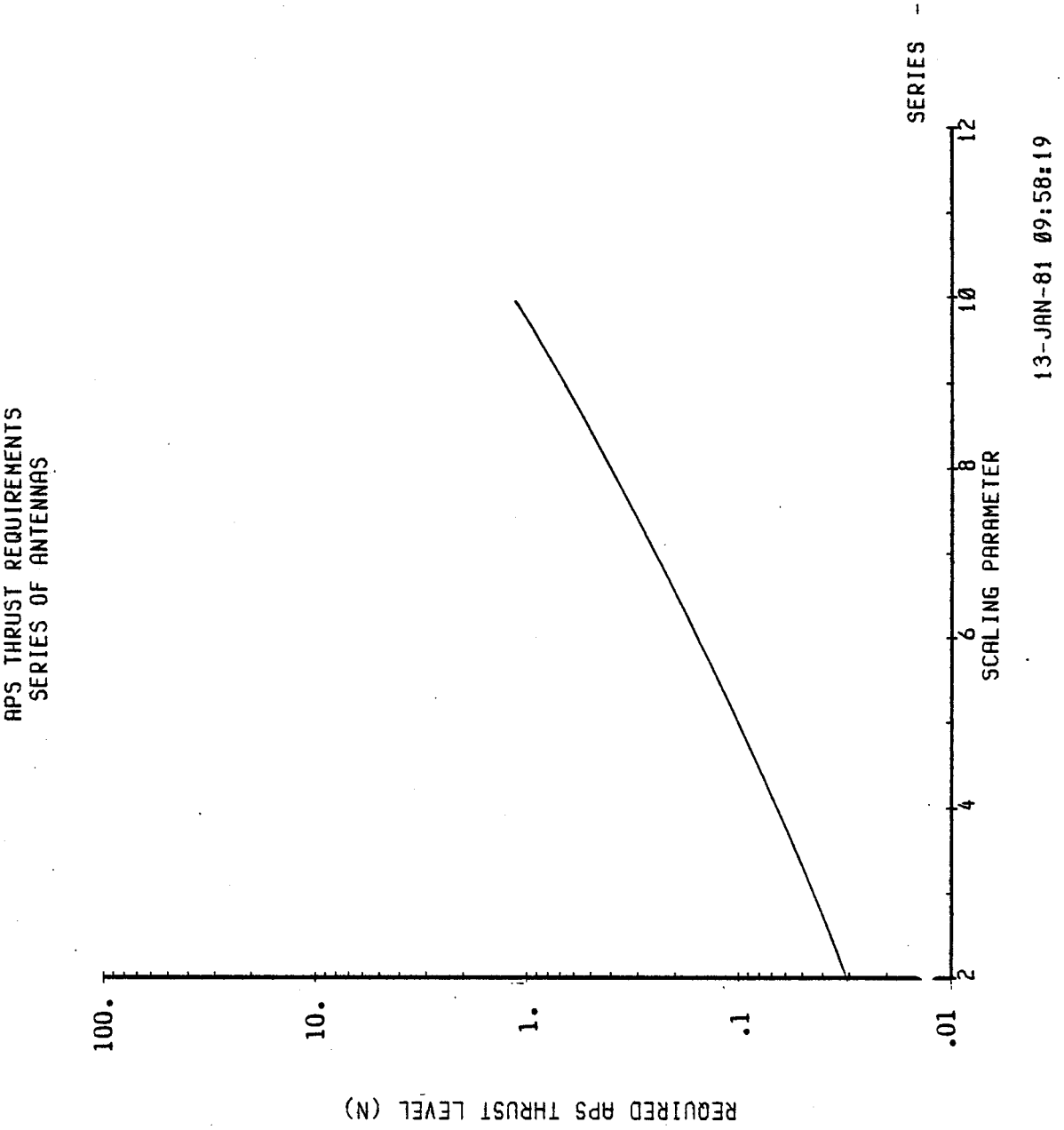

FIGURE 3-22 SERIES OF ANTENNAS APS THRUST REQUIREMENTS

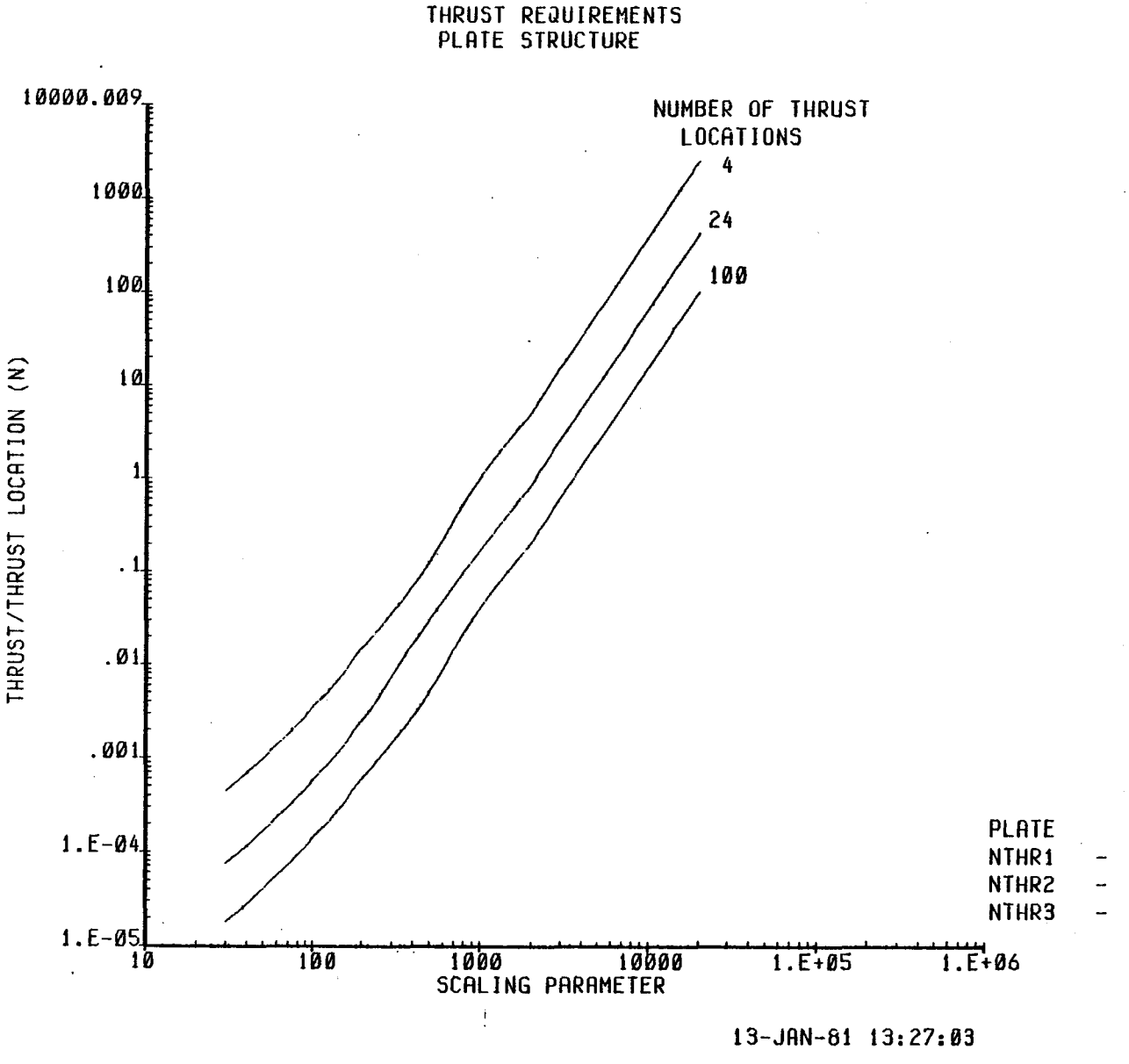

FIGURE 3-23 THRUST REQUIREMENTS PLATE STRUCTURE

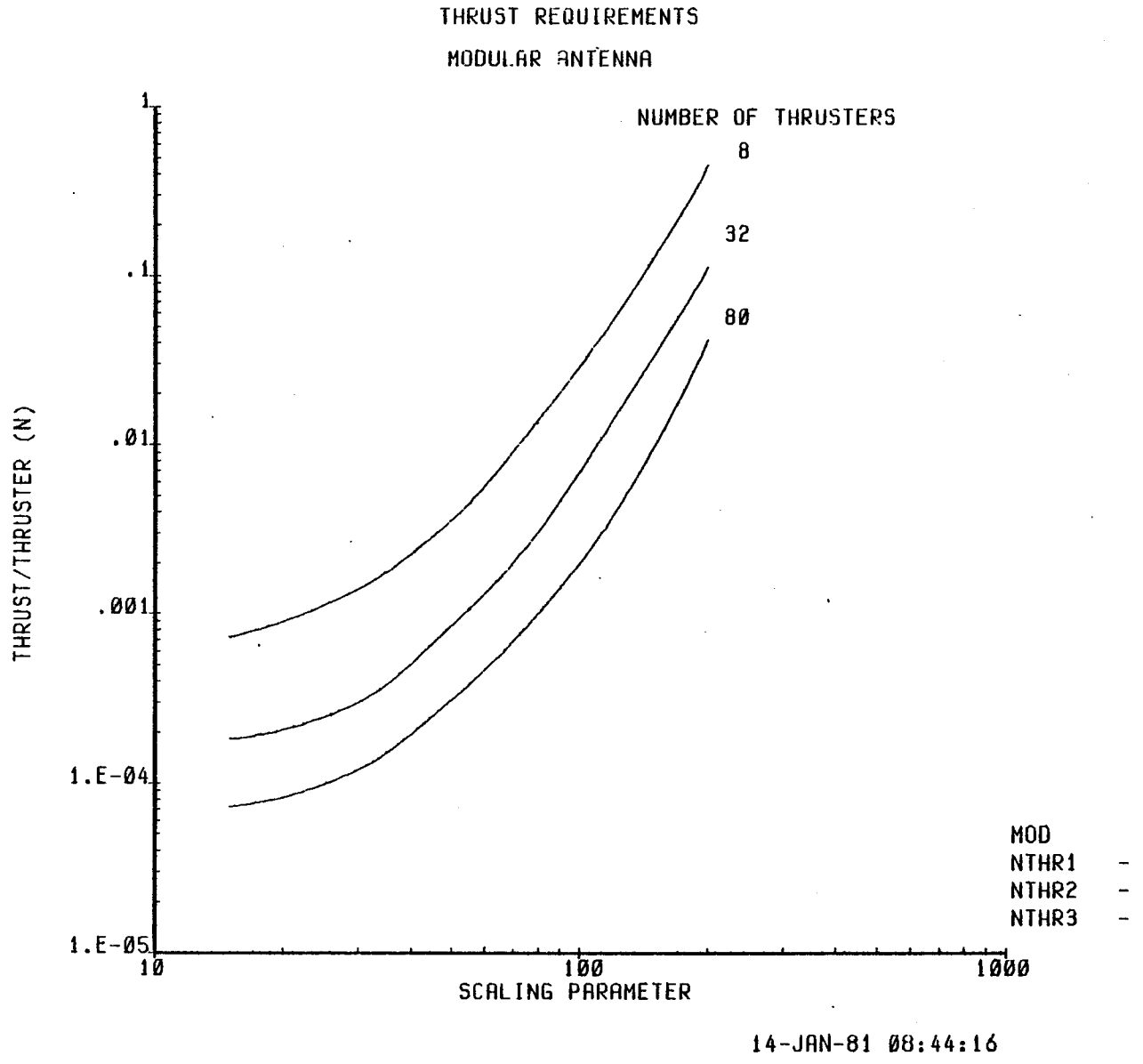

FIGURE 3-24 THRUST REQUIREMENTS MODULAR ANTENNA

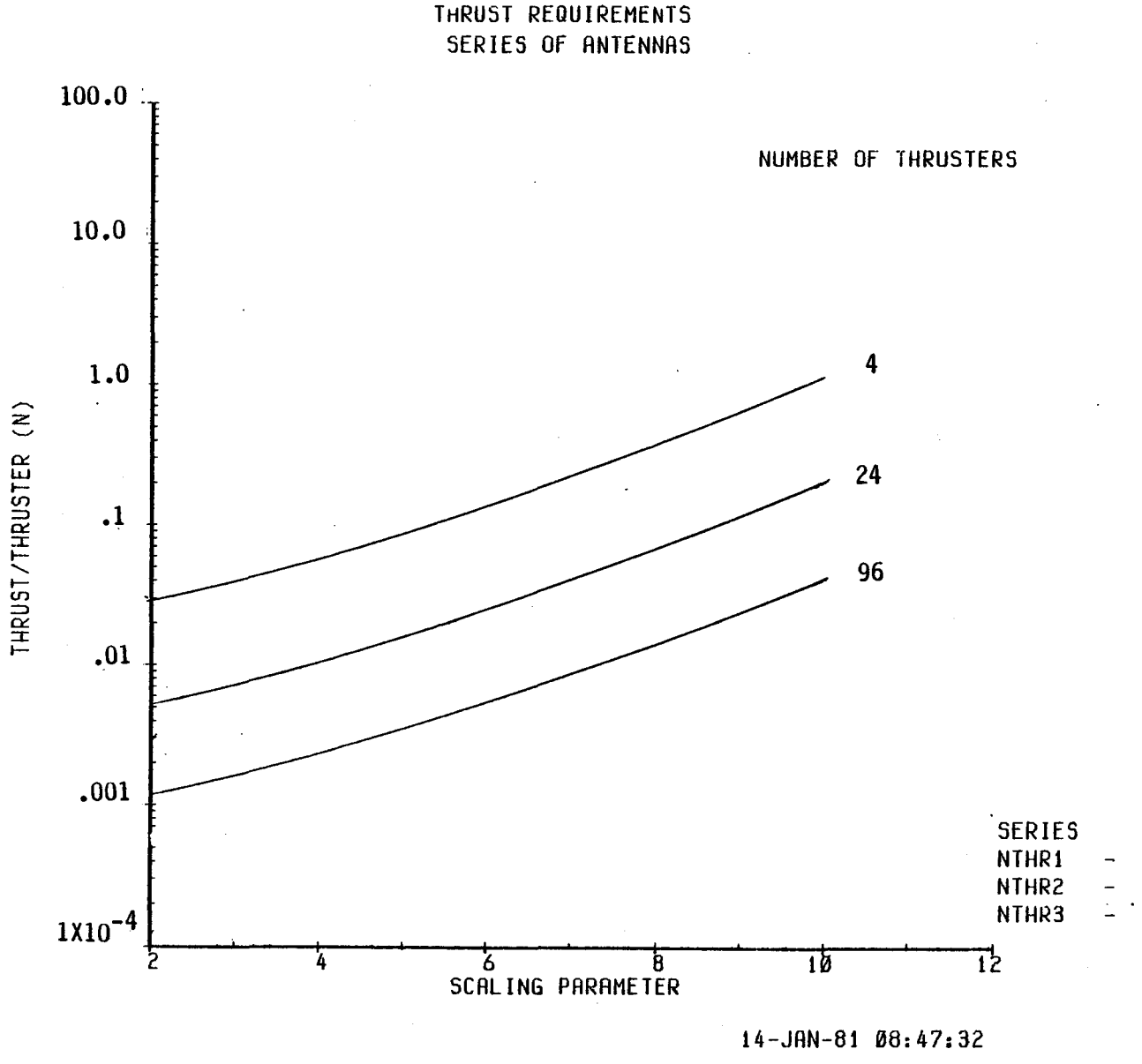

FIGURE 3-25 THRUST REQUIREMENTS SERIES OF ANTENNAS

change of the center of thrust as the number of thrusters is increased. It was assumed that this center of thrust was 1/4 of the major axis from the center which is true in an N + 1 distributed system with a large number of thrusters.

Until now the discussion of disturbance torques has been confined to geosynchronous orbit. If an APS were to be designed to counter the worst that low earth orbit could offer and yet still meet the geosynchronous requirements, a very large throttling ratio would be required. Throttling ratios can be achieved by having one throttlable thruster or a bank of thrusters that could have some members off and some on depending upon the need. Figure 3-26 shows the number of thrusters needed to get a given throttling ratio with each thruster having an individual throttling ratio of 4:1, 10:1 and 20:1. The actual throttling requirements for the three primary classes are shown in Figures 3-27, -28 and -29.

THIS PAGE INTENTIONALLY LEFT BLANK

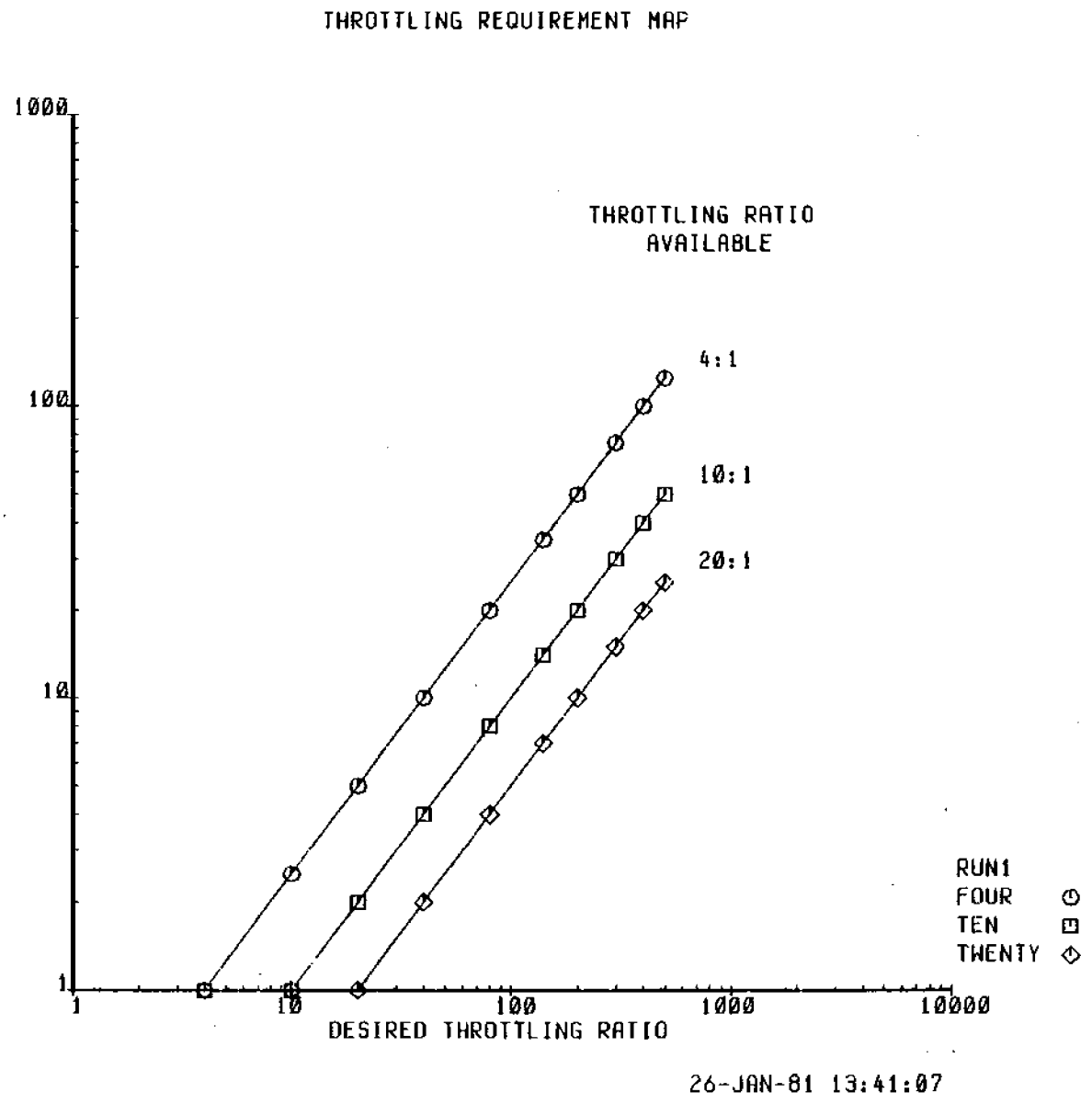

FIGURE 3-26 THROTTLING REQUIREMENT MAP

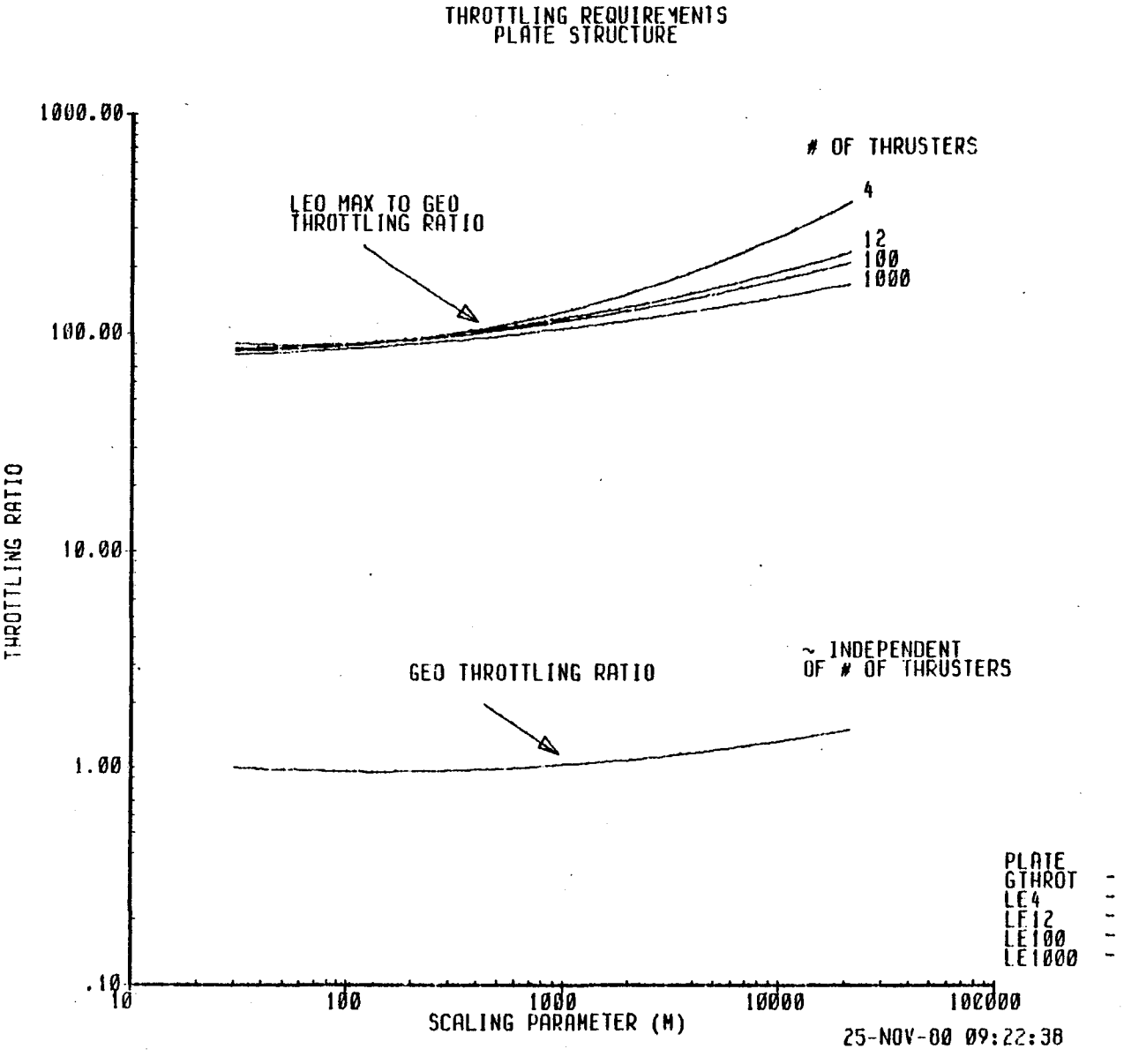

FIGURE 3-27 THROTTLING REQUIREMENTS PLATE STRUCTURE

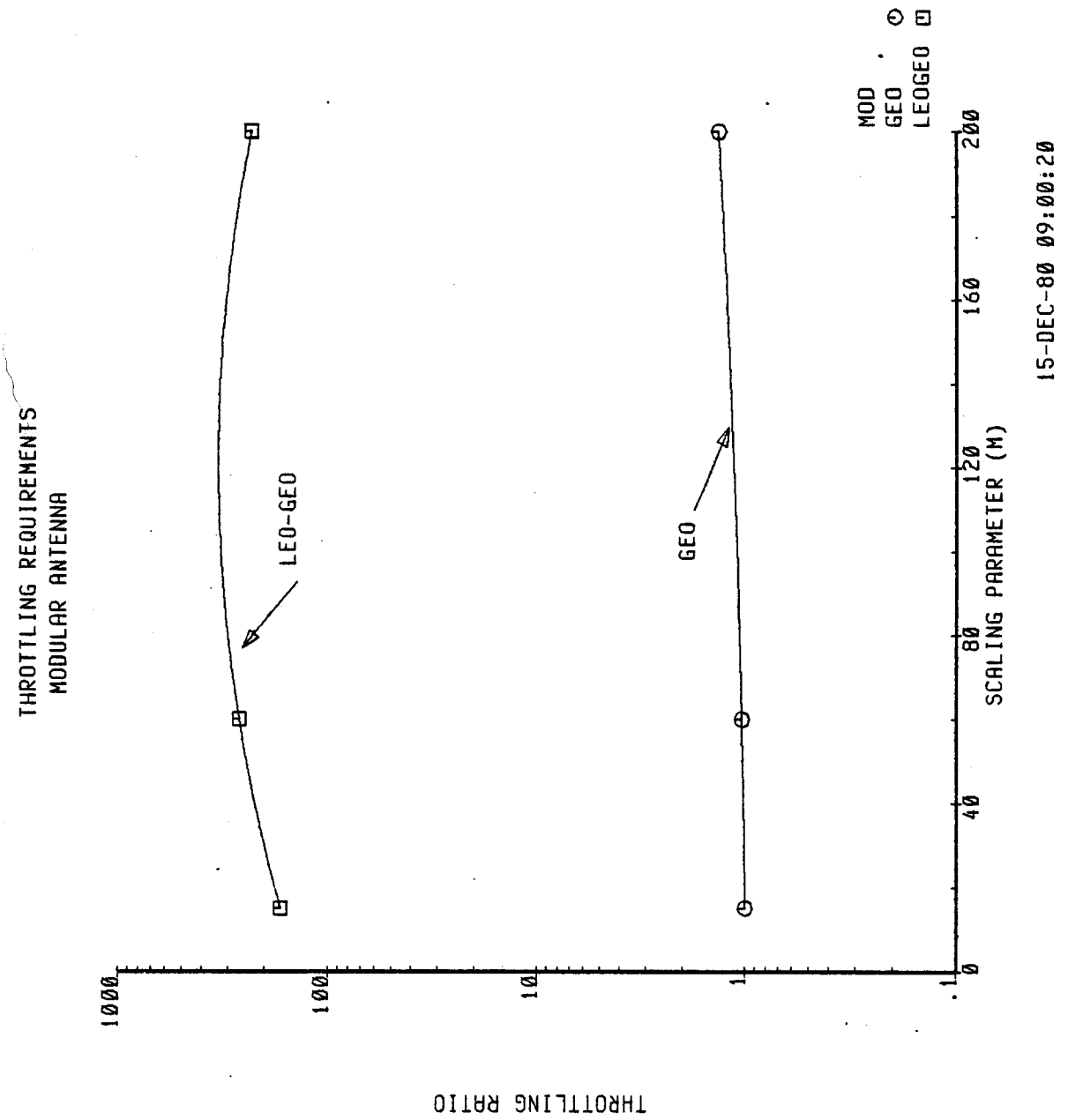

FIGURE 3-28 THROTTLING REQUIREMENTS MODULAR ANTENNA

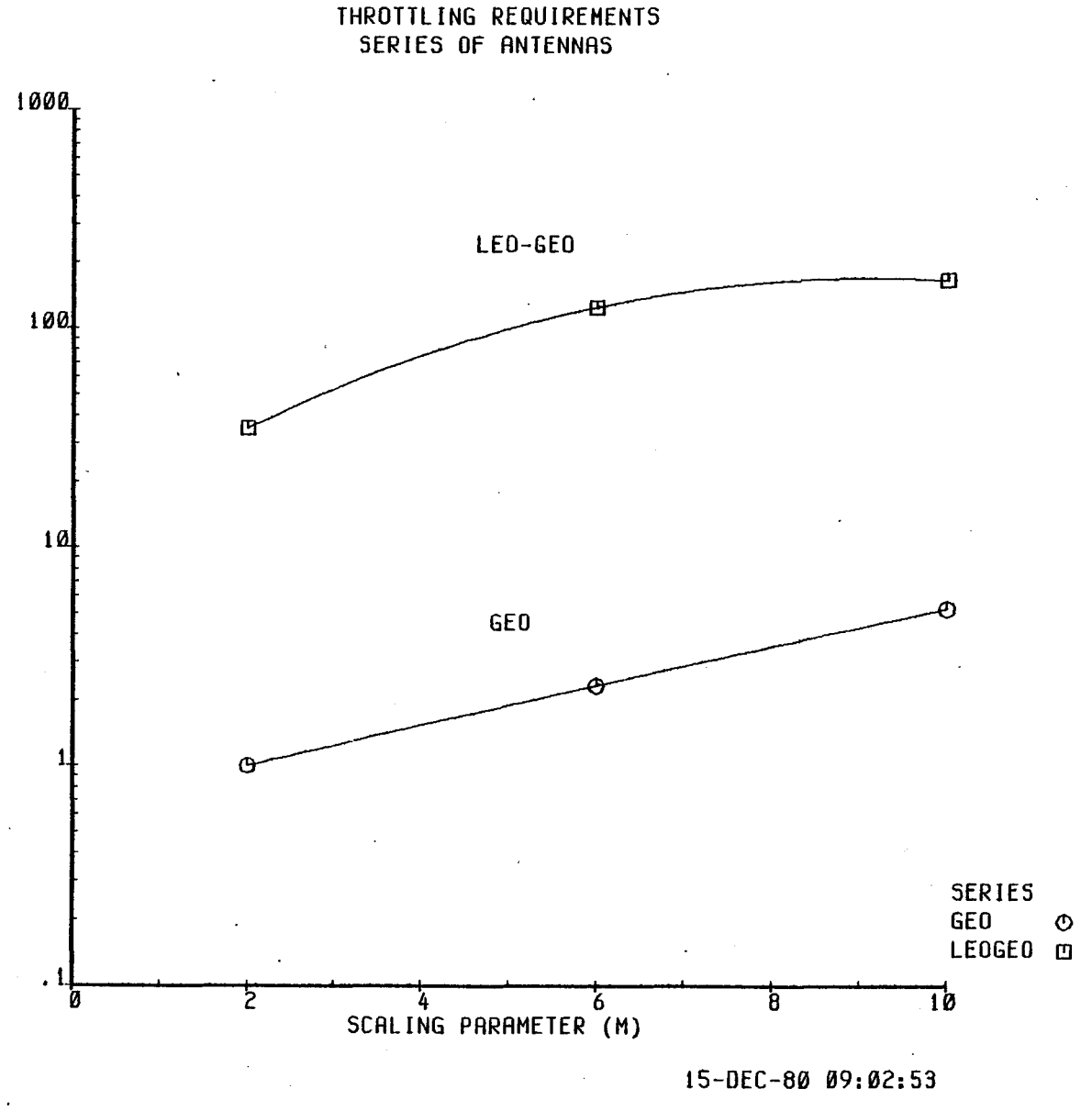

FIGURE 3-29 THROTTLING REQUIREMENTS SERIES OF ANTENNAS

3.2.2 Number and Distribution of Thrusters

An ideal auxiliary propulsion system would apply thrust throughout a spacecraft structure. These thrusts would cancel all disturbance effects and apply any necessary stationkeeping forces and maneuver torques. Such an ideal distributed system would be capable of perfect attitude, shape and stationkeeping control with no excitation of structural flexible modes. Such a system is obviously not feasible for many reasons - the difficulty of mounting, supplying and controlling a large number of thrusters, practical limits of thrust, power supply constraints, difficulties associated with deployable structures, etc. Very often a centralized auxiliary control system is used or proposed, located on a relatively rigid portion of the structure and avoiding locations on relatively flimsy and easily deformed components such as solar panel arrays and antennas. These facts have been tacitly assumed above in developing the maximum and minimum thrust levels required with the least number of thrusters.

However, the first three generic classes, IA, IIB, and IIA yield themselves to the concept of an ideal force distribution. On these structures, it is possible to determine separately the force distribution for each disturbance. For example, gravity gradient torques are ideally countered by equalling the force of gravity at each point on the structure. The forces that result are not equal or even linearly distributed. A maneuver torque, however, poses the least structural excitement if all forces are equal in magnitude and the force is equally distributed. These ideal distributions are to be integrated over small areas to characterize a given

thruster at a given location. Hence, it is necessary to find a force distribution over the entire surface, or in the case of the box structure (IIA) throughout the entire volume.

Generally, required forces are equally distributed throughout the structures, whereas torques will require non-equal and possibly varying direction forces. As an example, a solar pressure of 1 Newton can be ideally countered in a 100 m^2 plate by a force of 0.01 N/m^2 in the z direction throughout. However, a gravity gradient torque requires equal and opposite forces at each point depending on its attraction to the earth. Further, a maneuvering torque is ideally obtained by an equal force perpendicular to the radius from the axis about which you are to maneuver.

Torques require some further illumination. Gravity gradient torques are due to the unequal gravitational attraction of one part of the structure relative to the other. It is best illustrated by a plate seen edge on at a worst case angle of 45^o shown in Figure 3-30. The magnitude of the force at a distance x from the center is given by

$$dF(x) = GMdm\left(\frac{1}{r_o^2} - \frac{1}{(r_o - x/\sqrt{2})^2}\right)$$

This equation can be simplified by the following approximation:

$$\frac{1}{r_o^2} - \frac{1}{(r_o - x/\sqrt{2})^2} = \frac{r_o^2 - \sqrt{2}r_o x + x^2/2 - r_o^2}{r_o^2(r_o - x/\sqrt{2})^2}$$

$$= \frac{\sqrt{2}x}{r_o^3} \quad \text{assuming } r_o \sim r_o - \frac{x}{\sqrt{2}}$$

Therefore $$dF(x) \sim \pm \frac{GMdm\sqrt{2}x}{r_o^3}$$

The worst case orientation for gravity gradient torques about the x axis on the plate is shown in Figure 3-30 and the force is a function of y. The force is broken into F_z and F_y components to enter into the ideal distribution. Likewise, the worst case torques around the y and z axis are broken into F_x, F_z and F_x, F_y components respectively.

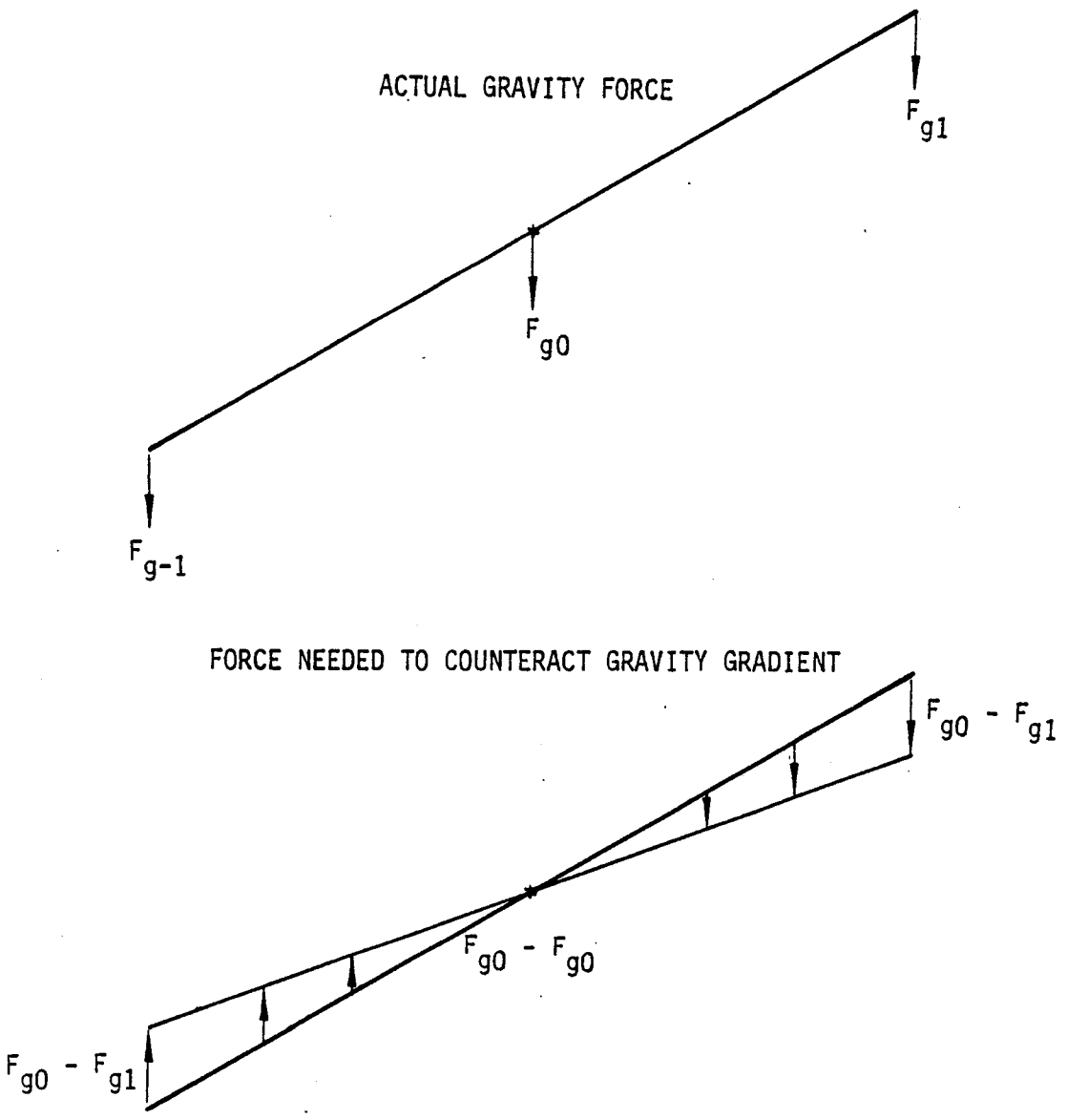

FIGURE 3-30 GRAVITY GRADIENT EQUALIZATION

In the box structure, x can be assumed measured from the center plane. For example, if the y and z axes are at 45^0 with respect to an earth center of mass line, x would be measured from the xz plane at the center. While this is an inexact formulation, it is sufficient for our purposes. The direction of these forces is at an angle of 45^0 to the y and z axis and therefore yields force contributions in both the y and z axis of equal magnitude and a factor of $\sqrt{2}/2$ times the absolute force magnitude.

Maneuvering torques about the y axis for the transfer trajectory are more complicated. Ideally, what is wanted is a force equally distributed throughout the structure which is perpendicular to a radial line drawn from the y axis. Once this force F is measured, the magnitude of the force vector in F_x and F_z can be calculated by measuring an angle θ from the x axis as follows:

$$F_x = |F_{CALC} \sin\theta|$$
$$F_y = |F_{CALC} \cos\theta|$$

To obtain $F_{calculated}$, the following equation must be solved:

$$T = 4\int_0^{w/2}\int_0^{\ell/2} F\sqrt{x^2+y^2}\,dx\,dy$$

for the plate and cross with w = width and l = length, and

$$T = 8\int_0^{\ell/2}\int_0^{w/2}\int_0^{h/2} F\sqrt{x^2+y^2}\,dx\,dy\,dz$$

for the box.

The solution to this equation is shown below for the plate and cross structure:

$$T = 2\left\{\frac{a}{2}\left[bK + a^2\ln(b+K) - a^2\ln a\right]\right.$$
$$+ \frac{b^3}{3}\ln\left(a+K - \frac{2}{3}\left(\frac{\sqrt{K+a}}{6}\sqrt{(K-a)^5}\right.\right.$$
$$+ \frac{3a\sqrt{K+a}}{24}\sqrt{(K-a)^3} - \frac{4b^2\sqrt{K+a}}{16}\sqrt{(K-a)}$$
$$\left.\left. + \frac{a^3}{2}\left[\ln\left(\sqrt{K+a} + \sqrt{K-a} - \ln(\sqrt{2}a)\right]\right)\right.\right.$$
$$\left. + \frac{b^3}{3}\ln b - \frac{b^3}{a}\right\}$$

where $K = \sqrt{a^2+b^2}$

where a = l/2 and b = w/2

For the box, it is necessary to multiply by 4w with a = l/2 and b = h/2.

The other forces; stationkeeping, aerodynamic, and radiation are added to the F_x, F_y or F_z components obtained from the torque analysis.

To summarize, the equally distributed forces necessary from solar pressure, aerodynamic pressure, and stationkeeping requirements are summed with the unequally distributed forces necessary to perform maneuvers and balance gravity gradient torques to identify the magnitude of force required over a given structure.

Figures 3-31 through 3-36 show the force/unit area for the plate and cross structures in the x, y and z directions. Figures 3-37 to 3-39 show the corresponding forces per unit volume for the box structure. For purposes of display, the force for gravity gradient was figured half way out on each object and the transfer force requirement was added at a worst case angle for each axis contribution.

3.3 Analysis of Auxiliary Propulsion System Characteristics Sensitivities

For each of the seven generic classes, there are three distinct control tasks to be performed; attitude control, shape control and stationkeeping. Each of these tasks may influence or be influenced by the five identified auxiliary propulsion characteristics. To determine the sensitivities each control function is examined in turn against the five auxiliary propulsion system characteristics.

First, it should be remembered that attitude control covers three basic functions; the cancellation of disturbance effects, maintaining pointing to the desired degree of accuracy and maneuvering. The relative importance of each function will vary from mission to mission and may also change significantly during the course of a mission. Consider, for example, a

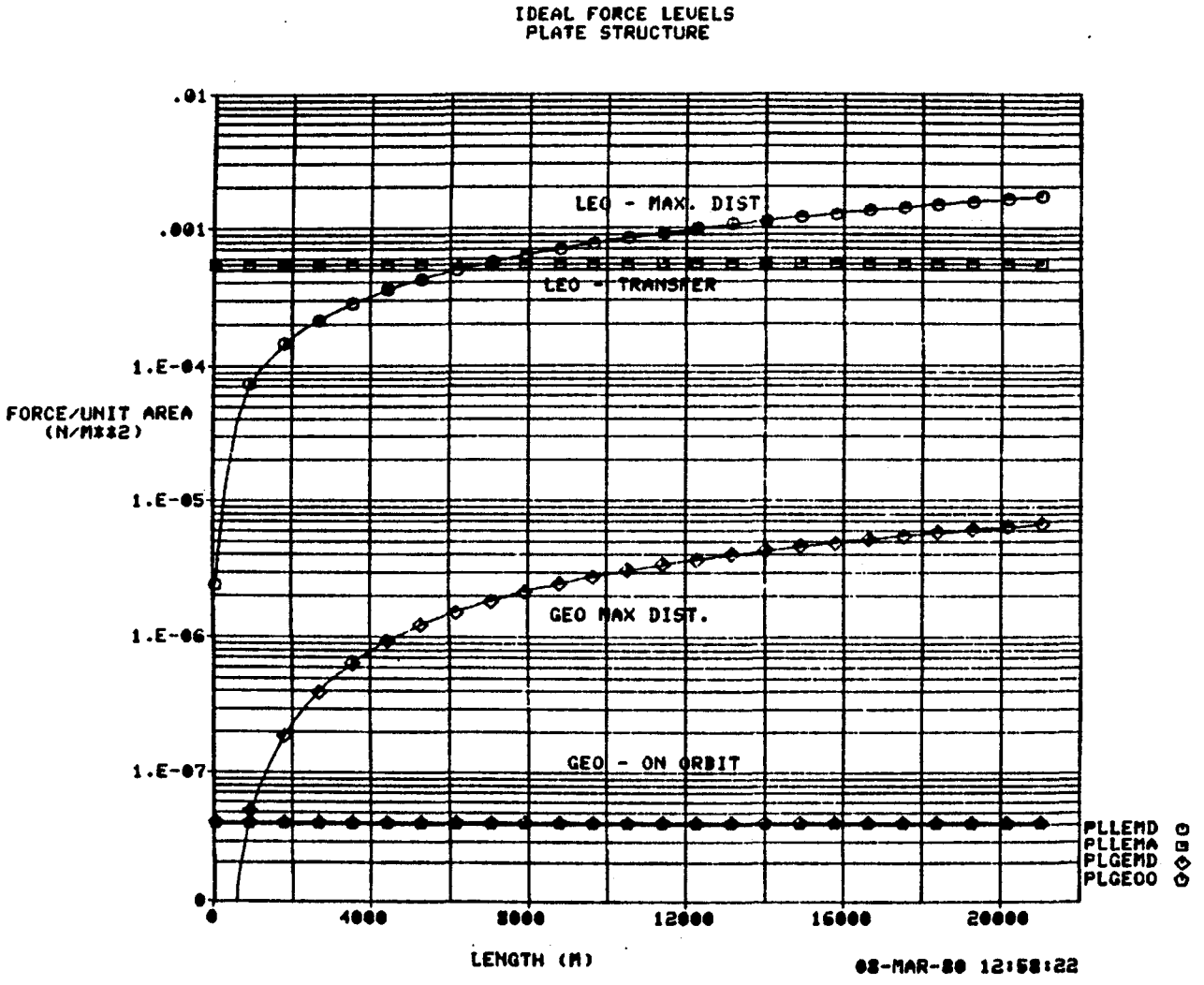

FIGURE 3-31 IDEAL FORCE LEVELS PLATE STRUCTURE - F_x

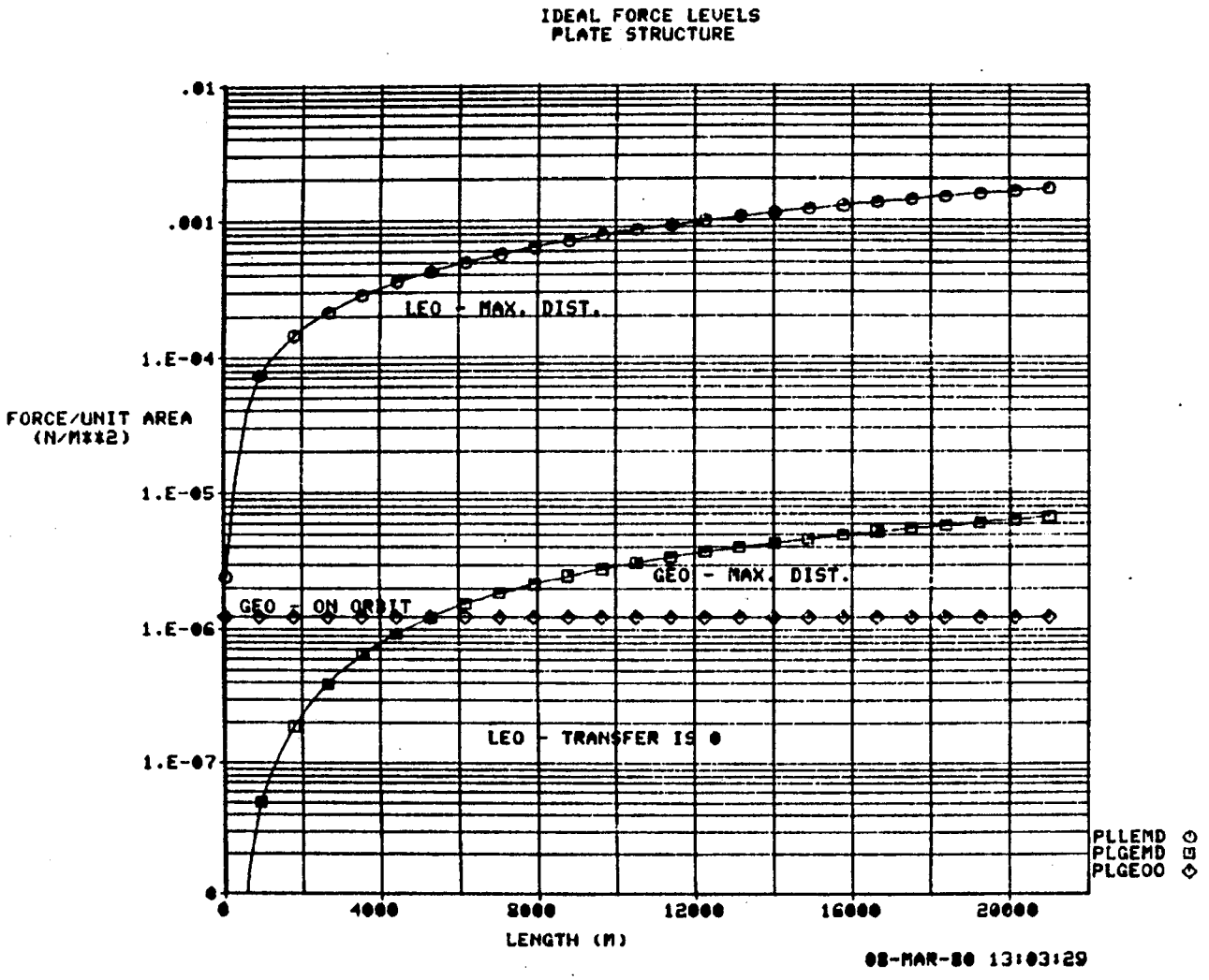

FIGURE 3-32 IDEAL FORCE LEVELS PLATE STRUCTURE - F_y

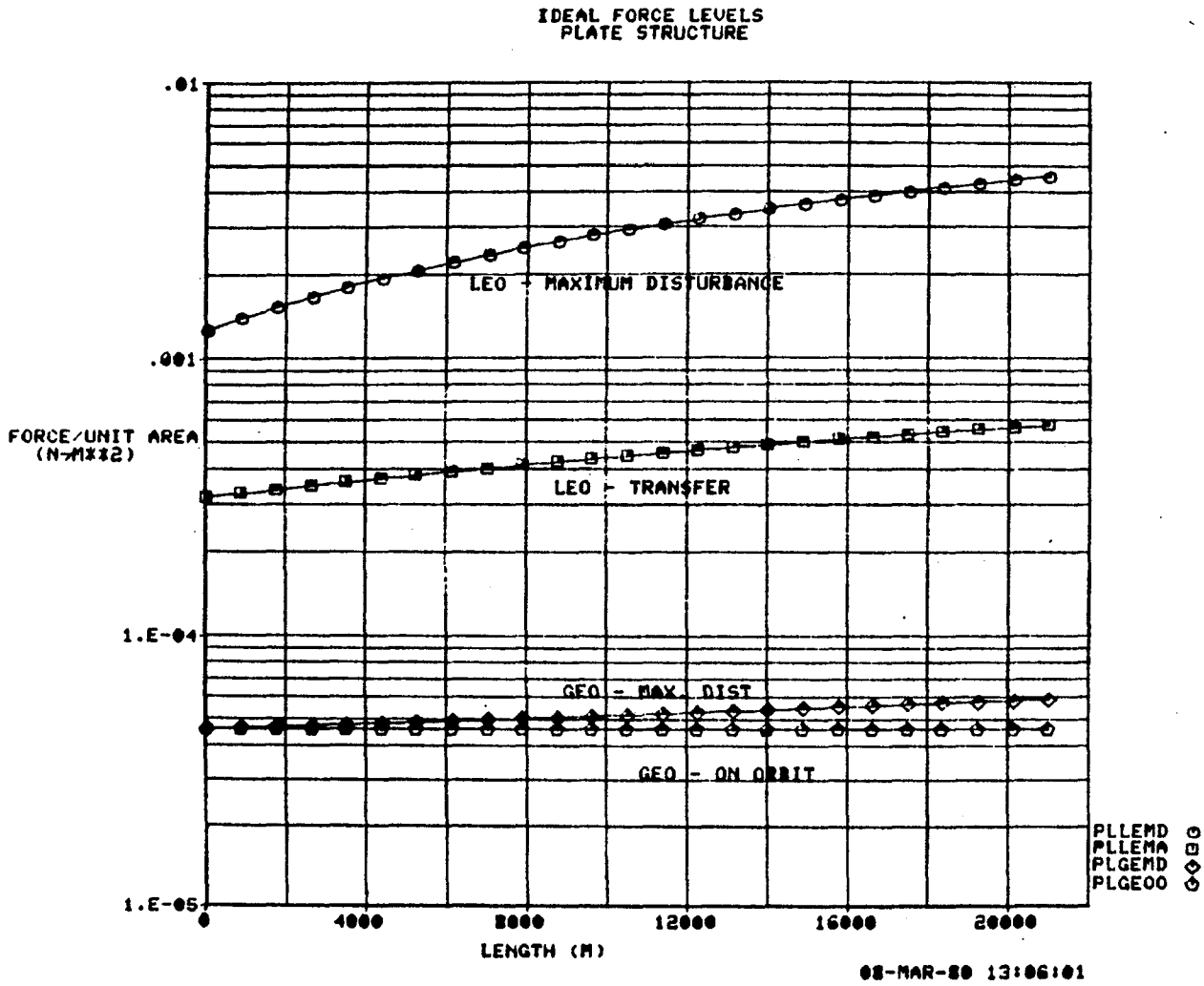

FIGURE 3-33 IDEAL FORCE LEVELS PLATE STRUCTURE - F_z

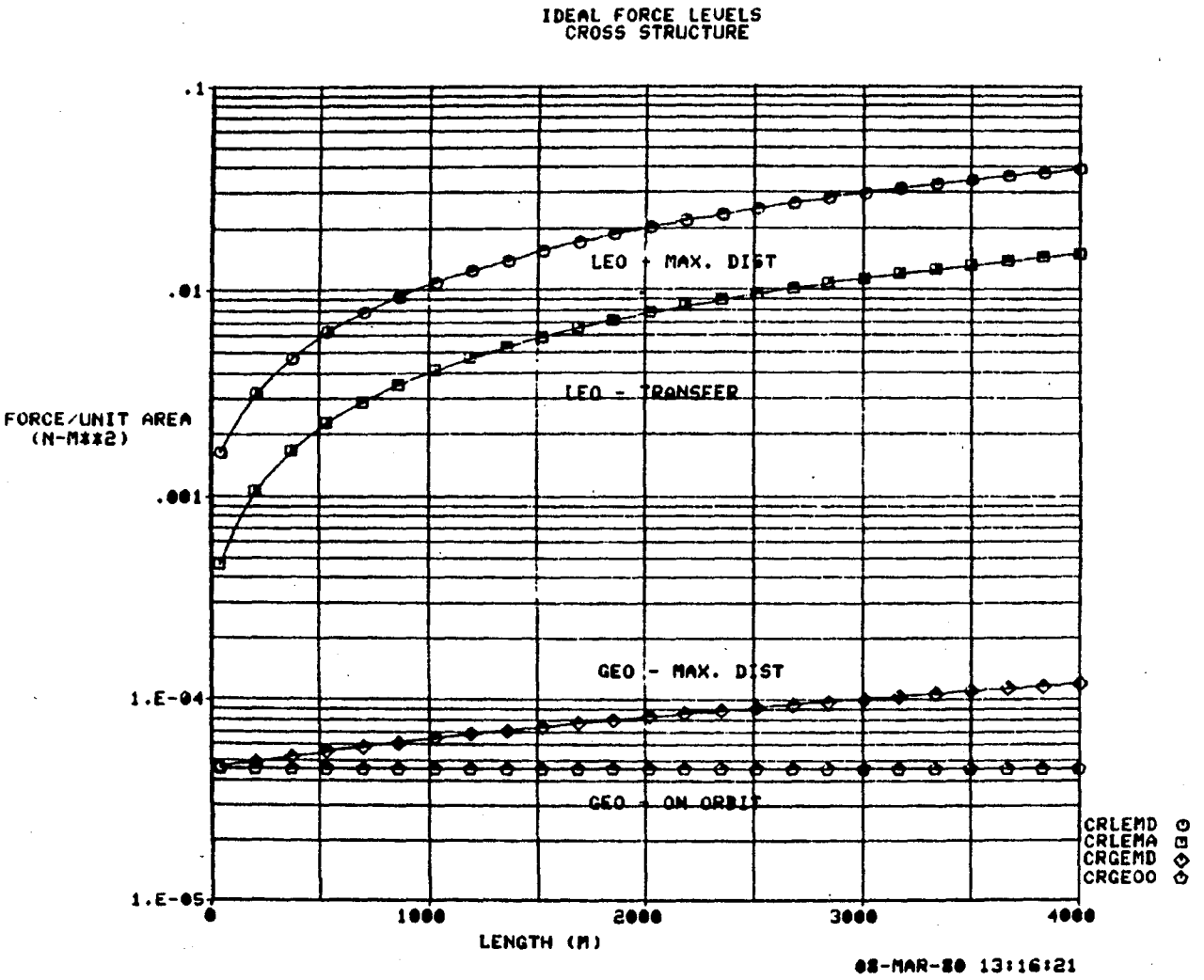

FIGURE 3-34 IDEAL FORCE LEVELS CROSS STRUCTURE - F_x

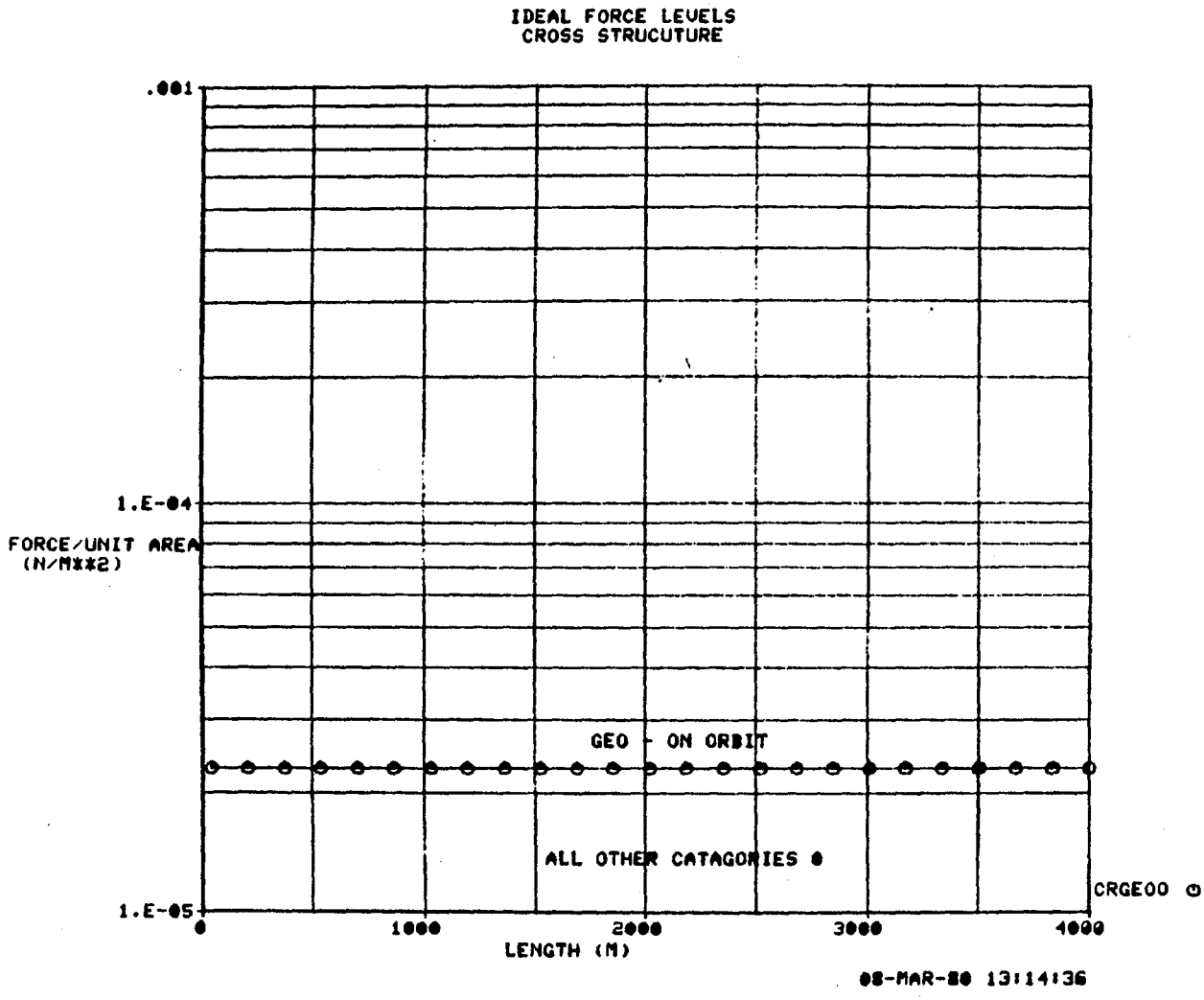

FIGURE 3-35 IDEAL FORCE LEVELS CROSS STRUCTURE - F_y

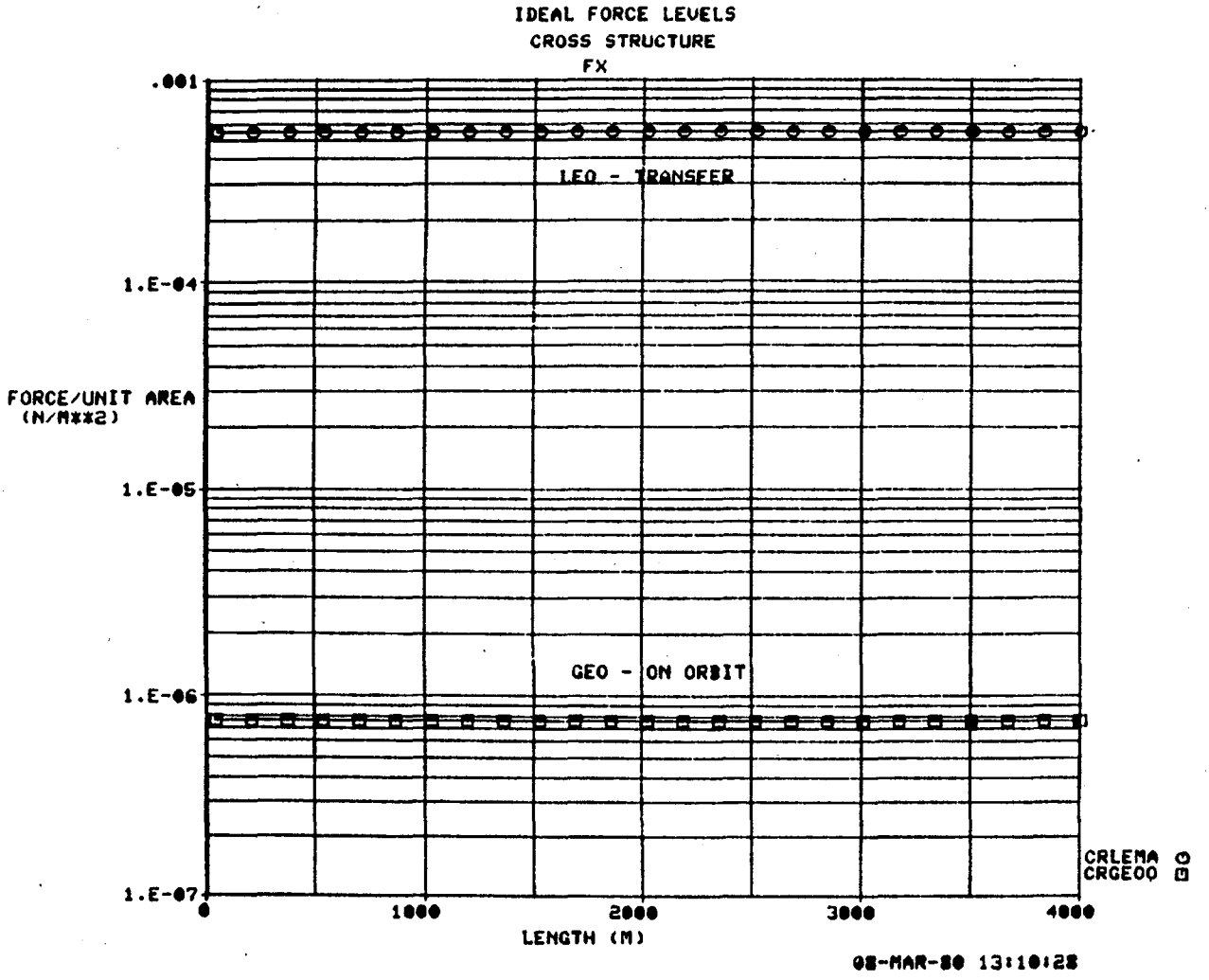

FIGURE 3-36 IDEAL FORCE LEVELS CROSS STRUCTURE - F_z

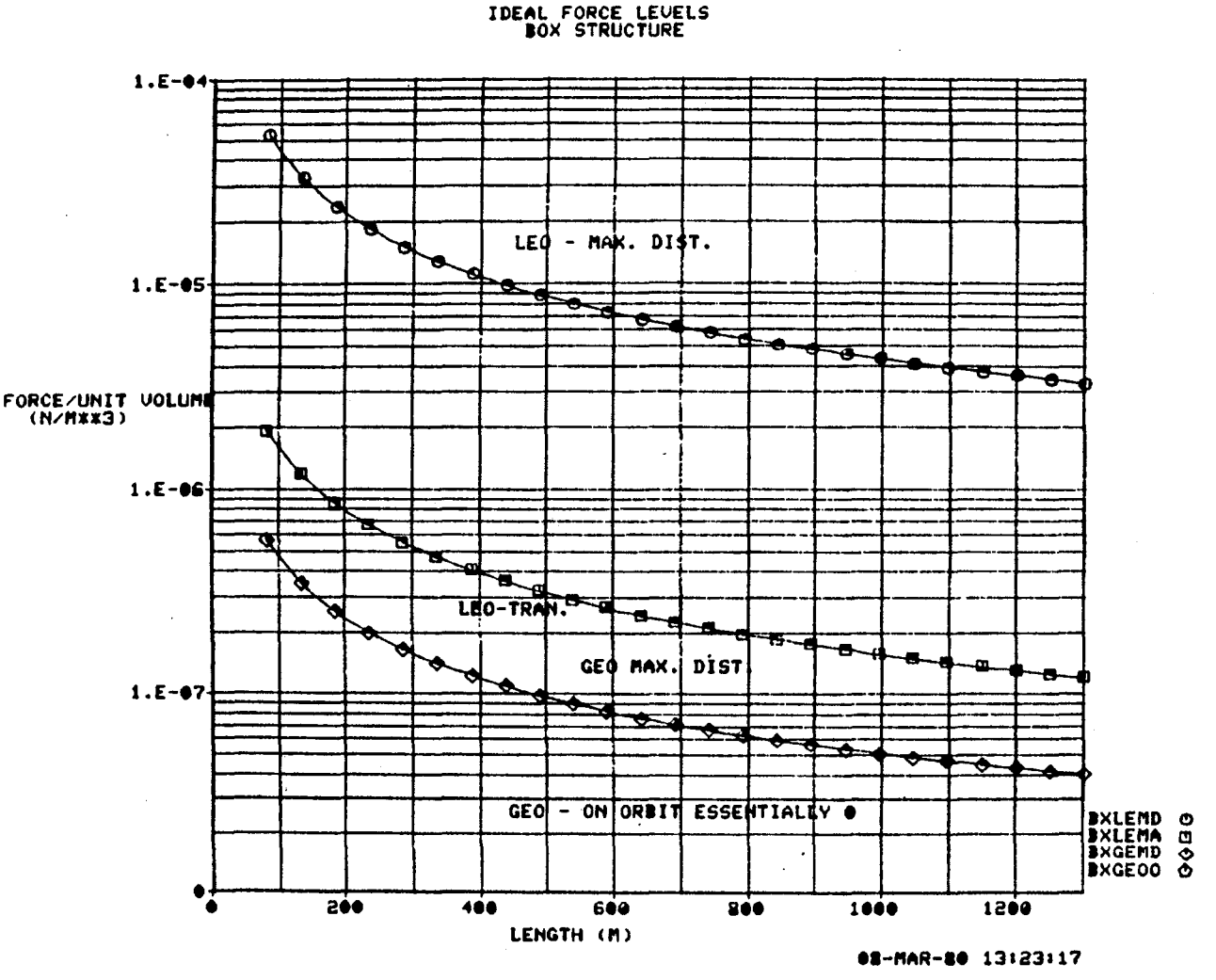

FIGURE 3-37 IDEAL FORCE LEVELS BOX STRUCTURE - F_x

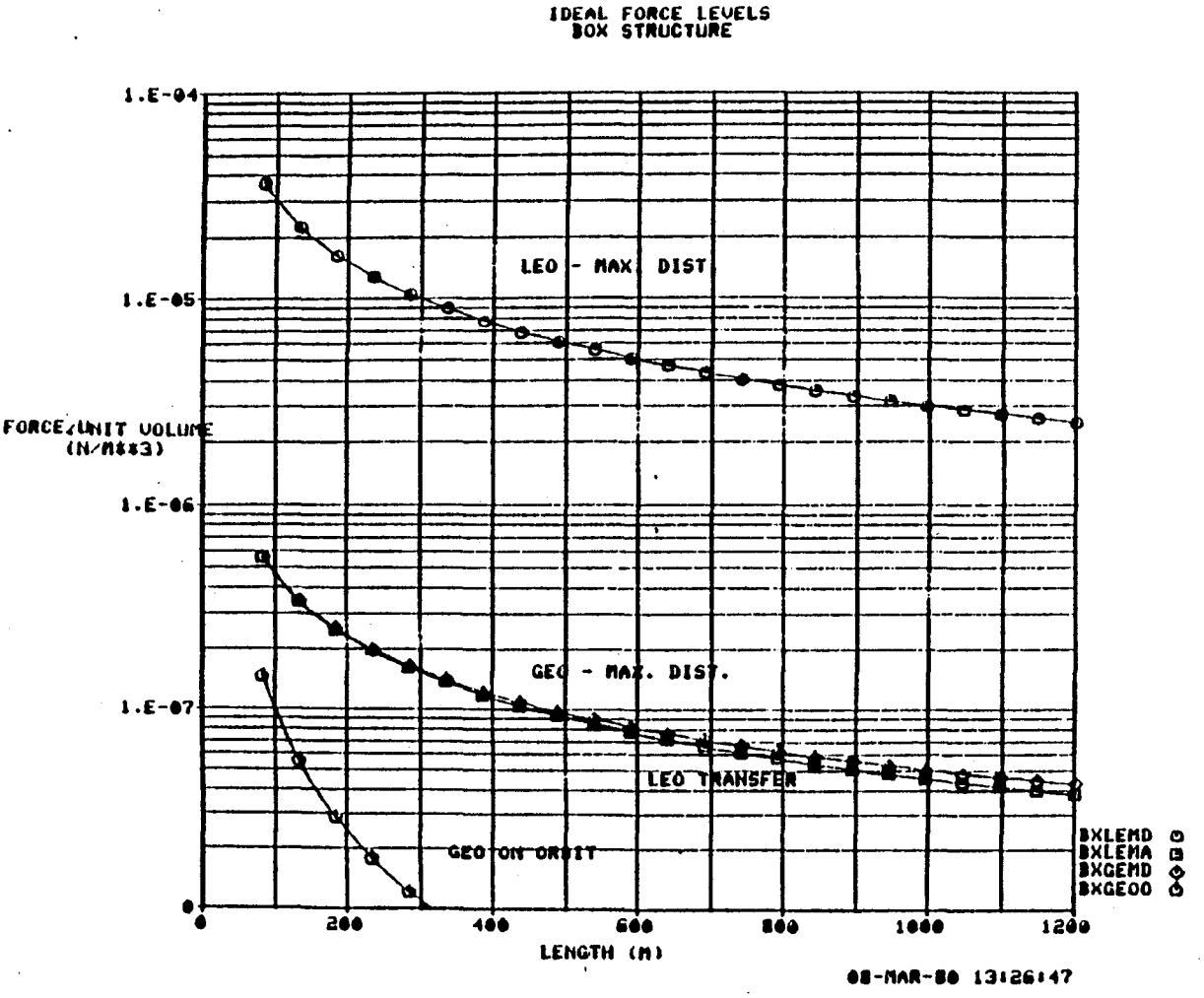

FIGURE 3-38 IDEAL FORCE LEVELS BOX STRUCTURE - F_y

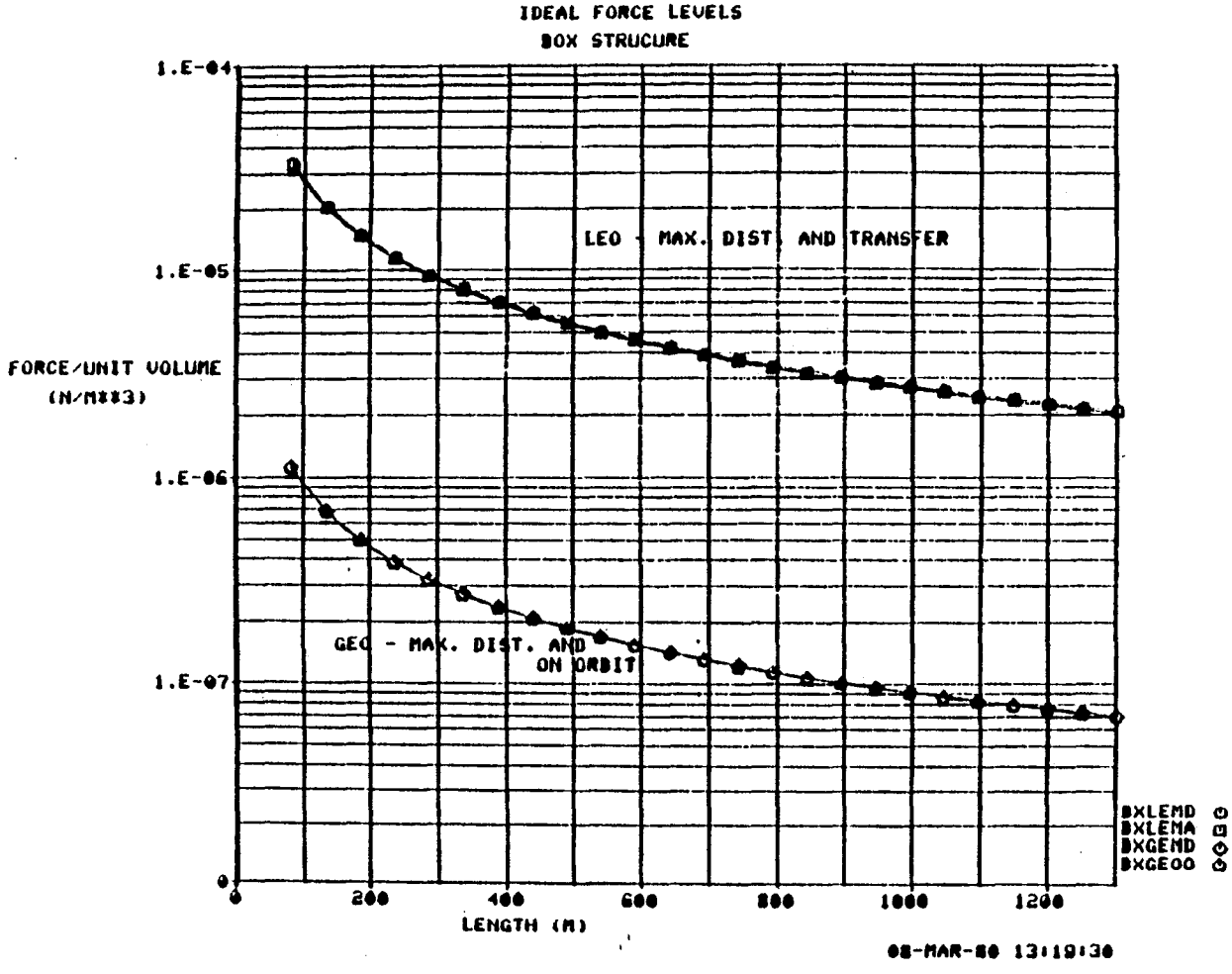

FIGURE 3-39 IDEAL FORCE LEVELS BOX STRUCTURE - F_z

large spacecraft built in low earth orbit then transferred to geosynchronous orbit to carry out its normal operations. During construction only rough pointing may be necessary and maneuver requirements will probably be minimal but disturbances must be countered and these may change considerably as construction proceeds. During transfer all three functions are needed; cancellation of disturbances, including perhaps torques introduced by misaligned prime propulsion units, pointing to achieve thrust vector control and maneuver if orbit plane changes are required. On orbit pointing will normally be an important function and disturbances must be opposed, including those introduced during periods of stationkeeping. Maneuvering demands may be zero.

Sensitivities then will be identified by looking at the five control functions (disturbance cancellation, pointing, maneuver, shape control and stationkeeping) in terms of the five auxiliary porpulsion system characteristics (number and distribution of thrusters, thrust levels, rise and decay characteristics, modulation and allowable mass).

It will be assumed that the spacecraft, including the auxiliary propulsion system, however configured, have been designed in a reasonably optimum fashion. For example, a required pointing accuracy can be achieved satisfactorily by systems with a wide range of numbers and distributions of thrusters. If properly designed, the effect of number and distribution on pointing accuracy is small. A poorly conceived system could however have too few thrusters of too large thrust and lead to inadequate pointing control of a flexible appendage.

A matrix of sensitivities is shown in Figure 3-40. The entries in the table are discussed below.

Thrust Level

Thrust level is a basic APS characteristic which influences or is influenced by all control functions and most LSS characteristics. Given a spacecraft configuration and mission requirements, the disturbance environment can be calculated and the pointing, maneuver, shape control, stationkeeping and desaturation requirements can be specified. Stationkeeping, shape control and disturbance force cancellation will

CONTROL FUNCTIONS AND LSS CHARACTERISTICS	APS CHARACTERISTICS				
	THRUST LEVEL	MODULATION	RISE AND DELAY TRANSIENTS	NUMBER AND DISTRIBUTION OF THRUSTERS	ALLOWABLE MASS
DISTURBANCE CANCELLATION	X	X		X	X
POINTING	X	X	X		
MANEUVER	X	X			
SHAPE CONTROL	X	X	X	X	X
STATIONKEEPING	X	X			X
DESATURATION	X	X			X
LSS SIZE	X	X	X	X	X
LSS MASS	X	X			X
LSS LIFETIME	X	X			
LSS STIFFNESS	X	X		X	
LSS STRENGTH	X				
THERMAL EXPANSION					

FIGURE 3-40 APS/LSS INTERACTIONS

establish bounds on the required thrust levels. Pointing, maneuver, disturbance torques and desaturation will define torque limits which are related directly to thrust level by the appropriate moment arms. Obviously thrust levels must be no lower than needed to overcome disturbance forces and torques. Upper bounds are more flexible because the necessary impulse can be generated, at least in principle, by large thrusts applied for a short time or lower thrusts applied for longer times. Practically, upper bounds may be set by a number of considerations. These include: minimum impulse bit requirements needed to meet pointing accuracies; limits imposed by shape control requirements; momentum exchange device control authority during desaturation and stationkeeping; excitation of flexible modes and stiffness and strength limitations. In short, thrust level impacts all control and LSS characteristics with the possible exception of thermal expansion.

Modulation

Just as widespread as thrust level in its interaction with control functions and LSS characteristics is modulation. Upper and lower thrust bounds can be found for any application but most of the time the thrust required will be between the bounds. For stationkeeping, desaturation and maneuver (except for tracking tasks) it may be possible to use maximum thrust for the necessary length of time to achieve the desired impulse. For disturbance cancellation, pointing and shape control, however, much more precise thrust levels are needed. Thus some form of modulation is essential for these control functions.

Two basic forms of modulation are amplitude and on-off. Amplitude modulation is the ideal but it will often be difficult to find an APS that has the necessary range. If clusters of thrusters can be used, the range will be considerably extended but there usually are nevertheless practical limitations on the range that can be achieved. As seen in the thrust level required curves (Appendix D) the range can be several orders of magnitude if the same APS is used for all phases of flight from LEO to GEO. On-off or pulse modulation achieves a desired mean thrust level by varying the time the thrust is applied and the time between pulses. In general, the effective thrust is

where DC is the duty cycle, or ratio of thrust on time to total time. The same duty cycle can be achieved with frequent short pulses or less frequent longer ones. The frequency may have to be quite closely constrained in practice to avoid exciting flexible modes, and for shape control, to match the structural frequency being damped.

On-off control has been used for many years to control relatively small spacecraft with chemical APS. The method is necessary because small chemical thrusters typically cannot be throttled. The method is quite successful if care is taken in design. A characteristic of on-off systems used for pointing is limit cycle operation in which the vehicle oscillates across a small deadband centered on the desired pointing position.

Rise and Decay Transients

Because of warm-up times, valve opening and closing times, fuel line capacitance and various other causes, APS thrusts typically do not start and stop when commanded to do so. The dealys are typically small, in the tenths or hundredths of a second range, for chemical APS but may be appreciable, up to half an hour, for electrical APS. In some applications, the delays can be compensated for by sending the start or stop signal appropriately early. This may be true, for example, during limit cycle operation if the accuracy requirements do not impose a very small deadband. For stationkeeping, desaturation, most maneuvers and disturbance cancellation tasks, the time delays are unimportant. None of the LSS characteristics interact significantly with transient effects except LSS size. During limit cycle operation, the larger vehicles are much more tolerant of time delays than smaller ones.

The most significant interaction of transients with control function occurs in shape control. In order to damp oscillations effectively, the APS thrust should be sinusoidal and accurately phased. Pulsed operation can also be used provided the pulses are precisely timed. Any lag in the continuous system or time delays in the pulsed system will degrade performance and may lead to instability.

Number and Distribution of Thrusters

It may often be necessary or convenient to replace a single thruster at a particular location by a cluster of units. This may be required, for example, when the maximum thrust needed is not available from a single thruster. Or where the range of thrust required is best achieved by multiple units. In these cases, the thrust/thruster will obviously be less than the total thrust level and will depend on the number of thrusters. Since this is the case, the number of thrusters, in a sense, interacts with all the control functions and LSS characteristics that thrust level interacts with. This, however, is a secondary effect. Primary interactions occur with the disturbance cancellation and, particularly, shape control functions. The LSS characteristic most affected is stiffness because of the close relation between shape control and stiffness.

Allowable Mass

APS mass will clearly affect total system mass. In fact the mass associated with the APS, which includes power processors and power generating weight penalty for electric systems and propellant and tankage for chemical systems, generally accounts for a large fraction of the total system mass.

A second effect is on shape control. The manner in which the APS mass is distributed will determine control accuracy and this again will depend on whether the thrusts are translational, for stationkeeping, or rotational, for disturbance torque cancellation or desaturation.

3.4 Single Shuttle Launch Impact on Auxiliary Propulsion System Characteristics

Utilizing the three generic deployable LSS, developed in Section 1.3 which can be launched with a single shuttle flight, a detailed thrust requirements study was performed. We considered in this study a 300 km, a 400 km, and a 500 km low earth orbit altitude as well as the geosynchronous orbit altitude. We also examined the effect of a range of LSS orientation angles on disturbance torque levels and thrust requirements.

To determine the thrust levels required, a set of groundrules was developed regarding disturbance torque calculation and thruster placement. These

assumptions are listed in Table 3-4. The first three assumptions deal with the calculation of disturbance torques and the last six concern thruster placement.

A center of pressure-center of gravity moment arm of 5 percent of the maximum dimension was decided to be representative of the designs considered. This moment arm is difficult to estimate accurately given the ideal nature of the generic classes. Actual distribution of system components on a given structure would determine the exact CG location. The 5 percent number was arrived at considering several large spacecraft proposed or currently flying. An estimate of the transmissivity of the truss work and antenna mesh was drawn from work done on solar array blockage factors on the SPS program.

The third assumption is actually an assumed operational philosophy. According to our structure orientation conventions, aerodynamic forces result from a vehicle being in a non-operational or disturbed orientation. It is assumed that one would reorientate the LSS as quickly as possible to a nominal orientation. To do this, only the aerodynamic torques would be countered and stationkeeping to maintain orbit position over long periods of time would be unnecessary.

The requirement for dual redundancy is necessary for the long mission life demanded of LSS. A ten year mission lifetime will stretch the limits of both electric and chemical system lifetime. Dual redundant systems are necessary to insure high mission reliability. Fixed orientation chemical thrusters are generally used on spacecraft because the added cost and weight of a gimballing mechanism is greater than simply adding more chemical thrusters. For electric thrusters, gimballing is appropriate because of the large cost and mass of a thruster unit. Gimballing helps to minimize thruster number, although there is some loss of control due to cosine losses for a limited freedom gimbal. A gimbal freedom of ± 45 degrees is assumed. This large freedom will minimize cosine losses and is physically realizable using current mechanism technology.

It is important to minimize the number of thrusters from a cost and mass standpoint. The goal of minimizing thruster number is tempered by the

criterion of redundancy and zero ΔV addition during maneuvering. A pair of opposing thrusters must be used which fire in opposing directions on opposite sides of the axis of rotation. Zero ΔV addition is necessry to achieve the tight stationkeeping requirements needed for many LSS. Finally, to minimize thrust requirements and APS mass, maximum moment arms for thrusters around large inertia axis are necessary.

The disturbance torques are presented as a function of LSS angle. This angle is defined in Figure 3-41. A zero degree orientation is the nominal orientation with antenna or platform surfaces facing the earth. A 45 degree orientation gives a maximum gravity gradient torque and a 90 degree orientation gives the maximum effective area for aerodynamic pressure.

Appendix D contains the disturbance torque requirements for each generic class. There are two sets of graphs included in the attachment. The first set (Figures D-27 through D-37) shows the torque composite breakdown for aerodynamic, solar, and gravity gradient disturbances at 300 and 500 km altitudes. Again, each graph in this set has an assumed CP-CG offset of five percent of the maximum dimension. Each graph in the first set has disturbance levels for a given LSS size as a function of LSS angle. The second set of graphs (Figures D-38 through D-49) has the total disturbance torque requirement as a function of LSS angle and altitude. The same CP-CG offset assumption used in set 1 applies to set 2. To condense the data presented in graphic form, a LEO disturbance torque summary has been generated and is shown in Table 3-5. Table 3-5 shows the disturbance torque level for each class and size under four conditions. There are two altitudes, 300 and 500 km and two LSS angles considered. The LSS angles are 10^{o} and an angle at which the structure receives the maximum disturbance level. A 10^{o} angle has been selected as a logical nominal LSS angle. This angle is one which encompasses any pointing errors with sufficient margin to assure control and is not so excessive as to force the APS size to unrealistic proportions. The worst case LSS orientation angle is also given for each structure and size. A worst case angle of 45 degrees indicates gravity gradient is the dominant disturbance. As the worst case angle approaches 90 degrees, aerodynamic torques dominate.

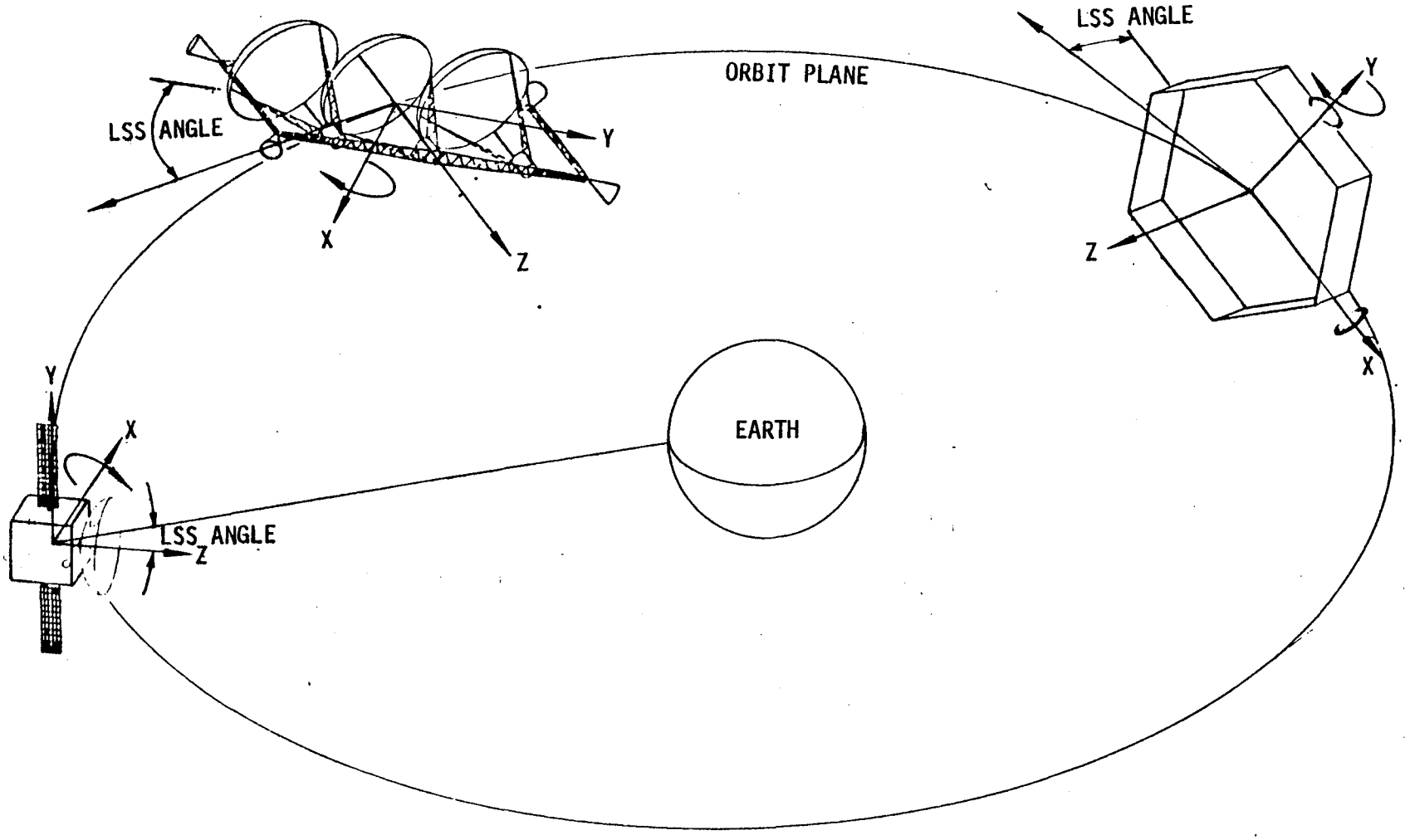

FIGURE 3-41 LSS ANGLE DEFINITION

1. Disturbance torque requirements used 5 percent of the maximum dimension CP-CG offset for all structures.
2. Truss work and antenna mesh was assumed to have a 95 percent transmission factor.
3. Only torques due to aerodynamic forces were considered, not the force itself.
4. Thrusters were located to assure dual redundancy.
5. Chemical systems have a fixed orientation (no gimbal freedom).
6. Electric thrusters have a ±45 degree gimbal capability.
7. The number of electric thrusters was minimized.
8. Thruster distribution was capable of zero ΔV adition maneuvering.
9. Maximum moment arms utilized where possible around large inertia axis.

TABLE 3-4 THRUST LEVEL DETERMINATION ASSUMPTIONS

CLASS	SIZE	ALTITUDE					
		300 km			500 km		
		LSS ANGLE		WORST CASE ANGLE (DEG)	LSS ANGLE		WORST CASE ANGLE (DEG)
		10° (N-m)	WORST CASE (N-m)		10° (N-m)	WORST CASE (N-m)	
PLATE W/O BLANKET	30 M	.055	.350	75	.014	.060	50
	100 M	1.80	11.2	75	.500	2.20	52
	250 M	22.0	205.	75	6.30	31.0	53
PLATE W/BLANKET	30 M	.810	6.80	90	0.12	.500	72
	100 M	32.0	230.	83	5.30	23.0	58
	150 M	112.	850.	80	28.0	108.	55
MODULAR ANTENNA	15 M	.170	1.20	90	.014	.088	86
	60 M	3.30	21.0	83	0.55	2.20	58
	200 M	46.0	305.	90	4.80	22.0	73
SERIES OF ANTENNAS	2	1.50	11.5	45	1.50	9.90	45
	3	9.50	61.0	45	9.50	53.0	45
	4	30.0	195.	45	30.0	160.	45

TABLE 3-5 LEO DISTURBANCE TORQUE SUMMARY

We can qualitatively see from Table 3-5 that a system sized for the worst case angle will have approximately an order of magnitude greater thrust level requirement than a system sized for nominal disturbances. We can also see that a system sized for a 300 km altitude will have a a thrust level of up to 10 times that of a system sized for 500 km. The factor varies depending upon the degree of domination of aerodynamic torques.

The LEO-GEO transfer maneuvering requirement is determined by the in and out-of-plane thrust vector control requirements imposed by a time-optimal continuous thrust transfer. The selection of axis about which the vehicle maneuvers is shown in Table 3-6. Table 3-7 shows the LEO-GEO transfer maneuvering requirements for each class and size. Qualitative conclusions can be drawn from Table 3-7 as follows:

- o Starting altitude does not significantly influence transfer maneuvering requirements
- o Transfer requirements are roughly equivalent to the 500 km worst case disturbance requirements except for the series of antennas

Appendix D also contains the Geosynchronous requirements in three sets of graphs. The first set (Figures D50-D54) show the total torque requirements as a function of LSS angle. Figure D50 shows the composite breakdown for one particular structure. The gravity gradient torque peaks at an LSS angle of 45 degrees while the solar torques remain constant over the range of LSS angles. The total torque profile for each graph in the first set will, therefore, have an identical shape to the top curve in Figure C1. The end points of each curve in Figures D51-D54 give the level of solar pressure torques. Table 3-8 summarizes these requirements for a 10 degree LSS angle and a worst case orientation. From this table, it is clear that electric propulsion can provide geostationary disturbance cancellation for the complete range of structures and sizes.

A second set of graphs details the mission energy requirements assuming a 10 year geosynchronous mission. Figures D55-D66 give a composite breakdown and D67-D70 summarize the total requirements. Each graph in this set is a function of duty cycle which is defined as the time of thrusting during a

TABLE 3-6 SELECTION OF PRIME THRUST AXIS

• MINIMUM INERTIAS USED

PLATE	PRIME THRUST AXIS	MANEUVER AXIS	MANEUVER AXIS INERTIAS		
			SMALL	MEDIUM	LARGE
W/O BLANKET	Z	Y OR X	23,700	8.42×10^5	1.1945×10^7
W/BLANKET	Z	Y OR X	52,390	5.995×10^6	3.7800×10^7
MODULAR ANTENNA	X	Y	18,483	4.707×10^5	5.161×10^6
SERIES OF ANTENNAS	X	Y	1.498×10^6	2.278×10^6	3.041×10^6

TABLE 3-7 LEO - GEO TRANSFER MANEUVERING TORQUE REQUIREMENTS

	START ALTITUDE	SMALL (N-m)	MEDIUM (N-m)	LARGE (N-m)
PLATE				
W/O BLANKET	300	.069	2.46	34.88
	400	.064	2.29	32.49
	500	.060	2.14	30.46
W/BLANKET	300	.153	16.306	96.39
	400	.142	15.189	89.79
	500	.134	14.240	84.18
MODULAR ANTENNA	300	.054	1.37	15.07
	400	.050	1.28	14.04
	500	.047	1.19	13.16
SERIES OF ANTENNAS	300	4.37	6.65	8.88
	400	4.07	6.19	8.27
	500	3.81	5.81	7.75

CLASS	SIZE	LSS ANGLE 10° (N-m)	LSS ANGLE WORST CASE (N-m)	WORST CASE ANGLE (DEG)
PLATE W/O BLANKET	30 M	.0003	.0004	45
	100 M	.013	.019	45
	250 M	.25	.280	45
PLATE W/BLANKET	30 M	.006	.007	45
	100 M	.23	.280	45
	150 M	.85	1.05	45
MODULAR ANTENNA	15 M	.0015	.002	45
	60 M	.022	.026	45
	200 M	.30	.320	45
SERIES OF ANTENNAS	2	.20	.800	45
	3	.065	.260	45
	4	.013	.042	45

TABLE 3-8 GEO DISTURBANCE TORQUE SUMMARY

correction orbit divided by the time of the correction orbit. A duty cycle of 0.1 is basically an impulsive correction whereas a duty cycle of 1.0 is continuous thrusting. Table 3-9 summarizes the mission energy requirements for three representative duty cycles.

The final set of graphs (D77-D74) in Appendix D illustrate the stationkeeping thrust level requirements as a function of both duty cycle and frequency of correction. The frequency of correction is the time between correction orbits. If a number of orbits occur between each successive correction, the thrust level required increases. To reduce operating time and complexity, a low duty cycle and infrequent corrections are desired. Obtaining these goals may require thrust levels of one newton or greater for the large structures. Table 3-10 summarizes the stationkeeping thrust level requirements.

The thruster locations on each class were determined based on the assumptions listed in Table 3-4. Because of the assumed gimballing capability of the electric thrusters, the number of electric thrusters needed was held to eight. The chemical thrusters varied in number from 13 to 17 depending upon the class considered. Figures 3-42, 3-43, and 3-44 show the thruster location assumptions.

Based on these thruster locations and the disturbance analysis previously presented, the thrust/thruster requirements were generated. These requirements are presented in Tables 3-11 and 3-12. The electric and chemical systems have different thrust/thruster requirements for two reasons. First, the distributions are different, hence moment arms for electric thrusters may be shorter for some axis. Second, the stationkeeping duty cycle that electric thrusters need to lower thrust level requirements down to currently achievable levels is around 40 percent. Chemical thrusters are not so limited by thrust and lower duty cycles will decrease the frequency of operation and increase lifetime of the system. Hence, a duty cycle of 10 percent was selected for chemical thrusters. A duty cycle less than 10 percent will cause the chemical thruster I_{sp} to lower as if it were operating in a pulsed mode.

CLASS	SIZE	STATIONKEEPING DELTA-V (M/S)		
		DUTY CYCLE		
		0.1	0.4	1.0
PLATE W/O BLANKET	30 M	539	576	835
	100 M	703	742	1078
	250 M	1062	1137	1672
PLATE W/BLANKET	30 M	953	1015	1480
	100 M	1093	1156	1701
	150 M	1123	1190	1742
MODULAR ANTENNA	15 M	578	617	904
	60 M	606	640	931
	200 M	734	781	1140
SERIES OF ANTENNAS	2	583	625	916
	3	583	625	916
	4	583	625	916

TABLE 3-9 MISSION ENERGY REQUIREMENTS

CLASS	SIZE	THRUST LEVEL REQUIRED (N)			
		ONCE/ORBIT		ONCE/WEEK	
		DUTY CYCLE		DUTY CYCLE	
		0.1	0.4	0.1	0.4
PLATE W/O BLANKET	30 M	.008	.002	.050	.015
	100 M	.027	.007	.190	.050
	250 M	.087	.022	.610	.170
PLATE W/BLANKET	30 M	.028	.008	.200	.050
	100 M	.290	.075	1.95	.530
	150 M	.620	.160	4.10	1.10
MODULAR ANTENNA	15 M	.030	.008	.250	.070
	60 M	.130	.032	.900	.250
	200 M	.300	.082	2.10	.600
SERIES OF ANTENNAS	2	.110	.020	.800	.210
	3	.160	.040	1.20	.310
	4	.230	.060	1.60	.420

TABLE 3-10 STATIONKEEPING THRUST REQUIREMENTS

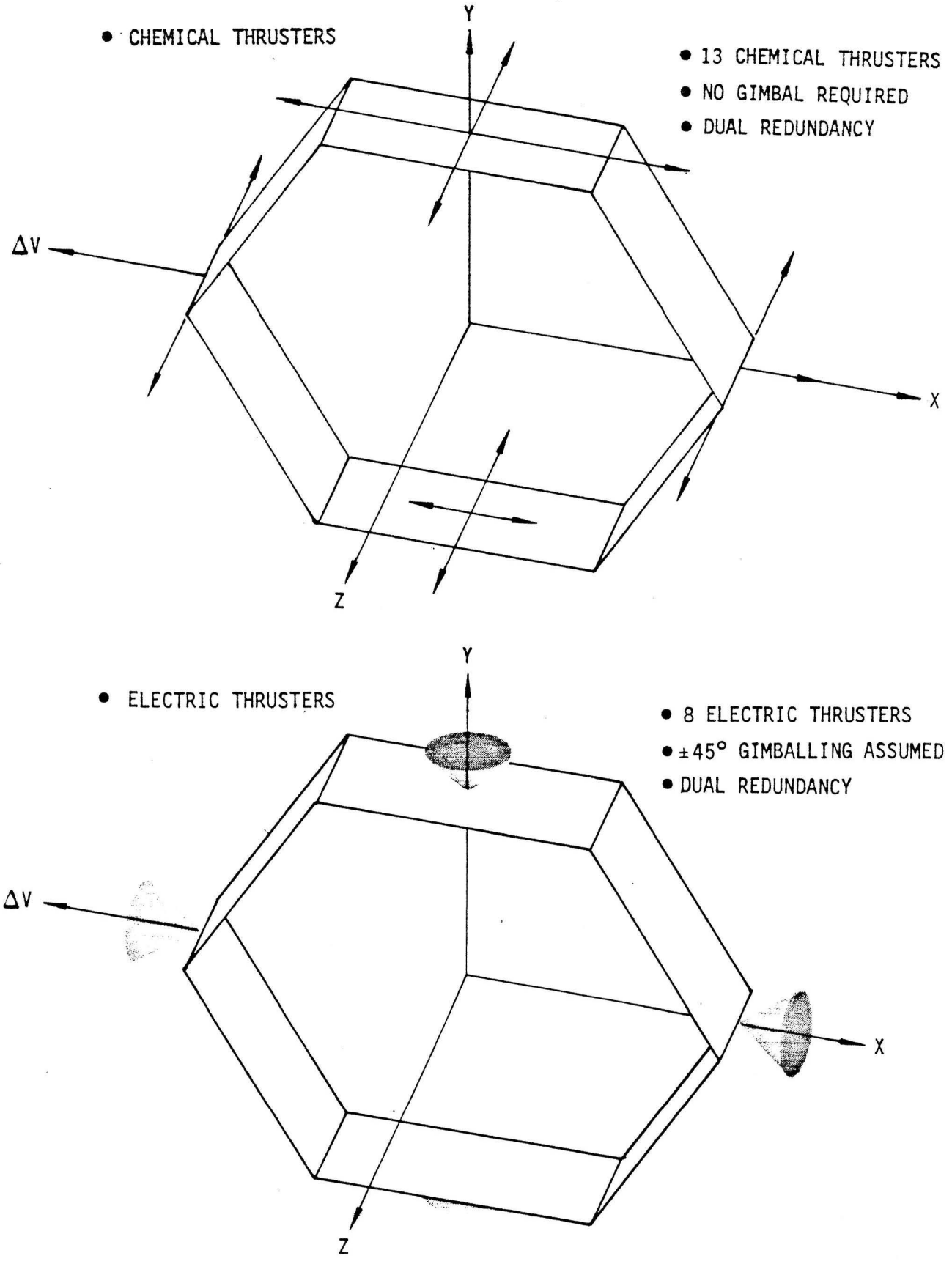

Figure 3-42

TETRAHEDRAL TRUSS THRUSTER LOCATIONS

• CHEMICAL THRUSTERS

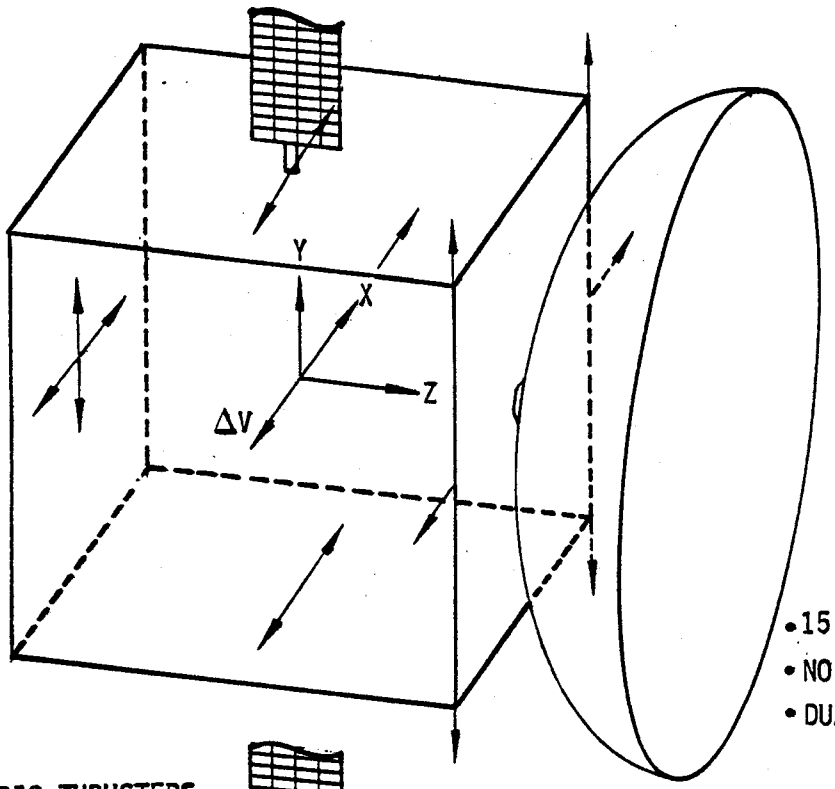

- 15 CHEMICAL THRUSTERS
- NO GIMBAL REQUIRED
- DUAL REDUNDANCY

• ELECTRIC THRUSTERS

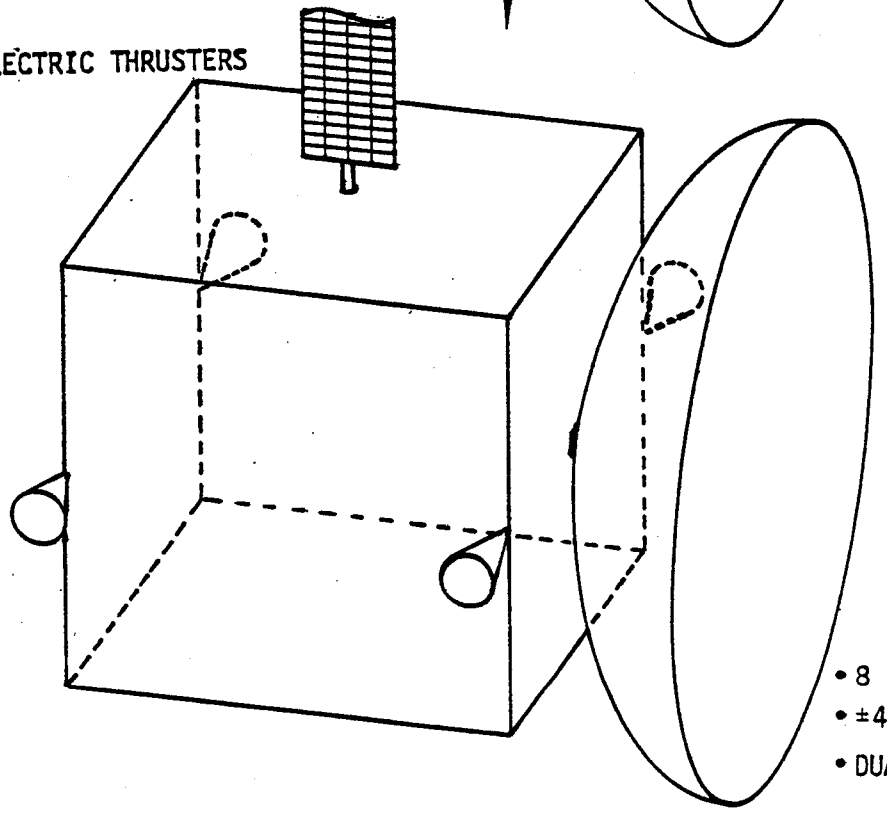

- 8 ELECTRIC THRUSTERS
- ±45 GIMBALLING
- DUAL REDUNDANT

FIGURE 3-43 MODULAR ANTENNA

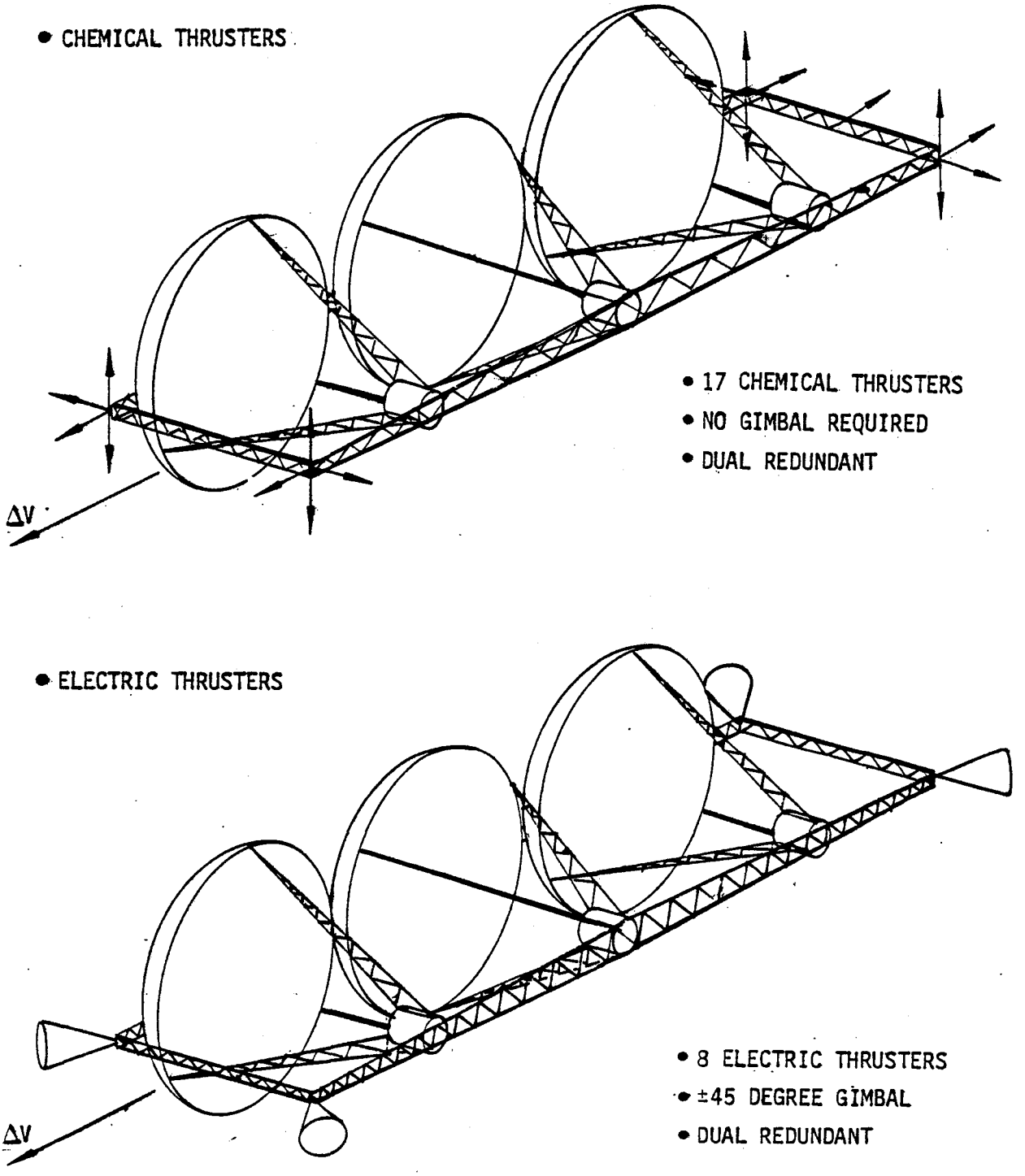

Figure 3-44 SERIES OF ANTENNAS

The thrust requirements have been given for two altitudes with two LSS orientations, a time optimal low thrust LEO-GEO transfer, a geosynchronous worst case orientation, and for GEO stationkeeping. The requirements for 400 km are available but were not displayed to save space and the number of parameters considered. If 400 km data is required, interpolation can suffice. An additional rationale for eliminating the 400 km start altitude is that the shuttle's capability does not vary significantly between 300 and 400 km. For 500 km, an additional OMS kit is necessary to achieve the higher altitude and there is a corresponding reduction of payload capability.

Table 3-11

CHEMICAL APS - THRUST/THRUSTER REQUIREMENTS SUMMARY

CLASS	SIZE	DISTURBANCE TORQUE 300 km		DISTURBANCE TORQUE 500 km		LEO - GEO TRANSFER	GEO DISTURBANCE	GEO STATIONKEEPING @ 0.1 DUTY CYCLE	
		10°	WORST CASE	10°	WORST CASE		WORST CASE	ONCE/ORBIT	ONCE/WEEK
PLATE W/O BLANKET	30 m	0.003	0.018	0.0005	0.003	0.0035	0.00005	0.008	0.050
	100 m	0.027	0.170	0.0075	0.035	0.0400	0.00030	0.027	0.190
	250 m	0.132	1.230	0.0380	0.185	0.2100	0.00170	0.087	0.610
PLATE W/BLANKET	30 m	0.040	0.340	0.0055	0.025	0.0075	0.00035	0.028	0.200
	100 m	0.480	3.450	0.0795	0.345	0.2445	0.00420	0.290	1.950
	150 m	1.120	8.500	0.2800	1.080	0.9640	0.01050	0.620	4.100
MODULAR ANTENNA	15 m	0.120	0.545	0.0100	0.060	0.0370	0.00150	0.030	0.250
	60 m	1.500	9.540	0.2500	1.000	0.6250	0.01150	0.130	0.900
	200 m	16.83	55.790	1.7550	8.050	5.5150	0.11700	0.300	2.100
SERIES OF ANTENNAS	2	0.025	0.192	0.0250	0.165	0.0730	0.00100	0.055	0.400
	3	0.106	0.680	0.1060	0.591	0.0740	0.00300	0.080	0.600
	4	0.250	1.625	0.2500	1.330	0.0740	0.00700	0.115	0.800

Table 3-12

ELECTRIC APS - THRUST/THRUSTER REQUIREMENTS SUMMARY

CLASS	SIZE	DISTURBANCE TORQUE 300 km 10°	DISTURBANCE TORQUE 300 km WORST CASE	DISTURBANCE TORQUE 500 km 10°	DISTURBANCE TORQUE 500 km WORST CASE	LEO - GEO TRANSFER	GEO DISTURBANCE WORST CASE	GEO STATIONKEEPING @ 0.4 DUTY CYCLE ONCE/ORBIT	GEO STATIONKEEPING @ 0.4 DUTY CYCLE ONCE/WEEK
PLATE W/O BLANKET	30 m	0.004	0.025	0.001	0.004	0.005	0.0001	0.002	0.015
	100 m	0.038	0.240	0.011	0.049	0.057	0.0004	0.007	0.050
	250 m	0.187	1.739	0.054	0.261	0.297	0.0020	0.022	0.170
PLATE W/BLANKET	30 m	0.056	0.480	0.008	0.035	0.011	0.0055	0.008	0.050
	100 m	0.700	4.880	0.112	0.488	0.346	0.0059	0.075	0.530
	150 m	1.584	12.020	0.396	1.527	0.346	0.0150	0.160	1.100
MODULAR ANTENNA	15 m	0.120	0.504	0.010	0.060	0.037	0.0115	0.004	0.035
	60 m	1.500	9.540	0.250	1.000	0.625	0.0115	0.016	0.125
	200 m	16.800	55.790	1.755	8.050	5.515	0.1170	0.041	0.300
SERIES OF ANTENNAS	2	0.035	0.272	0.035	0.233	0.103	0.0020	0.010	0.105
	3	0.150	0.962	0.150	0.836	0.105	0.0040	0.020	0.155
	4	0.353	2.298	0.353	1.880	0.105	0.0100	0.030	0.210

THIS PAGE INTENTIONALLY LEFT BLANK

4.0 INTERACTION BETWEEN AUXILIARY PROPULSION SYSTEM CHARACTERISTICS AND LARGE SPACE SYSTEM CHARACTERISTICS

The objective in this section is to establish the system-level characteristics required of auxiliary propulsion systems to enable them to meet the requirements of large space system, and from these, in Section 5, to determine the directions APS technology development should take. To accomplish this end, it is desirable to establish bounds on the values of the APS characteristics within which technologists will be required to work. Because these bounds are configuration and/or mission dependent, a useful output would be a set of parameter maps showing the functional dependence of the various parameters upon each other, upon the scaling parameter, and upon control accuracy, for each generic LSS class.

The original intent was to quantify each of the elements that indicate sensitivity in the matrix of Figure 3-40. In effect, to determine a collection of partial derivatives to define the functional relationship of each interaction. Unfortunately difficulties arise. The basic problem is that the parameters listed horizontally are not independent. For example, LSS mass is a function of size, stiffness, strength and perhaps, lifetime. Also the disturbances are obviously functions of LSS mass and size, and all three are functions of the scaling parameters derived in Task 3.1. It was concluded that an attempt to develop a matrix of partials would not be very productive. Instead, four separate, relatively independent, study areas were selected which would explore the complex interrelationship between APS and LSS characteristics. These areas are: Thrust Level, Thrust Modulation and Transient Effects, Number and Distribution of Thrusters, and Allowable Mass. The thrust level study was presented in Section 3.2.1 and the remaining three areas are investigated in the following sections. Although each investigation only treats certain aspects of of the problem, in sum they cover all the sensitivities identified in the Figure 3-40 matrix.

A second objective was to collect the results of the four studies to define optimum APS characteristics. The last subtask examined the impact of a single shuttle launch.

Proportional and pulse modulated systems were treated separately. In each case methods of implementation, transient effects and performance were examined to determine the interactions will LSS.

Large flat structures (generic class I) were studied to define interactions with the number and distribution of thrusters. Two aspects were found significant, attitude control and shape control. It became clear that performance improvement could be gained by distributing the thrusters over the structure. Doubling the minimum number of thrusters gave a marked improvement, a further doubling a smaller improvement and so on.

In the Allowable Mass subtask, scaling laws were collected for various APS components such as tanks, power processors, solar arrays, etc. These expressions were then used together with thrust and total impulse required data to determine APS mass as a function of specific impulse. This determinaion was made for small, medium and large vehicles in each generic class.

The results of the above studies were reviewed to single out the APS characteristics that have significant interactions with control functions and APS charactristics. This review identified the APS characteristics that are desirable and those that should be avoided.

The final subtask examined the impact of vehicles constrained to a single shuttle launch. This involved the redefinition of some of the scaling laws and the determination of APS masses for the single launch vehicles.

The results obtained in Task 4 established the system level APS characteristics needed to meet the requirements of LSS. They provide the information necessary to proceed with Task 5, the determination of the directions APS technology development should take.

4.1 Thrust Modulation and Transient Effects

Thrust modulation will affect to some extent all control functions. The ideal situation would be an APS capable of amplitude modulated thrusts all the way from the maximum required down to zero. Since this is presently not attainable some form of pulse modulation is necessary to obtain small effective thrust levels.

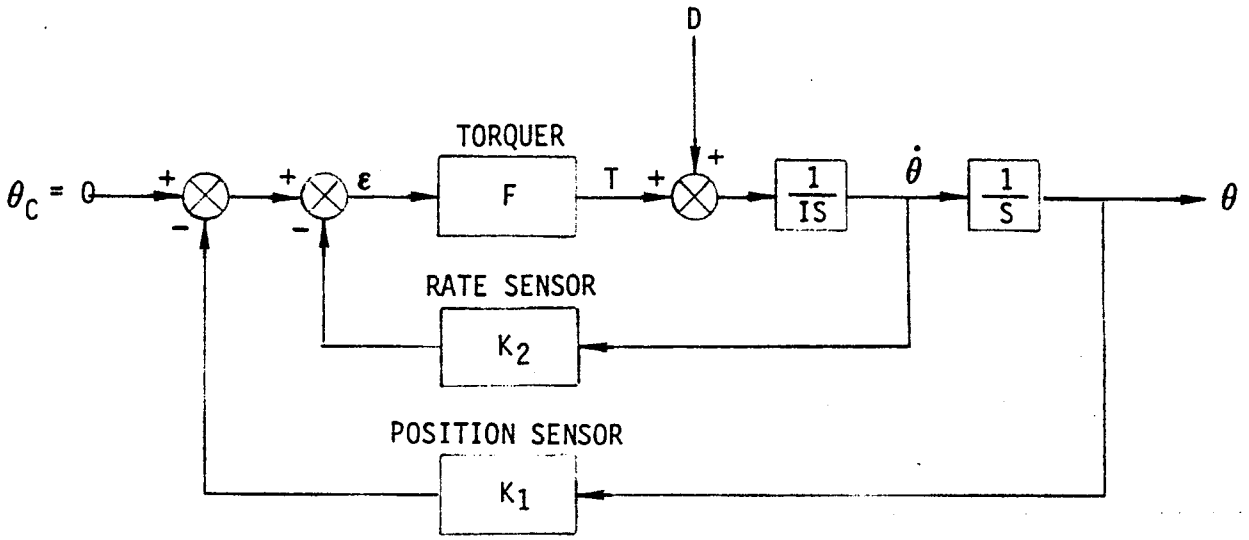

FIGURE 4-1 PROPORTIONAL SYSTEM BLOCK DIAGRAM

The rise and decay transients associated with APS will affect primarily the pointing and shape control functions. This is because these functions require thrust application at precise times. In some cases compensation can be made for transient effects but when this is not possible the system performance will suffer.

Variable thrust to enable disturbance torques to be exactly cancelled would provide optimum system performance. Such a system ideally can provide high accuracy and once the desired pointing has been achieved no effort over and above the cancellation of disturbance torques is needed to maintain pointing. A proportional system of this kind is only possible if the APS thrusts can deliver torques which closely approximate the applied disturbance torques. Not only must the control torques equal the magnitude of the disturbance torques but they must do so at all times. This requires the capability to change thrust at matching rates.

When the necessary thrust range and rates of change cannot be met pulse modulation can be used. This method can take several forms but the most likely is pulse-width modulation, also called on-off and bang-bang control. Thrusts of constant magnitude are turned on and off for varying lengths of time to achieve a desired mean thrust level.

4.1.1 Proportional Control

When proportional control is available the control thrust is determined as a function of system error, which is usually defined as a linear combination of rate and position error.

4.1.1.1 System Implementation

A typical implementation, in one axis, is shown in Figure 4-1. The rate and position errors are sensed and combined with appropriate gains to form the system error, ε . The control torque is commanded as a function of the error, summed with disturbance torques, D, and applied to the vehicle to produce an acceleration. Integration of the acceleration leads to the rate and position. The accuracy achievable in practice is determined primarily by the sensor characteristics. The control system shown in Figure 4-1 can drive the system error, as sensed, to very small values (actually to $\theta = D/kk_1$) when the disturbance is constant, and introduce only a small

additional error when the disturbance is changing. The system frequency and damping are functions of the gains.

Even better accuracy, if required, can be obtained by including an integral of position term in the system error formulation. Lower accuracy can be achieved by introducing deadzones in the system either at the thrust drivers, block F, or in the position sensor. There is no propellant penalty associated with accuracy provided the control torque is available over the range covering the maximum disturbance torque down to zero and provided the I_{sp} remains reasonably constant over this range.

Basic System Characteristics

The system equation, based on the block diagram of Figure 4-1, and assuming a control torque of T = K is:

$$(Is^2 + KK_2 s + KK_1)\bar{\theta} = \bar{D} \tag{4.1}$$

where I is the moment of inertia
D the disturbance torque, and
K_i are gains

The characteristic equation is that of a second order system. It follows that the system frequency (ω) and damping (ζ) are given by

$$\omega^2 = KK_1/I \tag{4.2}$$

$$2\zeta\omega = KK_2/I \tag{4.3}$$

If D is constant the response is given by

$$\bar{\theta}(s) = \frac{D}{s}\left(\frac{1}{Is^2 + KK_2 s + KK_1}\right) \tag{4.4}$$

which has the solution

$$\theta(t) = \frac{D}{I\omega^2}\left(1 - e^{-at}\cos bt - \frac{a}{b}e^{-at}\sin bt\right) \tag{4.5}$$

where $a = KK_2/I$, $(a^2 + b^2) = \omega^2 = KK_1/I$ (4.6)

It is often convenient to represent system response in the phase plane; i.e., a plot of θ vs $\dot{\theta}$. In the phase plane, solutions from various initial conditions have trajectories as shown in Figure 4-2 (reproduced from Reference 3).

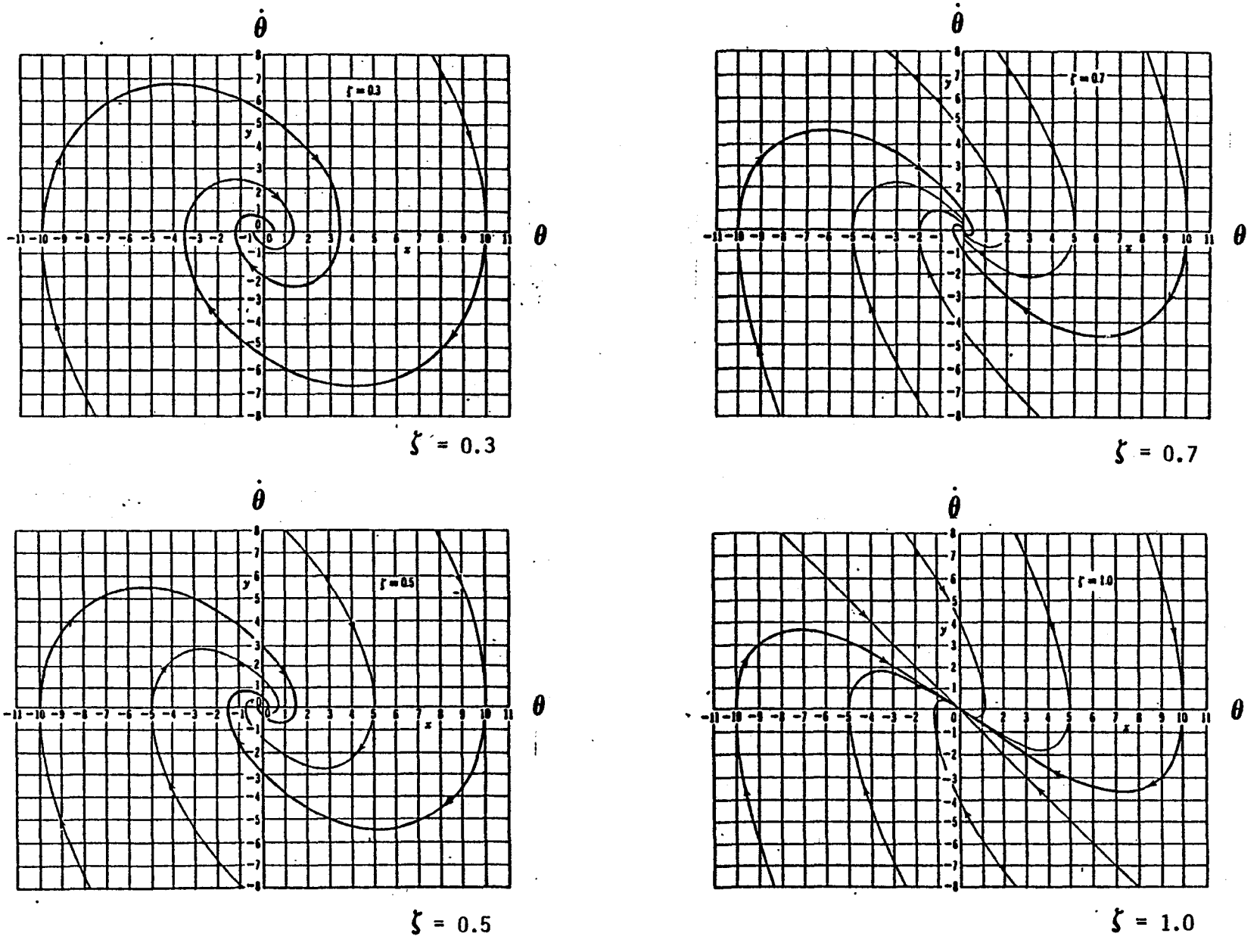

FIGURE 4- 2 PHASE PLANE TRAJECTORIES

The steady state error under a constant torque can be found by applying the final value theorem to (4)

$$\theta_{ss} = \frac{D}{s}\left(\frac{s}{Is^2+KK_2s+KK_1}\right)\Big/_{s=0}$$

$$= \frac{D}{KK_1} \text{ or } \frac{D}{I\omega^2} \qquad (4.7)$$

4.1.1.2 Transient Effects

Electric engines, which are the prime contenders for proportional control applications, typically offer a thrust range but only down to limiting value. If a lower thrust bound does exist there are several ways of configuring the control system to achieve desired results.

If there were no thrust bound the thrust vs error curve would take the form shown in Figure 4-3(a), that is a simple gain, or F = K in Figure 4-1. When limiting is present a relatively simple approach is to revert to pulse operation. If the thrust is set to zero when less than the limiting value is called for the F function takes the form shown in Figure 4-3(b). This method sacrifices accuracy but requires the same amount of propellant (assuming the same I_{sp}) as true proportional control. Continuous proportional control can be obtained, down to zero effective thrust, by using opposing thrusters. A possible thrust vs error relation is as shown in Figure 4-3(c). In this case accuracy is maintained but a propellant penalty is incurred.

Hybrid Proportional/Pulse Operation

The system is hybrid because it uses proportional control when

$$D \geq T_c$$

where T_c is the limiting control torque

and on-off control when $D<T_c$.

Assuming the system block diagram of Figure 4-1, the control law is

$$T = K(K_1\theta + K_2\dot{\theta})$$

In the phase plane, the lines indicating where the limiting value occurs are given by

$$\pm T_c = K(K_1\theta + K_2\dot{\theta}) \qquad (4.8)$$

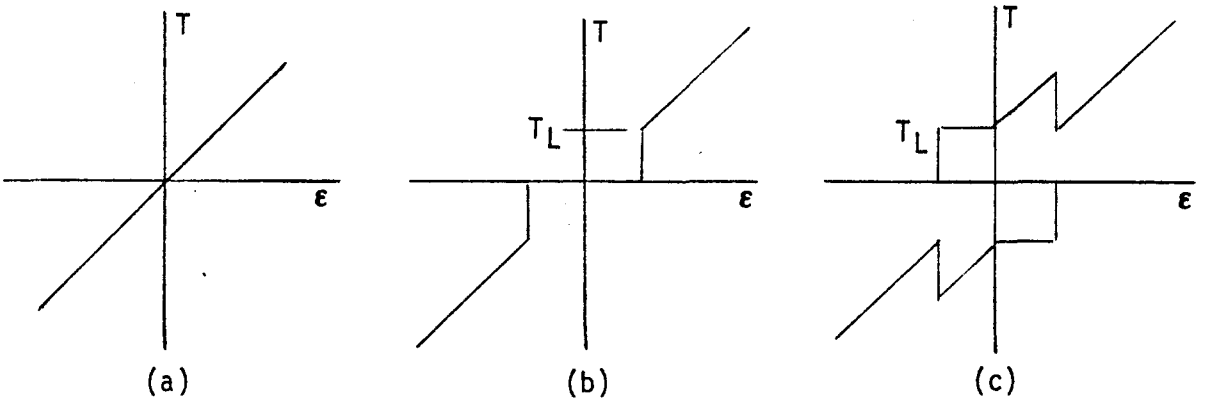

FIGURE 4-3 F FUNCTIONS

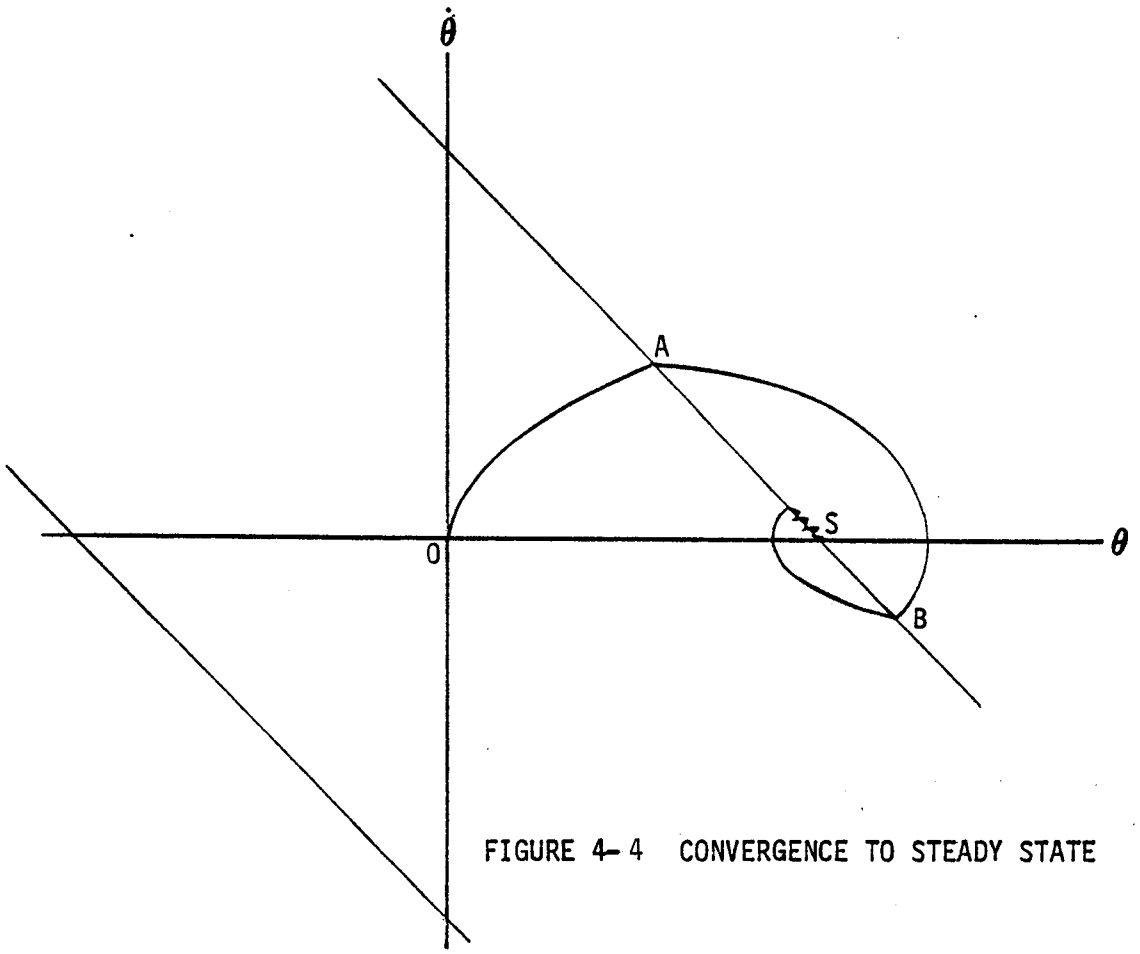

FIGURE 4-4 CONVERGENCE TO STEADY STATE

These are shown in Figure 4-4. The system trajectory, starting from 0 is also shown. Assuming D to be positive but less than T_c the system will follow the unpowered trajectory from 0 to A. The equation is given by

$$I\ddot{\theta} = I\dot{\theta}\frac{d\dot{\theta}}{d\theta} = D$$
$$\dot{\theta}^2 = 2D\theta/I \qquad (4.9)$$

that is, a parabola. At A the thrust is turned on taking the system to B. Arc AB is given by the solution to

$$I\ddot{\theta} + KK_2\dot{\theta} + KK_1\theta = D \qquad (4.10)$$

which is the same as equation (4.1) and is a distorted logarithmic spiral in the phase plane.

Successive on and off trajectory arcs will continue until the system converges to point S. Although the shapes of the converging trajectories will vary with the system parameters the result is always the value of at S; i.e., the solution of equation (4.8) with $\dot{\theta} = 0$

$$\theta_S = T_c/KK_1 = T_c/I\omega^2 \qquad (4.11)$$

(This value can be compared with $D/I\omega^2$ attainable with a fully proportional system.)

Once the steady state point has been reached, the system will automatically adapt a pulsing mode with a duty cycle (ratio of thruster on time to total time) of $\frac{D}{K}$.

Opposed Thrust

If an effective torque of T below T_c is required a torque of $T_c + T$ can be generated by one set of thrusters and a torque $-T_c$ by the opposing set. This will achieve a net torque T. The system will behave as a true proportional system in terms of pointing and disturbance cancellation but will incur a propellant penalty whenever the net torque is less than the limiting value.

Delayed Response

In a proportional system once an operating thrust has been achieved there may be delays when thrust changes are commanded. These may be simulated by introducing a first order lag. In effect, the block F in Figure 4-1 takes the form

$$F = \frac{1}{1+\tau s}$$

where τ is the time constant. The system equation becomes

$$\left(Is^2 + \frac{KK_2 s + KK_1}{1+\tau s}\right)\bar{\theta} = \bar{D}$$

or $$(I\tau s^3 + Is^2 + KK_2 s + KK_1)\bar{\theta} = \bar{D}(1+\tau s)$$

The steady state error under a constant torque remains the same although response will be a little sluggish. Under varying torques little change in response will occur provided τ is small compared to the times involved.

4.1.1.3 Performance

The basic accuracy and propellant consumption performance relations will be found below for pointing, shape control, maneuver and desaturation and stationkeeping control functions.

Pointing

Accuracy values have already been determined: For true proportional systems, including those using opposed thrust, and using simple rate and position feedback the steady state error under a constant (or slowly varying) torque is

$$\theta_{ss} = \frac{D}{I\omega^2}$$

When a lower torque limit of T_c applies the error rises to

$$\theta_{ss} = \frac{T_c}{I\omega^2}$$

The propellant consumption in a proportional system, with or without torque limiting, is that needed to counter the disturbance torque. Once the steady state position has been acquired no additional effort is necessary and no savings are obtainable by relaxing the accuracy.

Opposed thrust mechanizations in general impose a propellant consumption penalty. Assuming the method illustrated by Figure 4-3(c) the propellant required is that needed to overcome the disturbances plus that needed to achieve $2T_c$ whenever $T_c < D$.

To obtain an assessment of the penalty it is necessary to know what proportion of the time the disturbance torque is less than the limiting control torque. Since most disturbances will be sinusoidal in nature an example can be worked assuming

$$D = A\sin\omega t \quad , \quad T_c = kA$$

Using the opposed thrust technique the plus and minus torques needed to counter the disturbance will be as shown in Figure 4-5. Starting from zero the disturbance torque will build to T_c when

$$kA = A\sin\Omega t_1$$
$$t_1 = \frac{1}{\Omega}\sin^{-1}(k)$$

In disturbance cycle period the torque will be below T_c for a time $4t_1$ or $\frac{4}{\Omega}\sin^{-1}k$. since the period is $\frac{2\pi}{\Omega}$ the proportion of time the system will be in the opposed thrust mode is

$$\frac{\Omega}{2\pi} \times \frac{4}{\Omega}\sin^{-1}k = \frac{2}{\pi}\sin^{-1}k$$

The total torque impulse is represented by the shaded are in Figure 4-5, that is:

$$\text{Impulse} = 2\,(\text{ABCD} + \text{EFGH} + \text{GHI})$$
$$= 2\left[A\int_{t_1}^{\pi/2-t_1}\sin\Omega t\,dt + 6t_1kA + kA\int_{-t_1}^{t_1}(1+\sin\Omega t)\,dt\right] \qquad (4.12)$$

Now by inspection it is seen that

$$GHJ = \frac{1}{3}EFGH = 2t_1kA$$

Then Impulse $= 2A\int_{t_1}^{\pi/2-t_1}\sin\Omega t\,dt + 16t_1kA$

$$= \frac{2A}{\Omega}\int_{\sin^{-1}k}^{\pi-\sin^{-1}k}\sin\alpha\,d\alpha + 16t_1kA$$

$$= \frac{4A}{\Omega}\sqrt{1-k^2} + \frac{16kA}{\Omega}\sin^{-1}k \qquad (4.13)$$

The impulse with true proportional control would be

$$I = 2A\int_0^{\pi/2}\sin\Omega t\,dt = \frac{4A}{\Omega} \qquad (4.14)$$

The ratio is (4.13) divided by (4.14), i.e.,

$$R = \sqrt{1-k^2} + 4k\sin^{-1}k \qquad (4.15)$$

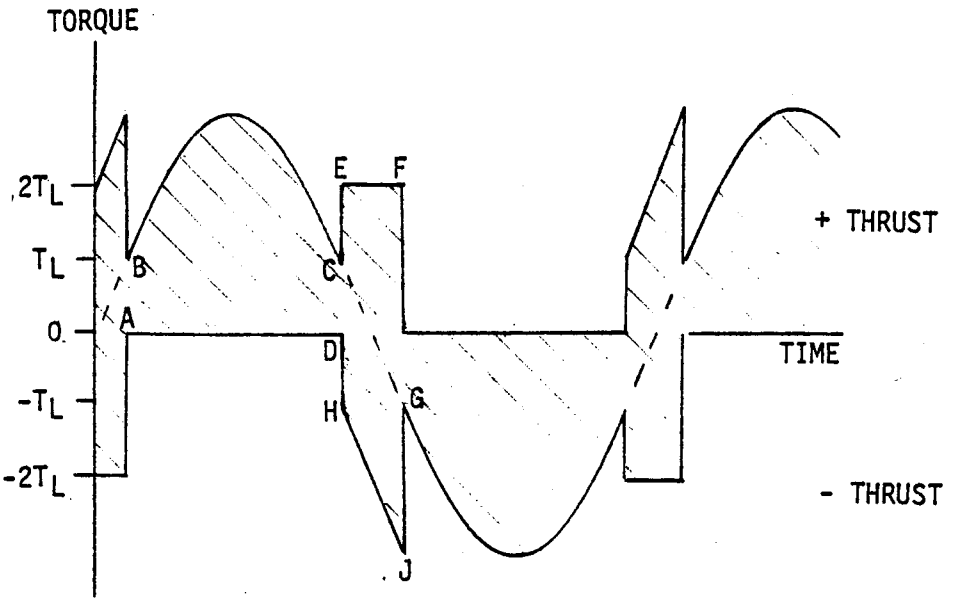

FIGURE 4-5 OPPOSED THRUST FIGURE

Since propellant consumption is proportional to impulse, R represents the ratio of consumption under a true proportional system. R is shown plotted against k in Figure 4-6. It is seen that the penalty is quite small for lower values of k (less than 10 percent for k less than 0.17, for example) but rises rapidly as k increases.

Shape Control

The theory of small oscillations about an equilibrium condition of an elastic body shows that the shape can be described by (Reference 4)

$$u(x) = \sum q_n \phi_n(x) \tag{4.16}$$

where q_n are the normal coordinates and

$\phi_n(x)$ the normal modes.

The normal coordinates are defined

$$q_n = \frac{\int \rho u \cdot \phi \, dv}{\int \rho \phi \cdot \phi \, dv} \tag{4.17}$$

taken over the entire body with

$\rho(x)$ representing the density, and

$dv(x)$ an element of volume.

It can be shown that the modes are orthogonal, that is

$$\int \rho \phi_i \cdot \phi_n \, dV = \begin{cases} 1, & i = n \\ 0, & i \neq n \end{cases} \tag{4.18}$$

Kinetic and elastic strain energies are given by

$$T = \frac{1}{2} \sum m_n \dot{q}_n^2 \tag{4.19}$$

$$V = \frac{1}{2} \sum m_n \omega_n^2 q_n^2 \tag{4.20}$$

where ω_n is the modal frequency and

m_n the generalized mass.

$$m_n = \int \rho \phi_n \cdot \phi_n \, dV \tag{4.21}$$

The generalized force is defined

$$Q_n = \int F \cdot \phi \, dV \tag{4.22}$$

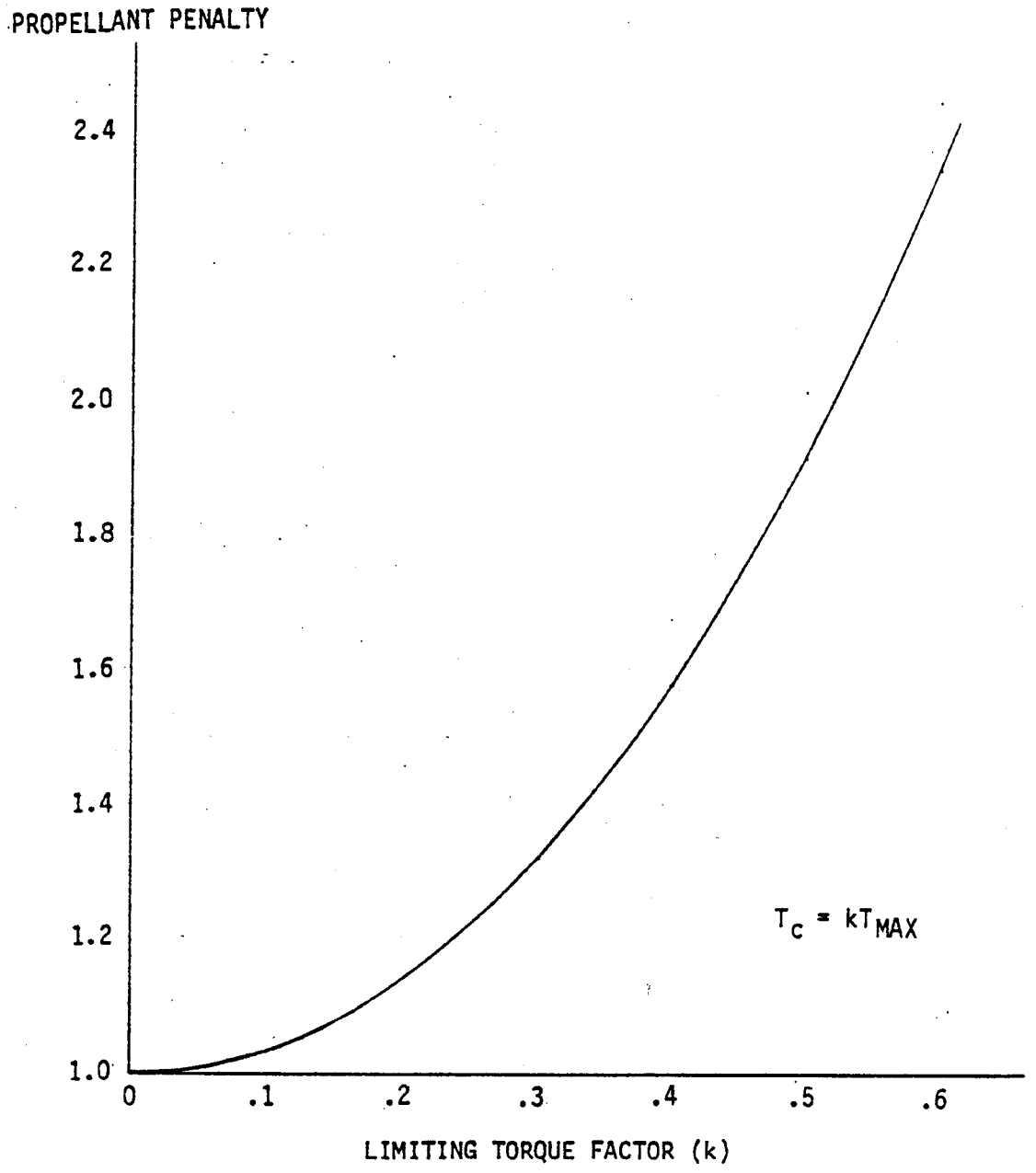

FIGURE 4-6 OPPOSED THRUST PROPELLANT PENALTY

where F is the force acting at x.

The above equations describe the system as a whole, but as a consequence of the orthogonality condition, equation (4.18), they also hold for each mode; that is, for particular values of n. This property will be used to gain insight into the problems of shape control by focussing attention on a single mode.

Lagrange's equations state

$$\frac{d}{dt}\left(\frac{\partial L}{\partial \dot{q}}\right) - \left(\frac{\partial L}{\partial q}\right) = Q \tag{4.23}$$

where the Lagrangian L is

$$L = T - V \tag{4.24}$$

Using (4.19), (4.20) and (4.21)

$$\frac{d}{dt}(m\dot{q}) + m\omega^2 q = F$$

$$\ddot{q} + \omega^2 q = \frac{F}{m} \tag{4.25}$$

A candidate for proportional control is to apply thrust according to

$$F = -km\dot{q} \tag{4.26}$$

Substituting this into equation (4.25)

$$\ddot{q} + k\dot{q} + \omega^2 q = F/m \tag{4.27}$$

This is the equation of a damped second order system. Taking the Laplace transform of (4.27)

$$(s^2 + ks + \omega^2)\bar{q} = (s+k)q_0$$

assuming an initial condition of $q(0) = q_0$, $q(0) = 0$. The solution is

$$q(t) = q_0 e^{-kt/2}\left(\cos bt + \frac{k}{2b}\sin bt\right) \tag{4.28}$$

$$b = \frac{1}{2}\sqrt{4\omega^2 - k^2}$$

Proportional control is thus effective in providing damping of structural oscillations (or increasing existing structural damping). The natural frequency is reduced slightly from ω to $\frac{1}{2}\sqrt{4\omega^2 - k^2}$. The damping time constant is directly related to the gain k in equation (4.26) and is equal to 2/k.

A basic equation of beam theory states

$$EI\frac{\partial^4 y}{\partial x^4} + \rho\frac{\partial^2 y}{\partial t^2} = 0 \tag{4.29}$$

where y is the deflection

x the location along the beam

E Young's Modulus

I the second moment of area, and

ρ the mass per unit length = $\frac{M}{L}$

Assuming the motion to be sinusoidal, y can be expressed

$$y = y_o \sin(\omega t + \phi) \tag{4.30}$$

where ϕ is a phase angle.

Substituting (4-30) into (4.29)

$$EI\, d^4y_o/dx^4 - \rho\omega^2 y_o = 0$$

If $n^4 = \rho\omega^2/EI$

$$d^4y_o/dx^4 - n^4 y_o = 0 \tag{4.31}$$

which has the solution

$$y_o = A \cos nx + B \sin nx + C \cosh nx + D \sinh nx$$

Applying the boundary conditions for a free-free beam leads to the equation

$$\cos nL \cosh nL = -1$$

which has solutions for various values of nL. These represent modes. Substituting into (4.32)

$$\omega_i = C\sqrt{\frac{EI(nL)_i^4}{ML^3}} \tag{4.32}$$

to define the modal frequencies. This equation applies to flat plates if motion is restricted to the xy plane. Frequencies for the first few modes are found to be

1st mode C = 3.56
2nd mode C = 9.82
3rd mode C = 19.2
4th mode C = 31.8

A plot of the first mode frequency vs. scaling parameter is shown in Figure 4-7. Two values of I are shown with E chosen for both graphite and aluminum.

Minimum Thrust Bound

If the control law, equation (4.26), is attempted with a bounded system, it becomes modified to

$$\frac{F}{m} = \begin{cases} -k\dot{q}, & |\dot{q}| > F_2/mk \\ 0, & |\dot{q}| \leq F_2/mk \end{cases} \qquad (4.33)$$

where F_2 is the limiting value

If k is small, the system frequency closely approximates the natural frequency and the motion can be expressed

$$q = q_0 \cos\omega t \ , \ \dot{q} = -\omega q_0 \sin\omega t$$

From (4.33) it follows that the thrust is on whenever

$$\omega t > \sin^{-1}|F_2/mk\omega q_0| \qquad (4.34)$$

and off when the angle is less than this, Figure 4-8.

Although the response can be calculated, it is clear that the only difference from an unlimited system will be a decrease in damping. Moreover the decrease will be small because the thrust is zero at the least effective parts of the cycle, when the velocity is minimum. It is concluded that limited thrust is not a serious problem for shape control.

Opposed Thrust

The use of opposed thrust could recover the damping lost by thrust limiting. Since, however, the loss is small the additional complication of opposed thrust hardly seems warranted particularly as switching would be required at relatively high frequencies and the method entails a propellant penalty.

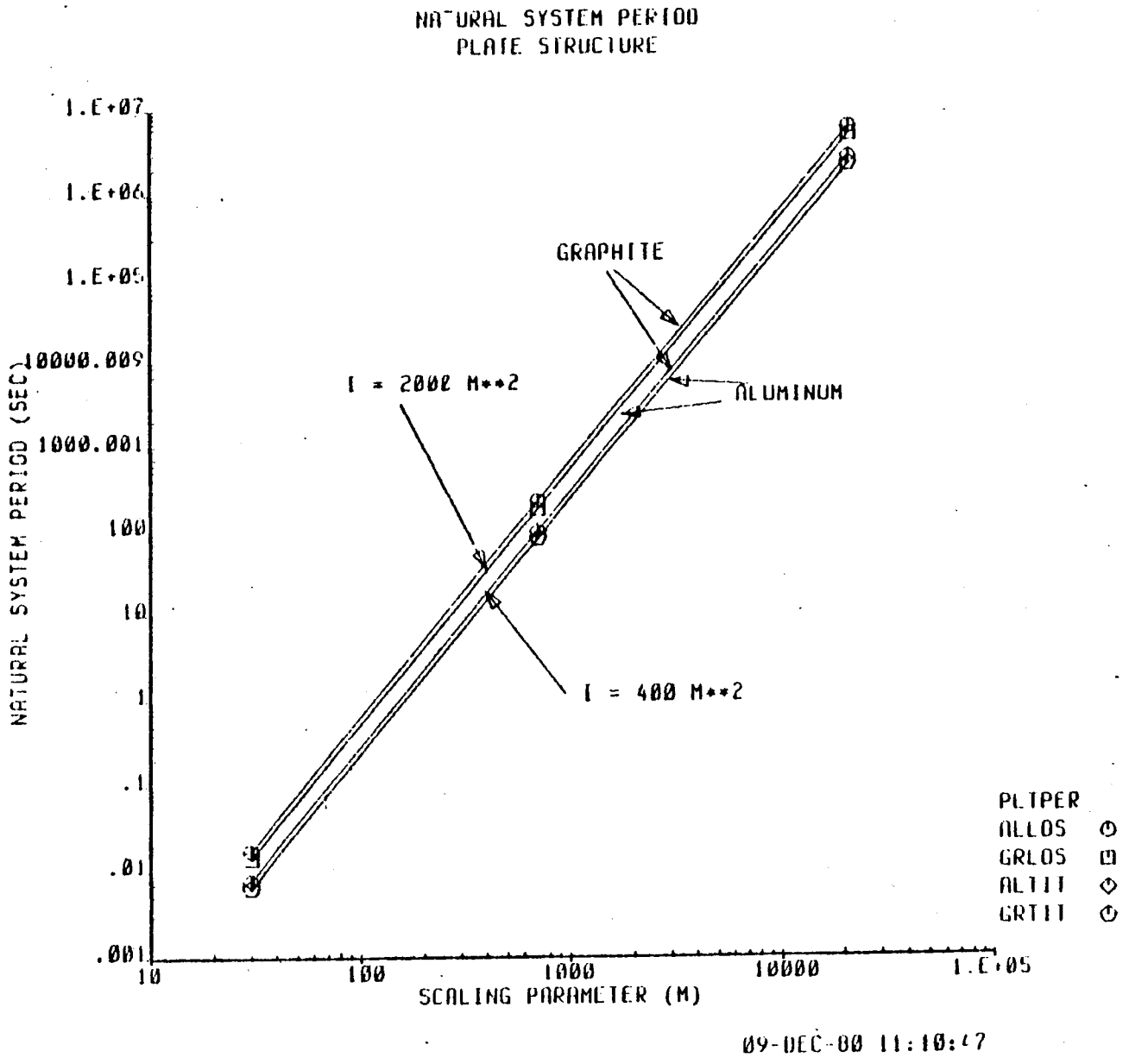

FIGURE 4-7 PLATE STRUCTURE NATURAL PERIOD

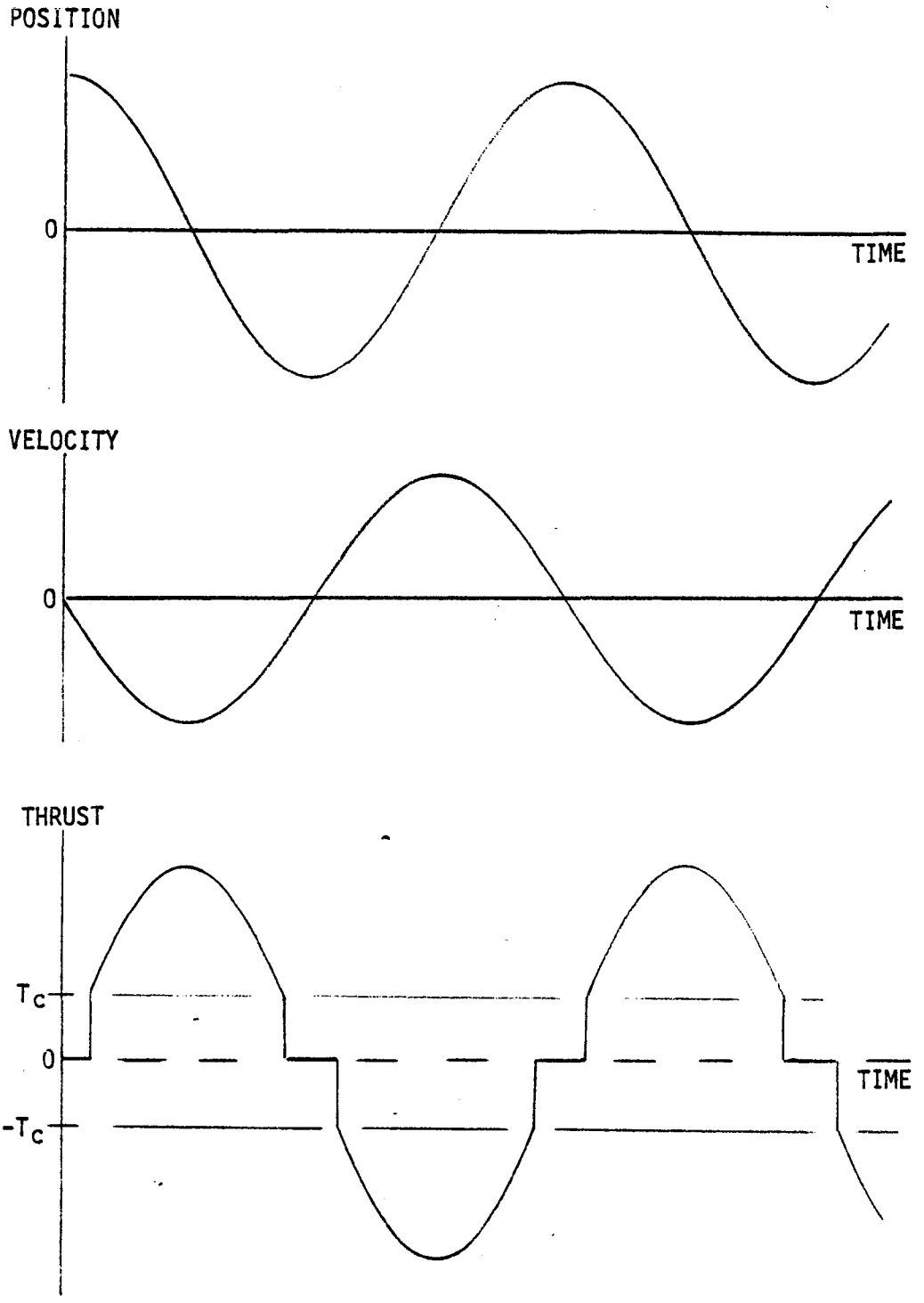

FIGURE 4-8 LOWER THRUST BOUND FIGURE

Delayed Response

If the delays can be represented as a first order lag the control law (4.26) becomes modified to

$$\frac{F}{m} = \frac{-k\bar{q}s}{1+\tau s} \tag{4.35}$$

and the system equation is

$$\left(s^2 + \frac{ks}{1+\tau s} + \omega^2\right)\bar{q} = IC \tag{4.36}$$

The equation can be expessed in the form

$$(\alpha+\tau s)\left[(s+a)^2+b^2\right]\bar{q} = (1+\tau s)IC \tag{4.37}$$

which has the solution

$$\bar{q} = \frac{(1+\tau s)IC}{(\alpha+\tau s)\left[(s+a)^2+b^2\right]}$$

By partial fractions

$$\bar{q} = (IC)\left[\frac{A}{\alpha+\tau s} + \frac{B(s+a)+C}{(s+a)^2+b^2}\right]$$

$$q(t) = (IC)\left[\frac{A}{\tau}e^{-\frac{\alpha t}{\tau}} + e^{-at}\left(B\cos bt + \frac{C}{b}\sin bt\right)\right] \tag{4.38}$$

The first term will decay to zero leaving the last two terms to represent the subsequent motion. It is seen that the damping ratio is given by

$$\zeta = a/\omega$$

The parameter a can be found by equating the left hand sides of equations (4.36) and (4.37)

$$\tau s^3 + s^2 + s(k+\omega^2\tau) + \omega^2 = \tau s^3 + s^2(2a\tau+\alpha) + s(\Omega^2\tau + 2a\alpha) + \Omega^2\alpha$$

where $\Omega^2 = a^2+b^2$

Equating coefficients of s^n

$$2a\tau + \alpha = 1$$

$$\Omega^2\tau + 2a\alpha = \tau\omega^2 + k$$

$$\Omega^2\alpha = \omega^2$$

substituting $\alpha = (1-2a\tau)^2$ and $\Omega^2 = \frac{\omega^2}{1-2a\tau}$ into the second equation yields

$$2a\tau(1-2a\tau)^2 = k\tau(1-2a\tau) - 2a\tau(\omega\tau)^2 \tag{4.39}$$

But $\omega = \frac{2\pi}{T}$ where T is the natural system period. If R is defined $\frac{\tau}{T}$, (4.39) can be rearranged to give

$$R^2 = \frac{k\tau(1-2a\tau) - 2a\tau(1-2a\tau)^2}{8\pi^2 a\tau} \tag{4.40}$$

Referring back to equation (4.28) the damping ratio of the continuous system is

$$\zeta = k/2\omega$$

The ratio of the damping ratios, delayed system over continuous non-delayed system, is

$$K = \frac{a}{\omega}\Big/\frac{k}{2\omega} = \frac{2a}{k} = \frac{2a\tau}{k\tau}$$

substituting this into (4.40) leads to

$$R^2 = \frac{1}{4\pi^2}\left(\frac{1}{K}(1-2a\tau) - (1-2a\tau)^2\right)$$

$$K = (1-2a\tau)/\left[4\pi^2R^2 - (1-2a\tau)^2\right] \qquad (4.41)$$

Now $a\tau$ will be a very small number in all practical applications. If $a\tau \ll 1$

$$K \sim 1/(1+4\pi^2R^2) \qquad (4.42)$$

This expression relates the ratio of the damping, delayed system to ideal system, to R which is the ratio of first order lag time constant to the natural oscillation period. It is shown plotted in Figure 4-9. For small lag time constants, say $\tau < .05T$, the delayed system can still achieve 90 percent or more of the ideal system. But the situation rapidly deteriorates; when $\tau = .5T$ only about 10 percent effectiveness remains.

Maneuver

Proportional control will allow maneuvering torques to be tailored to suit slew laws which can minimize structural oscillations. This may be important if the maneuver involves tracking some target. It may be of no consequence if the maneuver is simply a prelude to thrust application and there are no time constraints.

As an example of the reduction in oscillation amplitude attainable the response to a step and a ramp torque can be compared. For a system with very low damping the equation of motion can be approximated:

$$(s^2+\omega^2)\bar{\theta} = \bar{T}$$

For a step torque

$$\bar{\theta} = \frac{T}{s(s^2+\omega^2)}$$

$$\theta(t) = \frac{T}{\omega^2}(1-\cos\omega t)$$

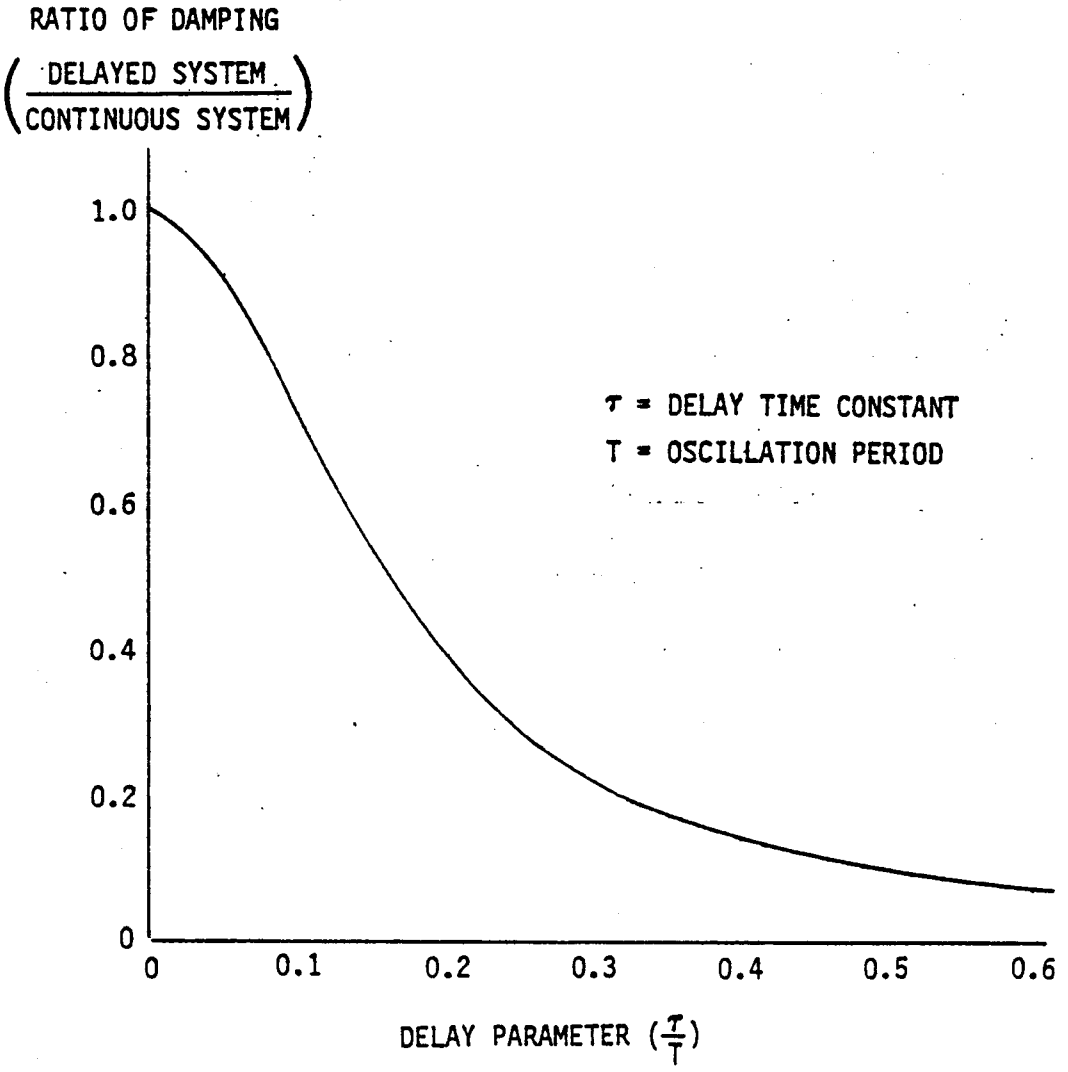

Figure 4- 9 EFFECT OF TIME DELAY ON DAMPING

For a ramp torque

$$\bar{\theta} = \frac{T}{s^2(s^2+\omega^2)}$$

$$\theta(t) = \frac{T}{\omega^2}\left(t - \frac{1}{\omega}\sin\omega t\right)$$

The ramp response has only $\frac{1}{\omega}$ the amplitude of the step response.

A thrust limited system means only that a step torque corresponding to the limiting thrust must be accommodated. The effects are minor. Similarly a delayed response will be unimportant unless the maneuver is related to accurate tracking.

Desaturation and Stationkeeping

These functions are usually not demanding. The impulse delivered is the important consideration and the time and rate of delivery are generally secondary. This being the case the advantage of an amplitude modulated APS is the ability to minimize structural oscillations. The comments under maneuver are applicable.

4.1.2 Pulse Modulated Control

Pulse width modulation will be the most likely pulse mode suitable for APS. In this method thrusts are turned on and off for various times but the thrust level, when on, is essentially constant. The impulse delivered to the system is determined by the on time and is controlled by varying this time. The effective thrust and impulse values are the constant thrust on values multiplied by the duty cycle, defined as the ratio of on time to total time.

When external torques are low the duty cycle becomes low. Better accuracy is obtained by frequent small pulses than infrequent larger pulses. As the torque gets smaller, the on times decrease and eventually a limit, called the minimum impulse bit, is reached. This is determined by physical APS characteristics such as valve actuation time, propellant metering, warm-up times, etc.

A consequence of on-off control is the phenomenon of limit cycling. In a zero disturbance situation position control is maintained by firing thrusts

of alternate sign. This causes a continual oscillation back and forth across the zero position error point. A plot of position against time is shown in Figure 4-10(a). A more convenient representation, especially for analysis, is the phase plane, Figure 4-10(b), which shows θ vs $\dot{\theta}$. The system oscillates between limits $\pm \theta_d$ which define a deadzone. The width of the limit cycle may or may not be symmetrical about the θ axis.

Considering one axis only, and assuming the limit cycle is symmetrical, the angular momentum of the vehicle as it coasts across AB, Figure 4-10(b), is

$$H_{AB} = I\dot{\theta}_d$$

Following the pulse, at C, the angular momentum is

$$H_{CD} = -I\dot{\theta}_d$$

The change is then $2I\dot{\theta}_d$ which must equal the impulse

$$\Delta H = 2I\dot{\theta}_d = Fe\tau$$

or

$$\dot{\theta}_d = Fe\tau/2I \tag{4.43}$$

where F is the thrust
τ the on time, and
e the moment arm

The propellant consumed in going from B to C is

$$W = \frac{F\tau}{I_{sp}}$$

and since there are two such burns in each cycle, the consumption is

$$2W = \frac{2F\tau}{I_{sp}} \quad \text{per cycle.} \tag{4.44}$$

To find the limit cycle period the coast times are necessary. The time to travel from C to D is

$$T_{CD} = \frac{2\theta_d}{\dot{\theta}_d}$$

thus the total limit cycle period is

$$T = 2\tau + T_{CD} + T_{AB}$$

$$= 2\left(\tau + \frac{2\theta_d}{\dot{\theta}_d}\right)$$

$$= 2\left(\frac{4\theta_d I}{Fe\tau} + \tau\right)$$

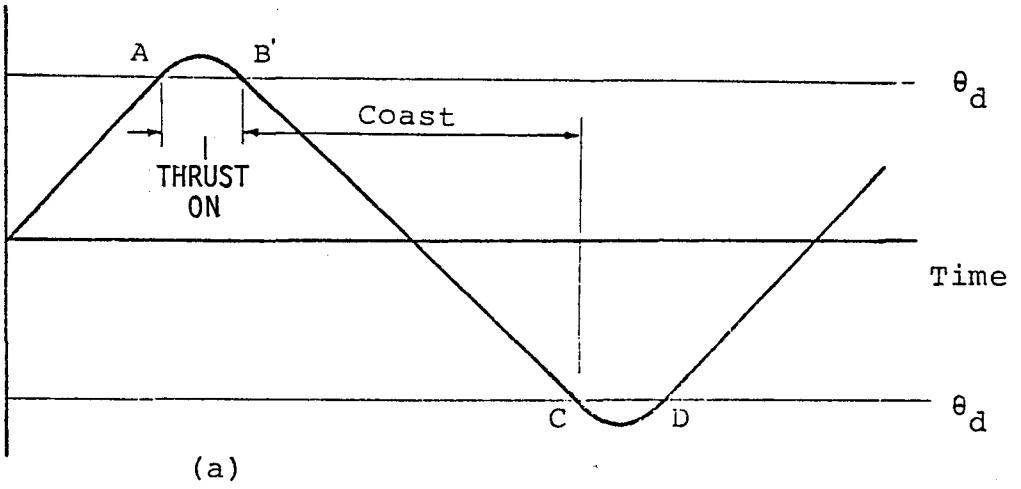

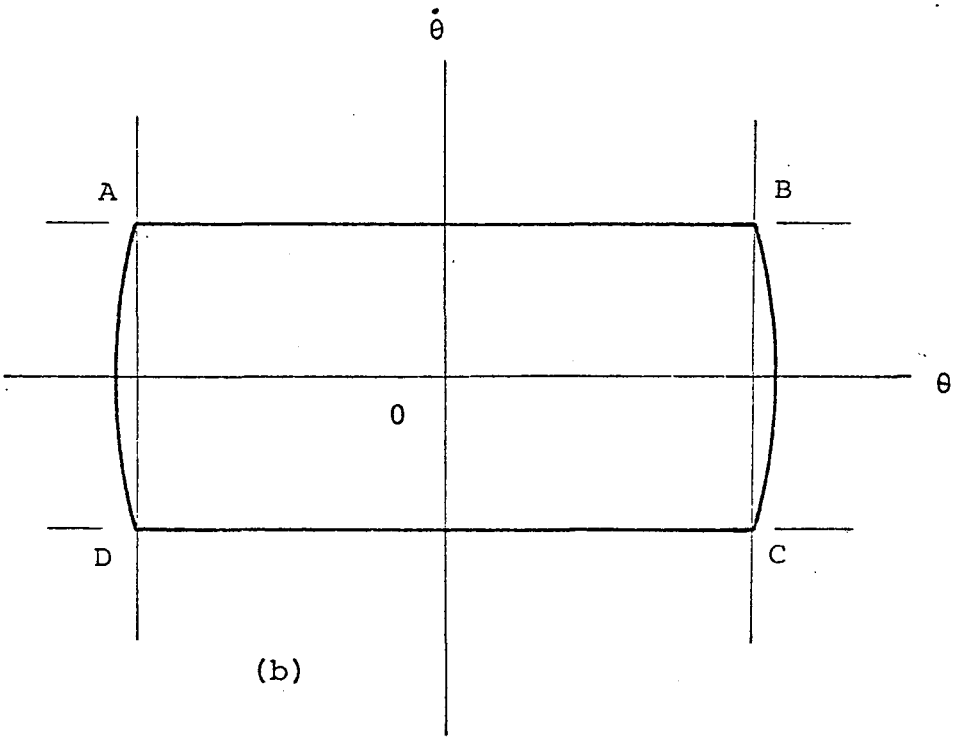

FIGURE 4-10 LIMIT CYCLE TRAJECTORIES

In general, the coast time T_{AB} or T_{CD} is very long compared to the burn time, τ. When this is the case

$$T \sim \frac{8I\theta_d}{F e \tau} \tag{4.45}$$

and the duty cycle; i.e., the ratio of on time to off time is

$$DC = 2\tau/T$$
$$= F e \tau^2 / 4 I \theta_d \tag{4.46}$$

The mean rate of propellant consumption is then

$$\dot{w} = DC \frac{F}{I_{sp}} = \frac{(F\tau)^2 e}{4\theta_d I I_{sp}}$$

or, using equation (4.43)

$$\dot{w} = \frac{I\dot{\theta}_d^2}{e\theta_d I_{sp}} \tag{4.47}$$

It is seen that propellant consumption is proportional to the impulse bit, $F\tau$, squared and inversely proportional to the width of the deadzone. There is thus considerable incentive to keep the impulse bit as small as possible.

If $\left(\frac{F\tau}{I_{sp}}\right)^2$ is denoted P, the propellant consumed can be expressed

$$\frac{W}{P} = \frac{et}{4\theta I}$$

Figure 4-11 shows W/P as a function of the scaling parameter for three pointing accuracies. A flat plate structure and 10 year lifetime were assumed.

4.1.2.1 System Implementation

In order to produce a limit cycle some means of turning the thrust on at points B and D of Figure 4-10(b) must be devised. This is achieved by using rate and position sensors and a relay or switching amplifier. A block diagram of a general system is shown in Figure 4-12. For the time being the sensors will be assumed ideal and the relay to have a simple deadzone as shown in Figure 4-13.

The signal going to the relay is

$$\epsilon = K_1\theta + K_2\dot{\theta}$$

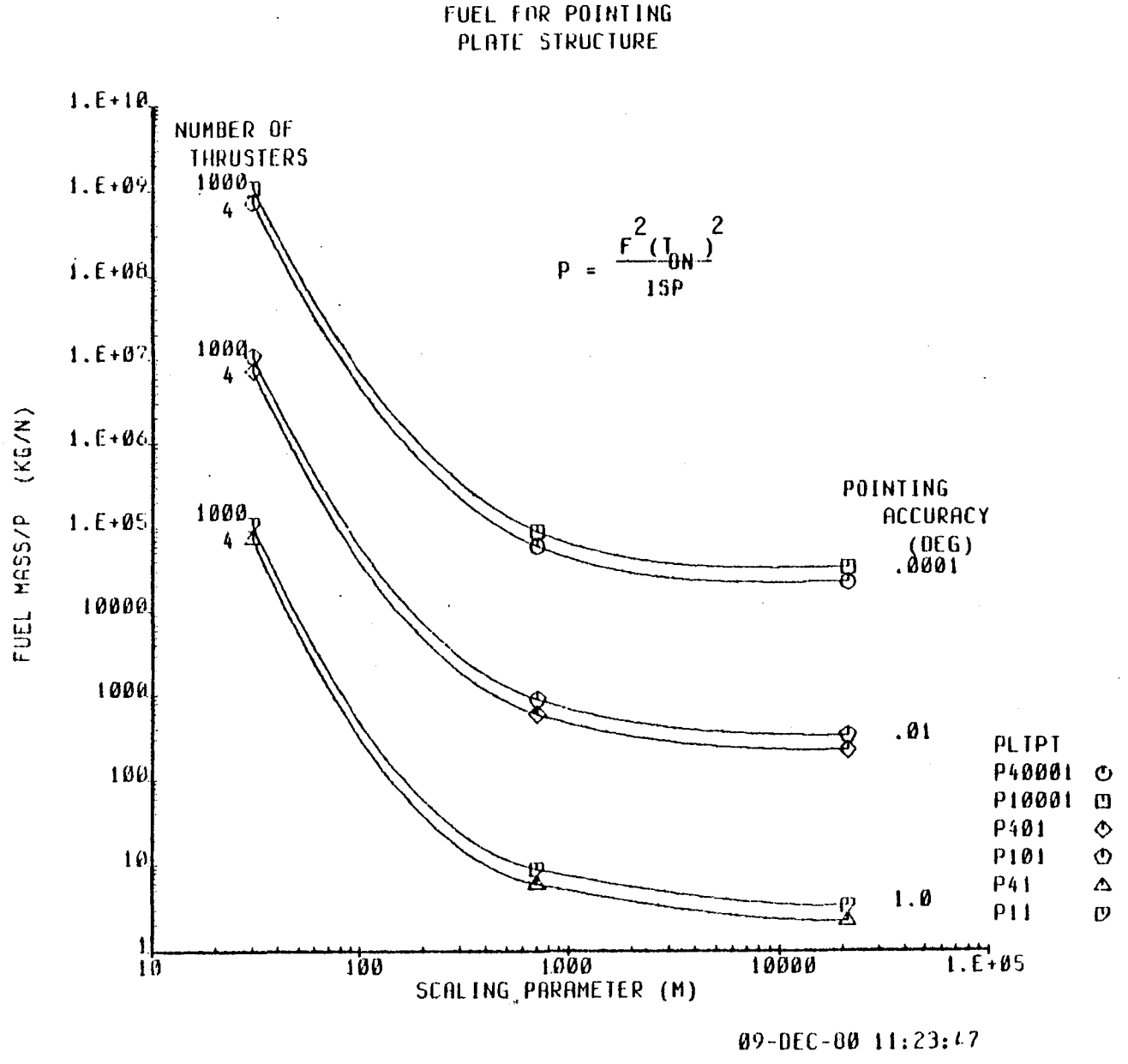

FIGURE 4-11 FUEL FOR POINTING PLATE STRUCTURE

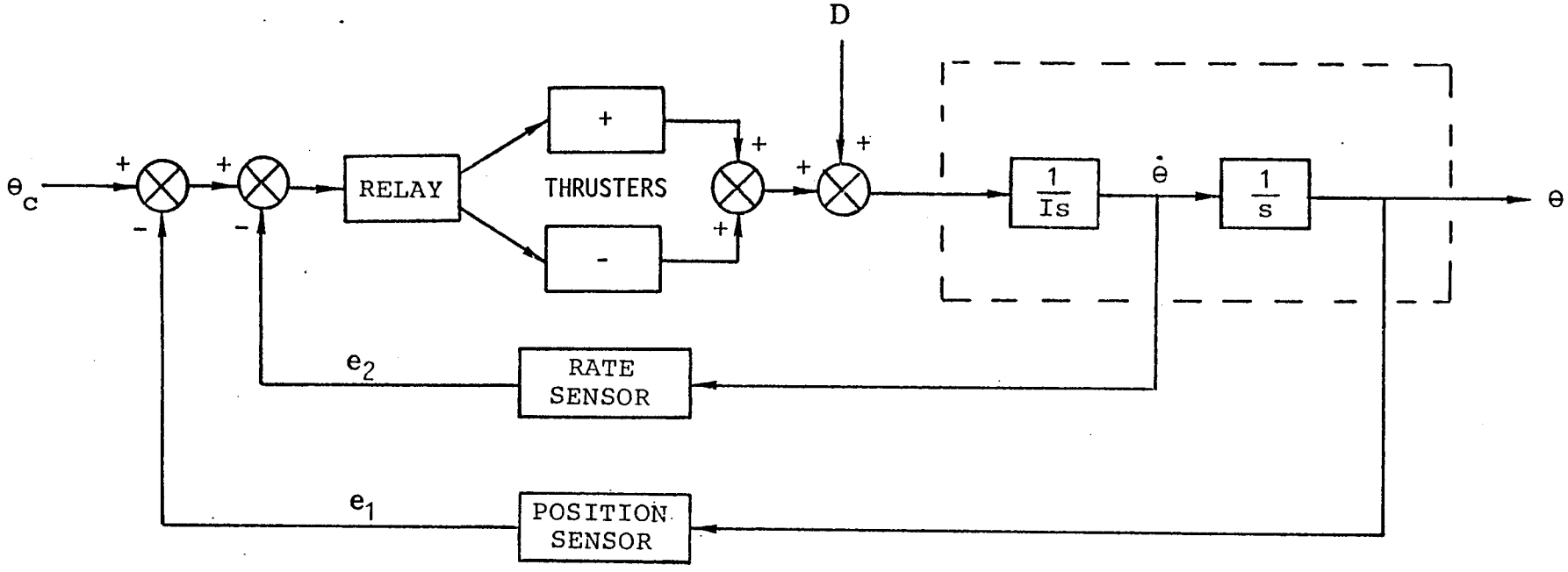

FIGURE 4-12 ON-OFF SYSTEM BLOCK DIAGRAM

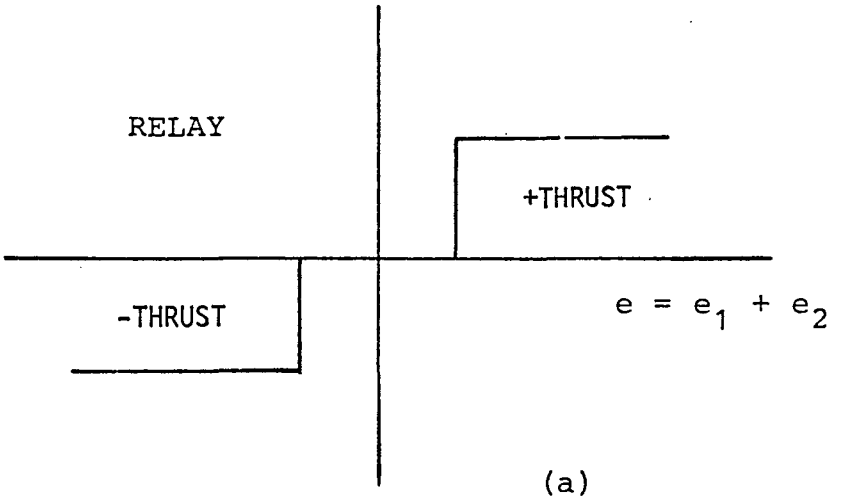

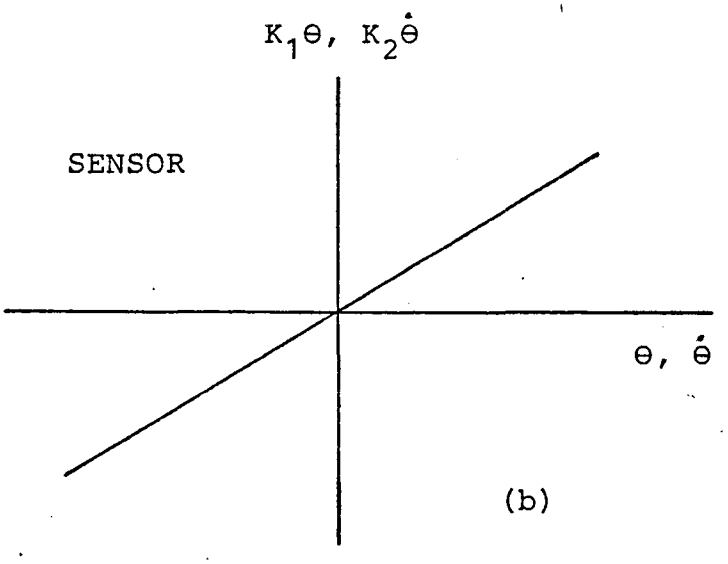

FIGURE 4-13 RELAY AND SENSOR CHARACTERISTICS

thus the minus thrust, defined as the thrust that produces a torque in a direction to decrease θ, will be switched on when

$$K_1\theta + K_2\dot{\theta} \geq \delta \tag{4.48}$$

Similarly, the plus thrust will be turned on when

$$K_1\theta + K_2\dot{\theta} \leq -\delta \tag{4:49}$$

and both thrusts will be zero in the range

$$-\delta < K_1\theta + K_2\dot{\theta} < \delta \tag{4.50}$$

Expressions (4.49) and (4.50) can be represented on the phase plane as two lines, Figure 4-14, known as switchlines. These divide the phase plane into three regions - a central band where no thrust is applied, the plus thrust region to the left of the central band and a minus thrust region to the right.

In the phase plane, when no torques are acting, the coast trajectories are straight lines. With torque, trajectory arcs are given by

$$I\ddot{\theta} = D \pm Fe$$

which integrates to give

$$\theta = \theta_0 + \dot{\theta}_0 t + \left(\frac{D \pm Fe}{I}\right)\frac{t^2}{2} \tag{4.51}$$

More conveniently for phase plane work

$$I\ddot{\theta} = I\dot{\theta}\frac{d\dot{\theta}}{d\theta} = D \pm Fe$$

leading to

$$\left(\dot{\theta}^2 - \dot{\theta}_0^2\right) = 2(D \pm Fe)(\theta - \theta_0) \tag{4.52}$$

This is the equation of a parabola, concave to the left for negative net torques and concave to the right for positive net torques.

Figures 4-15(a) and (b) show convergence of the system, in different ways, to a limit cycle about the origin. The convergence is a consequence of the negative slope of the switchlines introduced by the K_2 term in the error signal.

4.1.2.2 Transient Effects

There are a variety of imperfections in real life systems which can alter the form of the switchlines and modify limit cycle characteristics. Some of these nonlinearities and their effects will be examined in this section.

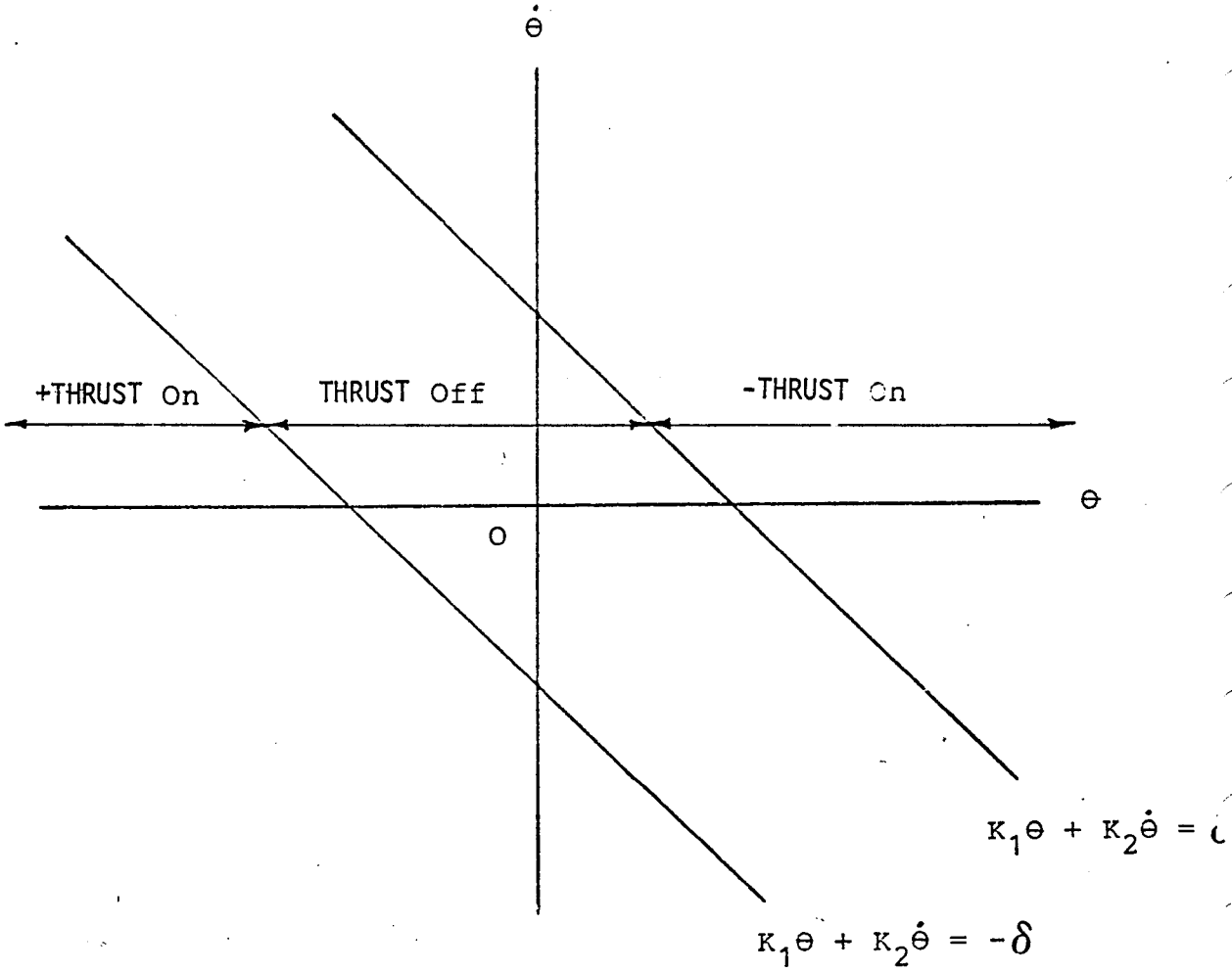

FIGURE 4-14 SWITCHLINES IN THE PHASE PLANE

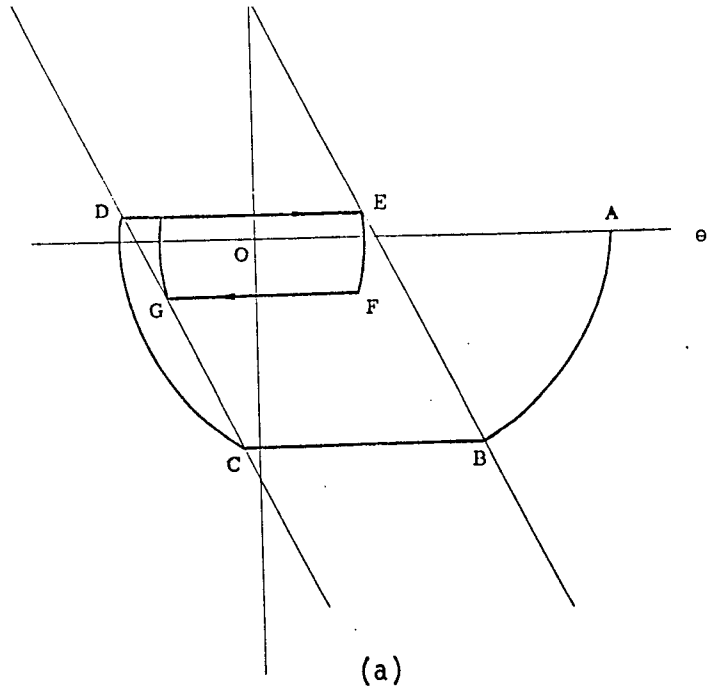

(a)

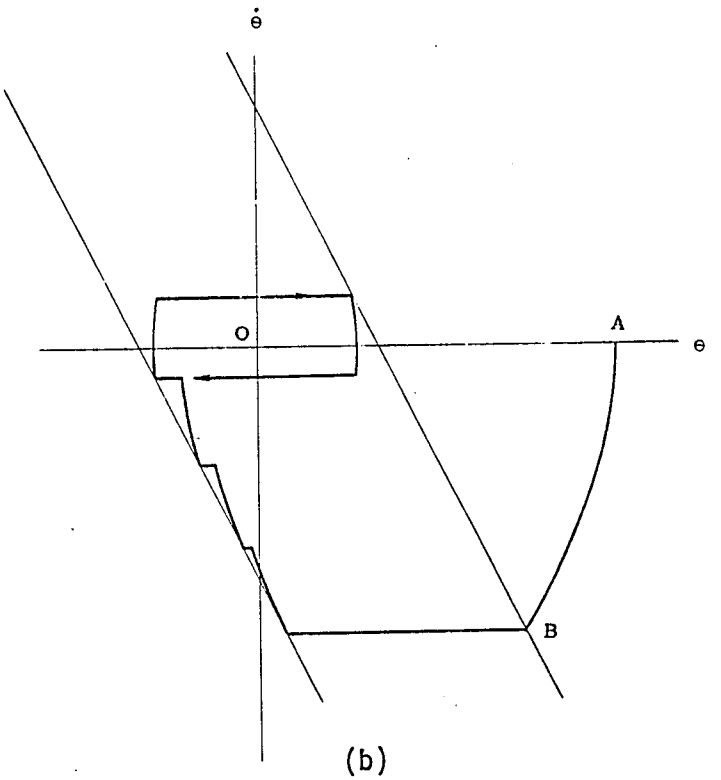

(b)

FIGURE 4-15 CONVERGENCE TO LIMIT CYCLE

The jet on pulse has to this point been assumed rectangular. In fact there will be rise and decay transients and the pulse is more likely to take the form shown in Figure 4-16. Perhaps surprisingly the rectangular approximation very closely matches the effect of a true pulse. The rise and decay simply round out the corners that are sharp in an idealized trajectory but have little effect on performance. There is a second effect that requires consideration however. If the thrust starts at B and the rectangular approximation (having the same area) starts at C there is a delay $t_C - t_B$. In fact thrust initiation at B was most likely delayed a short time after the on signal was generated at A. This type of delay can be caused by valve opening time, fuel line capacitance, warm up or ignition delays. The time $t_C - t_A$ can be used to combine the various contributions into one effective on delay, t_o. Similarly, if point D represents the time an off signal is generated and E the end of the rectangular approximation, $t_E - t_D$ can be taken as an effective off delay, t_f.

An on delay modifies the phase plane switchline by changing its slope. The jet on line occurs at $\Delta\theta = \dot{\theta} t_o$ beyond the signal on line as shown in Figure 4-17(a). The off delay is somewhat similar with the thrust off line being constructed by continuing trajectories past the signal off lines the distance travelled in time t_f, Figure 4-17(b).

In some cases it is possible to compensate for on and off delays by repositioning the switchlines so that the thrust comes on and goes off when required. This process requires moving the switchlines closer to the origin, that is, reducing the value of δ in equation (4.50) and modifying the gains K_1 and K_2. It is only possible if δ can be reduced. If δ is already at a minimum set by system parameters the on delay will tend to cause a degradation in accuracy and the off delay will increase propellant consumption. This is seen from equation (4.47)

$$\dot{w} = I\dot{\theta}_d^2 / e\theta_d I_{sp}$$

The on delay increases θ_d, the width of the deadzone. This actually reduces propellant consumption but usually the savings will be more than cancelled by the effective increase in $\dot{\theta}_d$ caused by the off delay.

The off delay problem can be avoided if the system is arranged to fire a minimum impulse bit when the on line is crossed and the rates are low.

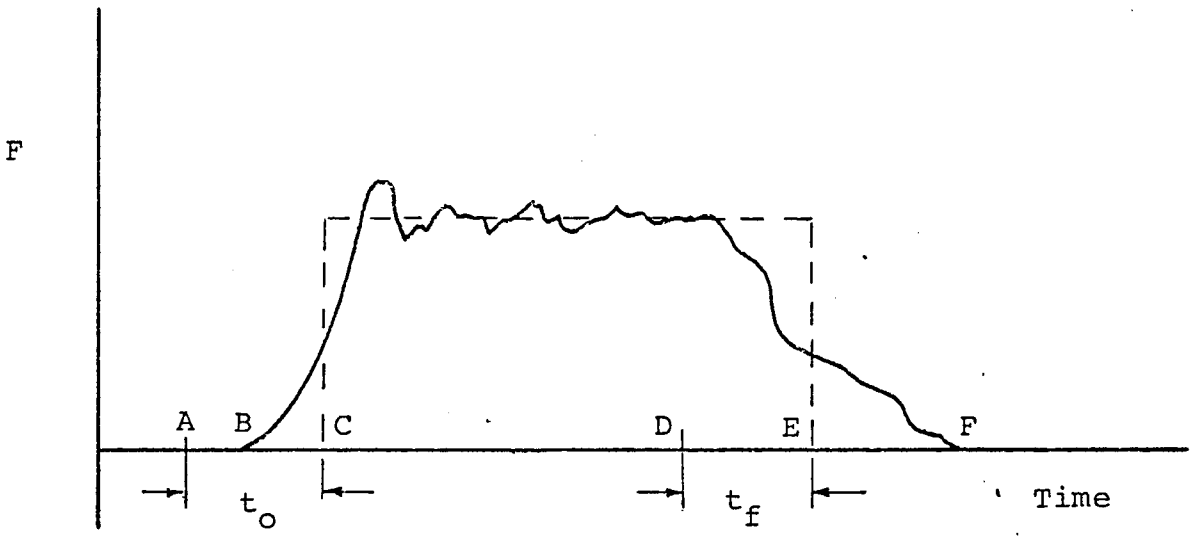

FIGURE 4-16 PULSE APPROXIMATIONS

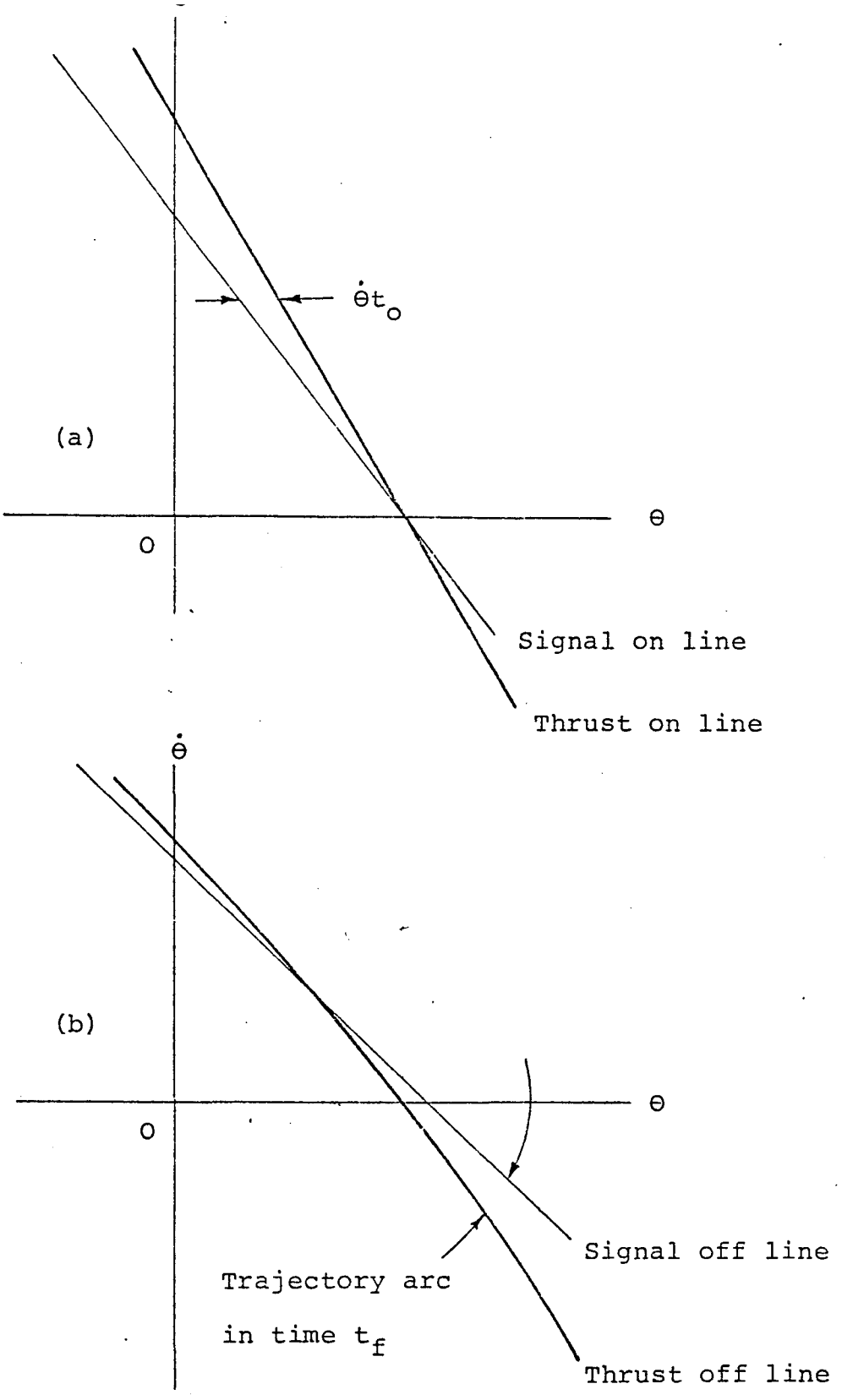

FIGURE 4-17 EFFECT OF TIME DELAYS ON SWITCHLINES

This avoids the need for an off line in the terminal limit cycle but requires additional system logic to implement.

4.1.2.3 Performance

The terminal limit cycles reached by the system with ideal sensors and a relay with deadzone are typically asymmetric. If the deadzone is traversed on one side, for example FG in Figure 4-15(a), at a rate R times the symmetric rate, $\dot{\theta}_s$, the time to cross is closely approximated by

$$T_{FG} = \frac{2\theta_d}{R\dot{\theta}_s}$$

and

$$T_{HE} = \frac{2\theta_d}{\dot{\theta}_s(2-R)}$$

The duty cycle is then

$$DC = \frac{2\tau}{T} = \frac{2\tau}{T_{FG} + T_{HE} + 2\tau}$$

$$\sim \frac{\tau\dot{\theta}_s R(2-R)}{2\theta_d} = \frac{F\tau^2}{4I\theta_d} R(2-R) \qquad (4.53)$$

$$\dot{w} = \frac{(F\tau)^2 e}{4\theta_d I I_{sp}} R(2-R) \qquad (4.54)$$

These are the symmetric duty cycle values factored by R(2 - R). The factor is shown plotted in Figure 4-18. The asymmetric cycle thus uses less propellant but since the asymmetric cycle rate is random the savings cannot be predicted except on a probability basis.

The limit cycle deadzone, θ_d, achieved by the relay deadzone of δ, is

$$\theta_d = \frac{\delta}{K_1} = \frac{K_2 F e \tau}{2IK_1} \qquad (4.55)$$

Pointing

When disturbance torques are present limit cycle trajectories are modified primarily because the thrust off trajectory arcs become parabolas rather than straight horizontal lines.

If the disturbance torque is positive and the minus thrust is used to counter the disturbance the limit cycle trajectory takes the form shown in Figure 4-19(a). The dotted lines represent the response to a larger torque

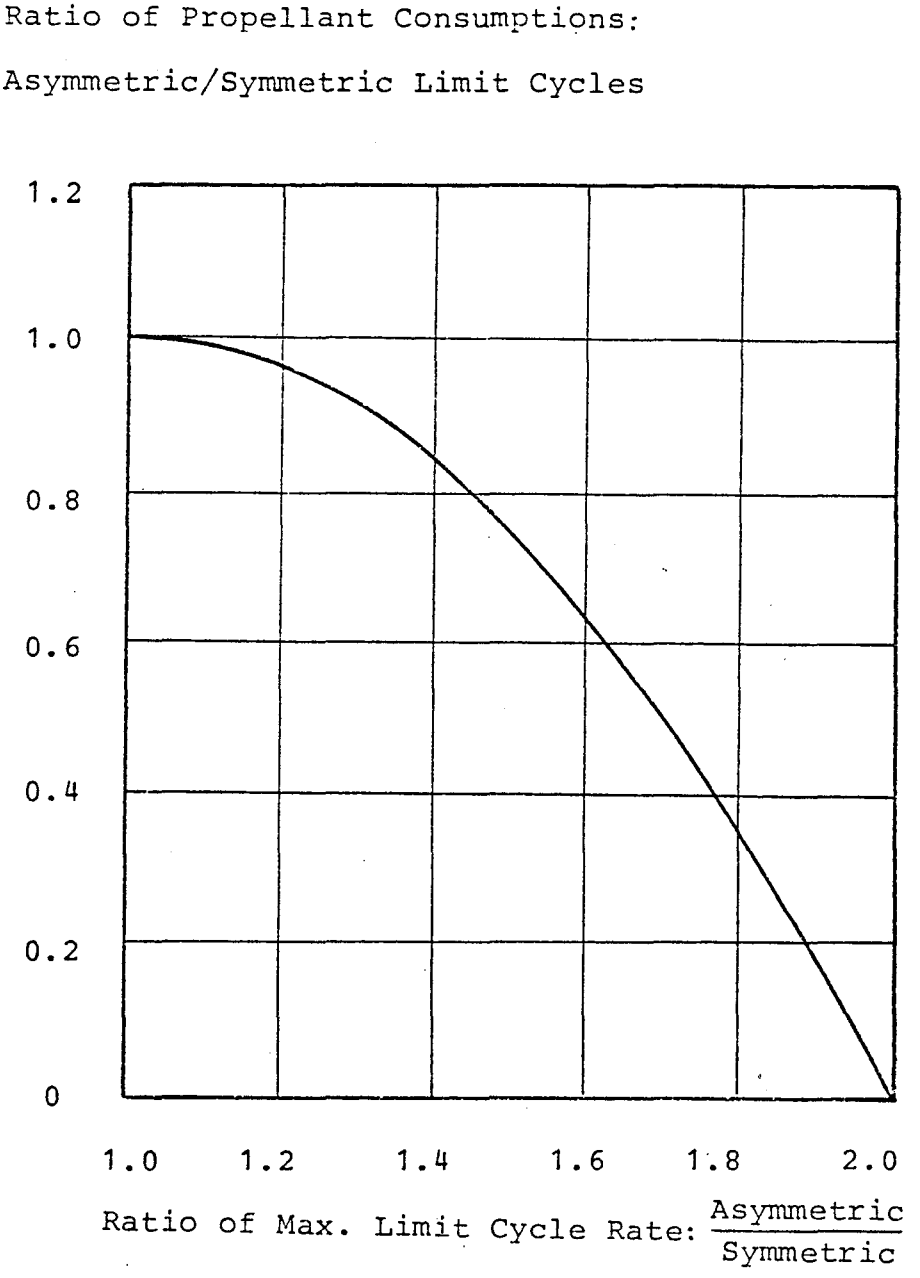

FIGURE 4-18 PROPELLANT CONSUMPTION IN ASYMMETRIC LIMIT CYCLES

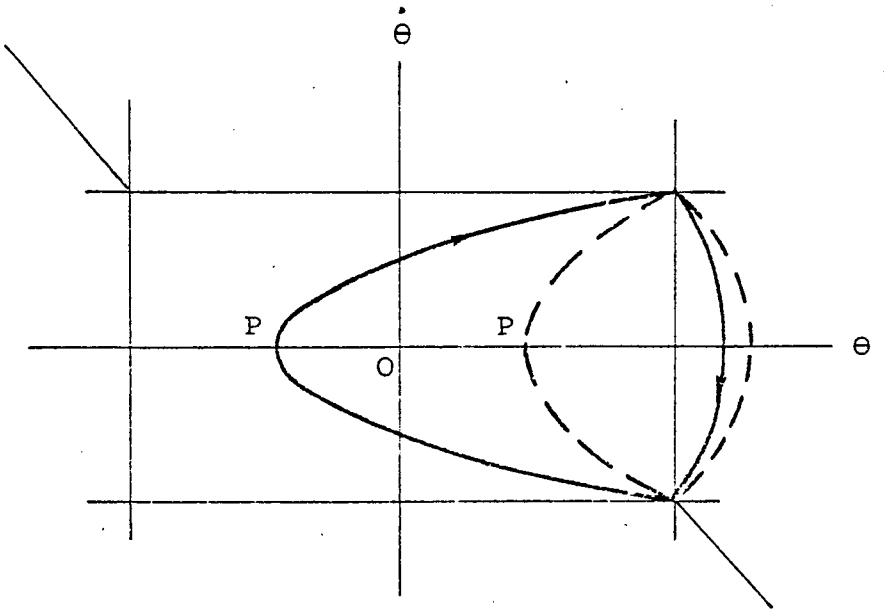

(a)

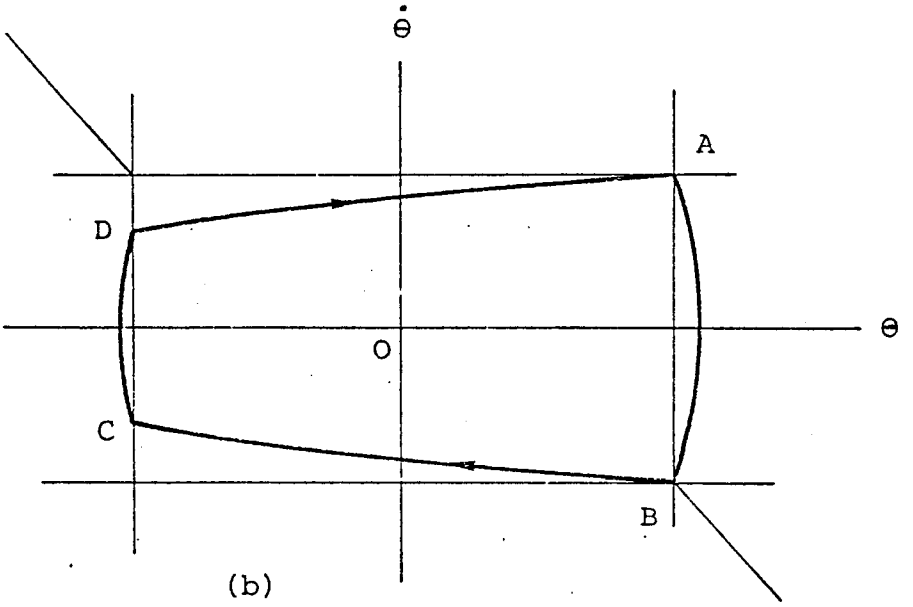

(b)

FIGURE 4-19 ONE AND TWO PULSE LIMIT CYCLES

than the solid lines. If D increases in magnitude the point P, where the trajectory crosses the axis inside the deadzone, will move to the right. Conversely as D gets smaller P will move to the left. At some level P will meet the left hand boundary of the deadzone. When this occurs the limit cycle will change from a one pulse cycle to a two pulse cycle which will adjust itself to take up the symmetrical shape shown in Figure 4-19(b).

To evaluate the performance in one and two pulse cycles consider the deadzone to be $2\theta_d$ by $2\dot{\theta}_d$ in size. Using equation (4.52) the trajectory inside the deadzone is

$$I(\dot{\theta}^2-\dot{\theta}_d^2) = 2D(\theta-\theta_d) \tag{4.56}$$

For the one pulse cycle the point P is given by setting $\dot{\theta} = 0$; i.e.,

$$-I\dot{\theta}_d^2 = 2D(\theta_p-\theta_d)$$

$$\theta_p = \theta_d - I\dot{\theta}_d^2/2D$$

In order to remain a one pulse cycle $\theta_p > -\theta_d$, that is provided

$$\theta_d - I\dot{\theta}_d^2/2D > -\theta_d$$

$$D > I\dot{\theta}_d^2/4\theta_d \tag{4.57}$$

This is the condition for a one pulse cycle.

The time on, from A to B is $\tau = -2\dot{\theta}_d/(D-Fe)$

while the time off, from B through P to A is

$$T_{AB} = 2\dot{\theta}_d/D$$

leading to a limit cycle period

$$T = T_{AB} + \tau = \frac{2\dot{\theta}_d}{Fe-D} + \frac{2\dot{\theta}_d}{D}$$

$$T = \frac{2\dot{\theta}_d + Fe}{Fe-D} \tag{4 58}$$

The mean propellant consumption is

$$\dot{W} = \frac{F\tau}{TI_{sp}} = \frac{D}{eI_{sp}} \tag{4.59}$$

Notice that the mean torque applied is $Fe\tau/T$, exactly equal to the disturbance torque. The one pulse cycle is thus very efficient and all the propellant used goes into countering the disturbance.

In the two pulse cycle, point C in Figure 4-19(b) is found by setting $\theta = \theta_d$ in (4.56)

$$I(\dot\theta_c^2 - \dot\theta_d^2) = -4D\theta_d$$

$$\dot\theta_c^2 = \dot\theta_d^2 - 4D\theta_d/I$$

The thrust on and off times are

$$\bar T_{AB} = 2\dot\theta_d/(Fe-D)$$

$$\bar T_{CD} = 2\dot\theta_d/(Fe+D)$$

$$\bar T_{BC} = \bar T_{DA} = (\dot\theta_d - \dot\theta_c)/D$$

The total on time is then

$$\bar T_{ON} = \frac{2\dot\theta_c}{Fe+D} + \frac{2\dot\theta_d}{Fe-D}$$

and the total off time

$$\bar T_{OFF} = \frac{2}{D}(\dot\theta_d - \dot\theta_c)$$

The limit cycle period is then

$$\bar T = \frac{2\dot\theta_c}{Fe+D} + \frac{2\dot\theta_d}{Fe-D} + \frac{2}{D}(\dot\theta_d - \dot\theta_c)$$

$$\bar T = \frac{2eD}{D(F^2e^2-D^2)}\left[\dot\theta_d(Fe+D) - \dot\theta_c(Fe-D)\right] \qquad (4.60)$$

and the propellant consumption rate

$$\dot w = \frac{F\bar T_{ON}}{\bar T I_{sp}}$$

$$= \frac{D}{eI_{sp}}\left(\frac{\dot\theta_d(Fe+D) + \dot\theta_c(Fe-D)}{\dot\theta_d(Fe+D) - \dot\theta_c(Fe-D)}\right)$$

$$= \frac{D}{eI_{sp}}\left(\frac{\dot\theta_d(1+R) + \dot\theta_c(1-R)}{\dot\theta_d(1+R) - \dot\theta_c(1-R)}\right) \qquad (4.61)$$

where $R = \frac{D}{Fe}$

Suppose now the critical value of D from (4.57) is written D_c

$$D_c = I\dot\theta_d^2/4\theta_d$$

It follows that the zero torque limit cycle propellant consumption from (4.47) is

$$\dot w eI_{sp} = 4D_c \qquad (4.62)$$

When $D = D_c$, the one pulse cycle under constant torque has

$$\dot w eI_{sp} = D \qquad (4.63)$$

and the two pulse cycle has

$$\dot w eI_{sp} = D\left(\frac{1+R + (1-R)\sqrt{1-D/D_c}}{1+R - (1-R)\sqrt{1-D/D_c}}\right) \qquad (4.64)$$

when R is small (4.40) can be approximated by

$$\dot{w}_e I_{sp} \sim D\left(\frac{1+\sqrt{1-D/D_c}}{1-\sqrt{1-D/D_c}}\right) \tag{4.65}$$

$\dot{w}_e I_{sp}$ is plotted against D/D_c in Figure 4-20. It is seen that the no torque consumption can be significantly higher than the consumption under a small torque (by a factor of 4 when $D = D_c$).

A pure time delay will increase the width of the deadzone. If there are no disturbance torques

$$\Delta\theta = \tau_D \dot{\theta}_L \tag{4.66}$$

where τ_D is the delay and
$\dot{\theta}_L$ the limit cycle rate

$$\dot{\theta}_L = \frac{\pi}{2I} \quad \text{radians/sec} \tag{4.67}$$

Substituting (4.67) into (4.66)

$$\Delta\theta = \frac{\tau_D \, MIB}{2I} \tag{4.68}$$

where MIB is the minimum impulse bit; i.e., $F\tau_{min}$

$\Delta\theta/MIB$ is shown in Figure 4-21 as a function of the scaling parameter for several time delays.

Shape Control

Shape control using discrete pulses can be achieved by applying a pulse in a direction to oppose the motion once every half cycle. The most effective time to deliver the pulse is when the velocity is a maximum. From (4.25) with F=0

$$q = q_0 \cos\omega t$$

Differentiating $\dot{q} = -\omega q_0 \sin\omega t$

which is maximum at $\omega t = \frac{n}{2}\pi$, n = 1, 2, 3....

At the maximum velocity points the amplitude is zero and the system energy is entirely kinetic. The momentum at such a point is

$$p_0 = m\omega q_0$$

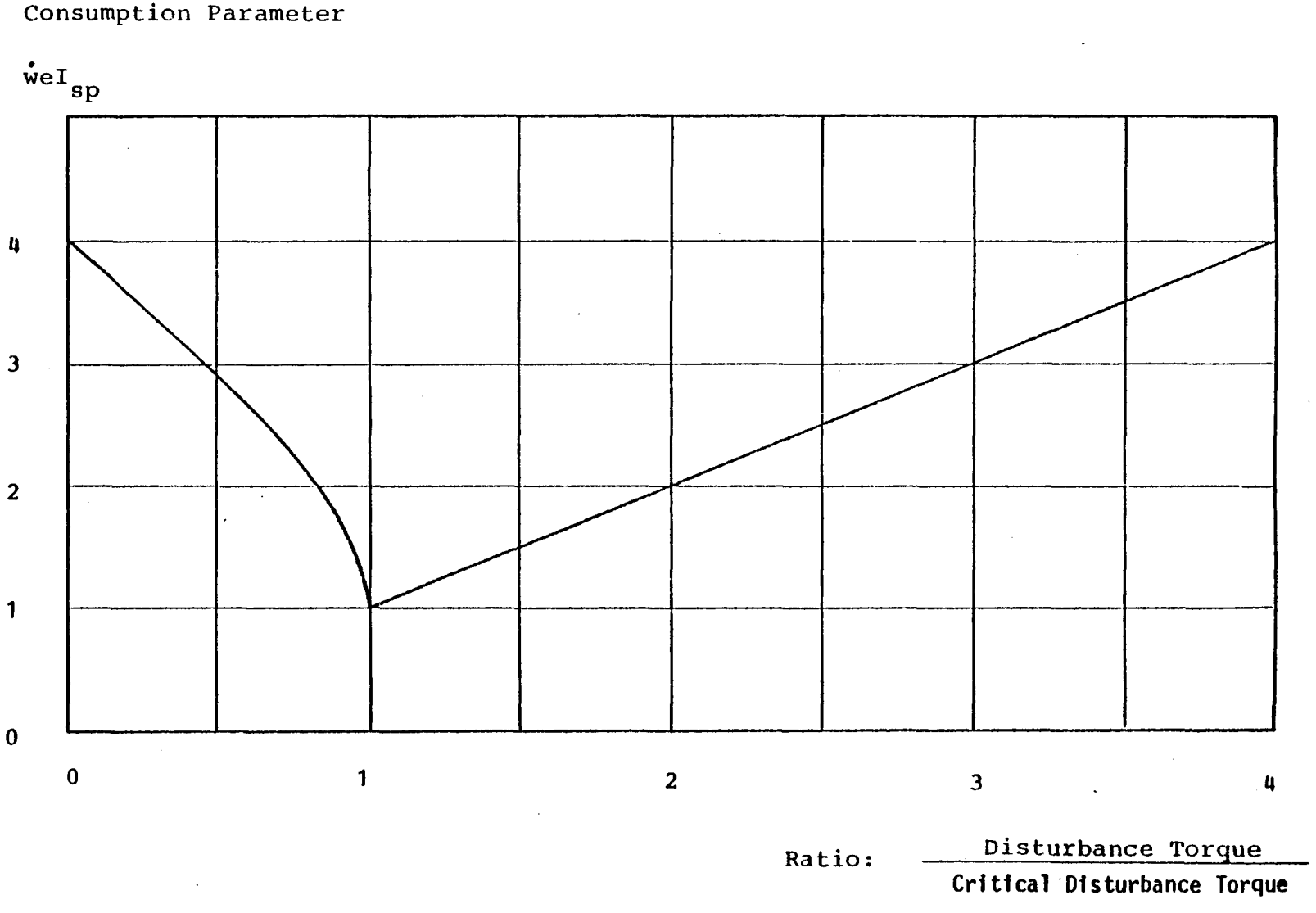

FIGURE 4-20 PROPELLANT CONSUMPTION UNDER SI DISTURBANCE TORQUES

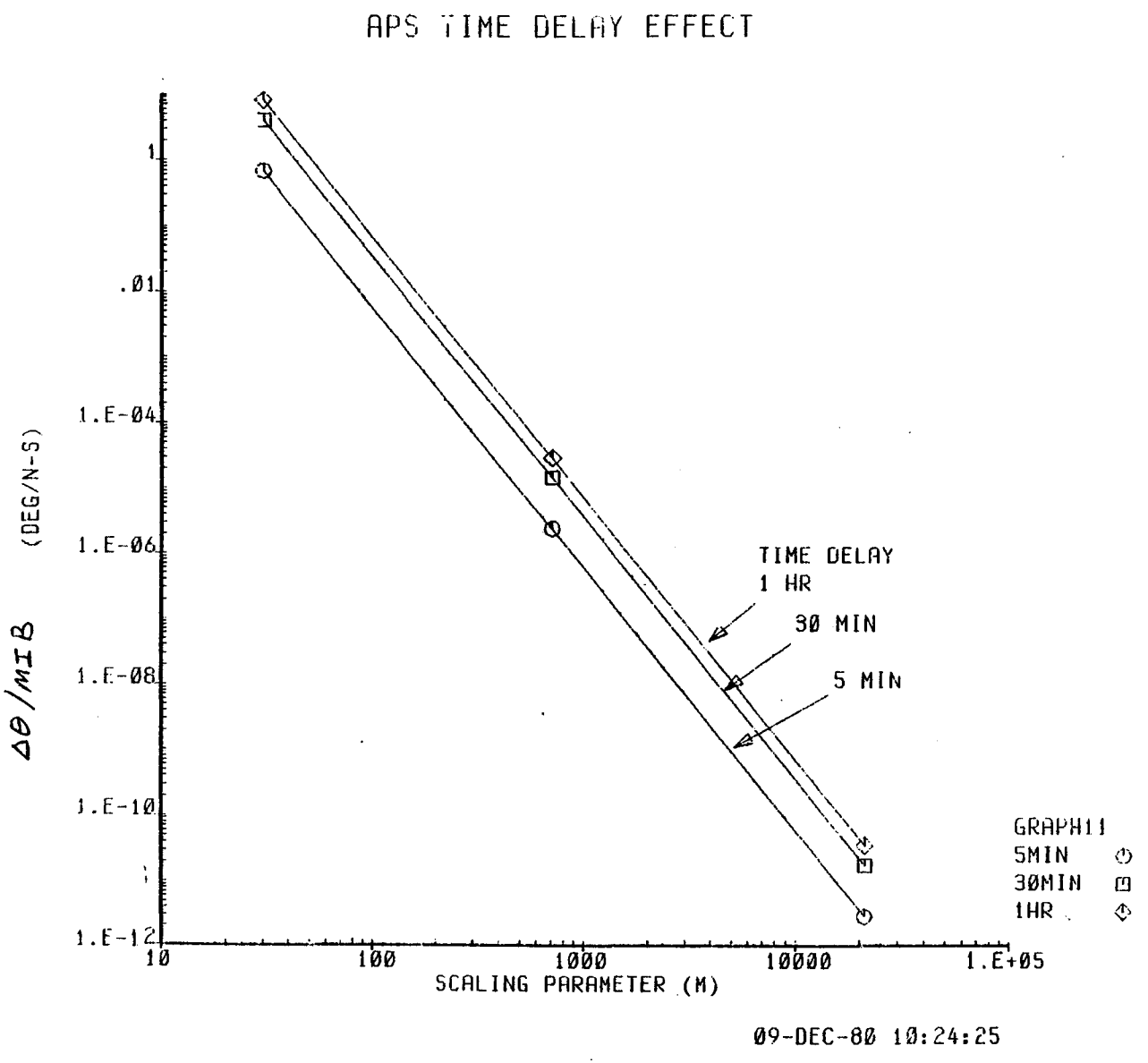

FIGURE 4-21 EFFECT OF APS TIME DELAY ON ACCURACY

Suppose at succeeding points an impulse of $F\tau$ is applied. The momentum after pulse application is

$$p_i = m\omega q_o - iF\tau \tag{4.69}$$

In particular, after one cycle and two pulse applications the momentum is

$$p_2 = m\omega q_o - 2F\tau$$

The corresponding energy is

$$T = \frac{1}{2}m\dot{q}^2 = \frac{1}{2}m\left(\frac{p_2}{m}\right)^2$$
$$= \frac{1}{2}m\left(\frac{m\omega q_o - 2F\tau}{m}\right)^2$$
$$= \frac{m}{2}\left(\omega q_o - \frac{2F\tau}{m}\right)^2 \tag{4.70}$$

This must equal the system strain energy; ie.e,

$$\frac{1}{2}Kq^2 = \frac{m}{2}\left(\omega q_o - \frac{2F\tau}{m}\right)^2 \tag{4.71}$$

Initially $$\frac{1}{2}Kq_o^2 = \frac{1}{2}m\omega^2 q_o^2 \tag{4.72}$$

Dividing (4.71) by (4.72)

Now q/q_o would equal $e^{-\zeta\omega t}$ if the process were continuous instead of discrete. However an approximate effective damping ratio can be found by equating

$$e^{-\zeta\omega t} = \frac{q}{q_o} = 1 - \frac{2F\tau}{m\omega q_o}$$

and taking t to be one cycle; i.e., $t = \frac{2\pi}{\omega}$

$$e^{-2\pi\zeta} \sim 1 - \frac{2F\tau}{m\omega q_o}$$

$$\zeta = \frac{1}{2\pi}\ln\left(\frac{1}{1 - 2F\tau/m\omega q_o}\right) \tag{4.73}$$

ζ as a function of $\frac{2F\tau}{m\omega q_o}$ is shown in Figure 4-22.

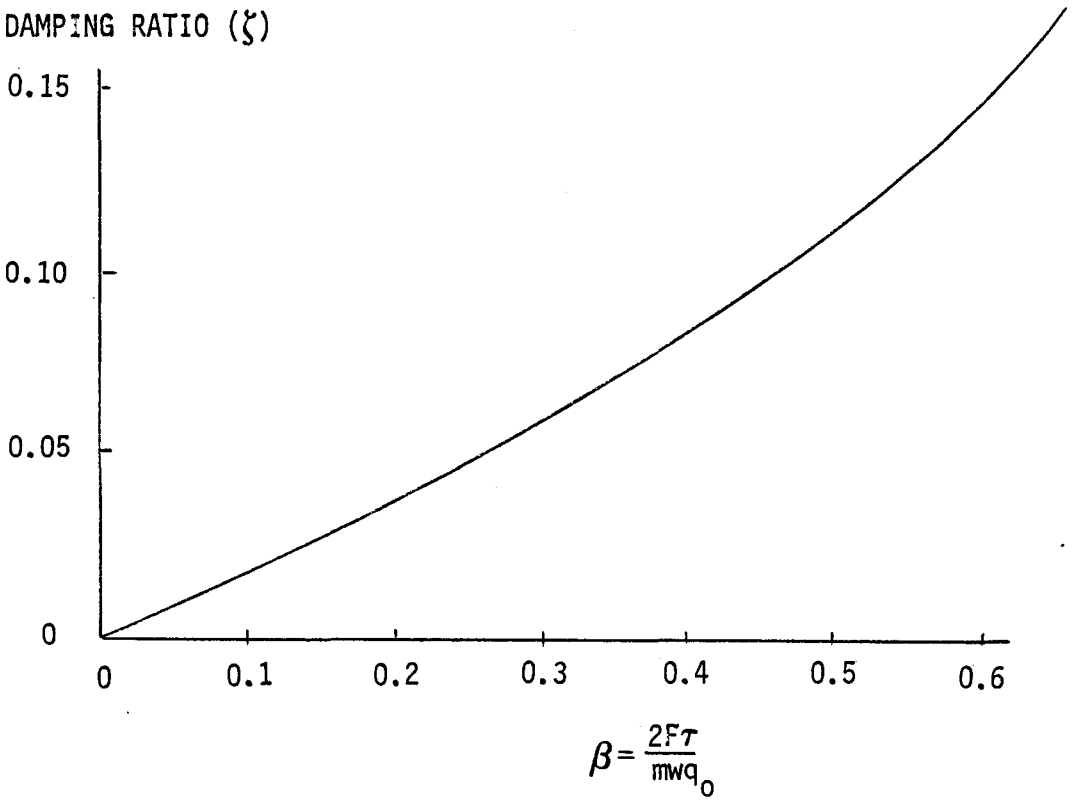

FIGURE 4-22 STRUCTURAL DAMPING WITH PULSE CONTROL

Since $m = \frac{M}{L}$ for the plate structure

$$\zeta = \frac{1}{2\pi} \ln\left(\frac{1}{1 - \frac{2F\tau L}{M\omega q_0}}\right)$$

This is shown in Figures 4-23, 4-24, and 4-25 for a small, medium and large plate structure assuming FE to be the minimum impulse bit.

It is seen that pulse control can be used as well as proportional control to damp structural oscillations. The pulse application must cease however when

$$m\omega\dot{q} \leq F\tau$$

or the pulses will induce an oscillation instead of damping it. The limiting value is found by equating the strain and kinetic energies

$$\frac{1}{2}Kq^2 = \frac{1}{2}m\omega^2 q^2 = \frac{1}{2m}(F\tau)^2$$

$$\frac{Kq^2}{m} = \left(\frac{F\tau}{m}\right)^2$$

But $\frac{K}{m} = \omega^2$ and the minimum amplitude can be expressed

$$q = \frac{F\tau}{m\omega} \tag{4.74}$$

Delayed Thrust

The pulse is ideally applied when $\omega t = \frac{n}{2}\pi$ but if there are on delays the pulse will be late. Suppose it is applied at $t = \frac{n}{2}\pi + \alpha$. The velocity at first pulse application is

$$\dot{q} = \omega q_0 \sin\left(\frac{\pi}{2} + \alpha\right)$$

and the momentum is

$$p = m\omega q_0 \sin\left(\frac{\pi}{2} + \alpha\right)$$

After two pulse applications; i.e., after one cycle

$$p = m\omega q_0 \sin\left(\frac{\pi}{2} + \alpha\right) - 2F\tau$$

and

$$\dot{q} = \omega q_0 \sin\left(\frac{\pi}{2} + \alpha\right) - \frac{2F\tau}{m}$$

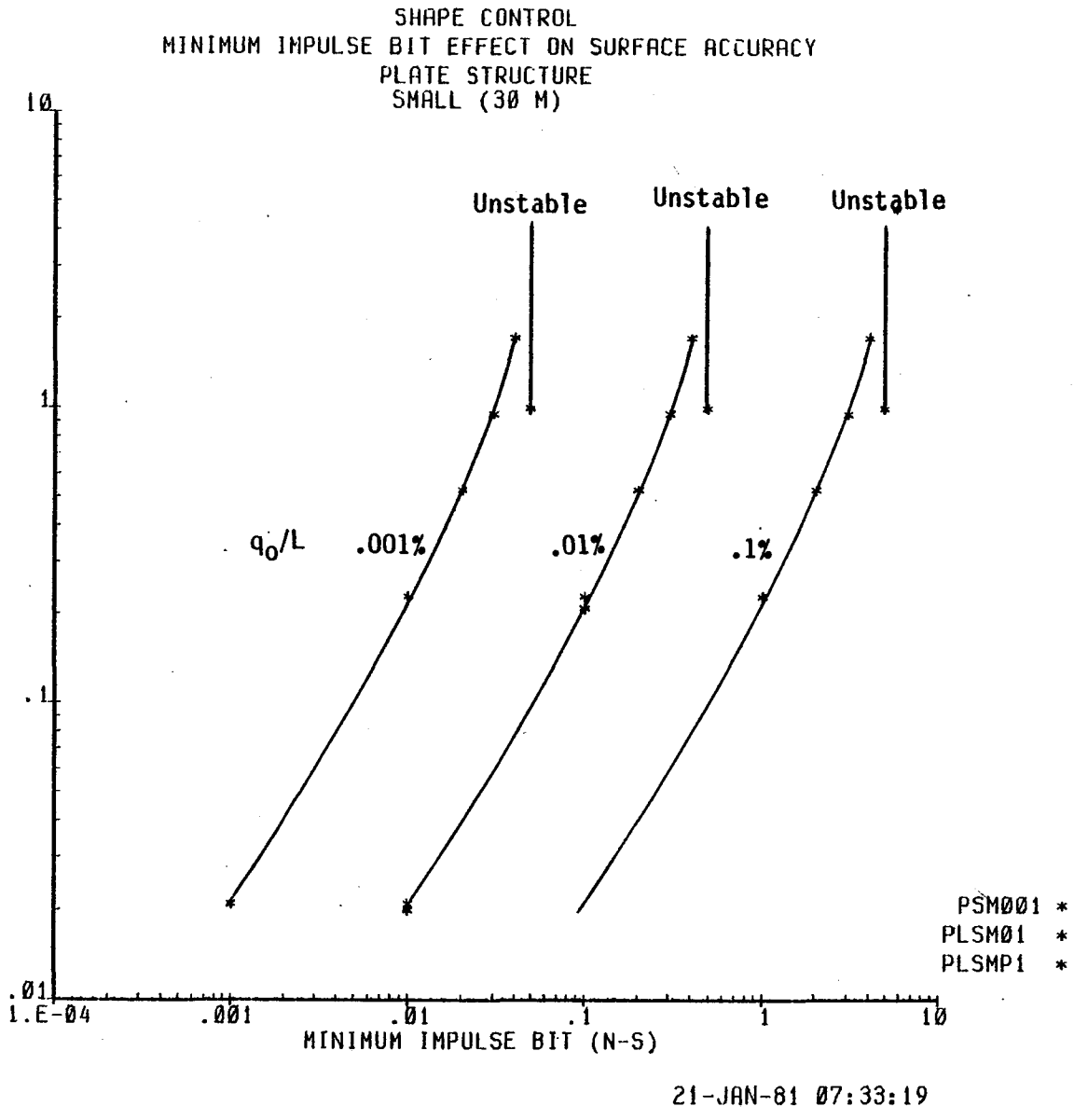

FIGURE 4-23 SHAPE CONTROL ACCURACY, SMALL PLATE STRUCTURE

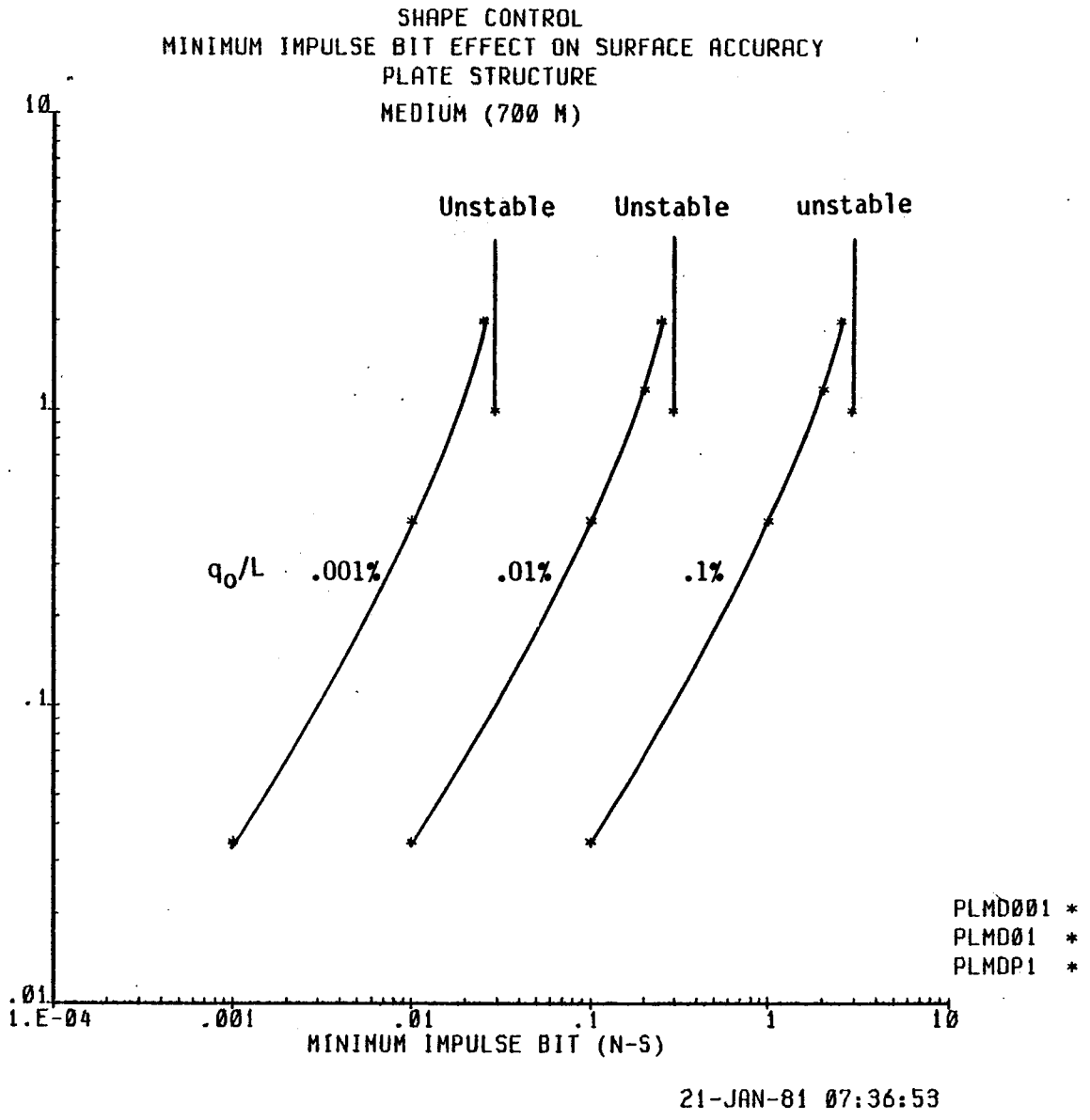

FIGURE 4-24 SHAPE CONTROL ACCURACY, MEDIUM PLATE STRUCTURE

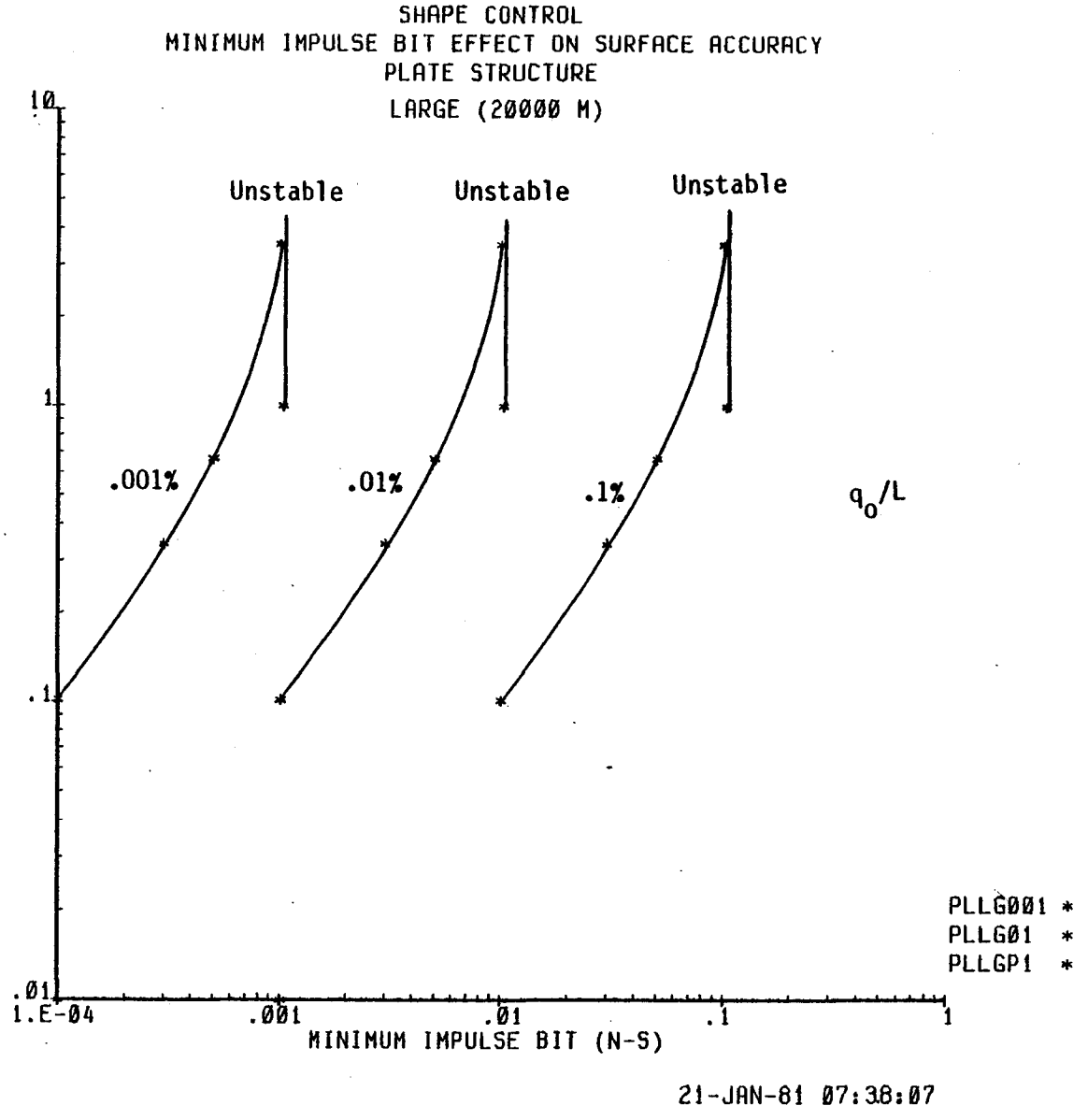

FIGURE 4-25 SHAPE CONTROL ACCURACY, LARGE PLATE STRUCTURE

The kinetic energy at this time is

$$T = \frac{m}{2}\left[\omega q_0 \sin\left(\frac{\pi}{2}+\alpha\right) - \frac{2F\tau}{m}\right]^2 \tag{4.75}$$

and the strain energy is

$$V = \frac{K}{2}\left[q_0 \cos\left(\frac{\pi}{2}+\alpha\right)\right]^2 \tag{4.76}$$

The total energy after one cycle is then the sum of T and V; i.e.,

$$E = \frac{1}{2}Kq_0^2\cos^2\left(\frac{\pi}{2}+\alpha\right) + \frac{m}{2}\left[\omega q_0 \sin\left(\frac{\pi}{2}+\alpha\right) - \frac{2F\tau}{m}\right]^2$$

and this must equal $\frac{1}{2}Kq^2$

$$Kq^2 = Kq_0^2\cos^2\left(\frac{\pi}{2}+\alpha\right) + m\left[\omega q_0 \sin\left(\frac{\pi}{2}+\alpha\right) - \frac{2F\tau}{m}\right]^2$$

$$\left(\frac{q}{q_0}\right)^2 = \cos^2\left(\frac{\pi}{2}+\alpha\right) + \frac{m}{K}\left[\omega \sin\left(\frac{\pi}{2}+\alpha\right) - \frac{2F\tau}{mq_0}\right]^2 \tag{4.77}$$

As before the damping ratio is given by

$$e^{-2\pi\zeta} = q/q_0$$

substituting (4.77) and using $K = m\omega^2$

$$\zeta = \frac{1}{4\pi}\ln\left[\frac{1}{\cos^2\left(\frac{\pi}{2}+\alpha\right) + \left[\sin\left(\frac{\pi}{2}+\alpha\right) - 2F\tau/mq_0\omega\right]}\right] \tag{4.78}$$

Curves of ζ vs α and $\frac{\tau}{T}$ for several representative values of $\frac{2F\tau}{m\omega q_0}$ are shown in Figure 4-26. As might be expected the effect of a time delay is to reduce the effectiveness.

It may be of interest to compare the relative effectiveness of the proportional and pulse methods of shape control. The impulse delivered per cycle by the proportional method is

$$I = 2\int_0^{\pi} F\,dt$$

$$= 2\int_0^{\pi} km q_0 \sin\omega t\,dt$$

$$= 4km q_0$$

and this provides a damping ratio of $\zeta = \frac{k}{2\omega}$

If J is defined $\frac{I}{m\omega q_0}$

$$\zeta = \frac{k}{2\omega} = \frac{I}{8m\omega q_0} = \frac{J}{8}$$

$$J = 8\zeta \tag{4.79}$$

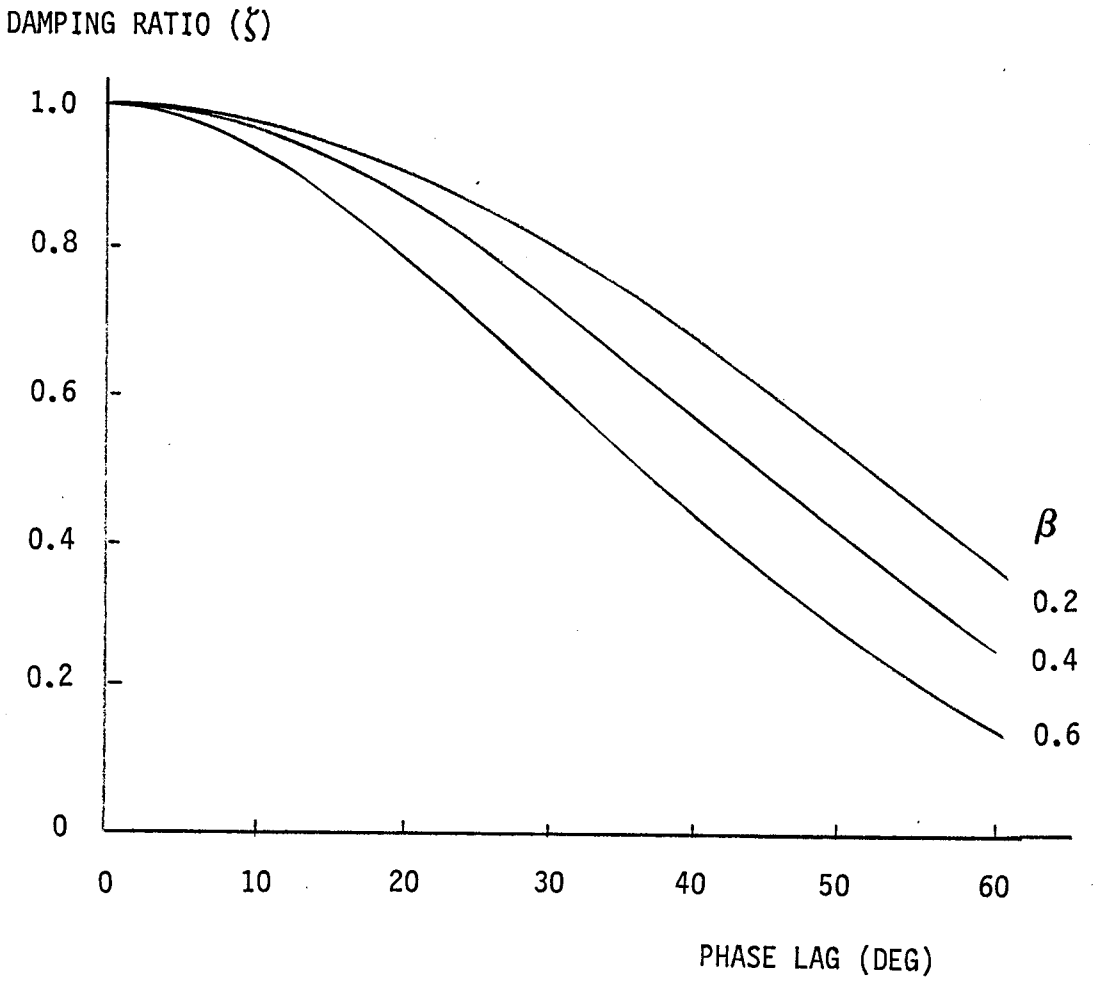

FIGURE 4-26 EFFECT OF TIME DELAYS ON DAMPING RATIO

The pulse method, from equation (4.73) has

$$e^{-2\pi\zeta} = 1 - J$$

$$J = 1 - e^{-2\pi\zeta} \qquad (4.80)$$

J is shown as a function of ζ in Figure 4-27. It is seen that the pulse method is the more efficient and becomes increasingly so as the damping is increased.

Maneuver

As shown in Section 4.2.1.3 proportional control has an advantage over an on-off control for maneuver in being more suited for implementing jerk limited slew laws. In general an on-off system will excite larger amplitude structural oscillations than a carefully tailored proportional system. When a train of pulses is used frequencies which will cause resonance must particularly be avoided.

Desaturation and Stationkeeping

Again the major drawback of an on-off system is greater excitation of structural oscillations.

4.2 Number and Distribution of Thrusters

In section 3.2.1 the thrust levels required to generate the total control forces and torques were determined. These assumed the minimum number of thrusters in the most favorable practical locations. In general this meant placing the thrusters as far apart as possible without mounting the units on parts of the solar panels or antennas. This approach is reasonable for generic classes IIB, IIC, IIIA and IIIB. The first three generic classes, IA, IB and IIA, however, lend themselves to distributed thruster configurations. This situation was addressed in Section 3.2.2 and force/unit area (for classes IA and IB) and force/unit volume (for class IIA) data were derived. In this section the distributed thruster concept will be examined in more detail.

It is clear that in practice the thrust distribution cannot be an ideal continuum but must be approximated by a finite, and probably relatively

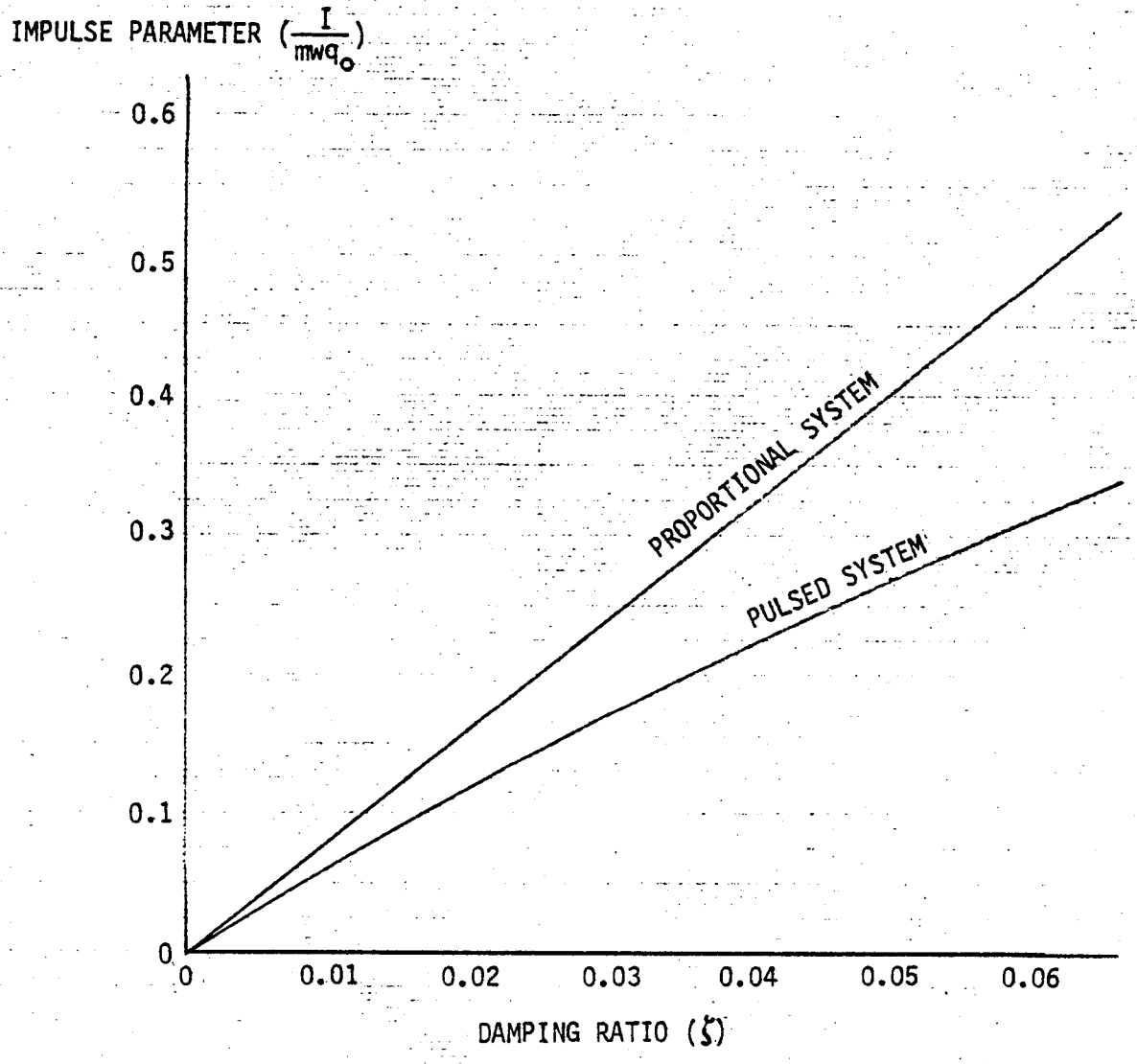

FIGURE 4-27 COMPARISON OF PROPORTIONAL AND PULSE CONTROL DAMPING

small, number of thrusters. Of interest are the effects of the number and location on ability to control shape, the merits of trading stiffness and strength against number of thrusters and the possible existence of minimum mass configurations. Although distributed systems are applicable to both plate and box type vehicles attention here will be restricted to plate type structures.

4.2.1 Attitude Control

To assess the effects of multiple thrusters the plate-like structure was represented as a uniform beam. Thrusters were placed uniformly along the length of the beam with each thrust assumed equal. The beam shape was then determined under two conditions: (1) when all thrusters were fired in the same direction (to represent translation) and (2) when the thrusters on one half were fired in one direction and those on the other side in the opposite direction (to repesent torque application).

Number of Thrusters - Two thruster spacings were used as shown in Figure 4-28. These are termed (N-1) where there is one less beam segment than the number of thrusters and there are thrusters at each end of the beam, and (N+1) in which there is one more beam element than thrusters. The (N+1) configuration is effectively the (N-1) configuration with the beam end thrusters left off.

The spacing of the thrusters will determine the effective moment arm during torque application. It can be shown that the effective distance is

$$\ell = \frac{NL}{4(N+1)} \quad \text{or} \quad \frac{NL}{4(N-1)} \tag{4.81}$$

for the (N+1) and (N-1) configurations respectively. Both expressions are asymptotic to l = .25L as N increases. The variation with N is shown in Figure 4-29.

The total impulse required to counter disturbance torques for small, medium and large plate structures (as defined in Table 4-1) are shown in Figure 4-30. The curves are fairly flat when presented in a semi-log format. Figure 4-31 repeats the small plate data with linear scales and shows that the variation with number of thrusters is quite considerable. These curves assume an (N+1) distribution and a CG-CP offset of 10 percent of the

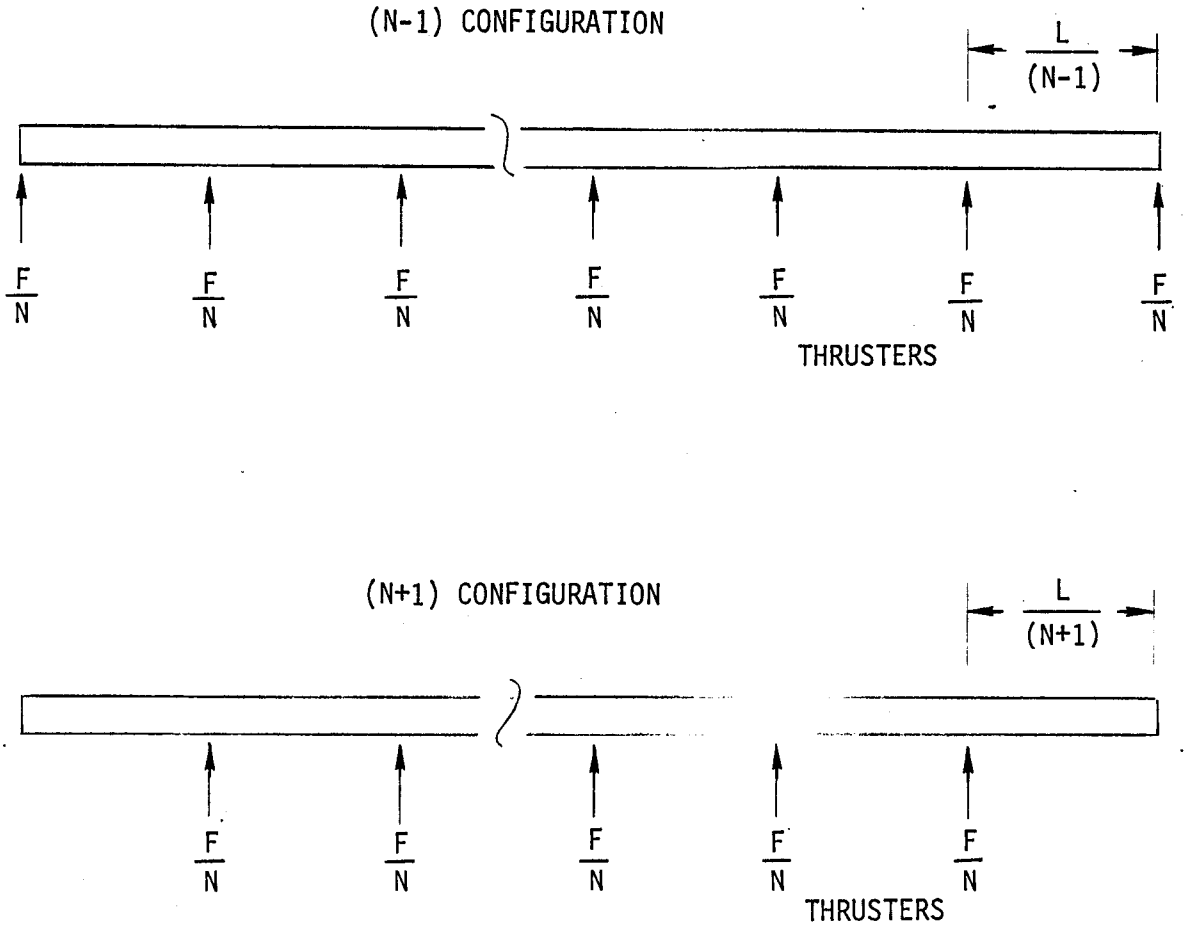

Figure 4-28 (N-1) AND (N+1) THRUSTER CONFIGURATION

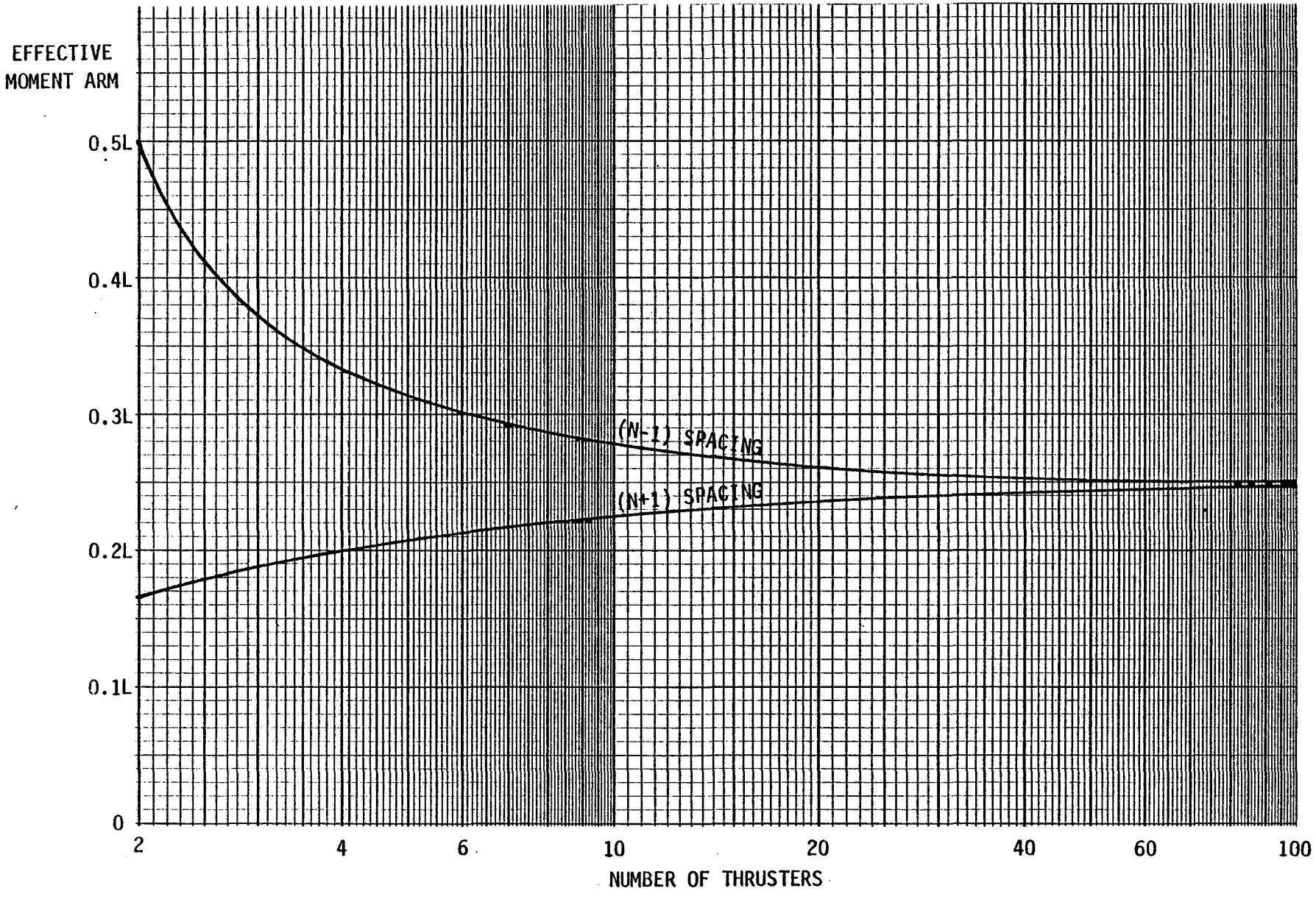

FIGURE 4-29 EFFECTIVE MOMENT ARM OF DISTRIBUTED THRUSTERS

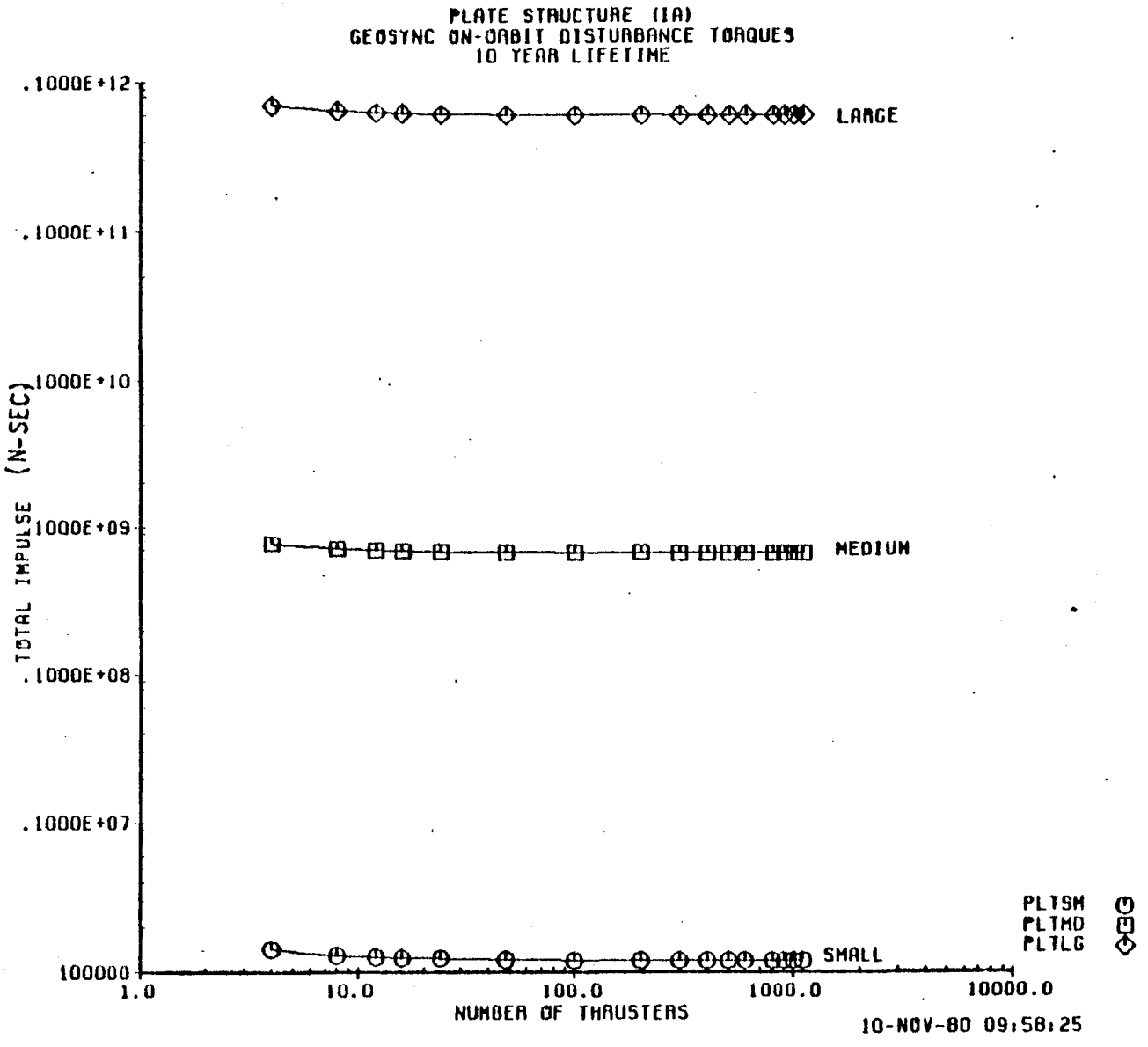

FIGURE 4-30 GEO ON-ORBIT DISTURBANCE IMPULSE, PLATE STRUCTURE (IA)

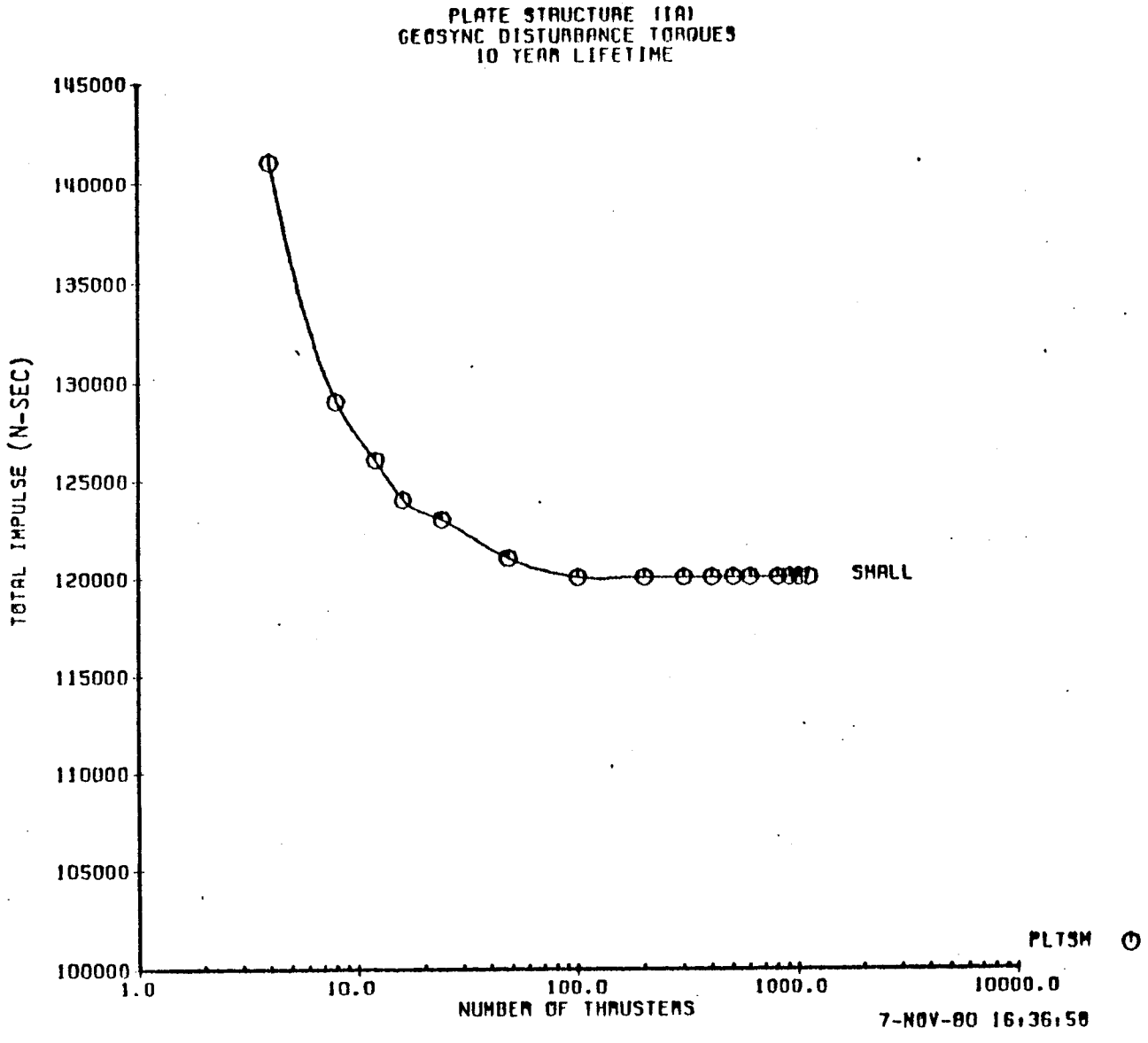

FIGURE 4-31 GEO ON-ORBIT DISTURBANCE IMPULSE, PLATE STRUCTURE (IA)

characteristic length. Figures 4-32 and 4-33 whow comparable curves for the cross and box structures.

4.2.2 Shape Control

Using normal modes, the dynamics of a flexible structure can be obtained by calculating the physical response of a point for each mode and then finding the total response using superposition. The differential equation for each mode is:

$$\ddot{q} + 2\zeta\omega_n \dot{q} + \omega_n^2 q = \frac{F}{m} \tag{4.82}$$

where: q = modal response
ω = modal frequency
ζ = modal damping ratio
m = generalized mass
F = generalized force
$= \sum_k T_k \phi_{Tk}$
T_k = Force at the k^{th} point on the structure
ϕ_{Tk} = mode shape at the point where T_k is applied

The response of the single degree of freedom modal equation (4.82) to a step generalized force, F, is:

$$q(t) = \frac{F}{m\omega_n^2}\left[1 - e^{ut}\left(\cos\omega t - \frac{u}{\omega}\sin\omega t\right)\right] \tag{4.83}$$

where: $u = -\zeta\omega_n$
$\omega_n = \omega\sqrt{1-\zeta^2}$

After solving each modal equation at time t, the physical response at a point on the structure is given by the summation of the responses in each of the modes:

$$y(t) = \sum_{i=1}^{N} \phi_i q_i(t) \tag{4.84}$$

where: ϕ_i = i^{th} mode shape at the point where responses are being calculated
$q_i(t)$ = i^{th} modal response from equation (4.83)

By solving equations (4.83) and (4.84) at successive time intervals, the maximum structural deflections can be found.

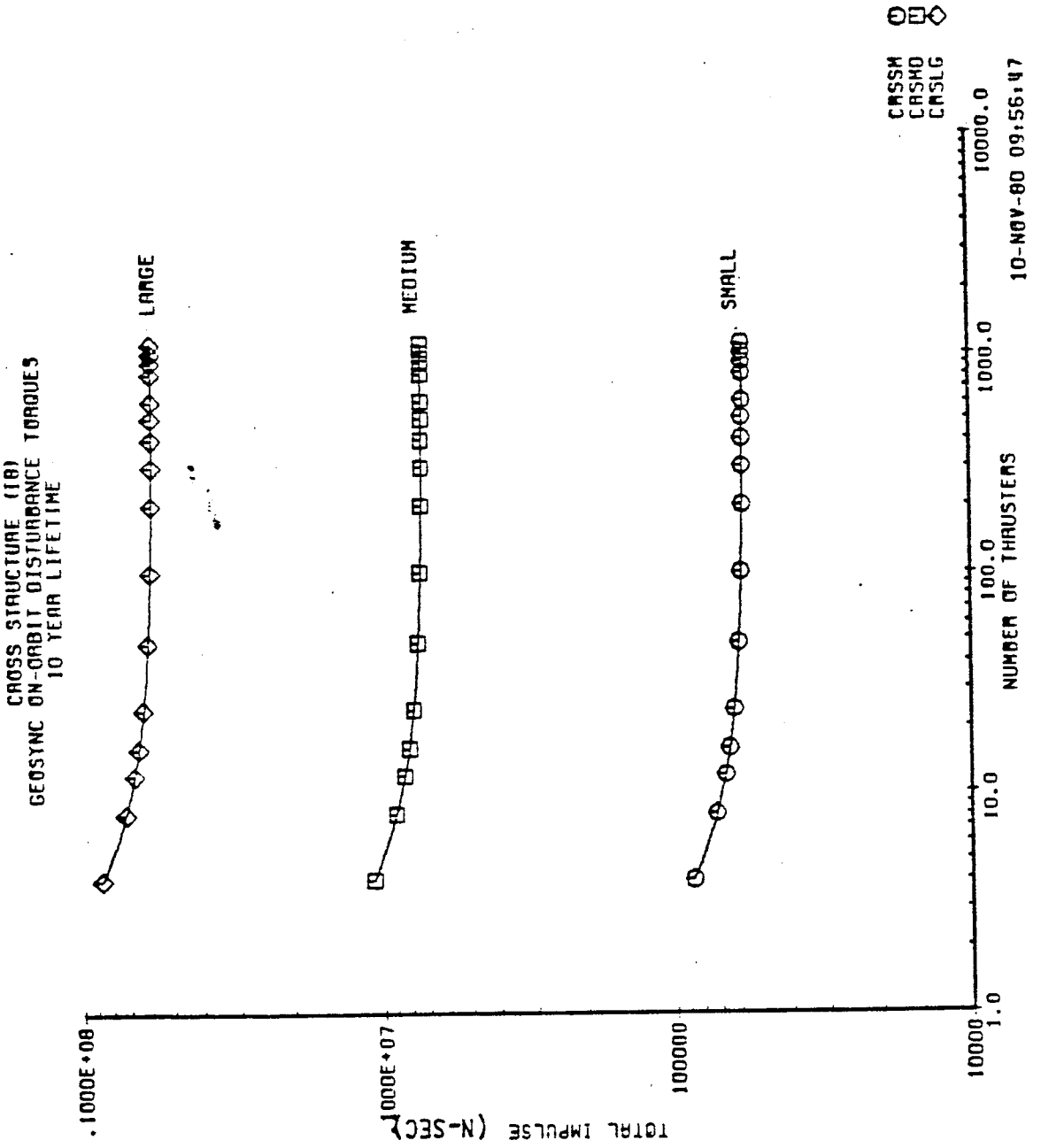

FIGURE 4-32 GEO ON-ORBIT DISTURBANCE IMPULSE, CROSS STRUCTURE (IB)

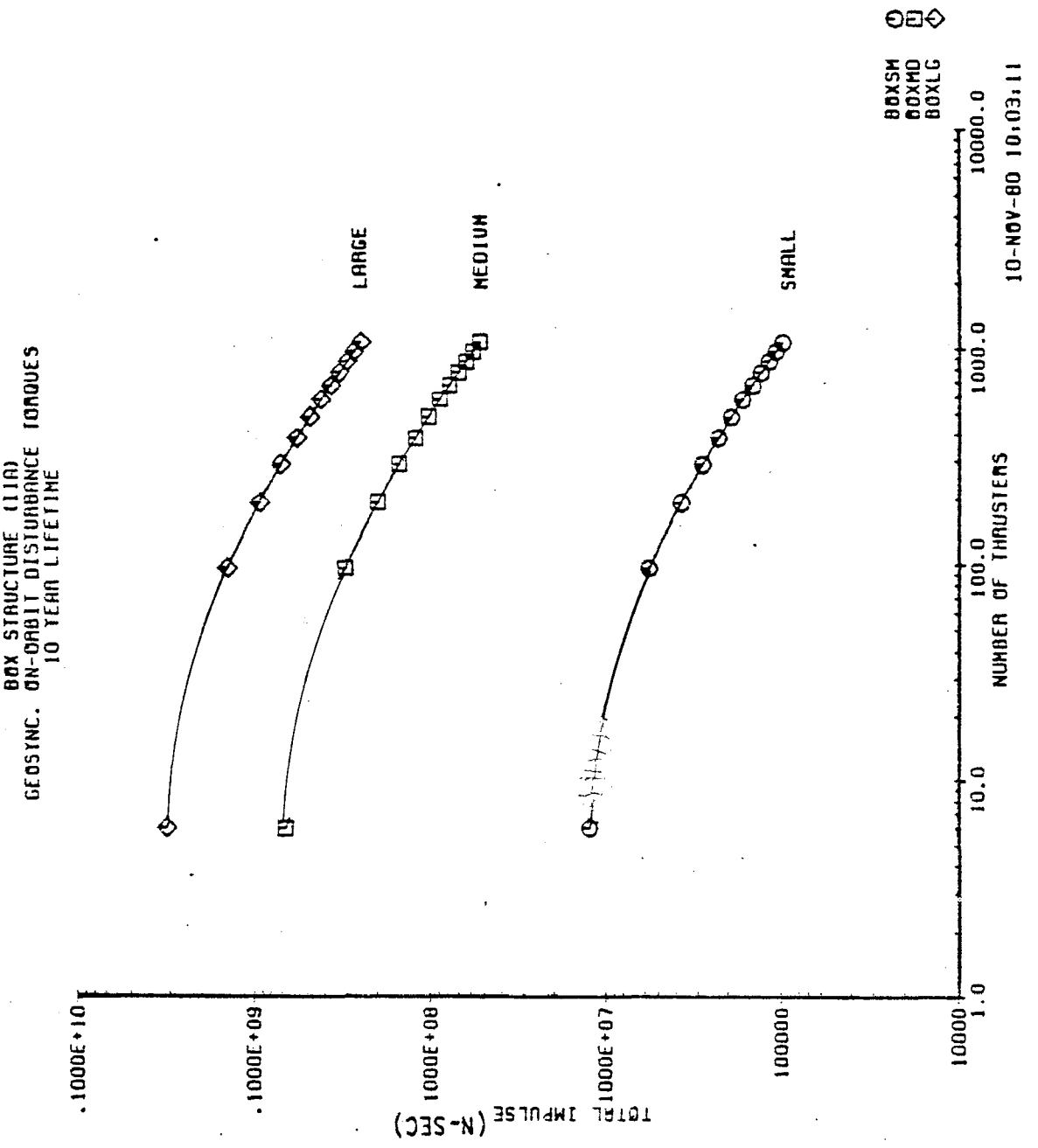

FIGURE 4-33 GEO ON-ORBIT DISTURBANCE IMPULSE, BOX STRUCTURE (IIA)

The steady state deflection due to a step force is found by letting t in equation (4.83). The steady state response of each mode is:

$$q_{ss} = \frac{F}{m\omega_n^2} \tag{4.85}$$

and the steady state physical response is:

$$y_{ss} = \sum_{n=1}^{N} \frac{\phi_i \cdot F_i}{m_i \omega_{ni}^2} \tag{4.86}$$

A computer program was written to determine the maximum and steady state elastic responses to step inputs from the thrusters. Ten free-free modes were used and the problem formulated in normalized form so that the results apply to beam-like structures of any size. The normalized deflection is defined:

$$\bar{y} = \frac{y}{F}\left(\frac{EI}{L^3}\right) \tag{4.87}$$

where: y = the elastic deflection
F = the total thrust
E = Young's modulus
I = the section 2nd moment of area
L = the beam length

The actual deflection is

$$y = \bar{y}\frac{L^3 F}{EI} \tag{4.88}$$

and shows that y is inversely proportional to EI. Length is an important parameter with y proportional to L^3.

Figure 4-34 shows the maximum dynamic deflection as a function of the number of thrusters, all firing in the same direction, for both the (N-1) and (N+1) configurations. As expected, the deflection decreases as the number of thrusters is increased. The decrease is rapid at first but then declines. Going from two to five thrusters ((N-1) curve) reduces the deflection by a factor of about 4:1. A further 4:1 reduction requires 14 thrusters.

Figures 4-35 and 4-36 show similar (N-1) and (N+1) curves for the torque case. The center thruster contributes nothing to torque when there are an odd number of thrusters and turning this one off leads to some improvement

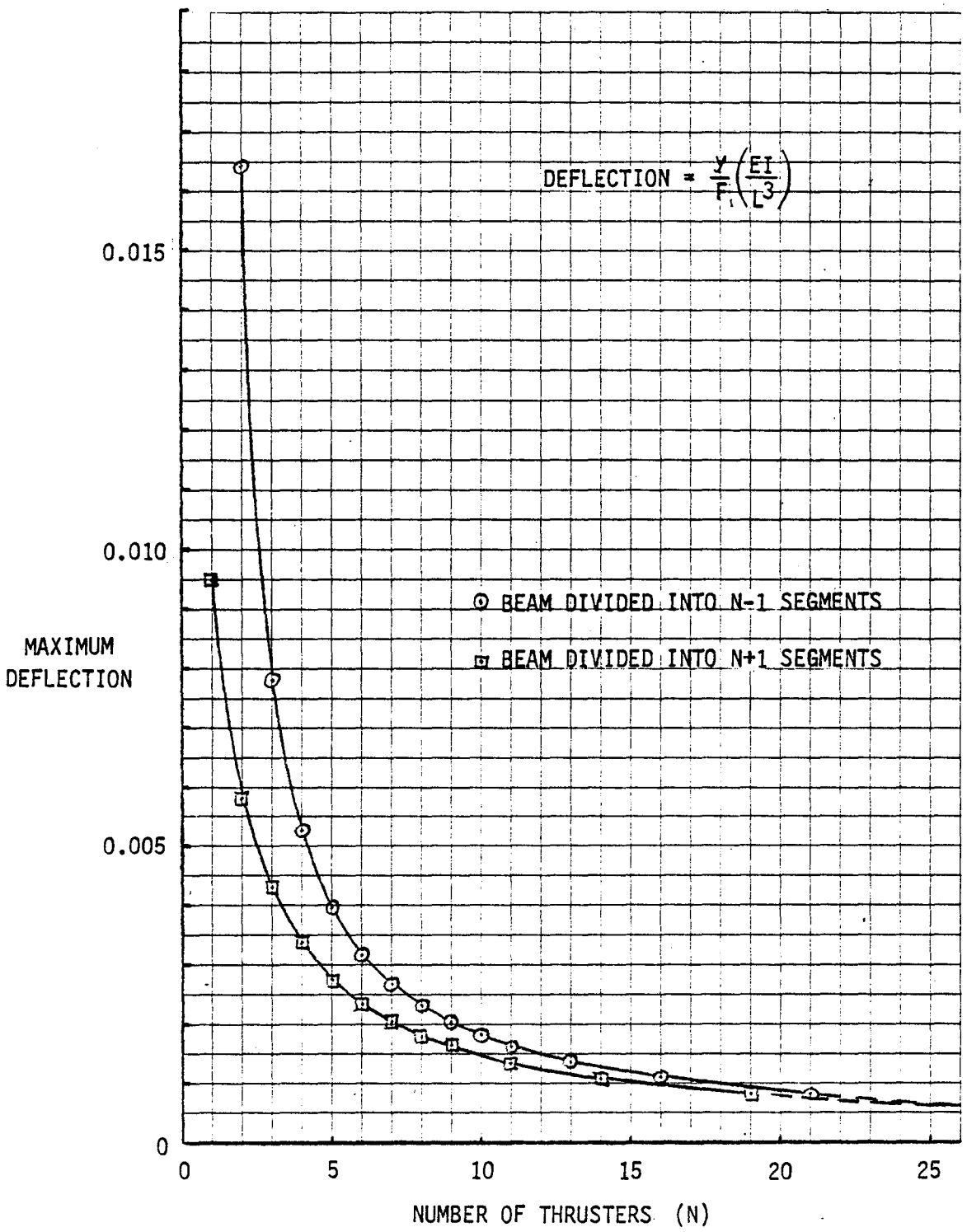

Figure 4-34 DEFLECTION DUE TO TRANSLATION

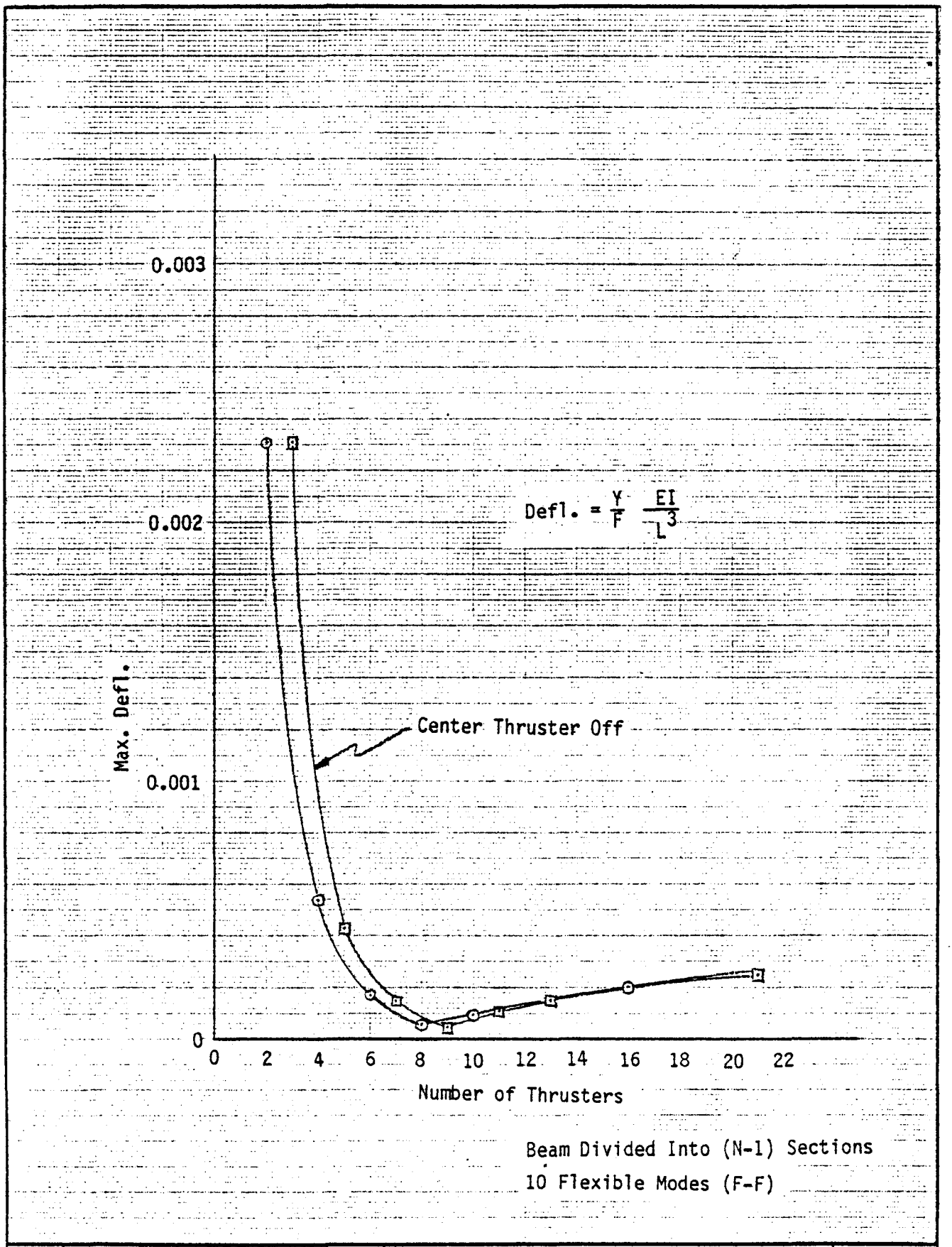

CALC			REVISED	DATE
CHECK				
APR				
APR				

Figure 4-35
Beam Deflections Due to Rotation

THE BOEING COMPANY

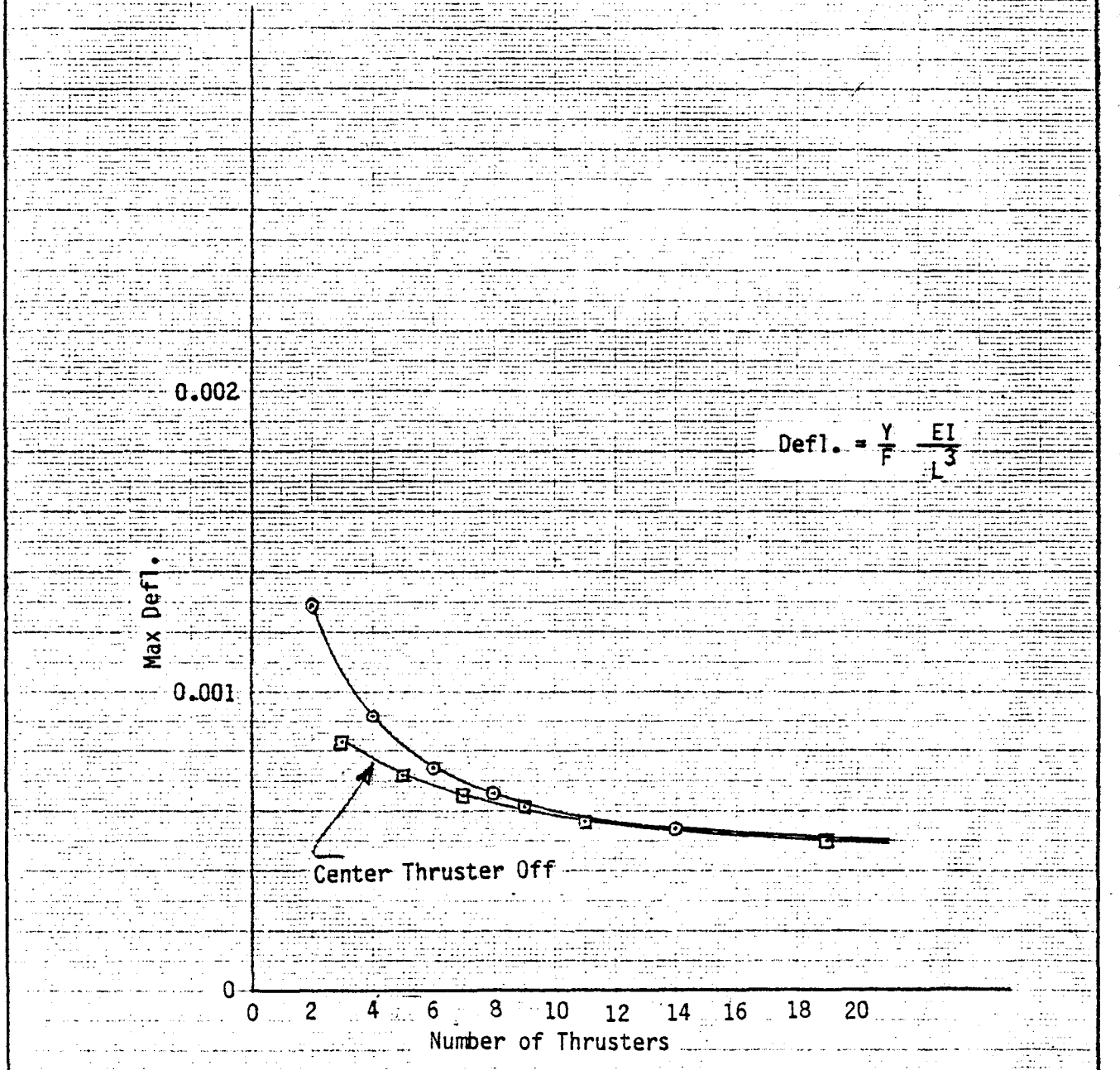

Beam Divided Into (N+1) Sections
10 Flexible Modes (F-F)

CALC			REVISED	DATE
CHECK				
APR				
APR				

Figure 4-36
Beam Deflections Due to Rotation

THE BOEING COMPANY

when there are only a few thrusters. In comparing the translational and rotational cases it is seen that the deflections are much larger when the thrusts are asymmetric.

Figures 4-34, 4-35 and 4-36 were constructed using the first ten bending modes. Values shown are the maximum deflections from the equilibrium (flat) state occurring at any point in the beam. Steady state values were about one half the maximums.

To determine if the number of modes used had any influence the calculations were repeated using fewer modes. Figures 4-37 and 4-38 show the change in maximum symmetric case deflections for the (N+1) and (N-1) configurations. Very little change is seen in the (N+1) case. In the (N-1) case some variation occurs but the curves are essentially flat for three or more modes.

Figures 4-39 and 4-40 show the asymmetric case and again there is no significant change above three modes. The curves indicate that little excitation of higher modes is taking place and analysis with as few as the first three modes will give reasonable answers for both symmetric and asymmetric thrusting.

Thruster Spacing - The effect of thruster location was examined by taking two thrusters, equally spaced from the center of the beam, and determining the maximum deflections with both symmetric and asymmetric thrust. The results are shown in Figure 4-41. Maximum deflections occurred when the thrusters were at the ends of the beam. Sharp minimums appeared in both cases and these were significantly lower than the maximums - by a factor of some 50 in the translational case and about 20 in the rotational. The shapes of the beams when the thrusters were located in the best position is shown in Figure 4-42.

Much additional work could be done on various combinations of location and thrust level to determine optimum configurations. These would be useful in a design environment but need not be pursued here where the primary interest is on APS characteristics and requirements. It is clear from the shape control point of view that distributed thrusters are desirable and location is important when a small number of thrusters are used.

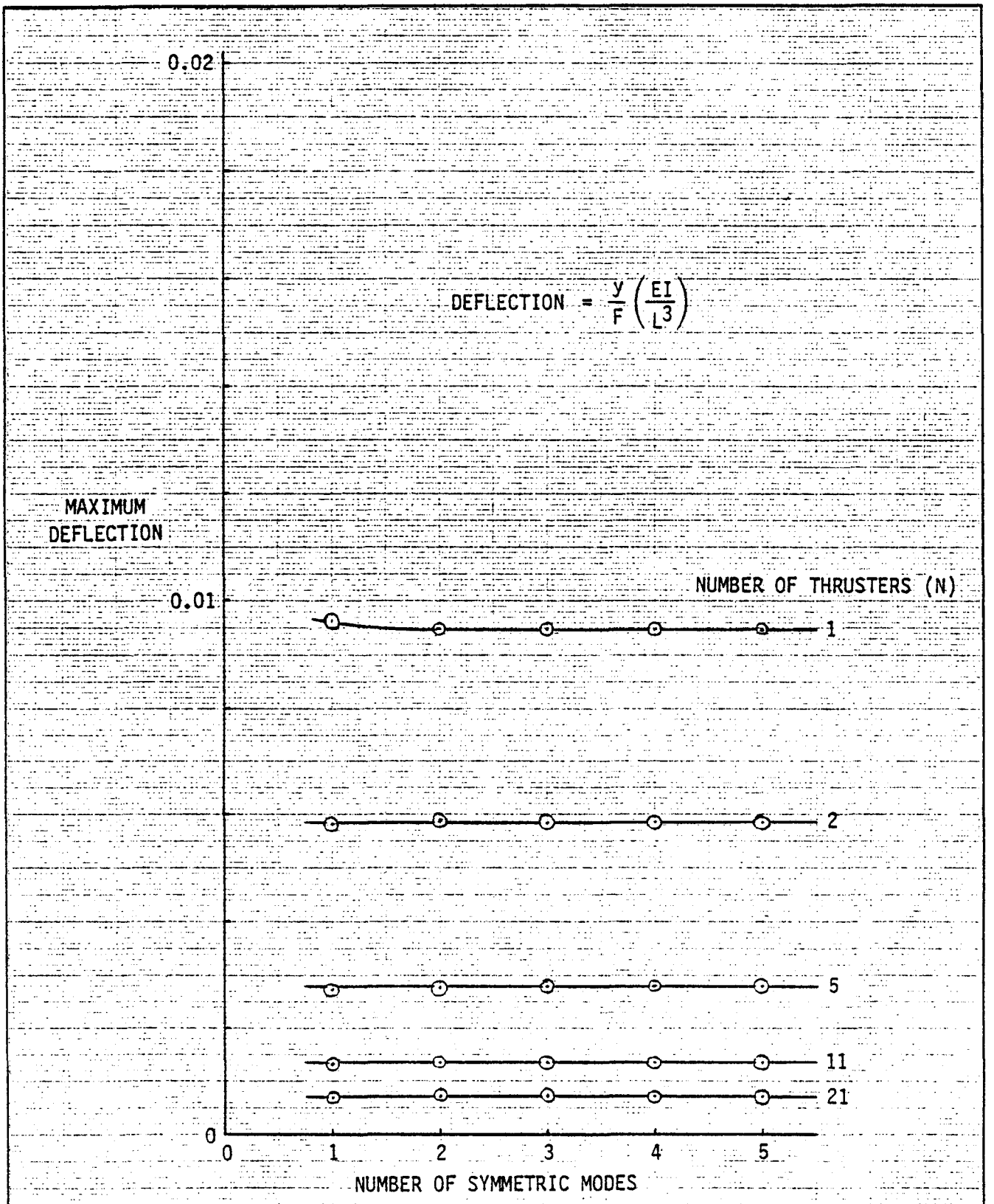

Figure 4-37 DEFLECTION DUE TO TRANSLATION, (N+1) SPACING, vs. NUMBER OF MODES

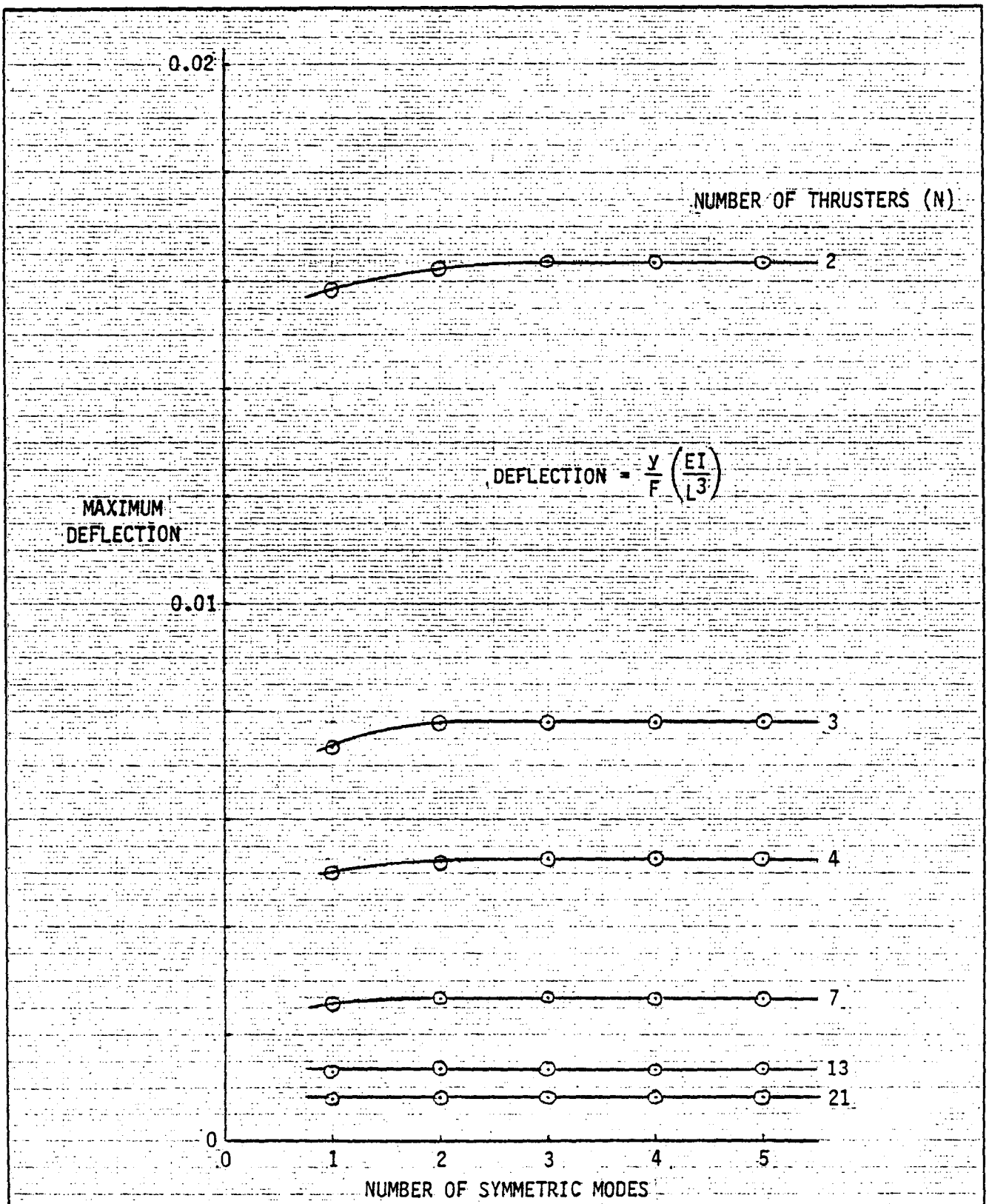

Figure 4-38 DEFLECTION DUE TO TRANSLATION, (N1-1) SPACING, vs. NUMBER OF MODES

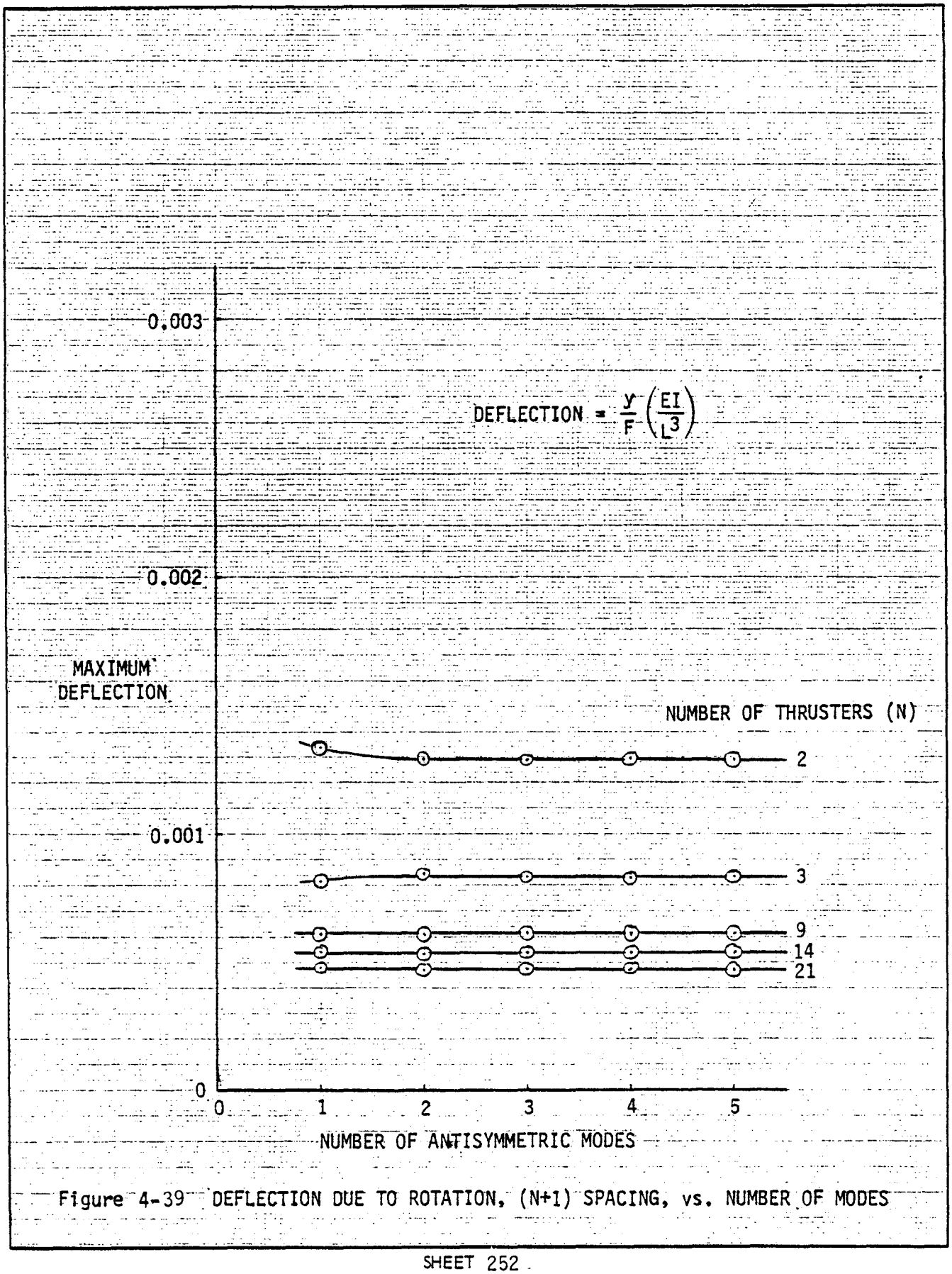

Figure 4-39 DEFLECTION DUE TO ROTATION, (N+1) SPACING, vs. NUMBER OF MODES

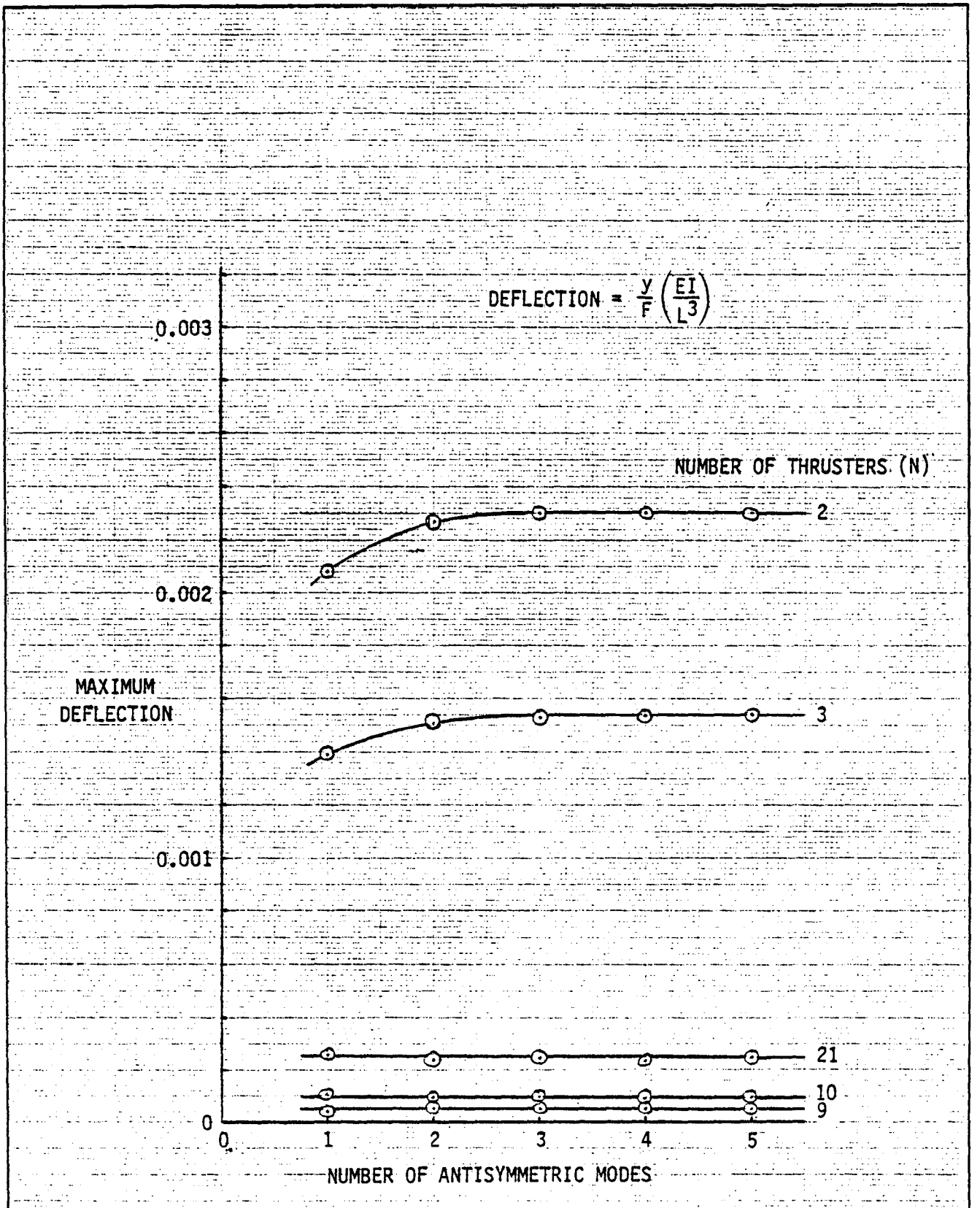

Figure 4-40 DEFLECTION DUE TO ROTATION, (N-1) SPACING, vs. NUMBER OF MODES

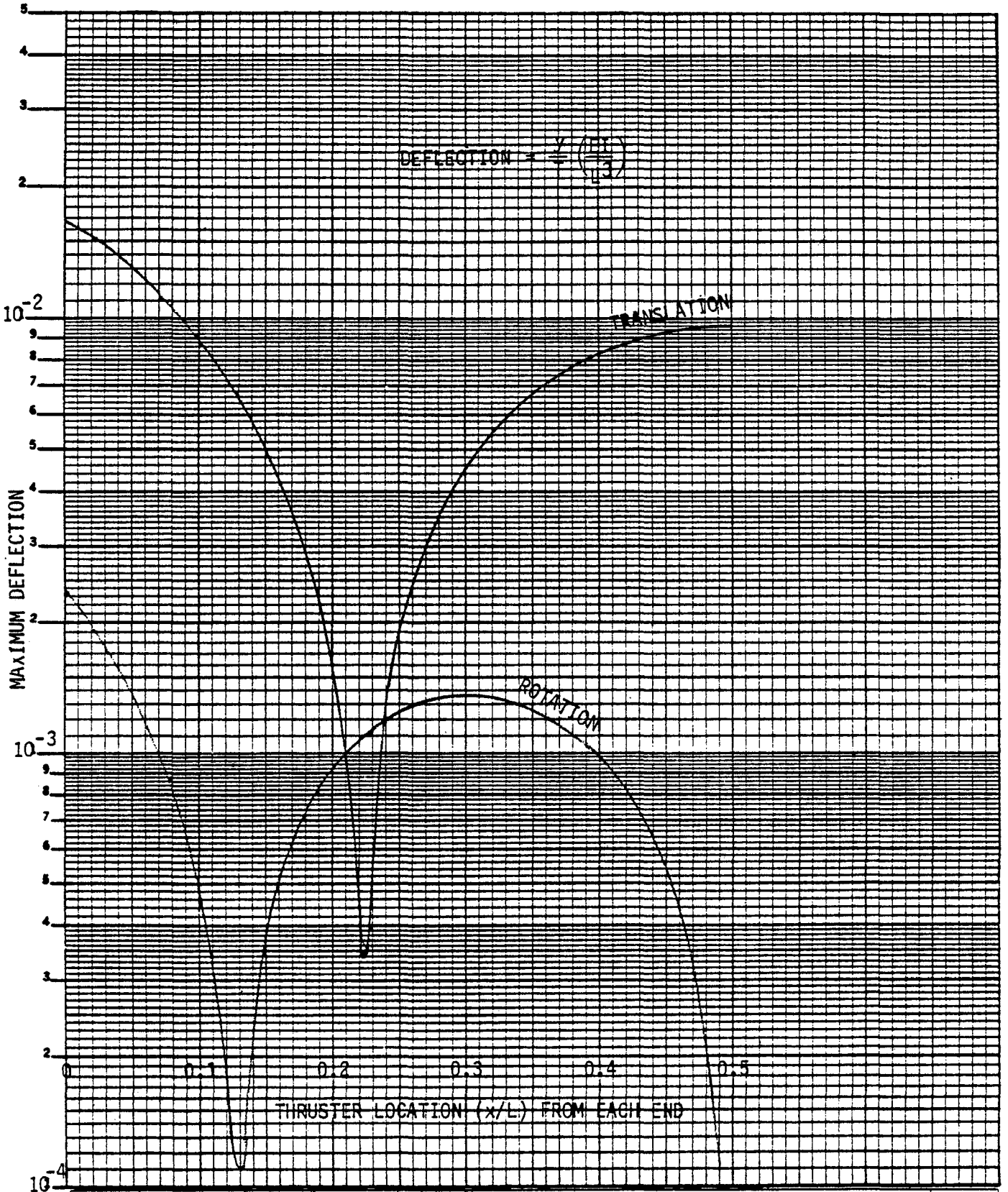

	INITIALS	DATE	REV BY INITIALS	DATE	TITLE	MODEL
CALC					Figure 4-41 MAXIMUM BEAM DEFLECTIONS FOR TWO THRUSTERS	
CHECK						
APPD						
APPD						

REV LTR _____

BOEING NO. 254

SH

$$\text{DEFLECTION} = \frac{y}{F}\left(\frac{EI}{L^3}\right)$$

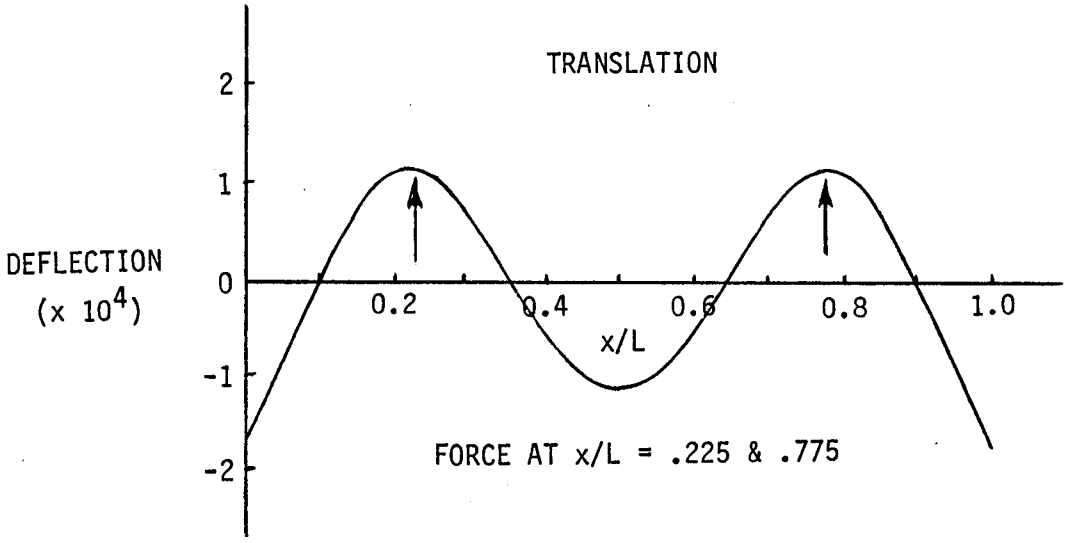

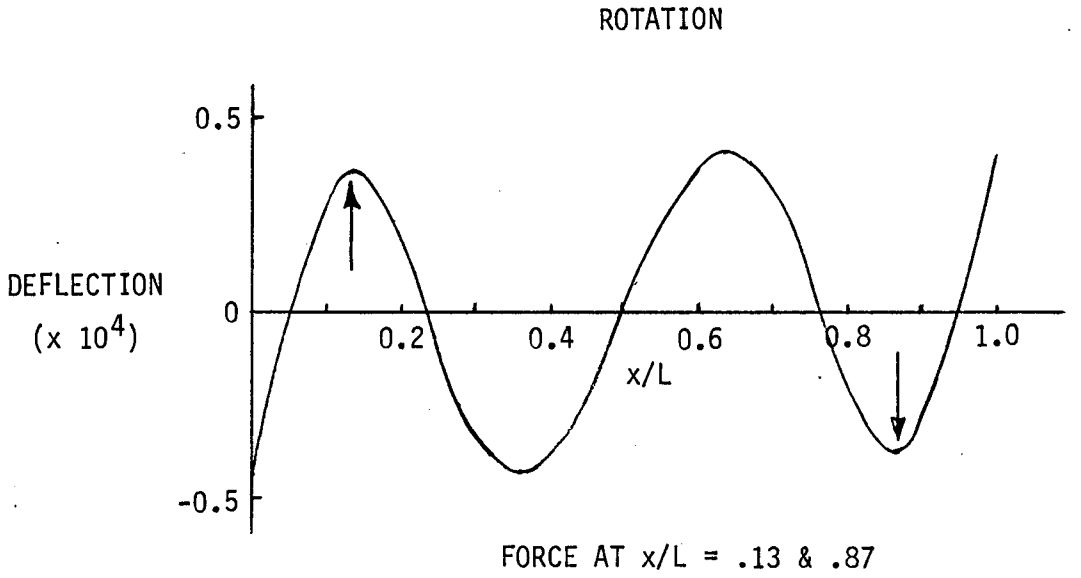

Figure 4-42 MINIMUM BEAM DEFLECTIONS FOR TWO THRUSTERS

Thrust Levels - The effects of thrust level on the surface flatness can be determined using equation (4.87)

$$\frac{F}{n} = \left(\frac{y}{L}\right)\frac{1}{n\bar{y}}\left(\frac{EI}{L^2}\right) \qquad (4.89)$$

This relates the thrust/thruster to the surface deflection as expressed by (y/L). Values have been claculated for small, medium and large flat plate structures with two values of I (400 and 2000 m^2) and for the values of E corresponding to aluminum and graphite. The curves are shown in Figures 4-43 and 4-44.

Stiffness/Number of Thruster Trades - From Equation (4.88) it is clear that increasing E or I will decrease the deflection. EI is a measure of the structure stiffness. Either aluminum or graphite composites currently seem the most likely materials. In any event, little control is available over E; the best material will be chosen to meet a number of criteria, which may include low thermal expansion, suitability for transportation and in-space construction in addition to low weight. Once the material is selected, E is fixed. The other component of stiffness, however, represented by I, depends on how the structural elements are configured. The value of I can also be increased by adding more structural material without a configuration change. The deflection in this case will decrease with lower I but the system weight too will increase.

4.3 Allowable Mass

The allowable mass study represents an examination of total system mass sensitivity to various APS parameters. Topics covered in this study includes the effect of APS mass distribution on the accuracy of shape control, auxiliary propulsion system mass determination, the identification of an optimum I_{sp} for electric systems, the effects of APS mass on total impulse requirements, and total system mass determination.

4.3.1 Shape Control

Surface accuracy of a plate type structure using distributed thrusters has been examined in Section 4.2. It was assumed that the structure was homogeneous. This implies that although the thrusts were applied at discrete points, the APS mass was distributed over the structure. The

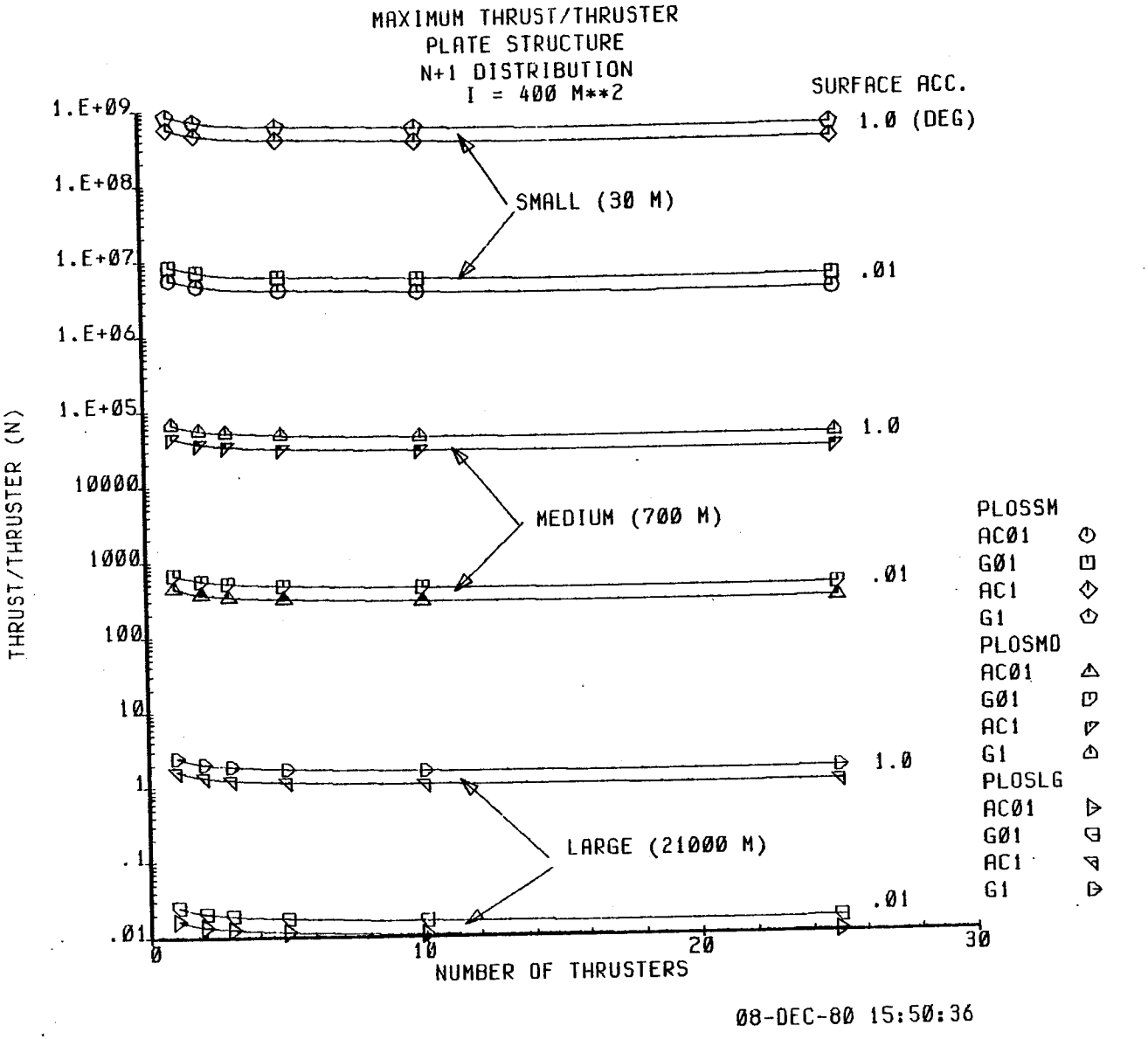

FIGURE 4-43 MAXIMUM THRUST/THRUSTER, PLATE STRUCTURE. SMALL I

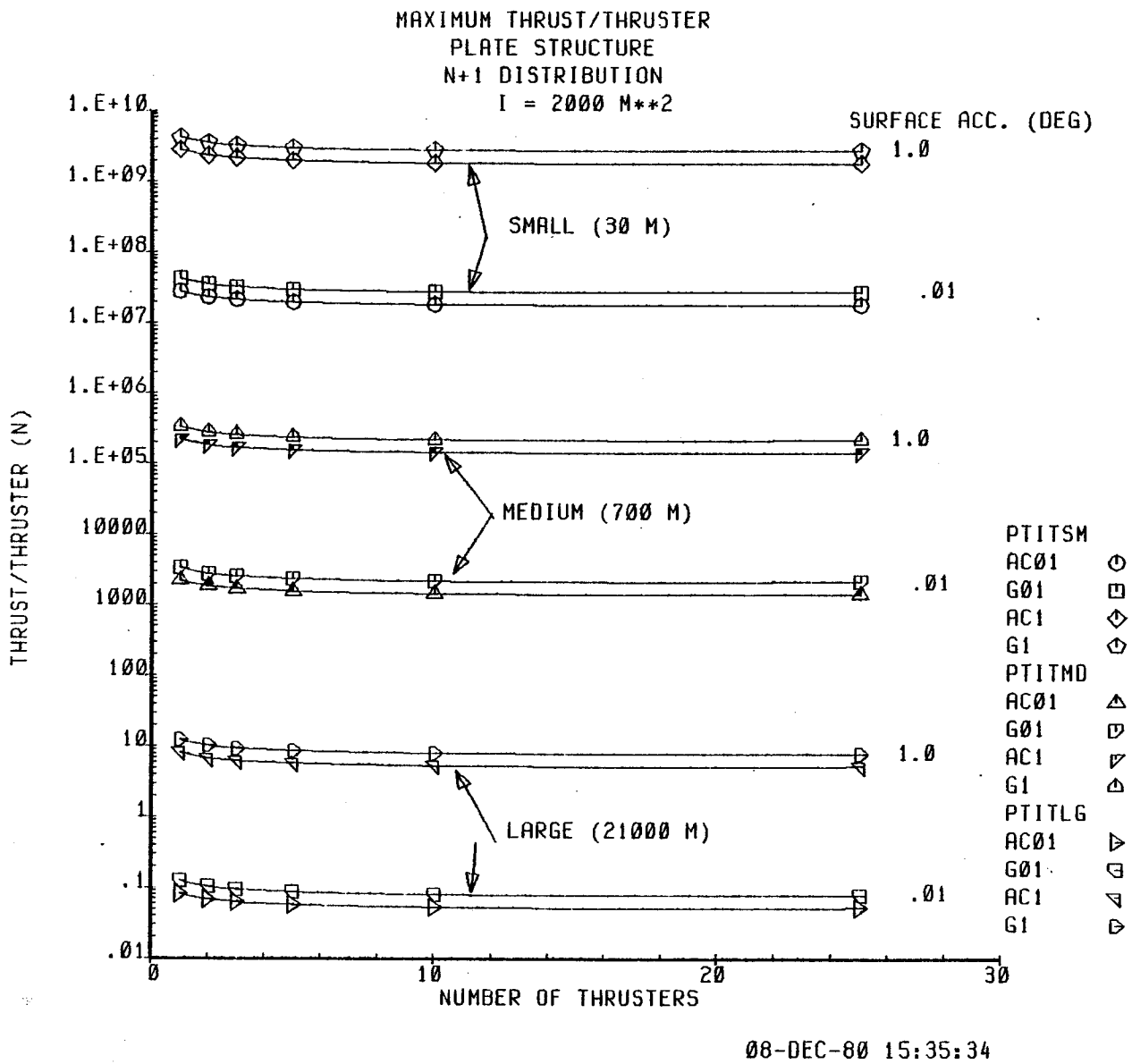

FIGURE 4-44 MAXIMUM THRUST/THRUSTER, PLATE STRUCTURE, LARGE I

study was extended to determine if there are allowable APS mass limitations associated with concentrated masses at the thruster locations.

To limit the number of parameters, an (N-1) distribution of thrusters was assumed. The number was taken as eight which corresponds to the minimum deflection case shown in Figure 4-35. The total LSS mass can be expressed as the sum of structure and APS masses

$$M = M_S + M_{APS} \tag{4.90}$$

and the ratio of the APS to structure mass can be expressed as a coefficient, K

$$K = M_{APS}/M_S$$
$$M = M_S(1+K) \tag{4.91}$$

The APS mass was assumed concentrated at the eight thruster locations with the structure mass equally distributed over the structure. Deflections were then recomputed for both translation (all thrusters firing in the same direction) and rotation (half the thrusters firing in opposite directions).

Three values of K were used: K = 1, 3 and 6. The resulting maximum deflections for translation and rotation are shown in Figure 4-45. Under rotation the maximum deflections increase as mass is added. This is caused by the fact that, for eight massless thrusters, the mode shapes and thruster locations result in a balance of forces which produce near minimum deflections. The addition of concentrated masses at the thruster locations results in a change in the mode shapes which upsets this balance and causes higher deflections. Note, however, that the maximum deflections due to rotation are less than or equal to those due to translation for all values of K used.

4.3.2 APS Mass Characteristics

The independent variables in this portion of the study were system efficiency and specific impulse. Thrust level and total impulse requirements were determined in Section 3.2.1. Propellant tank and thruster sizing were also predetermined by fixed parameter scaling laws which will be listed in a following paragraph.

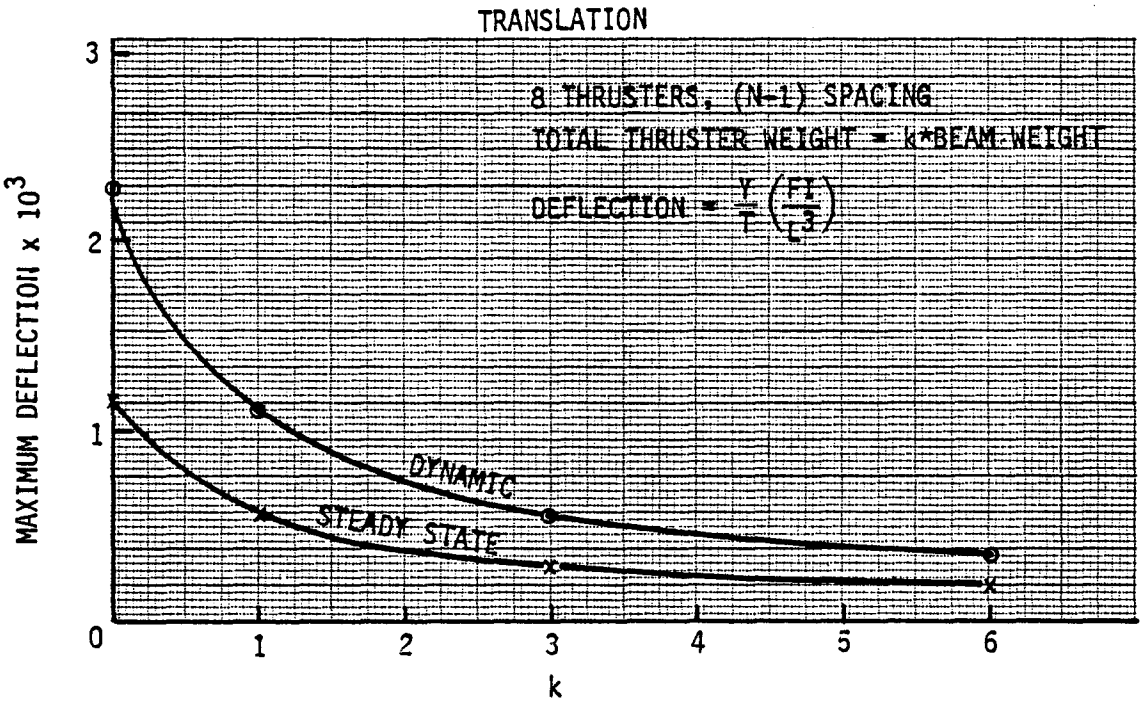

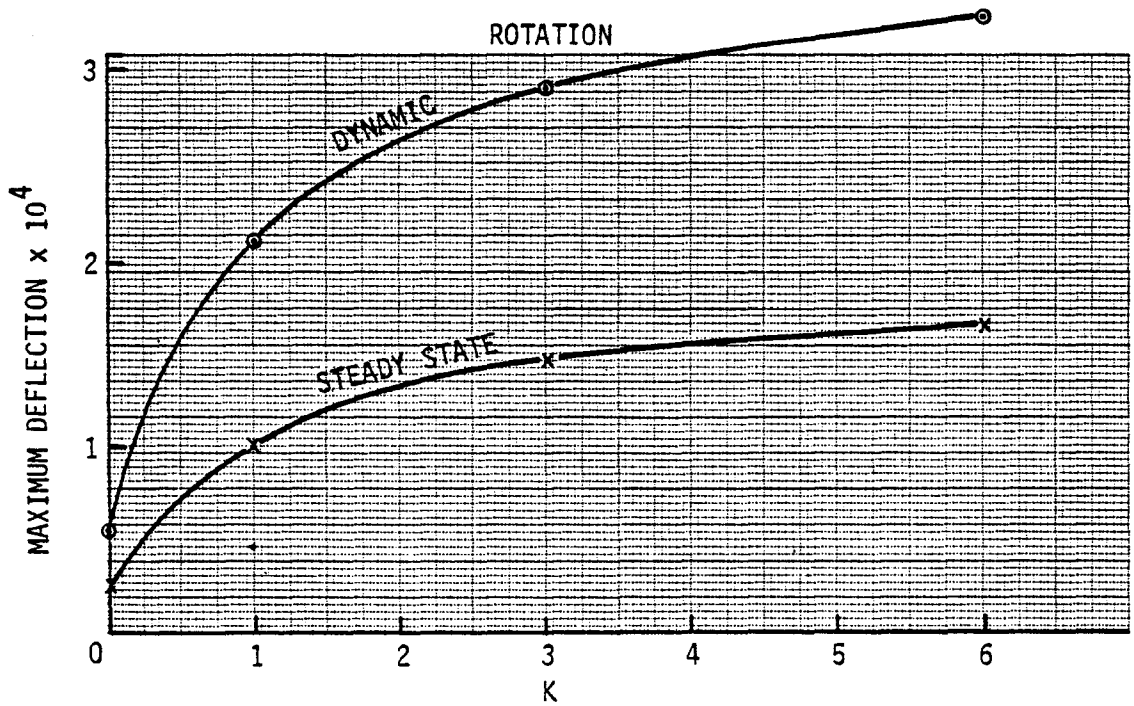

FIGURE 4-45 MAXIMUM BEAM DEFLECTIONS WITH CONCENTRATED THRUSTER MASSES

Determination of the auxiliary propulsion system mass was a six step process. The six steps are listed below in order of execution:

1. Total impulse determination
2. Thrust level determination
3. Fuel mass sizing
4. Fuel tank sizing
5. Thruster system sizing (thruster and any power system mass)
6. Summation of Fuel mass, Tank Mass, and thruster mass

Total impulse determination is outlined in Section 3.2.1. This analysis concluded that stationkeeping sources would comprise the total impulse needs for each class of LSS.

Stationkeeping sources include solar pressure perturbations, north/south solar and lunar gravity effects, and east/west stationkeeping due to earth triaxiality. Total impulse requirements result from the sum of these sources over a ten year lifetime. Table 4-1 contains the total impulse requirements for each class and size. The thrust level determination was shown in Section 3.2.1. These requirements are summarized in Table 4-2.

Fuel mass determination was a straight forward process using the following equation:

$$M_{Fuel} = \text{Total impulse}/(I_{sp} \times 9.8)$$

where M_{Fuel} in kilograms
Total impulse in Newton-seconds
I_{sp} in seconds

Specific impulse was treated as a parameter with a range of 0 to 60,000 seconds. This is an ambitious range of I_{sp}, however, in the context of defining technology advances a broad I_{sp} range seems appropriate.

Estimates of fuel tank mass depend on propellant type, tank material, tank back pressure, and an assortment of other variables. The following was assumed in estimating propellant tank mass:

Class/Size	Total Impulse Requirements (N - S)		
	Small	Medium	Large
Plate	1.199×10^5	6.50×10^7	5.86×10^{10}
Modular Antenna	1.104×10^6	4.561×10^6	1.657×10^7
Series of Antennas	2.063×10^7	6.19×10^7	1.031×10^8

Table 4-1 Total Impulse Requirements

TABLE 4-2 THRUST REQUIREMENTS

STRUCTURE	SIZE	# THRUSTERS	THRUST/THRUSTER REQUIRED			
			LEO MAXIMUM	LEO-GEO TRANSFER	GEO MAXIMUM	GEO NOMINAL
PLATE	SMALL (30 m)	4	.04	.0022	.0018	.0018
	MEDIUM (700 m)	4	21	20	.92	.92
		24	2.2	3.5	.16	.16
		100	.7	.9	.04	.04
	LARGE (21000 m)	4	610000	46000	6200	3310
		24	62000	8000	1080	570
		100	15100	1950	260	137
MODULAR ANTENNA	SMALL (15 m)	8	.14	.07	.009	.009
	MEDIUM (60 m)	8	1.2	.75	.034	.032
	LARGE (200 m)	8	62	60	.23	.105
		32	16	14	.06	.03
		80	6.4	5.6	.024	.012
SERIES OF ANTENNAS	SMALL (2)	4	.113	8.75	.04	.04
	MEDIUM (6)	4	6.75	32.5	.79	.48
		24	1.13	5.42	.13	.08
		96	.28	1.35	.03	.02
	LARGE (10)	4	26.3	54.0	2.80	.78
		24	4.4	9.0	.47	.13
		96	1.1	2.3	.12	.03

1. Propellant type is storable liquid: e.g., hydrazine, bipropellants, mercury, cesium, etc.

2. tank is of titanium with a pressure under 300 psi.

3. Tank wall thickness is 1.3 mm.

4. N # of tanks are used for N # thrusters in distributed systems.

5. One tank is used for non-distributed systems.

Sections 5.1 and 5.3 cover the current electric and chemical system characteristics. From these characteristics, scaling laws were derived for chemical and electrical engine mass. Utilizing References 3, 4 and 5, power processor and solar array scaling equations were also derived. These equations reflect state of the art technology and all specific masses and areas were fixed at these values. The independent variables were Thrust, I_{sp} and efficiency. Table 4-3 shows the auxiliary propulsion scaling laws used for the unlimited shuttle launch study. These scaling laws differ from the scaling laws used for the single shuttle launch study presented in Section 4.6. The PPU scaling equation used here fits high power PPU technology better than that used for the single shuttle launch. Likewise, thruster mass for the unlimited size study did not include factors for mounting structure and gimballing mechanism. These were included later for the single shuttle launch study.

Utilizing the scaling laws shown in previous paragraphs, total APS mass could be determined. For chemical systems, the process is free of independent variables. Electrical systems, however, have total system efficiency as a significant independent variable. Electric thruster efficiency was treated by three methods. First, efficiency was set at 80 percent which is representative of currently available ion propulsion systems. Second, efficiency (independent of I_{sp}) was treated as a parameter and set at five constant values: 20, 40, 60, 80 and 100 percent. The final treatment of efficiency considered the dependence in current systems of efficiency to specific impulse. The 30 cm thruster system was used as a model for this last method.

Electric Engine Scaling

$$M_e = 6169.4 \left(\frac{T}{I_{sp}}\right)^{.675} \quad \text{kg}$$

Power Scaling

$$P = \frac{9.807\ T\ I_{sp}}{2\eta} \quad \text{kw}$$

Power Processor Mass

$$M_{PPU} = 14.2\ (P)^{.52}$$

Solar Array Mass

$$M_{S/A} = 13.5\ (P)$$

Solar Array Area

$$A_{S/A} = 8.96\ (P)$$

Chemical Engine Scaling

$$M_e = .028\ (T) + .27 \quad \text{kg}$$

TABLE 4-3 APS SCALING LAWS

Figures E-1 through E-9 define the total APS mass as a function of I_{sp} for each primary structure. This mass is the "first pass" APS mass using GEO thruster sizing. The term "first pass" indicates that the effect of the APS mass itself on the total impulse requirements has not yet been included. This effect will be included in the total mass figures to be shown later. These later total mass figures yield the same optimum I_{sp} as the "first pass" APS mass data and can be safely used to examine APS mass to determine the optimum I_{sp}.

For the plate structure, an assumption was made that the solar array mass was free; i.e., the power generation mass was not charged to the APS mass but was assumed to be "left over" from the plate structures function. The relative masses of the electric and chemical APS for each class is shown in Appendix E. The thruster sizing used was for a geosynchronous worst case recovery. System efficiency for Figures E-1 through E-9 was set at 80 percent and did not vary with I_{sp}.

Optimum I_{sp} determination can be made for the primary structures from these graphs. The plate structure is an example where power is "free", hence, I_{sp} optimums tend to be far above currently available systems. As a general rule, an I_{sp} optimum of 10,000 to 50,000 sec is indicated for "free" power structures. The optimum is completely dependent on power processor mass.

The modular antenna and series of antennas structures show a considerably different set of optimum I_{sp} values than the plate structure. The trend is illustrated in Figure E-9. Optimum I_{sp}'s are close to 15,000 sec for small structures, 7000-10,000 sec for intermediate structures and 3000-7500 sec for very large structures.

A second treatment of efficiency used five values of η independent of I_{sp}. This parametric approach showed the sensitivity of optimum I_{sp} to efficiency. Figures E-10 through E-15 contain examples of the parametric study data. Generally, efficiency variations over a range of 60 to 100 percent do not appreciably change the optimum I_{sp}. A summary of the results of this study is shown in Table 4-4.

Structure	Size	Total System Efficiency 20%	60%	100%
Plate	Small (30m)	5100 sec	9500 sec	10000 sec
	Medium (700m)	30000 "	50000 "	>50000 "
	Large (21000m)	>50000 "	>50000 "	>5000 "
Modular Antenna	Small (15m)	6000 sec	10500 sec	13000 sec
	Medium (60m)	5800 "	10000 "	12500 "
	Large (200m)	1500 "	3200 "	4000 "
Series of Antennas	Small (2)	7500 sec	11000 sec	15500 sec
	Medium (6)	5000 "	9000 "	11500 "
	Large (10)	3600 "	7000 "	9000 "

Table 4-4 Optimum I_{sp} Sensitivity to System Efficiency

Structure	Size	Optimum I_{sp} (sec) Constant η = 80%	$\eta = f(I_{sp})$
Plate	Small (30m)	9800	10000
	Medium (700m)	>50000	>12000
	Large (21000m)	>50000	>12000
Modular Antenna	Small (15m)	12000	>12000
	Medium (60m)	10500	11500
	Large (200m)	3600	3950
Series of Antennas	Small (2)	15000	>12000
	Medium (6)	10500	10800
	Large (10)	7500	7800

Table 4-5 Optimum I_{sp} Comparison

As a final approach to system efficiency variation, the 30 cm J series thruster operating envelope was examined. The following Figure (4-46) shows the currently available system efficiency as a function of I_{sp}. Figure 4-47 shows the same data extrapolated to a range of 0 to 12,000 seconds I_{sp} and curve fit with a fourth order least squares routine. This curve fit was then incorporated into the optimum I_{sp} study.

Figures E-16 through E-18 illustrate the effect of the dependence of η on I_{sp}. The optimum I_{sp}'s found using this model are generally somewhat higher than the constant efficiency model. A comparison of the optimum I_{sp}'s found using a constant 80 percent efficiency and the I_{sp} dependent efficiency is shown in Table 4-5.

The set of "first pass" APS mass data was used to generate an added impulse factor over a 10 year lifetime of the LSS. The APS mass was added to the LSS mass along with any additional solar array area necessary for electric systems and the disturbance analysis was repeated. From this process, a new total impulse requirement was generated. Figures E-19 through E-22 show the impulse fractions relating the new total impulse to the "first pass" total impulse. From the figures, it can be seen that this new impulse is between 5 and 30 percent greater than the old or first pass data for I_{sp} between 300 and 10,000. For very low I_{sp} (<200 sec) and certain structures using electrical systems, the impulse fraction became quite large. These fractions were utilized in the total system mass determination in the next paragraph.

From the previous studies identifying the impact of the APS mass on total impulse needs and the optimum I_{sp} for the electric system, it is now possible to get a picture of the total system mass for each size of the three primary LSS. As another simplification, three APS systems were compared. These systems are 1) a chemical APS at 300 sec I_{sp}, 2) an electric APS at 3000 sec I_{sp}, and 3) an electric APS at the optimum I_{sp} identified for a specific class and size. The efficiency assumed for the electric systems was 80 percent.

The impulse fraction (new impulse/old impulse) was used as a correction factor to the first pass fuel mass number. Ideally, the entire loop of

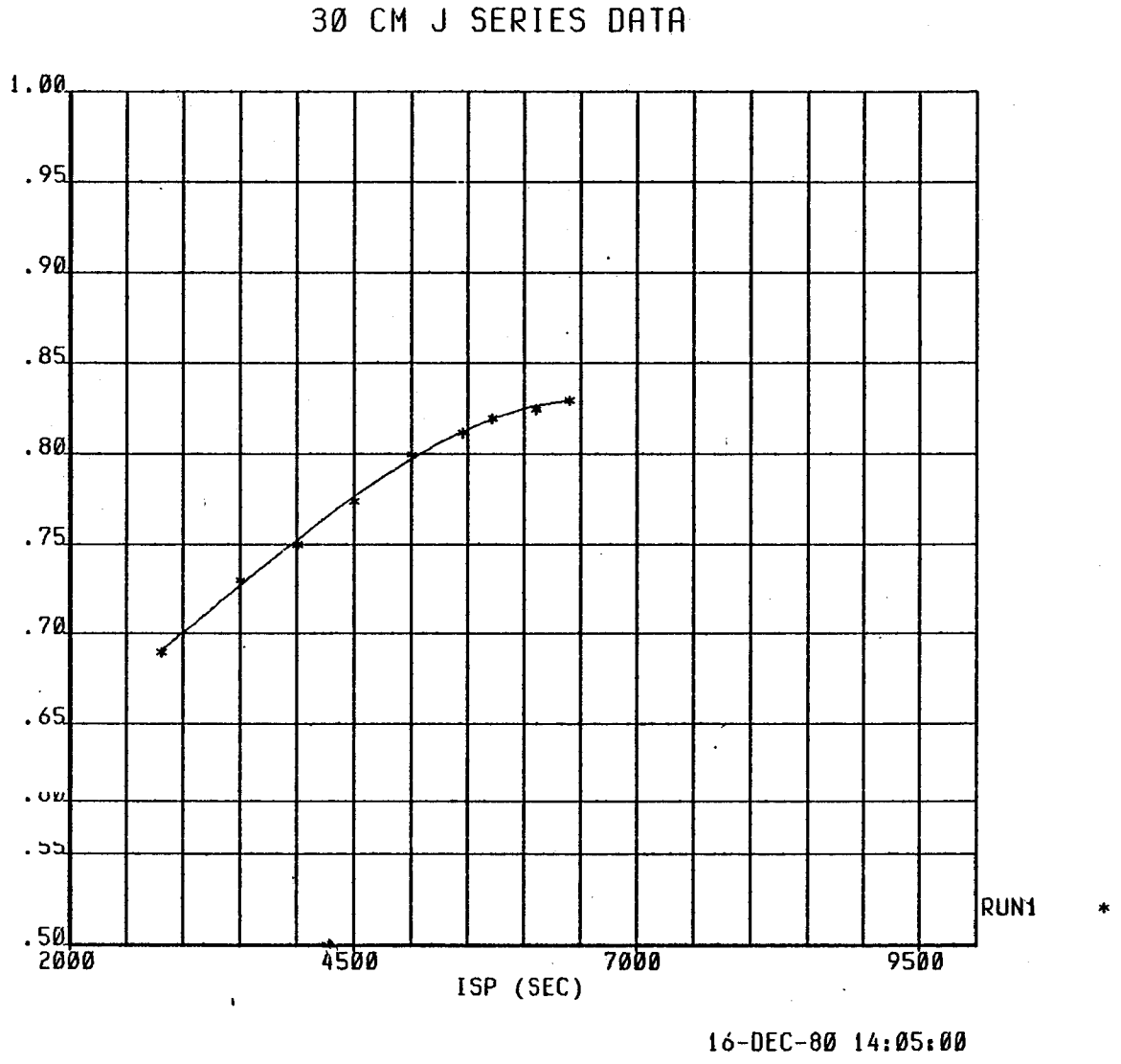

FIGURE 4-46 30 CM J SERIES DATA

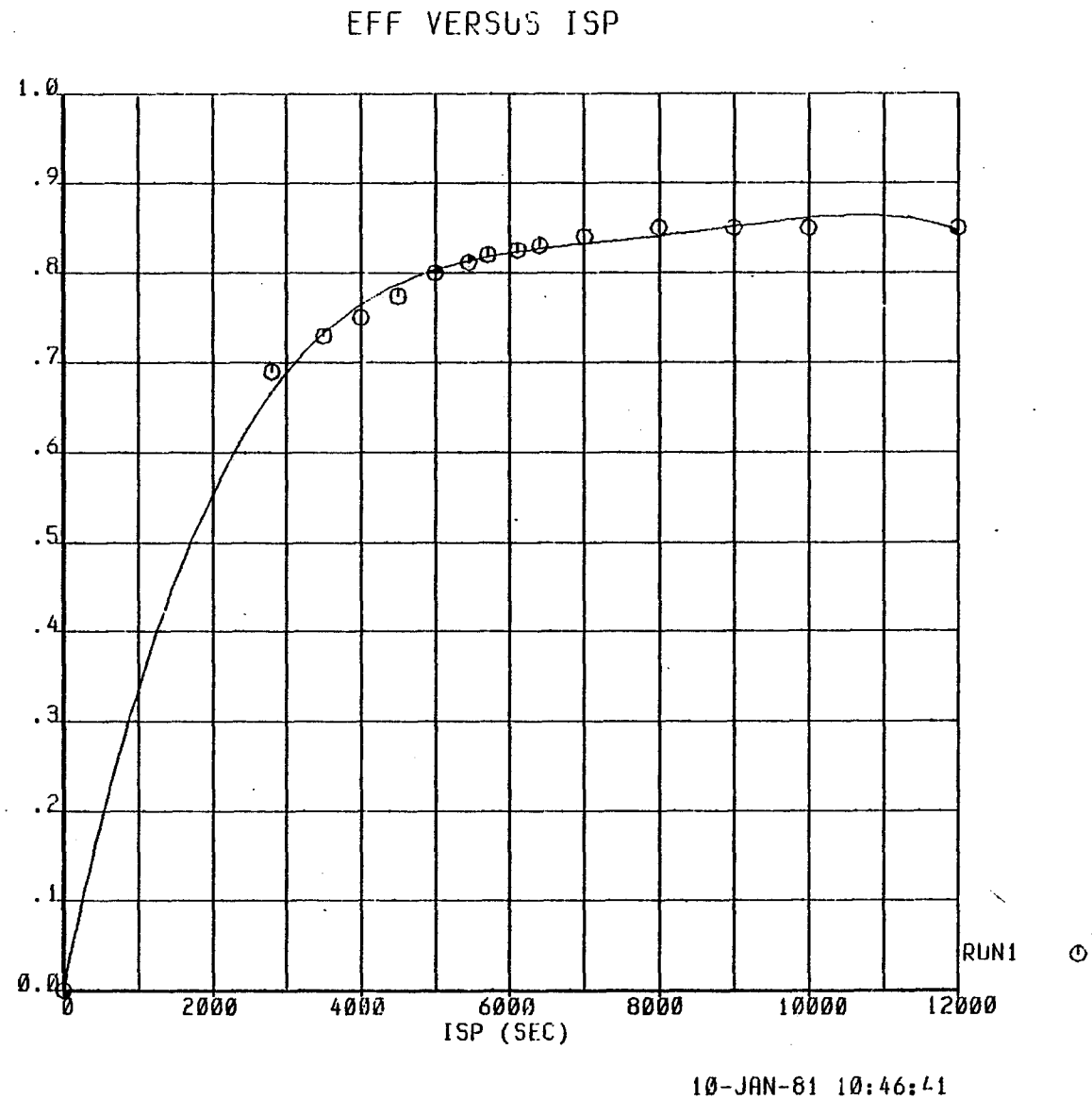

FIGURE 4-47 EFF VERSUS ISP

Parameter	PLATE			MODULAR ANTENNA			SERIES OF ANTENNAS		
	Small	Medium	Large	Small	Medium	Large	Small	Medium	Large
Scaling Parameter	30	700	21000	15	60	200	2	6	10
M_{LSS} (kg)	170	91880	$8.27X10^7$	2025	8100	27000	40270	$1.21X10^5$	$2.013X10^5$
Optimum I_{sp} (sec)	9800	>60000	>60000	12000	10500	3600	15000	10500	7500
$M_{Chem\ Eng + Tank}$ (kg) @ I_{sp} = 300 sec	19.4	730	70000	24.0	51.0	110	130	300	400
$M_{Elec\ Eng + Tank}$ (kg) @ I_{sp} = 3000 sec	5.3	260	50000	11.0	32.0	140	80	155	290
$M_{Elec\ Eng + Tank}$ (kg) @ I_{sp} = Optimum	5.3	300	30000	15	47.0	120	160	69	155
$M_{APS\ (including\ Fuel)}$ (kg) Chem Eng @ 300 I_{sp}	86.2	28920	$2.55X10^7$	537	2170	8720	10060	30100	50000
$M_{APS\ (including\ Fuel)}$ (kg) Elec Eng @ 3000 I_{sp}	9.7	2520	$2.08X10^6$	50	193	1350	810	3400	7100
$M_{APS\ (including\ Fuel)}$ (kg) Elec Eng @ I_{sp} = Optimum	6.9	410	130000	26.	95	1250	330	2300	3950

TABLE 4-6 SUMMARY OF MASS COMPONENTS

	Parameter	PLATE			MODULAR ANTENNA			SERIES OF ANTENNAS		
		Small	Medium	Large	Small	Medium	Large	Small	Medium	Large
	Scaling Parameter	30	700	21000	15	60	200	2	6	10
Chemical APS @ 300 sec	M_{Total} (kg)	256.2	$1.208X10^5$	$1.082X10^8$	2562	10270	34820	50330	$1.511X10^5$	$2.513X10^5$
	% M_{LSS}	66.3	76.06	76.4	79.04	78.9	77.5	80.0	80.1	80.1
	% M_{APS}	33.7	23.9	23.6	21.0	21.1	22.5	20.0	19.9	19.9
	% $M_{APS-Fuel}$	7.5	1.0	.1	1.2	.6	.4	.3	.2	.5
	% M_{Fuel}	26.2	22.9	23.5	19.8	20.5	22.1	19.7	19.7	19.4
Electric APS @ 3000 sec	M_{Total} (kg)	179.7	94400	$8.478X10^7$	2075	8293	28350	41080	$1.244X10^5$	$2.084X10^5$
	% M_{LSS}	94.4	97.3	97.5	97.6	97.7	95.2	98.0	97.3	96.6
	% M_{APS}	5.6	2.7	2.5	2.4	2.3	4.8	2.0	2.7	3.4
	% $M_{APS-Fuel}$	2.9	.2	.1	.4	.4	1.6	.2	.1	1.1
	% M_{Fuel}	2.7	2.5	2.4	2.0	1.9	3.2	1.8	2.6	2.3
Electric APS @ Opt. I_{sp}	M_{Total} (kg)	176.9	92290	$8.283X10^7$	2051	8195	28250	40600	$1.233X10^5$	$2.053X10^5$
	% M_{LSS}	96.0	99.6	99.8	98.7	98.8	95.6	99.2	98.1	98.0
	% M_{APS}	4.0	.4	.2	1.3	1.2	4.4	.8	1.9	2.0
	% $M_{APS-Fuel}$	3.0	.3	.04	.7	.5	3.0	.4	1.3	1.2
	% M_{Fuel}	1.0	.1	.16	.6	.7	1.4	.4	.7	.8

TABLE 4-7 COMPOSITE MAKEUP OF PRIMARY LSS CLASSES

determining total impulse needs would be run interactively until the fuel mass quantity converged. In the interest of time, the square of this factor multiplied by the first pass fuel mass was assumed to equal the final fuel mass. This method, while crude, yields a conservative total fuel mass number without sacrificing significant accuracy.

Table 4-6 is a collection of the raw mass component data for the three primary structures and the three APS types. Table 4-7 may add some insight into this raw data by showing the relative percent of the total mass of each component. It can be seen, for example, that the chemical system fuel mass makes up about 20 percent of the total system mass regardless of structure type or structure size. It is also true that for the electrical APS, the structure mass makes up 95 percent or more of the total system mass. For the chemical system, this number is closer to 78 percent. A more detailed examination of electrical system component mass is found in Figures E-23 through E-29.

4.4 Optimum Auxiliary Propulsion Characteristics

The quantitative data generated above were reviewed to single out the APS characteristics that have significant interactions with control functions and LSS characteristics. These are summarized below and identify the APS characteristics that are desirable and these that should be avoided.

4.4.1 Thrust Levels

In Section 3.2.1 thrust level requirements were investigated for each primary LSS class. There are three areas which contribute to an optimum APS determination. These are; 1) thrust level requirements, 2) throttling requirements, and 3) maneuvering thrust level requirements. Conclusions from each of these areas are somewhat mission specific and determination of an optimum APS is best dealt with in a parametric fashion.

The thrust level study pointed out that for certain sizes and classes of structures, the nominal mission (no maneuvering) thrust sizing criterion can be stationkeeping. Table 3-3 showed that for all small and some medium sized structures, stationkeeping accelerations were more significant than disturbance torques. This indicates that auxiliary propulsion rather than control moment gyros (CMG's) would be used on these structures for attitude

control. For very large sructures, the disturbance torques dominate stationkeeping except for the box structure. For these structures, CMG's of considerably greater mass and power requirements than currently available would have to be compared to an APS to decide which is optimal. For the purpose of this study, it is assumed auxiliary propulsion alone is required.

The thrust levels required for an optimum APS were given as a function of scaling parameter in Figures 3-23 through 3-25. To characterize the small, medium, and large primary class requirements, Table 4-2 in Section 4.3.2 was constructed. These thrust requirements were developed without regard to the effects on surface accuracy by relatively large thrust levels. In Section 4.2, the maximum allowed thrust/thrust location was identified for the plate structure. Figures 4-43 and 4-44 showed the allowed thrust for three plate sizes.

For each size and each second moment of area (I), the surface accuracy and material used varies. It is evident from Figures 4-43 and 4-44 that surface accuracy requirements are a bigger driver than material used, at least in the broad context of this study. An average tolerance number has been chosen for each size and surface accuracy and examined the thrust/thruster tolerance against the thrust/thruster required.

Figures 4-48 and 4-49 illustrate the relation between allowed and required thrust. The dependent variable in these graphs is the ratio of required to allowed thrust. When this ratio is greater than one, the surface accuracy requirement is violated. These graphs can be used to define a "maximum" size for 100 thrusters. The validity of the analysis for very large numbers of thrusters is not established because the allowed thrust study was run only to a relatively small (25) number of thrusters. Extrapolation to 100 thrusters, however, seems reasonable as a first estimate to "maximum" size. Table 4-8 displays the maximum size under the various conditions.

Clearly, the range of the second moment of inertia, I, studied for the Solar Power Satellite was not sufficient to meet the strength requirements of even 100 thrusters. Additional analysis is indicated for future studies.

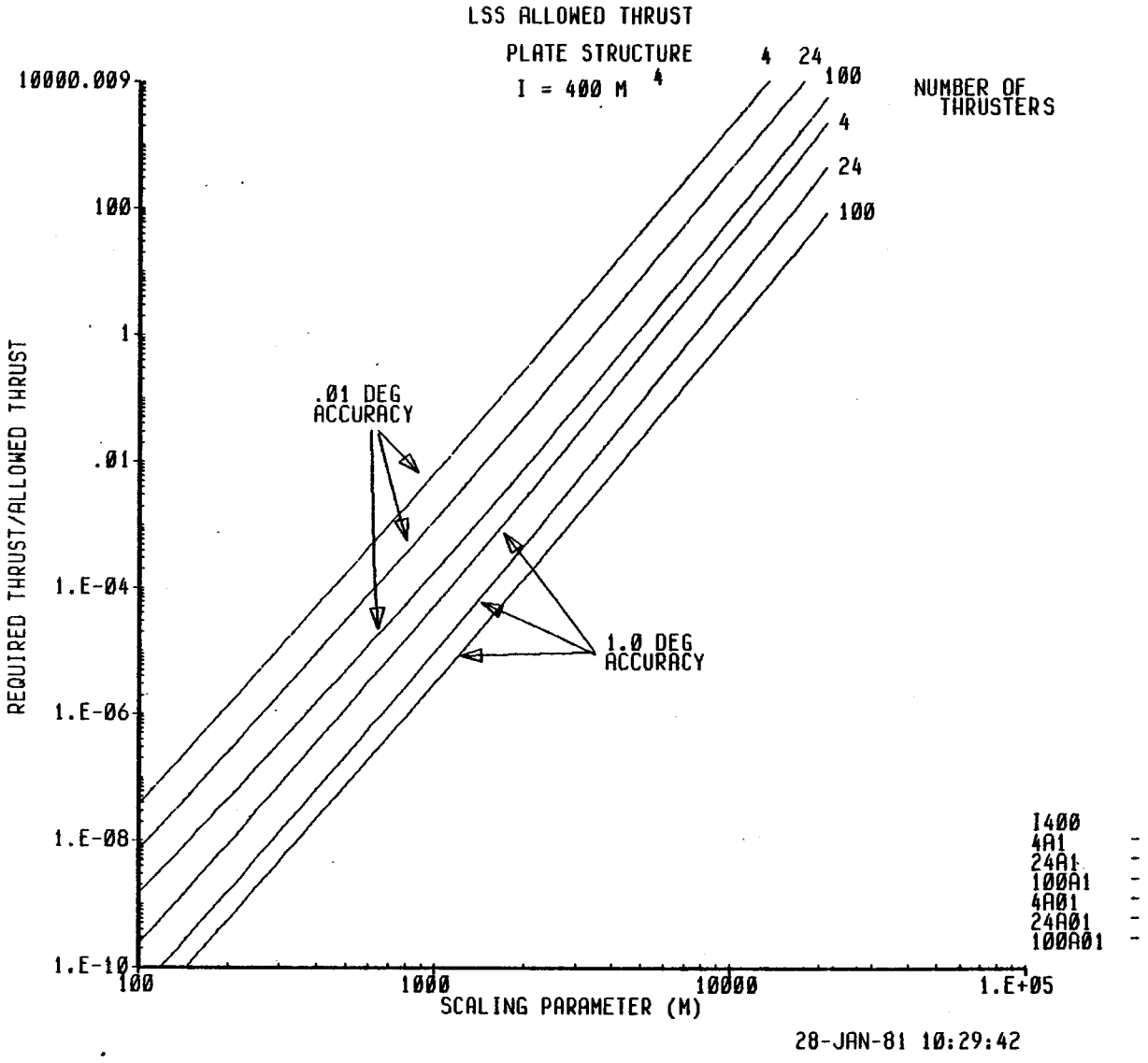

FIGURE 4- 48 LSS ALLOWED THRUST, PLATE STRUCTURE, SMALL I

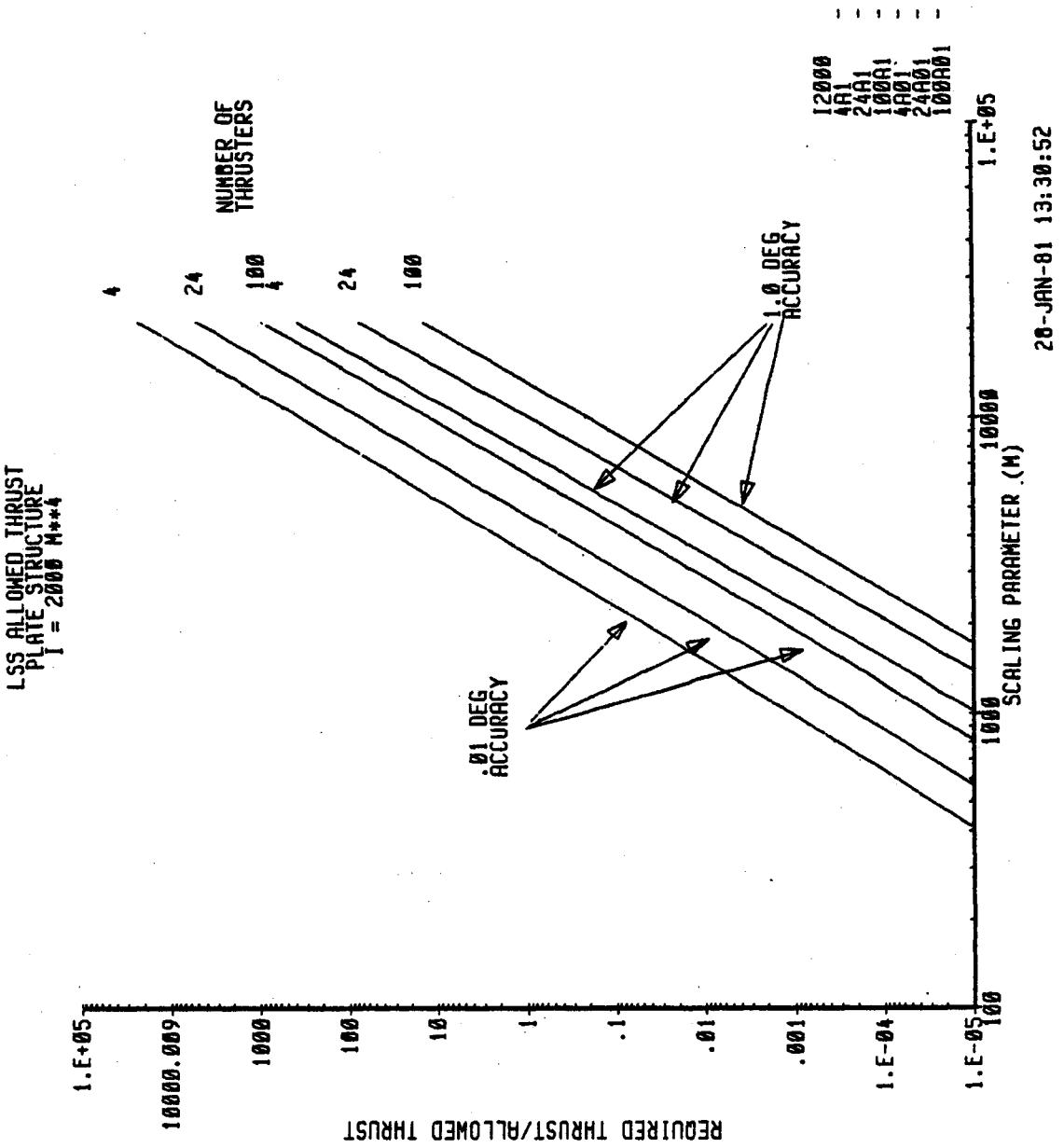

FIGURE 4- 49 LSS ALLOWED THRUST, PLATE STRUCTURE, LARGE I

	$I = 400\ m^4$		$I = 2000\ m^4$	
	Surface Accuracy (deg)			
Number of Thrusters	.01	1.0	0.1	1.0
4	2600	5800	3500	7600
24	3200	7500	4800	10000
100	4750	9700	6400	13000

Table 4-8 "Maximum" Allowed Size

The throttling requirements for the primary structures were examined in Figures 3-26 through 3-28. It can be concluded from these figures that geosynchronous operation with no maneuvering requires no more than a 5:1 throttling ratio and 4:1 or less is a sufficient ratio for all but the large series of antennas structure. Again, this ratio includes no maneuvering.

For a mission which requires stabilization at LEO, maneuvering control during LEO-GEO transfer, and nominal GEO operation, the throttling ratio was considerably higher. For the plate structure, this ratio is in a range of 90:1 for very small structures, to over 300:1 for large structures with a small number of engines. For the modular antenna, this ratio is between 100:1 and 200:1. A somewhat smaller range of throttling ratios is found for the series of antennas structures. These results were obtained using a judicious choice of axis for plane change maneuvers in LEO-GEO transfer. Nonetheless, the required throttling ratio is from 35:1 to 110:1.

Throttling ratios are entirely mission dependent and indicate only a rough guess at the ratios necessary. It can be said, however, that most probably two ranges of auxiliary propulsion and perhaps two entirely different types of auxiliary propulsion are dictated for a mission requiring both LEO and GEO operation.

It can be concluded that for moderately high speed slews, the thrusting requirements for maneuvering rather than disturbance cancellation may size the auxiliary propulsion system. For this study, the thrust levels shown in Table 4-2 will set the standard to compare existing technology.

4.4.2 Modulation

Disturbance cancellation, pointing and shape control are the control functions most affected by modulation. Accurate pointing requires the exact cancellation of disturbance torques. Since these vary in magnitude, typically from some maximum value all the way down to zero, the control torques should have the same capability. Shape control requires accurate timing or phasing and there are limitations on impulse delivered if active damping is to be effective. Maneuver, stationkeeping and desaturation are, in general, insensitive to modulation effects.

The two most practical forms of modulation for APS are amplitude and pulse. The requirements and characteristics are different for each form and are best treated separately.

Amplitude Modulation

Proportional control becomes possible with full amplitude modulation. Once the steady state condition has been reached, this type of system generates control torques which match the disturbances. The method is thus efficient in expending no more energy than necessary.

Pointing accuracies are compromised if modulation is not possible down to zero. If T_c is a lower torque bound a hangoff error occurs, given by equation (4.11); i.e.,

$$\theta_s = T_c/I\omega^2$$

This error can be eliminated if necessary, either by using opposed thrusts to generate very low and zero torques or by reverting to on-off operation. Both will incur propellant penalties as shown in Figures 4-6 and 4-11. A wider thrust range than is possible with one thruster can be achieved by clustering several units of low thrust. Generally this will incur a weight penalty.

Shape control requires a thrust in phase with the structure velocity at the thruster location. A minimum thrust bound is relatively unimportant and results only in a small decrease in damping.

Pulse Modulation

By varying the time on to total time ratio (the duty cycle) any effective thrust can theoretically be attained. Pulsed operation may be less desirable than proportional, however, because the discrete pulses may excite structural oscillations and the time between pulses, for very low effective values, may be excessively long. Proportional operation can be approximated at high duty cycles by a pulsed system but below a certain level of disturbance torque, given by equation (4.57),

$$D < I\dot{\theta}_d^2/4\theta_d$$

it is necessary to use limit cycle operation. This is not fuel efficient, in fact at zero disturbance torque, the propellant used will be four times the minimum (corresponding to D/eI_{sp}) as shown in Figure 4-20. Propellant consumption can be lowered in limit cycle operation by decreasing the minimum impulse bit, MiB. This is particularly effective in the smaller vehicles as shown in Figure 4-11.

Table 4-9 shows the minimum impulse bit required to achieve specified pointing accuracies for small, medium and large plate structures. These data were developed from Figures 4-11 and 4-48 assuming 5 percent of the propellant mass is used for limit cycling. The minimum impulse bits required should prevent no problem in most cases. Burn times can be found by dividing the minimum impulse bits by the thrust levels given in Table 4-2. Typically the minimum burn times are on the order of a second.

Shape control by a pulsed system is actually more efficient than using an amplitude modulated system as shown in Figure 4-27. There are, however, minimum impulse bit limitations. Pulsing must cease when

$$F\tau = m\omega g$$

as found by rewriting equation (4-74), to avoid exciting an oscillation instead of damping it. This implies that there is a limiting oscillation amplitude below which active damping is not possible with a pulse modulated APS.

Disturbance cancellation, maneuver, stationkeeping and desaturation are not significantly affected by pulse modulation system parameters.

4.4.3 Rise and Decay Transients

Pointing and shape control are the control functions most affected by rise and decay transients because they are sensitive to the time of application.

Accurate and efficient pointing in limit cycle operation is degraded by jet time on and time off delays. As shown in Figure 4-17 the delays distort the switchlines. Time on delays tend to increase the width of the deadzone and thus decrease accuracy. This is shown in Figure 4-21. Time off delays increase the limit cycle rate and this increases propellant consumption.

		Pointing Accuracy (Deg)		
		.0001	.01	1.0
Size	I_{sp}	Min Bit Req (N - S)		
Small	300	1.095×10^{-3}	.1095	10.95
	3000	7.75×10^{-4}	.0775	7.75
Medium	300	2.05	205	20500
	3000	1.84	184	
Large	300	112.7	1.127×10^{4}	1.127×10^{6}
	3000	100.7	1.007×10^{4}	1.007×10^{6}

Table 4-9 Minimum Impulse Bit Requirements

Time lags in proportional systems are generally unimportant for disturbance cancellation because the disturbances generally change slowly. A possible exception might occur during entry and exit from occultation. Even here the time taken to pass from full sunlight to full darkness in a geosynchronous orbit is over two minutes.

Shape control is particularly sensitive to the time of thrust application. In proportional systems a time lag causes a phase shift and tends to decrease damping, Figure 4-9. Table 4-10 shows the time constants permitted to achieve various levels of damping. The damping is expressed as the ratio of the damping for the delayed system divided by the damping of a perfect system. In pulsed system on delays have a similar effect as shown in Figure 4-18. Table 4-11 shows the delays permitted to achieve a given damping ratio. The data assumes a $\beta = 2F/m\, q_o$ of 0.4. Since large structures have lower frequencies and longer periods of oscillation, it is the smaller vehicles that will be most sensitive to time lags and on delays.

4.4.4 Number and Distribution of Thrusters

Shape control is the primary control function to interact with the number and distribution of thrusters. It is clear from Figure 4-26 that the greater the number of thrusters the lower the deflection during translation. In rotation, there appears to be a minimum in the 8 to 10 range, Figure 4-27. However, data in Figures 4-48 and 4-49 indicate that the number of thrusters may have to be very large to perform stationkeeping and keep deflections within limits for very flexible vehicles. The need for distributed thruster arrays brings up questions of implementation. Should commands be generated in a centrol computer or spread among distributed microprocessors? Should the thrusters be self contained units with their own tanks, propellant, PPU's etc., or should support equipment be centralized?

Secondary effects of distributed thrusters relate to efficiency. The effective moment arm for an (N-1) spacing decreases from 0.50L to 0.25L as the number of thrusters increases, Figure 4-21. An (N+1) shows improvement as the number increases, but from a low of 0.166L at N=2 to the asymptotic value of 0.25L for a large number. This means increased propellant

SIZE	SMALL	MEDIUM	LARGE	SMALL	MEDIUM	LARGE
RATIO OF DAMPING RATIOS	I = 400 m^4			I = 2000 m^4		
	DELAY TIME CONSTANT					
	msec	sec	hr	msec	sec	hr
1.0	0	0	0	0	0	0
0.9	0.90	11.5	86.5	0.41	5.2	38.7
0.8	1.36	17.4	131	0.62	7.8	58.4
0.7	1.77	22.7	170	0.80	10.1	75.9
0.6	2.21	28.3	212	1.00	12.7	94.9
0.5	2.70	34.7	260	1.22	15.5	116
0.4	3.32	42.5	318	1.50	19.0	142
0.3	4.13	53.0	397	1.87	23.7	177
0.2	5.41	69.3	519	2.45	31.0	232
0.1	8.11	104	779	3.67	46.5	348

Table 4-10 Effect of Time Delays on Shape Control of Aluminum Plate Structures, Continuous System

SIZE	SMALL	MEDIUM	LARGE	SMALL	MEDIUM	LARGE
DAMPING CONSTANT	I = 400 m^4			I = 2000 m^4		
	TIME DELAY					
	msec	sec	hr	msec	sec	hr
1.0	0	0	0	0	0	0
0.9	0.83	10.4	78.5	0.37	4.7	35.1
0.8	1.24	15.7	118	0.56	7.1	52.7
0.7	1.56	19.6	14.8	0.70	8.9	66.1
0.6	1.85	23.4	176	0.83	10.6	78.9
0.5	2.15	27.1	204	0.96	12.3	91.3
0.4	2.45	30.8	232	1.09	14.0	104
0.3	2.76	34.8	262	1.23	15.8	117
0.2	3.11	39.1	295	1.39	17.7	132

Table 4-11 Effect of Time Delays on Shape Control of Aluminum Plate Structures, Discrete System

consumption to obtain the same torques for a distributed system over that for a rigid vehicle with a minimum number of thrusters. There appears to be a need for optimum placement to obtain the best combination of low deflection with efficient operation. Figure 4-41, for just two thrusters, shows that performance can be very sensitive to thruster location.

4.4.5 Mass and I_{sp} Considerations

There were three areas investigated in Section 4.3 which contribute to optimum auxiliary propulsion system characteristics. These areas are mass distribution, optimum I_{sp}, and a chemical/electrical system mass comparison. As in previous discussions of optimum charactristics, the areas covered in this section are ultimately mission specific. The scaling laws leading to the optimum I_{sp} determinations and the chemical/electrical mass comparison are not design specific. They can only offer gross trends in design considerations rather than specific design characteristics.

Two methods of APS mass distribution were examined in Sections 4.2 and 4.3.1 for the distributed thruster classes. An equal distribution of mass along a beam was compared with 8 concentrated masses in an N-1 distribution. The parameter used for comparison was surface deflection. Results obtained from this study show that for a vehicle undergoing a rotation under torque, distributed mass provides significantly less surface deflection than concentrated mass. Under translation, concentrated masses at thruster locations provide less deflection than an equally distributed system.

An optimum distribution scheme depends on what function the APS must provide. If this function is primarily stationkeeping, mass concentrated at thruster locations is the best answer. If this function is maneuvering or disturbance cancellation, distributed mass provides the optimum answer.

Specific impulse sensitivity was the subject of Section 4.3.2. Three separate studies determined the optimum I_{sp} for electrical auxiliary propulsion systems. The optimum I_{sp} for a chemical system is very simply as high as possible.

Each method indicated similar trends for the optimum I_{sp}. For the plate structure, very high I_{sp}, greater than 10000 sec, was indicated for each size of structure regardless of the efficiency scaling laws used. This is true of all systems where the power is "free". For the modular antenna and series of antennas, the optimum I_{sp} is dependent on size. For small structures, the optimum I_{sp} is 10000 to 13000 seconds as shown in Table 4-6. As structures reach their respective maximum scaling parameter values, the optimum I_{sp} falls to 3500-4000 for the modular antenna and 800 to 1600 for the series of antennas. This indicates that optimum I_{sp}'s may be very sensitive to size and specific design.

4.5 Single Shuttle Launch Impact on APS Mass

The thrust level requirements for the single shuttle launch deployable vehicles were developed in Section 3.4. These requirements were then used to generate APS mass values for each scaling asumption. For the single shuttle limited structure study, a slightly different set of scaling assumptions was used than for the erectible structures. The system modelling equations also contain some differences for the deployable structures. These variations are described below.

Four system mass sizing assumptions were used for the single shuttle launch category. These classes have three altitudes - 300 km, 500 km and geosynchronous orbit as well as two LSS angles considered. The 300 km altitude was considered with a 10 degree LSS angle only. A worst case angle at 300 km altitude requires a thrust level that cannot be met by current state of the art (SOA) electric thrusters and was eliminated in favor of considering a 10^{o} offset. At 500 km, both a 10 degree offset and a worst case angle were considered. The geosynchronous thrust requirement for a worst case angle can be met by current electric thrusters and was included as a prudent requirement for on-orbit applications.

The system modelling equations used for deployable structure APS sizing are shown in Table 4-12. The thruster and PPU mass include factors for the mounting structure and gimbal mechanism. These equations were utilized with the thrust/thruster requirements in Table 3-11 and 3-12 to develop a set of APS system mass comparisons for chemical and electric systems.

TABLE 4-12 SYSTEM MODELING EQUATIONS

COMPONENT	UNITS	EQUATION
FUEL MASS	kg	M_p = TOTAL IMPULSE / (I_{sp} x 9.81)
TANK MASS	kg	$T_v = M_p$ / SPECIFIC VOLUME OF PROPELLANT[1]
		$T_r = \sqrt[3]{\frac{3\,T_v}{4\,\pi}}$
		$T_a = 4\,\pi\,T_r^2$
		$M_T = 5.62 \times T_a$
THRUSTER MASS	kg	$M_{Elec.\ eng.} = 12400.\ (T / I_{sp})^{.675}$
		$M_{Chem.\ eng.} = .056\ (T) + .54$
POWER	kw	$P = 9.807\ (T)\ (I_{sp}) / 2\eta_{sys}$
SOLAR ARRAY MASS	kg	$M_{S/A} = 13.5\ (P)$
SOLAR ARRAY AREA	m^2	$A_{S/A} = 8.96\ (P)$
POWER PROCESSOR MASS	kg	$M_{PPU} = 2.1 \times 6.5 \times (P)$

1 V_{SP} = 1 gm/cc CHEMICAL

V_{SP} = 13.5 gm/cc ELECTRICAL

Appendix E contains the single shuttle launched LSS total system mass breakdown data in Figures E-30 through E-41. Chemical and electric systems are compared using two chemical I_{sp}'s and three electric I_{sp}'s. The chemical I_{sp}'s of 250 and 500 represent the SOA and approximately the theoretical limit of chemical engines. Electric I_{sp}'s of 1000, 3000, and 10000 sec were considered. All three electric I_{sp}'s were graphed when they would fit on the same scale. In those cases where the 1000 sec or 10000 sec I_{sp} scaling yielded answers that were not comparable to 3000 seconds, only two electric I_{sp}'s were graphed. The APS mass was obtained in an iterative fashion by assuming a total LSS mass, calculating a required mission V, and then sizing an APS and fuel mass. The calculated hardware and fuel mass were added together with the constant (assumed) structure mass to get a new total LSS mass. The estimated LSS mass was compared with the calculated mass and a new total mass estimate derived. This process continued until the calculated mass was within one percent of the estimated mass. The number of iterations to converge on a system mass was never more than four and often only one or two.

The information contained in Figures E-30 through E-41 is summarized in tabular form in Table 4-13. In this table, the system having the lowest mass is given for each class, size and scaling assumption. Chemical SOA capability is assumed to be 250 sec I_{sp}. The electric SOA scaling data is presented later. The table ignores the thrut level limitations discussed above and shows only the comparison of systems mass. The I_{sp} indicated by the electric systems is the I_{sp} giving the least electric system mass.

TABLE 4-13

APS MASS COMPARISON FOR SOA CAPABILITY

ORBIT ALTITUDE	300 km	500 km	500 km	GEO
LSS ANGLE	10	10	WORST CASE	WORST CASE
SMALL STRUCTURES				
PLATE W/O BLANKET	ELECTRIC*, 3000 sec	ELECTRIC*, 10,000 sec	ELECTRIC*, 3000 sec	ELECTRIC, 10,000 sec
PLATE W/BLANKET	ELECTRIC*, 10,000 sec	ELECTRIC, 3000 sec	ELECTRIC, 3000 sec	ELECTRIC, 3000 sec
MODULAR ANTENNA	ELECTRIC*, 1000 sec	ELECTRIC, 3000 sec	ELECTRIC*, 3000 sec	ELECTRIC, 10,000 sec
SERIES OF ANTENNAS	ELECTRIC, 3000 sec	ELECTRIC, 3000 sec	ELECTRIC*, 3000 sec	ELECTRIC, 3000 sec
MEDIUM STRUCTURES				
PLATE W/O BLANKET	ELECTRIC*, 3000 sec	ELECTRIC, 3000 sec	ELECTRIC*, 3000 sec	ELECTRIC, 10,000 sec
PLATE W/BLANKET	ELECTRIC, 1000 sec	ELECTRIC, 3000 sec	ELECTRIC, 3000 sec	ELECTRIC, 3000 sec
MODULAR ANTENNA	CHEMICAL	ELECTRIC*, 3000 sec	CHEMICAL	ELECTRIC, 10,000 sec
SERIES OF ANTENNAS	ELECTRIC*, 1000 sec	ELECTRIC*, 1000 sec	CHEMICAL	ELECTRIC, 3000 sec
LARGE STRUCTURE				
PLATE W/O BLANKET	ELECTRIC*, 1000 sec	ELECTRIC, 3000 sec	ELECTRIC*, 1000 sec	ELECTRIC, 3000 sec
PLATE W/BLANKET	ELECTRIC, 1000 sec	ELECTRIC, 3000 sec	ELECTRIC, 1000 sec	ELECTRIC, 3000 sec
MODULAR ANTENNA	CHEMICAL	ELECTRIC*, 1000 sec	CHEMICAL	ELECTRIC, 3000 sec
SERIES OF ANTENNAS	ELECTRIC, 1000 sec	ELECTRIC, 1000 sec	CHEMICAL	ELECTRIC, 3000 sec

*ELECTRIC SYSTEMS HAVE LOWER MASS THAN CHEMICAL SYSTEMS AT 250 sec I_{SP}, BUT NOT AT 500 sec I_{SP}

THIS PAGE INTENTIONALLY LEFT BLANK

5.0 TASK 5 - DETERMINATION OF ELECTRIC AND CHEMICAL TECHNOLOGY ADVANCES REQUIRED

The objective in Task 5 is to bring together the information developed in previous tasks to determine the advances auxiliary propulsion technology should take.

Electrical propulsion system characteristics are reviewed in the first subsection. Each significant characteristic has been addressed and the system components, such as power source and power processor, were examined. The process was then repeated for chemical propulsion systems. A comparison of the required APS characteristics needed to support LSS against the charactristics presently available is made in the last subsection. Analysis is presented which shows areas of adequacy and deficiency for both electric and chemical propulsion systems. The deficient regions show where technology efforts should be directed to make present day APS more suitable for future LSS.

5.1 Review of Current Electric Propulsion System Characteristics

The present technology level of electric propulsions system (EPS) concepts has been determined and evaluated in the context of their applicability to satisfy the requirements for LSS auxiliary propulsion. This section will be a detailed review of existing EPS charactristics and will include examination of the following topics:

- o Thrust Level
- o Overall Efficiency
- o Start-Up Requirements
- o Specific Impulse
- o Power Levels
- o Propellant Type
- o Life Characteristics

Baseline Technology Review - In a chemical propulsion system (CPS), the inherent performance is directly related to the energy released during combustion (or decomposition) of the propellants, and the expansion of bases through a supersonic nozzle. In the case of EPS concepts, energy is applied from an external source and there are no inherent constraints on the exhaust velocity that can be achieved. Therefore, the system

performance can be optimized, within limits, to maximize performance, minimize weight, or minimize costs.

The basic propulsion system components are the electric power source, a power processor to convert raw power into the various forms required by the thruster, and the thruster itself. Devices typifying the present state of the art are illustrated in Figure 5-1. A typical systems diagram is shown in Figure 5-2. The application of auxiliary propulsion systems to LSS will generally require broadly distributed units. Thus, the technology associated with propellant storage and distribution concepts, power cabling, and thermal control are important and will be reviewed.

Thruster Characterization - The key issue in characterizing any EPS concept is selection of the type and size of the basic thruster. From this selection follows the basic requirements for power processing and overall system efficiency, and it also determines the feasible specific impulse range for any given propellant type. Since LSS can generally be assumed to require long, multi-year mission dirations, it follows that a high specific impulse propulsion system will be desired. Only the electrostatic ion thruster concept is capable of satisfying high performance requirements in the near future; therefore, the study and application of these devices will be emphasized.

An indication of electric thruster technology status is illustrated in Figures 5-3, 4 and 5. Figures 5-4 and 5-5 show two currently available ion thrusters which can be characterized by accepted theory. Only the ion thruster is, in essence, a device that has a wide latitude for beam currents ranging from 0.5 amps to about 6.0 amps, and screen voltages of 1000 to 4000 volts. These operating parameters correspond to a specific impulse range on the order of 2900 to 5000 seconds; performance trends with constant beam current are shown in Figure 5-6. A reduced specific impulse on the order of 2000 seconds or less can be achieved (if desired) by the incorporation of a third (deceleration) grid. Performance values as high as 20,000 seconds have been demonstrated by other ion thrusters.

Power System Definition - Technology options for solar arrays have been characterized as suggested by the specific weight trends shown in Figure

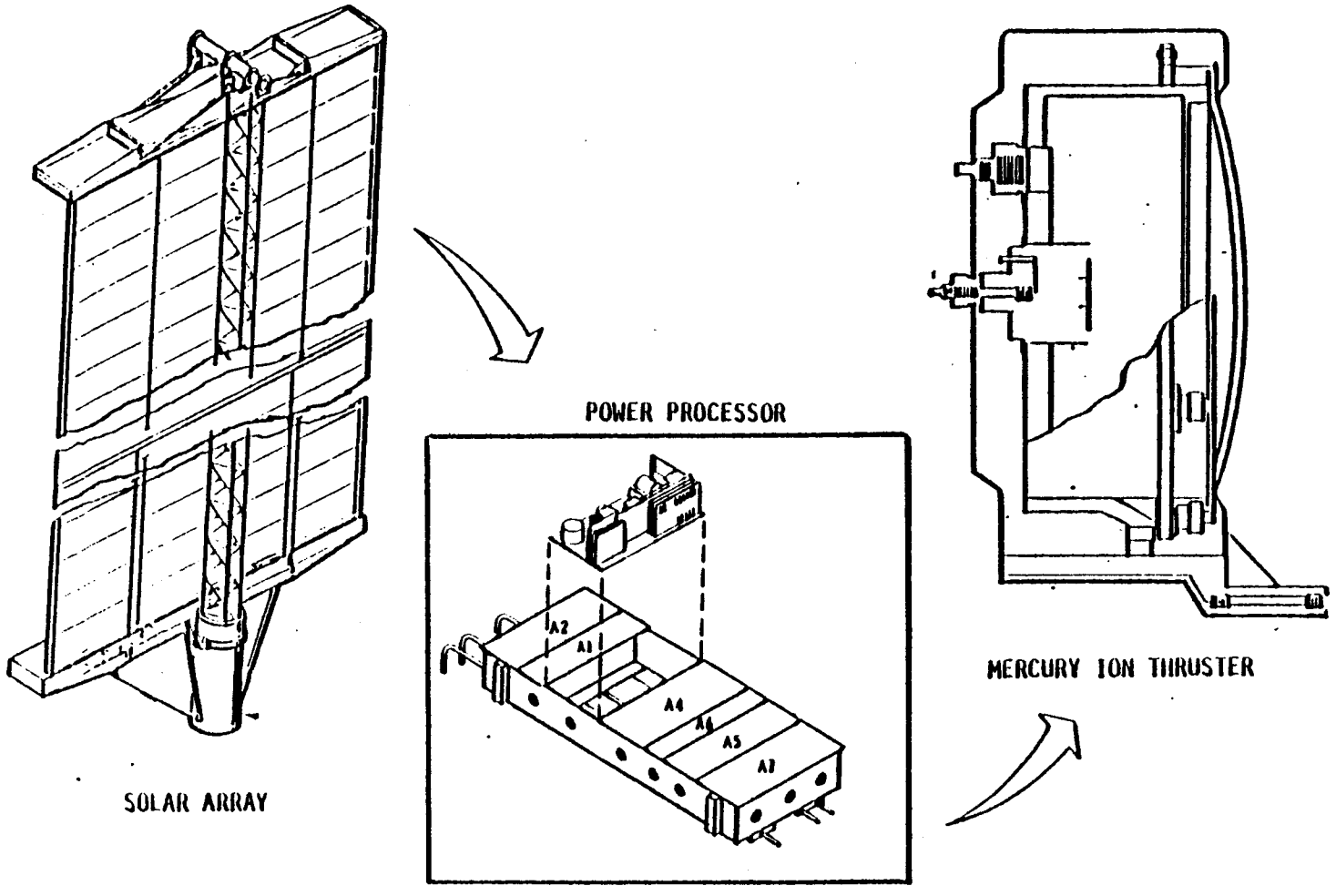

FIGURE 5-1 CURRENT ELECTRIC PROPULSION SYSTEM ELEMENTS

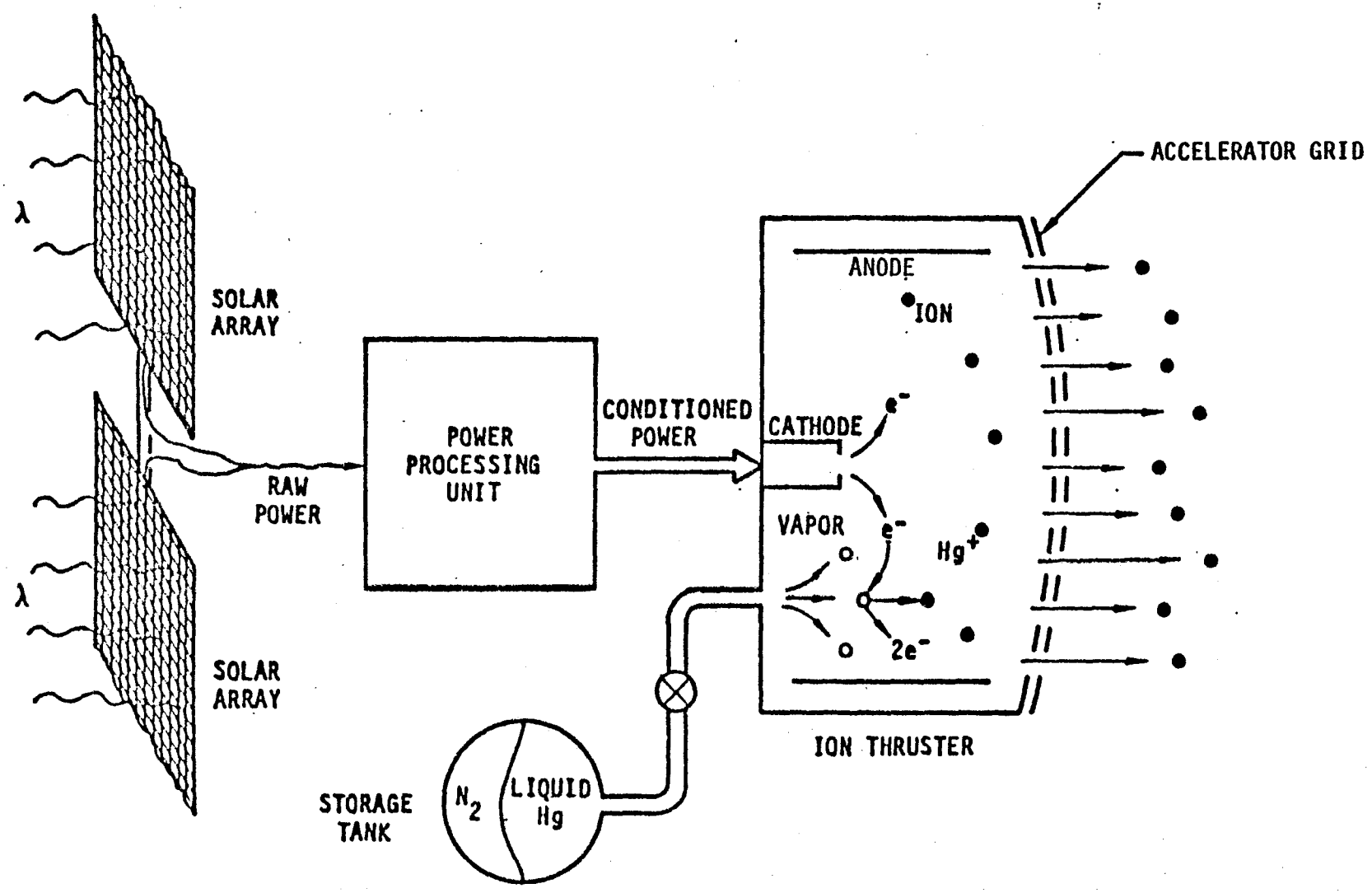

FIGURE 5-2 Ion Propulsion Functional Diagram

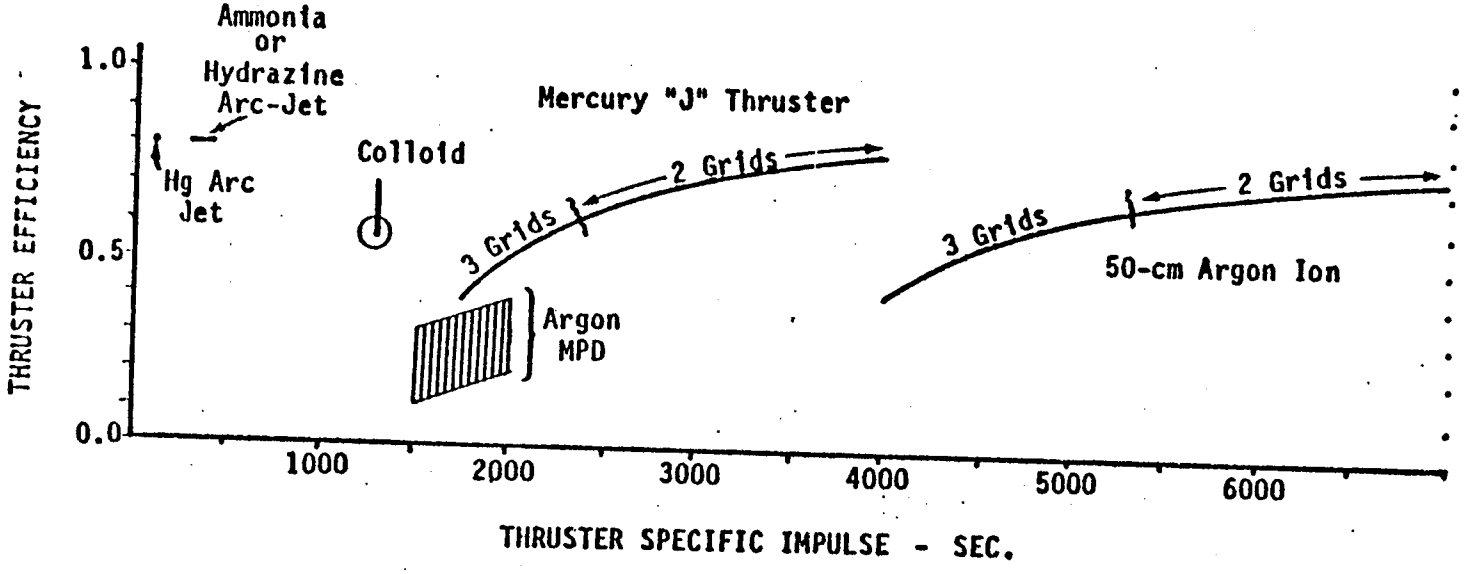

FIGURE 5-3 COMPARISON OF DEMONSTRATED ELECTRIC THUSTER EFFICIENCIES

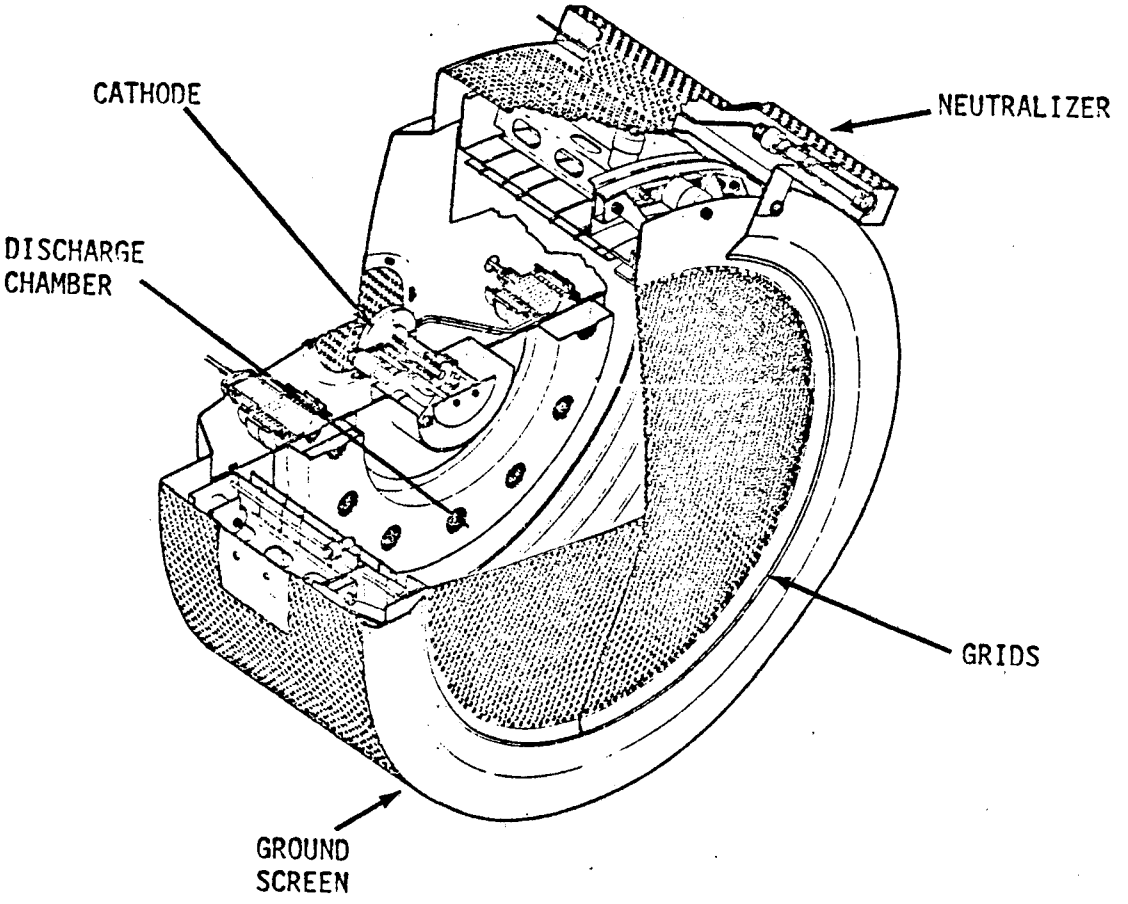

FIGURE 5-4 Cutaway of the 30cm Ion Thruster

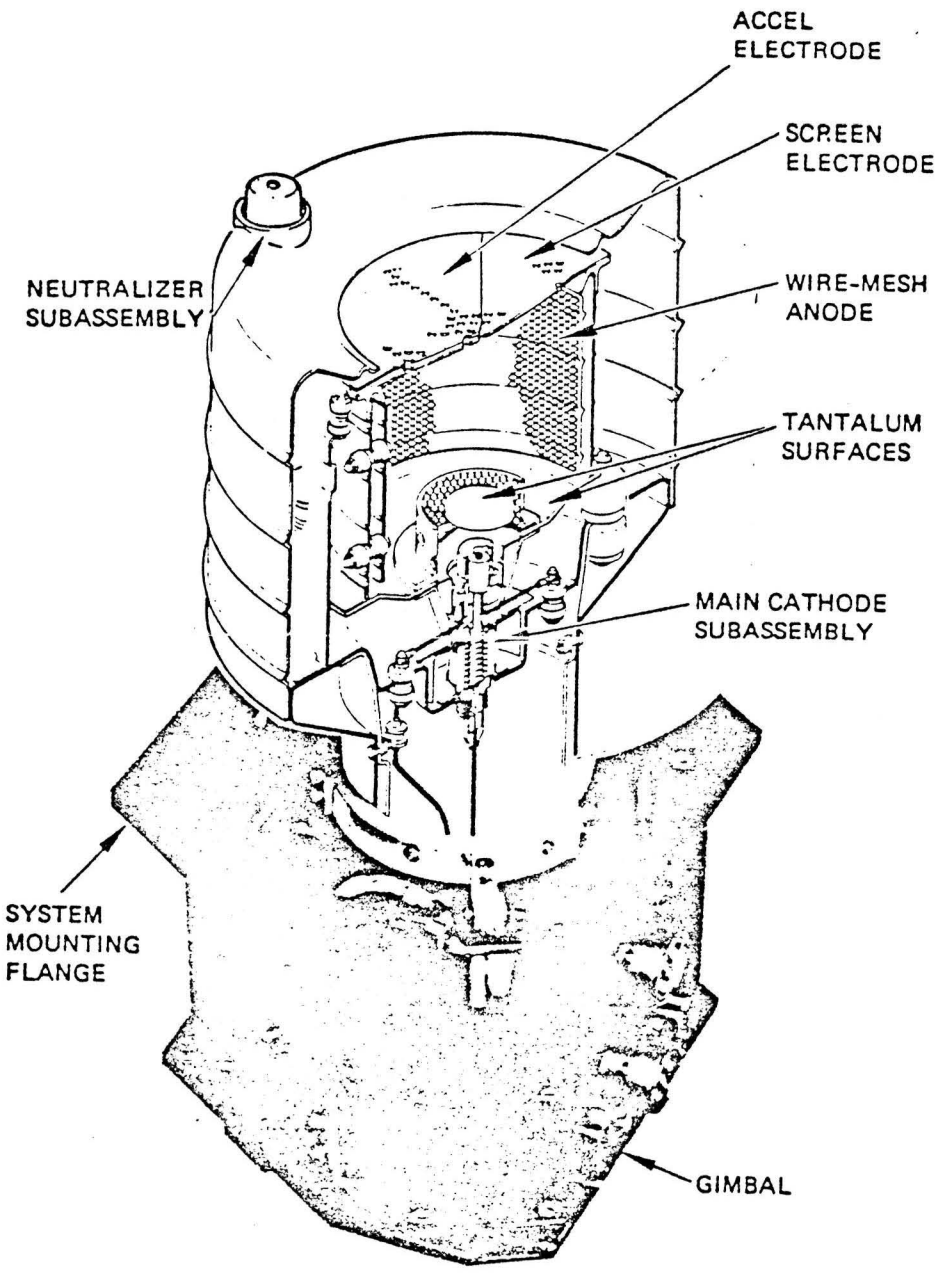

FIGURE 5-5 Isometric of EM 8-cm Thruster and Gimbal

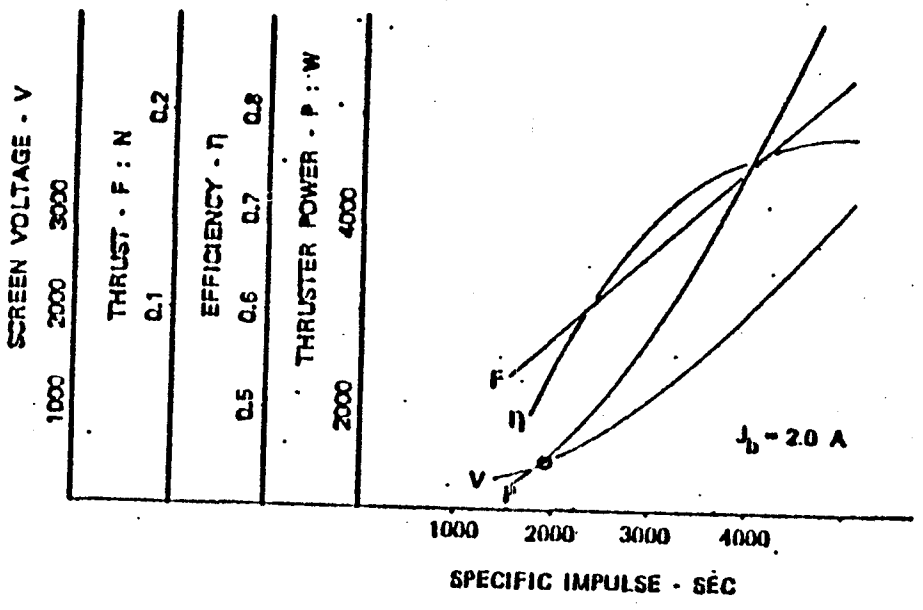

30-CM MERCURY ION J-TYPE THRUSTER CHARACTERISTICS

FIGURE 5-6 PERFORMANCE CHARACTERISTICS OF THE 30-cm J TYPE MERCURY ION THRUSTER AT A BEAM CURRENT OF 2.0 AMPERES

5-7. Variations from the SOA arrays are based on the NASA/MSFC 25 kw array updated to include the benefits of on-orbit fabrication; this latter assembly technique is particularly applicable if power requirements are determined to be on the order of 200 kw or higher. Sizing of the arrays was based on end-of-life characteristics thus allowing for life-cycle degradation.

Present ion thruster technology requires fairly complex power processing for proper operation; however, design and technology improvements are known, particularly for earth orbit missions. The functional module power is approximately 13 kg/kw. By simplifying power regulation requirements (for earth orbit operations), integrated heaters, and utilizing capacitor-diode voltage multipliers, the specific weight may be reducible to the order of 9 kg/kw. Power processor characterization trends are shown in Figure 5-8. A more ambitious approach to the auxiliary propulsion power system definition would be to utilize the array output directly, without the complexity of intermediate power processing - this approach can be considered only in the case of dedicated arrays. Minimization of power processing weight and cost is easily the most significant option for improving the utility of electric propulsion.

Starting Charactristics - The startup characteristics of an ion thruster are generally dictated by the thermal response parameters asociated with heaters and propellant vaporizers. Unless auxiliary power supplies are incorporated into the propulsion system design for continuous operation, a shutdown/startup sequence must be considered for each solar occultation occurrence. For low earth orbits, the thruster startup charactristics can require a considerable portion of the available sunlit period. For high orbits such as geosynchronous, however, the occultation period is minimal and a lengthy start sequence can be accommodated by simply anticipating thrust requirements. Figure 5-9 illustrates a typical start sequence for a 30 cm thruster; note that preheat operations account for the majority of the time, but that individual thermal response trends are on the order of 15 minutes. A 15 minute start sequence has been demonstrated with 8 cm mercury ion thrusters, and such an interval would appear to be acceptable to most, if not all, anticipated LSS control requirements.

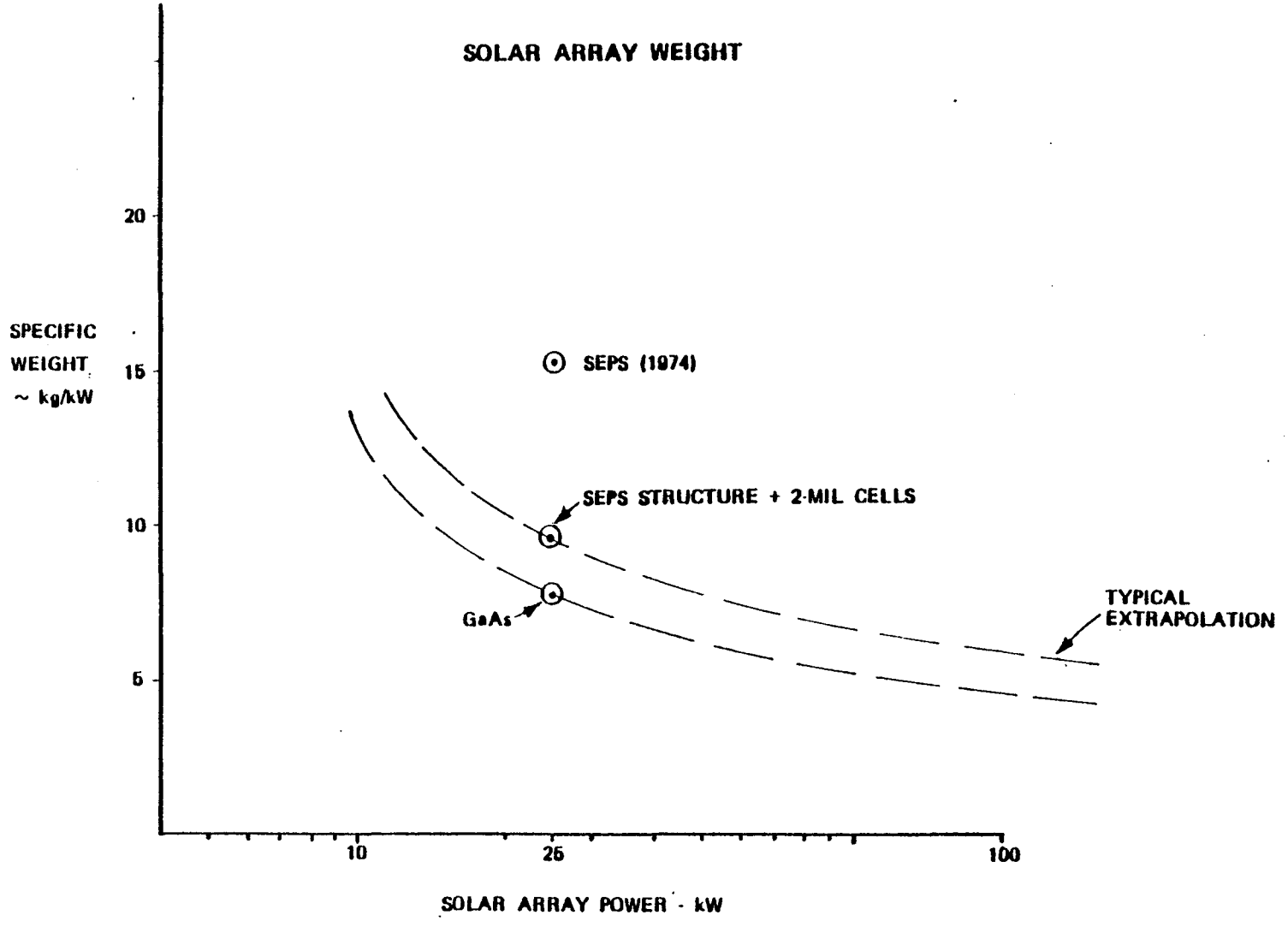

FIGURE 5-7 CONTEMPORARY SOLAR ARRAY TECHNOLOGY OPTIONS

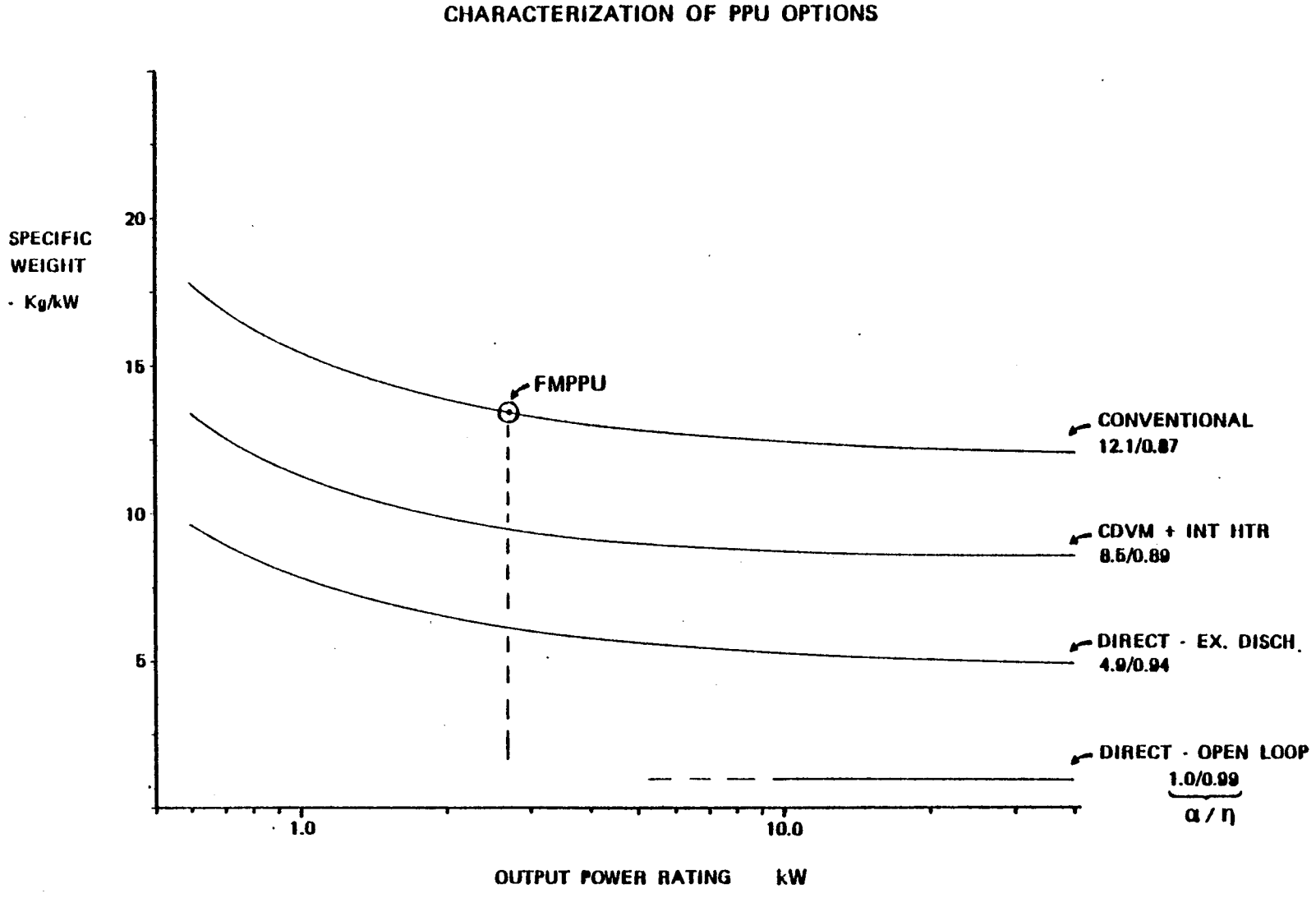

FIGURE 5-8 POWER PROCESSOR TECHNOLOGY OPTIONS AND BENEFITS

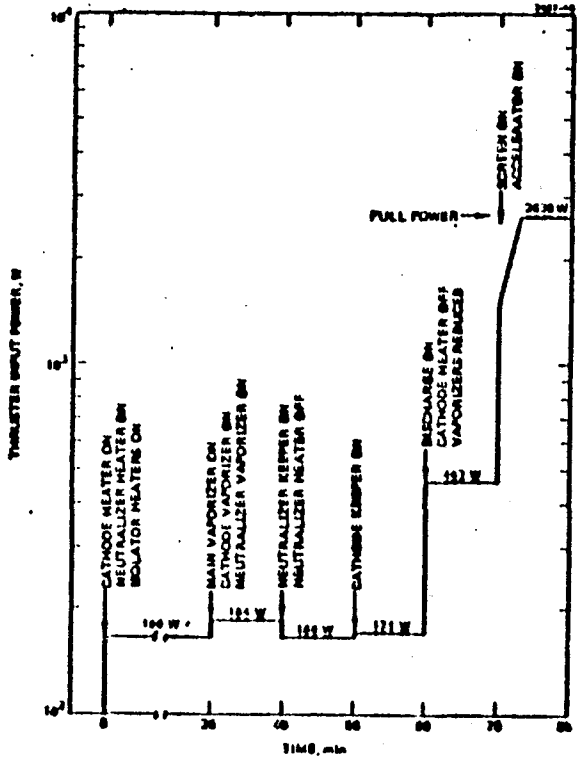

POWER REQUIREMENTS

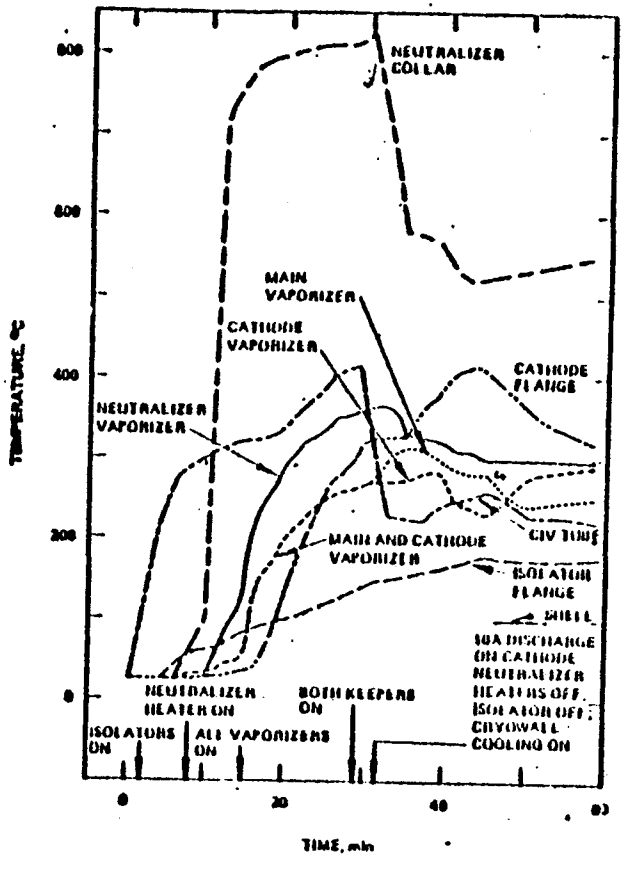

THERMAL RESPONSE

FIGURE 5-9 LABORATORY START SEQUENCE FOR A 30-cm MERCURY ION THRUSTER

Propellant Options - The current technology for ion propulsion systems, and near term anticipated program applications, envision the use of mercury or cesium as the system propellant. These are favored because of their high density which permits rather simple packaging and storage concepts, and their high atomic mass numbers that result in improved thruster performance characteristics. However, LSS vehicles may require large quantities of propellant for auxiliary propulsion and, as such, the preferred heavy metal propellant types may be environmentally unacceptable.

Electric Propulsion System Life Factors - A major life factor in ion thrusters is the double ion production rate, its relationship to beam current, and the erosion rate of elements within the device. Thruster lifetime characteristics are predicted by a bulk-averaged-plasma analysis. These analyses estimate plasma losses as a function of propellant type and thruster diameter. From this, efficiency and erosion life, including double ion effects, are determined. To illustrate this approach, consider the conceptual design of a 50 cm mercury ion thruster as shown in Figure 5-10. This design was analyzed to determine the effects of beam current on delivered specific impulse, thruster efficiency, and predicted life - these characteristics are shown in Figure 5-11. At this time, thruster life predictability as detrmined by analysis provides only trend data - this follows from the fact that double ion production is known to be sensitive to minor varitions in some thruster set-points such as cathode flowrate.

The following Table (5-1) provides summary of the thruster characteristics used in this study. Thes numbers are representative of ion thruster technology.

5.2 Review of Current Chemical Propulsion System Characteristics

A review of contemporary chemical propulsion system technology includes examination of the following characteristics:

- o Propellant Type
- o Thrust Level
- o Propellant Storage and Distribution
- o Specific Impulse
- o Transient Response
- o Life Limitations

	Technology Area	Currently Available
I	Thrust Levels	.001 - .13 N
II	Throttling Ranges	4:1 w/o clustering
III	Distribution Capability	Centralized systems with dedicated tank and power processor
IV	Time Constants	Instantaneous after warmup
V	Time Delays	15 minutes to 1 hour
VI	Minimum Impulse Bit	$< 1 \times 10^{-4}$ N-S for small thrusters
VII	I_{sp} Available	1500 to 6500 sec
VIII	Efficiency Range	Function of I_{sp} 60 to 85%
IX	Lifetime	~15000 hours (@ 2 Amps Beam Current)

Table 5-1 Technology Areas Considered

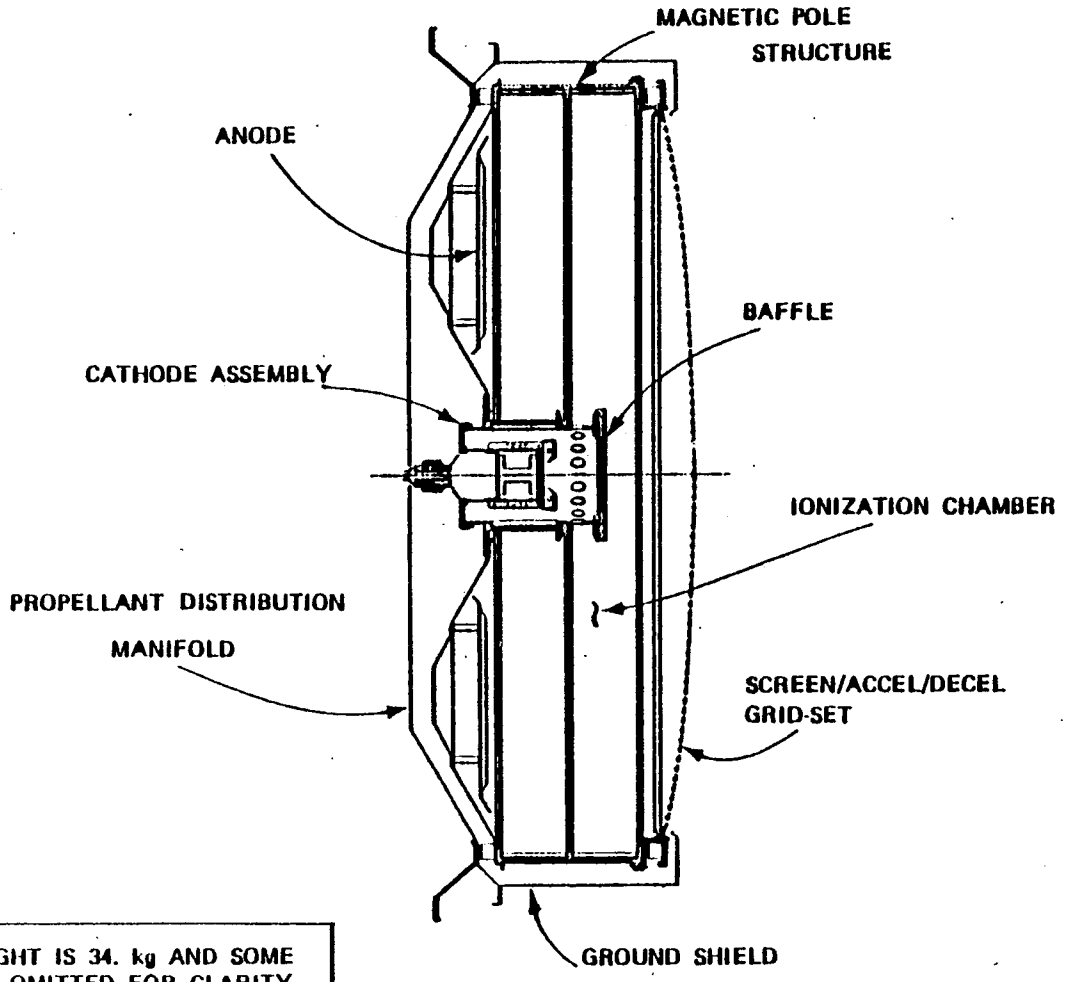

FIGURE 5-10 CONCEPTUAL 50-cm MERCURY ION THRUSTER

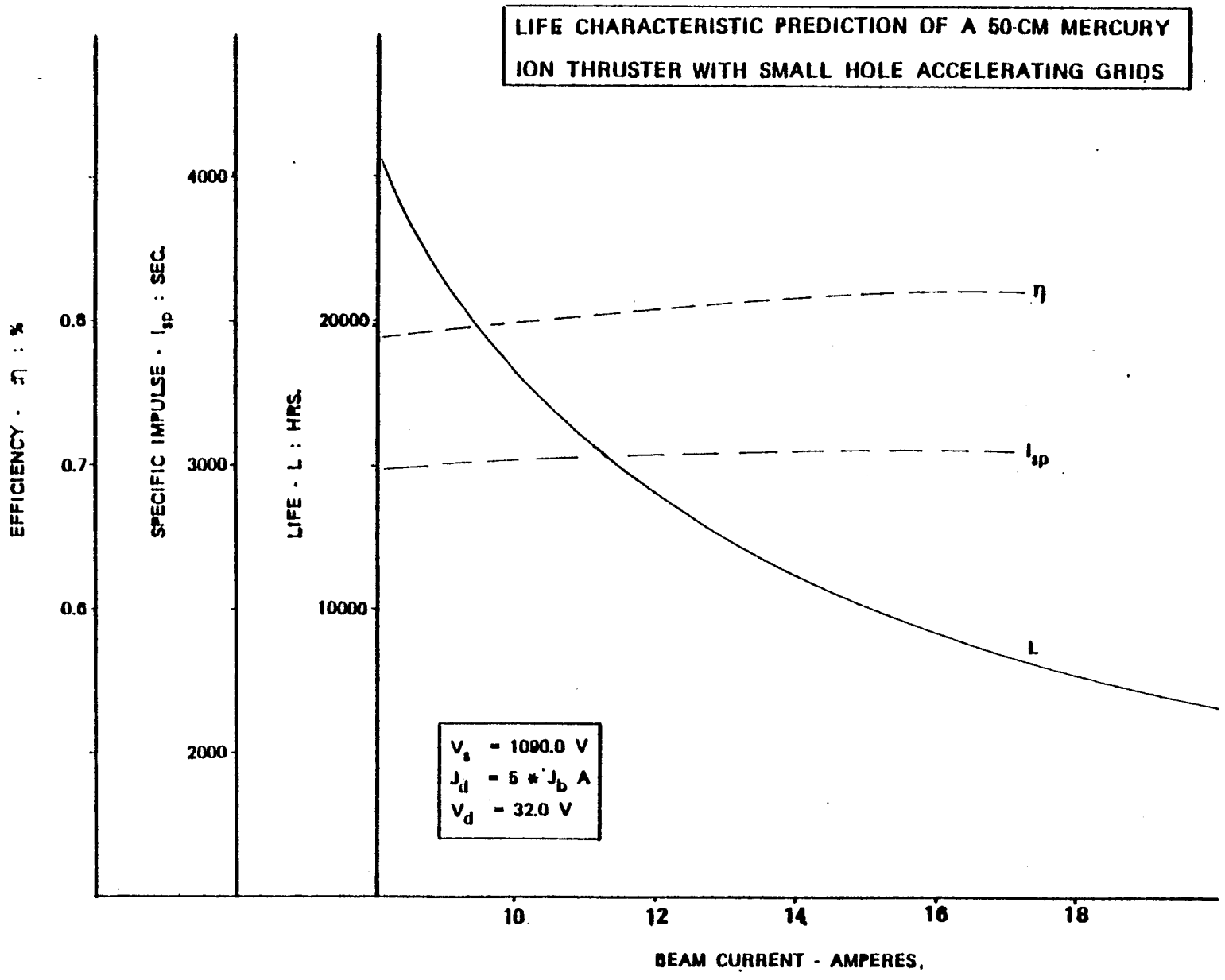

FIGURE 5-11 EFFECT OF BEAM CURRENT ON THRUSTER LIFT FOR A CONCEPTUAL 50-cm MERCURY ION THRUSTER

Baseline Technology Review - Chemical propulsion system concepts that have been developed encompass the gamut of cold gas, monopropellant, bipropellant, and solid propellant types, with sub-types consisting of variations in working fluid, and performance enhancement options. The general characteristics of these chemical concepts are summarized in a qualitative manner by generalized thrust/total impulse operating regimes as shown in Figure 5-12. These regimes are dictated by considerations of system weight, complexity and reliability, and cost.

Contemporary Thrust & Performance Characteristics - The performance attainable from a chemical thruster is basically dependent on the working fluid selection. Smaller variations within these groups are related to the specifics of any given thruster design such as injector details, nozzle expansion ratio, and compustion chamber characteristic length.

Early spacecraft development utilized monopropellant cold gas or hydrogen perozide (H_2O_2). With the development of Shell 405 catalyst in the early 1960's offering spontaneous thermal decomposition of hydrazine (N_2H_4), the use of this monopropellant has largely supplanted the lower performance monopropellants. N_2H_4 thrusters for attitude control systems have been developed over a thrust range from 0.1 to 2000 lb; however, most systems are less than 150 lb thrust. Examples of typical systems and their performance are listed in Table 5-2. Propellant flow rate increases with increased thrust level and catalyst bed volume also inceases to provide the required catalyst surface to decompose the propellant. Propellant shut-off valves can act in 10 - 20 milliseconds almost independent of size, so that minimum impulse bit will increase with thrust size as dictated by the amount of propellant in the catalyst bed.

Pulsing I_{sp} of an N_2H_4 thruster varies with pulse width due to the percentage of total impulse occurring during thrust buildup and tailoff. The pulsing I_{sp} is also a function of the duty cycle (ratio of on-time to off-time) due to the effect on catalyst bed temperature. I_{sp} may degrade to less than 30 percent of steady state I_{sp} at minimum pulse widths and duty cycles < 10 percent. To improve low duty cycle performance and prevent propellant freezeup (freezing point of $N_2H_4 \sim 36^{o}F$) some thruster designs have catalyst bed heaters. A 200 msec pulse every 15 minutes is programmed for IUS RCS thrusters to maintain catalyst bed temperatures.

TABLE 5-2 CURRENTLY AVAILABLE CHEMICAL SYSTEMS

PROPELLANTS	THRUST LEVEL – lb.	I_{SP} – sec. STEADY STATE	I_{SP} – sec. PULSE MODE	MIN. IMPULSE BIT – lb./sec.	COMMENTS
• MONOPROPELLANTS					
• H_2O_2	6	155			OPERATIONAL ON CENTAUR
• N_2H_4	0.1 – 2000				
TYPICAL THRUSTERS WITH SHELL 405 CATALYST	0.2	226	178 @ 70m/sec PULSE WIDTH	2.5×10^{-3}	OPERATIONAL, 7 PROGRAMS DEMONSTRATED 400,000 PULSES
	5.0	234	220	0.07	OPERATIONAL, NATO III, NRL/MSD ETC. 10 YR ON ORBIT LIFE
	30.0	235	100 – 200 @ .01 – 10% DUTY CYCLE	0.38	DEV. – IUS, DEMONSTRATED 3800 SEC. ON-TIME
	125	235	185 – 225 @ 1 – 10% D.C.	2.5 20 MS.	IR&D LONG LIFE DEV. – 8000 SEC. ON-TIME
	300 – 3000				DEV. FOR VELOCITY CONTROL – POTENTIAL CANDIDATE RCS THRUSTERS
	5	232	198 @ 50 MS.	0.75	IR&D – ELECTROTHERMAL DECOMPOSITIONS, POTENTIAL LIFE > 1×10^6 CYCLES, IMPROVED PERFORMANCE OVER CATALYST AT LOW DUTY CYCLE
• BIPROPELLANTS					
• MMH/N_2O_4	0.5 – 1600				
	0.5	270	180	0.004	DEV. ENGINE – PROBABLE LOWER LIMIT ON THRUST
	5.0	289	190 @ Min. BIT	0.02	INTELSAT – 1, 10,000 SEC. ON-TIME
	25.0	272, ϵ = 21	240 @ 40 MS.	0.85	SPACE SHUTTLE RCS DES. LIFE = 125,000 SEC TOTAL ON-TIME 500,000 CYCLES
• MMH/N_2O_4	100	310, ϵ = 150	190	0.55	APOLLO LUNAR, SERVICE MODULE RCS,
TYPICAL THRUSTER APPLICATIONS	300	282		120	VIKING ORIBTER MAIN ENGINE, POTENTIAL RCS ENGINE
	600	285, ϵ = 40	210 @ 50 MS.	30	SPACE SHUTTLE RCS DESIGN STUDY DESIGN GOAL = 100,000 SEC. ON-TIME 200,000 PULSES
	872	281, ϵ = 22	190 @ 40 MS.	35	SPACE SHUTTLE PRIMARY RCS DES. LIFE = 20,000 SEC. 60,000 CYCLES
• H_2/O_2	25 – 1500				
• LH_2/LO_2	25	400	348	0.5	DEMONSTRATION ENGINE – SPACE SYSTEM RCS STUDY
• GH_2/GO_2	1500	435	368	60	TECHNOLOGY PROGRAM – ADVANCED SPACE SYSTEM STUDIES

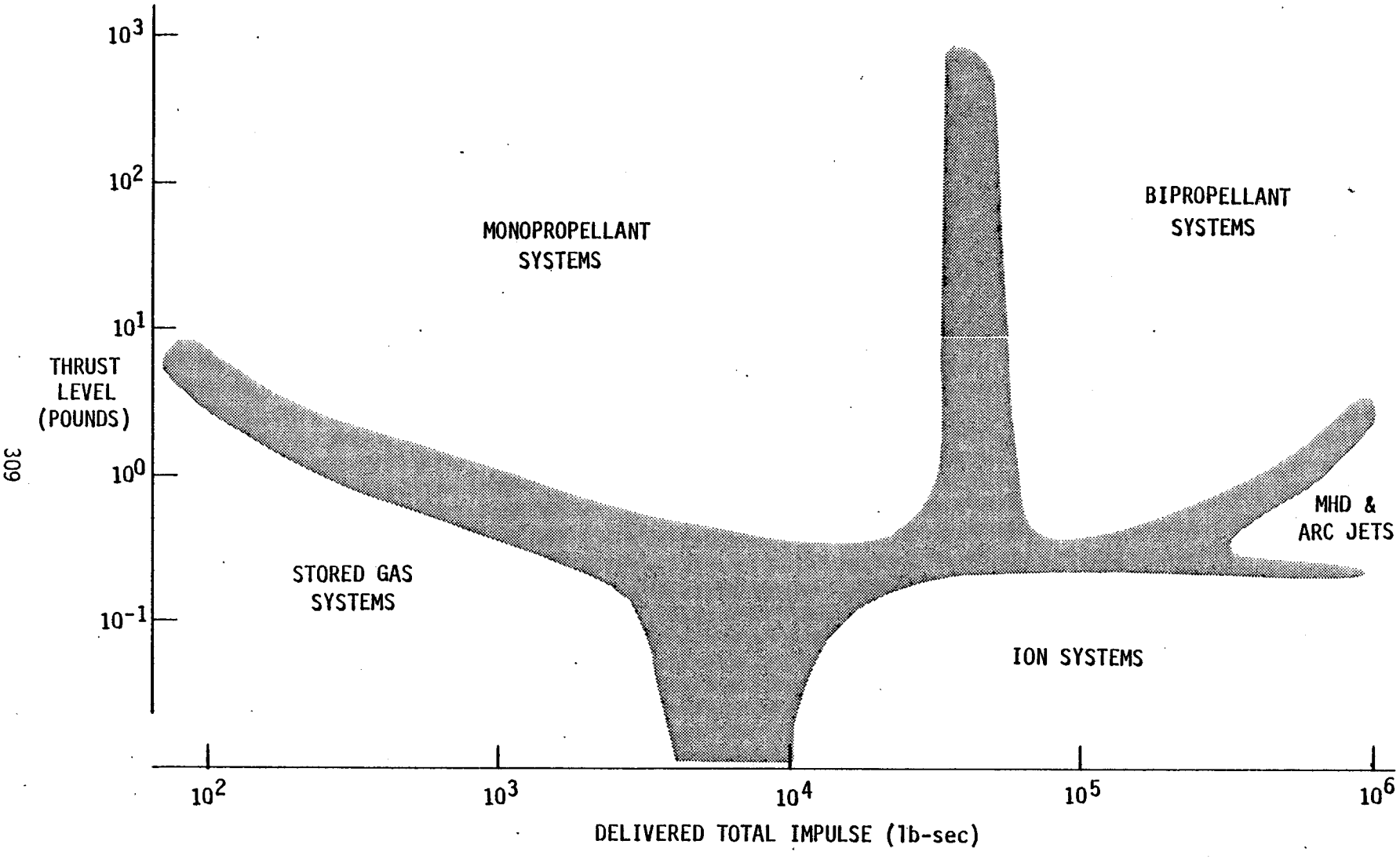

FIGURE 5-12 THRUST/TOTAL IMPULSE OPERATING REGIMES

Development work to improve catalyst bed life directed toward long thruster life has demonstrated up to 8000 seconds of cumulative operational time. Another long life development program substituted electrothermal decomposition employing a 20 watt resistance heater for the catalyst bed demonstrated 40 hours of steady state on-time and more than 10^6 cycles at the 5 lb thrust level. The performance of this thruster is shown in Table 5-2.

Bipropellant attitude control systems have been developed for applications where total impulse requirements have shown the advantage of higher performance over the simplicity of monopropellant systems. Current bipropellant systems utilize monomethyl hydrazine (MMH) and nitrogen tetroxide hypergolic propellants. Thruster size ranges from 0.5 lb to 1600 lb have been developed. Examples of typical system performance are listed in Table 5-2. Minimum thruster size in bipropellant thrusters is limited by current manufacturing techniques in drilling injector holes (0.004" dia) and is somewhat larger than N_2H_4 thrusters. As was characteristic of monopropellant thrusters, bipropellant thruster minimum impulse bit increases with thrust level due to injector head and propellant passage volumes. Minimum pulse width and pulsing I_{sp}, not limited by catalyst bed characteristics, become limited by material limitations to thermal cycling and for nozzle erosion.

Small size ($F < 5$ lb) bipropellant thruster performance may be degraded by boundary later cooling losses due to small chamber volume. At the higher thrust levels these losses are minimized and performance variations shown in Table 5-2 are a function of the thruster nozzle area ratio (ε). The space shuttle RCS thruster nozzles are severely limited by installation requirements and the performance shown is a result of the low nozzle area ratios.

H_2 and O_2 propellants are candidates for attitude control systems in advanced space system studies where these propellants may be available and the potential of higher performance is desirable. Performance of H_2/O_2 thrusters that have been demonstrated in prototype hardware have been included in Table 5-2. It should be noted that the H_2/O_2 propellant feed to the thrusters may either be gaseous or liquid and that the conditioning

of the propellant to maintain the feed in a single phase will be the most critical problem in the design of an H_2/O_2 attitude control system.

Thrust levels as low as 30 micro-pounds have been demonstrated with flight-proven ammonia resistojet systems. Thrust levels progress upwards from that point, with cold gas systems developing thrusts from a few millipounds up to about 10 pounds. The low I_{sp} of these systems - 140 to 170 for resistojets, 40 to 70 for cold gas - make them noncompetitive for long life LSS applications. Mono- and bi-propellant systems are summarized in Table 5-2.

Propellant Storage and Distribution - A key feature of propellant storage characteristics is the manner in which liquid propellant orientation and expulsion is managed in the zero-G environment. Care must be taken to ensure that the propellant flow to the system thrusters is free of entrained gases in order to provide smooth and efficient combustion. Both "active" and "passive" propellant orientation options are available for consideration and have proved flight experience. Table 5-3 summarizes some of the pertinent characteristics of active propellant orientation and expulsion techniques. Three of the listed types have an extensive qualification history:

o Bladders	Extensive Teflon bladder experience manned and unmanned spacecraft auxiliary propulsion since Mid-1960's
o Metallic Bellows	Minuteman-III post-boost propulsion subsystem
o Elastomeric Diaphragms	Extensive application in unmanned spacecraft of monopropellant hydrazine propulsion system

The reliability of an active propellant orientation and expulsion technique is always of concern and must be considered in any design selection evaluation study. Reliability factors include long term propellant compatibility, susceptability to leakage and/or rupture, and cycle life. The storage life of metallic bellows systems is approaching ten years in the Minuteman-III system, and operational lifetimes of elastomeric diaphragms is approaching seven years in the Pioneer-10 spacecraft.

TABLE 5-3

POSITIVE EXPULSION SYSTEM CHARACTERISTICS

EXPULSION SYSTEM	STRONG POINTS	PROBLEM AREAS
Pistons	Positive displacement; variable initial ullage gas volumes	Heavy; leakage; jamming due to cocking or corrosion; limited to cylindrical tanks
Bladders	Much development and flight experience; adaptable to most tank geometries and initial gas ullage volume	Long term compatibility; gas permeation; poor expulsion efficiency; folding geometry conducive to pinhole leaks
Metallic Bellows	Good compatibility; predictable performance adaptable to varying tank geometries and initial ullage volumes	High weight; cocking during expulsion
Elastomeric Diaphragm	Good expulsion efficiency; trouble free and repeatable diaphragm geometry during expulsion	Poor wear characteristics during prolonged propellant slosh; poor long life compatibility; limited to spherical tank geometry with significant initial ullage volume
Metallic Diaphragm	Good compatibility; not sensitive to propellant slosh	Limited to spherical tank geometry with significant initial ullage volume; high ΔP required for expulsion
Rolling Diaphragm	Good compatibility; not dependent on initial ullage volume	High ΔP required for expulsion; limited to cylindrical tank geometry

Passive techniques of propellant orientation are based on the surface tension properties of the propellant, thereby eliminating many of the reliability concerns associated with positive expulsion. The design of such a device requires complete knowledge of acceleration environments, propellant properties, temperatures and flowrates, and also pressurant charactristics. An abbreviated summary of the various phenomena associated with surface tension propellant acquisition, performance requirements, and design considerations are listed in the functional matrix of Table 5-4.

System Life Considerations - The primary concern is the quantity of expendables required, which requires definition of operational duty cycles and their relation to delivered specific impulse. The more subtle aspects of mission life requirements include long term propellant compatibility, age limits on materials of constrution (primary seals), valve cycle life, and exhaust plume contamination effects on other elements of the space vehicle.

A major life consideration for monopropellant hydrazine systems is that of the catalyst bed. Contemporary bed designs involve the mechanical packing of Shell 405 catalyst, generally with layered strata of fine and coarse granules. Prolonged operation results in the mechanical working of particles against each other, spalling, and eventual ejection from the reactor. The effective reduction in decomposition activity thus impairs transient response and steady state performance characteristics.

The cycle life of thruster valving may be an inherent limitation, at the present technology level, for application to the control of LSS. This would be particularly true in the case of limit cycle reaction control stabilization with small pointing tolerances as opposed, for instance, to momentum wheel control. Repetitive valve cycling ultimately leads to fatigue failures, high seat leakage rates, and poor response. Present technology places valve cycle life characteristics in the 10^5-cycle category, and is approaching 10^6 cycles on some units.

Thruster exhaust plume charactristics are not a life consideration for propulsion systems, but their effects must be considered in the placement on the vehicle. Plume impingement heating rates must be evaluated, and the

TABLE 5-4

SURFACE TENSION PROPELLANT ACQUISITION SYSTEM PHENOMENA

	EVENT								
	Pad Hold	Boost	Coast	Maneuver	Propellant Transfer	Thruster Start	Thruster Burn	Thruster Shutdown	Propellant Depletion
● PHENOMENA INVOLVED IN EVENT									
Capillary retention: steady and shock acceleration, steady and transient flow (normal and back-up mode operation)			X	X	X	X	X	X	
Pressure loss: in terms of pressure delivered to thruster and in terms of maintaining capillary control					X	X	X		
Filtration: filtration, stoppage					X		X		
Structural integrity: due to body acceleration, forming, welding, assembly, handling, installation, pressurization		X							
Gas entrapment in outlet: due to wetting of dip suppressor/filter assembly before downstream propellant filling		X							
● REQUIREMENTS AFFECTING PERFORMANCE OF EVENT									
Propellant quantity: quantity initially loaded and in tank at start of final burn			X	X	X	X	X	X	
Propellant flowrate: max at any time and max at depletion – propellant transfer max					X	X	X		
Propellant temperature: relative to retention, boilout, gumming, icing, and low g orientation			X						
Body acceleration: important to retention, orientation, depletion, structural strength, etc.	X	X	X	X	X				
Sequence of events: order and duration – transient profiles									
● DESIGN ELEMENTS INVOLVED IN EVENT									
Fill and drain system: relative to gallery hole seal-off and gas entrapment in outlet	X	X							
Pressurization system: relative to condensation and to gas entrapment in outlet	X								
Capillary fill vent screen: relative to heat transport, prevention of condensate sealing and hole gumming	X	X	X						
Gallery windows: hole diameter, location, open area, ratio of hole diameter to material thickness, and wicking	X	X	X	X	X	X	X	X	X
Gallery wall surface finish: relative to condensate sealing/seal-breaking and									
Gallery cross section area: relative to gallery capillary fill									

deposition of exhaust products on sensitive vehicle surfaces and equipment may be a life-limiting characteristic. Equipment that has shown sensitivity to plume contamination include solar arrays, thermal control paints, louvers, and second surface reflectors, and also any optical sensors that are a part of the control subsystem or payload.

5.3 Required Technology Advances

The intent of this section and those that immediately follow is to define the areas of technology which need improvement to meet the requirements of large space systems. To accomplish this objective we will examine five areas which have emerged as central issues in the auxiliary propulsion of large space systems. These are listed below:

- o Thrust Level
- o Start-Up Characteristics
- o Number and Distribution of Thrusters
- o System Mass
- o APS Lifetime

Each area above is discussed in the next five sections to define the chemical or electrical technology needs. The adequacy or inadequacy of currently available technology will depend greatly on the assumptions used in the requirements analysis. Technology needs will depend on the LSS class, the LSS size, and the system sizing assumptions (i.e., LEO operation, GEO operation, LSS orientation, etc.).

5.3.1 Thrust Level Technology Needs

In Tasks 3 and 4 we have examined the thrust level requirements of both the large erectable structures and the single shuttle launchable deployable structures. In addition to thrust level requirements we looked at throttling requirements and the effect of thrust levels on surface accuracy. The large erectable structures technology needs are presented first with deployable structures results following.

Table 4-2 listed the thrust requirements for four scaling assumptions and for each LSS class and size. In comparing the thrust/thruster requirements with the thrust levels currently available from chemical and electric

systems one finds that chemical systems are necessary to meet the low earth orbit needs under the assumptions used in generating Table 4-2. LEO altitude was assumed to be 300 km.

With the exception of the very large plate structure using a small number of thrusters, the SOA chemical thrust levels are adequate. Electric thrusters, however, are inadequate to meet the majority of missions. Table 4-2 has been restated in Table 5-5 to show this result.

In Table 5-5 we have put the available SOA ion thrusters plus the 50 cm conceptual design in the slots where their thrust levels are sufficient. For thrust levels above 0.4 N, the thrust needed is printed. There exists a clear need for increased electric thruster thrust levels for LEO operation and for medium and large erectable structures in GEO.

Throttling requirements were developed for the three main classes in Task 3. Figures 3-26 through 3-29 examined the difference in thrust level requirements from LEO to GEO and the difference in the maximum GEO and nominal GEO requirements. It is clear from these charts that no system available is capable of providing the up to 300:1 throttling ratios required for LEO and GEO operation. The GEO throttling ratios are far more manageable and the current electric propulsion throttling capability of 4:1 is adequate. For chemical systems the lack of throttlability is offset by the excess thrust level that can be provided. Effective thrust is varied by simply pulsing the thrusters at different duty cycles. Pulsing thrusters has the disadvantage of limit cycling (see Section 4.1.2) and some fuel waste. Another disadvantage is that if the thrust levels are very high, the structural deformation caused by each pulse can cause a degradation of mission performance or, in some cases, actual structural damage.

Figures 4-43, 4-44, 4-48 and 4-49 addressed the question of structural deformation for the plate structure. These figures showed that a plate structure of 2000 to 10000 meters in length had some structural deformation with the required thrust levels. For structures above 10000 meters in length this interaction was very significant. Deflections of greater than one degree were calculated even with graphite epoxy structures. For structures smaller than 1000 meters deflections were not significant.

TABLE 5-5 CURRENT ELECTRIC THRUSTER CAPABILITY FOR LARGE ERECTABLE STRUCTURES

			THRUST/THRUSTER REQUIRED			
STRUCTURE	SIZE	# THRUSTERS	LEO MAXIMUM	LEO-GEO TRANSFER	GEO MAXIMUM	GEO NOMINAL
PLATE	SMALL (30 m)	4	30cm	8cm	8cm	8cm
	MEDIUM (700 m)	4	21 n	20 n	.92 n	.92 n
		24	2.2 n	3.5 n	50cm	50cm
		100	.7n	.9 n	30cm	30cm
	LARGE (21000 m)	4	610000 n	46000 n	6200 n	3310 n
		24	62000 n	8000 n	1080 n	570 n
		100	15100 n	1950 n	260 n	137 n
MODULAR ANTENNA	SMALL (15 m)	8	50cm	30cm	8cm	8cm
	MEDIUM (60 m)	8	1.2 n	.75 n	30cm	15cm
	LARGE (200 m)	8	62 n	60 n	50cm	30cm
		32	16 n	14 n	30cm	15cm
		80	6.4 n	5.6 n	15cm	15cm
SERIES OF ANTENNAS	SMALL (2)	4	30cm	8.75 n	30cm	30cm
	MEDIUM (6)	4	6.75 n	32.5 n	.79 n	.48 n
		24	1.13 n	5.42 n	30cm	30cm
		96	50cm	1.35 n	15cm	15cm
	LARGE (10)	4	26.3 n	54.0 n	2.80 n	.78 n
		24	4.4 n	9.0 n	.47 n	30cm
		96	1.1 n	2.3 n	30cm	15cm

Single shuttle launched deployable structures have thrust requirements significantly below those of the larger erectible structues. Tables 3-11 and 3-12 illustrated these requirements. Current electric thrusters are adequate for a majority of the assumptions and LSS sizes studied. Table 3-12 is restated in Table 5-6 in the same manner as Table 5-5 to show this result.

5.3.2 Startup Characteristics

The effect of APS startup delays on the pointing accuracy of the plate structure was investigated in Section 4.1.2.3. In this section the relationship of pointing accuracy, minimum impulse bit, LSS size, and startup dime delay was derived. Figure 4-21 showed that as the structure size increased, time delays of up to one hour did not significantly effect pointing accuracy. For structures of a few hundred meters or less, this effect is noticable. The minimum impulse bit of electric thrusters is somewhat ill-defined because even during startup periods a small amount of thrust is produced. Nominal electric thruster shutdowns are not "clean" but have a period of throttling down to the shut-off point. If one assumes a minimum impulse bit of 0.1 N-S, a 30 minute startup delay indicates a 0.45 degree accuracy loss which is unacceptable for some missions. Additional research to define the electric propulsion minimum impulse bit is needed before the full impact of startup delays can be evaluated.

5.3.3 Number and Distribution of Thrusters

After analysis of thrust level requirements had been performed, it became clear that for the medium and large size structures the use of SOA electric propulsion units required large numbers of thrusters which for shape control reasons should ideally be equally distributed throughout the structure. Even with the larger thrust levels available with chemical thrusters, distribution of thrusters for classes IA (plate), IB (cross), IIA (box) is required for medium and large structures.

The number of thrust locations needed to minimize deflection reaches a point of diminishing returns. This facts was pointed out in Figure 4-34. In this figure it was shown that after approximately 10 thrusters were distributed equally across a beam, the reduction in deflection by adding an additional thruster is minimal. Specific designs must be analyzed to study

TABLE 5-6

CURRENT ELECTRIC THRUSTER CAPABILITY FOR
SINGLE SHUTTLE LAUNCHED DEPLOYABLE SPACECRAFT

CLASS	SIZE	DISTURBANCE TORQUE 300 km 10°	DISTURBANCE TORQUE 300 km WORST CASE	DISTURBANCE TORQUE 500 km 10°	DISTURBANCE TORQUE 500 km WORST CASE	LEO - GEO TRANSFER	GEO DISTURBANCE WORST CASE	GEO STATIONKEEPING @ 0.4 DUTY CYCLE ONCE/ORBIT	GEO STATIONKEEPING @ 0.4 DUTY CYCLE ONCE/WEEK
PLATE W/O BLANKET	30 m	8cm	15cm	8cm	8cm	8cm	8cm	8cm	15cm
	100 m	30cm	50cm	15cm	30cm	30cm	8cm	8cm	30cm
	250 m	50cm	1.7n	30cm	50cm	50cm	8cm	15cm	50cm
PLATE W/BLANKET	30 m	30cm	.48n	8cm	30cm	15cm	8cm	8cm	30cm
	100 m	.7n	4.9n	30cm	.49n	50cm	8cm	30cm	.53n
	150 m	1.6n	12.n	.4n	1.5n	50cm	15cm	50cm	1.1n
MODULAR ANTENNA	15 m	30cm	.5n	15cm	30cm	30cm	15cm	8cm	30cm
	60 m	1.5n	9.5n	50cm	1.0n	.63n	15cm	15cm	30cm
	200 m	17.n	55.n	1.7n	8.1n	5.5n	30cm	15cm	50cm
SERIES OF ANTENNAS	2	30cm	50cm	30cm	50cm	30cm	8cm	8cm	30cm
	3	50cm	.96n	50cm	.84n	30cm	8cm	8cm	50cm
	4	50cm	2.3n	50cm	1.9n	30cm	8cm	15cm	50cm

the interaction between beams on total surface deflections, however, this result may be applied generally in that there will always be a point of dimenishing returns for the distribution of thrusters.

Distributing thruster systems requires a distribution of system components over what may be very long distances. In the case of chemical systems, this poses no particular problem. For chemical systems, tanks, valves, and thrusters can easily be located as a unit with no interconnection between the units except for control electronics. Electric thrusters are a different matter. The high power required and inherently higher inert system mass for each APS unit dictates significantly greater system integration problems. Additional study to analyze these problems is indicated.

5.3.4 System Mass

Throughout this study, specific impulse was treated as a variable for both chemical and electrical APS. We found in Sections 4.3.2 and 4.5 that electric systems optimized over a wide range of specific impulse. Chemical systems have no power level dependence, hence always optimized at the highest achievable I_{sp}. In comparing the chemical and electric system mass for the large erectable structures using a geosynchronous requirement thruster sizing, it was found that in all cases electric systems had lower mass than chemical systems providing the optimum I_{sp} for the electric systems could be achieved.

Tables 4-4 and 4-5 presented the electric I_{sp} optimums under various assumptions. Under the assumptions used here, specific impulse range of current electric systems must be extended to much higher ranges than available. The plate structure needed higher than 50000 sec I_{sp} to optimize assuming the power source was not charged to the APS. If power mass was charged to the APS, a range of 3600 to 15000 sec I_{sp} is required to optimize system mass. For deployable structures, Table 4-13 provided a comparison for each class for four different mission assumptions. This study only looked at 1000, 3000 and 10000 second specific impulse levels for electric systems. The conclusions for geosynchronous orbit are the same for the deployable as well as the larger erectable structures. Electric systems have lower mass when sized for geosynchronous operation than do chemical systems.

LEO operation for deployable structures indicates that electric systems still have a mass advantage over chemical systems at an I_{sp} of 250 seconds. Chemical systems at 500 seconds, however, offset this advantage in many cases. LEO operation also requires lower specific impulse for electric systems. I_{sp}'s as low as 1000 seconds are indicated for LEO missions.

For both erectable and deployable structures, a general trend in specific impulse requirements is apparent. As the structure size increases, the optimum I_{sp} decreases. It is also true that as operational altitude decreases, optimum I_{sp} decreases. These facts are an indication that the thrust level demands at lower altitudes and for larger LSS sizes cause the power level demands, hence, power system mass to dominate fuel mass. At geosynchronous altitude and for smaller structures, the power system mass required does not dominate the fuel mass required until very high specific impulses.

5.3.5 Lifetime

The lifetime and reliability demands on all systems comprising LSS are drivers in LSS designs. System lifetimes of ten years or more with very high (> 95 percent) reliability will be required. These requirements indicate a need for redundancy management and operational schemes, both of which deserve future study. This study did not directly addess these issues but a set of requirements for electric and chemical thrusters has been developed.

For chemical systems, long term cryogenic propelland storage is a major issue. The specific impulse studies revealed that a chemical system of greater than 250 seconds I_{sp} is needed to compete with electric systems for single shuttle launched vehicles. This indicates a need for additional study to minimize the cost and system mass needed for 10 year or greater cryogenic storage. The second issue for chemical systems is hardware lifetime. Thruster value cycling and catalyst bed wear over the lifetime of the mision can be significant factors. Up to 100000 valve cycles will be needed for limit cycle operation over a 10 year mission. This does not appear to pose a problem for medium (1 - 10 N) thrusters; however, higher thrust cycling for 10^5 - 10^6 cycles has yet to be demonstrated. If hydrazine systems are used, catalyst bed life will have to be extended from 5 - 7 years up to 10 years.

Electric thruster lifetime and reliability are significant problems. For the 40 percent duty cycle proposed for geosynchronous orbit a thrust system lifetime of 35000 hours is indicated. Current systems have a lifetime of less than half this amount. Lifetime extension and verification testing as well as redundancy management analysis is indicated.

THIS PAGE INTENTIONALLY LEFT BLANK

6.0 DISCUSSION OF RESULTS

The comparison, in Section 5, of required APS characteristics for each generic class of LSS over a wide range of sizes has identified areas of deficiency in current systems. The removal or alleviation of these deficiencies are goals that technology development should address to develop APS suitable for future LSS applications.

In addition to results specifically concerning APS, general conclusions emerged in the course of the study that apply to the control of LSS. These may not guide APS technology development but will perhaps indicate some operational approaches that will be required to place LSS in orbit in a cost effective manner.

The study results are summarized below. First the general conclusions, then those that relate specifically to electric and chemical auxiliary propulsion systems. The APS results are condensations of those given in Section 5.

6.1 General Conclusions

Four general conclusions became apparent in the course of the study and were to some extent unexpected:

1. It had been assumed that many LSS would use momentum exchange devices such as inertia wheels and control moment gyros (CMG's) for attitude control. The trend towards this type of system seemed established in many of the preliminary design analyses conducted in recent years for vehicles which are large by present day standards; for example, the Solar Electric Propulsion System (SEPS) and the Space Operations Center (SOC). The momentum exchange systems are generally best when cyclic disturbances predominate or maneuvers are required. The LSS generic classes studied, however, showed that in most cases the stationkeeping requirements are equally as demanding as disturbances. Stationkeeping requires external forces which in GEO (and most LSS operational orbits were GEO) consist of both north-south and

east-west components. Attitude control including disturbance cancellation, can be combined with stationkeeping (in two axes) and both functions can be performed simultaneously to a large extent, by careful system design. This means that little additional impulse is needed for attitude control if the stationkeeping requirements are satisfied. This being the case, momentum exchange devices lose their advantage. The implication is that, far from being relegated to the relatively simple stationkeeping and desaturation role, APS for LSS will be required to do the more demanding tasks of attitude control, and in some instances shape control.

2. The literature survey conducted in Task 1 to identify generic classes of LSS showed that a majority would operate in geosynchronous orbits (GEO). Generally, they would be built in low earth orbit (LEO) and transferred to GEO to perform their mission. In examining thrust requirements, it became clear that the thrusts required varied by orders of magnitude with the higher values associated with LEO and transfer. This being the case, the study groundrule, that thrust vector control (TVC) during transfer be supplied by APS, may, with benefit of hindsight, be unrealistic. It will probably be more cost effective to assume that TVC will be supplied by the prime propulsion system or that transfer will be achieved by a tug so that TVC on the LSS itself becomes unnecessary.

   Another consideration is the big difference between nominal and maximum thrust requirements particularly in LEO. For example, many of the LSS considered had relatively small disturbance torques in their normal operating attitude but could experience very large torques in a worst case orientation. A case in point is gravity gradient torques. A solar power satellite (SPS) type vehicle flying parallel to the earth experiences zero gravity gradient torques although it is in a position of unstable equilibrium. If,

however, the SPS somehow gets into a 45^{o} pitch orientation, the gravity gradient torques are huge. This problem is particularly severe with large structures since gravity gradient torques are functions of the inertias which go up with the square of linear size. In the past, the conventional wisdom held that APS would be sized to handle worst case situations. It may be time to abandon that guideline for large erectible LSS. If APS were sized to handle on-orbit nominal disturbances, plus some prudent reserve for contingencies, but not worst case conditions the APS requirements would be considerably eased. Worst case orientations could be treated as follows:

- o Design the system so that the probability of loss of control is sufficiently small that the danger of reaching a worst case condition is acceptable.
- o Carry a secondary APS for emergency use only. This could, for example, be a high thrust chemical system. Presumably, emergencies would be infrequent so that the propellant needed, and thus the weight penalty, would be small.
- o Assume that a rescue vehicle would be available to effect emergency recoveries.

Any of these approaches would most likely be more cost effective than designing the APS to handle both the long term nominal torques and the short term emergency situations.

3. The study indicates that distributed thrusters and clusters of thrusters will be facts of life for LSS APS. This means that methods of controlling arrays of thrusters need to be developed. Questions of implementation, centralized vs. decentralized control, shared PPU's, location of tanks, redundancy management, etc., need to be addressed and solutions found.

4. The question of LEO vs. GEO assembly for such large structures as the SPS can be answered by looking at the control requirements at LEO versus those at GEO. Thrust level requirements for worst case orientations of very large structures in LEO proved to be nothing less than overwhelming. Thrusters of 10^4 to 10^5 Newtons simply for disturbance cnacellation were required. These thrust levels would cause significant structural deformation on the truss work. It is unlikely that structures greater than approximately 5000 meters in maximum dimension can be constructed and controlled in a 300 km orbit unless it can be guaranteed that a worst case disturbance orientation will never be encountered.

6.2 Electrical Auxiliary Propulsion Systems

There are four technology advances which, if achieved, would widen considerably the efficient application of electrical APS. These are:

- o Increased thrust
- o Reduced startup time
- o Higher I_{sp} for low thrust applications
- o Lower I_{sp} at higher efficiency for high thrust applications
- o Longer life

1. Many LSS applications show the need for thrusts well above those presently available. If higher thrusts do not become available, the only recourse is to cluster the units which introduces a weight penalty. In addition, the need, in general, for thrust components, plus and minus, in each of three axes means gimballed thrusters or two thrusters per axis. Either is difficult to implement if there are clusters of thrusters at each location.

2. Two basic modes of operation for pointing and disturbance cancellation are proportional and pulsed. Proportional control requires thrust modulation, ideally down to zero

thrust. Present day engines have a throttling capability of about 4:1 but the effective ratio can be greatly increased if there are multiple units. When the lower limit is reached either a hang-off error has to be accepted, opposed thrust techniques can be implemented or control has to revert to on-off, limit cycle, operation. Opposed thrust tends to introduce propellant penalties. Limit cycle operation is more efficient and can achieve good pointing accuracy if time-on delays are kept within bounds. Although limit cycle periods are long for LSS, 15 - 60 minute delays produce significant errors for large LSS.

Shape control requires the application of correcting forces at precise times. Again, shorter start up times would make EPS more effective.

3. Low thrust APS, typically those for support of on-orbit operations only, require higher I_{sp}'s for the smaller LSS than currently available to realize a minimum mass of the total system.

4. Results for some of the LSS classes, specifically those that require high thrusts and in which the power for EPS operations must be charged against the EPS, show that a different I_{sp}/efficiency relationship is desirable. Optimum systems, in the sense of minimum weight, occur at lower I_{sp} and higher efficiency than currently obtainable. The ability to trade I_{sp} and efficiency would be very beneficial for tailoring EPS to a particular LSS.

5. Future LSS almost invariably demand long life. Ten years is a typical minimum. Present day electric propulsion units are limited to about 15000 hours - less than two years. Increased life capability would be very beneficial in reducing the number of redundant thrusters needed to meet lifetime requirements.

6.3 Chemical Auxiliary Propulsion Systems

Two general areas need improvement to make chemical systems better suited for control of LSS. These are:

- o Increased I_{sp}
- o Longer life

1. Chemical APS have many desirable characteristics for control of LSS but in nearly every case they cannot compete with electrical systems because the total system weight becomes excessive. The chemical system thrusters and auxilliary equipment, such as tanks and valves, are generally light compared to electrical systems. They also have high thrust capability and short delay times. They lose out in long life applications because of the weight of propellant necessary. This would be reduced if the I_{sp} could be increased. Experimental oxygen/hydrogen combinations, both liquid and gaseous, show promise of reaching specific impulses up to 500 sec. This is about twice the value presently available.

   Chemical APS operate almost exclusively in a pulsed mode and pulsing is accompanied by a drop in achieved I_{sp}. The drop may be as high as 70 percent. In addition to seeking improvement in system I_{sp}, it may be as important, or even more important, to develop improved pulsing mode I_{sp} values.

2. Life is a limiting factor in chemical systems as well as electrical. Limitations stem from two sources, valve cycles and catalyst bed life. Valves are limited presently to about 500,000 cycles, thus the lifetime depends on the pulsing rate. If the limit cycle period exceeds 21 minutes, 500,000 cycles are enough for 10 years of operation. From this point of view, CPS have better life expectancy that EPS.

   Monopropellants currently use catalyst beds to cause ignition. These deteriorate with time and use and may be

life limiting. Hypergolic bipropellants do not need catalysts and so are free from this restriction. LSS mission lifetime may, therefore, dictate the use of bipropellants rather than the normally used hydrazine or other monopropellants.

THIS PAGE INTENTIONALLY LEFT BLANK

7.0 SUMMARY OF RESULTS

The objective of the study was to determine the electrical and chemical propulsion characteristics and technology advances necessary to meet auxiliary propulsion system (APS) requirements established for large space structures (LSS).

The study was subdivided into five tasks. Task 1 was devoted to determining LSS characteristics. A literature survey was conducted and uncovered about a hundred reports dealing with planned and projected LSS. It was found that the systems could be grouped into three main generic classes - flat, plate-like structures, modular antenna systems and series of antennas systems. Each group was then further divided into two or three sub groups. Each generic class was characterized by a scaling parameter and generalized expression for weight, area, moments of inertia, etc. were generated as functions of the parameter.

In Task 2, disturbance characteristics were determined with the aid a literature search. The disturbances depended, in general, on the vehicle mass properties and area distribution. Thus, the general expressions derived above allowed the disturbance torques to be calculated in terms of the scaling parameter. These disturbances defined the attitude control requirements and were used in Task 3 together with stationkeeping and maneuver requirements to define the total system control requirements. These were then used to determine the important APS characteristics and to identify areas of APS/LSS interaction.

In Task 4, the various APS/LSS interactions were quantified by four interrelated studies. These covered thrust levels, transients and modulation effects, number and distribution of thrusters and allowable mass. From these data, optimum APS characteristics were determined for each generic LSS class as a function of the scaling parameter.

Task 5 consisted of reviews of the current state of the art in both electrical and chemical APS. Available characteristics were then compared with the desired characteristics, found in Task 4, to define areas of acceptability and deficiency. The deficiencies indicated directions APS

technology advances should take to make future APS better suited for control of upcoming LSS.

Although the deficiencies varied with generic class and scaling parameter, general conclusions concerning needed technology advances can be summarized relatively concisely:

Electrical APS Technology Advances Desirable

- o Increase thrust
- o Reduce start up times
- o Increase specific impulse (low thrust applications)
- o Improve efficiency at lower specific impulses (high thrust applications)
- o Increase lifetime

Chemical APS Technology Advances Desirable

- o Increase specific impulse
- o Increase lifetime

Some general conclusions also emerged from the study. Although these do not directly impact APS, they may be important in pointing out changes in philosophy which seem to be necessary for future LSS operations. The general conclusions and their implications are as follows:

1. Stationkeeping requirements tend to dominate

   - o APS will be essential
   - o Control moment gyros and inertia wheels may not be used on LSS
   - o Much attitude control effort can be obtained free by combining attitude control and stationkeeping functions.

2. Thrust requirements vary very widely from construction in low earth orbit through transfer and operations in geosynchronous orbit

- o Hybrid systems (chemical plus electrical) may be indicated with electrical systems for nominal operation and chemical for recovery from worst case orientations.
- o APS requirements imposed by thrust vector control for transfer are very demanding. It may be best to use prime propulsion for thrust vector control.

3. Distributed thrusters or clusters of thrusters will be required.

   - o Redundancy management and implementation techniques need development.

THIS PAGE INTENTIONALLY LEFT BLANK

REFERENCES

1. Large Space Structures - Configuration Packaging, and Response Studies, Final Report, Boeing Aerospace Company, Seattle, Washington, September 1978 (Contract # NAS1-13967)

2. Freeland, R. E., Industry Capability for Large Space Antenna Structures, JPL Document 710-12, May 25, 1978

3. Graham, D. and McRuer, D., Analysis of Nonlinear Control Systems, Wiley; 1961

4. Jung, Y. C., The Theory of Aeroelasticity, Wiley; 1955

5. Poeschel, et al, High Power and 2.5 KW Advanced Technology Ion Thrusters, Final Report NASA CR-135,163, February 1977

THIS PAGE INTENTIONALLY LEFT BLANK

APPENDIX A

Bibliography, Large Space Structures

1. A FLEXIBLE PASSIVE SPACE ARRAY W/SPRINGS, J.V.Breakwell et.al., A78-12095

2. A REVIEW OF LARGE AREA SPACE SYSTEMS TOWARD IDENTIFICATION OF CRITICAL OR LIMITING TECHNOLOGY, M.A.Dienman et.al., General Electric Co., May 1978, X78-10214 (NASA CR 145339)

3. A STUDY TO DEFINE CRITICAL DESIGN CRITERIA FOR LARGE SPACE STRUCTURES, M.F.Card, Astro Research Corp., Santa Barbara,Calif., June 1979, 78K10974 (NASA CNT# : NAS1-15347)

4. A TECHNOLOGY PROGRAM FOR LARGE AREA SPACE SYSTEMS, A.Guastaferro(NASA Langley Research Center Hampton,Va.) and L.M.Jenkens(NASA,Johnson Space Center,Spacecraft Design Div.,Houston,Tex) April 1978, A79-16145 (Canaveral Council of Technical Societies,1978,p.6-42 to 6-53)

5. ACTIVE DAMPING OF MODAL VIBRATIONS BY FORCE APPORTIONING, R.Miserentino, Virginia Polytechnic Inst. and State Univ., Blacksburg, June 1979, 78K10854 (NASA CNT # : NSG-1526)

6. ADVANCED SPACE SYSTEM CONCEPTS AND THEIR ORBITAL SUPPORT NEEDS(1980-2000). VOL.1:EXECUTIVE SUMMARY, N76-30244 (NASA CR 148704)

7. ADVANCED SPACE SYSTEM CONCEPTS AND THEIR ORBITAL SUPPORT NEEDS(1980-2000) VOL.2:FINAL REPORT, N76-30245 (NASA CR 148703)

8. ADVANCED SPACE SYSTEM CONCEPTS AND THEIR ORBITAL SUPPORT NEEDS(1980-2000) VOL.3:DETAILED DATA, N76-30246 (NASA CR 148710)

9. ADVANCED TECHNOLOGY REQUIREMENTS FOR LARGE SPACE STRUCTURES,PART 3:FLIGHT DESCRIPTION,FINAL REPORT, E.Katz et.al., Rockwell International Corp. Downey,Calif., June 1977, X78-10058 (NASA CR 145256)

10. ADVANCED TECHNOLOGY REQUIREMENTS FOR LARGE SPACE STRUCTURES. PART 5: ATLAS PROGRAM REQUIREMENTS ,FINAL REPORT, E.Katz,A.N.Lillenas,J.A.Broddy, Rockwell International Corp.,Downey,Calif.,Space Division, Sep 1977, (NASA CR 159014;SD-77-AP-0162-PT-5)

11. AN ACTIVE MODAL CONTROL SYSTEM PHILOSOPY FOR A CLASS OF LARGE SPACE STRUCTURES, M.J.Balas,et.al., A78-12099

12. AN ENTREE FOR LARGE SPACE ANTENNAS, R.V.Powell and A.R.Hibbs, Calif. Inst. of Technology,Jet Propulsion Laboratory,Pasadena,Calif., Dec. 1977, Astronautics and Aeronautics,vol. 15,p.58-64.

13. AN INVESTIGATION OF THE NEEDS AND THE DESIGN OF AN ORBITING SPACE STATION WITH GROWTH CAPABILITIES,FINAL REPORT, M.T.Borelli, Rice Univ.,Houston Tex., 77N27169 (NASA CR 151450, CNT # : NASW-2776)

14. ANALYTICAL STUDY OF DESIGN TECHNIQUES FOR STABILIZATION AND CONTROL OF VERY LARGE SPACE STRUCTURES, M.T.Borelli, National Aeronautics and Space Administration,Marshall Space Flight Center,Huntsville,Ala.,Grumman Aerospace Corp.,Bethpage,N.Y., May 1978, 77K11425 (NASA CNT # : NAS8-32587)

15. APPLICATION OF STATION KEPT ARRAY CONCEPTS TO SATELLITE SOLAR POWER STATION DESIGN.FINAL REPORT VOL I,II,III, The Aerospace Corporation, FEB 1977, ATR-76-(7575)-2 (NAS8-31842)

16. ATTITUDE CONTROL OF LARGE SOLAR POWER SATELLITES, R.E.Oglevie, North American Space Operations,Rockwell International Corp.,Downey Calif., AIAA paper 78-1266.

17. ATTITUDE STABILITY OF FLEXIBLE SOLAR ELECTRIC SPACECRAFT-A PARAMETRIC STUDY, E.L.Marsh, Calif. Institute of Technology,Jet Propulsion Laboratory, Pasadena,Calif., Feb 1974, Journal of Spacecraft and Rockets,vol.11,p.89-96 (Contract No. NAS7-100)

18. AUTOMATED FABRICATION OF LARGE STRUCTURES, D.J.Powell and L.Browning, General Dynamics Corp.,Convair Div.,San Diego,Calif., Oct. 1978, Astronautics and Aeronautics,vol.16,p.24-29.

19. BIG COMSATS FOR BIG JOBS AT LOW USER COST, I. Beckey, Astronautics & Aeronautics, Feb. 1979.

20. CONTINUUM MODELING OF THREE-DIMENSIONAL TRUSS-LIKE SPACE STRUCTURES, A.H.Nayfeh and M.S.Hefzy, University of Cincinnati,Cincinnati,Ohio, Aug 1978, AIAA Journal, A78-44901

21. CONTROL CONCEPTS FOR LARGE SPACE STRUCTURES, R.C.Quartararo, Rockwell international Corp.,El Segundo,Calif., 1978, Langley Res. Center Large Space Systems Technol.,Vol.2 1978,p.935-957.

22. CONTROL TECHNOLOGY FOR LARGE SPACE STRUCTURES, J.Canavin, C.Stark Draper Lab,Cambridge,Mass., Sep 1978, AIAA paper 78-1691.

23. CONTROL SYSTEM TECHNOLOGY AND TRADE-OFFS FOR LARGE SPACE STRUCTURES, J.C.Blair, NASA Marshal Space Flight Center,Ala., Sep 1978, AIAA paper 78-1686.

24. DAMPING AUGMENTATION FOR LARGE SPACE STRUCTURES, T.C.Hendeson and J.R. Canavin, C. Stark Draper Lab.,Cambridge,Mass., AIAA paper 78-490.

25. DECENTRALIZED CONTROL OF LARGE SPACE STRUCTURES VIA FORCED SINGULAR PERTURBATION, J.R.Sesak and T.Coradetti, General Dynamics Corp.,Convair Division,San Diego Calif., Jan 1979, AIAA paper 79-0195.

26. DEPLOYABLE ORBITAL SERVICE PLATFORM CONCEPTUAL SYSTEMS STUDY, Mac. Doug., Mar 1979, Report no. MDC G7832 (NASA CR 159091)

27. DESIGN AND BEHAVIOR OF RIBLESS SOLAR REFLECTORS, Roderich A.Hyde, L.Livermore Lab.,Livermore Ca., Dec 1976, UCRL - 52191.

28. DESIGN CONCEPTS OF GEOSTATIONARY PLATFORMS, E.C.Hamilton and W.T.Carey Jr, NASA Marshall Space Flight Center,Ala., Sep 1978, AIAA paper 78-1642.

29. DESIGN CONCEPTS AND PARAMETRIC STUDIES OF LARGE AREA STRUCTURES, Astro Research Corp., Mar 1976, ARC-R-1008.

30. DESIGN CONSIDERATIONS FOR LARGE SPACE ANTENNAS, R.Johnson Jr., McDonnel-Douglas Corp.,ST. Louis,Mo., 1978, N79-10085 , NTIS HC A23/MF A01, CSCL 22B.

31. DESIGNING STRUCTURES FOR LARGE SPACE SYSTEMS, R.H.Christensen, McDonnel-Douglas Astronautics Co.,St.Louis,Mo., 79N10082.

32. DEVELOPMENT OF CONTROLLER DESIGN METHODOLOGY FOR LARGE FLEXIBLE SPACE STRUCTURES, N.J.Groom, Old Dominion Univ.,Norfolk,Va., Nov 1979, 78K10059 (NASA CNT # : NSG-1473)

33. DISTRIBUTED SURFACE CONTROL FOR LARGE SPACE STRUCTURES, R.C.Montgomery, Virginia Polytechnic Inst. and State Univ.,Blacksburg, Nov 1979, 78K10857 (NASA CNT # : NSG-1527)

34. DYNAMICS AND CONTROL OF LARGE SATELLITES, R.J.Herzberg,K.F.Johansen,R.C. Stroud, Lockheed Missiles and Space Co.,Inc.,Sunnyvale,Calif., Oct 1978 Astronautics and Aeronautics,Vol.16,p.35-39.

35. DYNAMICS AND CONTROL OF LARGE SPINNING SPACE CRAFT, J.N.Juang and M.Bolas, Martin Marietta Aerospace,Denver,Colo., Aug 1978, AIAA paper 78-1420.

36. DYNAMICS,CONTROL, AND STRUCTURAL FLEXIBILITY RESULTS FROM THE HERMES MISSION, F.R.Vigneron, Dept. of Communications,Communications Research Centre,Ottowa,Canada, Oct 1978, International Astronautical Congress, 29th,Dubrovnik,Yugoslavia,Oct 1-8,1978, Paper 78-101.

37. DYNAMICS OF A FLEXIBLE BODY IN ORBIT, V.K.Kumar and P.M.Bainum, Howard University,Washington,D.C., AIAA paper 78-1418.

38. ECONOMICS OF ION PROPULSION FOR LARGE SPACE SYSTEMS, T.D. Masek,J.W. Ward, Hughes Resarch Center, Malibu,Calif, V.K.Rawlin, Nasa,Lewis Research Center,Cleveland,Ohio, 27 Apr 1978, AIAA Paper 78-698

39. EFFICIENT CONCEPTS FOR LARGE ERECTABLE SPACE STRUCTURES, M.F.Card, H.G.Bush,W.L.Heard,Jr.,M.M.Mikulas,Jr., 79N10100.

40. ELECTRIC PROPULSION FOR AUXILIARY CONTROL OF LARGE SPACE SYSTEMS, F. Teren, National Aeronautics and Space Administration,Lewis Research Center, Cleveland,Ohio, 79W70256

41. ELECTRON BOMBARDMENT PHOPULSION SYSTEM CHARACTERISTICS FOR LARGE SPACE SYSTEMS, D.C. Byers and V.K. Rawlin,National Aaeronautics and Space Administration,Lewis Research Center,Cleveand,Ohio, 17 Nov 1976, NASA-TM-X-73554;E-8992

42. ERECTABLE SPACE STRUCTURES AND APPLICATIONS PLATFORM STUDY, Rockwell International, Feb. 1979.

43. GEOSYNCHRONOUS INFORMATION SERVICES PLATFORMS IN THE YEAR 2000, Wolbens & Shepphind, AIAA # 78-1636.

44. HIGH RESOLUTION SOIL MOISTURE RADIOMETER, T.T. Wilheit, National Aeronautics and Space Administration,Goddard Space Flight Center,Greenbelt, Md., 1978, NASA Vol. 1 1978 p.177-194

45. HYBRID COMPUTER SIMULATION OF TWO NONLINEAR ATTITUDE CONTROLLERS FOR FLEXIBLE SPACECRAFT, T.M.M. Abdel-Rahman, Spar Aerospace Products,Ltd Toronto,Canada, P.C. Hughes, Toronto University,Downsview,Ontario,Canada, 28 April 1978, vol 9 Proceedings of the Ninth Annual Pittsburgh Confreence p. 1229-1236

46. LARGE ADVANCED SPACE SYSTEMS (LASS) COMPUTER PROGRAM, L.B. Garrett, National Aeronautics and Space Administration,Langley Research Center, Hampton,Va., 1 July 1979, 78K11161(CNT#: NAS1-15462)

47. LARGE ANTENNA STRUCTURE TECHNOLOGIES REQUIRED FOR 1985-2000, W.R. Wannlund, TRW Defense and Space Systems Group,Redondo Beach,Calif., 1978, NASA Vol.1 1978,p221-241

48. LARGE COMMUNICATION-SATELLITE ANTENNA, J. Schultz, Grumman Aerospace Corp., Bethpage, N.Y., June 1977. 78A27020.

49. LARGE SPACE DEPLOYABLE ANTENNA SYSTEMS, Lockheed Missiles and Space Co., Sunnyvale, Calif., 1978. 79N10087.

50. LARGE SPACE ERECTABLE ANTENNA STIFFNESS REQUIREMENTS, J.A. Fager, General Dynamics Corp., San Diego Calif., April 1978. 78A322929, AIAA 78-590.

51. LARGE SPACE SYSTEMS TECHNOLOGY, VOLUME 1, E.C. Naumann and A. Butterfield, NASA, Langley Research Center, Hampton, Va., Jan. 1978. N79-10078 (NASA-CP-2035-Vol-1).

52. LARGE SPACE SYSTEMS TECHNOLOGY, VOLUME 2, E.C. Naumann and A. Butterfield, NASA, Langley Research Center, Hampton, Va., Jan. 1978. N79-10097 (NASA-CP-2035-Vol-2).

53. LIBRATIONAL DYNAMICS OF SATELLITES WITH THEMALLY FLEXED APPENDAGES, V.J. Modi and K. Kumar, British Columbia University, Vancouver, Canada, July 1973. A74-17602.

54. MANEUVERING AND POINTING FLEXIBLE VEHICLES, Douglas C. Fosth, Boeing Aerospace Co., Seattle, Wash. N79-10111.

55. MODEL VERIFICATION OF LARGE STRUCTURAL SYSTEMS, L.T. Lee et al., J.H. Wiggins Co., Redondo Beach Calif.,July 1978. N78-31464 (NASA-CR-150811).

56. MISSION REQUIREMENTS FOR ORBIT TRANSFER OPERATIONS, FINAL REPORT, VOL. II, Aerospace Report #ATR=79(7723)-1. NASA CNT # NASW 3134.

57. NASA FORECAST OF SPACE TECHNOLOGY (1980-2000), Jan. 1976. NASA-SP-387.

58. OAST SPACE THEME WORKSHOP, VOLUME 2, NASA, Langley Research Center, Hampton, Va., April 1976. N79-15118 (NASA-TM-80006).

59. OAST THEME WORKSHOP, VOLUME 3,NASA, Langley Research Center, Hampton, Va., April 1976. N79-15127 (NASA-TM-80015).

60. ORBITAL ANTENNA FARMS, B.I. Edelson and W.L. Morgan, COMSAT Lab., Clarksburg, Md., Sept. 1977. A77-47268.

61. ORBITING DEEP SPACE RELAY STATION(ODSRS): DSN FEASIBILITY STUDY REPORT, Tom Thornton and John Hunter, Jet Propulsion Lab., Pasadena, Calif., 1978. N79-10083.

62. OVERVIEW OF THE LARGE SPACE SYSTEMS TECHNOLOGY PROGRAM, A. Guastaferro, NASA, Langley Research Center, Hampton, Va., 1978. 79N10079.

63. PERIODIC ANALYSIS OF LARGE SPACE STRUCTURES, R.W. Fralich, NASA, Langley Research Center, Hampton, Va., December 1979. 77K10066.

64. PLATFORM DESIGNED FOR NUMEROUS USES, C. Covault, June 1978. A78-42509.

65. PLANNING FOR LARGE CONSTRUCTION PROJECTS IN SPACE, J.H. Disher, NASA, Office of Space Flight, Wash., D.C., Oct. 1977. A79-20767.

66. POINTING AND CONTROL TECHNOLOGY NEEDS FOR FUTURE AUTOMATED SPACE SYSTEMS, J.B. Dahlgren and S.M. Gunter, Jet Propulsion Laboratory, Pasadena, Calif., Sept. 1978. A78-52748 (NASA CNT # NAS7-100).

67. PRACTICAL DESIGN OF LOW-COST LARGE SPACE STRUCTURES, J.M.Hedgepeth, Astro Research Corp., Carpinteria, Calif., M.M. Mikulas, Jr., NASA, Langley Research Center, Hampton, Va., and R.H. MacNeal, MacNeal-Schwendler Corp., Los Angeles, Calif., Oct. 1978. A79-10508.

68. PRELIMINARY DEFINITION AND EVALUATION OF ADVANCED SPACE CONCEPTS, Aerospace Report #ATR-78(7674)-1 /Vol II. N78-28107 (NASA CNT # NASW-3030).

69. PRELIMINARY INVESTIGATIONS INTO THE ACTIVE CONTROL OF LARGE SPACE STRUCTURES, M.F. Card, NASA, Langley Research Center, Hampton, Va., June 1979. 76K10972 (NASA CNT #NSG-1279).

70. PROPULSION OPTIONS FOR ORBITAL TRANSFERS IN CIS-LUNAR SPACE, J.P. Layton, Techno-Systems Analysis Corp., Princeton, N.J., May 1977. A78-27931.

71. REDUCED ORDER CONTROL OF LARGE STRUCTURES IN SPACE, M.J. Balas, Bolt Beranek and Newman, Inc., Cambridge, Mass., Jan. 1979. A79-19593, AIAA 79-0196.

72. SATELLITE POWER SYSTEM (SPS) CONCEPT DEFINITION STUDY, Rockwell International Corp.,NASA 8-32475.

73. SELF POWERED ELECTRIC PROPULSION OF SATELLITE POWER SYSTEMS, J.B. Wedded, W.W. McRae and S.T. Cerni, Rockwell International Downey, Calif., April 1978. AIAA 78-694.

74. SERVING THE PUBLIC VIA PLATFORMS IN SPACE, R. Fleisig and J.L. Bernstein, Grumman Aerospace Corp. Bethpage, N.Y., March 1978. A79-11557, AAS 78-015.

75. SIZE, PERFORMANCE AND COST TRADES OF LARGE SOLAR ELECTRIC PROPULSION SYSTEMS, H.F. Meissinger, TRW Defense and Space Systems Group, Redondo Beach, Calif. April 1978. A78-37440, AIAA 78-687.

76. SOME DESIGN CONSIDERATIONS FOR LARGE SPACE STRUCTURES, H.G. Bush, M.M. Mikulas, Jr., and W.L. Heard, Jr., NASA, Langley Research Center, Hampton, Va., 1977. 77A25747, AIAA 77-395.

77. SPACE CONSTRUCTION SYSTEM ANALYSIS, Rockwell International Corp., April 1979. NASA CNT # NAS9-15718.

78. SPACE WILL BE THE NEXT BIG CONSTRUCTION SITE, G. Bylinsky, Feb. 1979. A79-24450.

79. SPOKED WHEELS TO DEPLOY LARGE SURFACES IN SPACE, R. F. Crawford & J. M. Hedgepeth, AIAA # 74-1267.

80. STRUCTURAL & ASSEMBLY CONCEPTS FOR LARGE ERECTABLE SPACE SYSTEMS, 1977. AAS # 77-205.

81. STRUCTURAL ATTACHMENTS FOR LARGE SPACE STRUCTURES, W.R. Britton, R.A. Spencey, M.D. Thulson, Martin Marietta Corp., Denver, Colo., July 1978. N78-30168, (NASA CNT #NAS8-32654).

82. STRUCTURAL DESIGN CONCEPT FOR FUTURE SPACE MISSIONS, J.H. Launchner, University of Southern Illinois, Carbondale, Ill., Oct. 1966. 77X78426, NASA-CR-154700, NASA CNT # NGR-14-008-002.

83. STRUCTURAL EFFICIENCY OF LONG LIGHTLY LOADED TRUSS AND ISOGRID COLUMNS FOR SPACE APPLICATIONS, M.M. Mikulas, Jr.,July 1978. N78-33480.

84. STRUCTURES FOR SOLAR POWER SATELLITES, R.H. Nansen and H. di Ramio, Boeing Aerospace Co., Seattle, Wash., A79-10513.

85. SURVEY OF FUTURE REQUIREMENTS FOR LARGE SPACE STRUCTURES, FINAL REPORT, John M. Hedgepeth, NASA, Washington, D.C., Jan. 1976. N76-15500, NASA-CR-2621, NASA CNT #NAS1-13178.

86. TAKING A NEW APPROACH TO THE SPACE SOLAR POWER STATION, L.J. Cantafio, V.A. Chobotov, and M.G. Wolfe, The Aerospace Corporation, Nov.1979, GSSPS

87. TECHNOLOGY ASSESSMENT AND OUTLOOK, M.F. Card, E.T. Kruszewski, and A. Guastaferro, NASA, Langley Research Center, Hampton, Va. A79-10512.

88. TECHNOLOGY FOR ACCURATE SURFACE AND ATTITUDE CONTROL OF A LARGE SPACEBORNE ANTENNA AND MICROWAVE SYSTEM, John B. Dahlgren, Jet Propulsion Lab., Pasadena, Calif., 1978. N79-10092.

89. THE DYNAMICS AND CONTROL OF LARGE FLEXIBLE SPACE STRUCTURES, H.A, Hamer, HASA, Langley Research Center, Hampton, Va., May 1977. 77K11190, NASA CNT # NSG-1414.

90. THE PRODUCTION OF ULTRATHIN POLYMIDE FILMS FOR THE SOLAR SAIL PROGRAM AND LARGE SPACE STRUCTURES TECHNOLOGY (LSST), A FEASIBILITY STUDY, R.H. Forester, Midwest Research Inst., 1978. N78-30657 (NASA-CR-157569).

91. THE TECHNOLOGY OF LARGE MULTI-FUNCTION COMMUNICATION SATILLITES IN THE POST INTELSAT V ERA, C.L. Cuccia, Ford Aerospace and Communication Corp., Palo Alto, Calif., Oct. 1978. A79-11320.

92. THE CONTROL OF SPACECRAFT VIBRATIONS USING MULTIVARIABLE OUTPUT FEEDBACK, J.K. Canavin, C. Stark Draper Lab., Cambridge Mass., Aug. 1978. AIAA 78-1419.

93. THE OAF CONCEPT EXTENDED, W.L. Morgan and B.I. Edelson, COMSAT Laboratories, Clarksburg, Md., April 1978. A78-32891, AIAA 78-546.

94. THREE-AXIS ATTITUDE CONTROL FOR SOLAR-POWERED ELECTRIC PROPULSION SPACECRAFT, H.K. Bouvier, Jet Propulsion Lab., Pasadena, Calif., Oct. 1974. A75-22946.

95. WEIGHT OPTIMIZATION OF ULTRA LARGE SPACE STRUCTURES, R.P. Reinert Boeing Aerospace Company, MAY 1979. SAWE 1 01 (NASA CNT # NAS9-15196).

APPENDIX B

MASS PROPERTIES AND DISTURBANCE FORCE AND TORQUE DATA

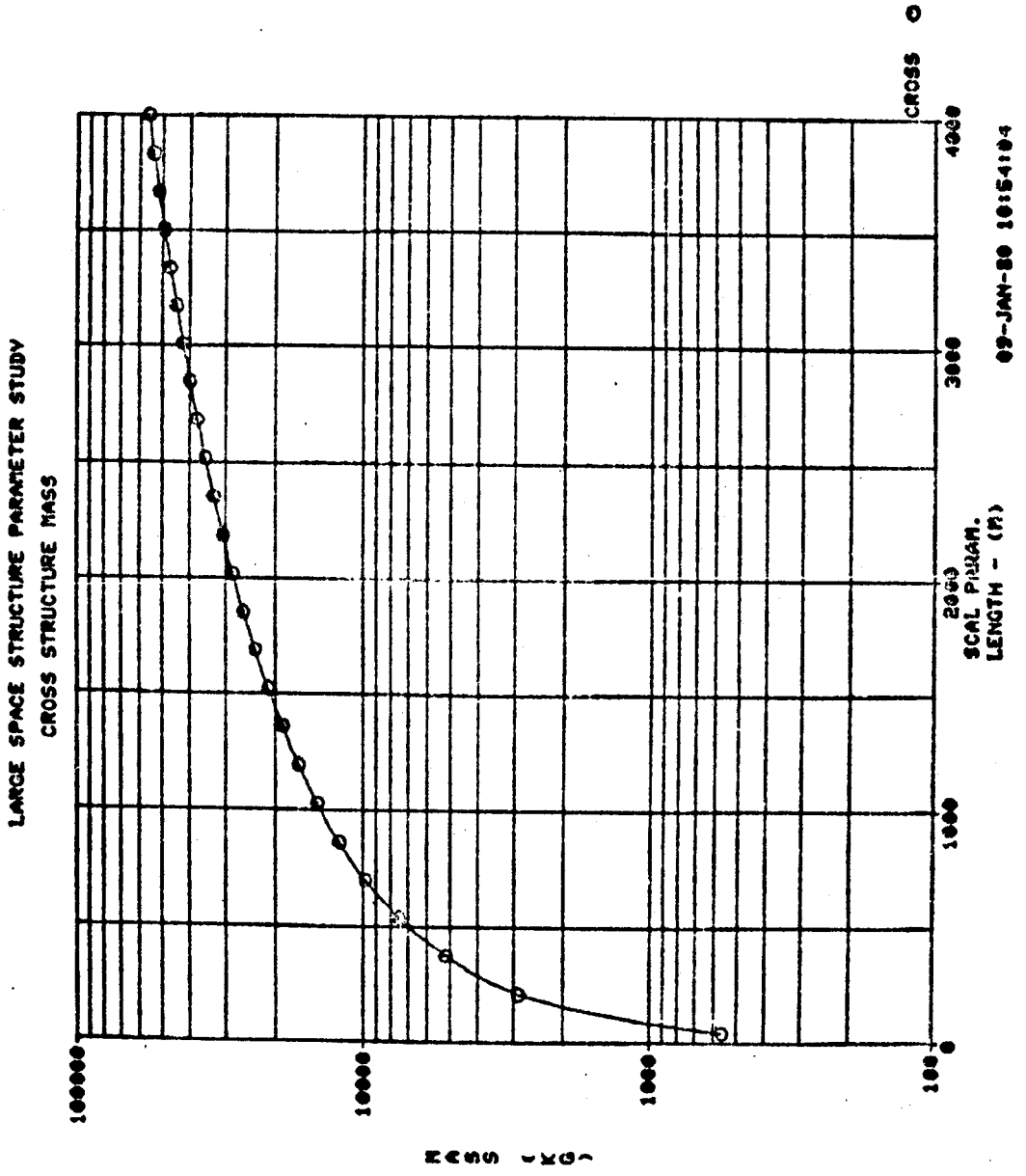

FIGURE B-1 LARGE SPACE STRUCTURE PARAMETER STUDY
PLATE STRUCTURE MASS

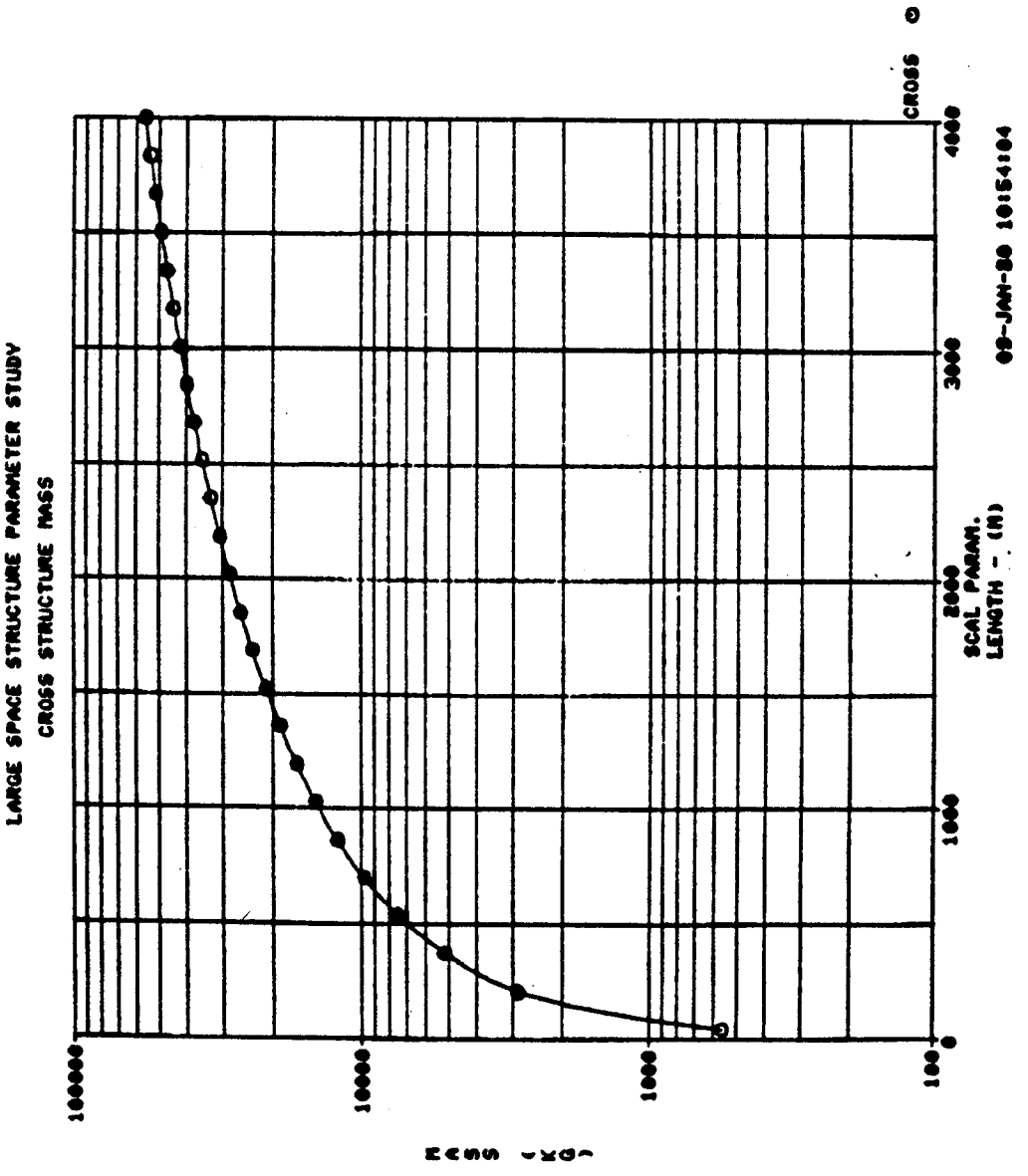

FIGURE B-2 LARGE SPACE STRUCTURE PARAMETER STUDY
CROSS STRUCTURE MASS

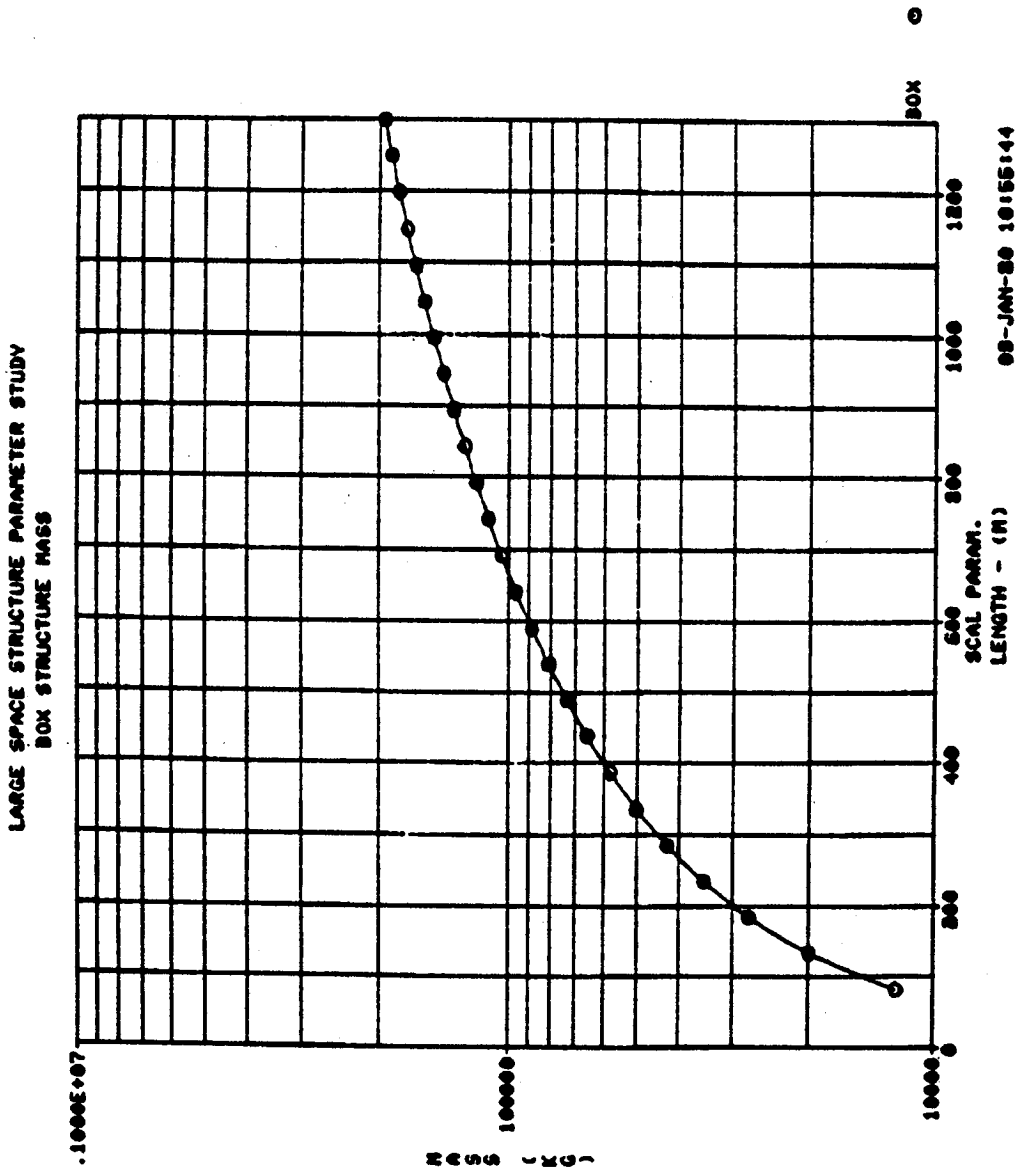

FIGURE B-3 LARGE SPACE STRUCTURE PARAMETER STUDY
BOX STRUCTURE MASS

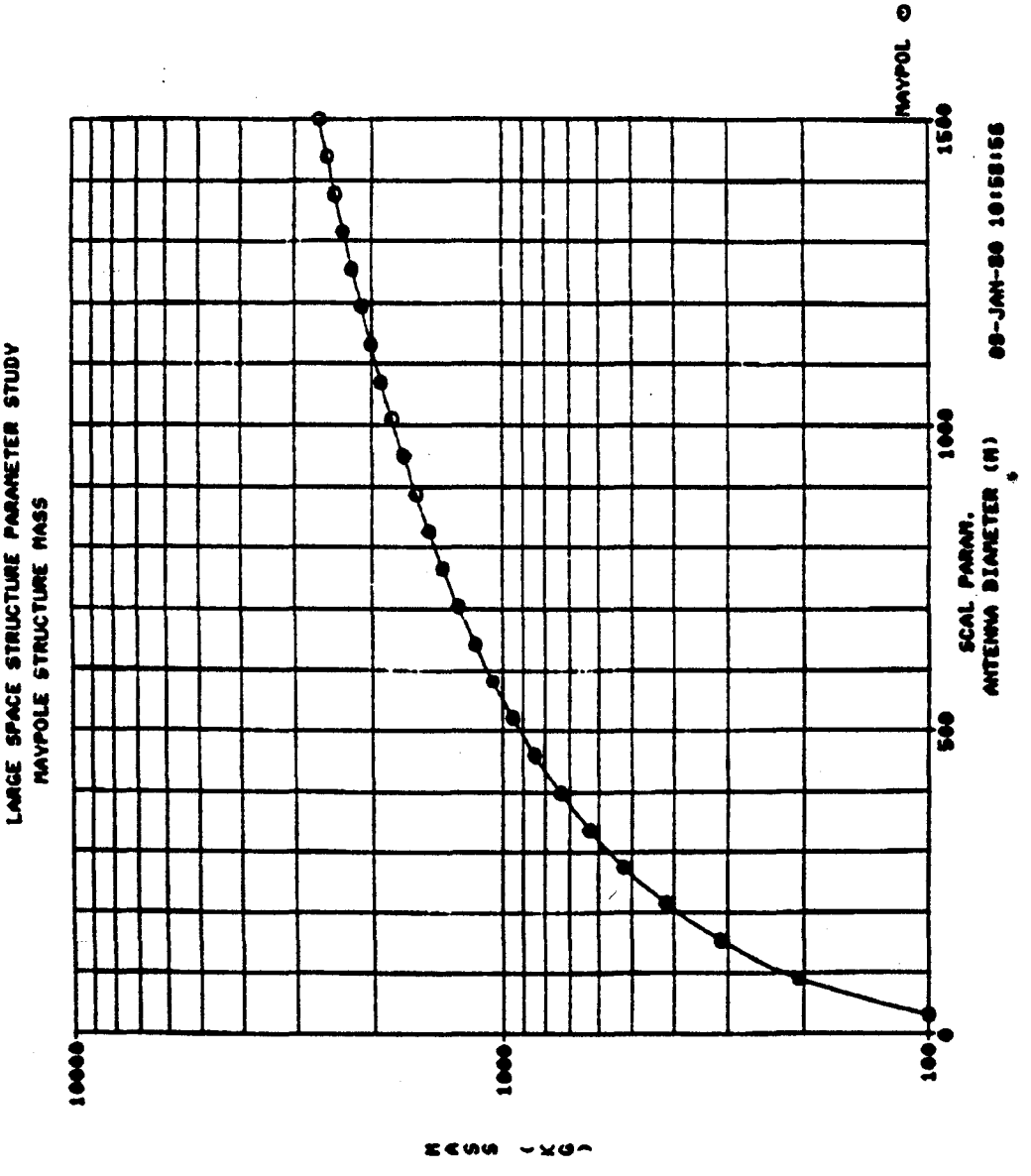

FIGURE B-4. LARGE SPACE STRUCTURE PARAMETER STUDY
SINGLE MODULAR ANTENNA STRUCTURE MASS

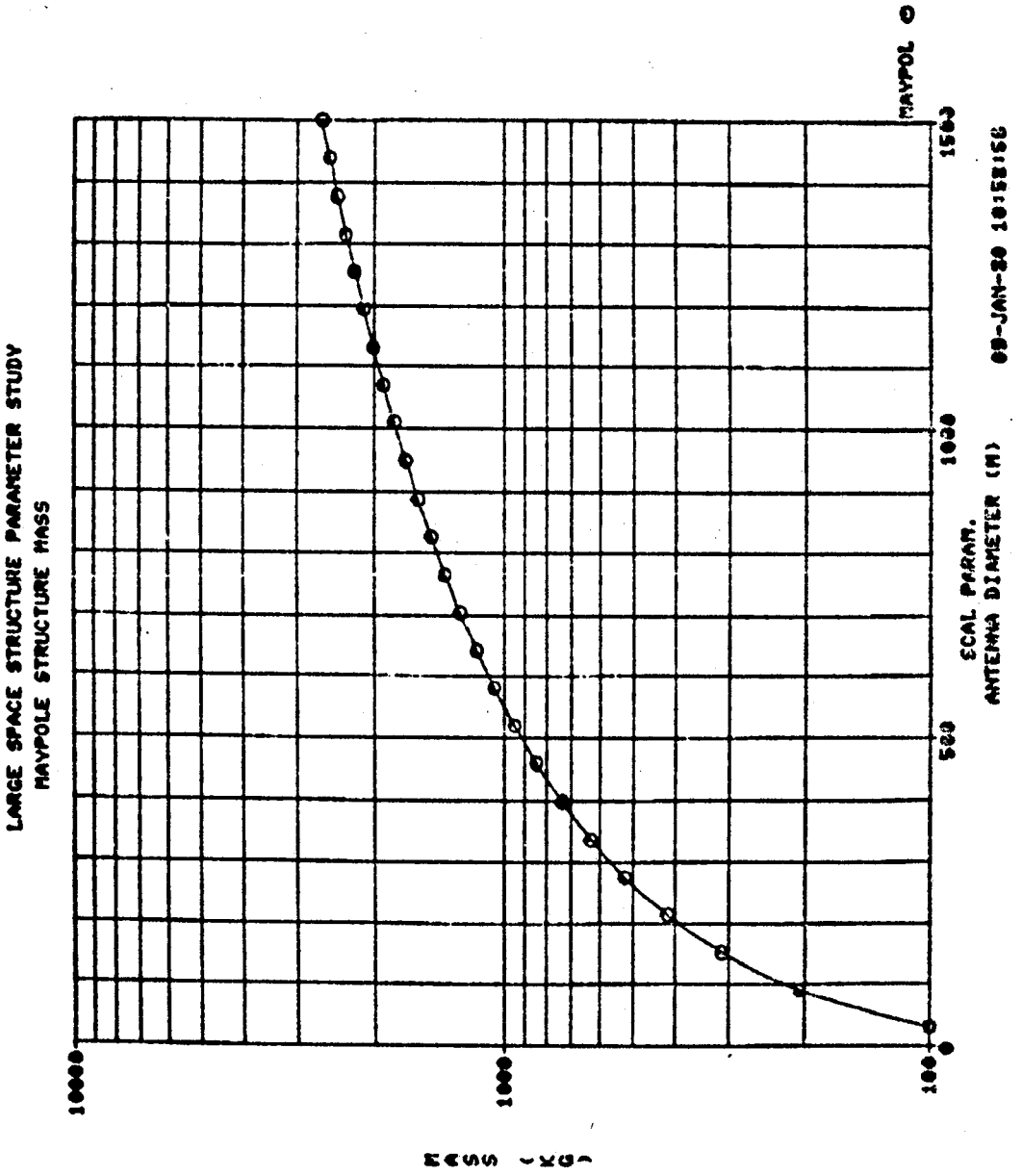

FIGURE B-5 LARGE SPACE STRUCTURE PARAMETER STUDY
MAYPOLE STRUCTURE MASS

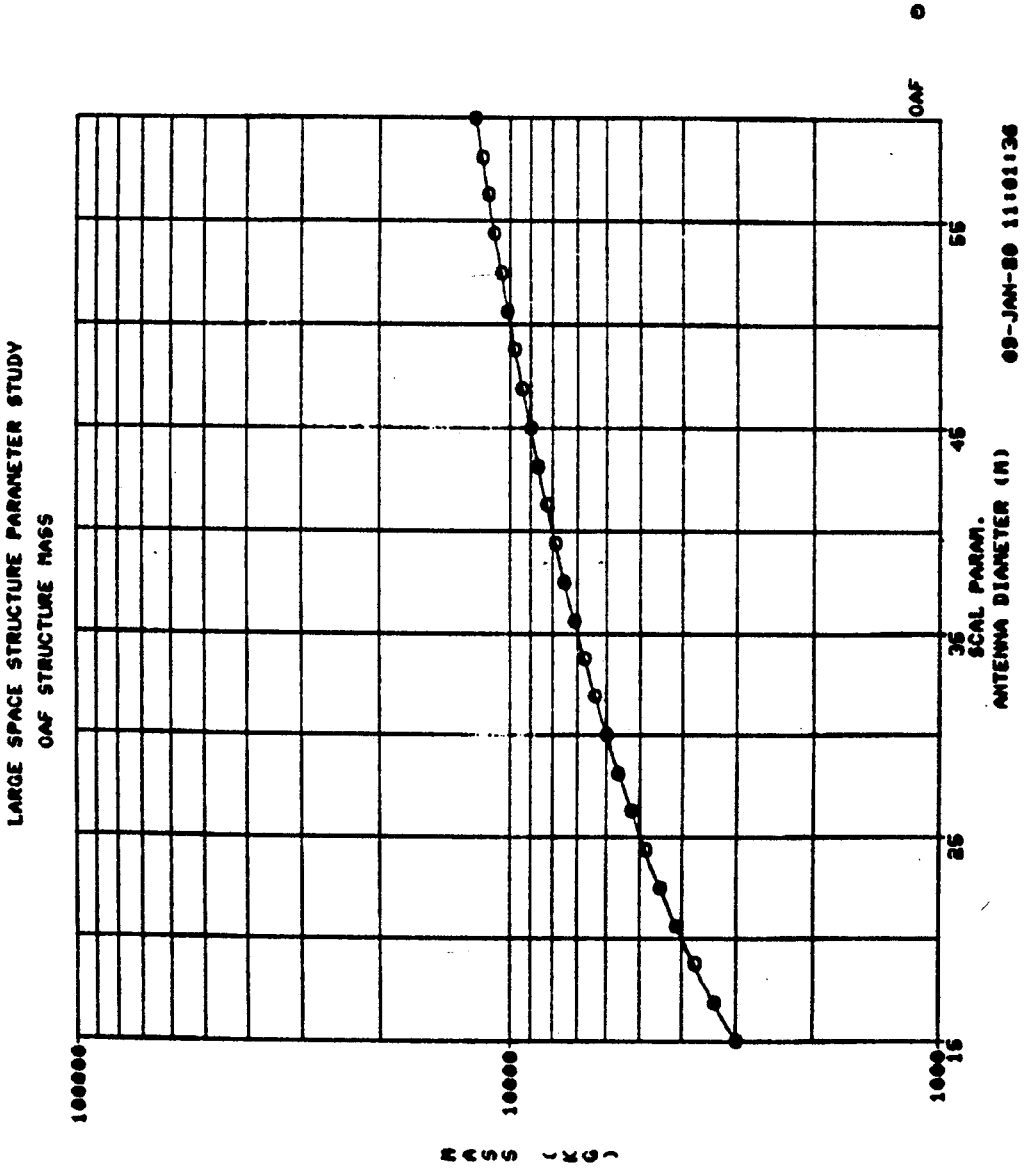

FIGURE B-6 LARGE SPACE STRUCTURE PARAMETER STUDY
OAF STRUCTURE MASS

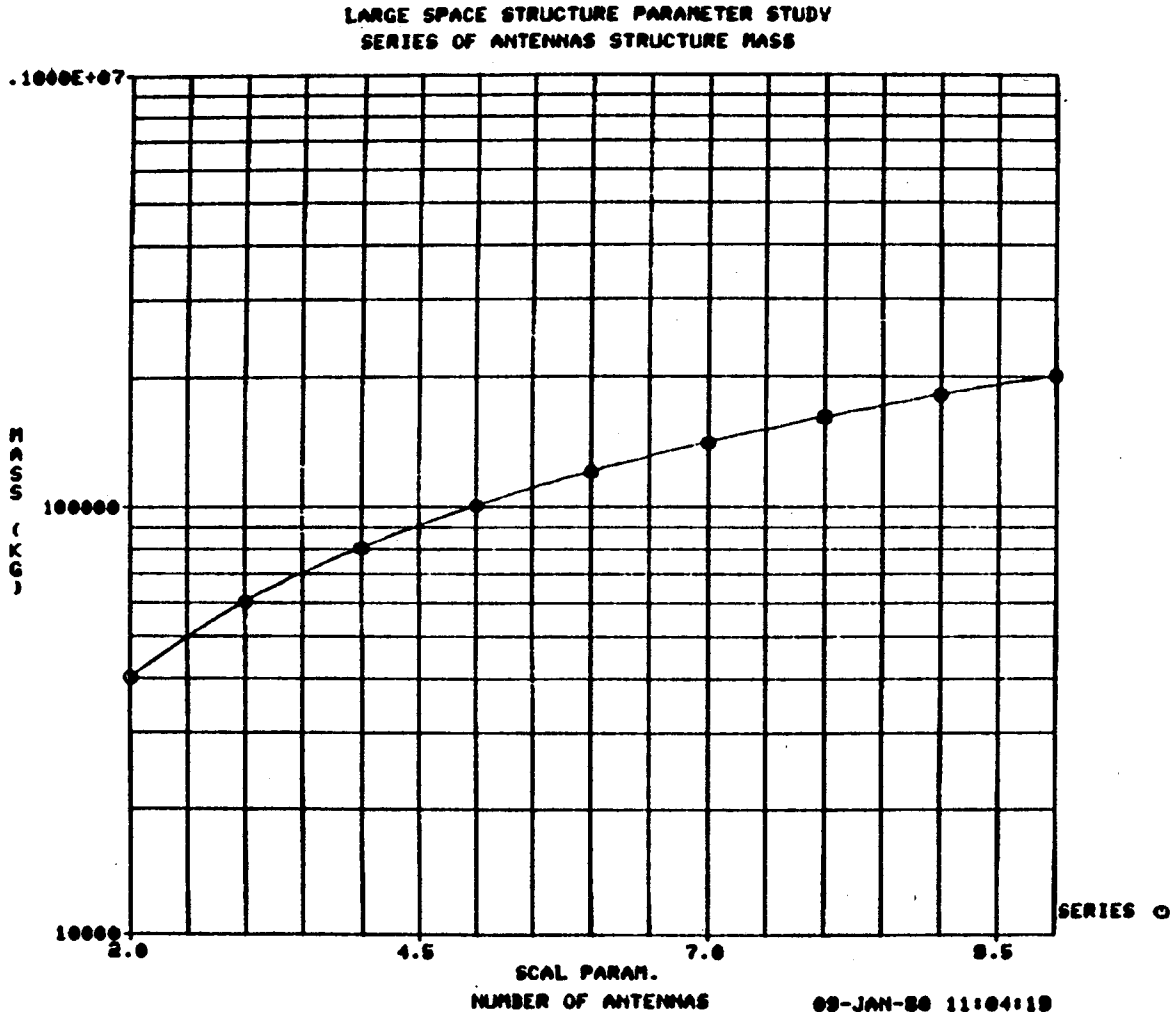

FIGURE B-7 LARGE SPACE STRUCTURE PARAMETER STUDY
SERIES OF ANTENNAS STRUCTURE MASS

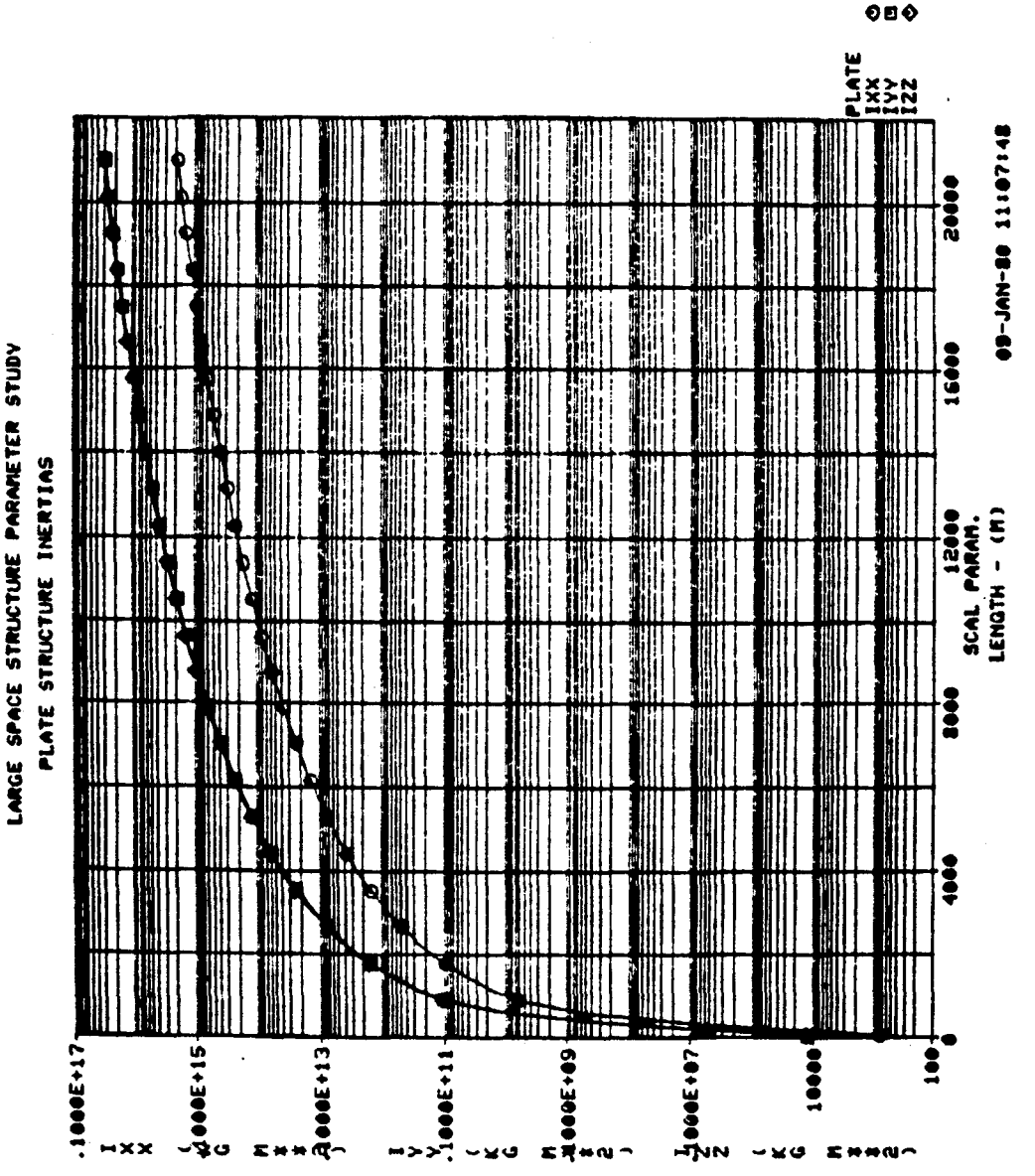

FIGURE B-8 LARGE SPACE STRUCTURE PARAMETER STUDY
PLATE STRUCTURE INERTIAS

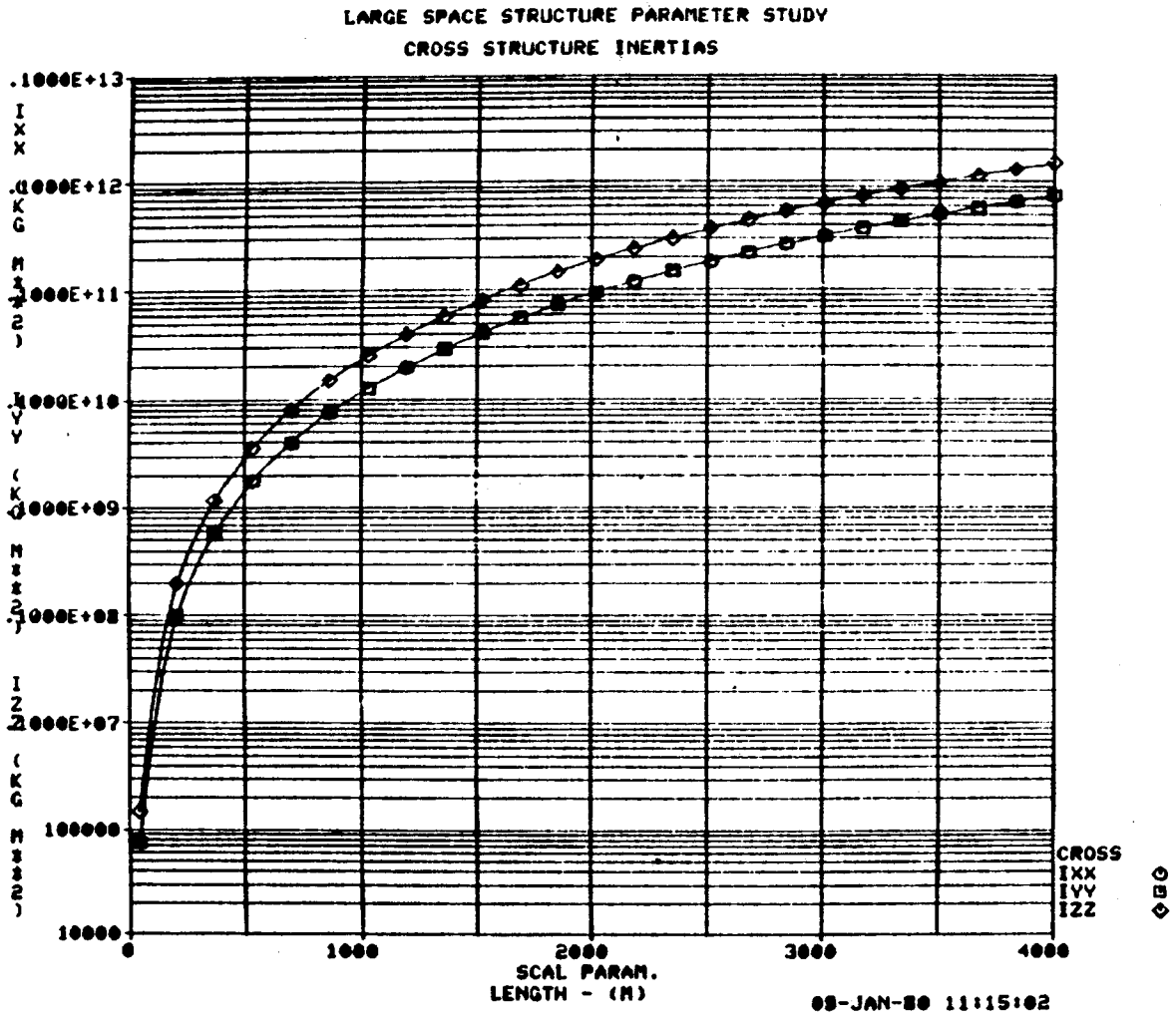

FIGURE B-9 LARGE SPACE STRUCTURE PARAMETER STUDY
CROSS STRUCTURE INERTIAS

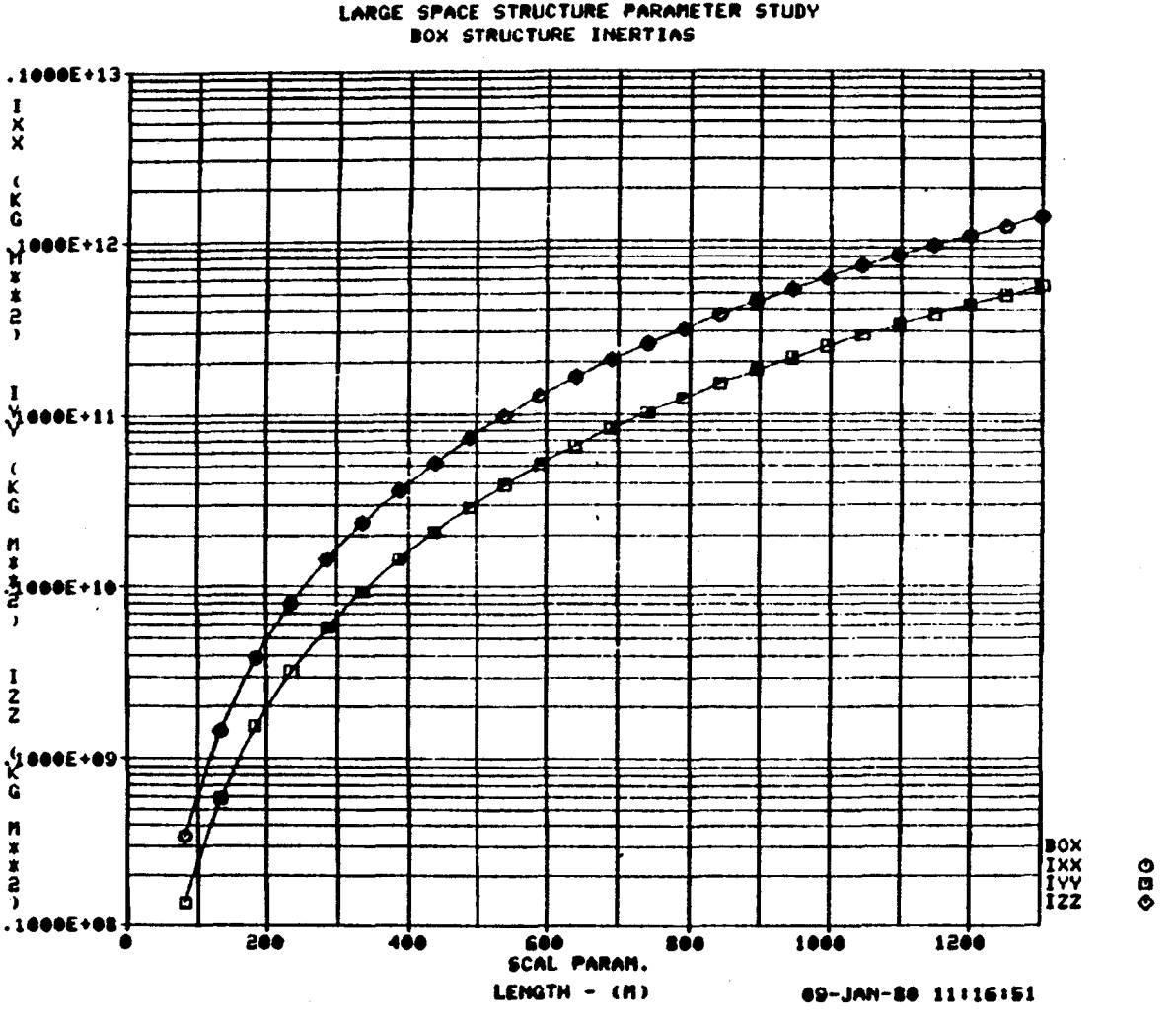

FIGURE B-10 LARGE SPACE STRUCTURE PARAMETER STUDY
BOX STRUCTURE INERTIAS

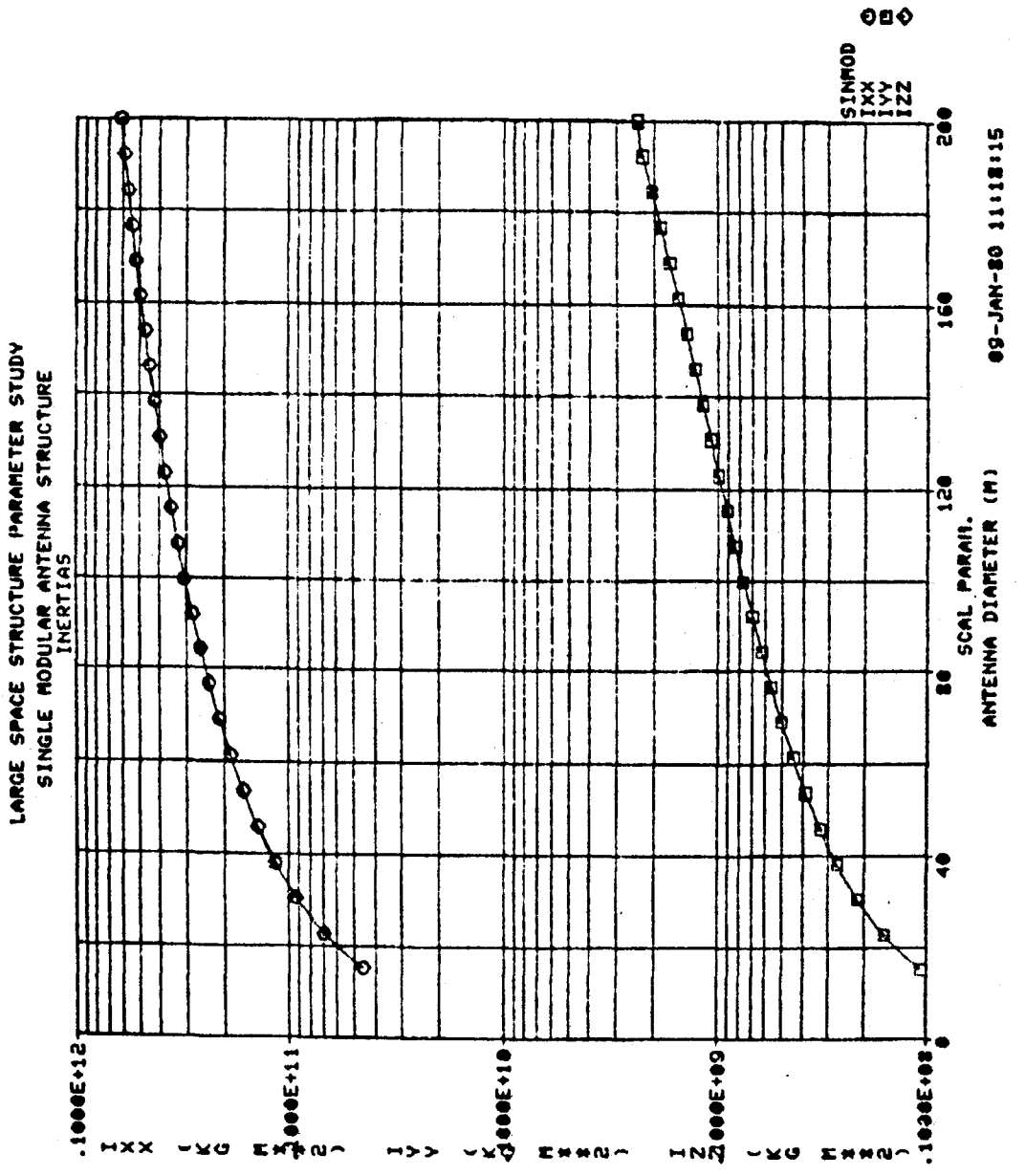

FIGURE B-11 LARGE SPACE STRUCTURE PARAMETER STUDY
SINGLE MODULAR ANTENNA STRUCTURE INERTIAS

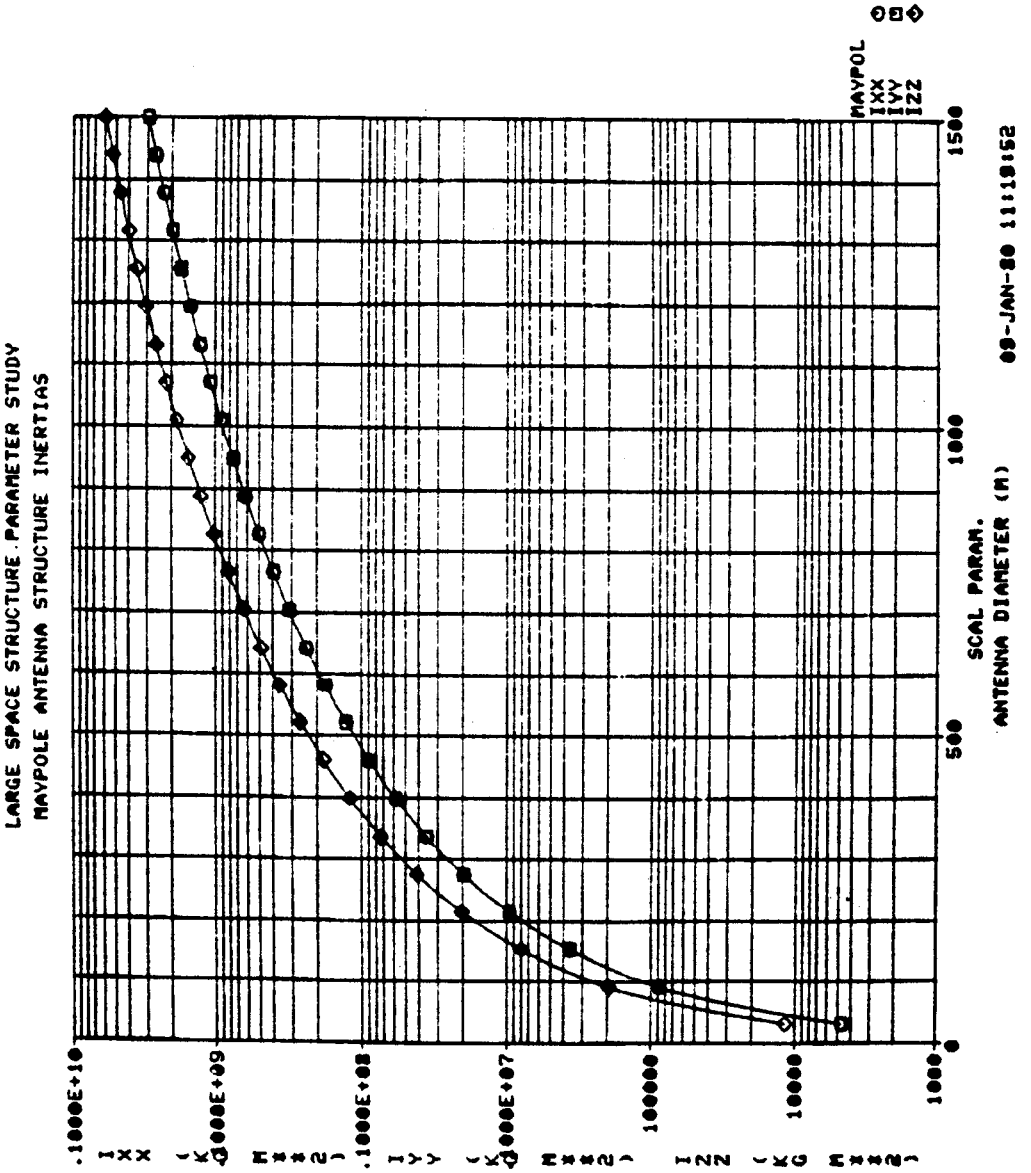

FIGURE B-12 LARGE SPACE STRUCTURE PARAMETER STUDY
MAYPOLE ANTENNA STRUCTURE INERTIAS

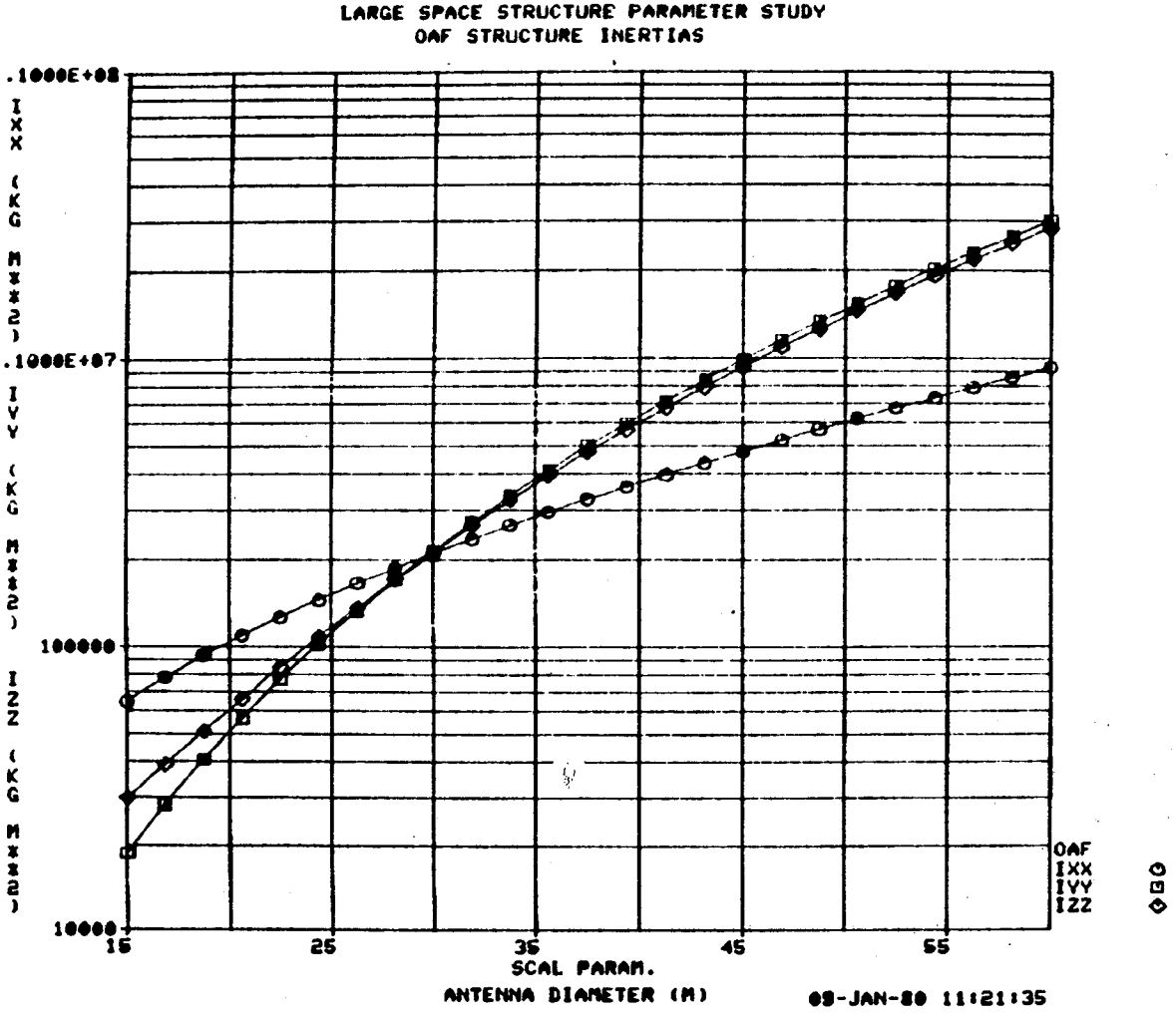

FIGURE B-13 LARGE SPACE STRUCTURE PARAMETER STUDY
OAF STRUCTURE INERTIAS

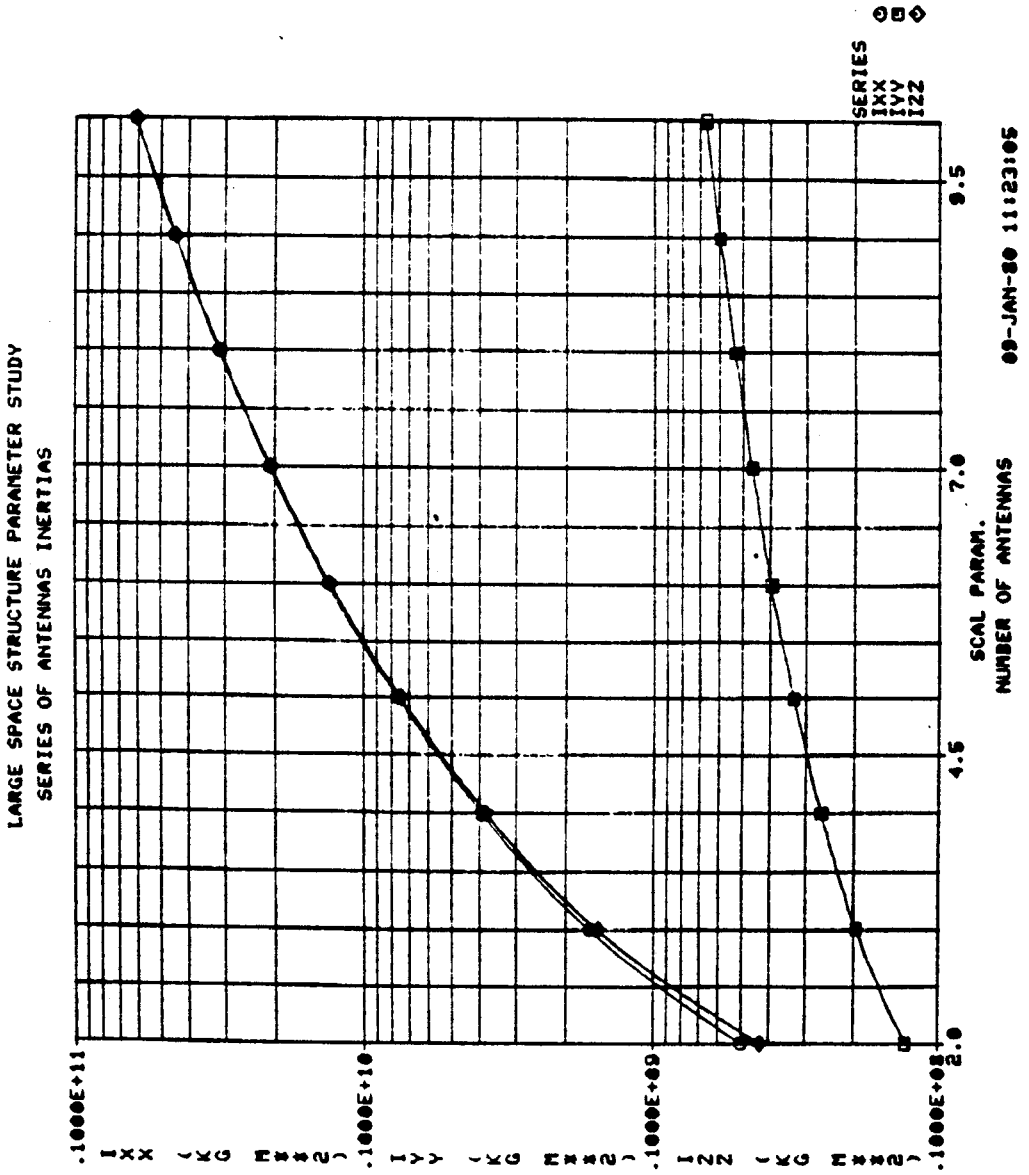

FIGURE B-14 LARGE SPACE STRUCTURE PARAMETER STUDY
SERIES OF ANTENNAS INERTIAS

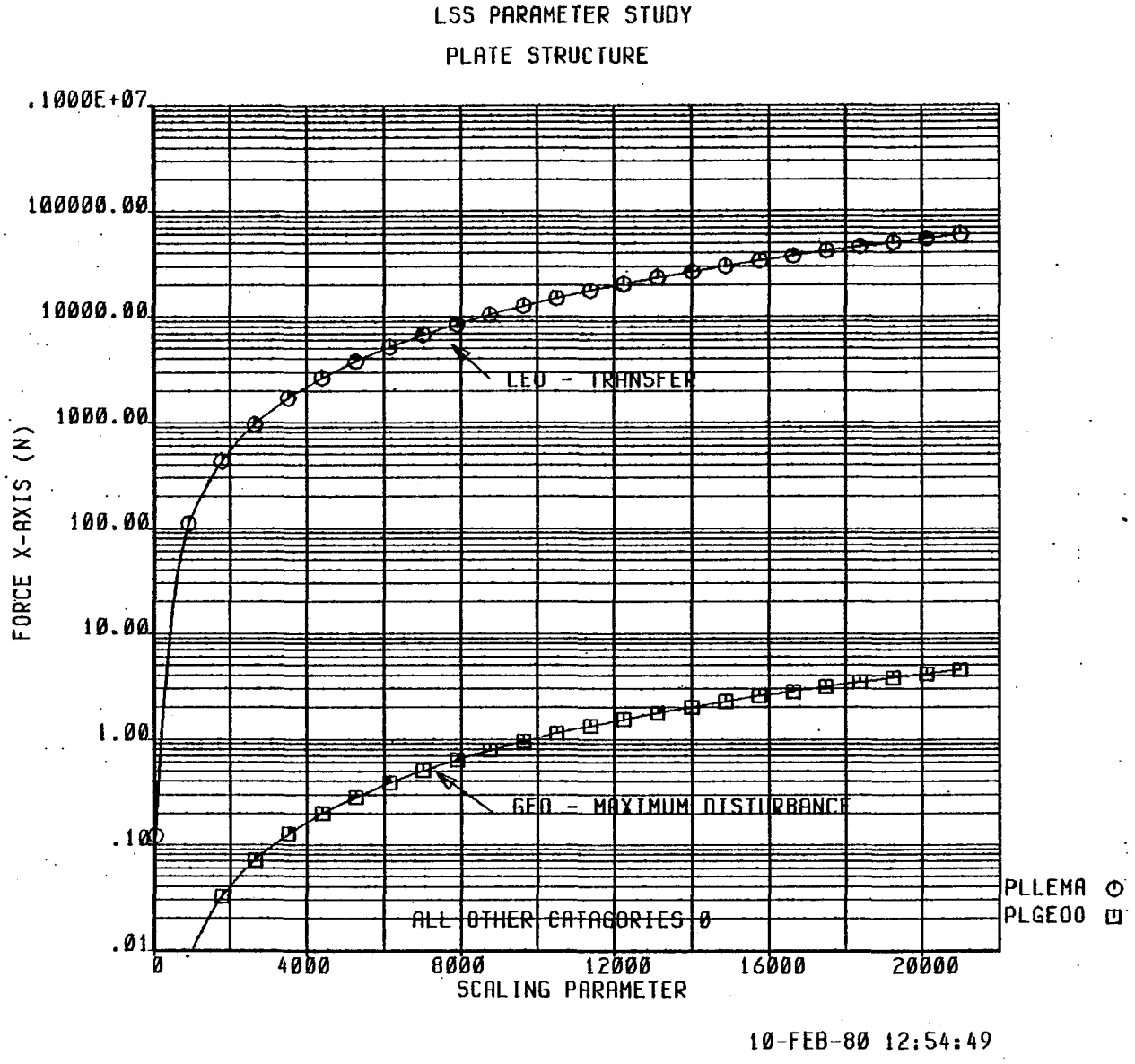

FIGURE B-15 LSS PARAMETER STUDY PLATE STRUCTURE FORCES - X AXIS

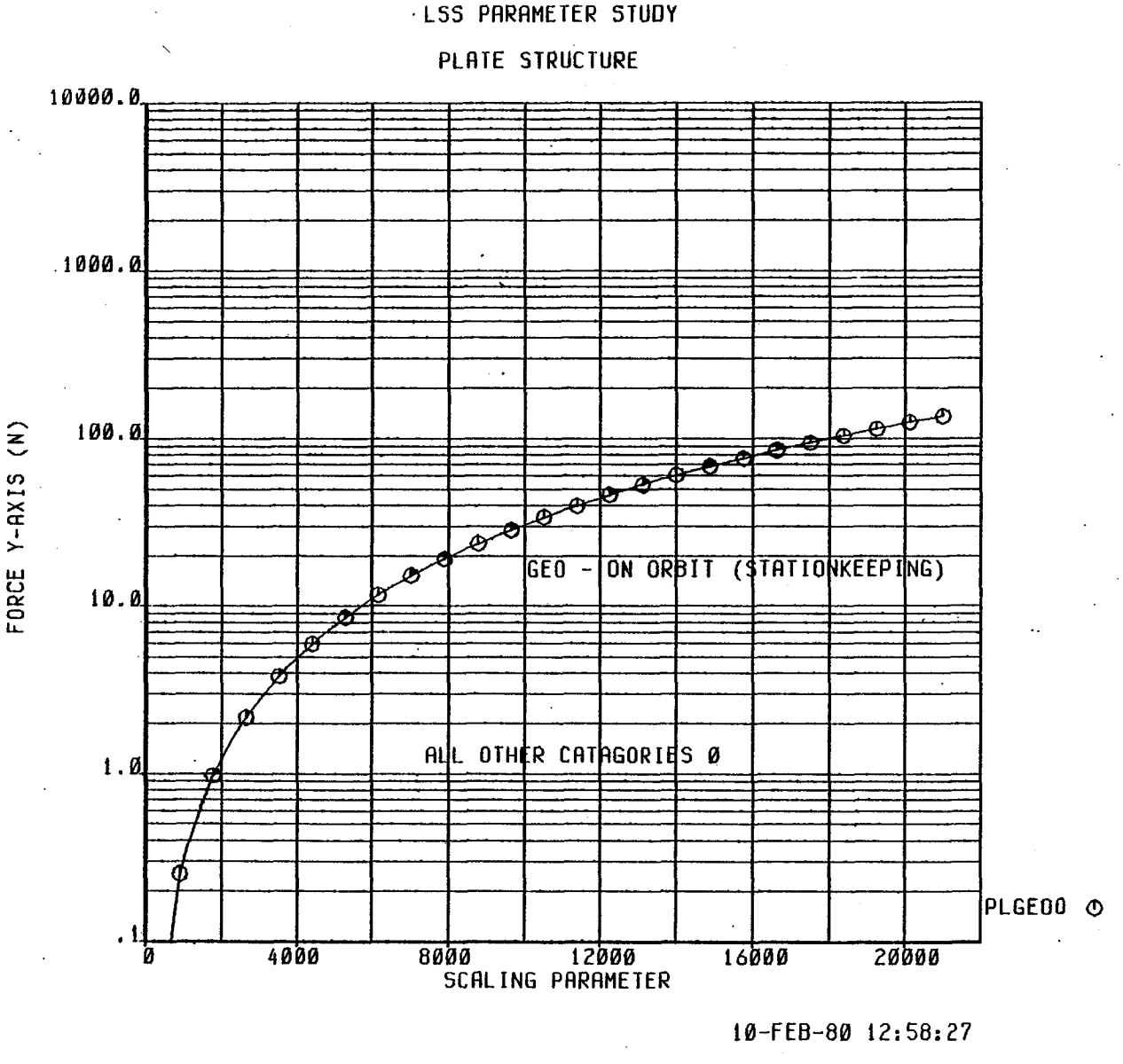

FIGURE B-16 LSS PARAMETER STUDY PLATE STRUCTURE FORCES - Y AXIS

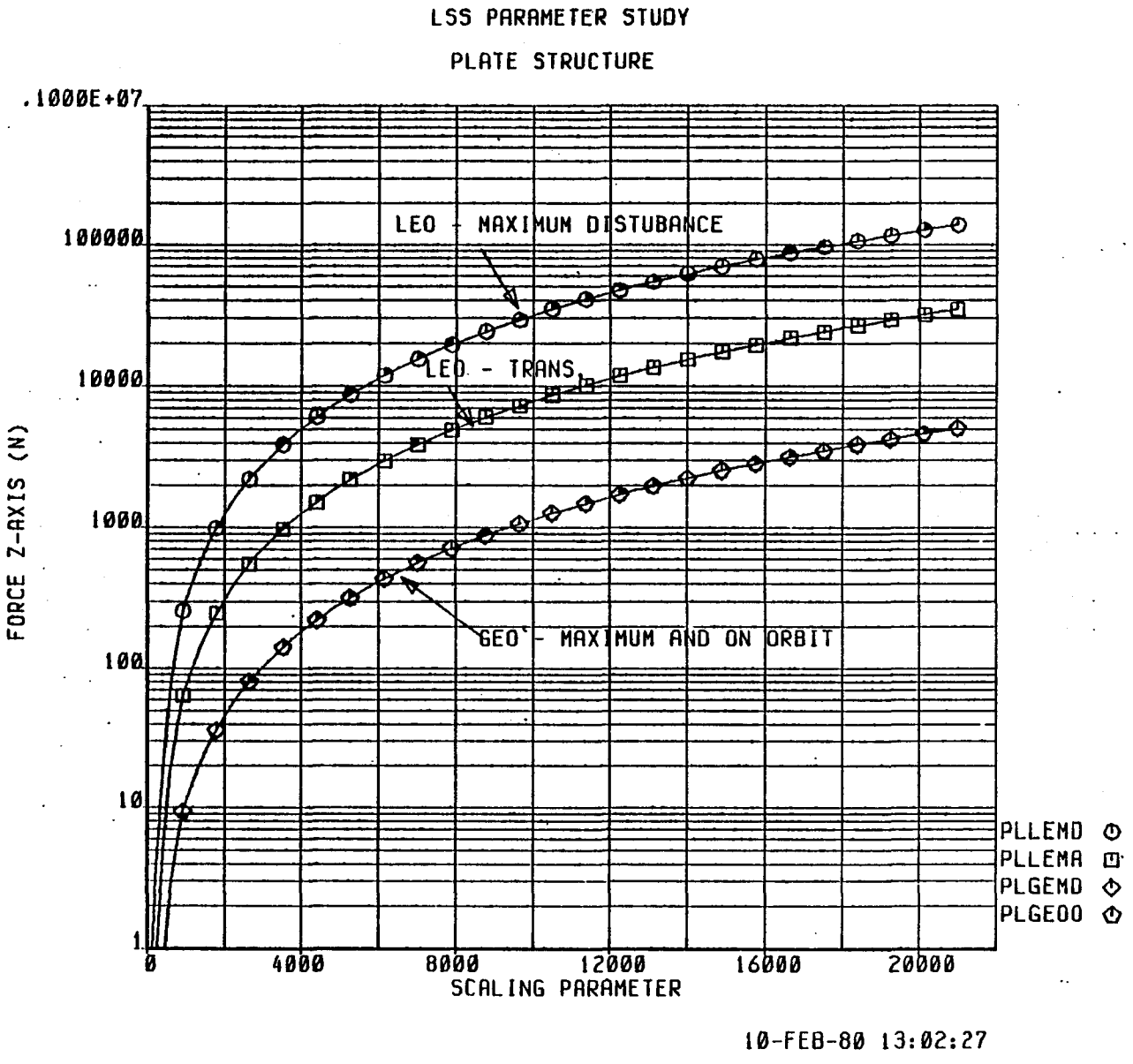

FIGURE B-17 LSS PARAMETER STUDY PLATE STRUCTURE FORCES - Z AXIS

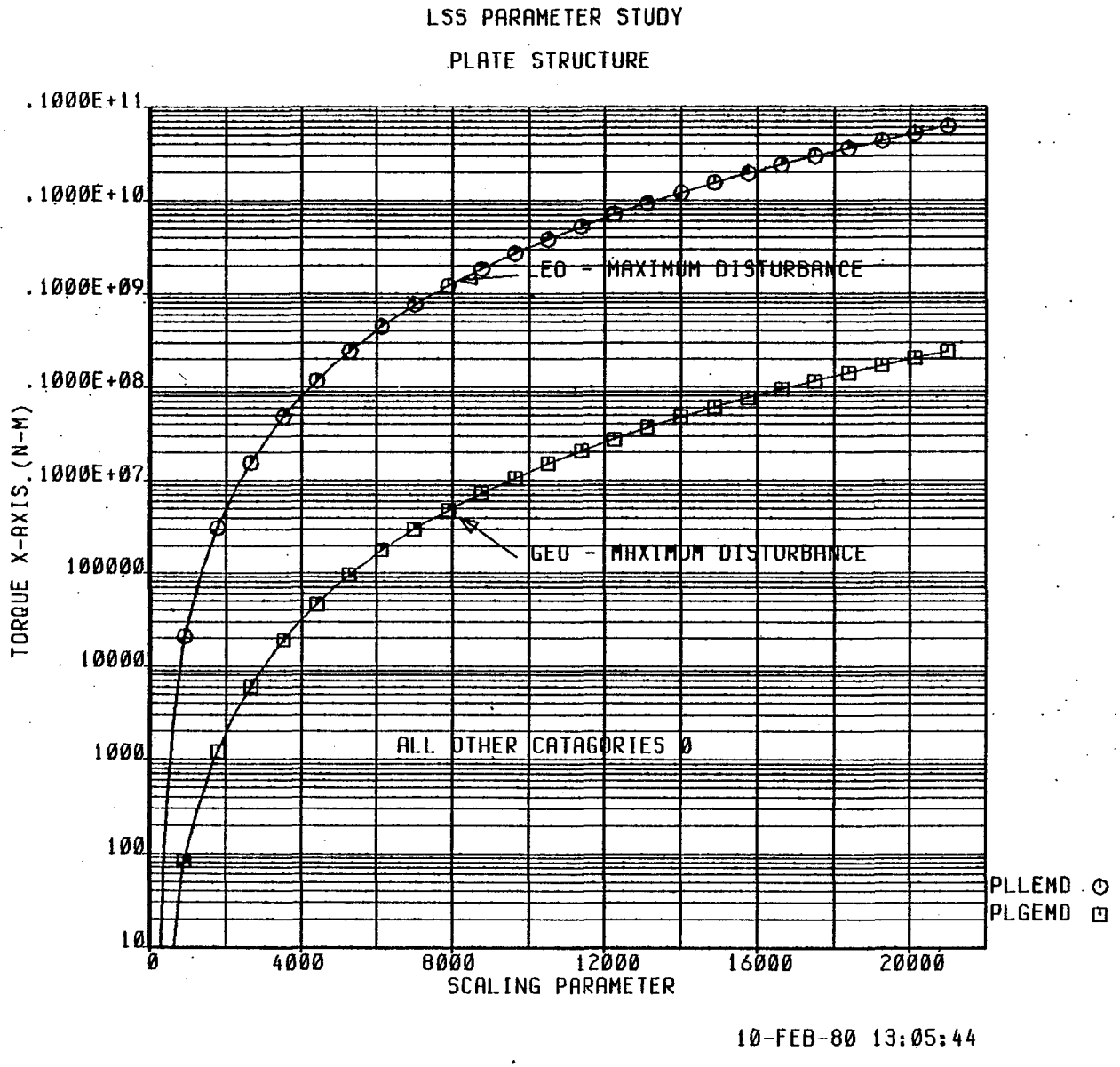

FIGURE B-18 LSS PARAMETER STUDY PLATE STRUCTURE TORQUES - X AXIS

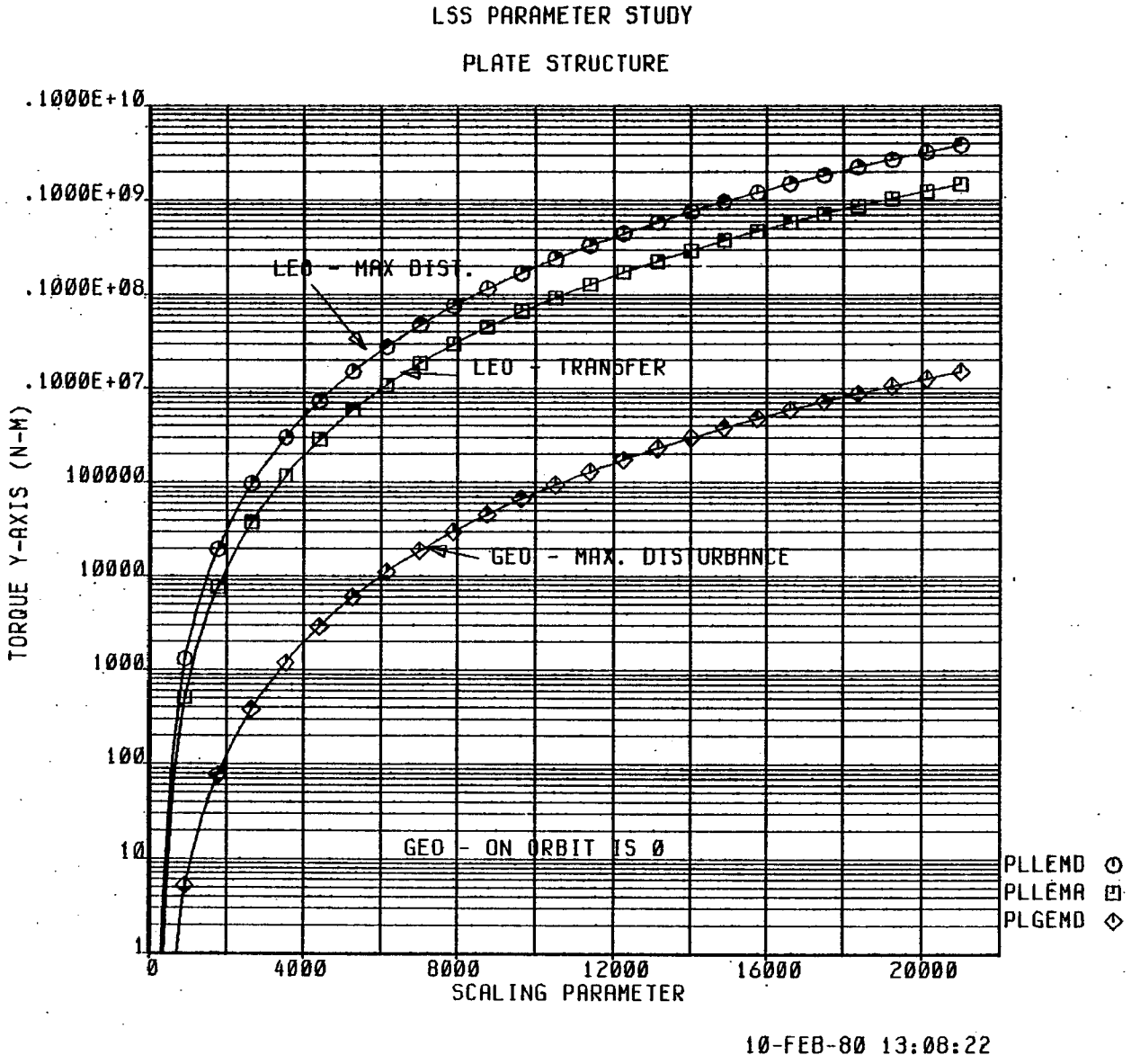

FIGURE B-19 LSS PARAMETER STUDY PLATE STRUCTURE TORQUES - Y AXIS

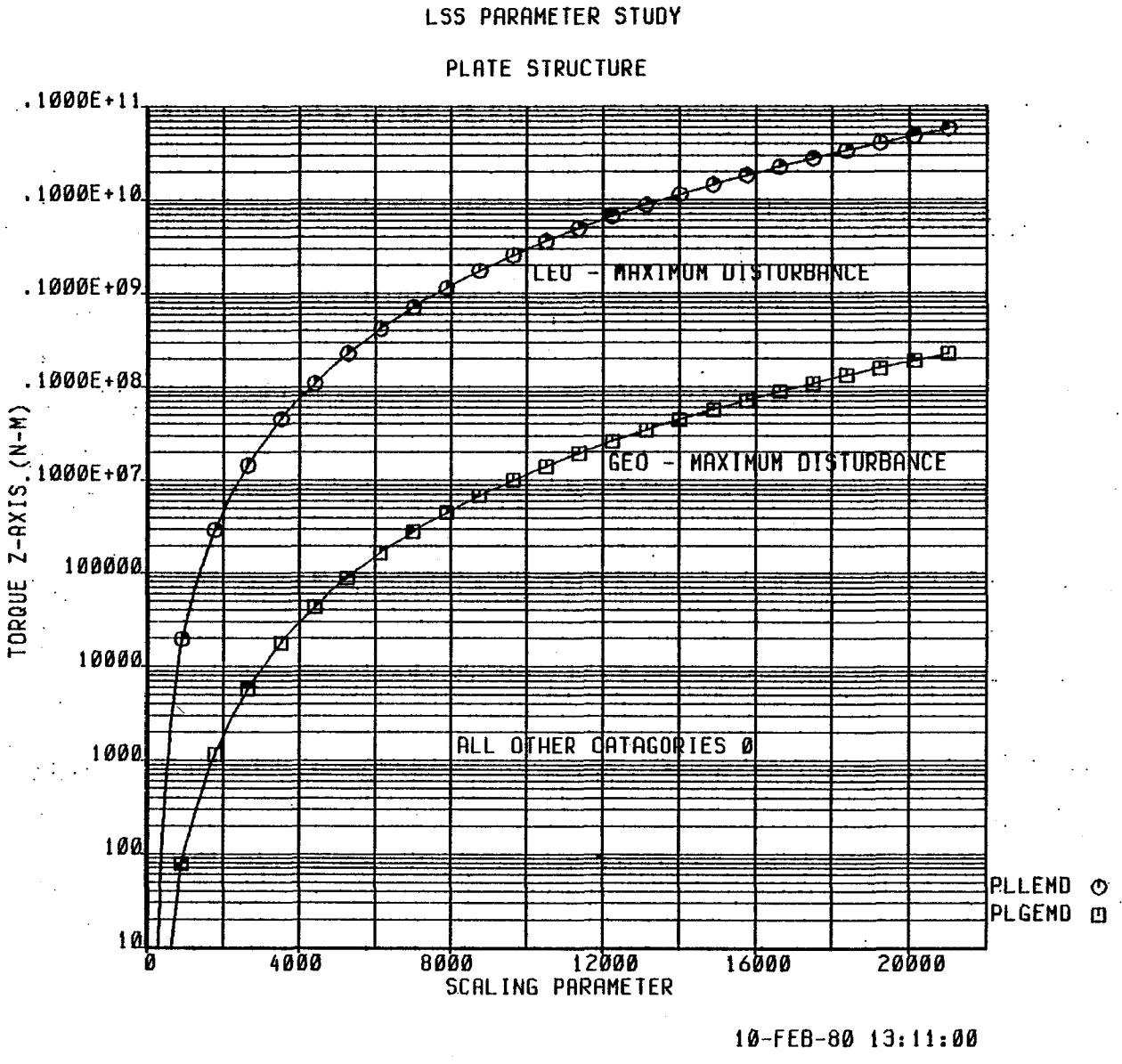

FIGURE B-20 LSS PARAMETER STUDY PLATE STRUCTURE TORQUES - Z AXIS

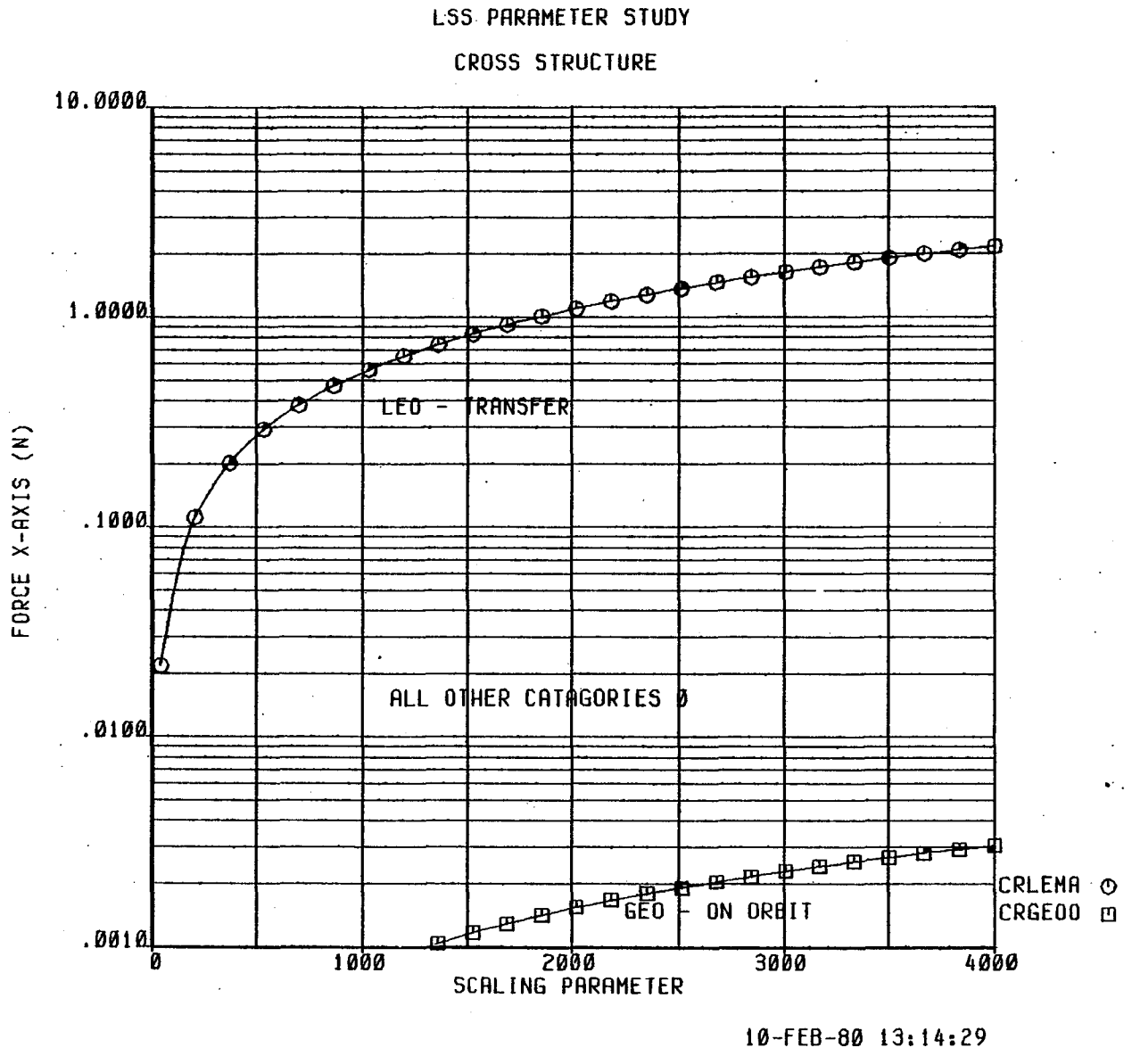

FIGURE B-21 LSS PARAMETER STUDY CROSS STRUCTURE FORCES - X AXIS

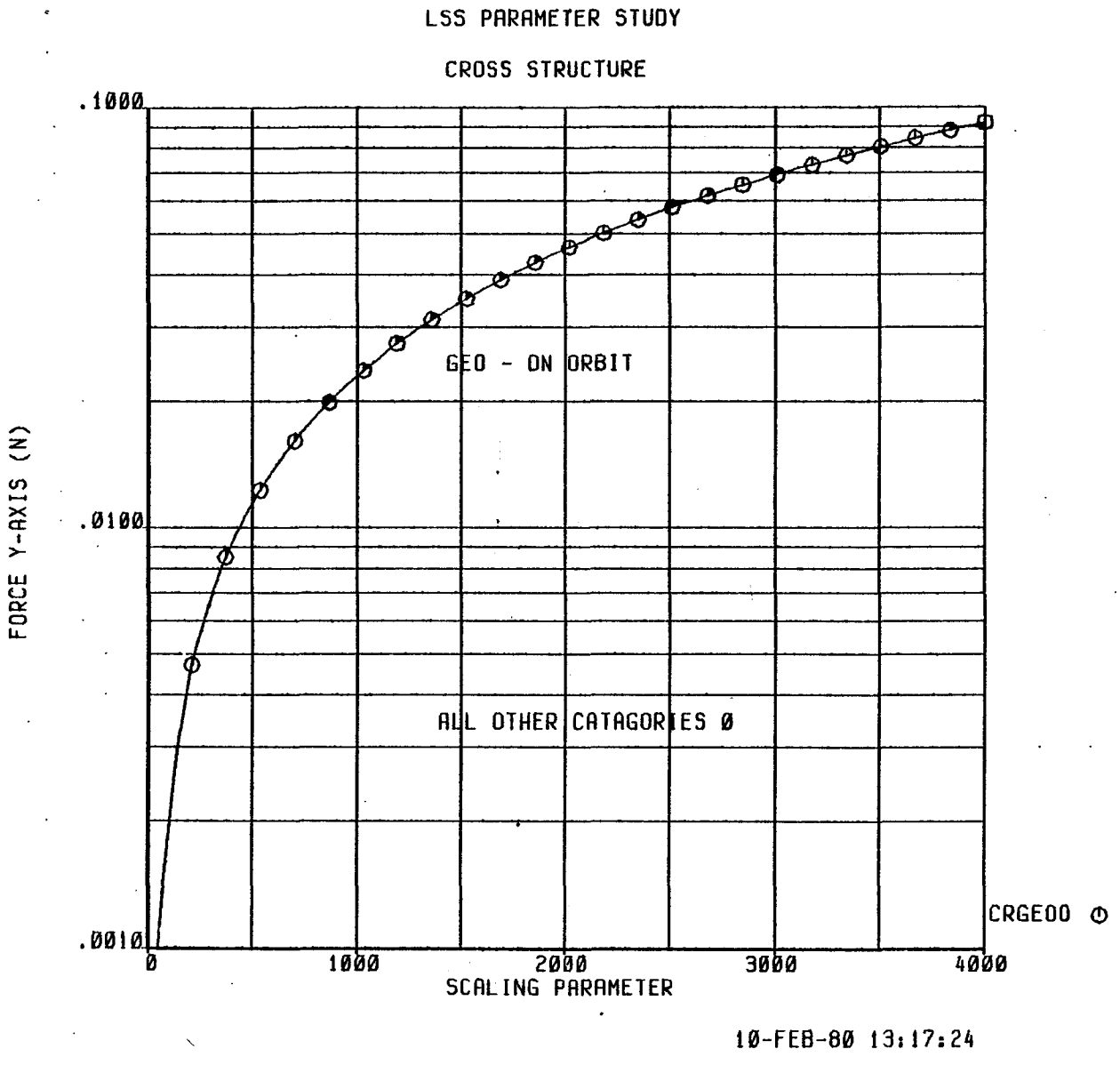

FIGURE B-22 LSS PARAMETER STUDY CROSS STRUCTURE FORCES - Y AXIS

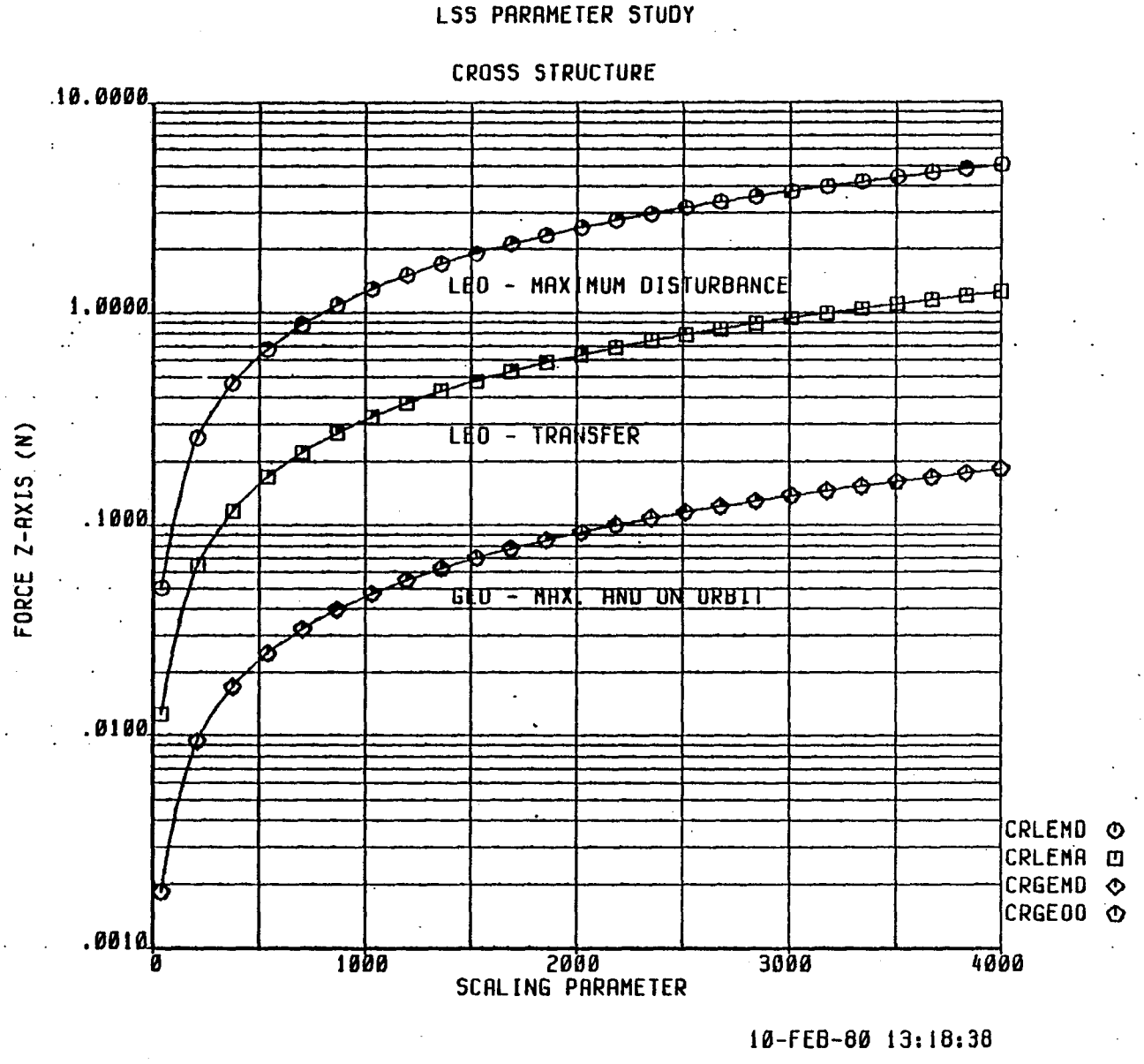

FIGURE B-23 LSS PARAMETER STUDY CROSS STRUCTURE FORCES - Z AXIS

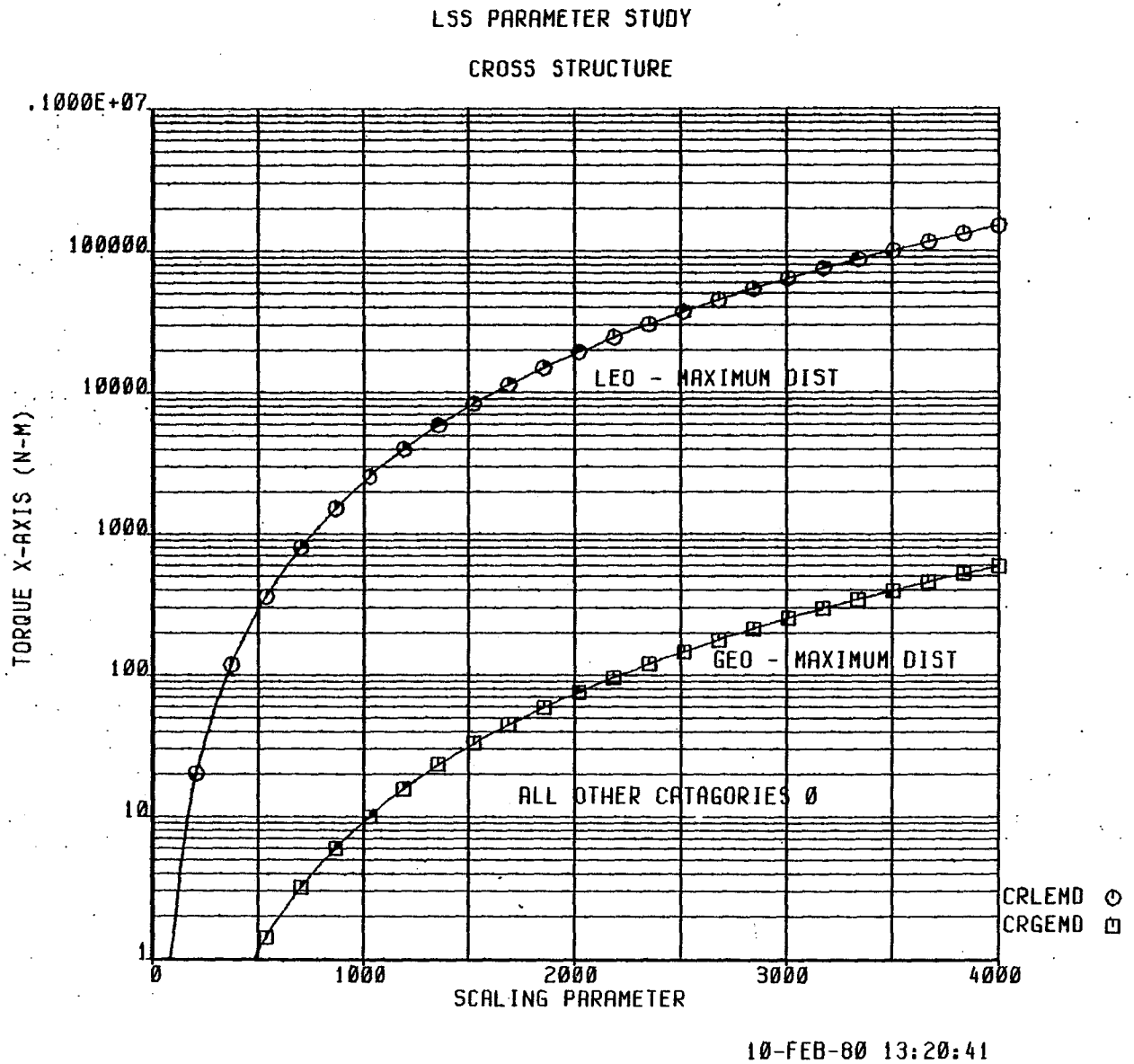

FIGURE B-24 LSS PARAMETER STUDY CROSS STRUCTURE TORQUES - X AXIS

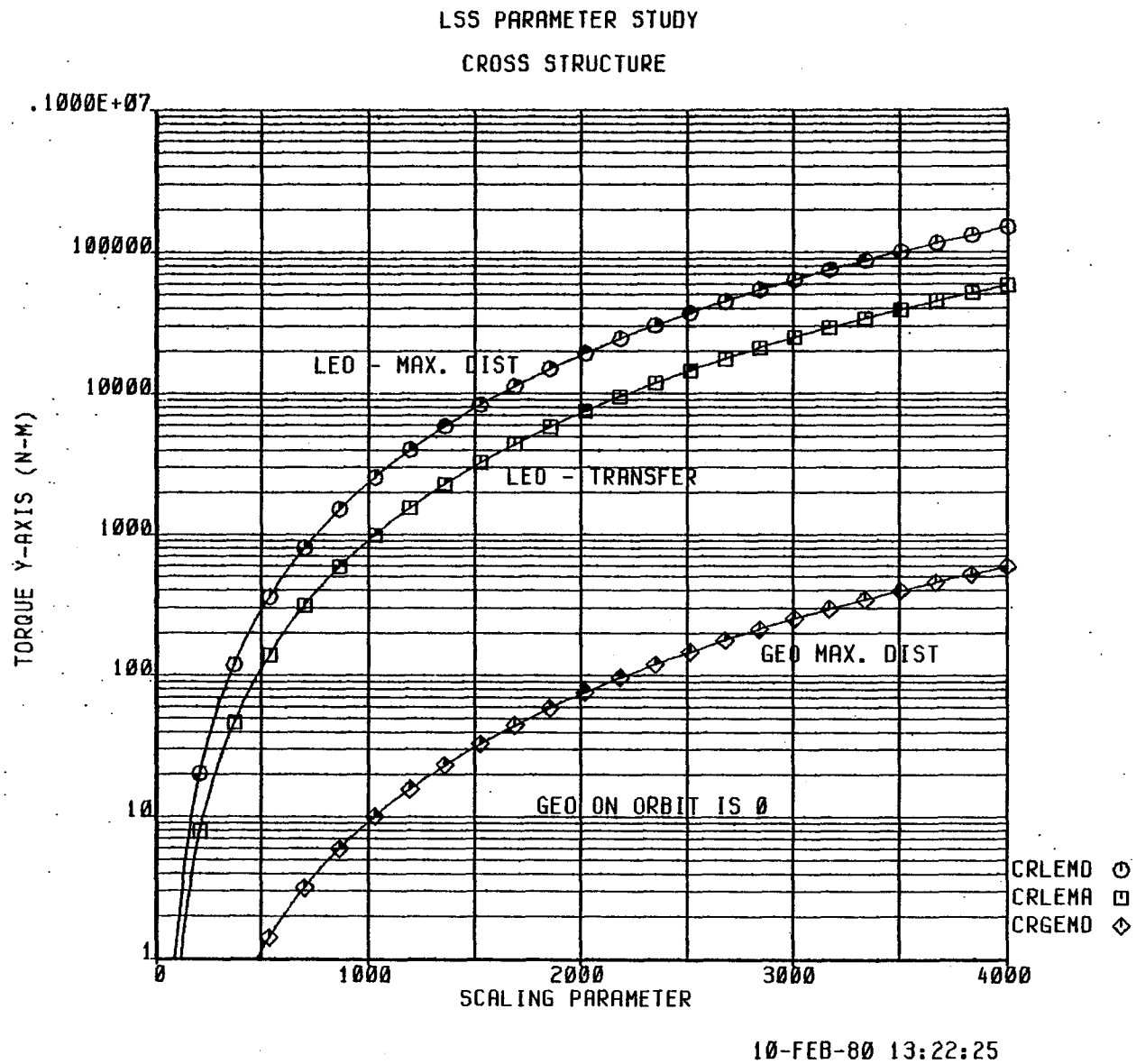

FIGURE B-25 LSS PARAMETER STUDY CROSS STRUCTURE TORQUES - Y AXIS

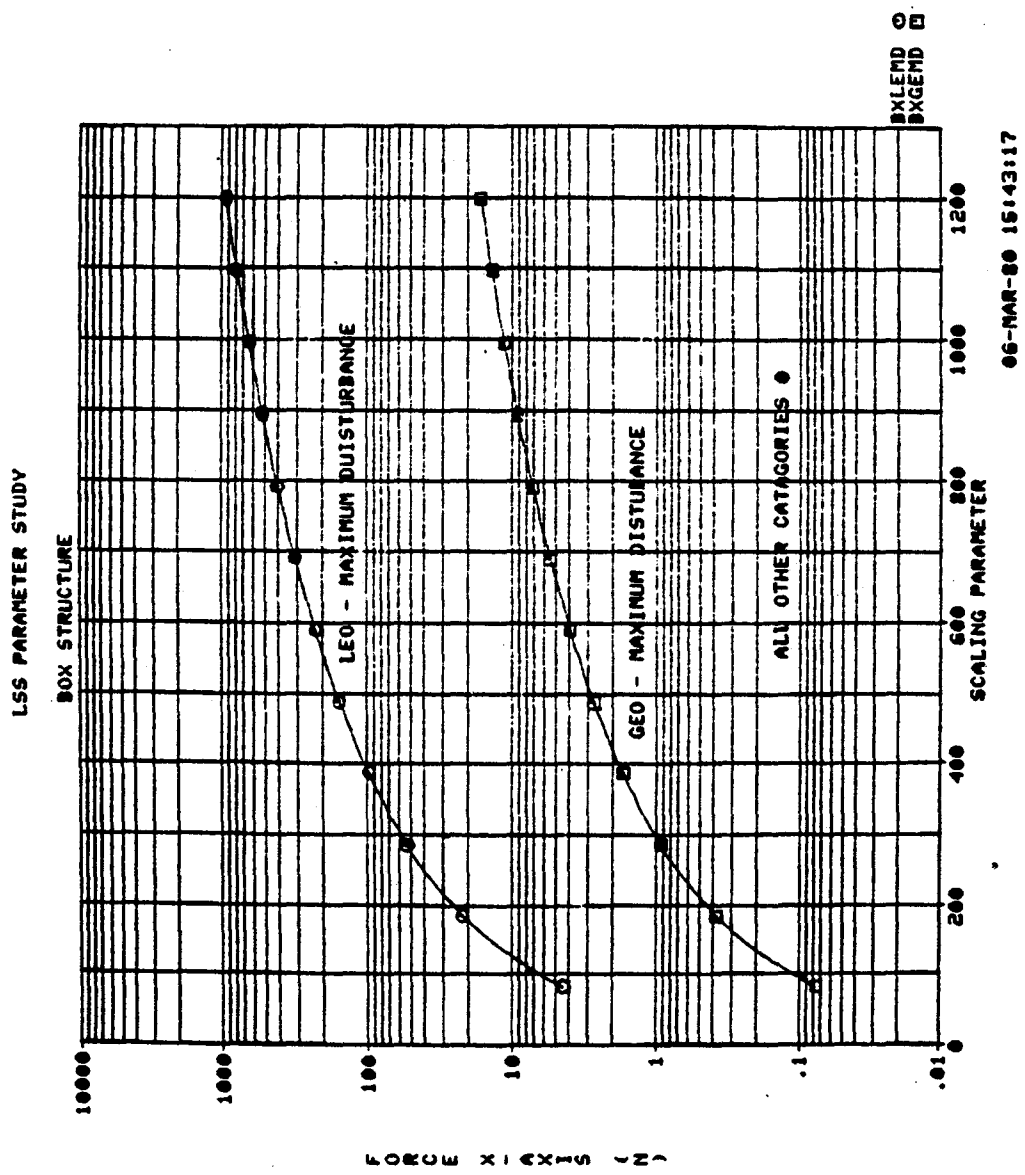

FIGURE B-26 LSS PARAMETER STUDY BOX STRUCTURE FORCES - X AXIS

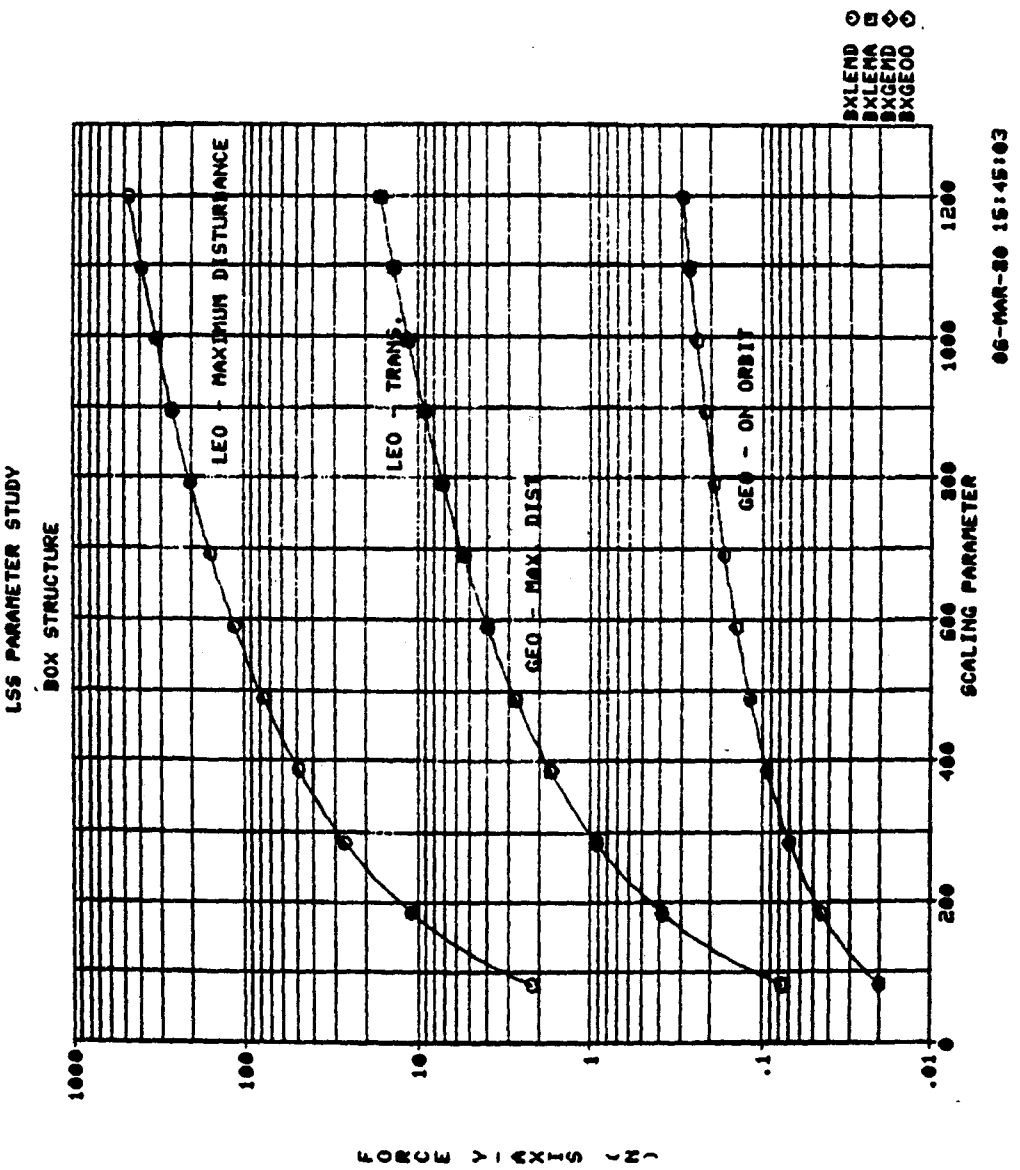

FIGURE B-27 LSS PARAMETER STUDY BOX STRUCTURE FORCES - Y AXIS

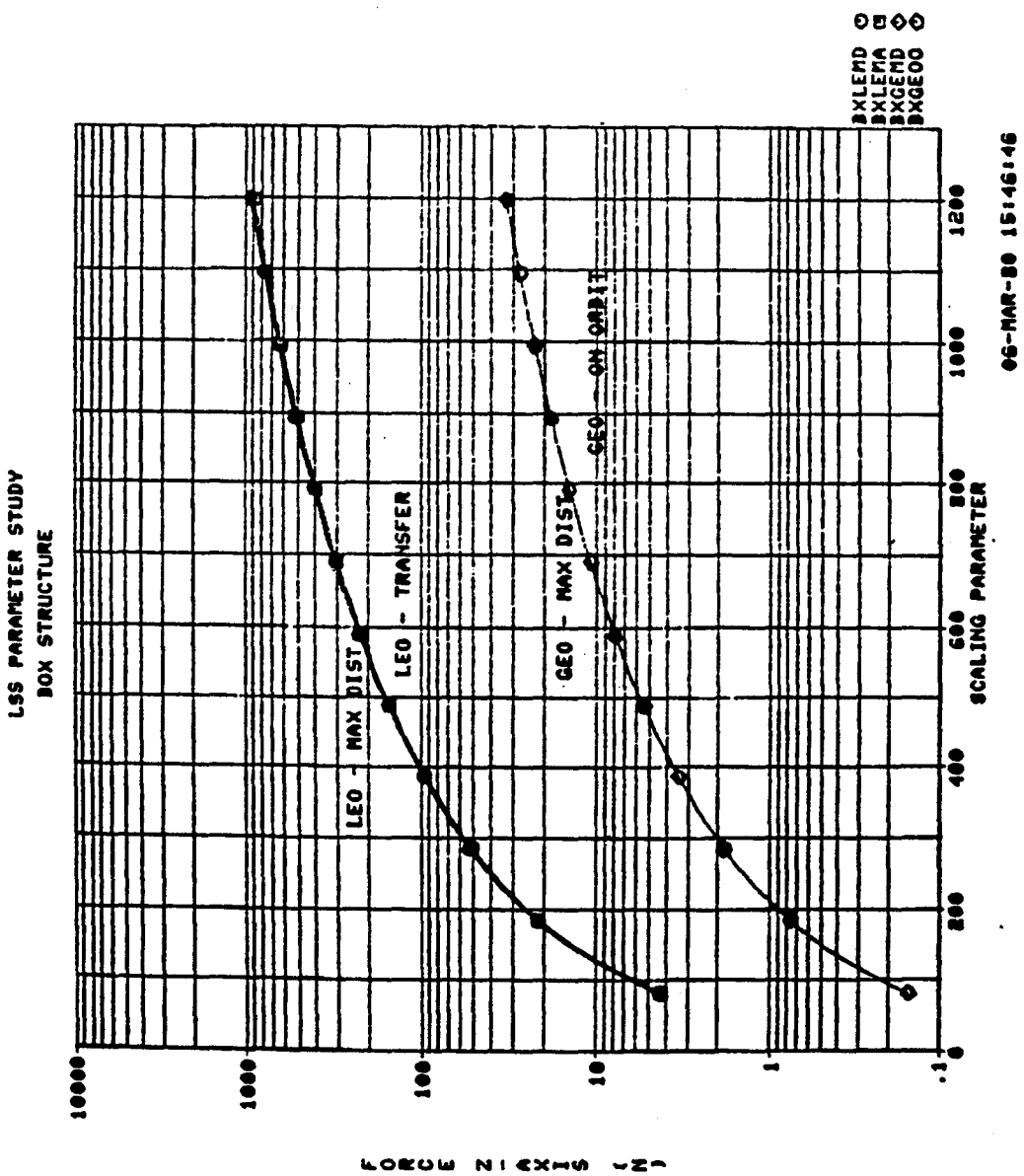

FIGURE B-28 LSS PARAMETER STUDY BOX STRUCTURE FORCES - Z AXIS

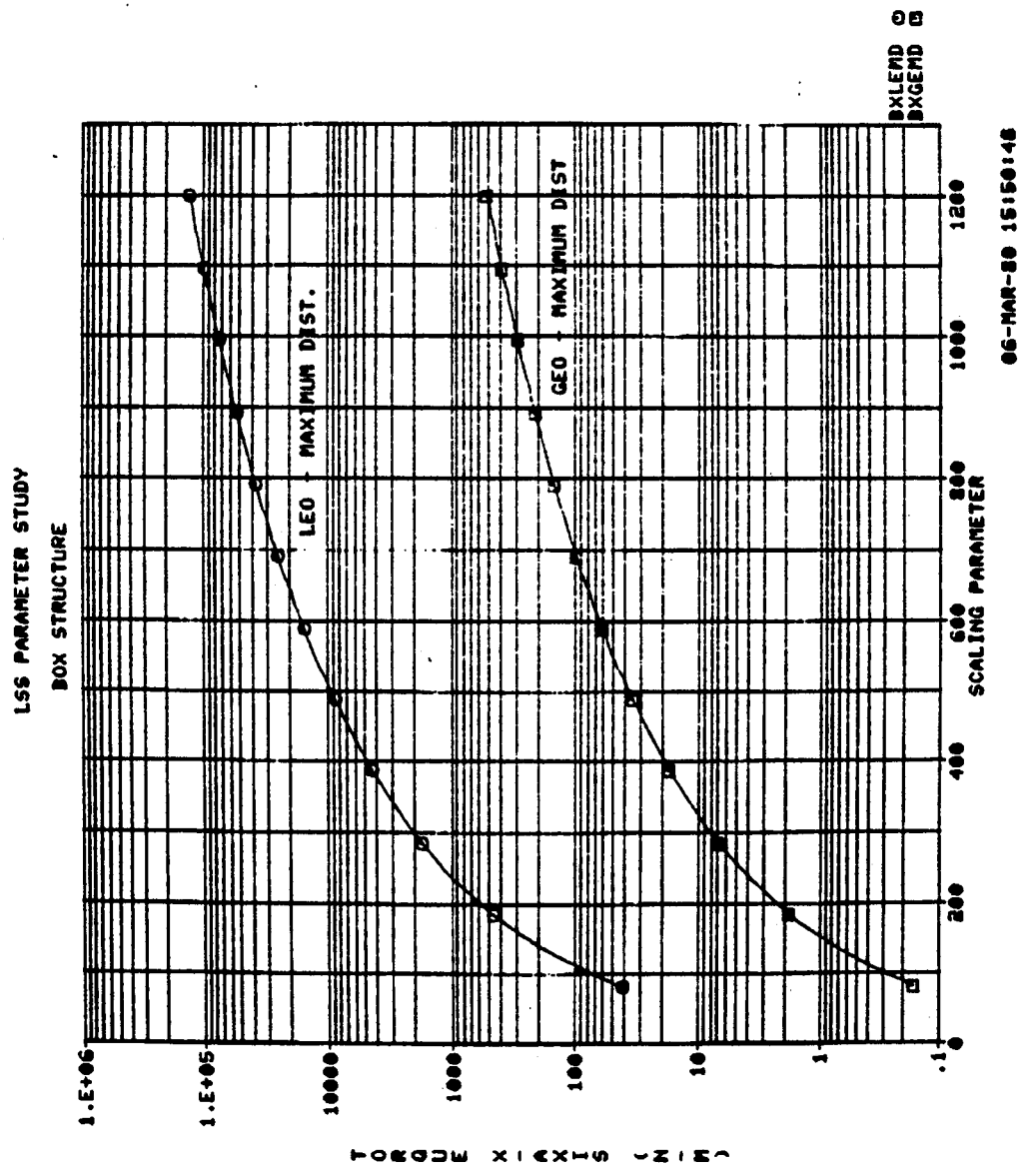

FIGURE B-29 LSS PARAMETER STUDY BOX STRUCTURE TORQUES - X AXIS

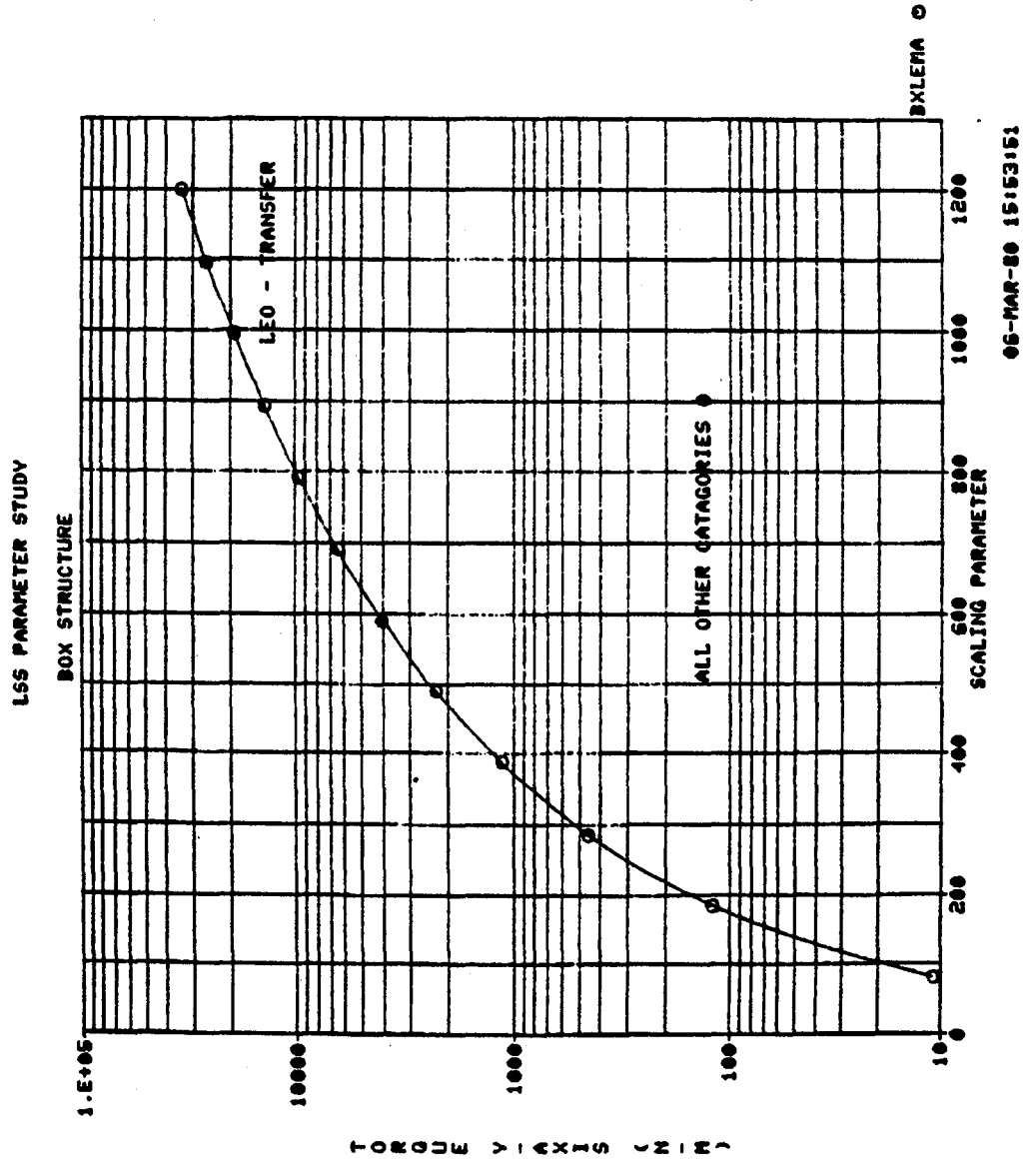

FIGURE B-30 LSS PARAMETER STUDY BOX STRUCTURE TORQUES - Y AXIS

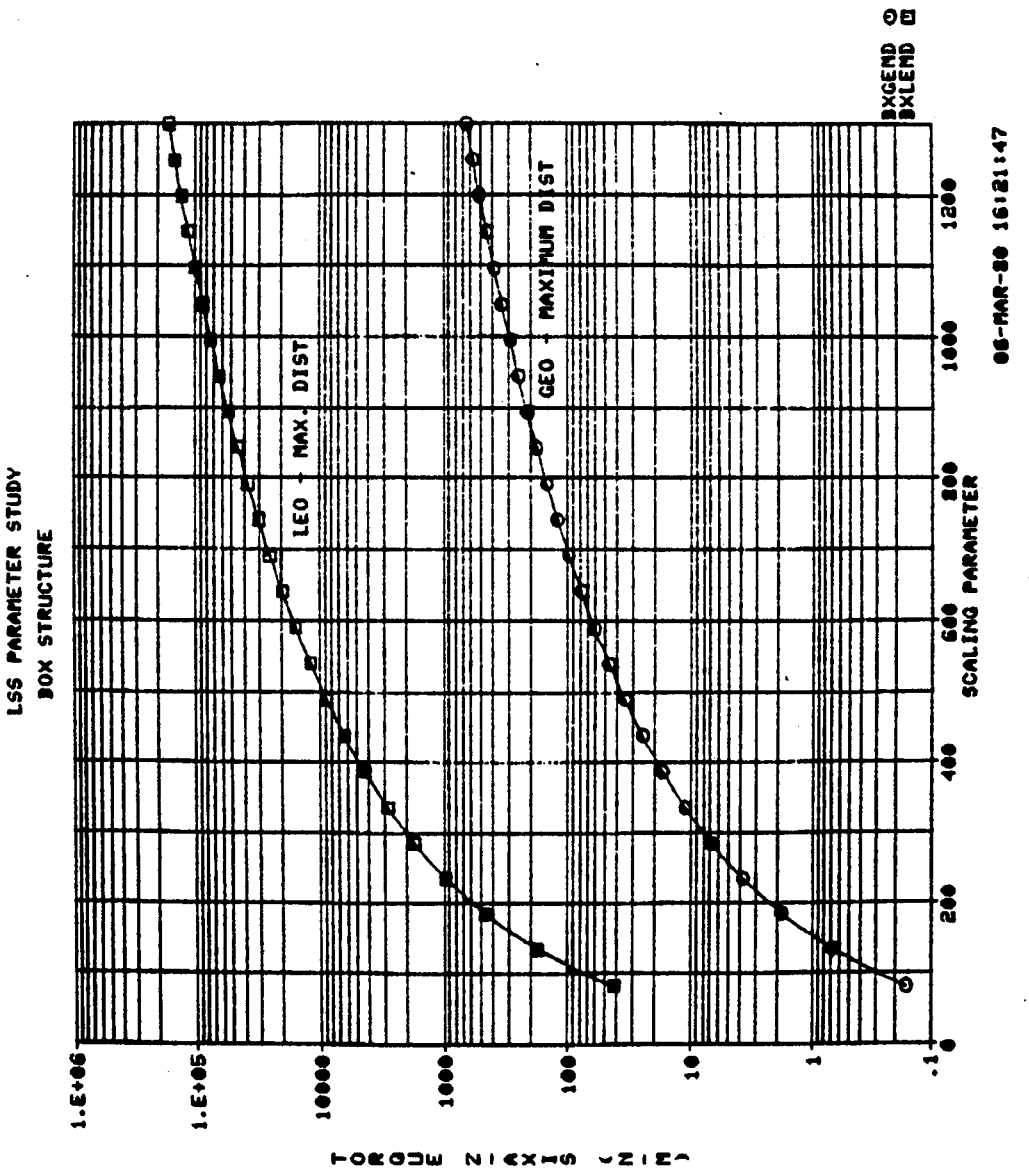

FIGURE B-31 LSS PARAMETER STUDY BOX STRUCTURE TORQUES - Z AXIS

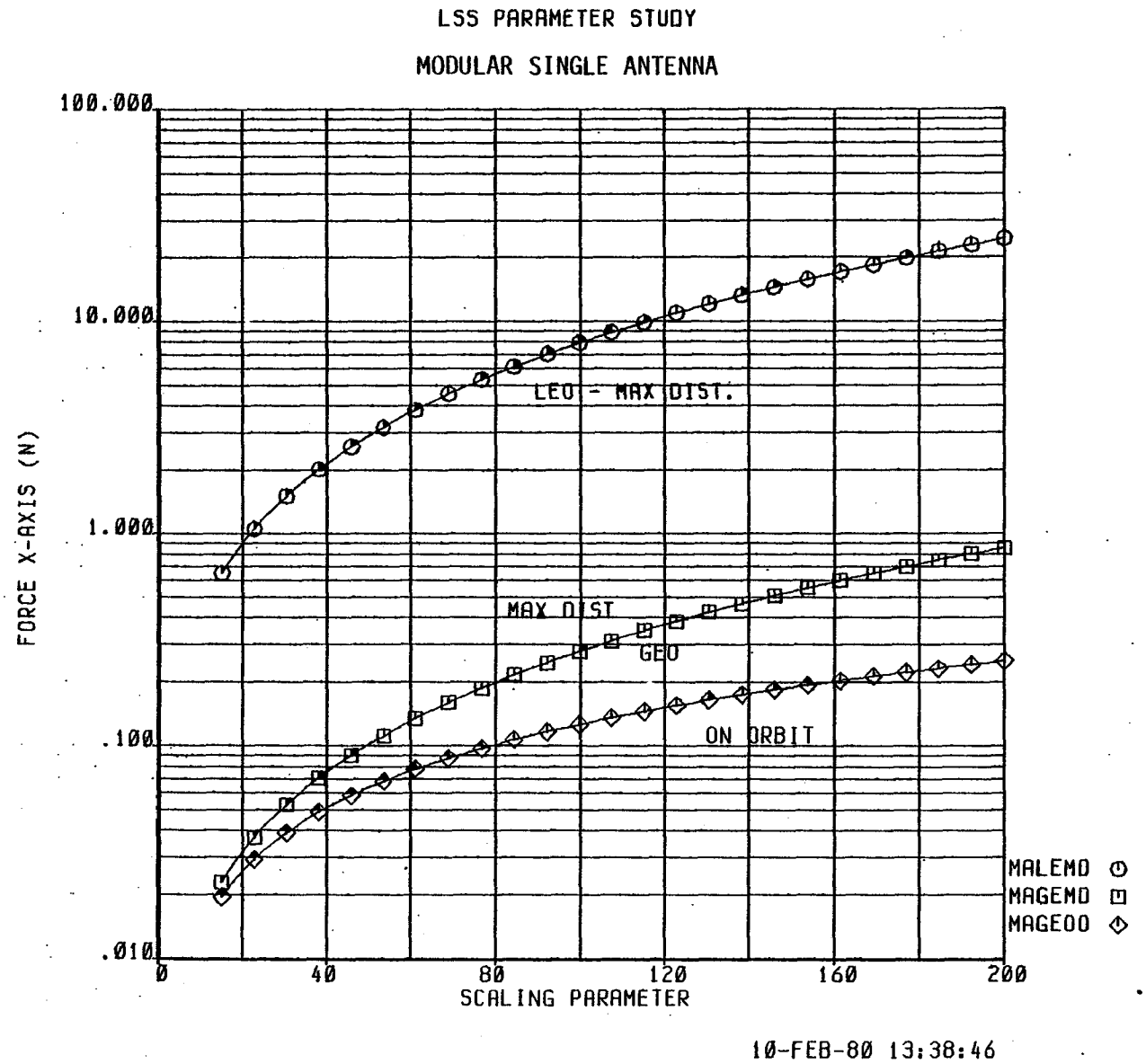

FIGURE B-32 LSS PARAMETER STUDY MODULAR SINGLE ANTENNA FORCES - X AXIS

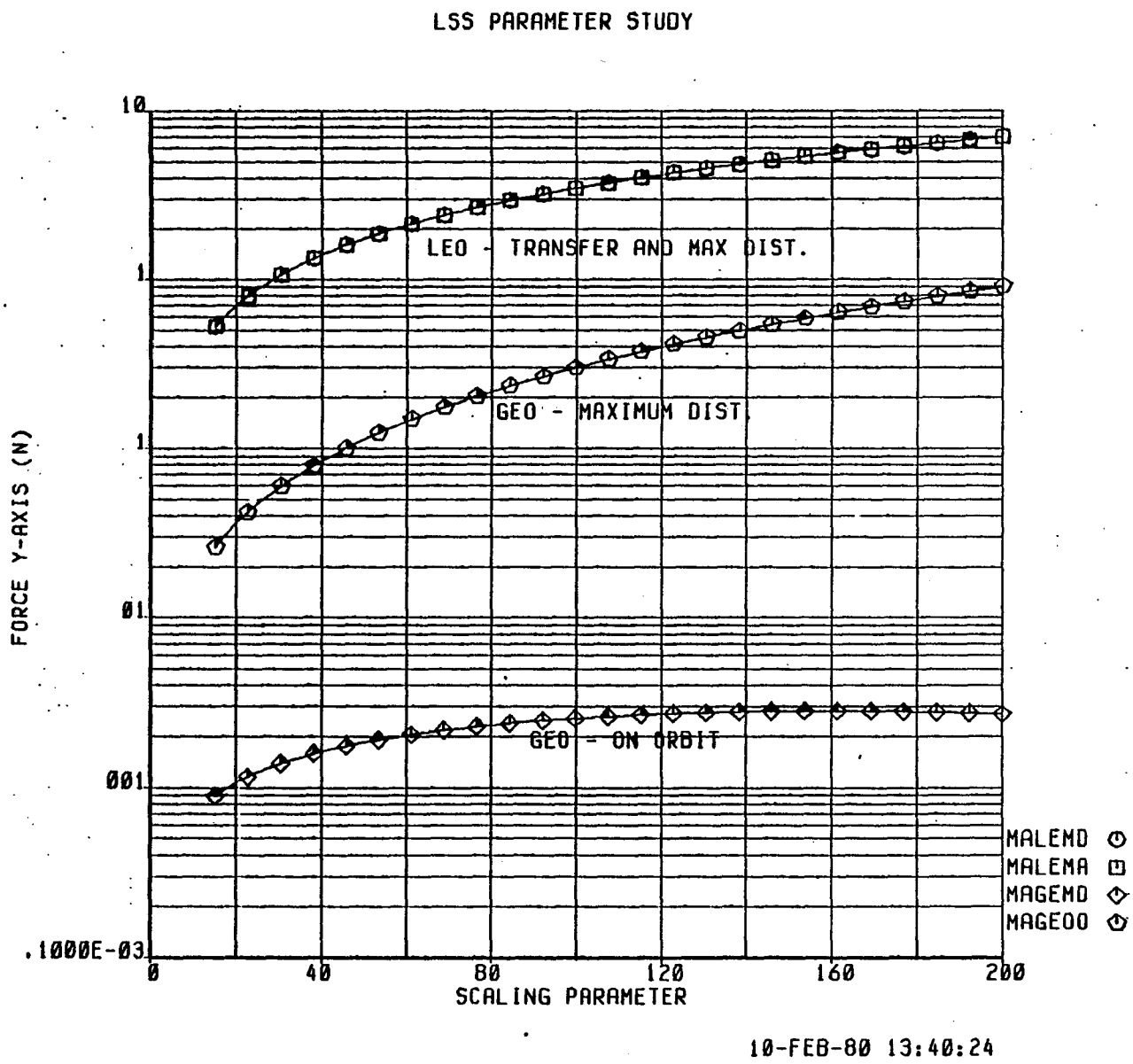

FIGURE B-33 LSS PARAMETER STUDY MODULAR SINGLE ANTENNA FORCES - Y AXIS

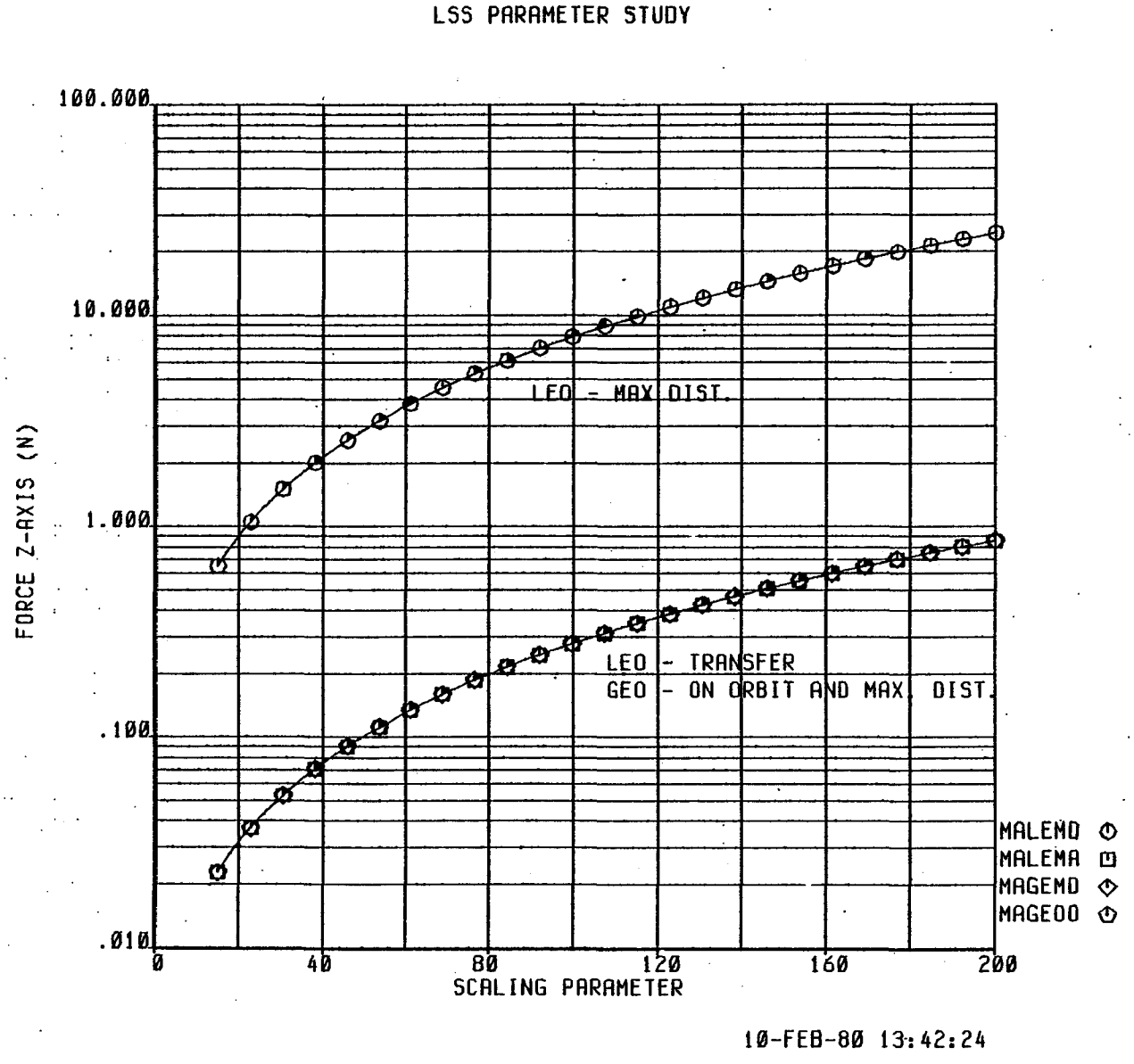

FIGURE B-34 LSS PARAMETER STUDY MODULAR SINGLE ANTENNA FORCES - Z AXIS

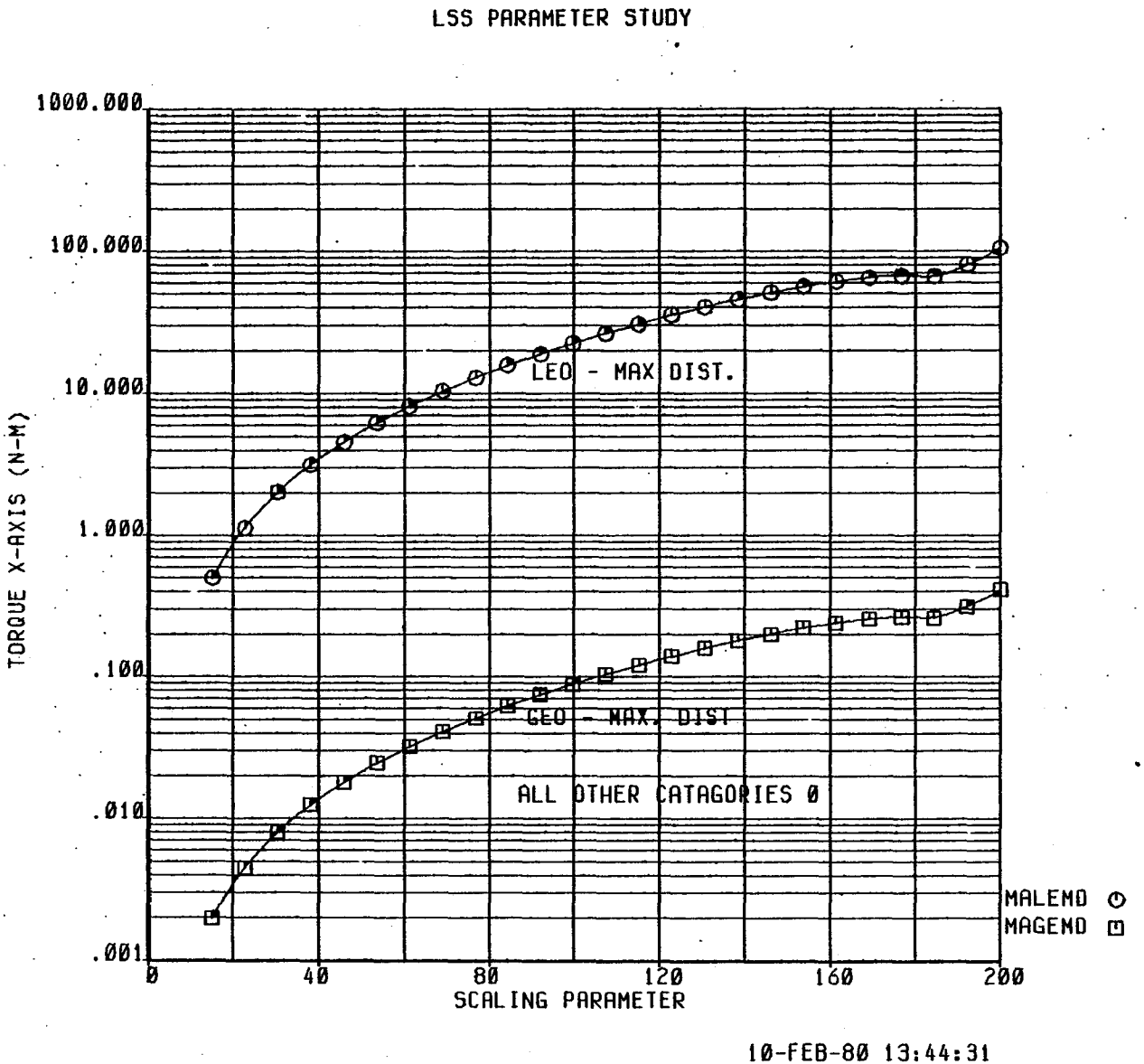

FIGURE B-35 LSS PARAMETER STUDY MODULAR SINGLE ANTENNA TORQUES - X AXIS

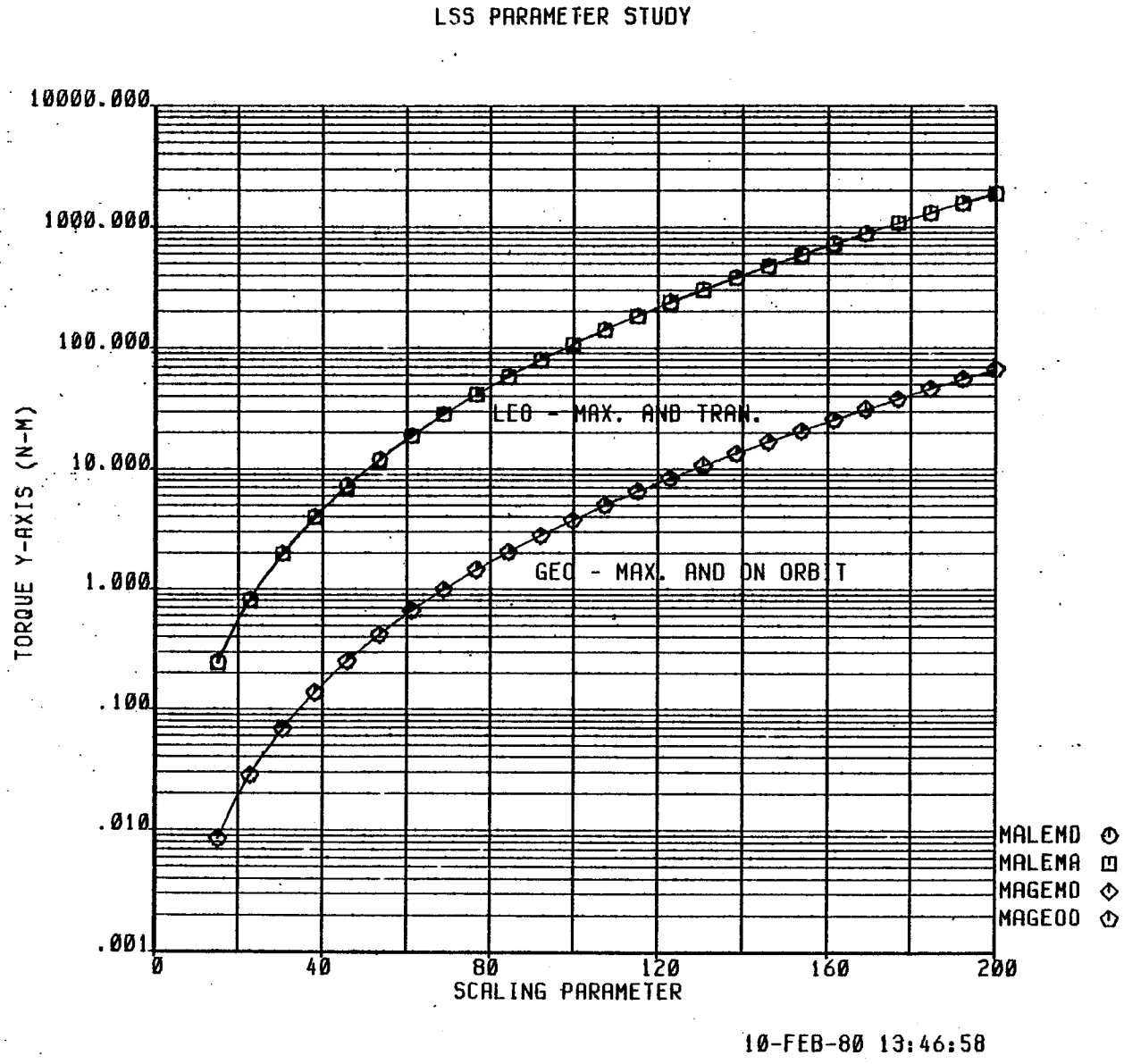

FIGURE B-36 LSS PARAMETER STUDY MODULAR SINGLE ANTENNA TORQUES - Y AXIS

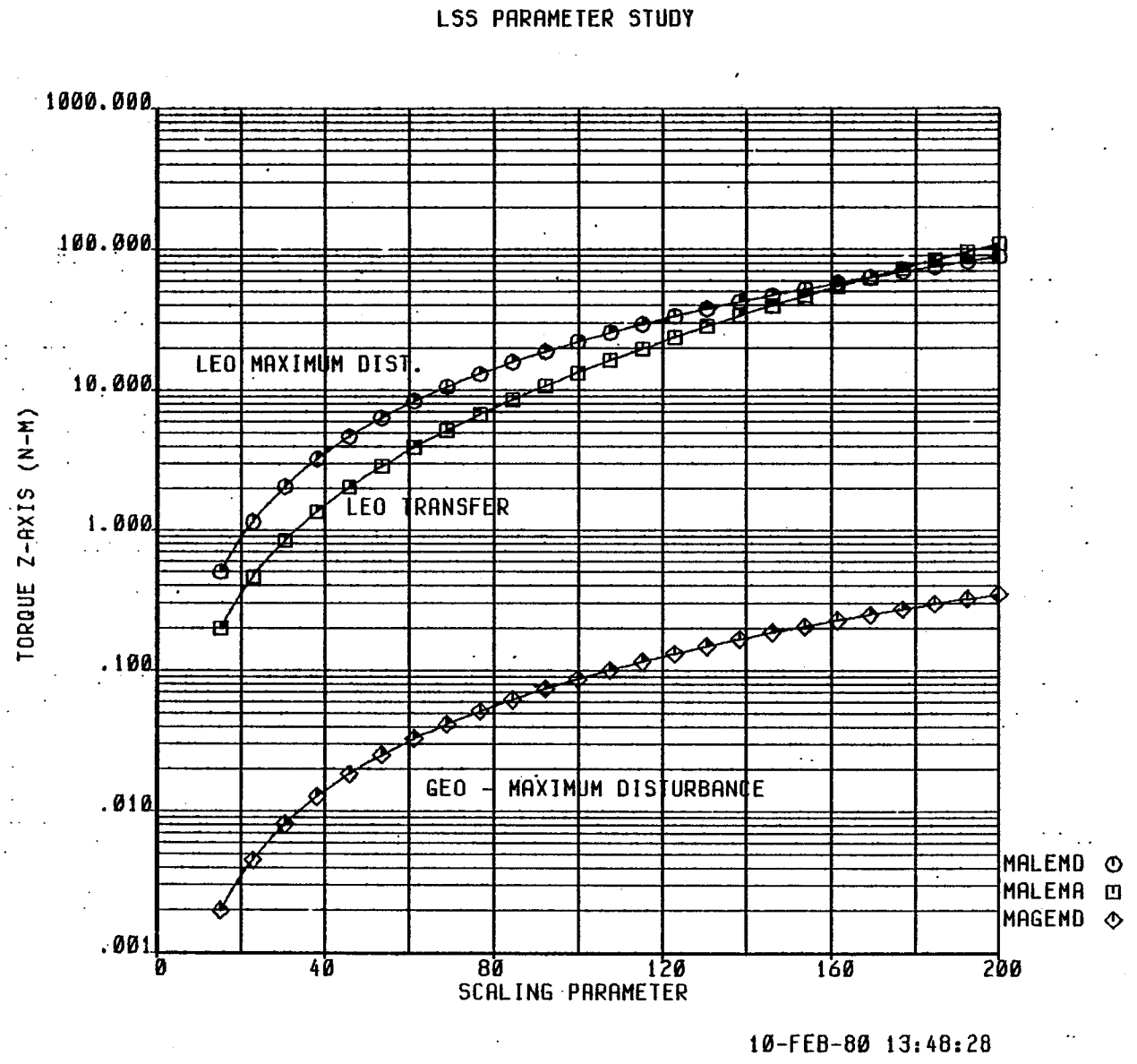

FIGURE B-37 LSS PARAMETER STUDY MODULAR SINGLE ANTENNA TORQUES - Z AXIS

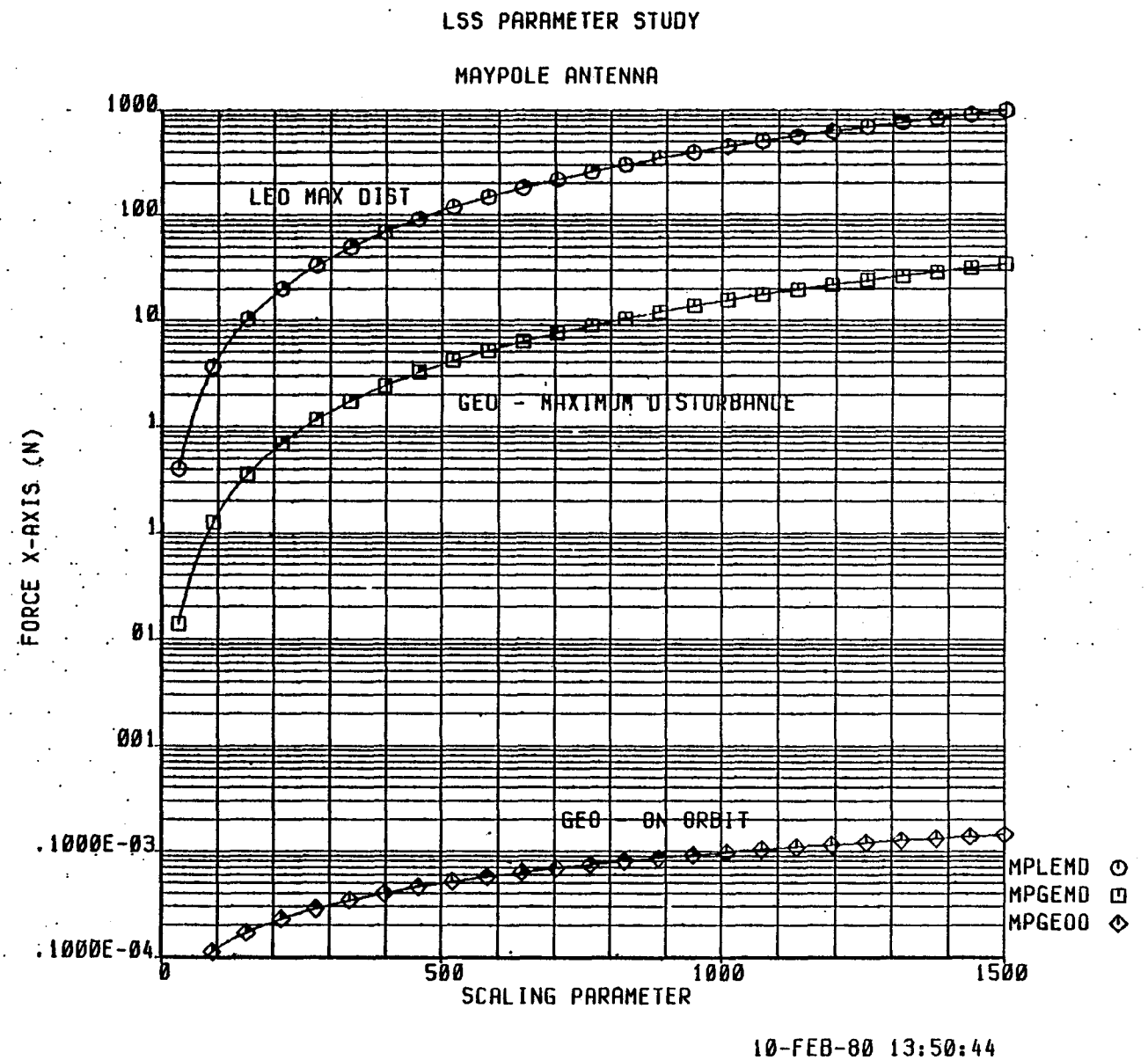

FIGURE B-38 LSS PARAMETER STUDY MAYPOLE ANTENNA FORCES - X AXIS

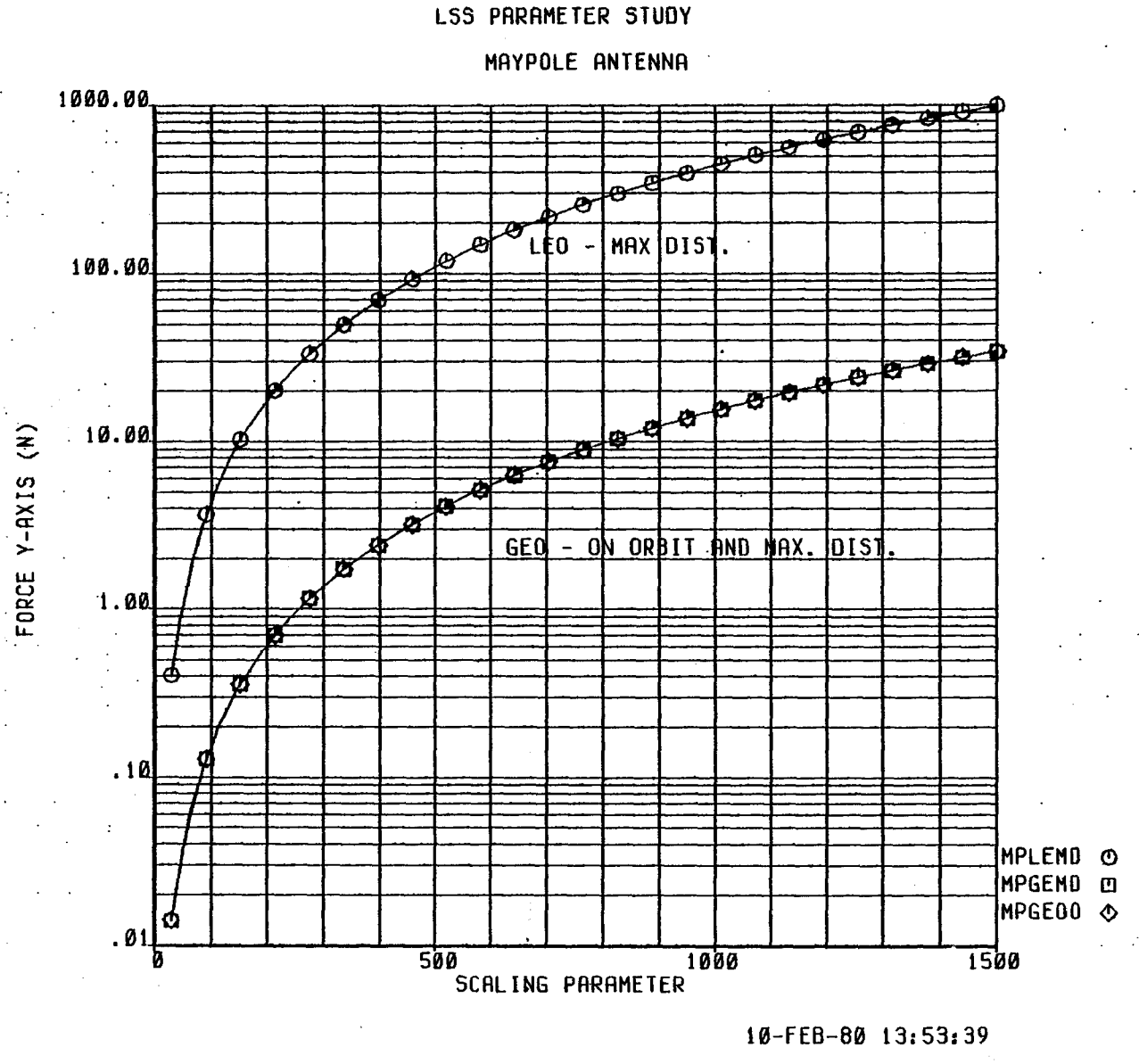

FIGURE B-39 LSS PARAMETER STUDY MAYPOLE ANTENNA FORCES - Y AXIS

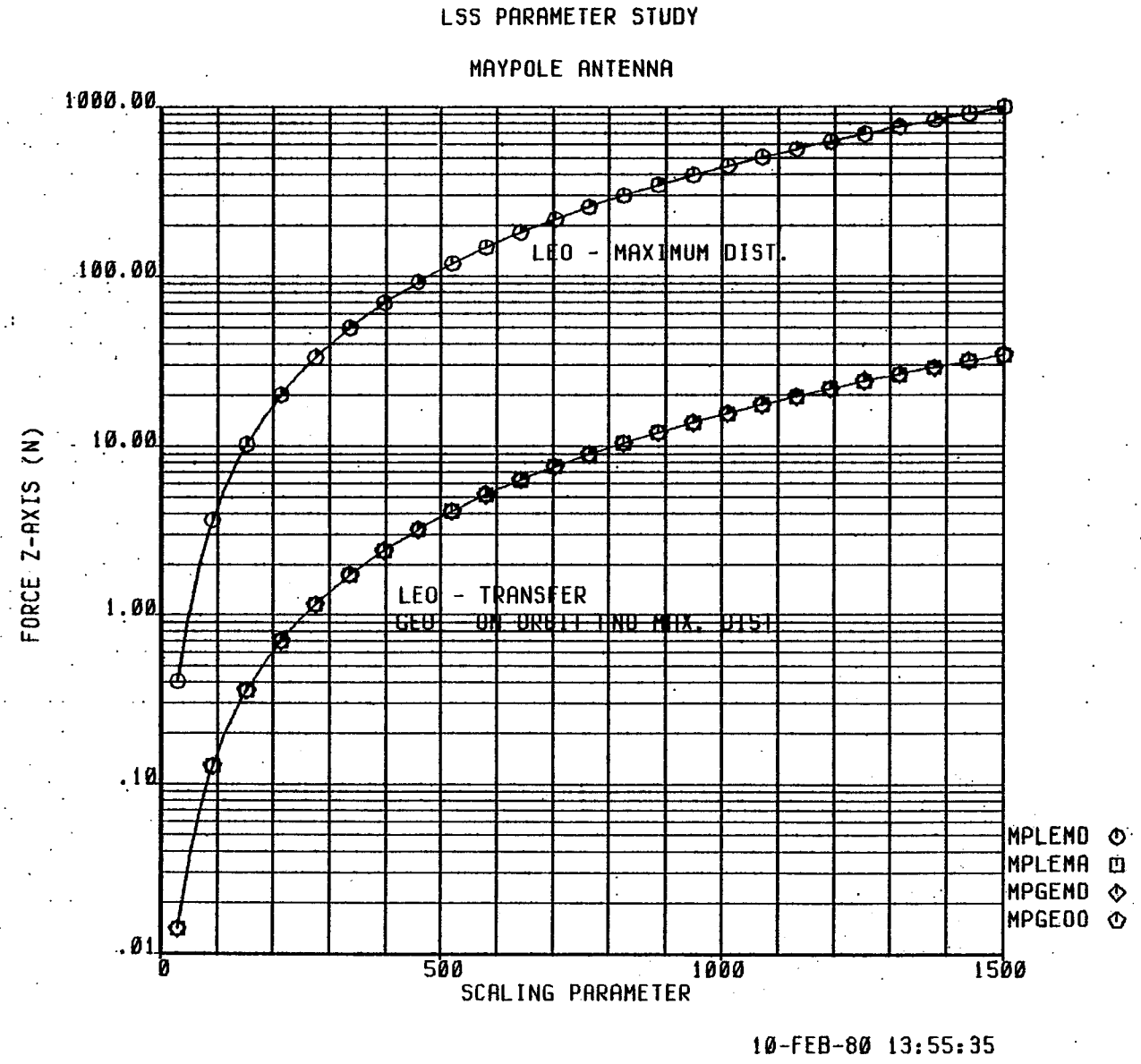

FIGURE B-40 LSS PARAMETER STUDY MAYPOLE ANTENNA FORCES - Z AXIS

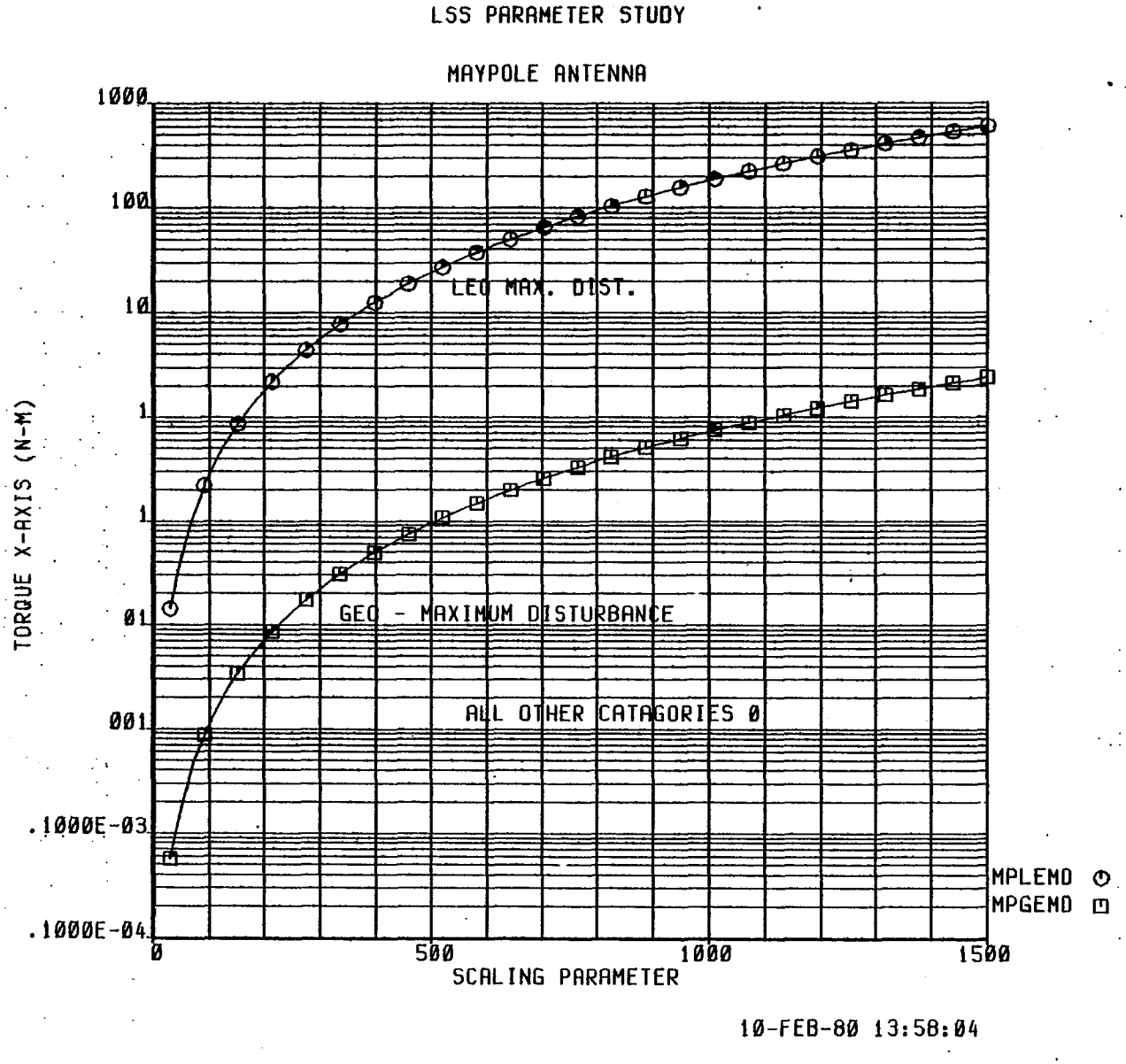

FIGURE B-41 LSS PARAMETER STUDY MAYPOLE ANTENNA TORQUES - X AXIS

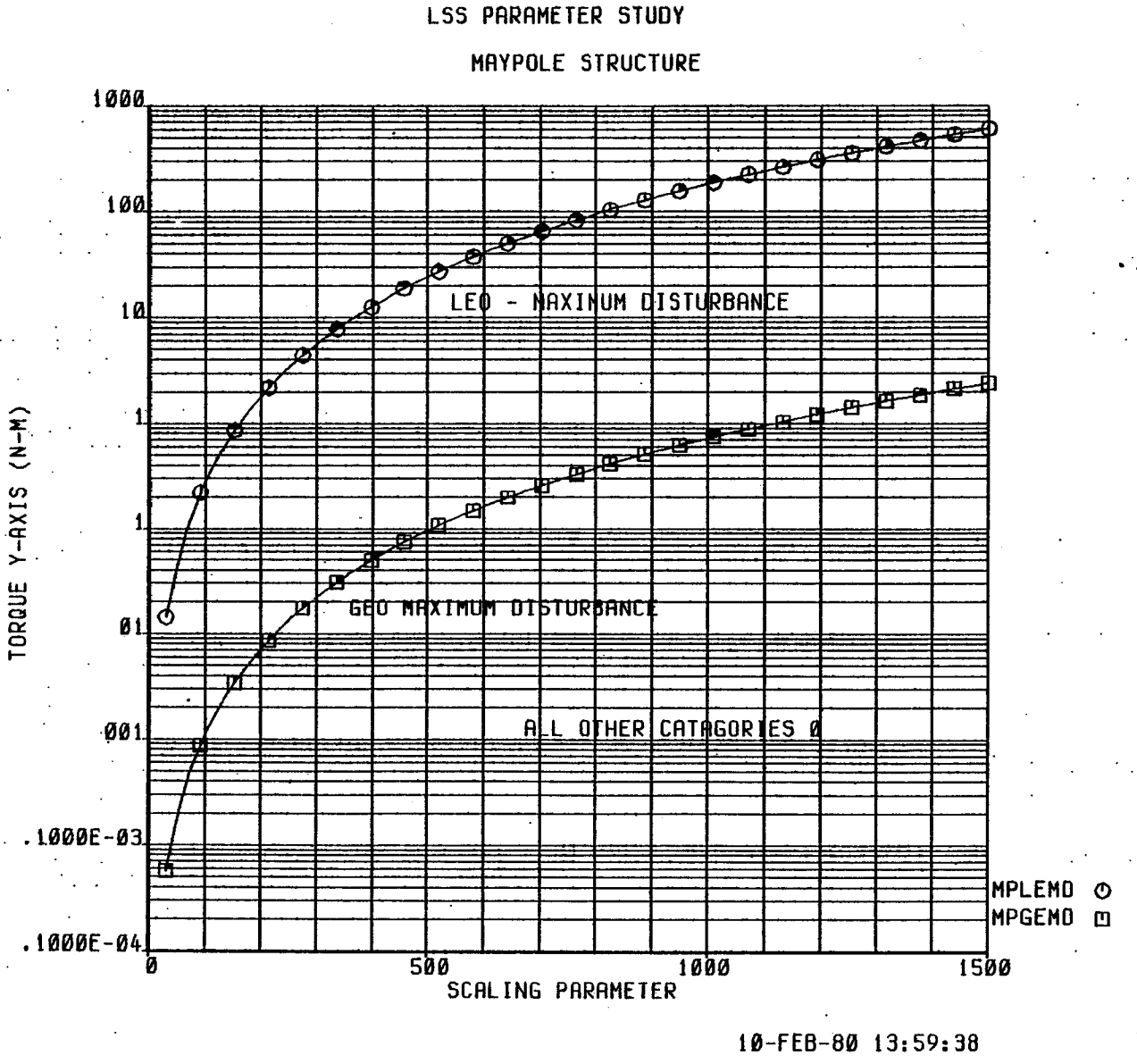

FIGURE B-42 LSS PARAMETER STUDY MAYPOLE ANTENNA TORQUES - Y AXIS

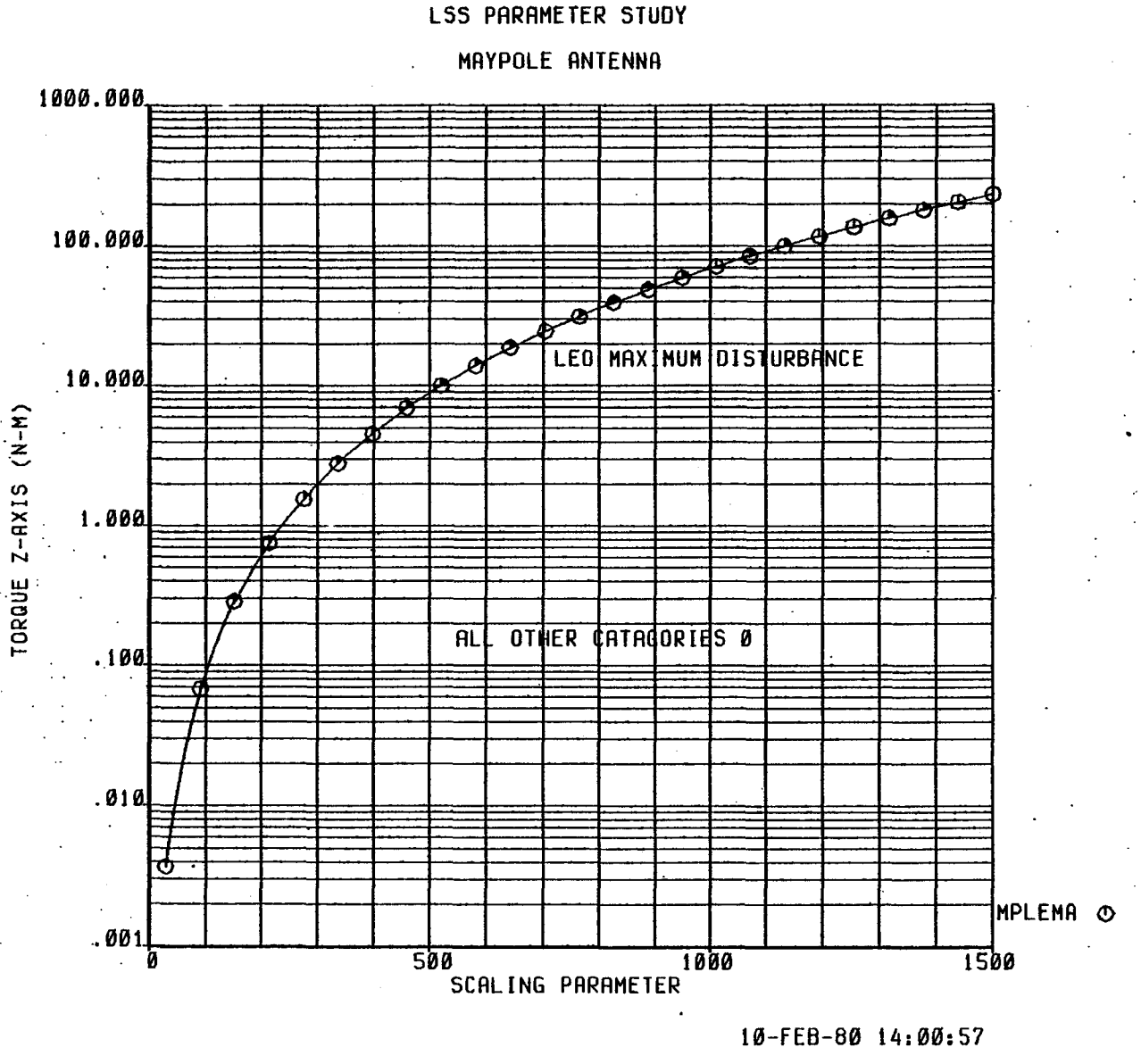

FIGURE B-43 LSS PARAMETER STUDY MAYPOLE ANTENNA TORQUES - Z AXIS

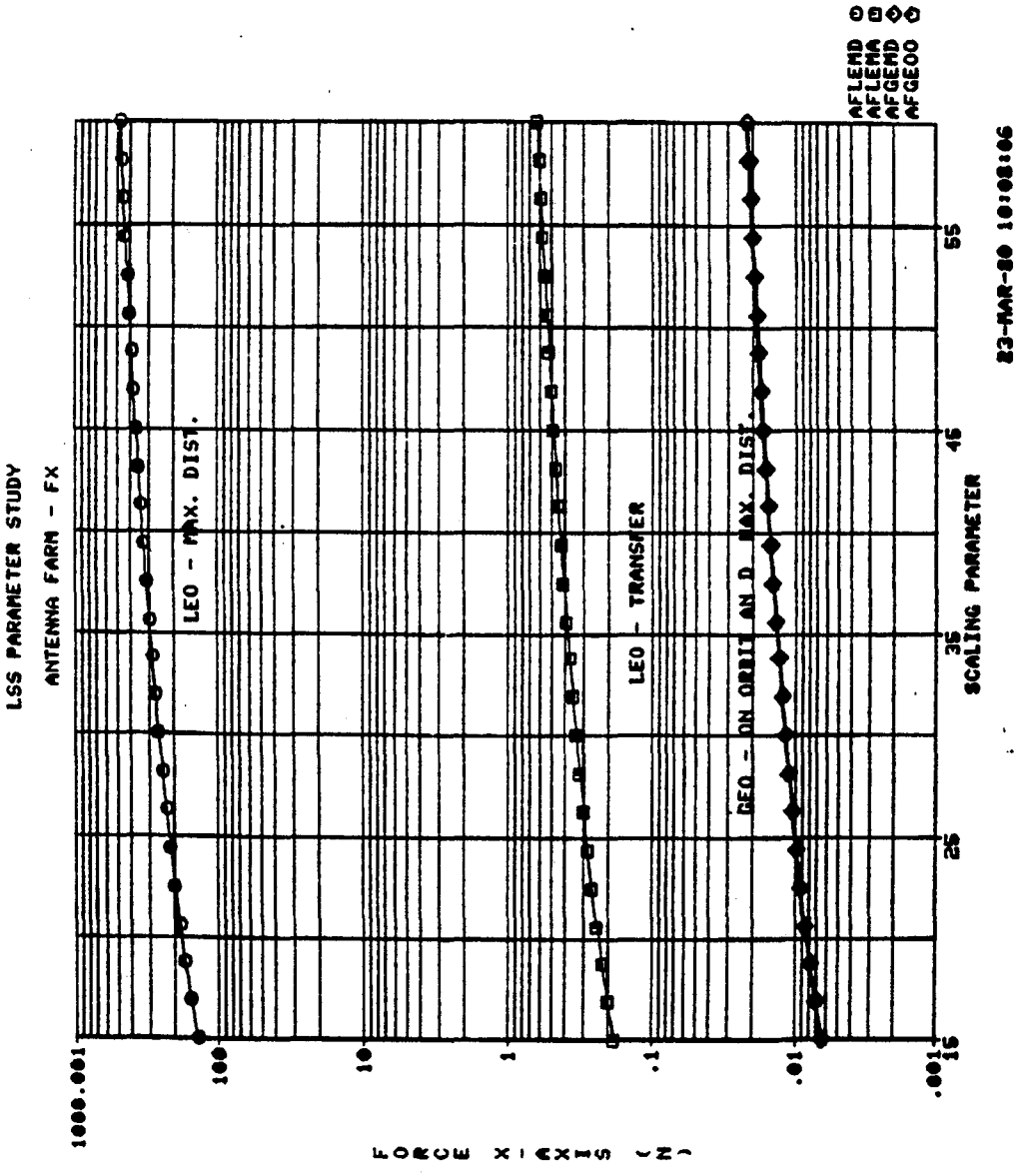

FIGURE B-44 LSS PARAMETER STUDY ANTENNA FARM FORCES - X AXIS

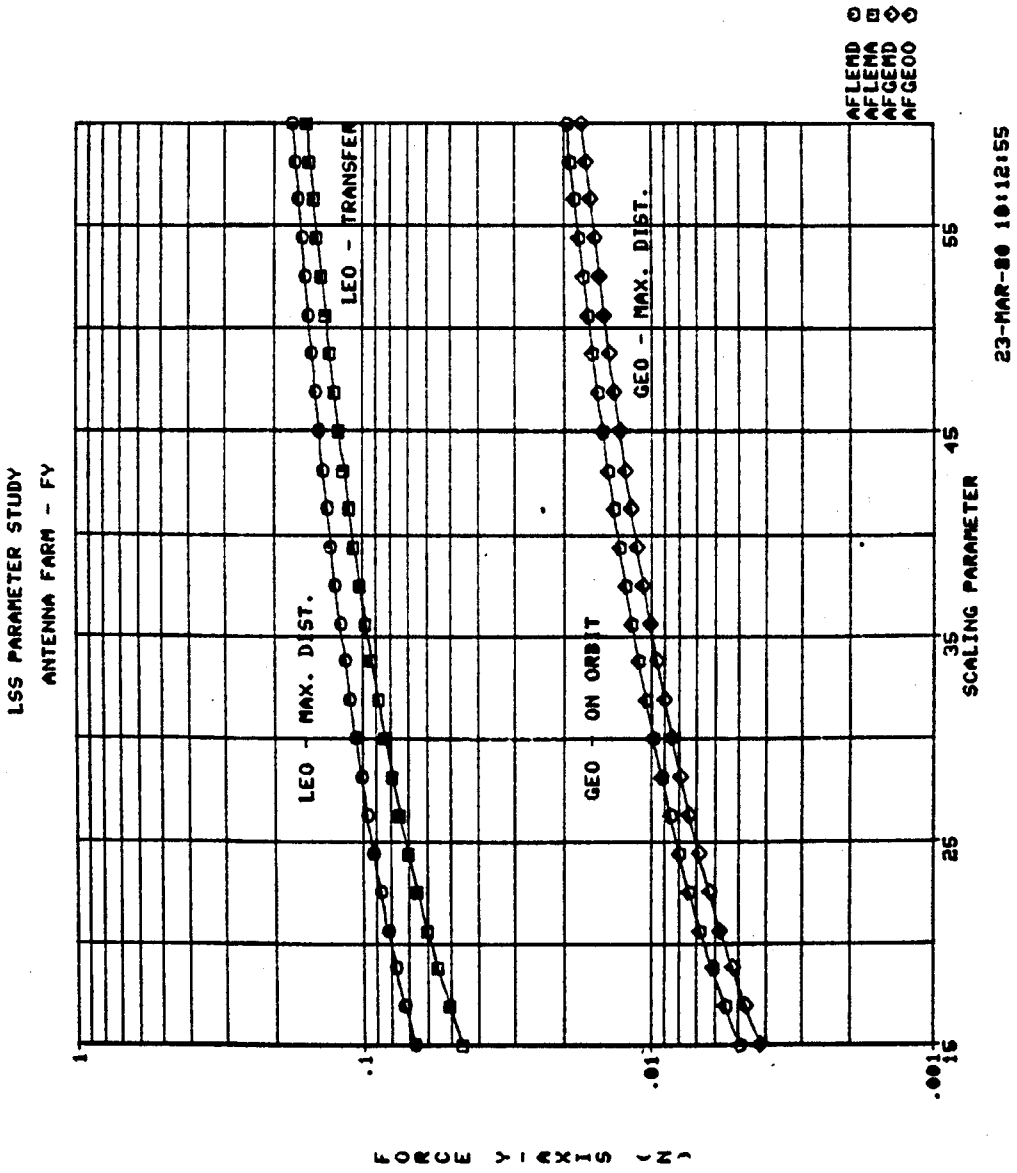

FIGURE B-45 LSS PARAMETER STUDY ANTENNA FARM FORCES - Y AXIS

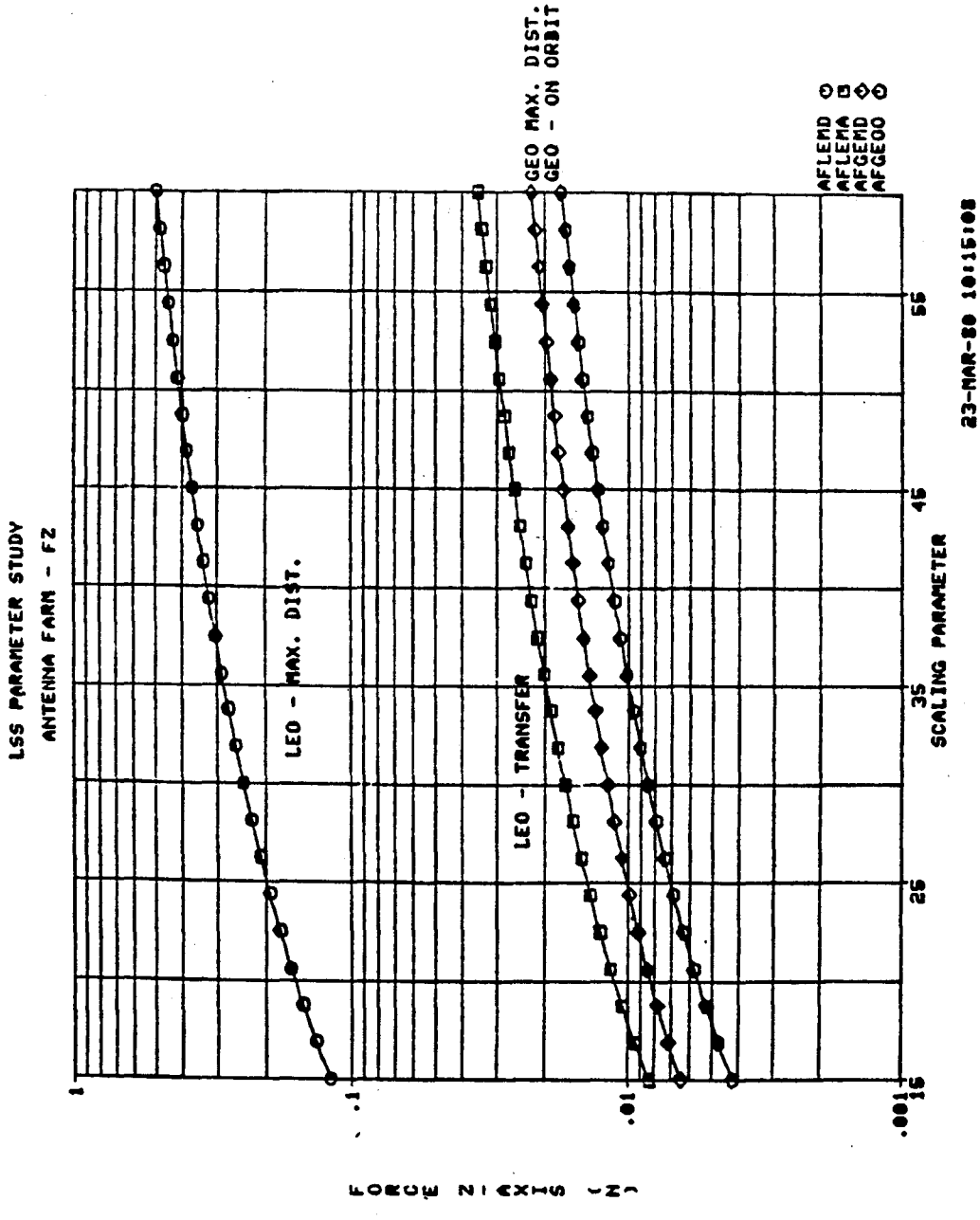

FIGURE B-46 LSS PARAMETER STUDY ANTENNA FARM FORCES - Z AXIS

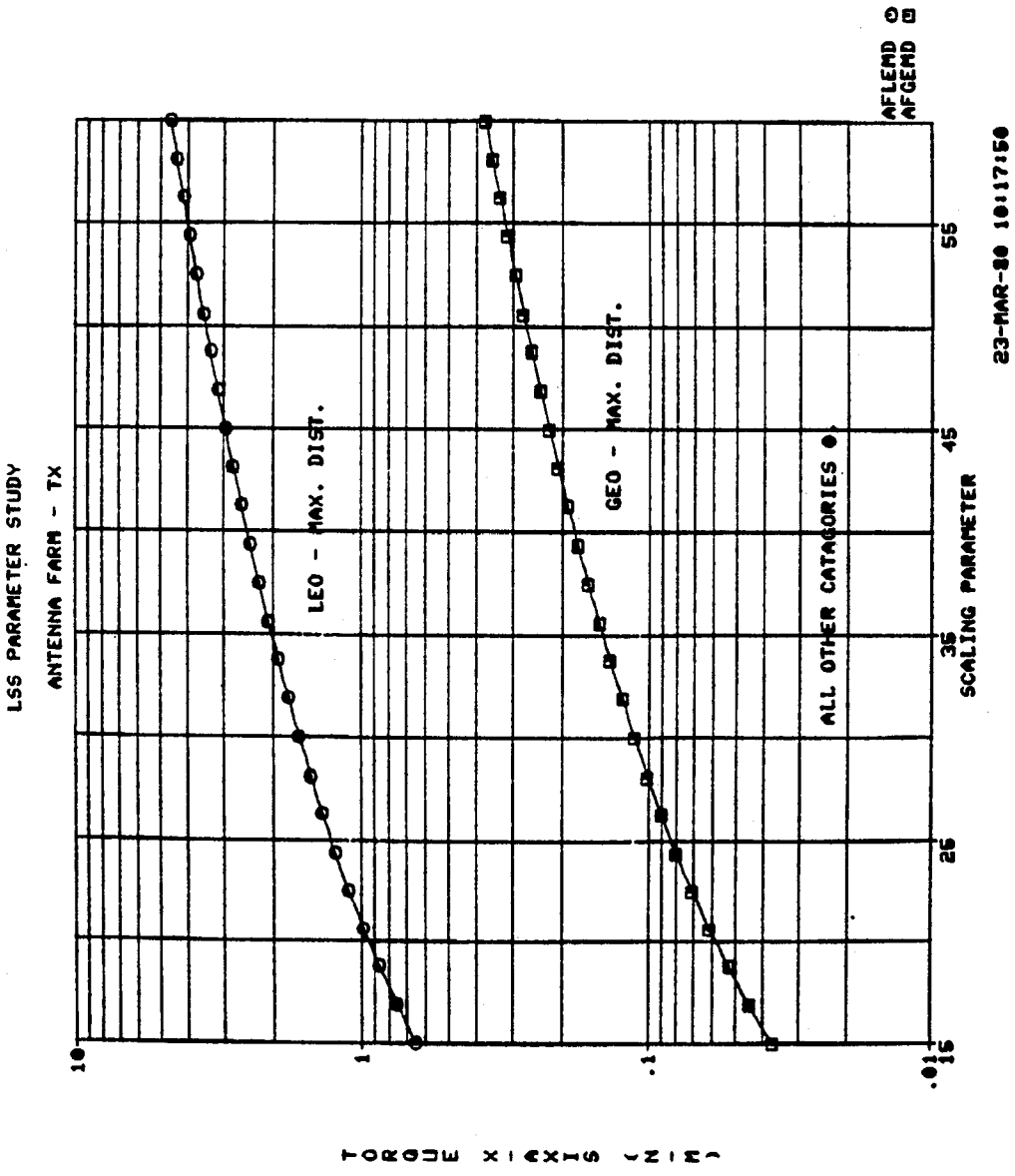

FIGURE B-47 LSS PARAMETER STUDY ANTENNA FARM TORQUES - X AXIS

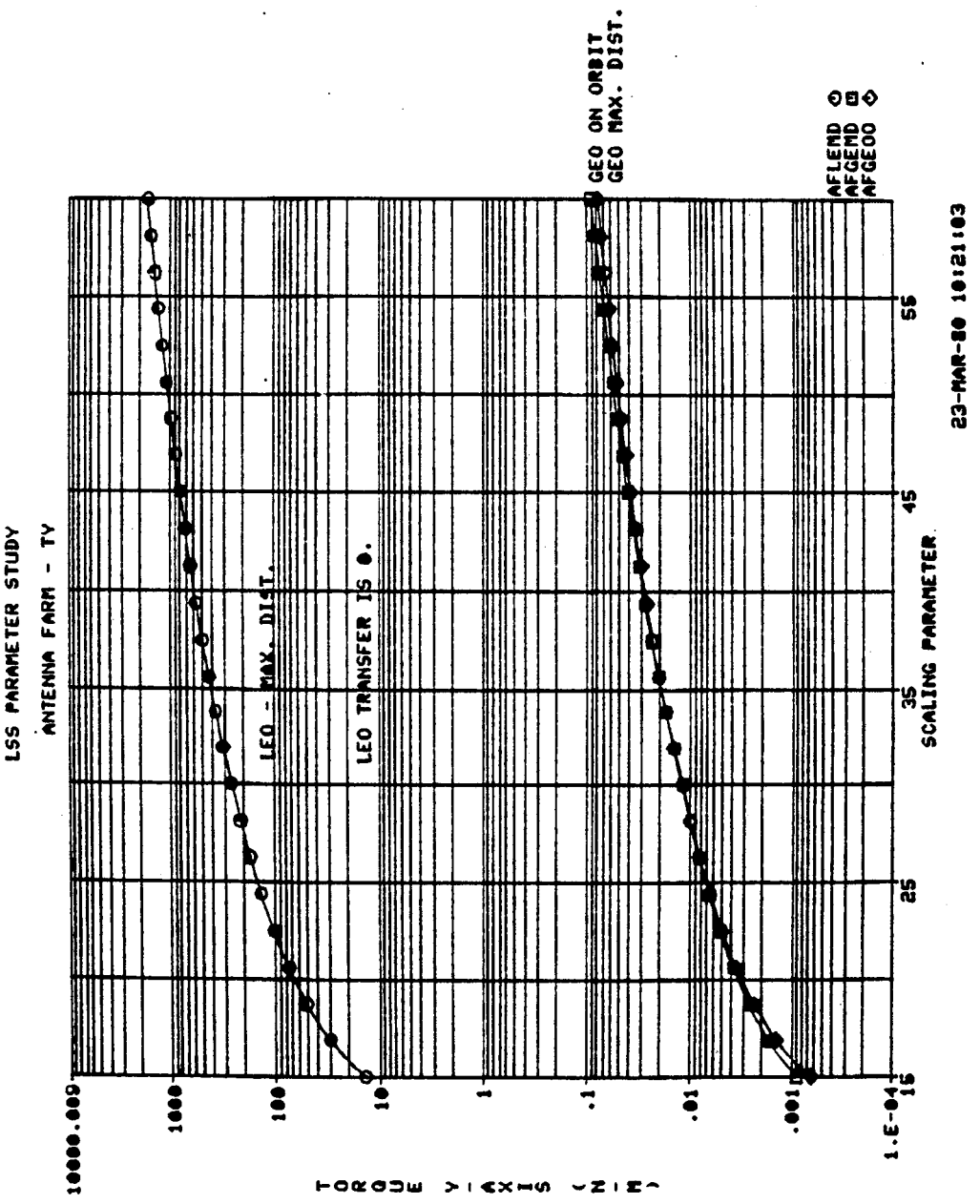

FIGURE B-48 LSS PARAMETER STUDY ANTENNA FARM TORQUES - Y AXIS

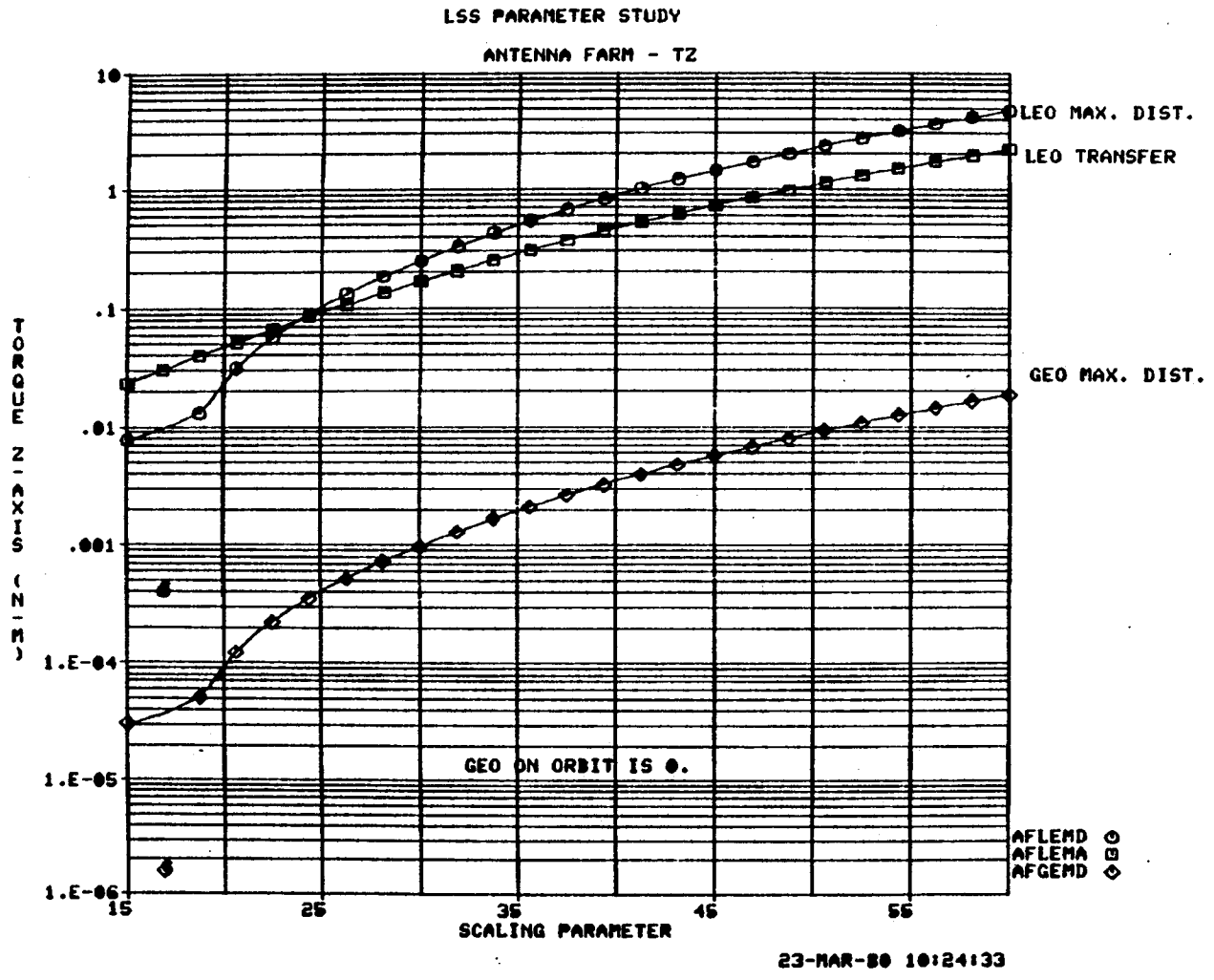

FIGURE B-49 LSS PARAMETER STUDY ANTENNA FARM TORQUES - Z AXIS

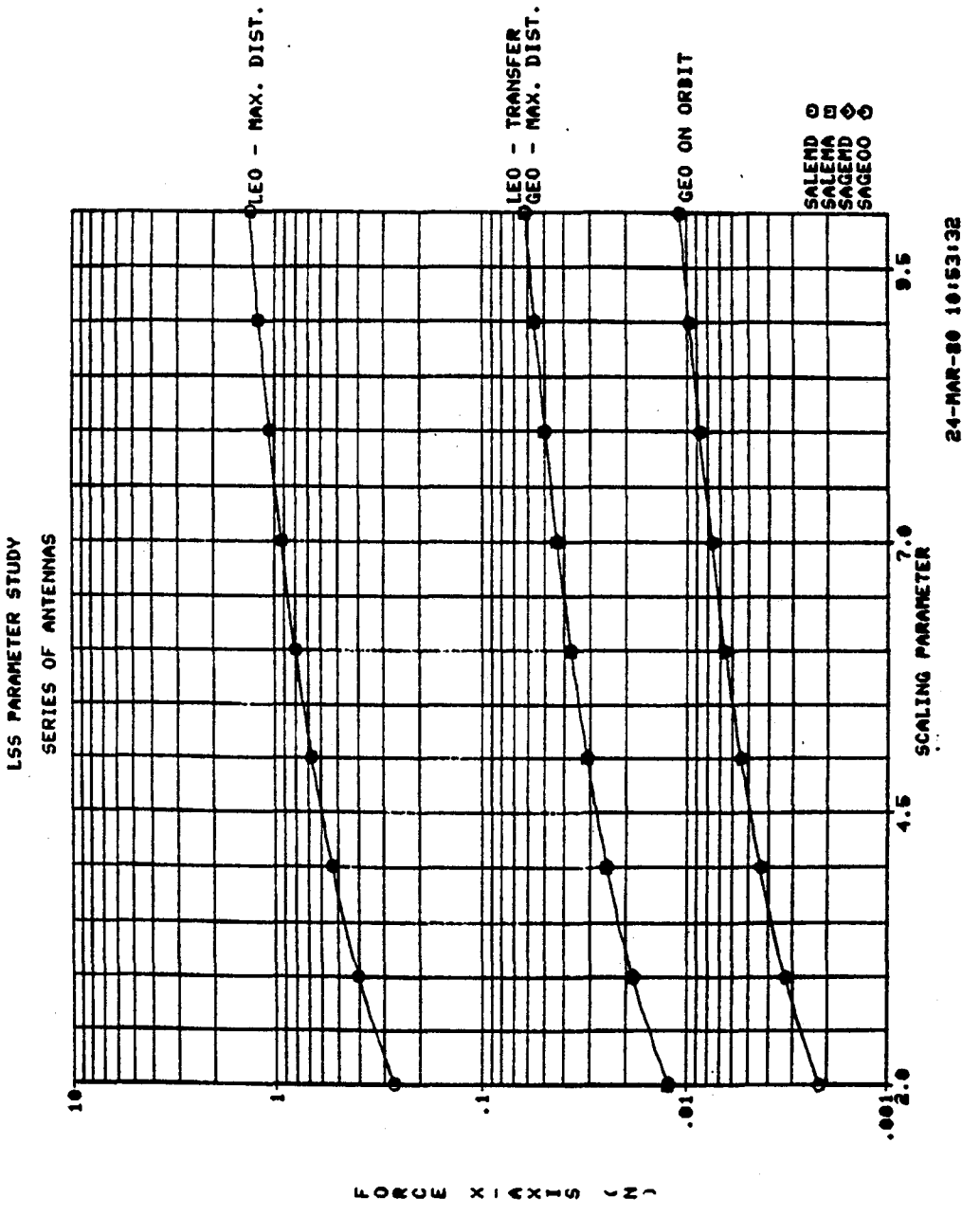

FIGURE B-50 LSS PARAMETER STUDY SERIES OF ANTENNAS FORCES - X AXIS

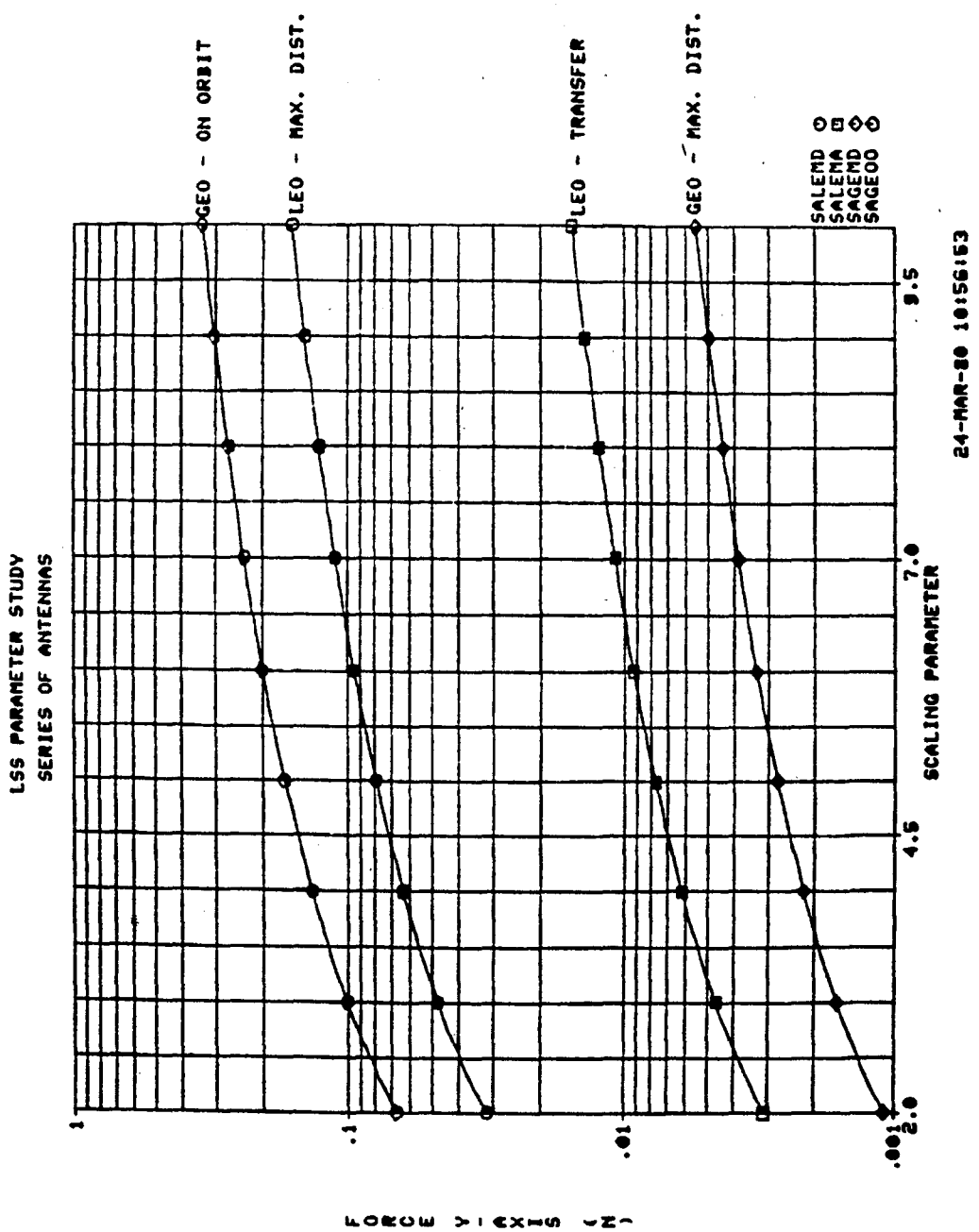

FIGURE B-51 LSS PARAMETER STUDY SERIES OF ANTENNAS FORCES - Y AXIS

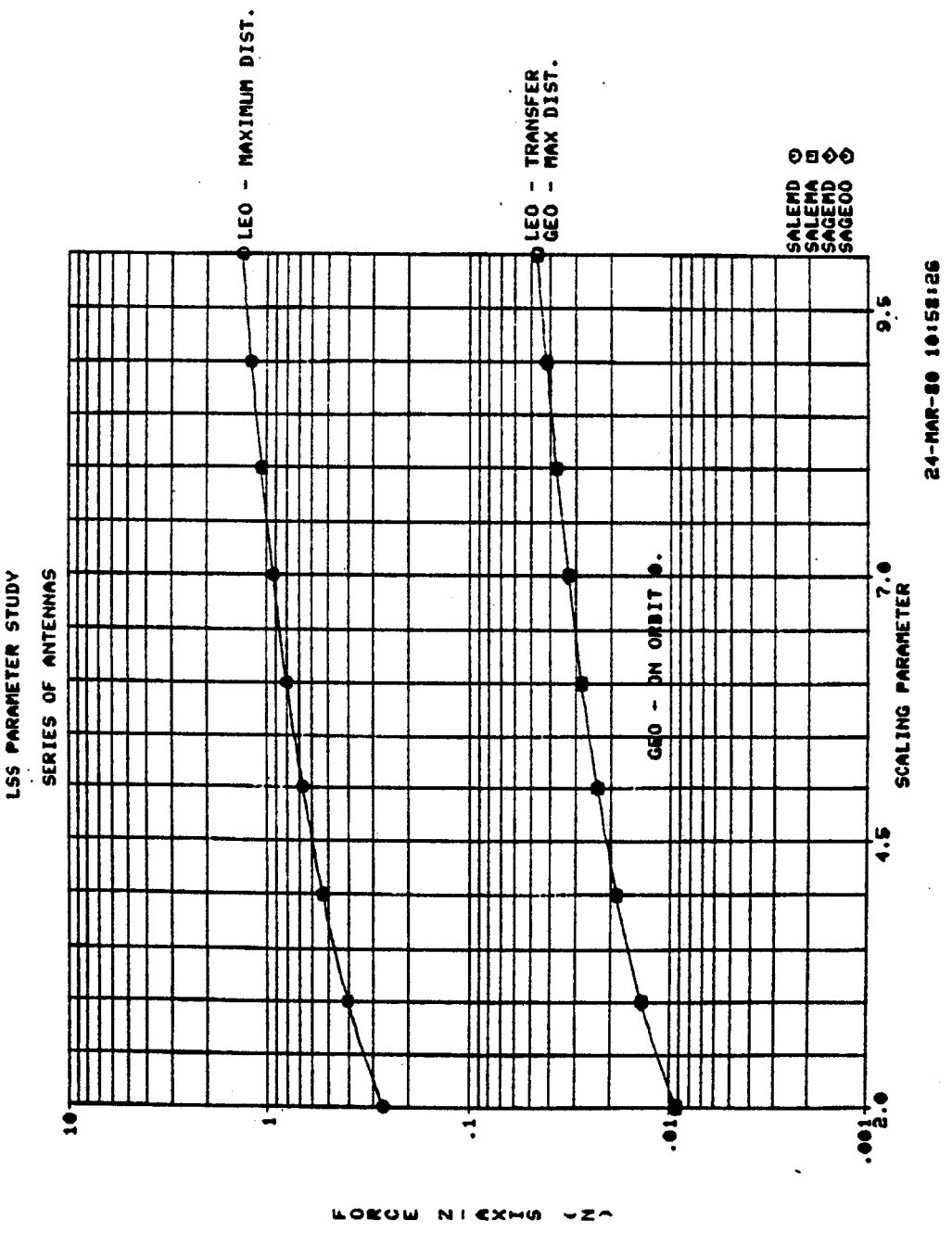

FIGURE B-52 LSS PARAMETER STUDY SERIES OF ANTENNAS FORCES - Z AXIS

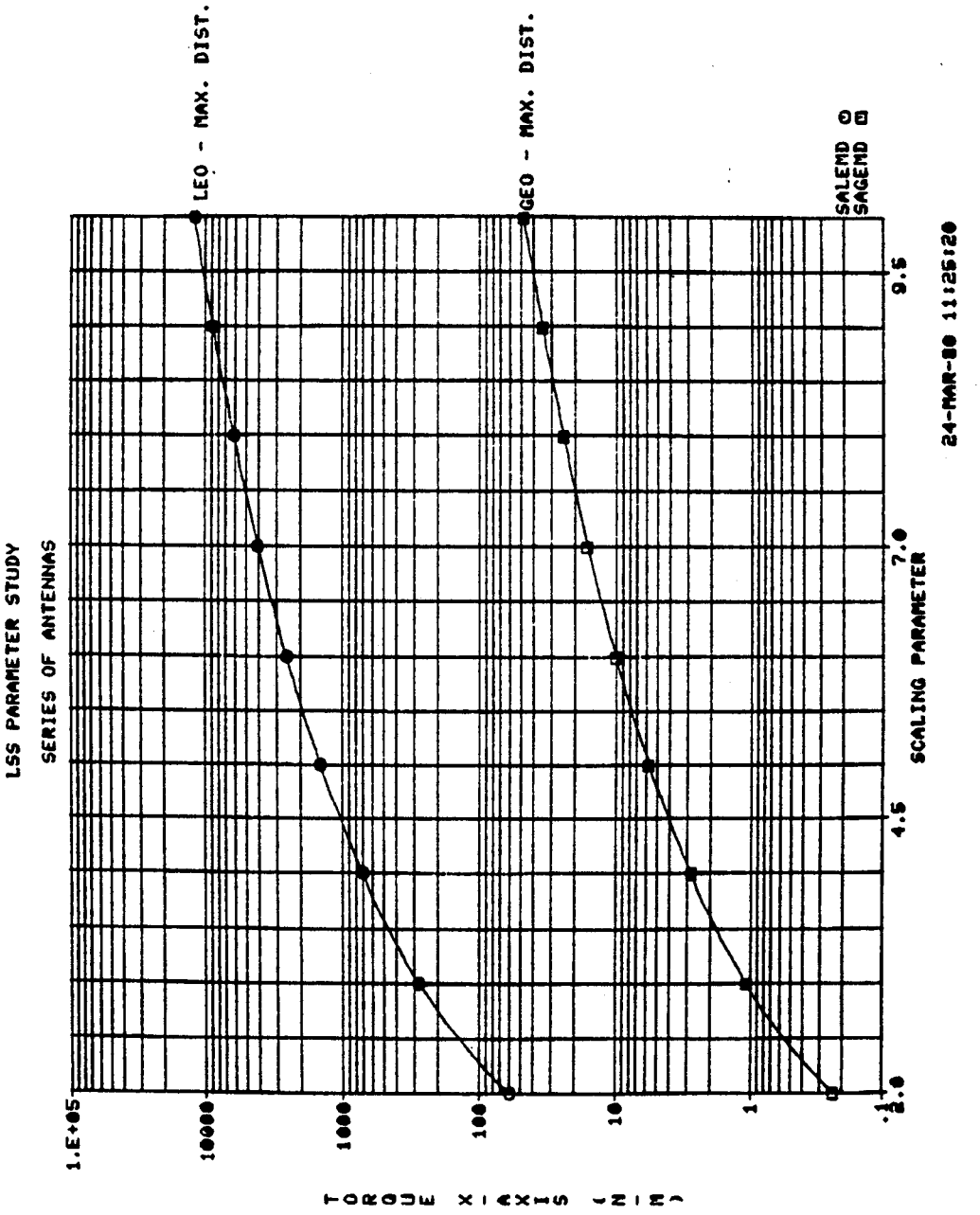

FIGURE B-53 LSS PARAMETER STUDY SERIES OF ANTENNAS TORQUES - X AXIS

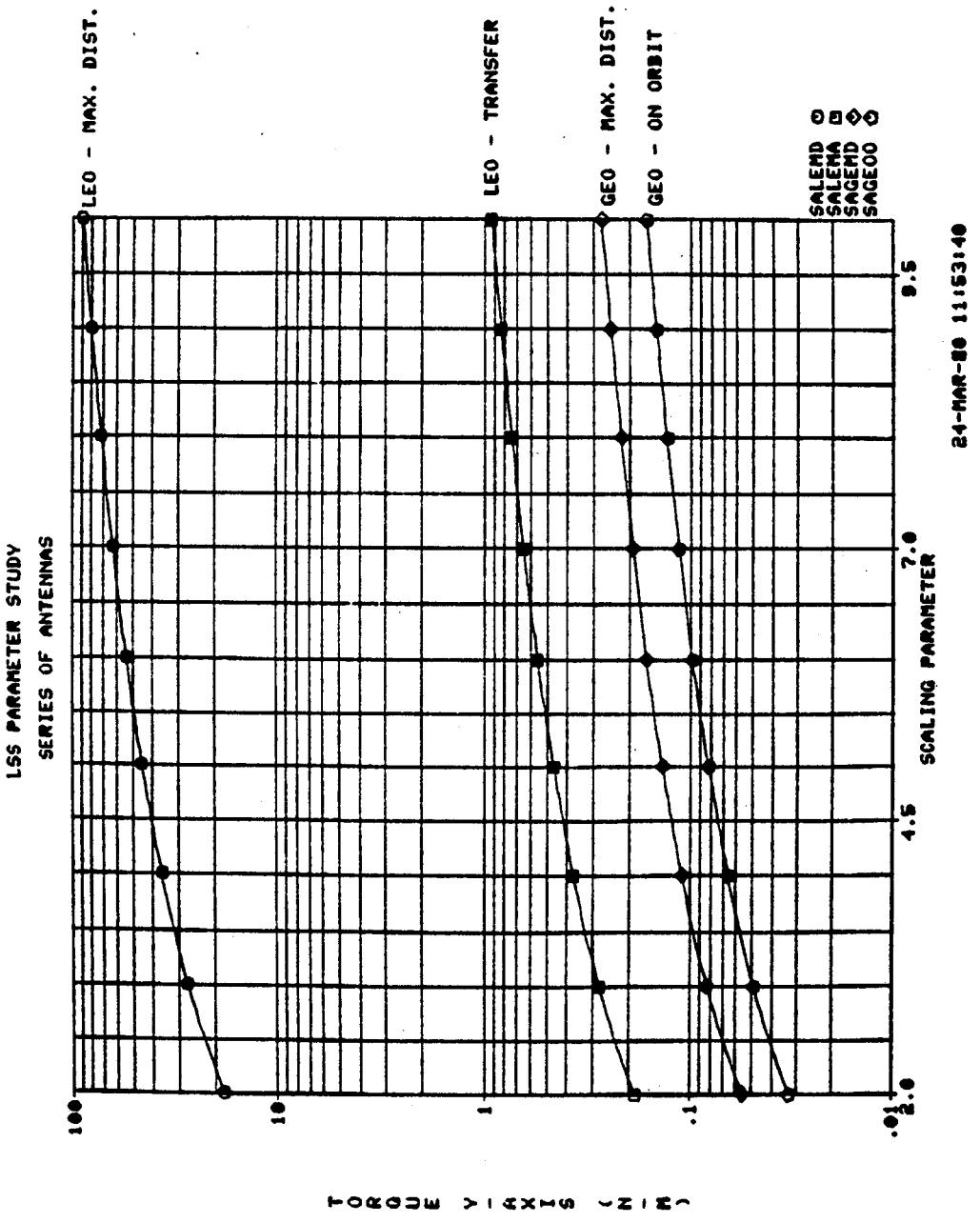

FIGURE B-54 LSS PARAMETER STUDY SERIES OF ANTENNAS TORQUES - Y AXIS

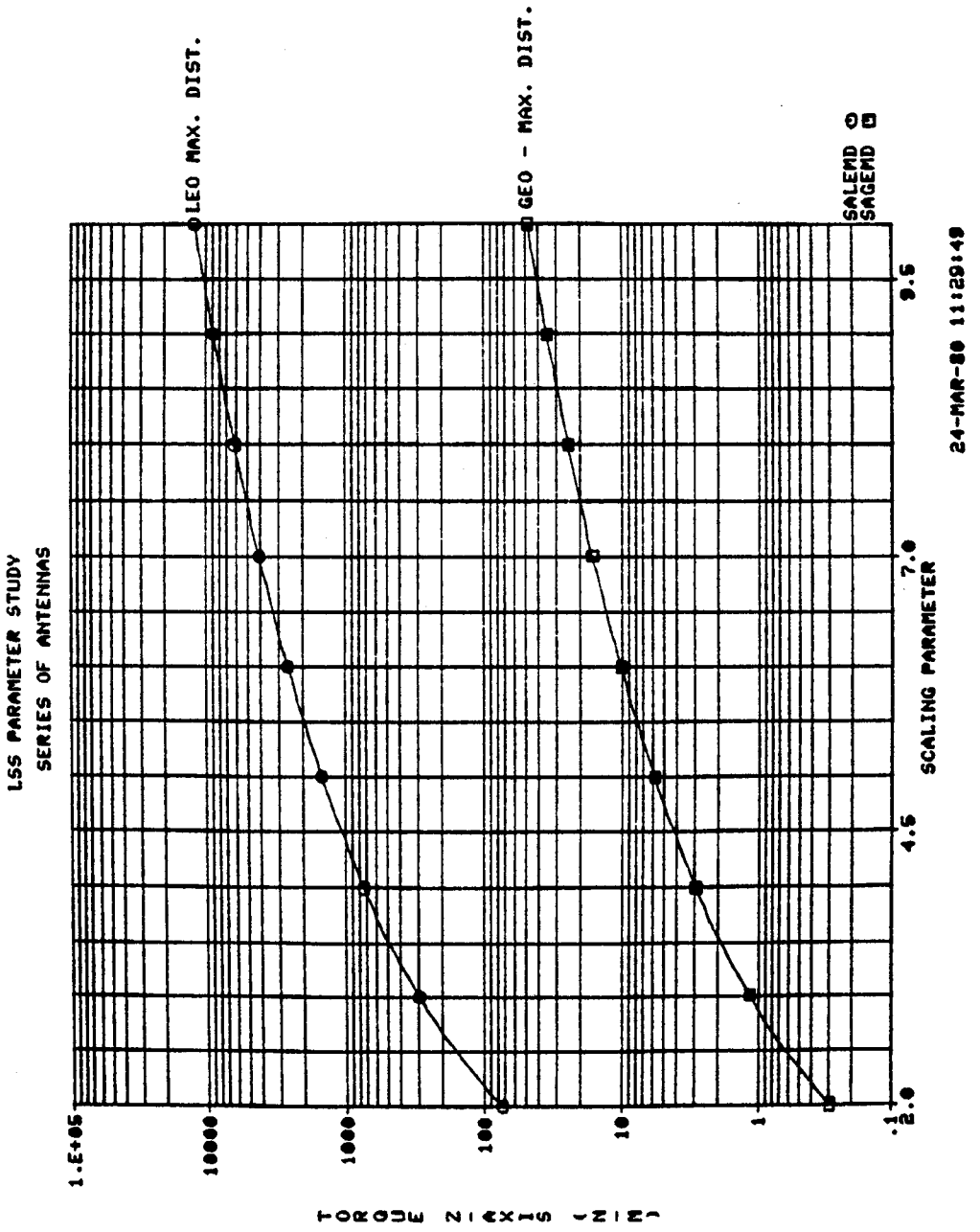

FIGURE B-55 LSS PARAMETER STUDY SERIES OF ANTENNAS TORQUES - Z AXIS

APPENDIX C

Bibliography, Disturbance Forces And Torques

GENERAL SURVEYS

ADVANCED SPACECRAFT STABILIZATION AND CONTROL TECHNIQUES, A. E. Sabroff, Journal of Spacecraft and Rockets, Vol. 5, December 1968

ATTITUDE CONTROL FOR SATELLITES, P. E. G. Cope, Flight International, Vol. 89, June 23, 1966

ATTITUDE CONTROL OF EARTH SATELLITES, R. K. Whitford, Control Engineering, Vol. 9, February, 1962 and April, 1962

ATTITUDE STABILIZATION AND CONTROL OR EARTH SATELLITES, D. H. Gerlach, Space Science Reviews, Vol. 4, 1965

CONTROL AND STABILIZATION OF SPACECRAFT, A. Kesserlring, et. al., ESRO SP-16, June, 1967

DESIGN GUIDE TO ORBITAL FLIGHT, J. Jensen, G. Townsend, J. Kork and D. Kraft, McGraw-Hill, 1962

DYNAMICS AND CONTROL OF ADVANCED SPACE VEHICLES, P. W. Likins, NASA CR-124272, April, 1973

HANDBOOK OF GEOPHYSICS AND SPACE ENVIRONMENTS, S. L. Valley (Ed), McGraw-Hill, 1965

HANDBOOK OF SATELLITES AND SPACE VEHICLES, G. Merril (Ed), Van Nostrand, 1965

METHODS FOR THE CONTROL OF SATELLITES AND SPACE VEHICLES, R. E. Roberson, WADC TR 60-643, July, 1960

PRINCIPLES AND DEVELOPMENTS IN PASSIVE ATTITUDE CONTROL, D. B. Debra, American Astronautical Society Science and Technology Series, Vol. 9, AAS Publications, 1966

SPACE FLIGHT, K. Ehricke, Van Nostrand, 1960

STABILIZATION AND ATTITUDE CONTROL OF SATELLITE VEHICLES, W. E. Frye and E. V. B. Stearns, American Rocket Society Journal, Vol. 29, December, 1959

RELATIVE MAGNITUDE OF THE SPACE ENVIRONMENT TORQUES ON A SATELLITE L. E. Wiggins, AIAA Journal, Vol. 2, 1964

RADIATION

AERODYNAMIC AND RADIATION DISTURBANCE TORQUES ON SATELLITES HAVING COMPLEX GEOMETRY, W. T. Evans, in Torques and Attitude Sensing In Earth Satellites, Academic Press, 1964

CORPUSCULAR RADIATION AND THE ACCELERATION OF ARTIFICIAL SATELLITES, L. G. Jacchia, International Geophysical Year Annals, Vol. 12, 1960

DETERMINATION OF FORCES AND MOMENTS DUE TO LIGHT PRESSURE ACTING ON A BODY IN MOTION IN COSMIC SPACE, A. A. Karimov, Journal of Applied Mathematics and Mechanics, Vol. 26, March, 1963

DETERMINATION OF SOLAR RADIATION FORCES OF SATELLITE MATERIALS, F. Shahroki and H. T. Clark, AIAA Journal, Vol. 5, August, 1968

EARTH REFLECTED SOLAR RADIATION INCIDENT UPON AN ARBITRARILY ORIENTED SPINNING FLAT PLATE, F. G. Cunningham, NASA TN D-1842, July, 1963

EARTH REFLECTED SOLAR RADIATION INPUT TO SPHERICAL SATELLITES, F. G. Cunningham, NASA TN D-1099, October, 1961

THE EFFECT OF SOLAR RADIATION ON THE MOTION OF AN ARTIFICIAL SATELLITE, R. W. Bryant, NASA TN D-1063, September, 1961

EFFECTS OF SOLAR RADIATION PRESSURE UPON SATELLITE ATTITUDE CONTROL, R. J. McElvain, American Rocket Society Preprint 1918-61, August, 1961

THE EFFECT OF TERRESTIAL RADIATION ON SATELLITE ORBITS, S. P. Wyatt, in Dynamics of Satellites, Academic Press, 1963

INFLUENCE OF THE SOLAR RADIATION PRESSURE ON THE MOTION OF AN ARTIFICIAL SATELLITE, P. Musen, Journal of Geophysical Research, Vol. 65, May, 1960

RADIATION FORCES ON A FLAT PLATE IN ELLIPTIC NEAR-EARTH ORBITS, R. C. Flanagan and V. J. Modi, Canadian Aeronautics and Space Institute Trans., Vol. 3, September, 1970

RADIATION STRESSES ON REAL SURFACES, D. K. Edwards and J. T. Bevans, AIAA Journal Vol. 3, March, 1965

SOLAR PHYSICS AND SOLAR RADIATION, L. Larmore, in Space Physics, Wiley, 1964

SOLAR RADIATION ON INCLINED SURFACES, H. Heywood, Nature, Vol. 204, November, 1964

THE SOLAR RADIATION PRESSURE FORCE AND TORQUES MODEL, B. M. Georgevic, American Astronautical Society Paper 71-352, August, 1971

SPACECRAFT RADIATION TORQUES, NASA SP-8027, October, 1969

GRAVITY GRADIENT

CONTRIBUTION OF EARTH OBLATENESS TO GRAVITY TORQUE ON A SATELLITE, L. B. Schlegel, AIAA Journal, Vol. 4, November, 1966

EFFECT OF INERTIA PRODUCT TERMS ON SATELLITE GRAVITATIONAL TORQUES, J. L. Tietze, Journal of Spacecraft and Rockets, Vol. 3, October, 1966

GENERALIZED GRAVITY GRADIENT TORQUES, R. E. Roberson, in Torquers and Attitude Sensing in Earth Satellites, Academic Press, 1964

THE GRAVITATIONAL FIELD ENVIRONMENT OF AN EARTH SATELLITE, C. Adamson, NASA TN D-1270, August, 1962

GRAVITATIONAL TORQUE IMPULSE ON A STABILIZED SATELLITE, P. F. Hultquist, American Rocket Society Journal, Vol. 31, November, 1961

GRAVITATIONAL TORQUE ON A SATELLITE OF ARBITRARY SHAPE, R. A. Nidey, APS Journal, Vol. 31, November, 1961

GRAVITATIONAL TORQUE ON A SATELLITE VEHICLE, R. E. Roberson, Journal of the Franklin Institute, Vol. 265, January, 1958

GRAVITATIONAL TORQUE ON A SMALL RIGID BODY IN AN ARBITRARY FIELD, C. D. Pengelley, American Rocket Society Journal, Vol. 32, March, 1962

GRAVITATIONAL INTERACTION TORQUES, T. R. Kane, Journal of Spacecraft and Rockets, Vol. 9, October, 1972

GRAVITY GRADIENT TORQUES ON ARTIFICIAL SATELLITES - A METHOD OF CALCULATION, R. W. Raymond, Astronautica Acta, Vol. 12, January-February, 1966

GRAVITY TORQUE EFFECTS, T. R. Kane and R. T. Robe, AIAA Journal, Vol. 4, August, 1966

GRAVITY TORQUE ON AN ORBITING VEHICLE, B. F. Coolin, NASA TN D-70, September, 1959

THE INFLUENCE OF THE MAGNETIC AND GRAVITATIONAL FIELDS OF THE EARTH ON THE OSCILLATIONS OF A SATELLITE ABOUT ITS CENTER OF MASS, A. A. Khontor, Cosmic Research, Vol. 5, July-August 1967

ON THE GRAVITY GRADIENT AT SATELLITE ALTITUDES, W. Kohnlein, Smithsonian Astrophysical Observatory Special Report 246, July, 1967.

THE POTENTIAL ENERGY OF A SMALL RIGID BODY IN THE GRAVITATIONAL FIELD OF AN OBLATE SPHERIOD, R. E. Roberson and D. Tatistcheff, Journal of the Franklin Institute, Vol. 32, September, 1956

PLANETARY GRAVISPHERES, H. Struyhold, Astronautics, Vol. 7, January, 1962

SECULAR GRAVITATIONAL TORQUE ON A SATELLITE IN A CIRCULAR ORBIT, R. A. Nidey, American Rocket Society Journal, Vol. 31, July, 1961

SPACECRAFT GRAVITATIONAL TORQUES, NASA SP-8024, May, 1969

TORQUE ON A SATELLITE IN A GENERAL GRAVITATIONAL FIELD, R. E. Roberson, AIAA Journal, Vol. 6, March, 1968

AERODYNAMIC

AERODYNAMIC AND RADIATION DISTURBANCE TORQUES ON SATELLITES HAVING COMPLEX GEOMETRY, W. T. Evans, in Torques and Attitude Sensing in Earth Satellites, Academic Press, 1964

AERODYNAMIC MOMENT ON BODIES MOVING AT HIGH SPEED IN THE UPPER ATMOSPHERE, W. A. Gustafson, American Rocket Society Journal, Vol. 29, April, 1959

APPLICATIONS OF THE THEORY OF FREE MOLECULE FLOW TO AERONAUTICS, H. Ashley, Journal of the Aeronautical Sciences, Vol. 16, Feburary 1949

APPROXIMATE FREE MOLECULE AERODYNAMIC CHARACTERISTICS, D. M. Schrello, American Rocket Society Journal, Vol. 30, August, 1960

ATMOSPHERIC DRAG ON NON-SPHERICAL ARTIFICIAL SATELLITES, R. E. Zadunaisky, Smithsonian Astrophysical Observatory Special Report 65, July, 1961

AN ATMOSPHERIC DENSITY MODEL FOR APPLICATION IN ANALYTICAL SATELLITE THEORIES, A. C. Mueller, NASA CR-151605, November 1977

ATMOSPHERIC DRAG ON THE SATELLITE, R. Jastrow and C. A. Pearse, JGR, Vol. 62, September, 1957

ATMOSPHERIC PRESSURE, DENSITY, TEMPERATURE AND WIND VARIATIONS BETWEEN 50 AND 200 KM, C. G. Justus and A. Woodrum, NASA CR-2062, May, 1972

THE DETERMINATION OF ATMOSPHERIC DRAG ON ARTIFICIAL SATELLITES, L. G. Jacchia, in Dynamics of Satellites, Academic Press, 1963

DYNAMIC ATMOSPHERIC EFFECTS UPON SATELLITE MOTION AND SATELLITE LIFETIME, R. W. Bruce, 5th International Space Science Symposium, Flopence, May, 1964

EFFECT OF THE DIURNAL ATMOSPHERIC BULGE ON SATELLITE ACCELERATIONS, S. P. Wyatt, Smithsonian Astrophysical Observatory Special Report 63, May, 1961

EFFECTS OF AERODYNAMIC TORQUE ON AN ASYMMETRIC GRAVITY STABILIZED SATELLITE, G. S. Nurre, Journal of Spacecraft and Rockets, Fol. 5, September, 1968

KINETIC THEORY OF GASES, E. H. Kennard, McGraw-Hill, 1938

MECHANICS OF RAREFIED GASES in Handbook of Supersonic Aerodynamics, S. A. Schaaf and L. Talbot, Navord Report 1488 (Vol. 5), February, 1959

MODELS OF THE EARTH'S ATMOSPHERE (120 to 1000 km), NASA SP-8021, May, 1969

MOLECULAR FLOW OF GASES, G. N. Patterson, Wiley, 1956

SPACECRAFT AERODYNAMIC TORQUES, NASA SP-8058, January, 1971

THEORETICAL AERODYNAMIC CHARACTERISTICS OF BODIES IN A FREE-MOLECULE-FLOW FIELD, J. R. Stadler and V. J. Zunick, NASA TN 2423, July, 1961

A WORKING MODEL FOR THE UPPER ATMOSPHERE, L. G. Jacchia, Nature, Vol. 192, December, 1961

MAGNETIC

ASSESSMENT AND CONTROL OF SPACECRAFT MAGNETIC FIELDS, NASA SP-8037, September 1970

DESCRIPTIONS OF THE GEOMAGNETIC FIELD, R. K. C. Luke, SSD-TR-67-32, January, 1967

THE ELECTROMAGNETIC TORQUES ON SPHERICAL EARTH SATELLITES IN A RAREFIED PARTIALLY IONIZED ATMOSPHERE, F. Hohl, NASA TR-R-231, February 1966

AN EVALUATION OF VARIOUS GEOMAGNETIC FIELD EQUATIONS, H. C. Euler and P. E. Wasko, NASA Marshall Space Flight Center Report MTP-AERO 63-60, July, 1963

FERROMAGNETISM, R. M. Bozarth, Van Nostrand, 1951

GEOMAGNETIC AND INTERPLANETARY MAGNETIC FIELD ENVIRONMENT OF AN EARTH SATELLITE, NASA TN D-1019, 1962

THE GEOMAGNETIC FIELD, L. J. Cahill, in Space Physics, Wiley, 1964

GEOMAGNETISM, G. J. Dressler, in Satellite Environment Handbook, Stanford University Press, 1965

INTERPLANETARY MAGNETIC FIELDS, E. J. Smith, in Space Physics, Wiley, 1964

MAGNETIC FIELD EFFECTS ON ARTIFICIAL SATELLITES, R. H. Wilson, Sky and Telescope, Vol. 20, August, 1960

MAGNETIC FIELDS - EARTH AND EXTRATERRESTRIAL, NSAS SP-8017, March, 1969

MAGNETIC FIELDS IN INTERPLANETARY SPACE, L. J. Cahill, Science, Vol. 147, February, 1965

MAGNETIC FIELDS IN THE MAGNETOPAUSE AND VICINITY AT SYNCHRONOUS ALTITUDE, W. D. Cummings and P. J. Coleman, Institute of Geophysics and Planetary Physics, Pub. 654, February, 1968

MAGNETIC PROPERTIES OF SELECTED SPACECRAFT MATERIALS, Proceedings, Symposium on Space Magnetic Exploration and Technology, Engineering Report No. 9, 1967

THE MAGNETOSPHERE, L. J. Cahill, Scientific American, Vol. 212 March, 1965

ON THE PROBLEM OF THE INTERACTION BETWEEN A SATELLITE AND THE EARTH'S MAGNETIC FIELD, Yu. V. Zonov, NASA TT P-37, May, 1960

REVIEW OF ELECTROMAGNETIC EFFECTS ON SPACE VEHICLES, K. P. Chopra, Journal of the Astronautical Sciences, Vol. 9, Spring, 1962

ROTATIONAL MAGNETODYNAMICS AND STEERING OF SPACE VEHICLES, R. H. Wilson, NASA TN D-566, September 1961

SPACECRAFT MAGNETIC TORQUES, NASA SP-8018, March, 1969

THERMAL

A REVIEW OF THERMAL RADIATION PROPERTIES AND MEASURING TECHNIQUES, J. T. Bevans, Space Technology Laboratories, TN-60-0000-09096, June, 1960

SIMPLIFIED THERMAL ESTIMATION TECHNIQUES FOR LARGE SPACE STRUCTURES. E. W. Grogren, D. L. Barclay and J. W. Straayer, NASA CR-145253, October, 1977

EFFECT OF SURFACE THERMAL RADIATION CHARACTERISTICS ON THE TEMPERATURE PROBLEM IN SATELLITES, in Surface Effects in Spacecraft Materials, Wiley, 1960

TEMPERATURE EQUILIBRIA IN SPACE VEHICLES, R. A. Cornog, in Advances in Astronautical Sciences, Vol. 3, Plenum Press, 1958

MISCELLANEOUS

THE DYNAMIC ATTITUDE EQUATIONS FOR AN N-BODY SATELLITE, W. Hooker and G. Margulies, Journal of the Astronautical Sciences, Vol. 12, Winter 1965

EFFECTS OF STRUCTURAL FLEXIBILITY ON CONTROL SYSTEMS, NASA SP-8016, April, 1969

METEOROID ENVIRONMENT MODEL-1969, NASA SP-8013, March, 1969

NATURAL VIBRATION MODAL ANALYSIS, NASA SP-8012, September, 1968

SPACECRAFT MASS EXPULSION TORQUES, NASA SP-8034, December, 1969

TORQUES ON A SATELLITE VEHICLE FROM INTERNAL MOVING PARTS, R. E. Roberson, American Rocket Society Journal, Vol. 6, June, 1958

ORBIT DRIFT

LONGITUDINAL STATIONKEEPING OF NEARLY GEOSTATIONARY SATELLITES, N. C. Ostrander, Rand Corp., RM-6166-PR, November, 1969

APPENDIX D

Thrust/Thruster Requirements, Torque Composite Breakdown, and Delta-V Requirements Summary

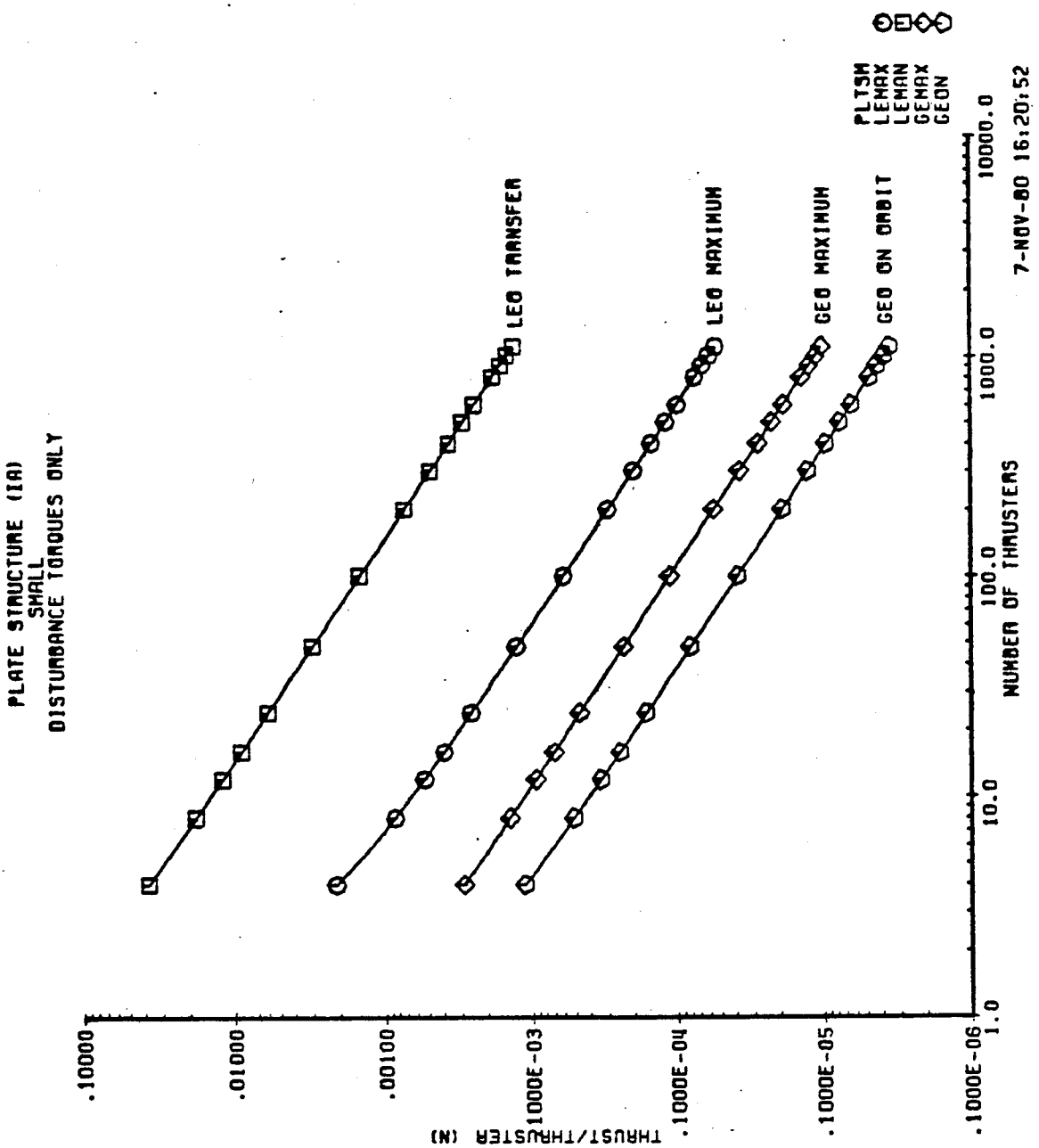

FIGURE D-1 SMALL PLATE STRUCTURE THRUST/THRUSTER REQUIREMENTS DUE TO DISTURBANCE TORQUES

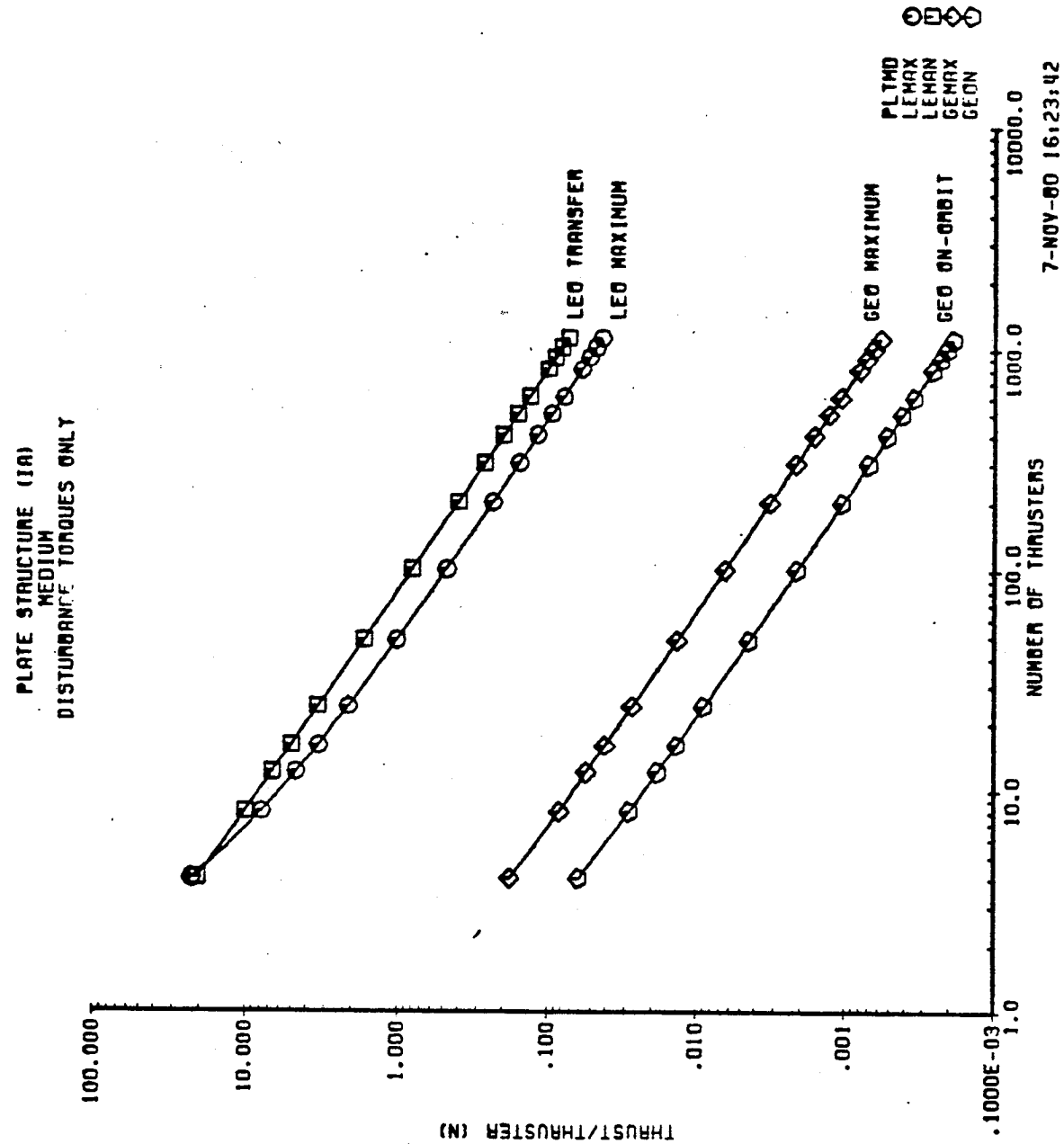

FIGURE D-2 MEDIUM PLATE STRUCTURE THRUST/THRUSTER REQUIREMENTS DUE TO DISTURBANCE TORQUES

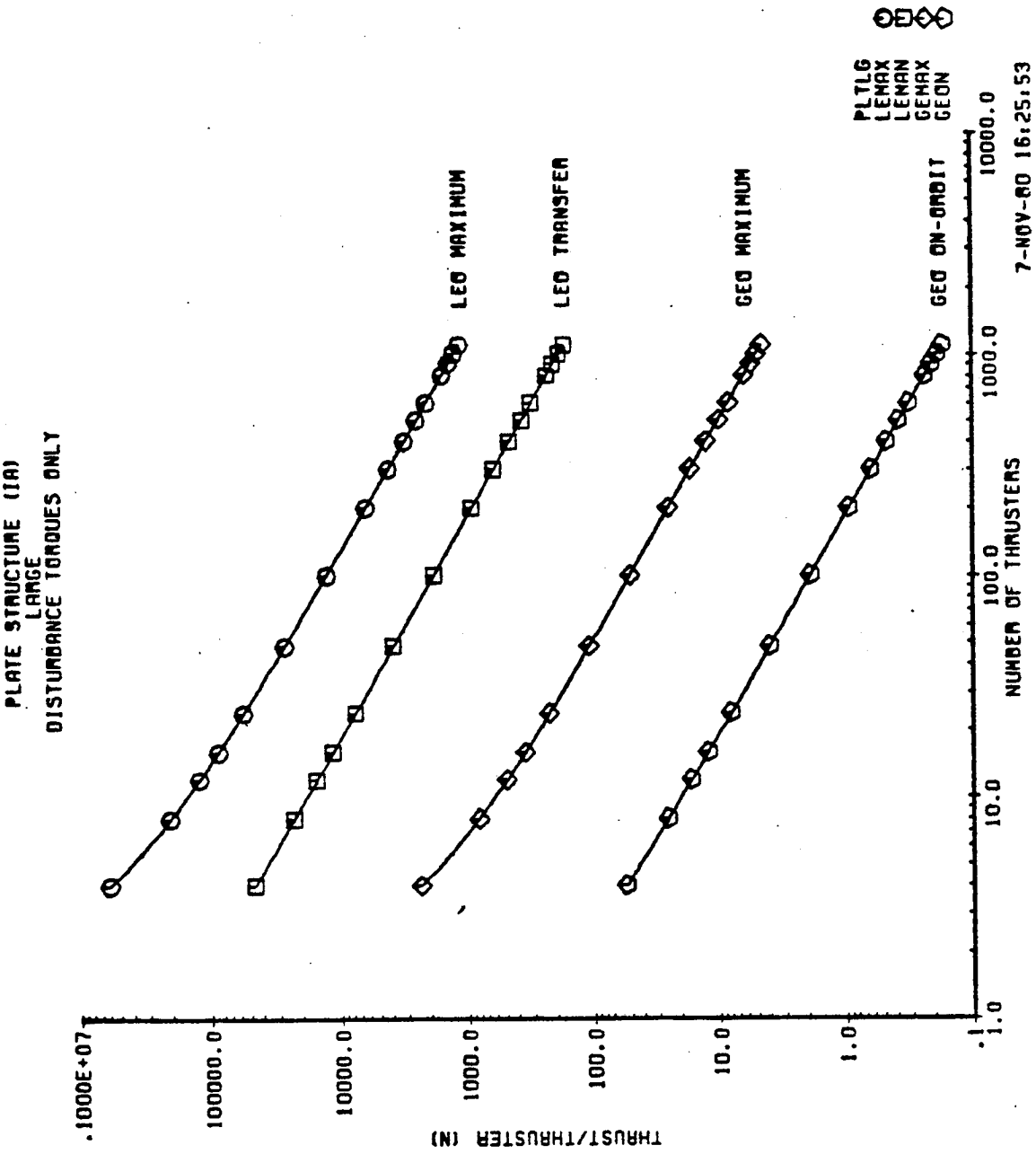

FIGURE D-3 LARGE PLATE STRUCTURE THRUST/THRUSTER REQUIREMENTS DUE TO DISTURBANCE TORQUES

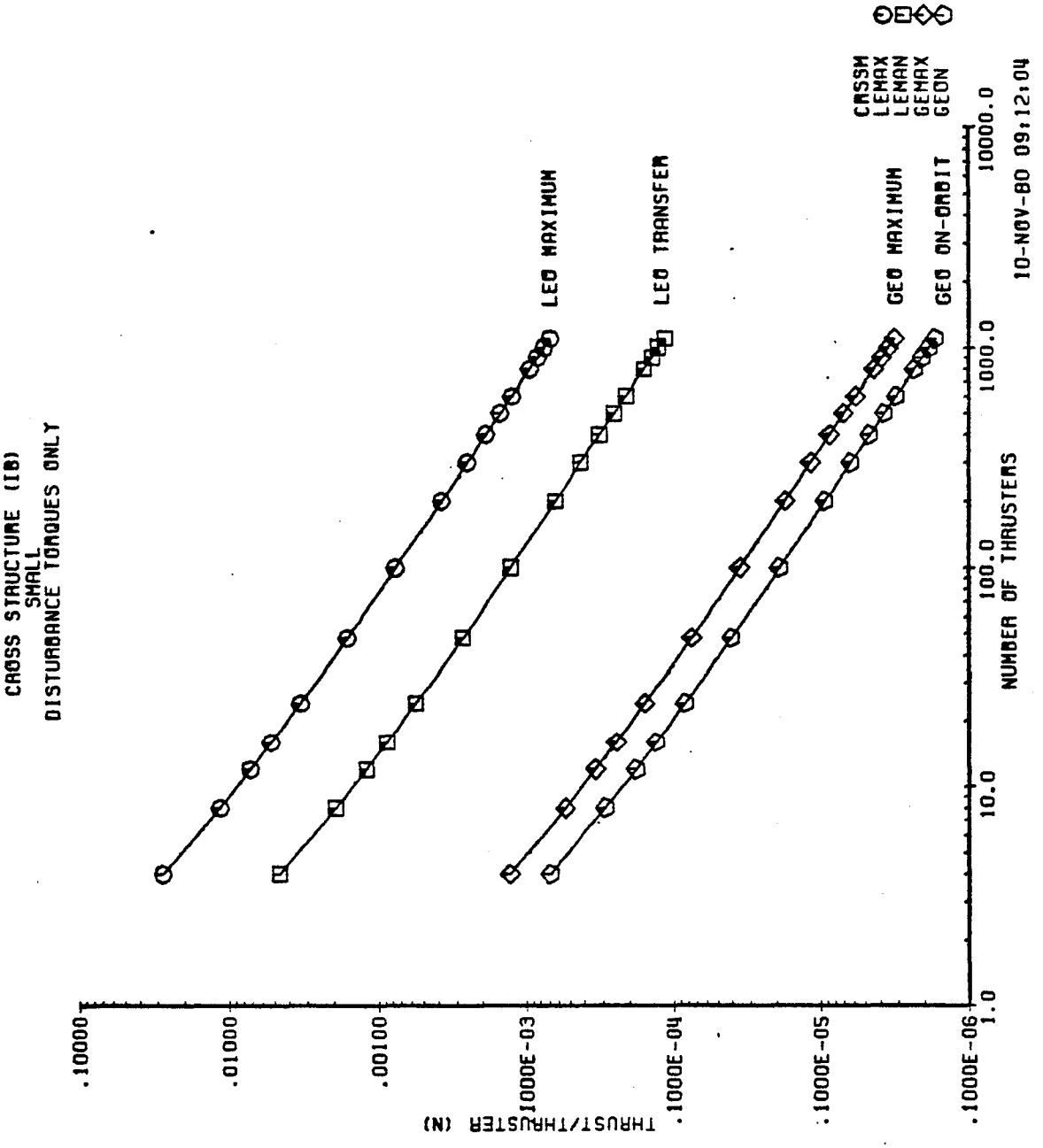

FIGURE D-4 SMALL CROSS STRUCTURE THRUST/THRUSTER REQUIREMENTS DUE TO DISTURBANCE TORQUES

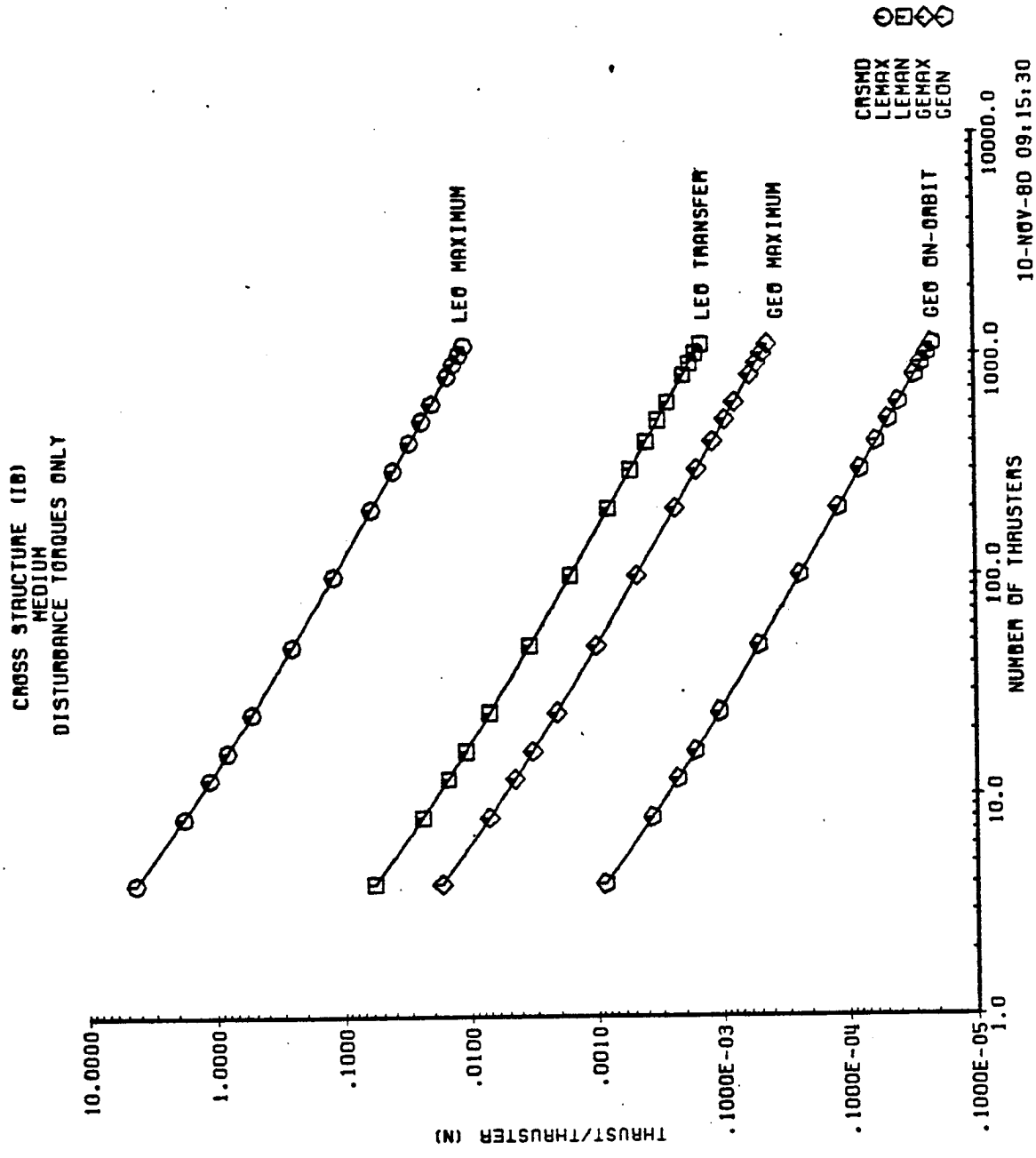

FIGURE D-5 MEDIUM CROSS STRUCTURE THRUST/THRUSTER REQUIREMENTS DUE TO DISTURBANCE TORQUES

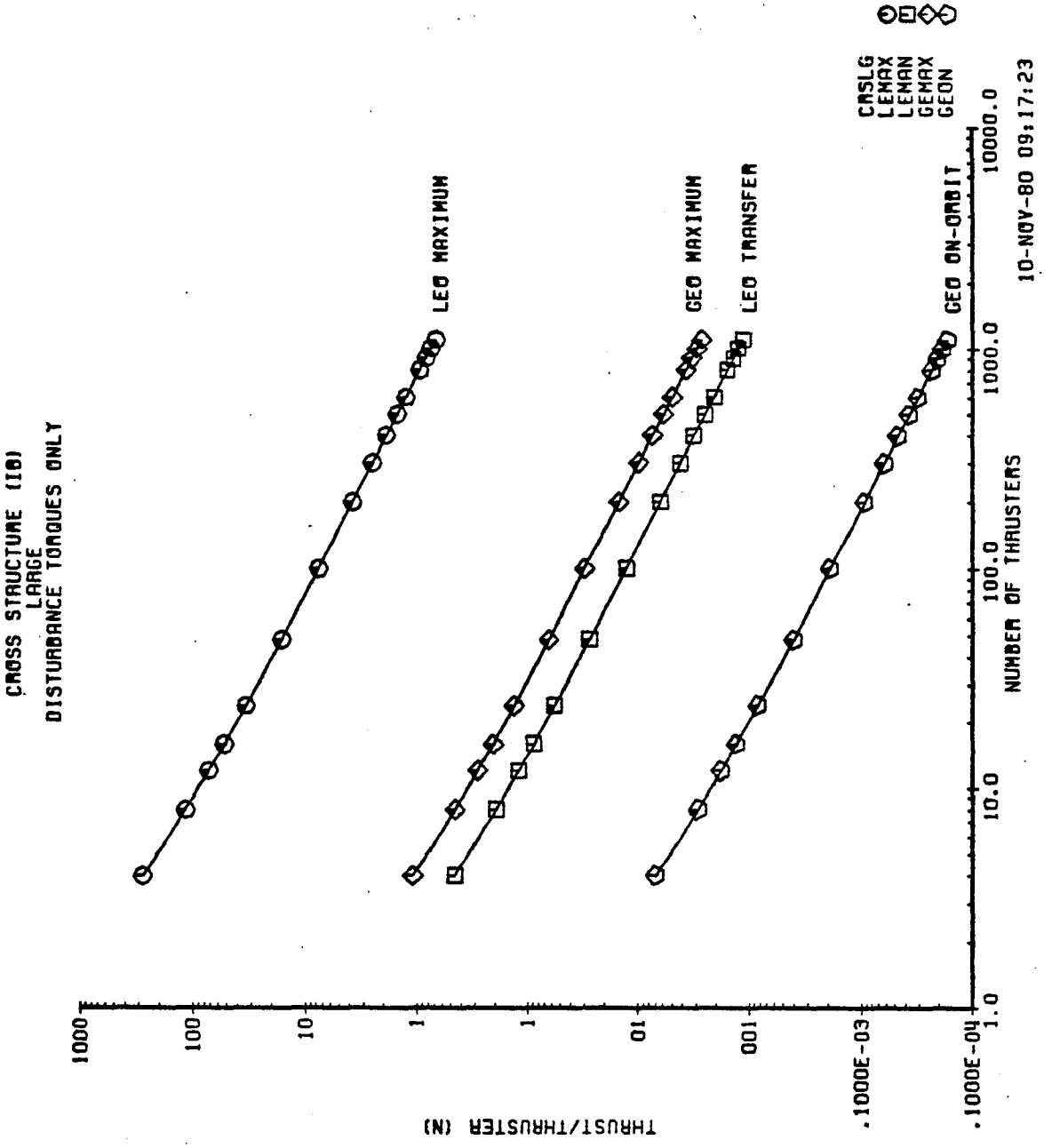

FIGURE D-6 LARGE CROSS STRUCTURE THRUST/THRUSTER REQUIREMENTS DUE TO DISTURBANCE TORQUES

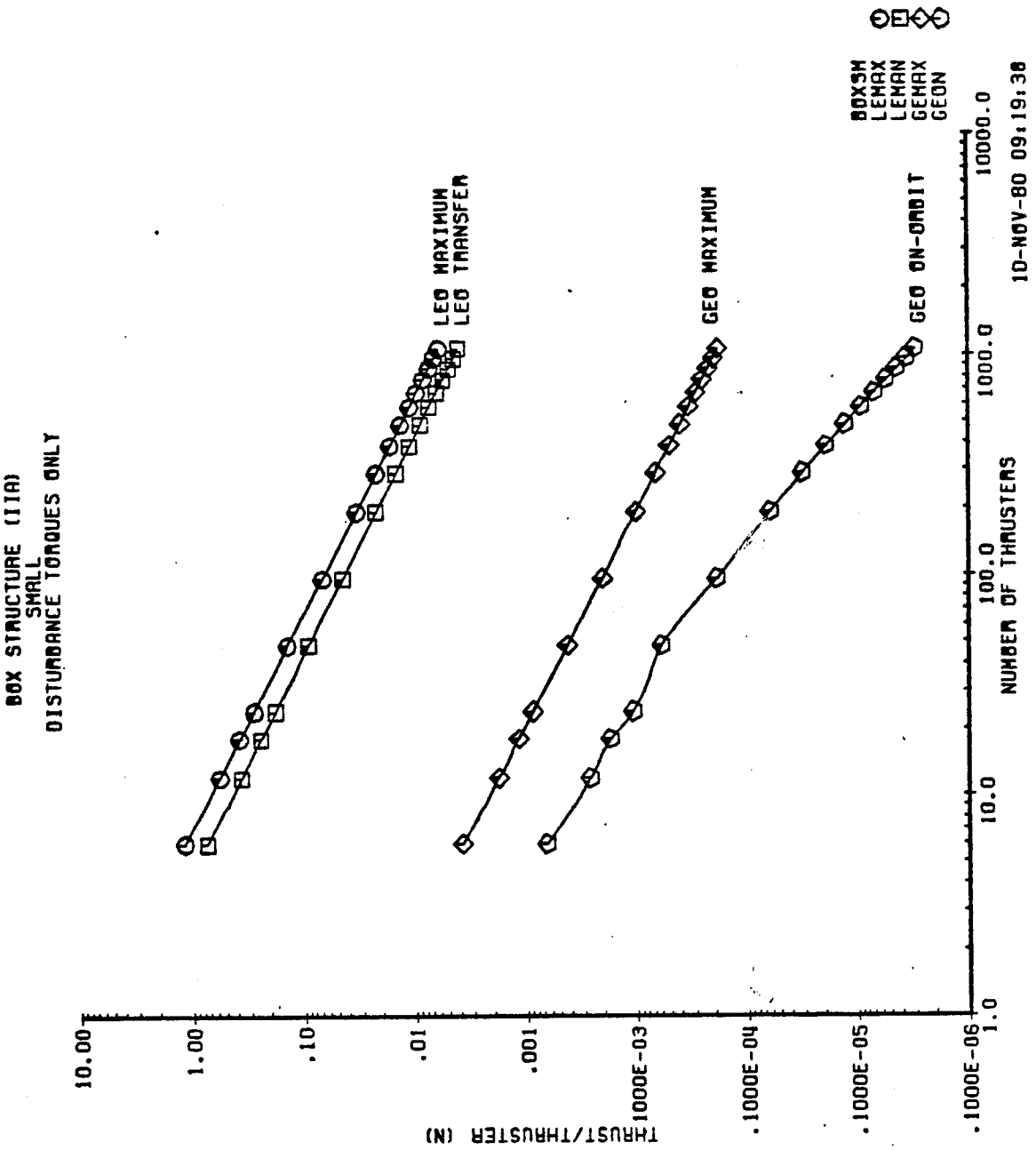

FIGURE D-7 SMALL BOX STRUCTURE THRUST/THRUSTER REQUIREMENTS DUE TO DISTURBANCE TORQUES

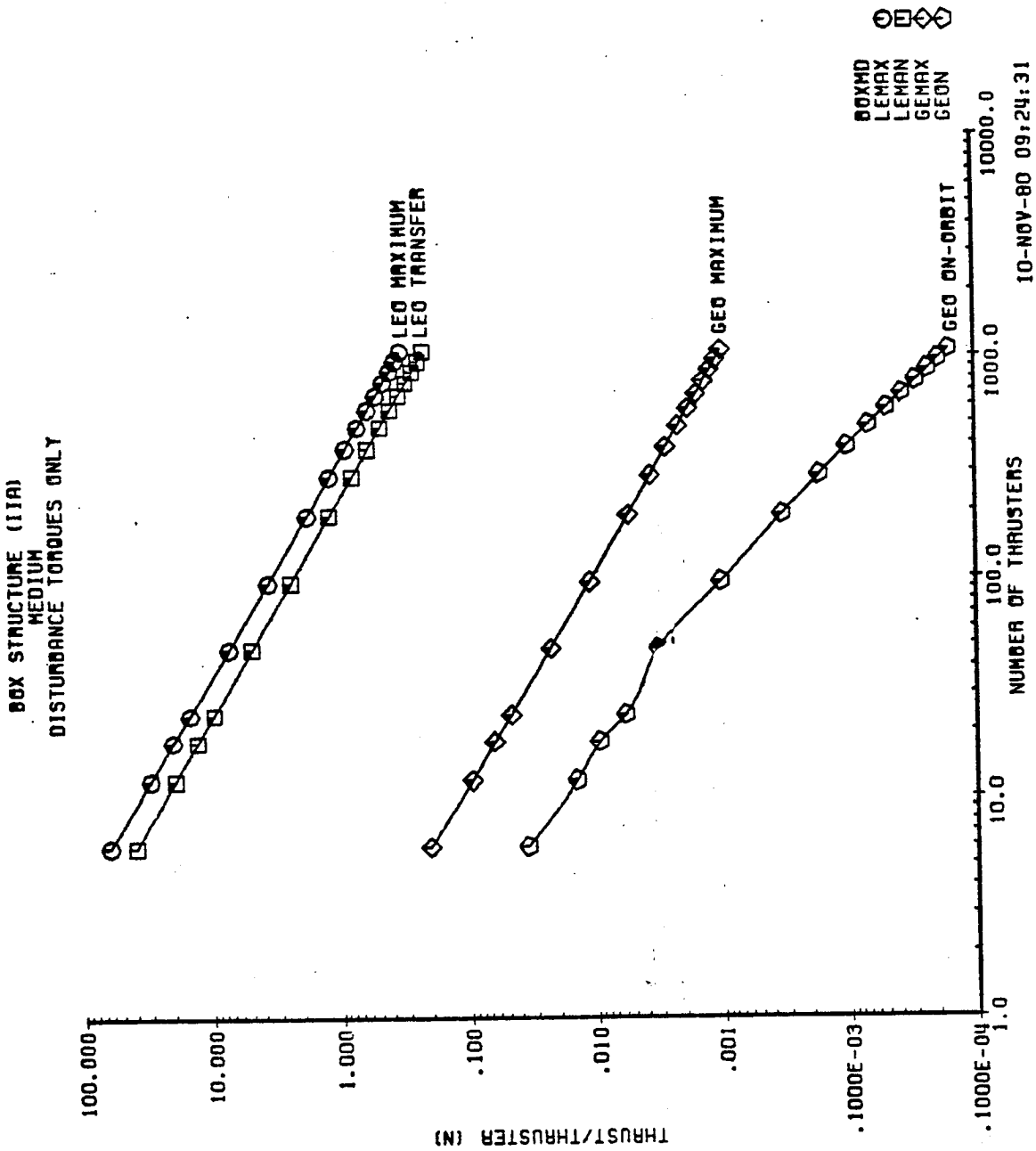

FIGURE D-8 MEDIUM BOX STRUCTURE THRUST/THRUSTER REQUIREMENTS DUE TO DISTURBANCE TORQUES

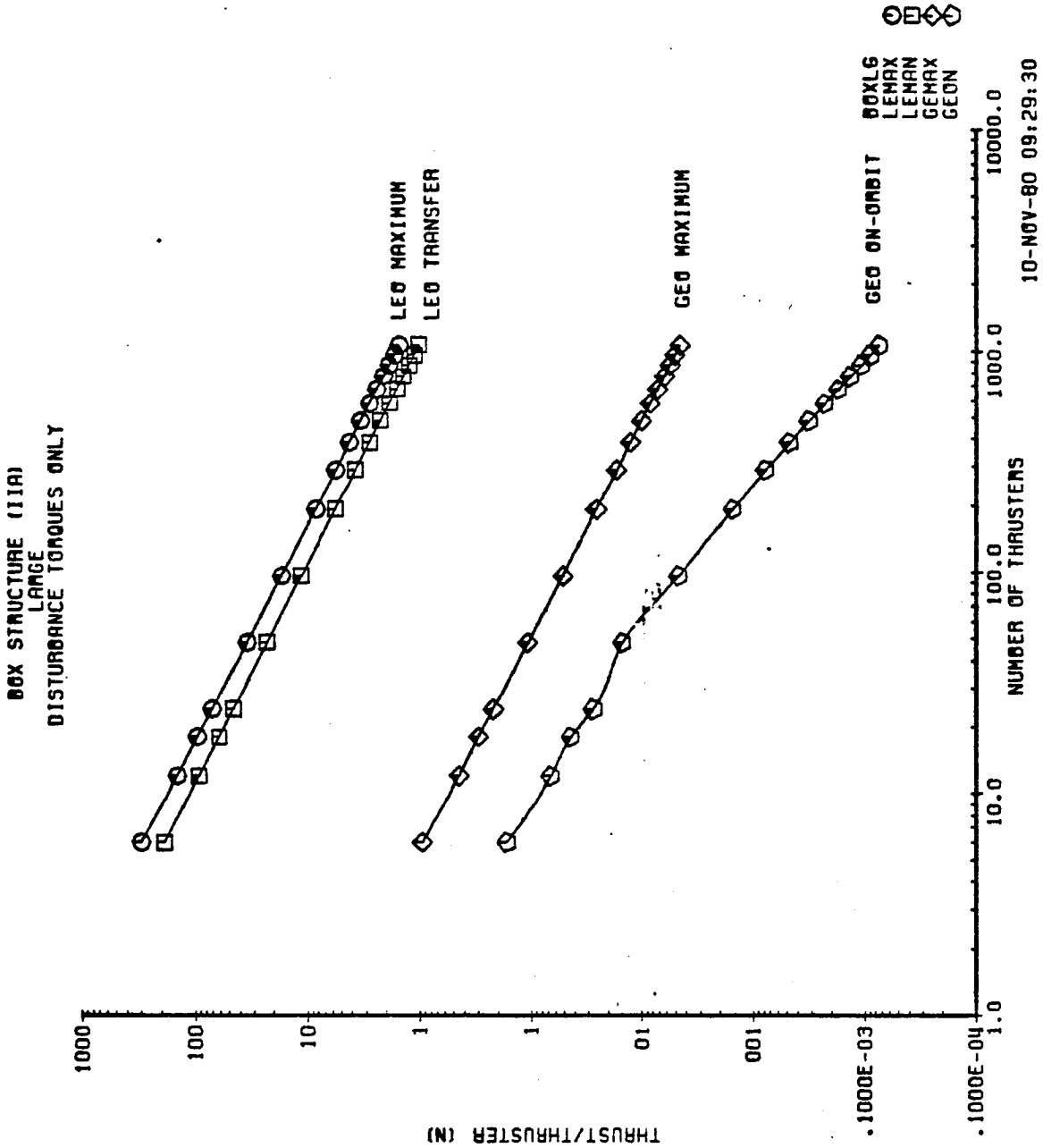

FIGURE D-9 LARGE BOX STRUCTURE THRUST/THRUSTER REQUIREMENTS DUE TO DISTURBANCE TORQUES

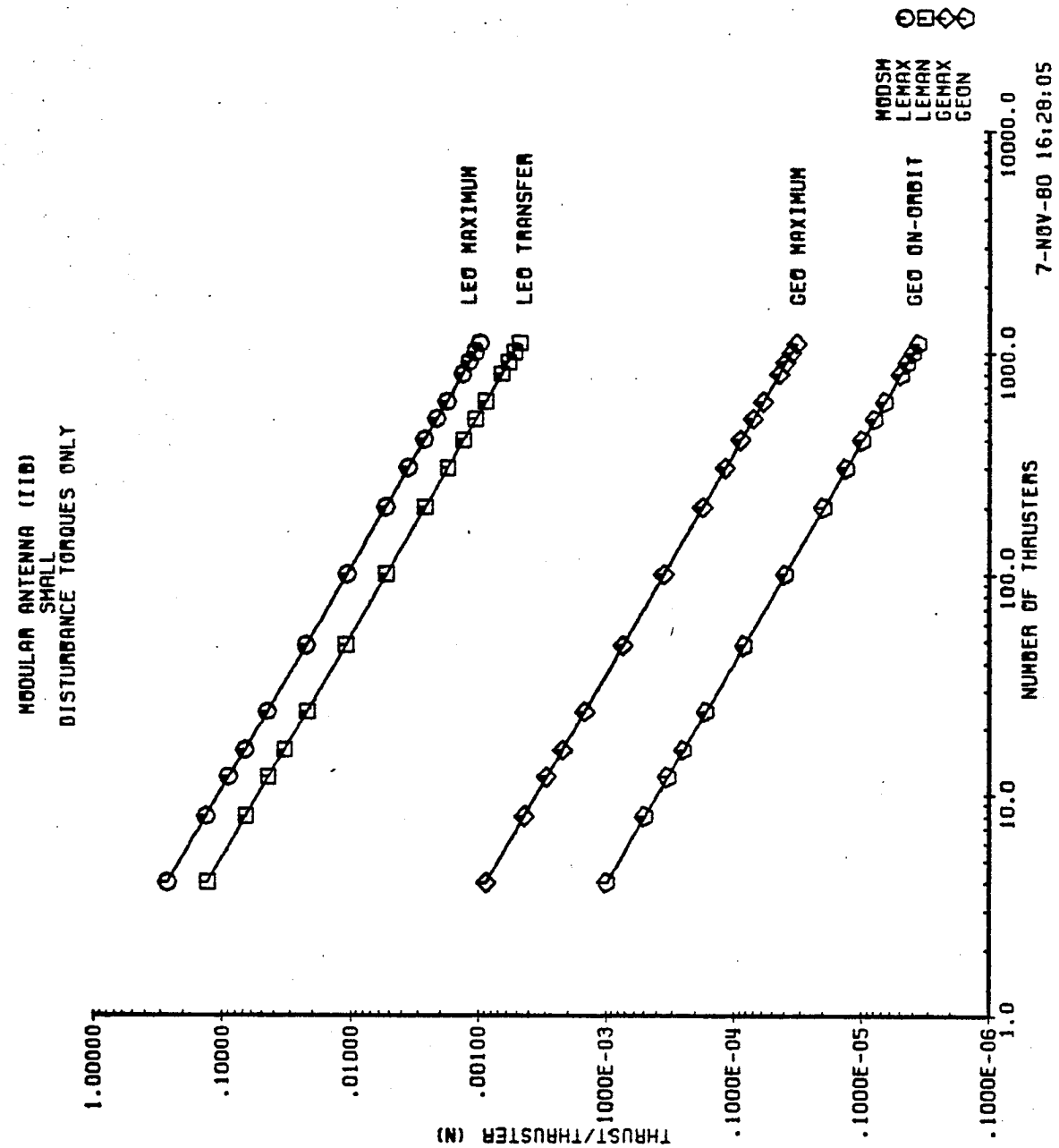

FIGURE D-10 SMALL MODULAR ANTENNA THRUST/THRUSTER REQUIREMENTS DUE TO DISTURBANCE TORQUES

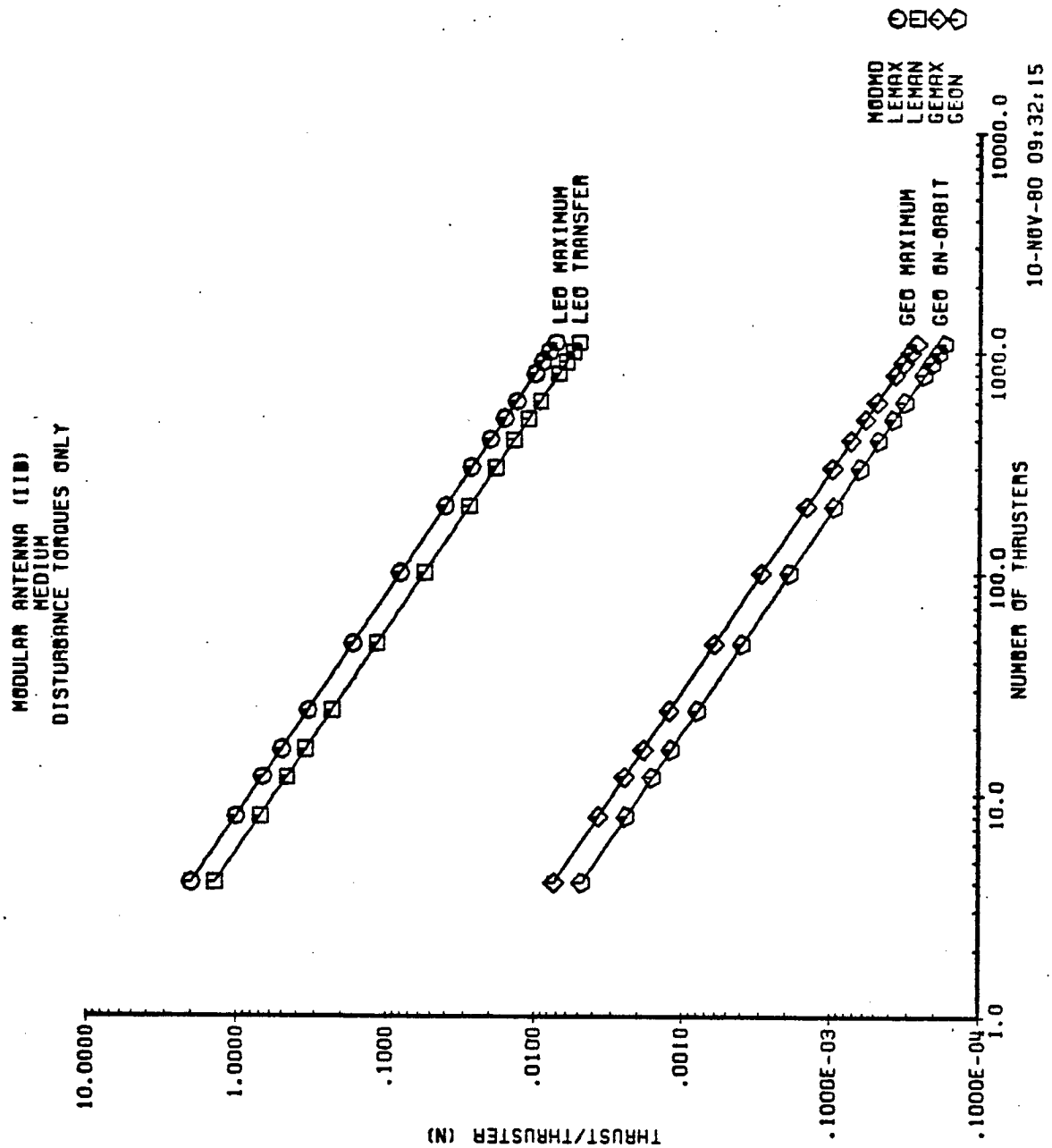

FIGURE D-11 MEDIUM MODULAR ANTENNA THRUST/THRUSTER REQUIREMENTS DUE TO DISTURBANCE TORQUES

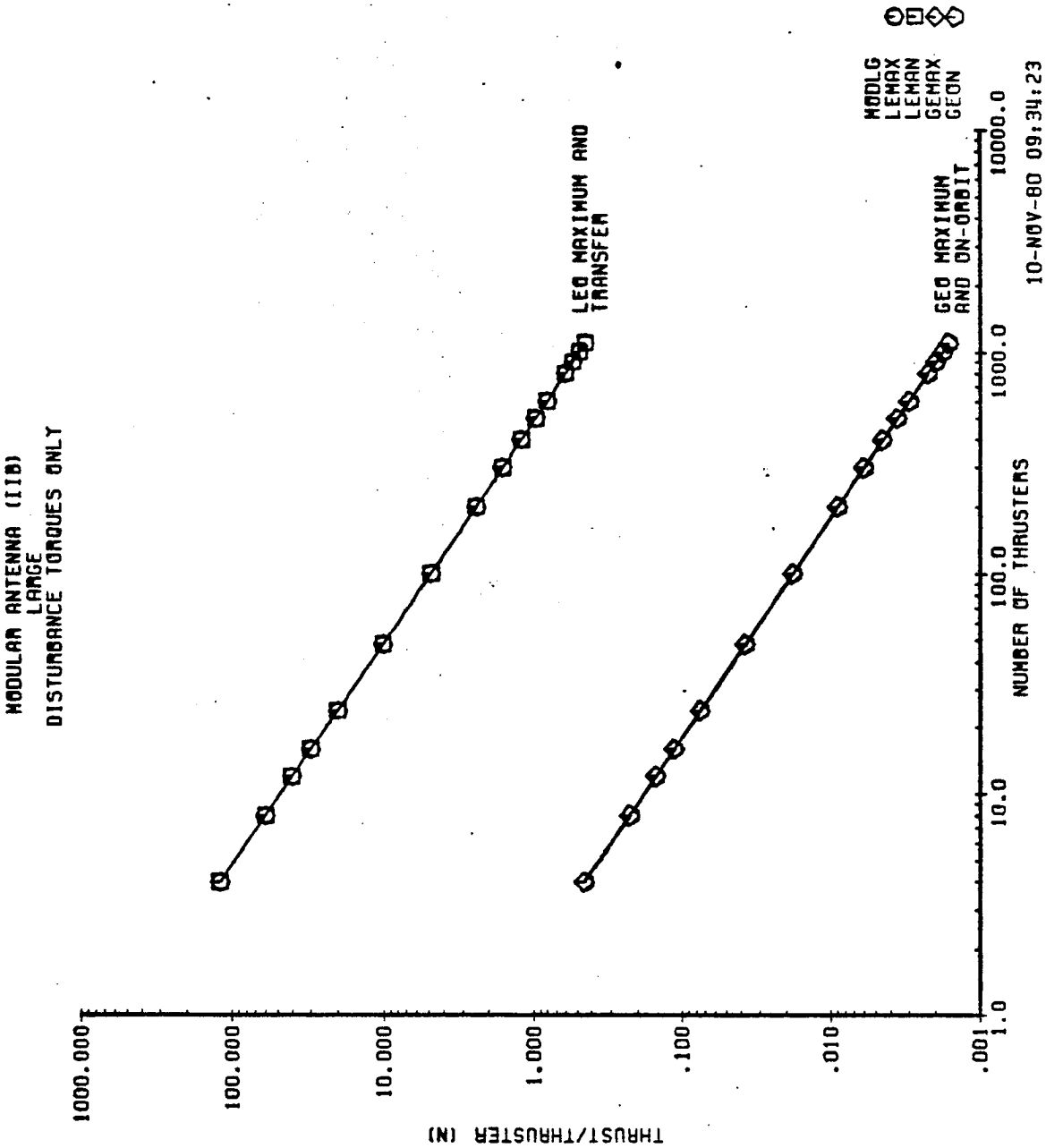

FIGURE D-12 LARGE MODULAR ANTENNA THRUST/THRUSTER REQUIREMENTS DUE TO DISTURBANCE TORQUES

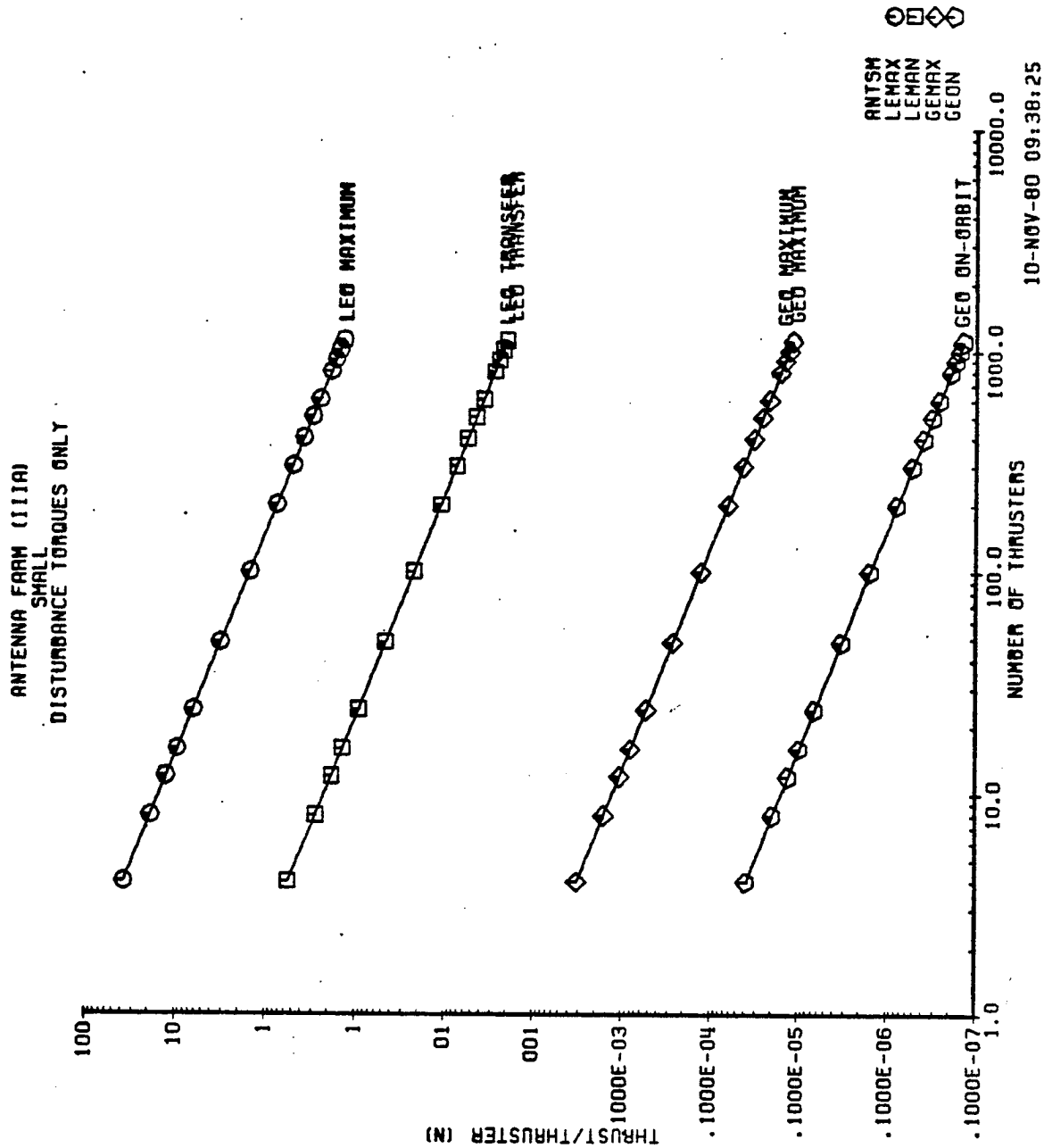

FIGURE D-13 SMALL ANTENNA FARM THRUST/THRUSTER REQUIREMENTS DUE TO DISTURBANCE TORQUES

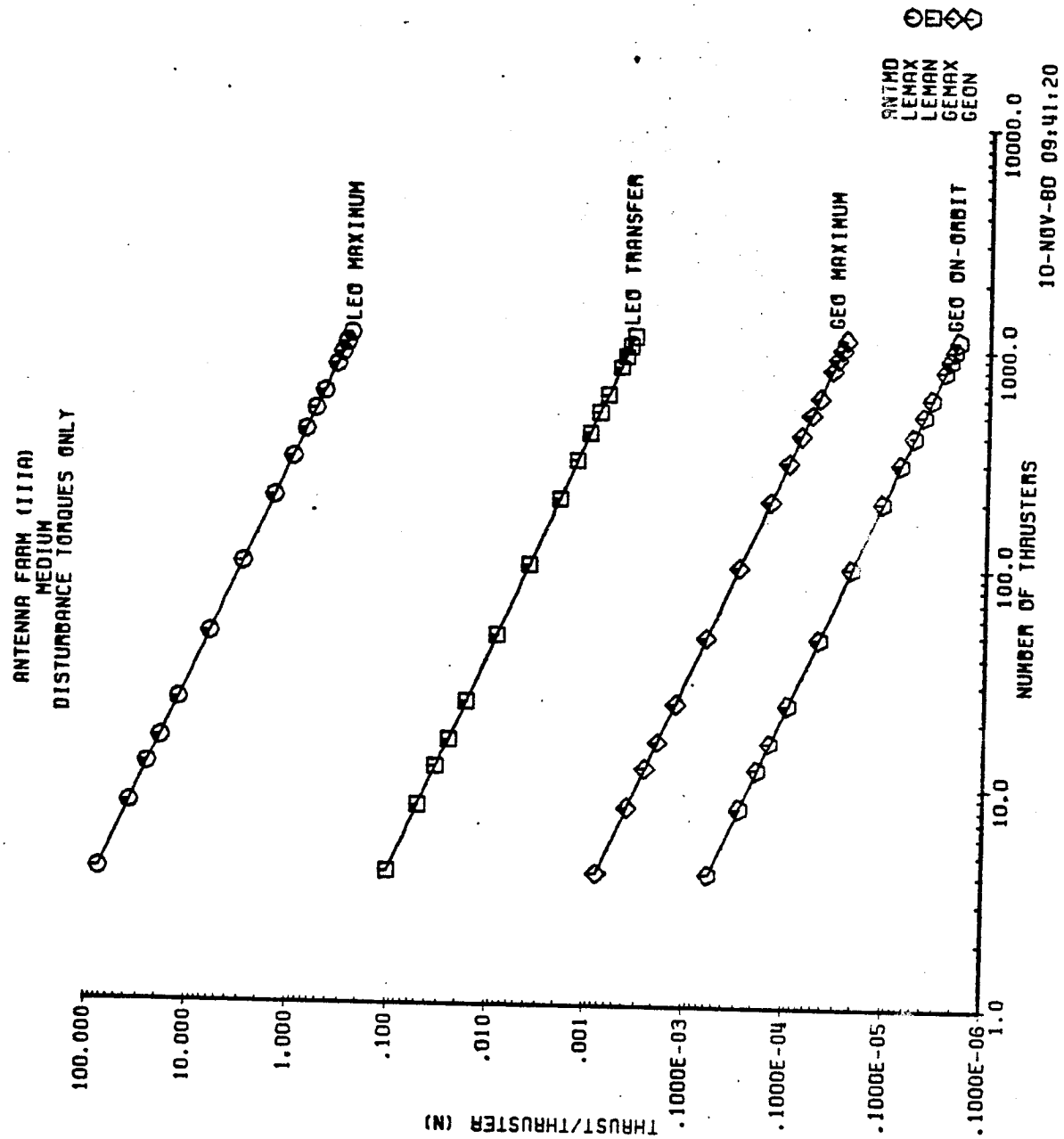

FIGURE D-14 MEDIUM ANTENNA FARM THRUST/THRUSTER REQUIREMENTS DUE TO DISTURBANCE TORQUES

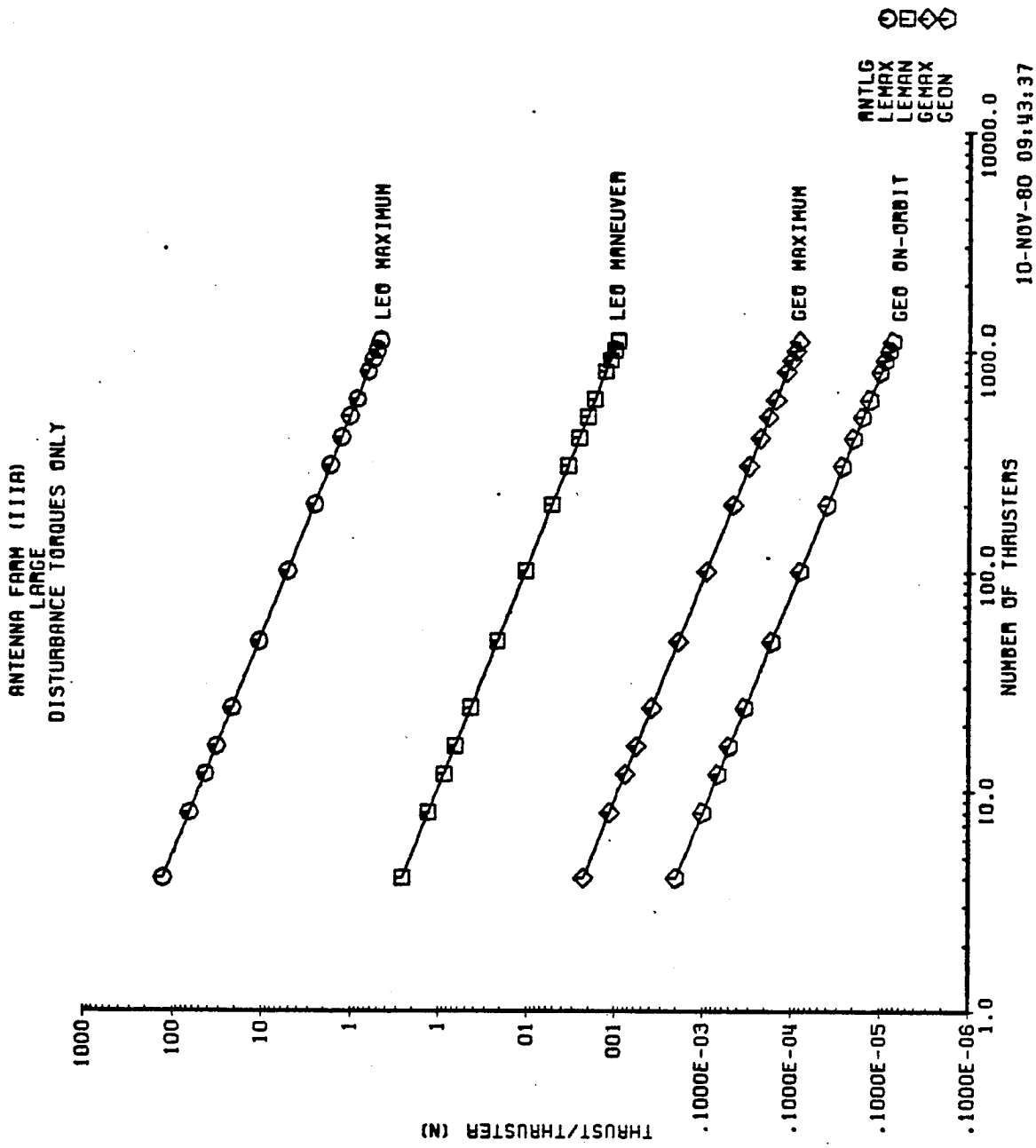

FIGURE D-15 LARGE ANTENNA FARM THRUST/THRUSTER REQUIREMENTS DUE TO DISTURBANCE TORQUES

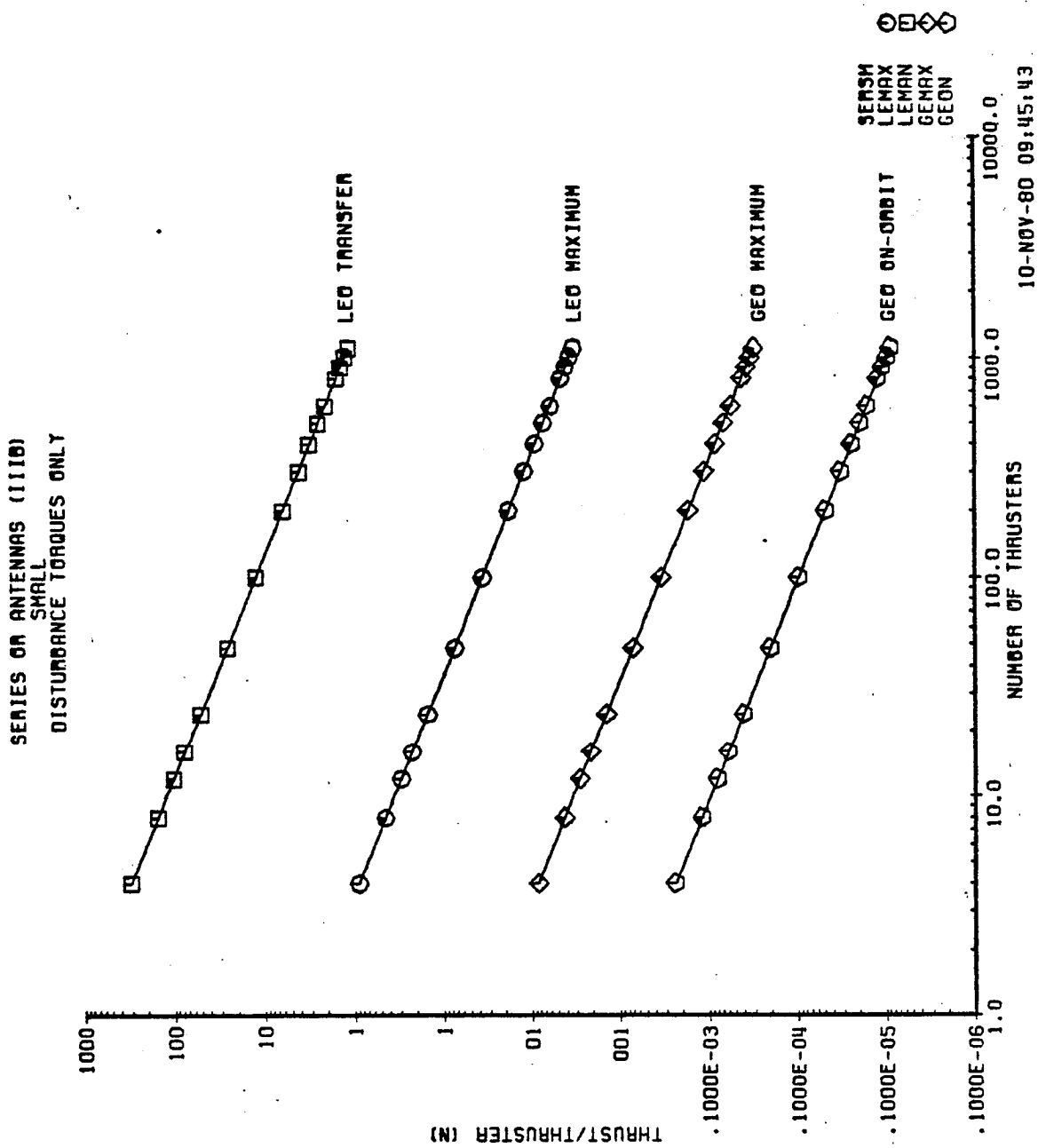

FIGURE D-16 SMALL SERIES OF ANTENNAS THRUST/THRUSTER REQUIREMENTS DUE TO DISTURBANCE TORQUES

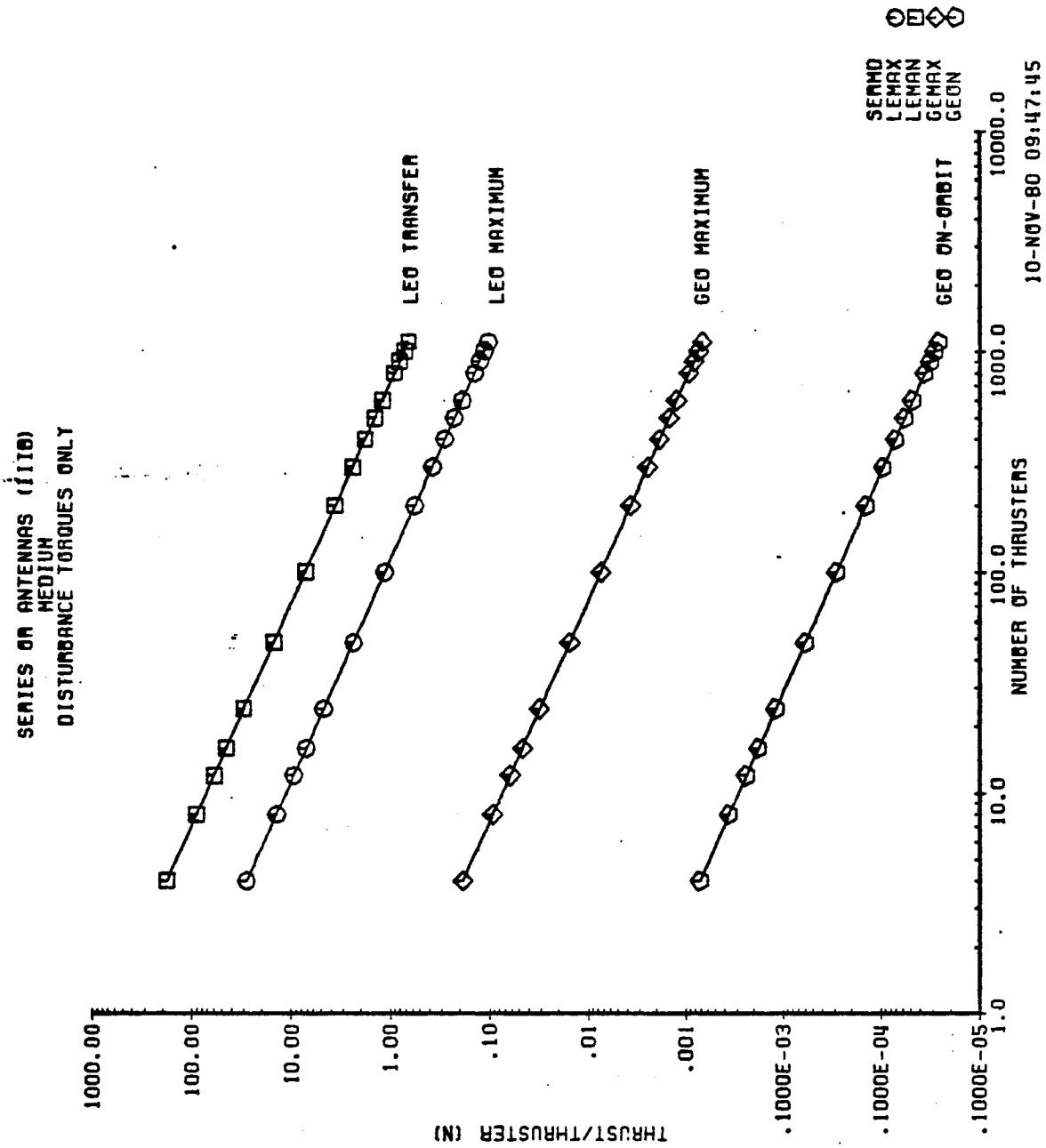

FIGURE D-17 MEDIUM SERIES OF ANTENNAS THRUST/THRUSTER REQUIREMENTS DUE TO DISTURBANCE TORQUES

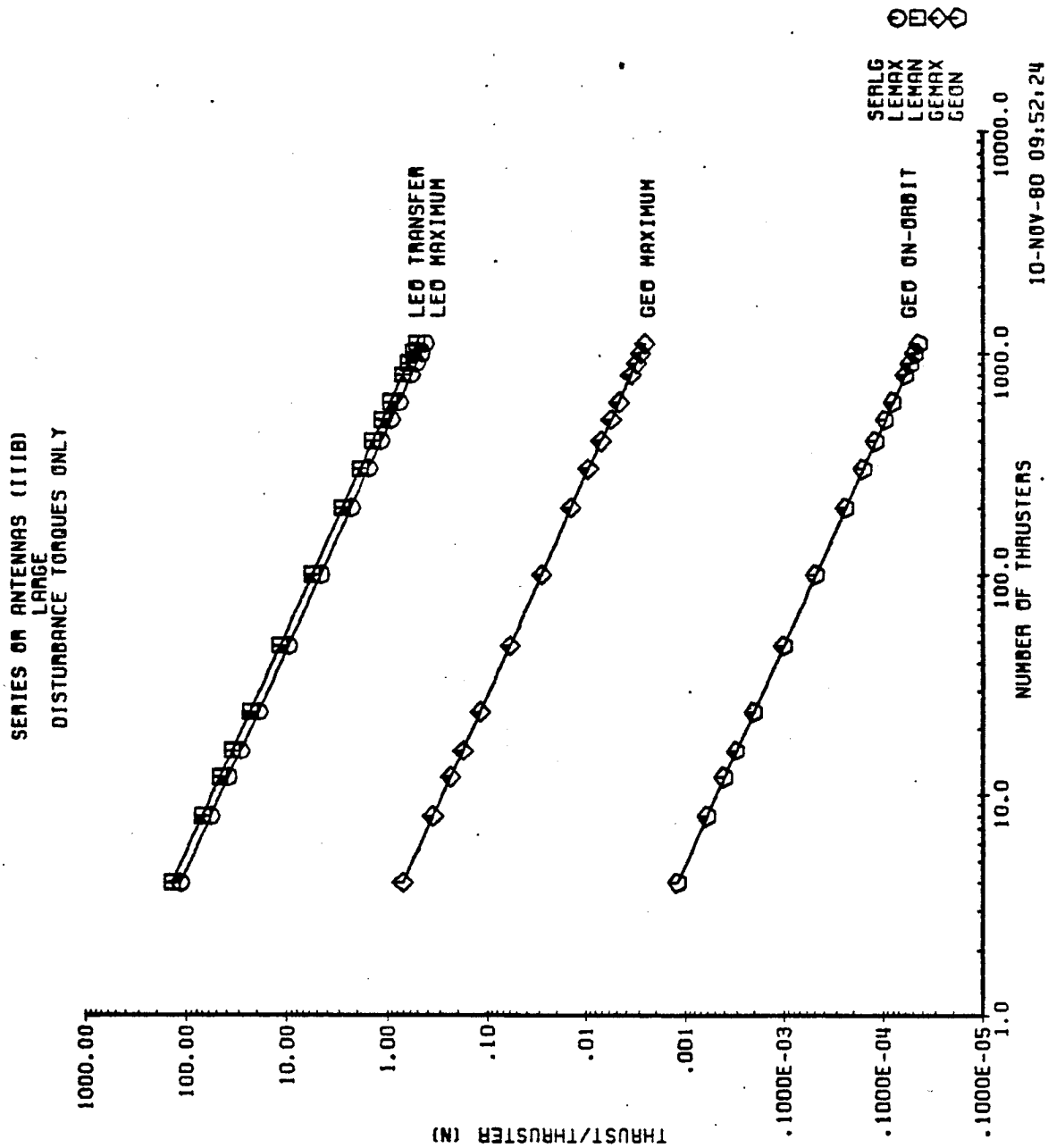

FIGURE D-18 LARGE SERIES OF ANTENNAS THRUST/THRUSTER REQUIREMENTS DUE TO DISTURBANCE TORQUES

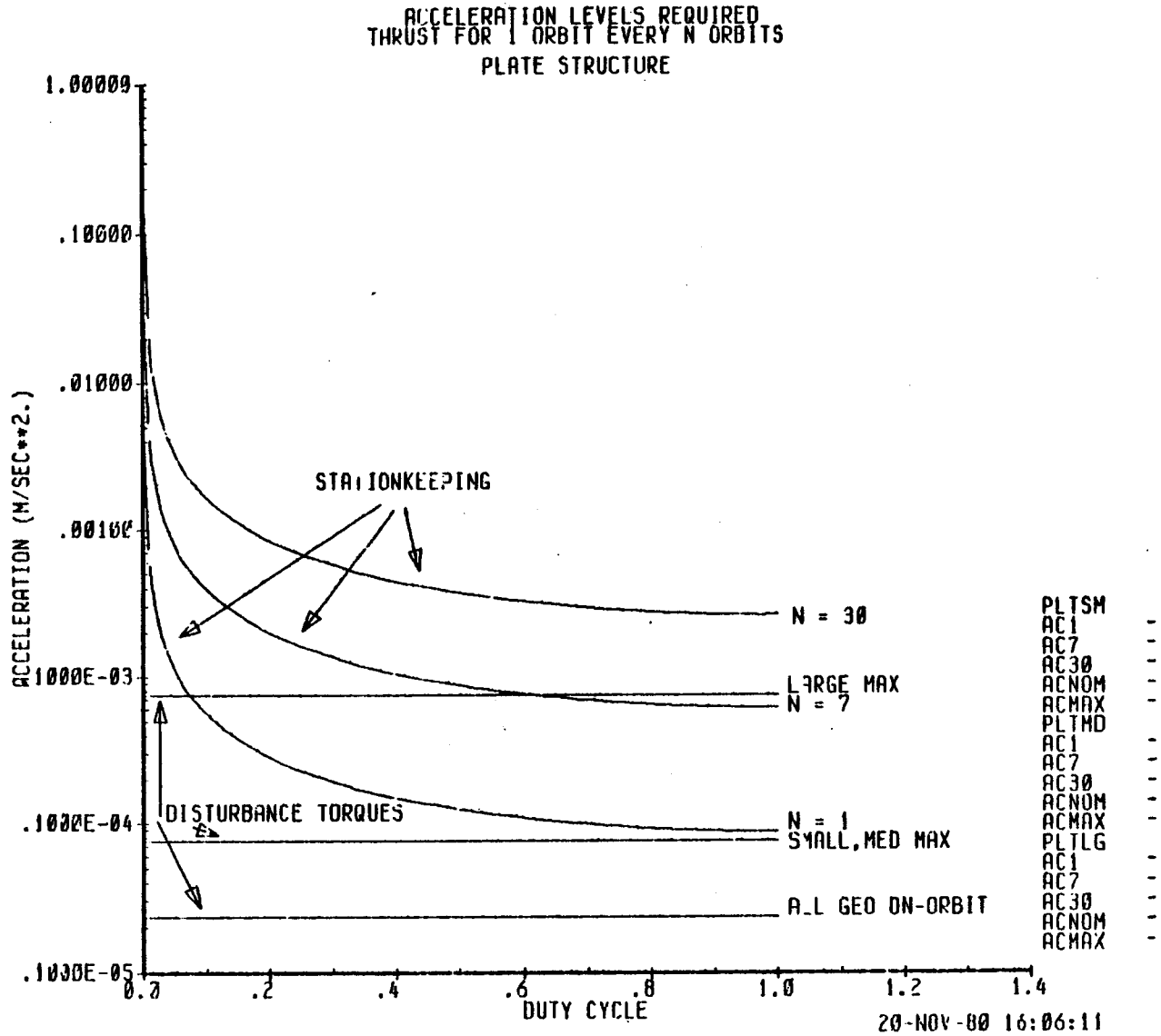

FIGURE D-19 PLATE STRUCTURE ACCELERATION LEVELS REQUIRED

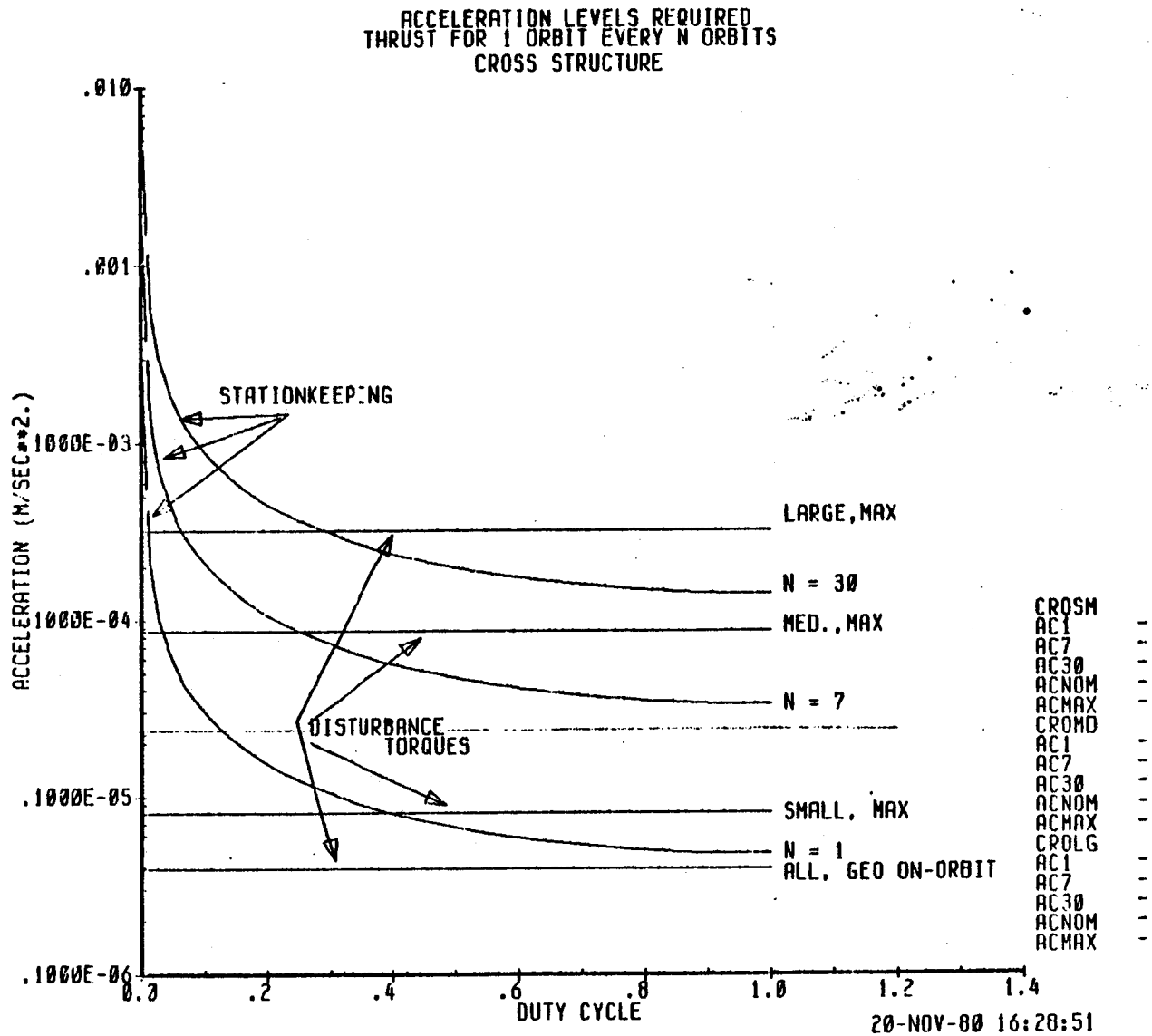

FIGURE D-20 CROSS STRUCTURE ACCELERATION LEVELS REQUIRED

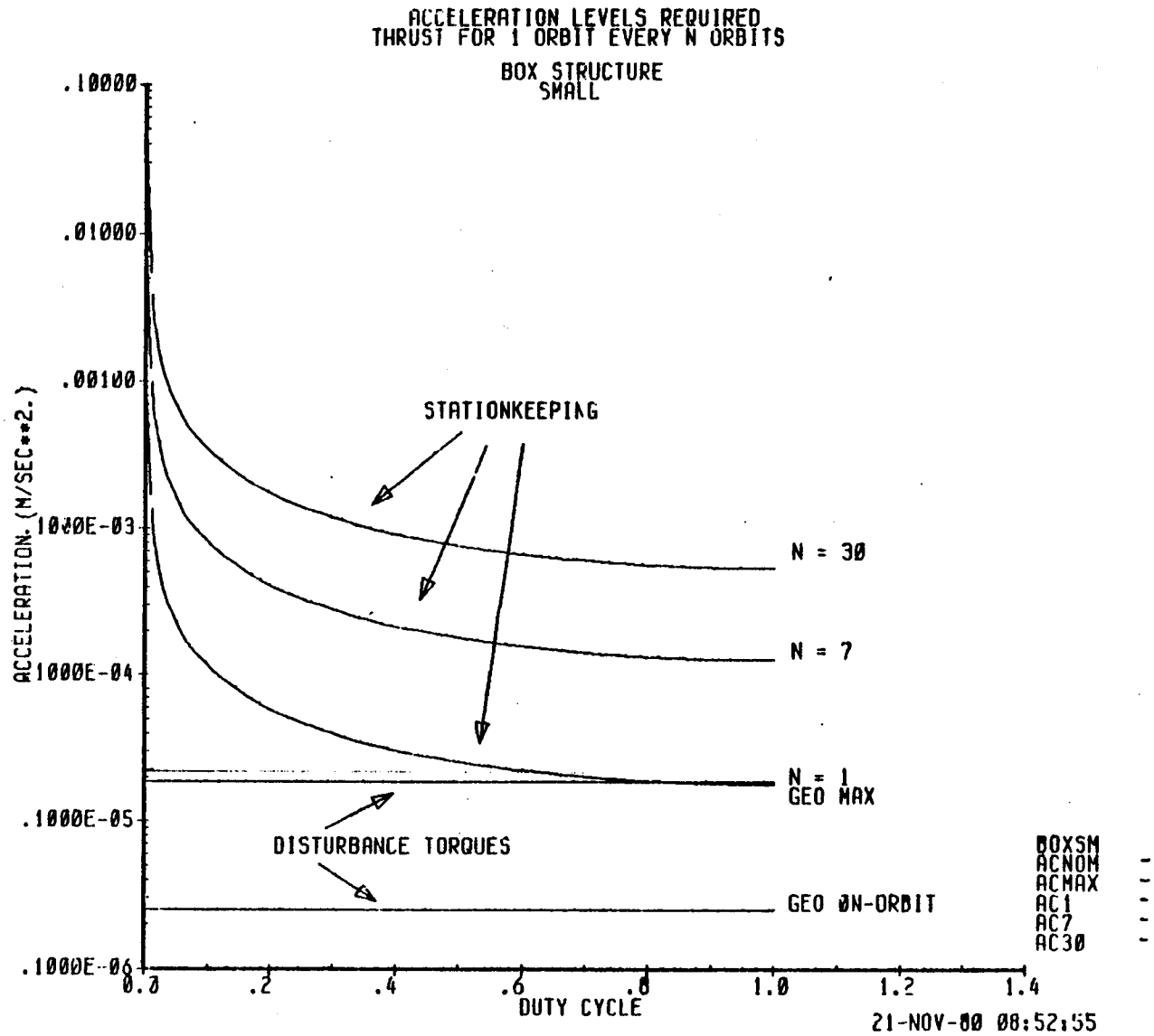

FIGURE D-21 SMALL BOX STRUCTURE ACCELERATION LEVELS REQUIRED

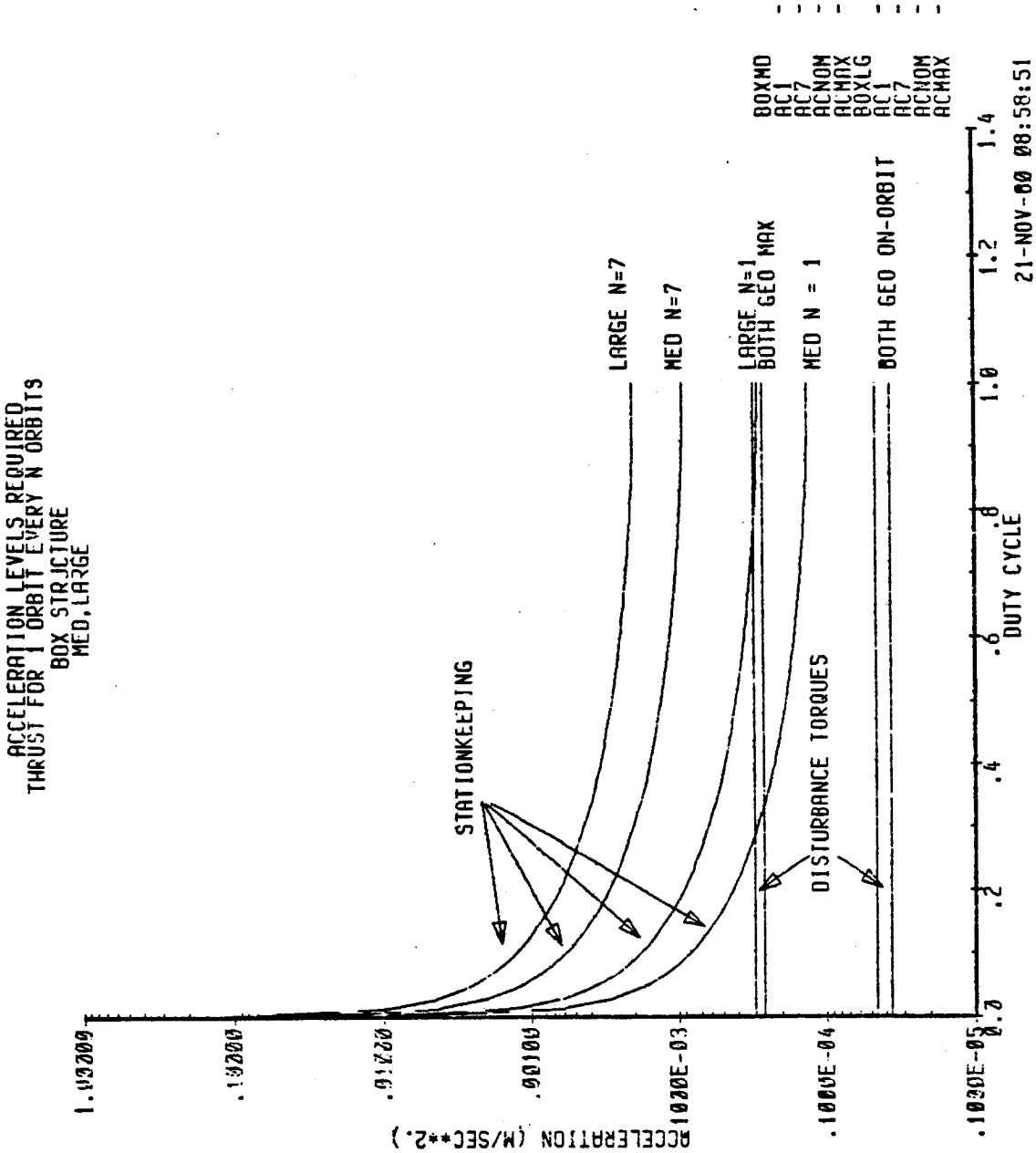

FIGURE D-22 MED & LARGE BOX STRUCTURE ACCELERATION LEVELS REQUIRED

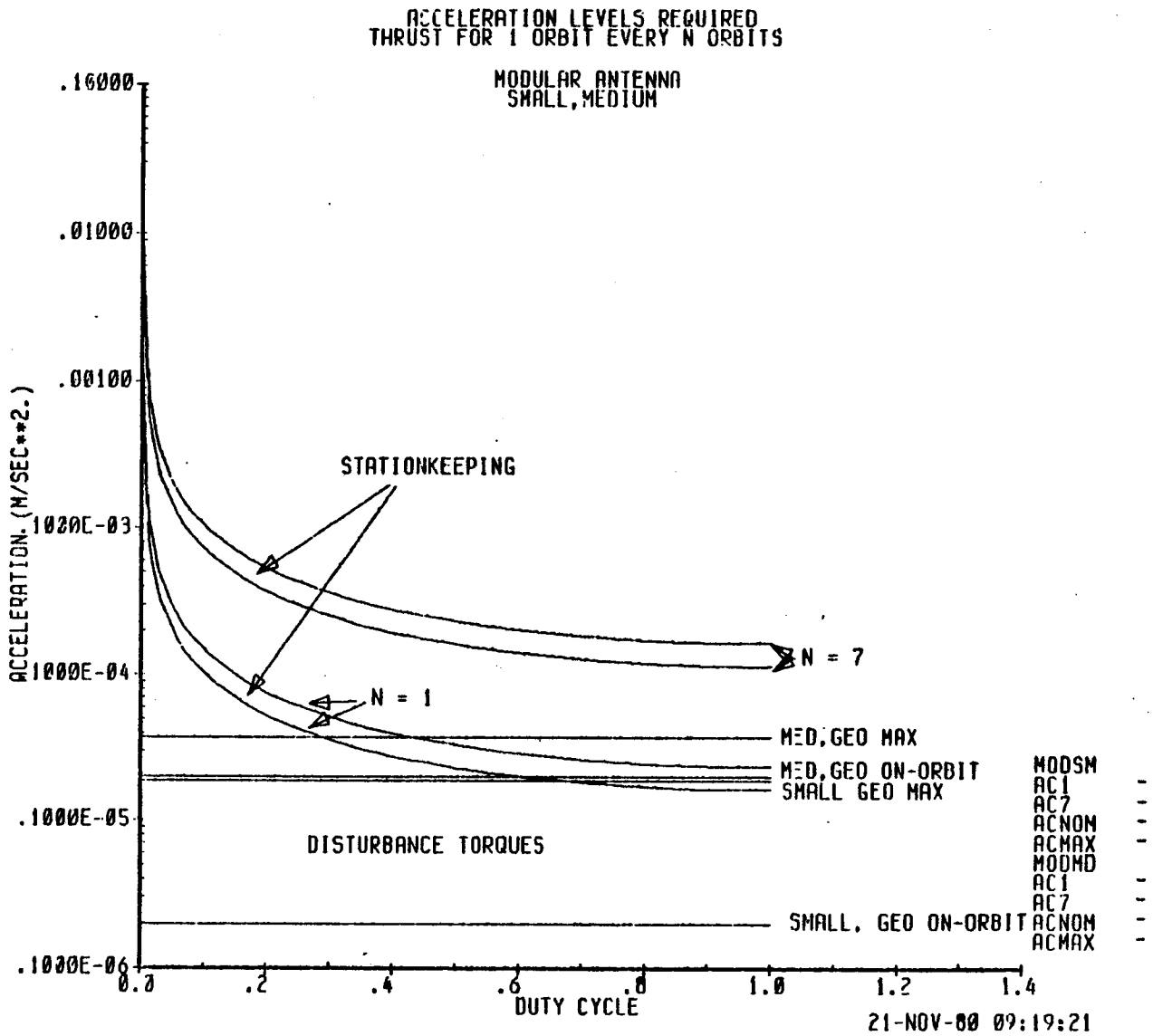

FIGURE D-23 SMALL & MED MODULAR ANTENNA ACCELERATION LEVELS REQUIRED

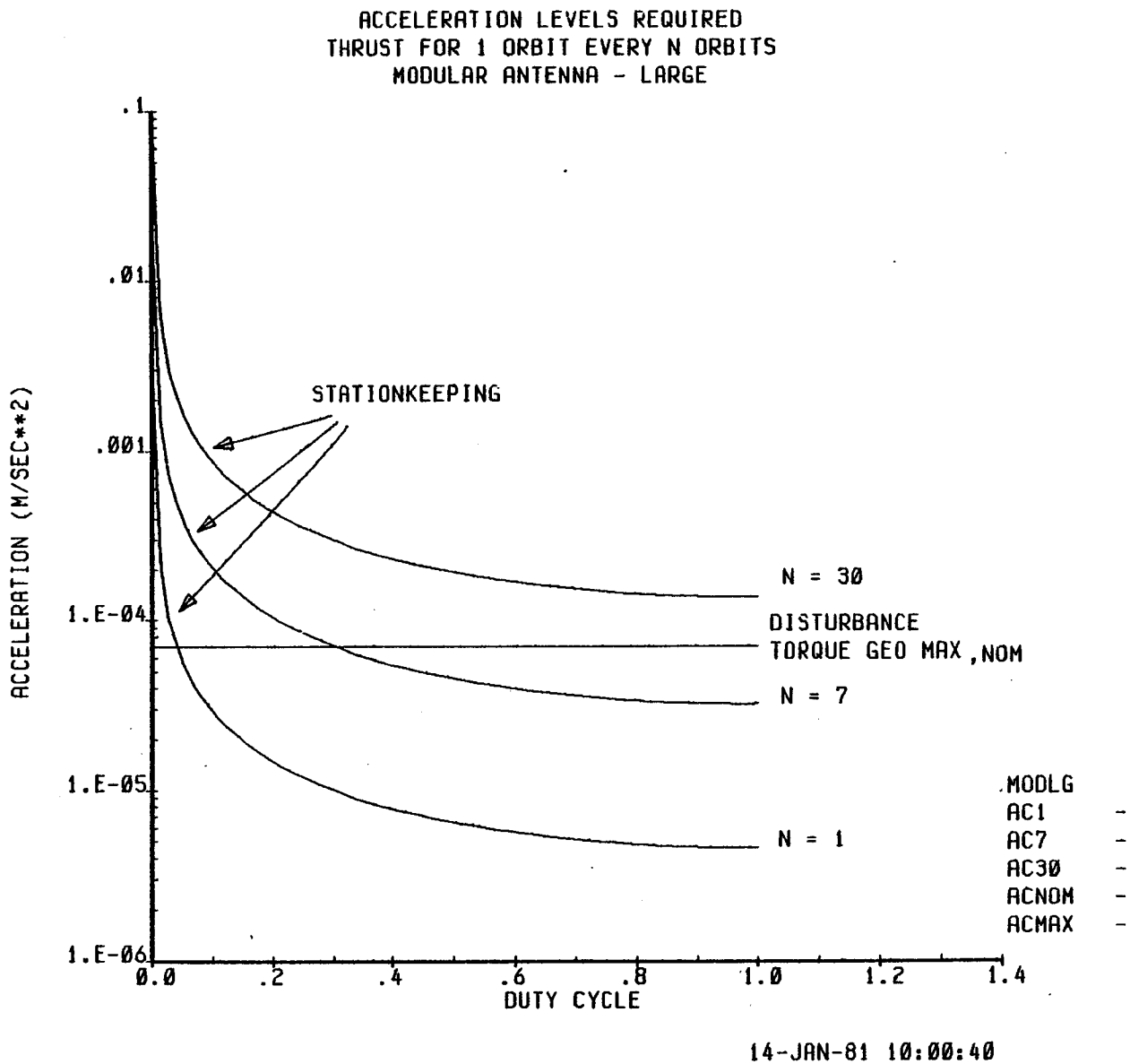

FIGURE D-24 LARGE MODULAR ANTENNA ACCELERATION LEVELS REQUIRED

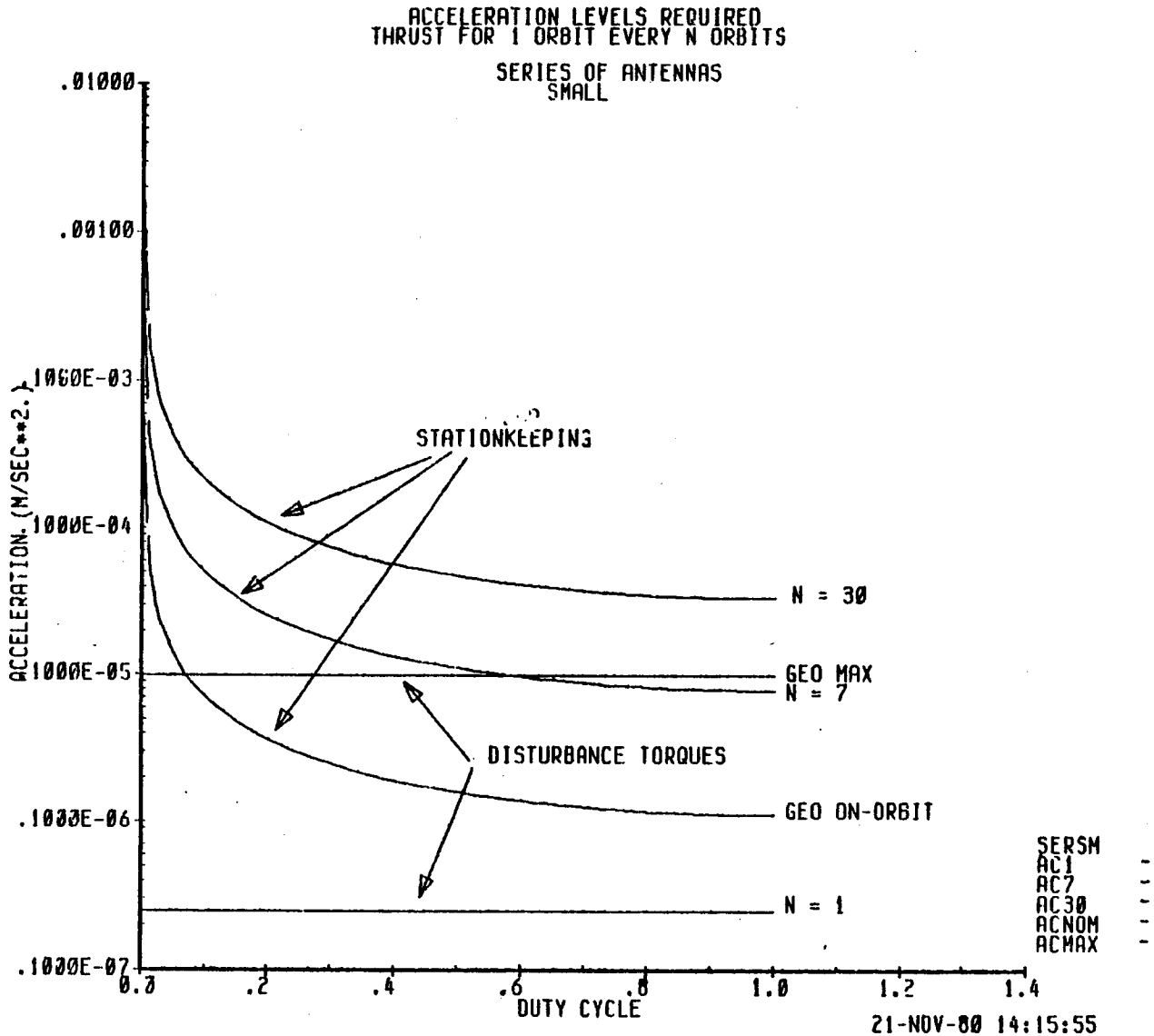

FIGURE D-25 SMALL SERIES OF ANTENNAS ACCELERATION LEVELS REQUIRED

Figure 6.6

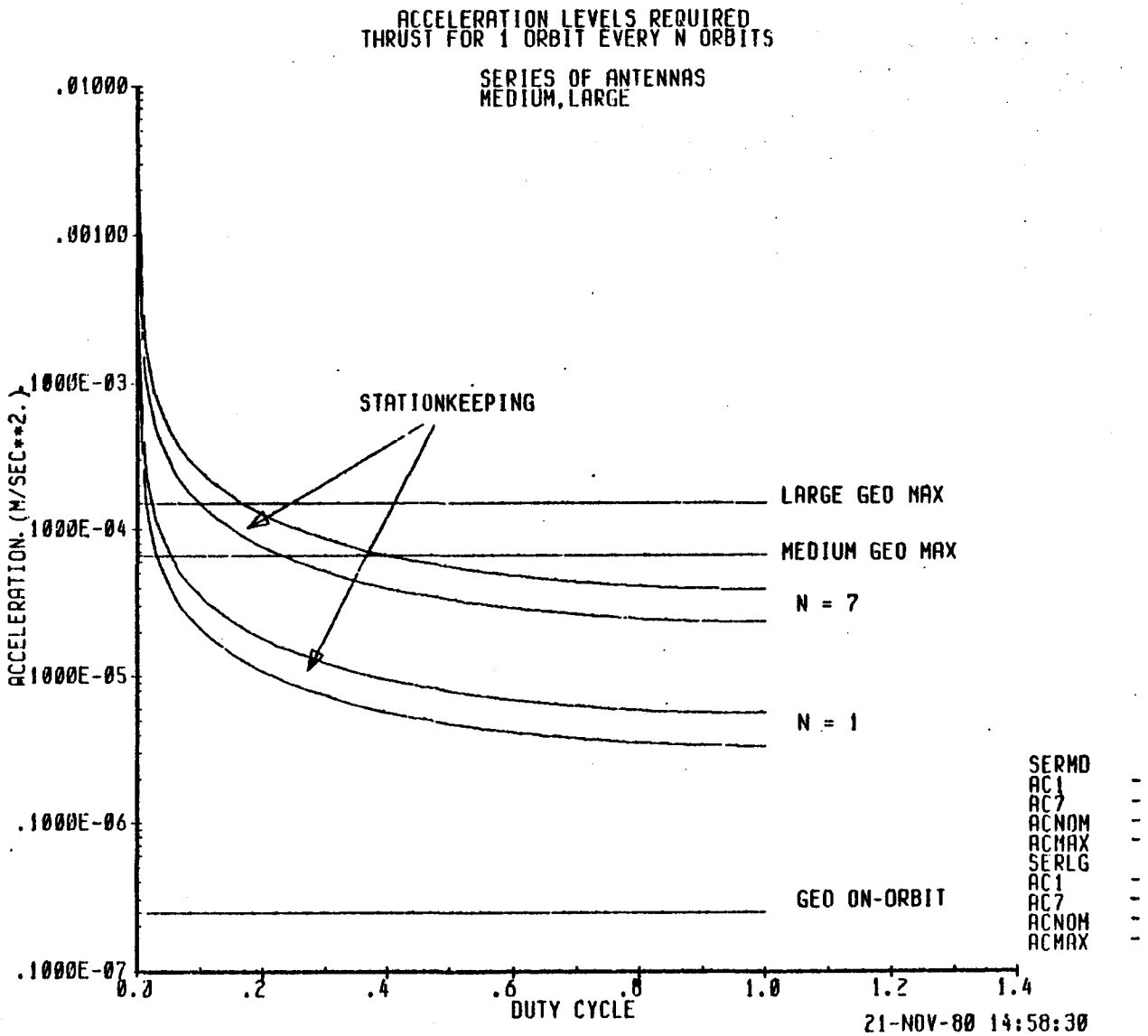

FIGURE D-26 MED & LARGE SERIES OF ANTENNAS ACCELERATION LEVELS REQUIRED

Figure 6.7

FIGURE D-27

TORQUE COMPOSITE BREAKDOWN
PLATE STRUCTURE W/O BLANKET - SMALL (30 M)
CP-CG = 5% OF MAX. DIM.

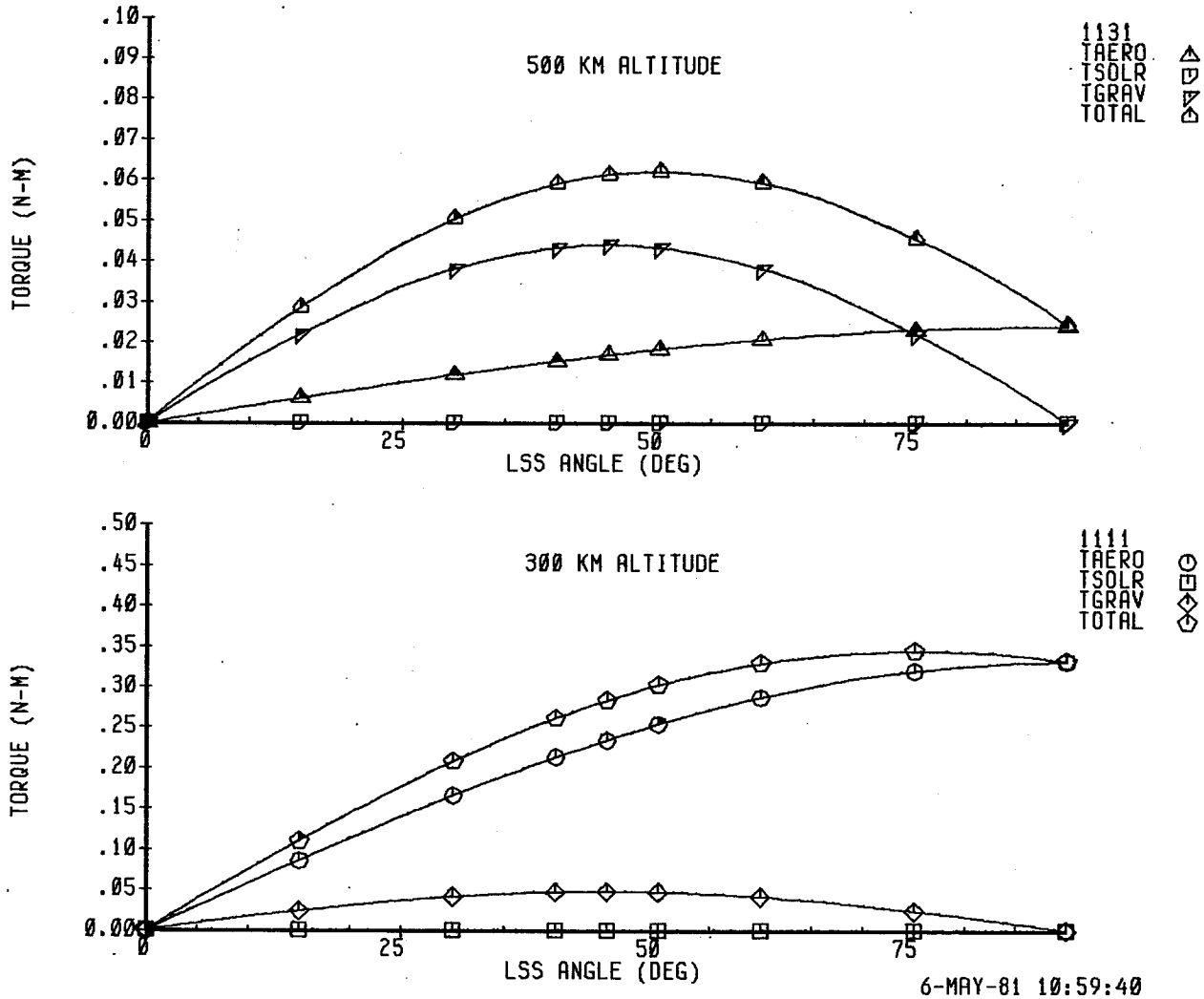

FIGURE D-28

TORQUE COMPOSITE BREAKDOWN
PLATE STRUCTURE W/O BLANKET - LARGE (250 M)
CP-CG = 5% OF MAX. DIM.

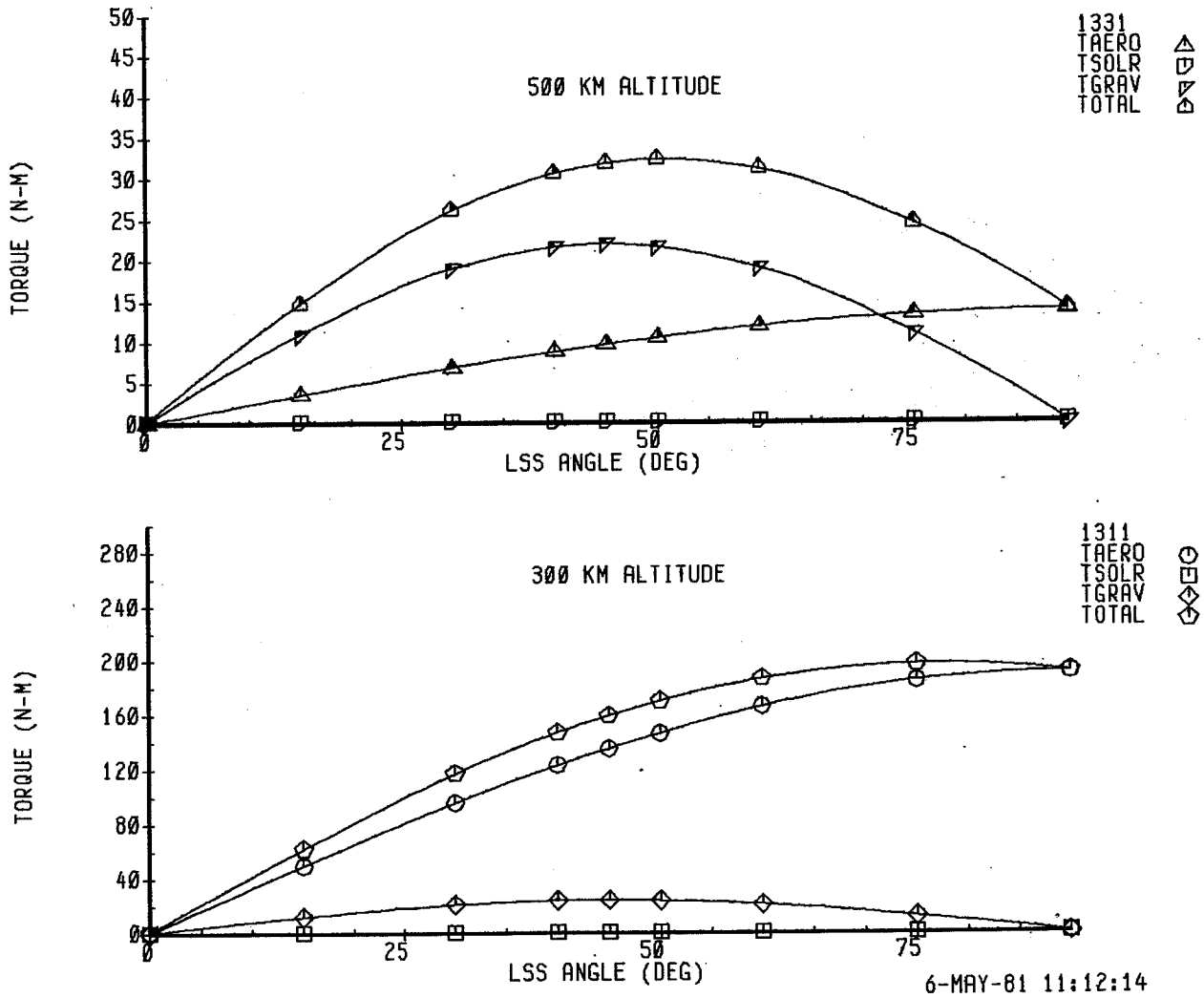

FIGURE D-29
TORQUE COMPOSITE BREAKDOWN
PLATE STRUCTURE W/BLANKET - SMALL (30 M)
CP-CG = 5% OF MAX. DIM.

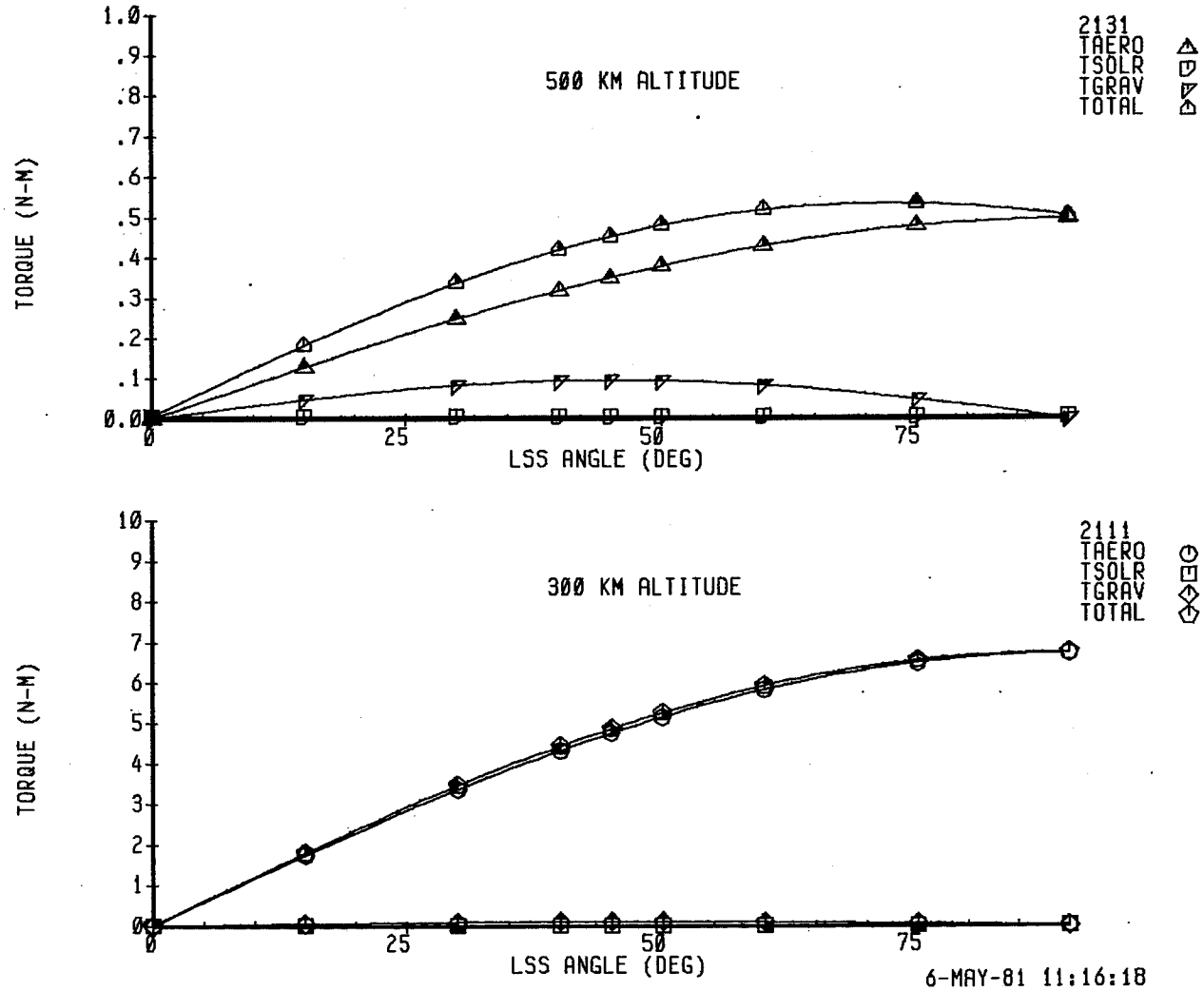

FIGURE D-30
TORQUE COMPOSITE BREAKDOWN
PLATE STRUCTURE W/BLANKET - MEDIUM (100 M)
CP-CG = 5% OF MAX. DIM.

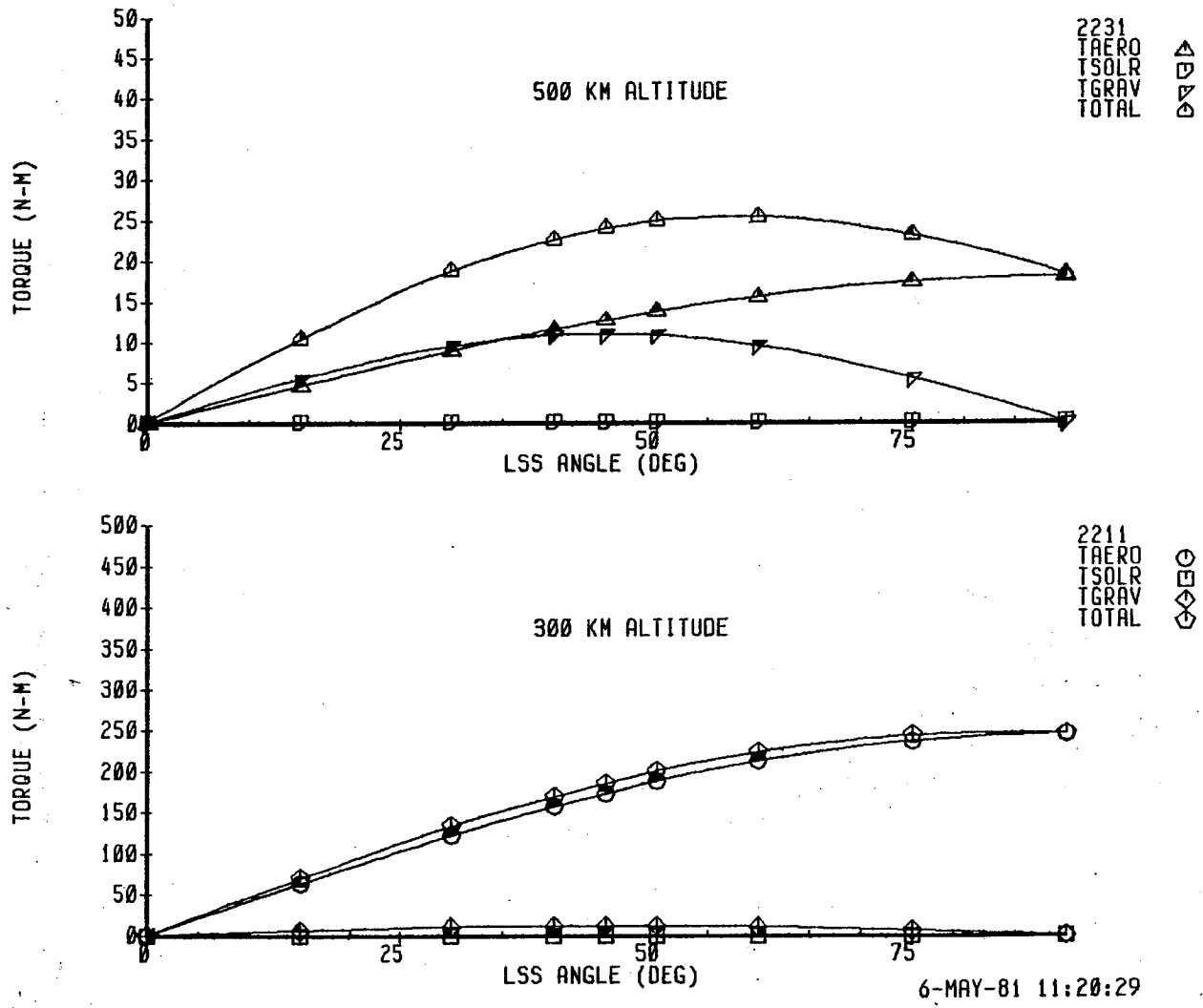

FIGURE D-31
TORQUE COMPOSITE BREAKDOWN
PLATE STRUCTURE W/BLANKET - LARGE (150 M)
CP-CG = 5% OF MAX. DIM.

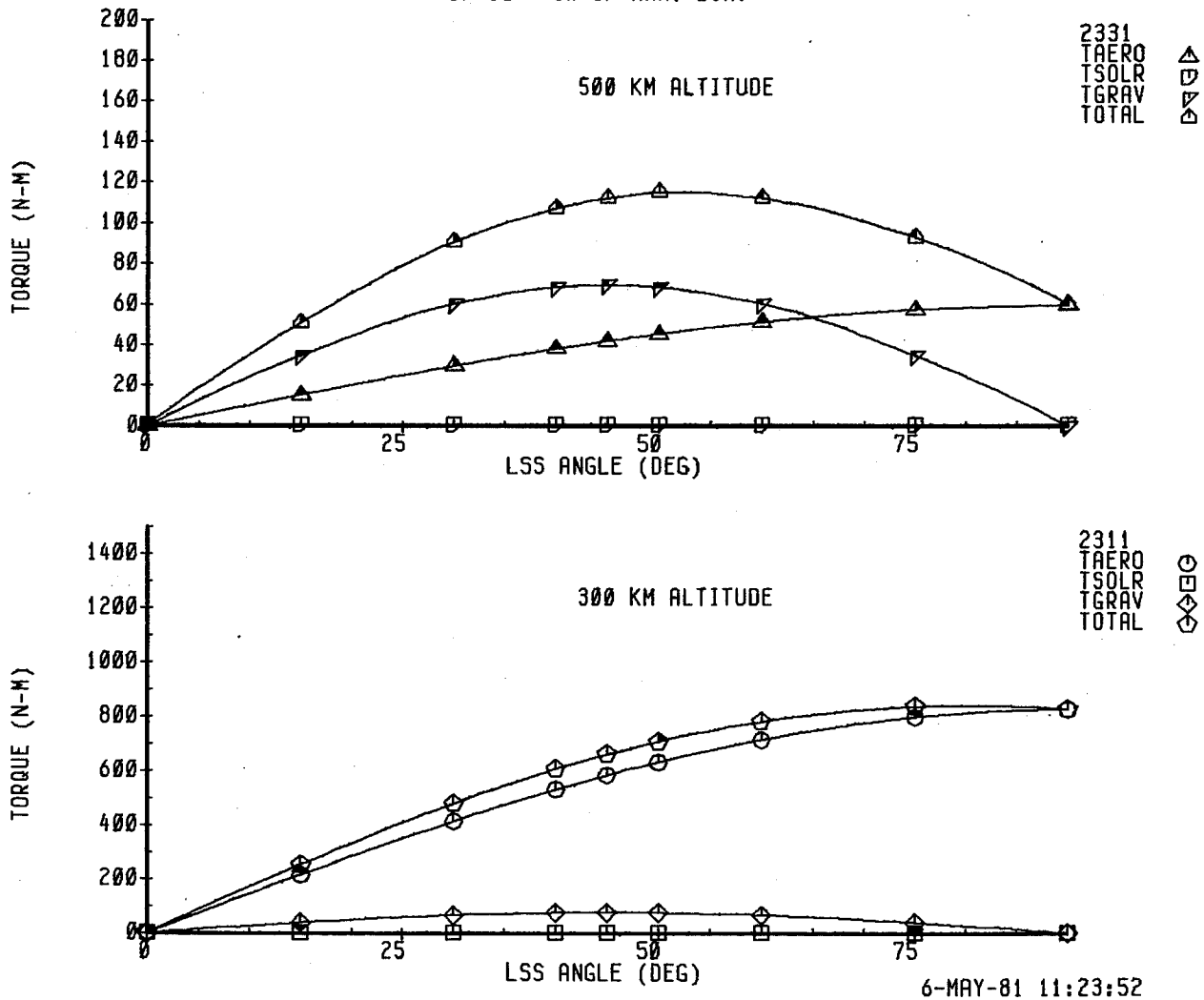

FIGURE D-32
TORQUE COMPOSITE BREAKDOWN
MODULAR ANTENNA - SMALL (15 M)
CP-CG = 5% OF MAX. DIM.

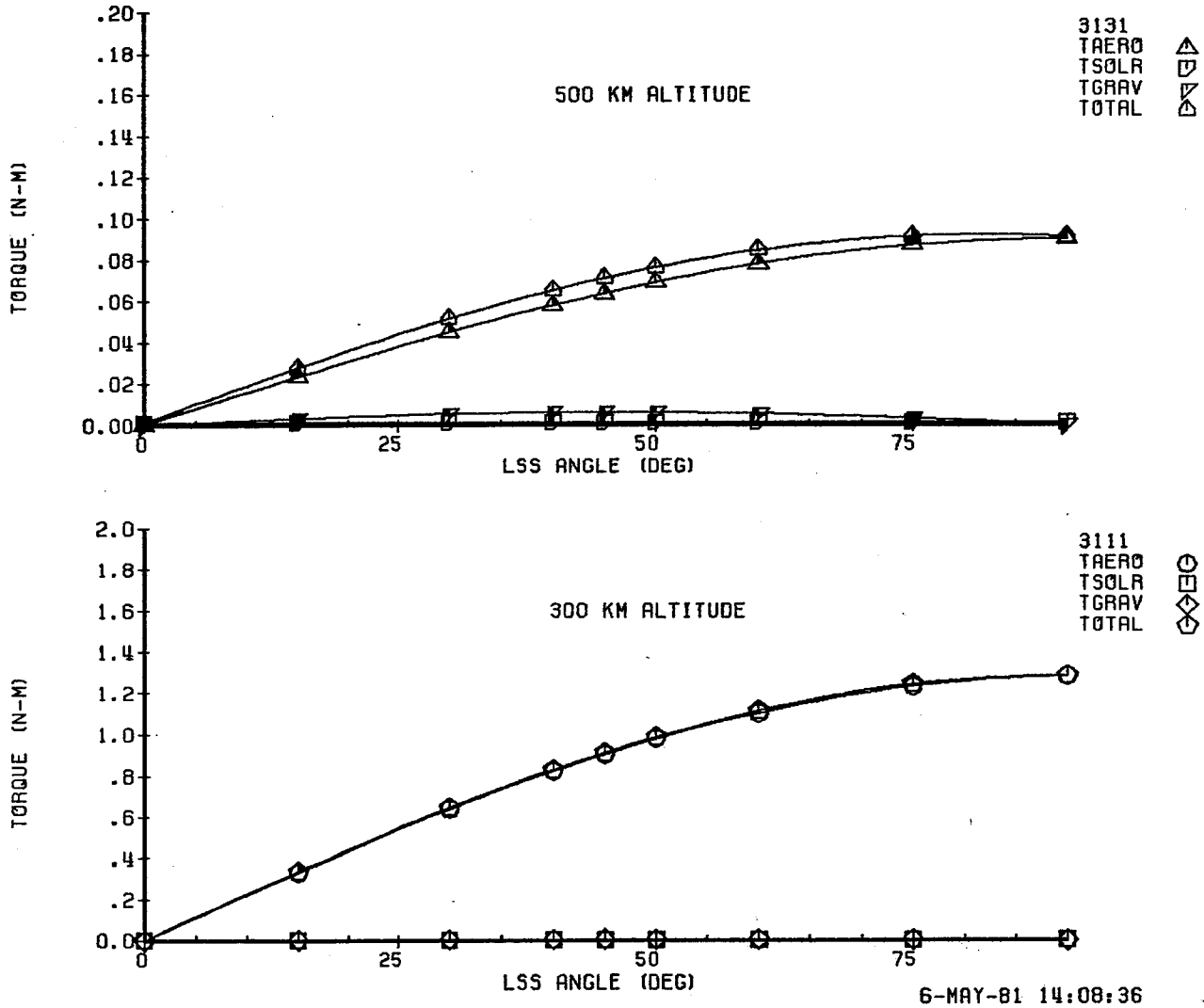

FIGURE D-33
TORQUE COMPOSITE BREAKDOWN
MODULAR ANTENNA - MEDIUM (60 M)
CP-CG = 5% OF MAX. DIM.

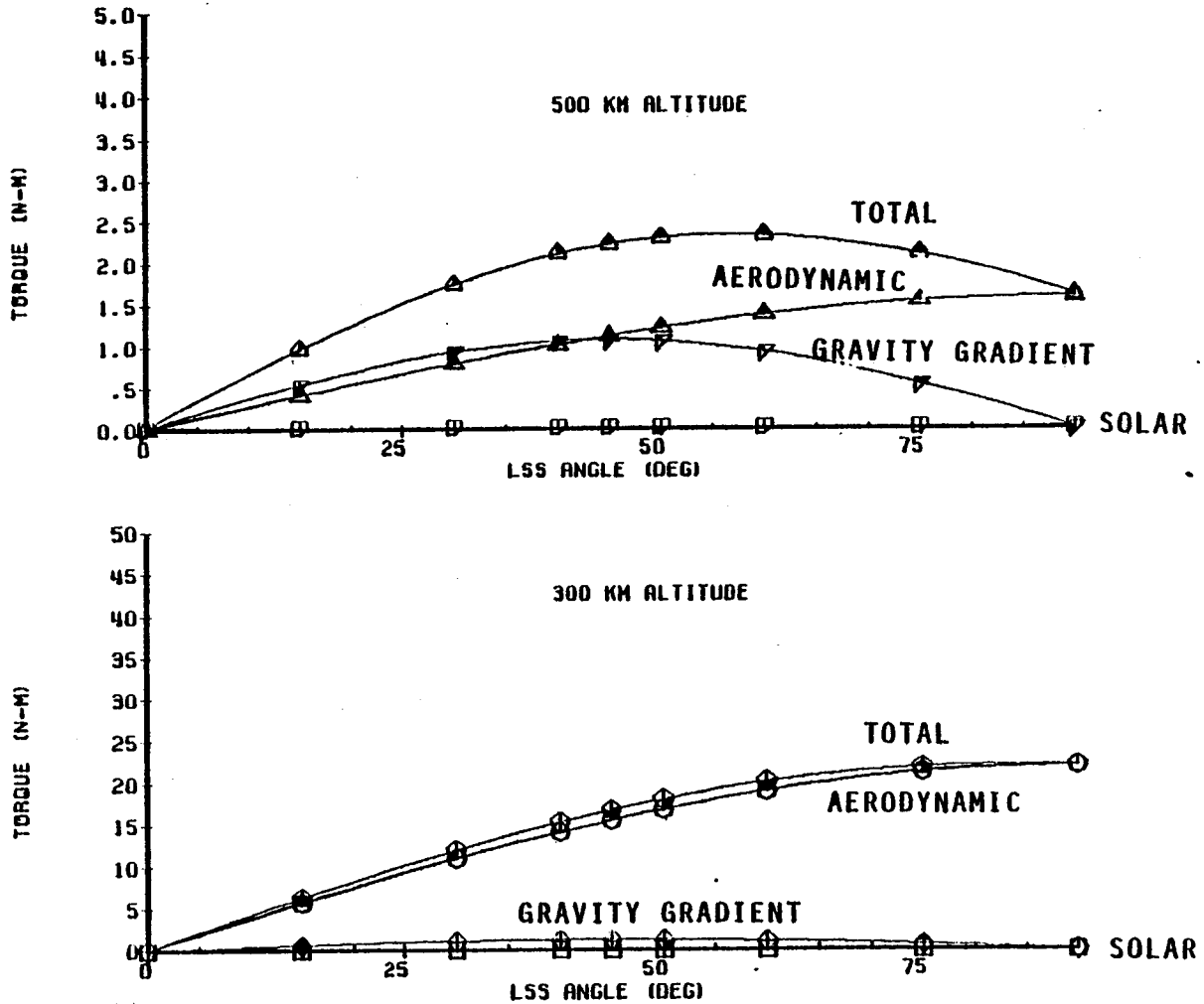

FIGURE D-34
TORQUE COMPOSITE BREAKDOWN
MODULAR ANTENNA - LARGE (200 M)
CP-CG = 5% OF MAX. DIM.

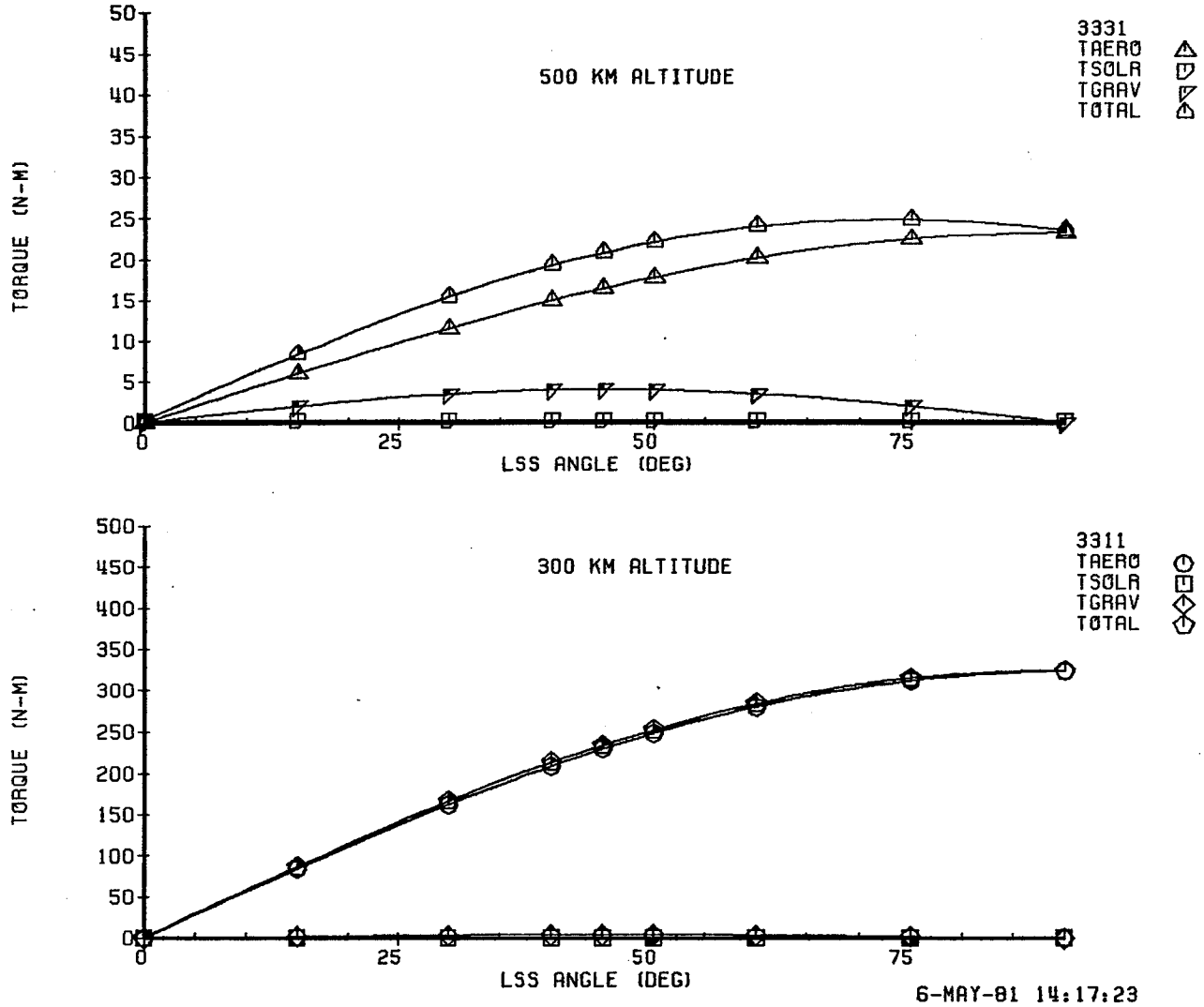

PAGE
D35 & D36
MISSING

FIGURE D-37
TORQUE COMPOSITE BREAKDOWN
SERIES OF ANTENNAS - LARGE (4)
CP-CG = 5% OF MAX. DIM.

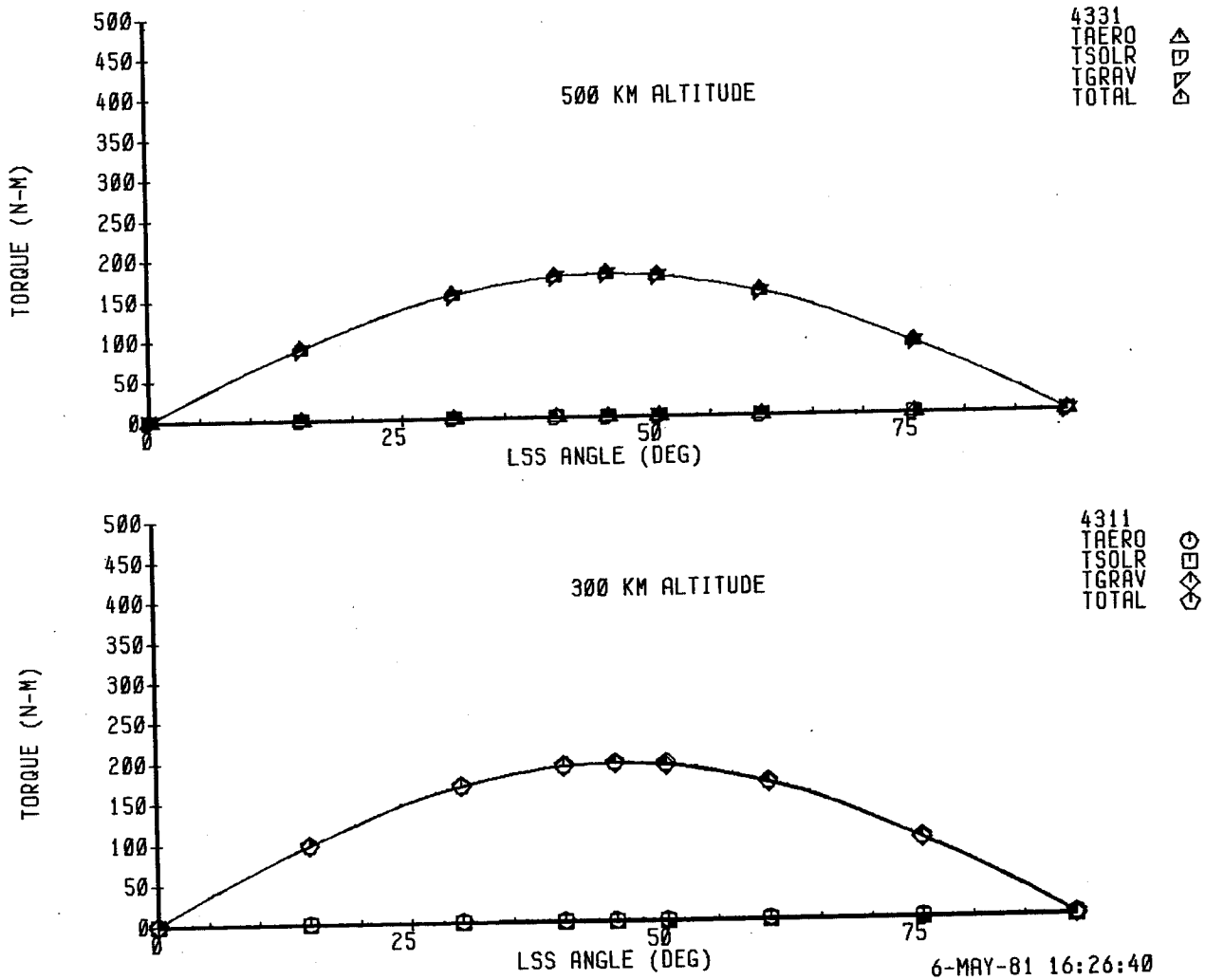

FIGURE D-38
TOTAL TORQUE REQUIREMENT
PLATE STRUCTURE W/O BLANKET - SMALL (30 M)
CP-CG = 5% MAX. DIM.

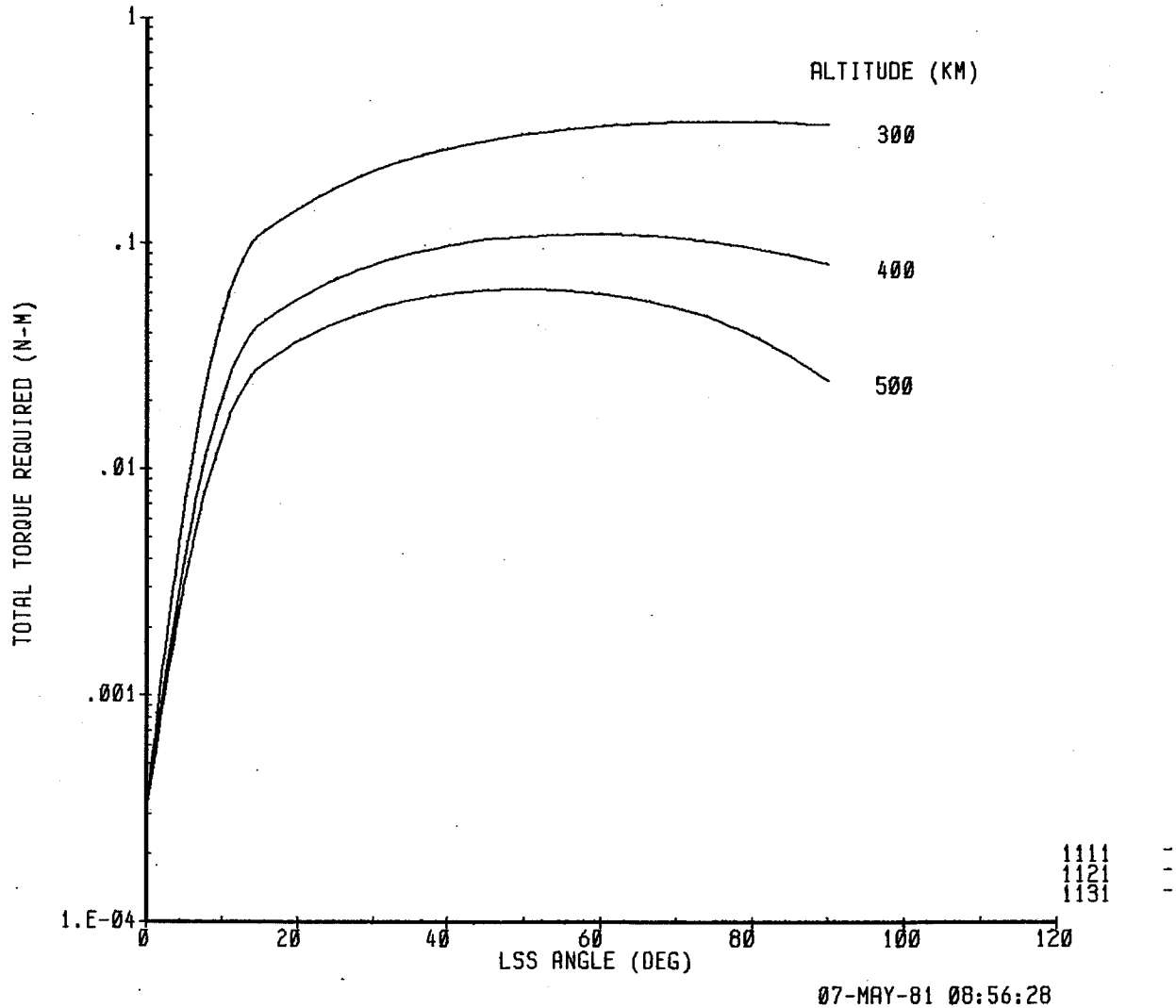

FIGURE D-39
TOTAL TORQUE REQUIREMENT
PLATE STRUCTURE W/O BLANKET - MEDIUM (100 M)
CP-CG = 5% MAX. DIM.

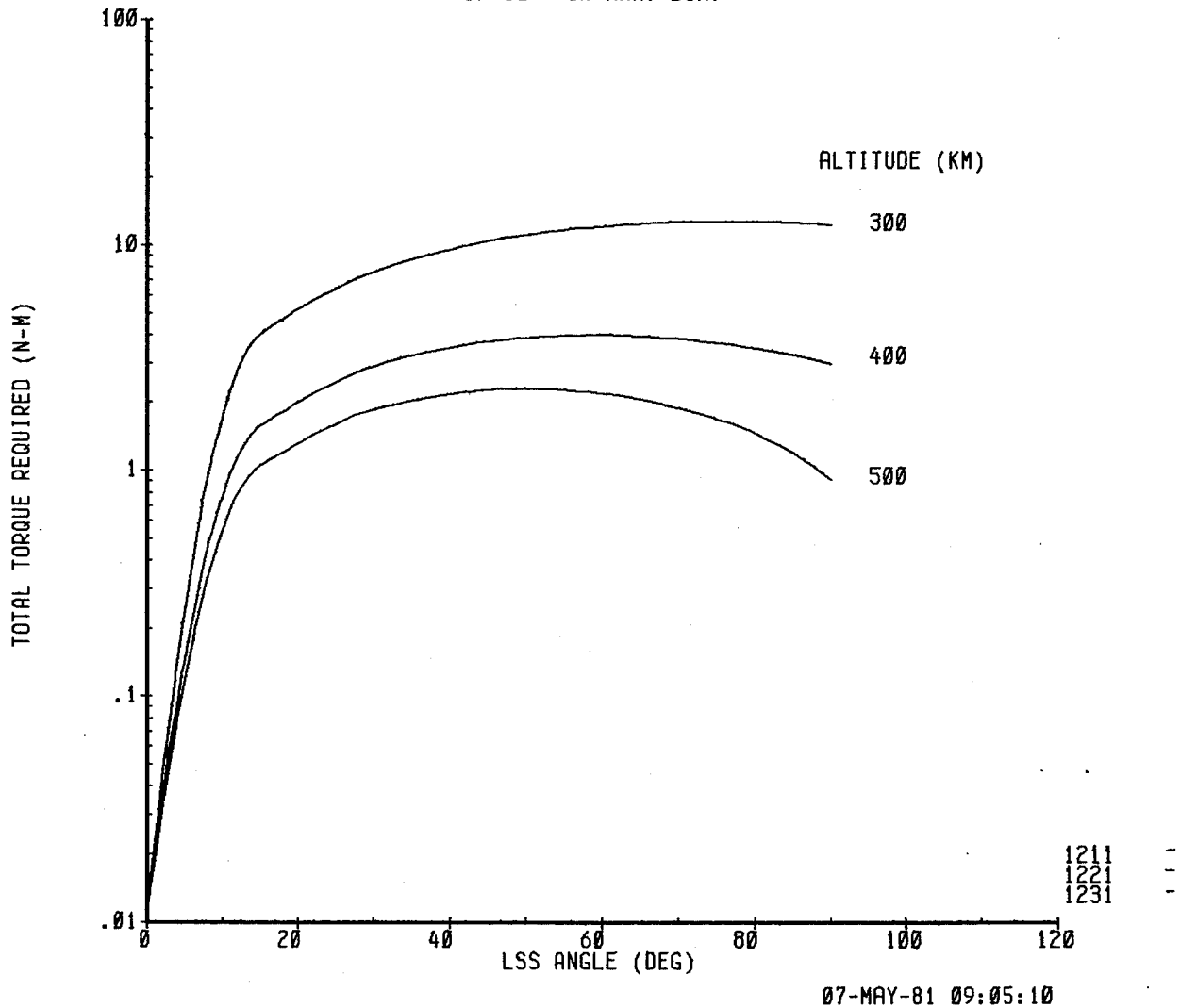

FIGURE D-40
TOTAL TORQUE REQUIREMENT
PLATE STRUCTURE W/O BLANKET - LARGE (250 M)
CP-CG = 5% MAX. DIM.

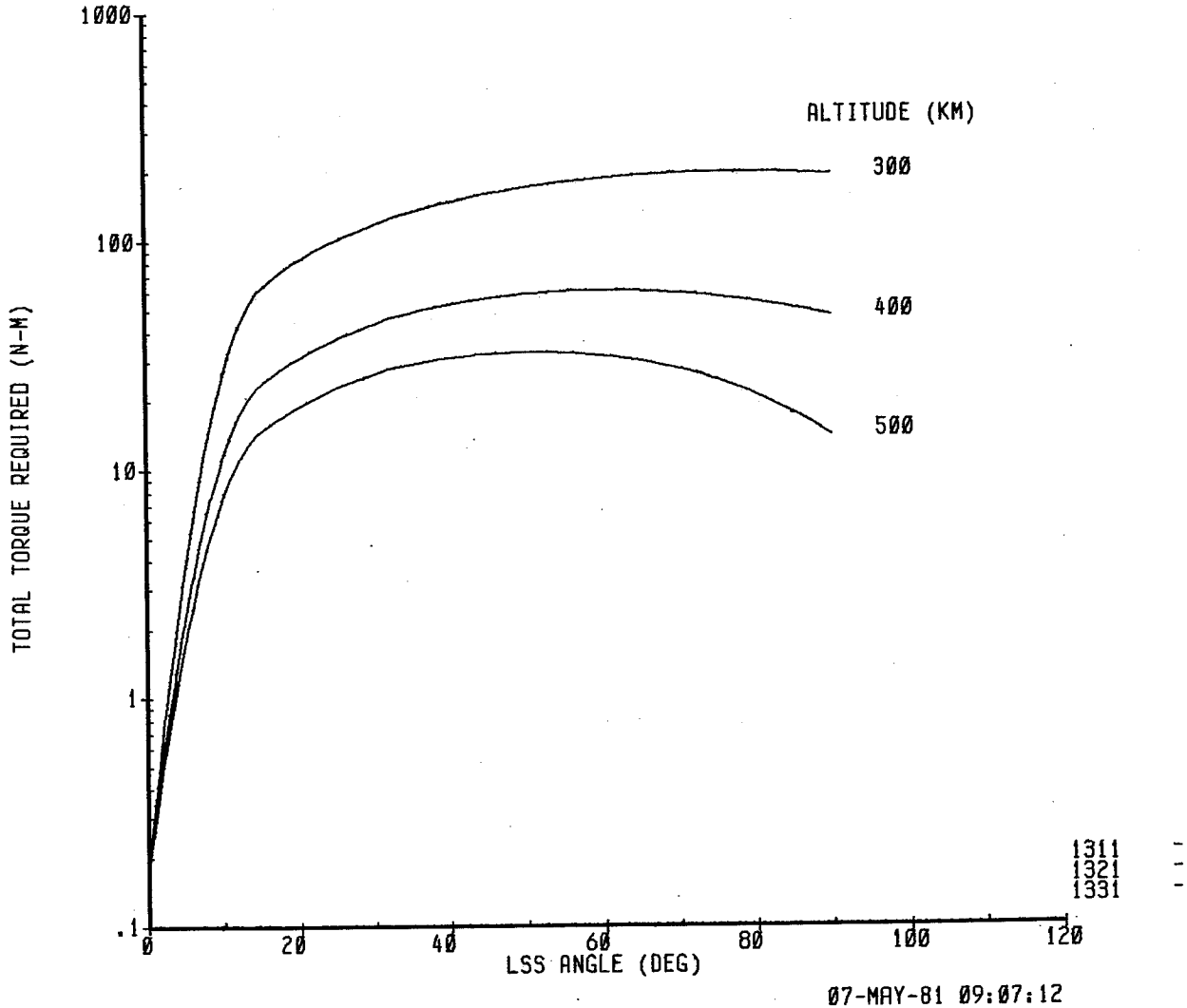

FIGURE D-41

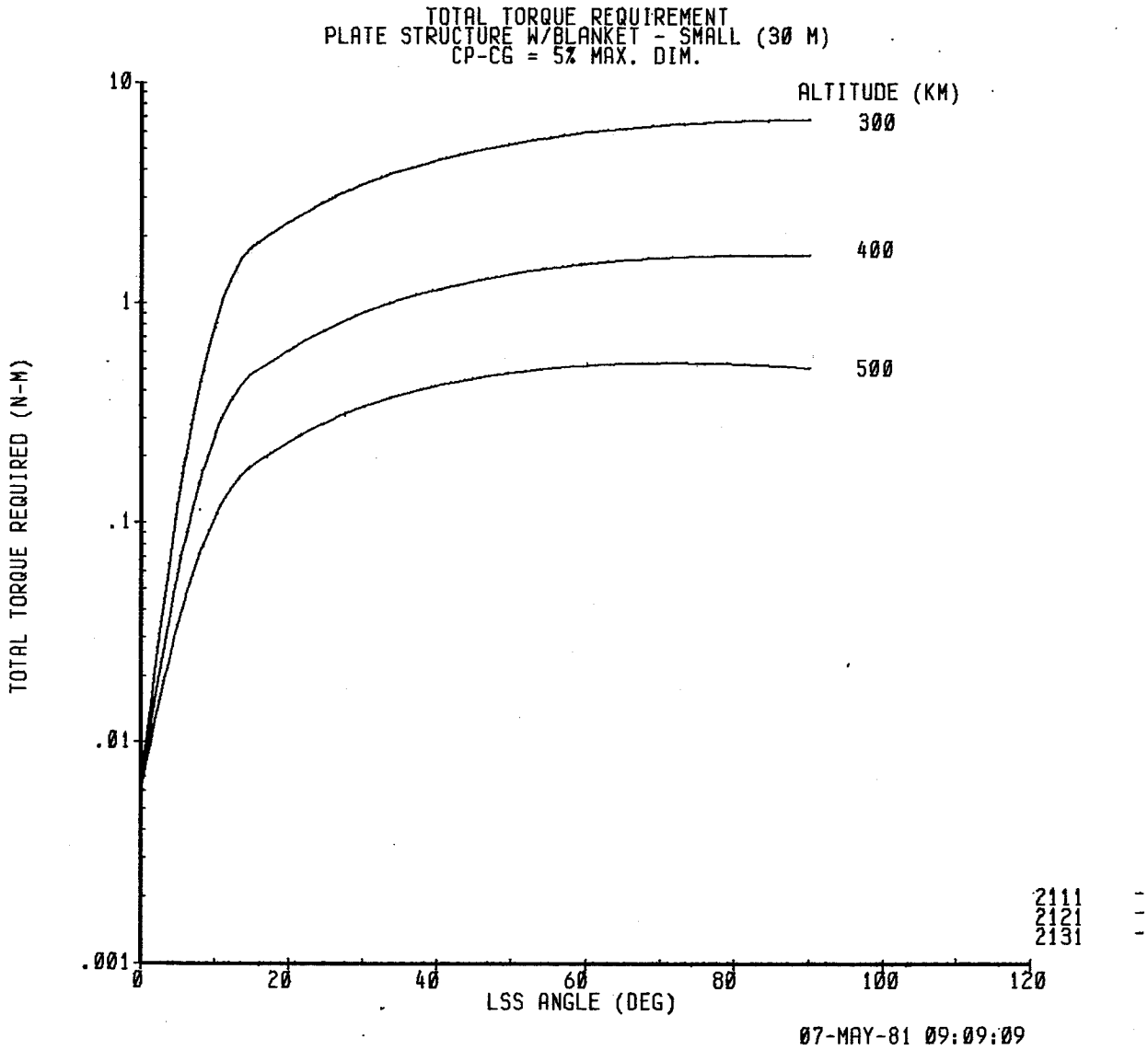
TOTAL TORQUE REQUIREMENT
PLATE STRUCTURE W/BLANKET - SMALL (30 M)
CP-CG = 5% MAX. DIM.
ALTITUDE (KM)
300
400
500
TOTAL TORQUE REQUIRED (N-M)
10
1
.1
.01
.001
0
20
40
60
80
100
120
LSS ANGLE (DEG)
2111
2121
2131
07-MAY-81 09:09:09

FIGURE D-42

TOTAL TORQUE REQUIREMENT
PLATE STRUCTURE W/BLANKET - MEDIUM (100 M)
CP-CG = 5% MAX. DIM.

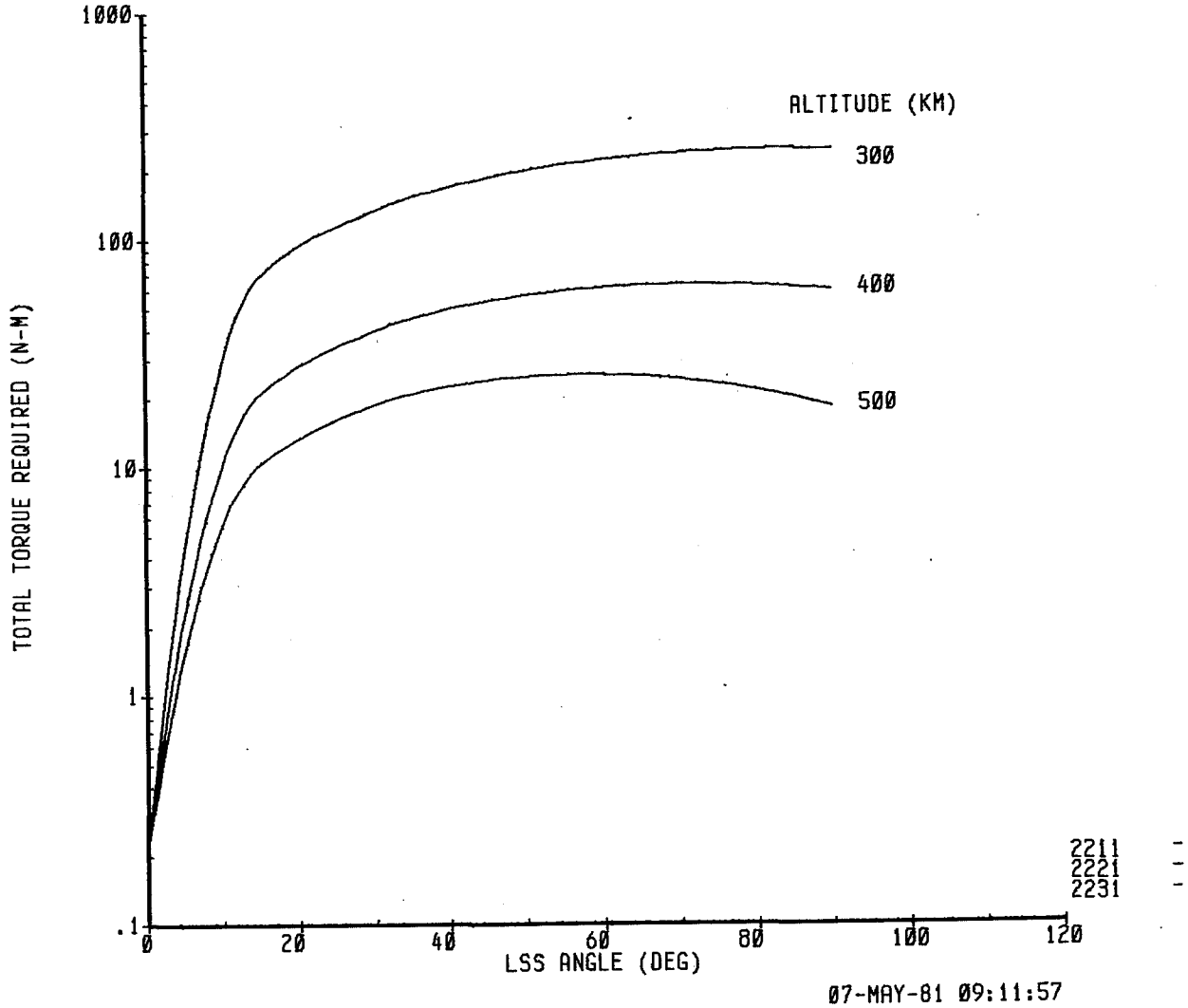

FIGURE D-43
TOTAL TORQUE REQUIREMENT
PLATE STRUCTURE W/BLANKET - LARGE (150 M)
CP-CG = 5% MAX. DIM.

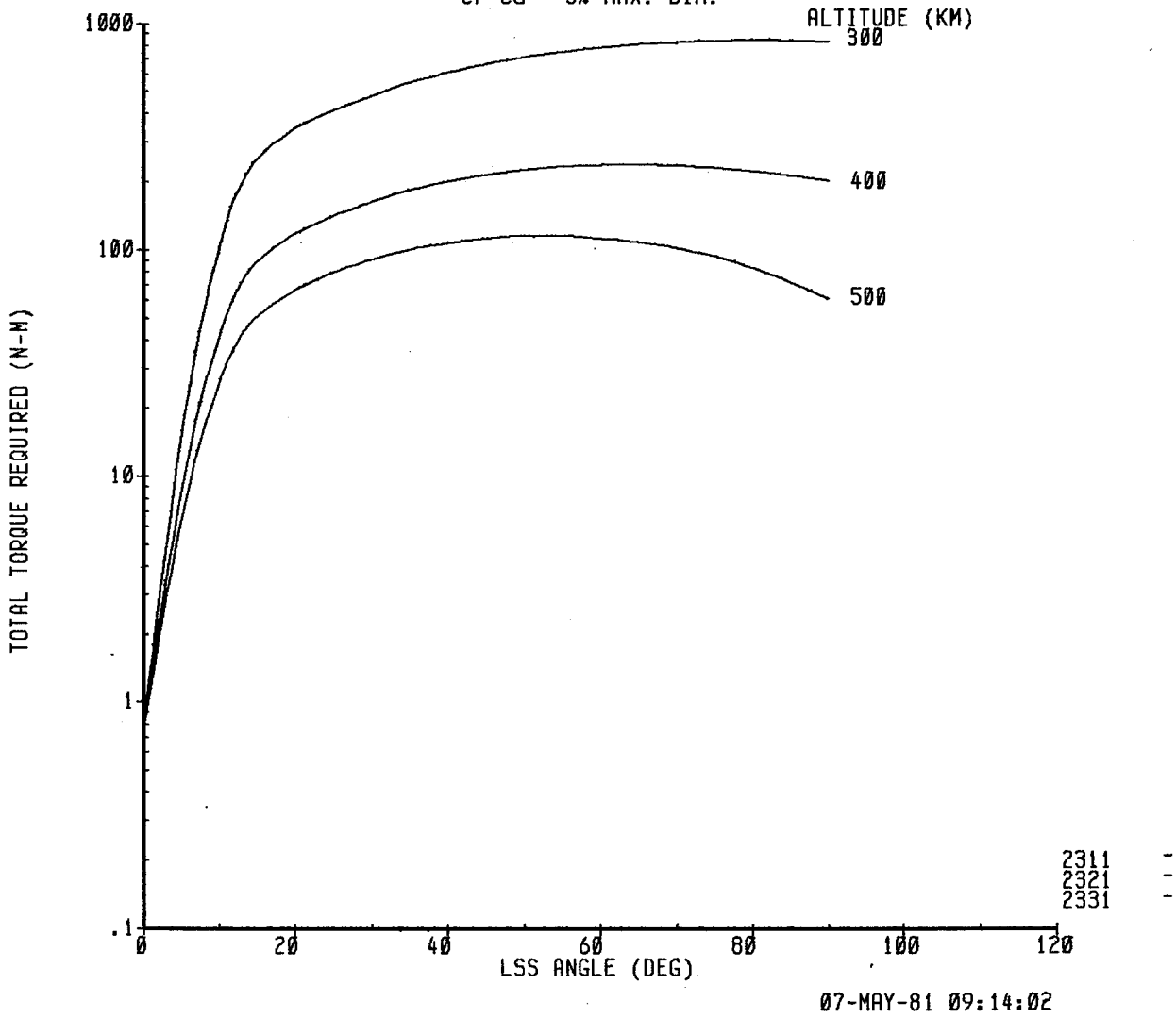

FIGURE D-44
TOTAL TORQUE REQUIREMENT
MODULAR ANTENNA - SMALL (15M)
CP-CG = 5% MAX. DIM.

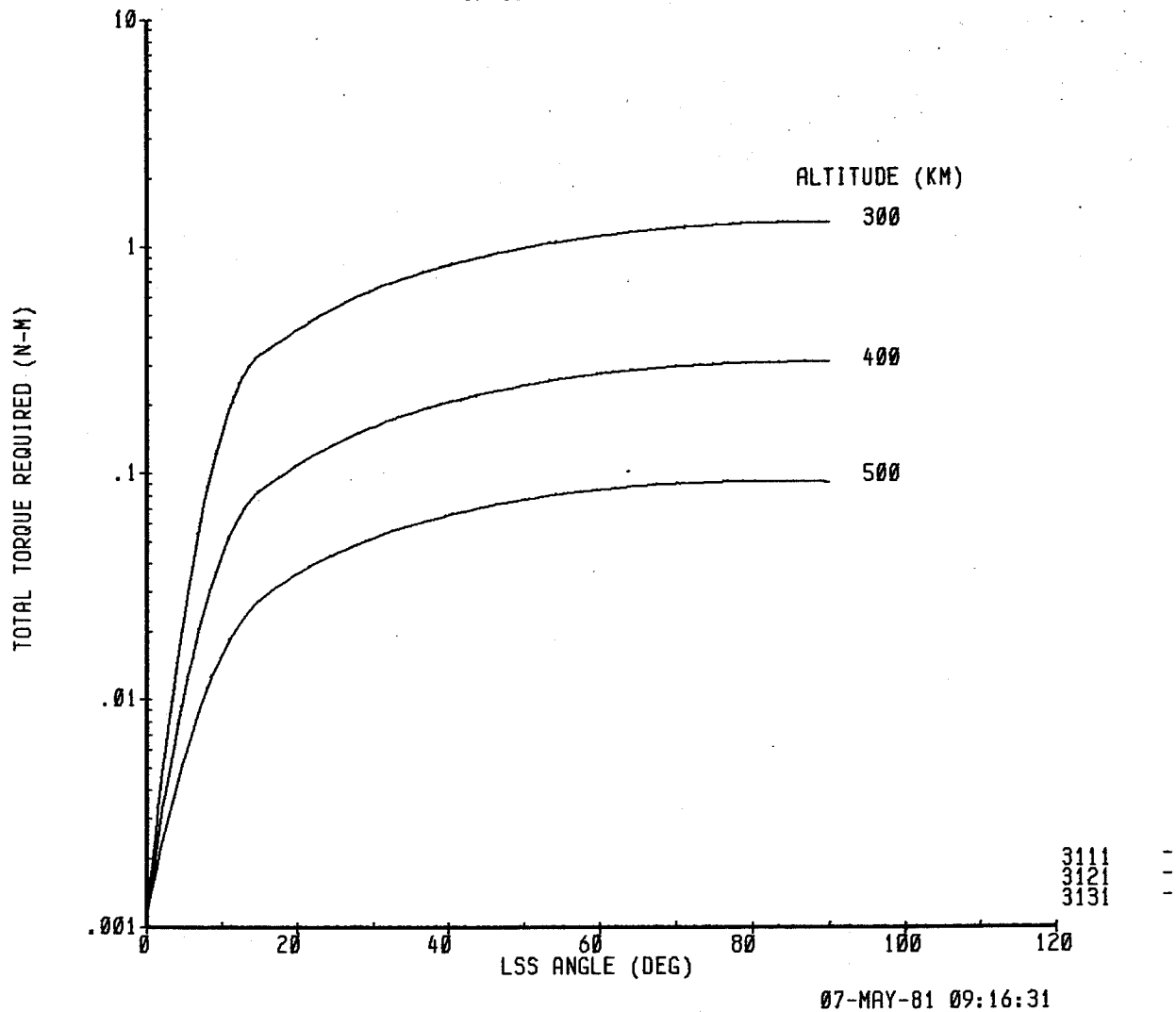

FIGURE D-45
TOTAL TORQUE REQUIREMENT
MODULAR ANTENNA - MEDIUM (60 M)
CP-CG = 5% MAX. DIM.

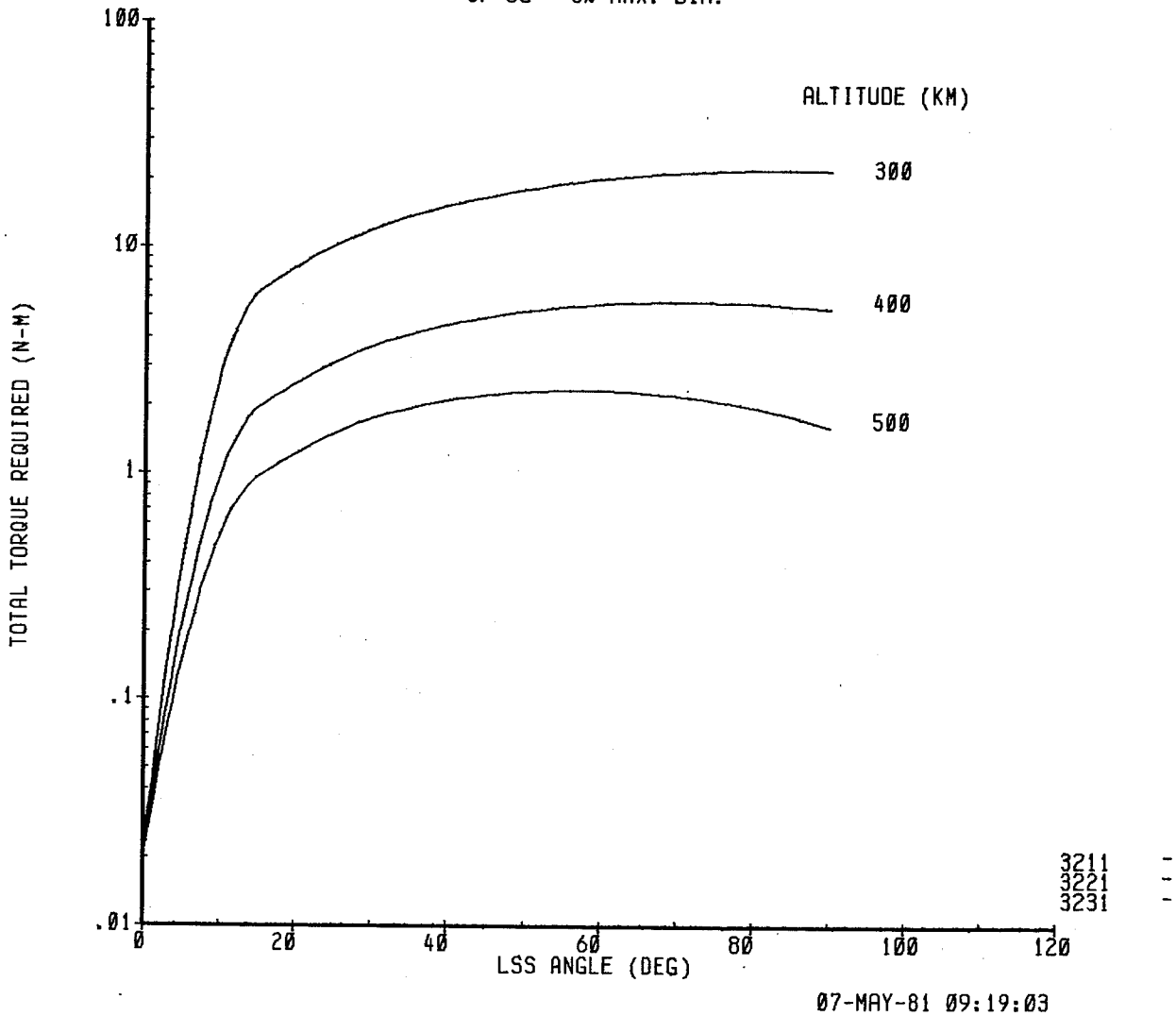

FIGURE D-46

TOTAL TORQUE REQUIREMENT
MODULAR ANTENNA - LARGE (200 M)
CP-CG = 5% MAX. DIM.

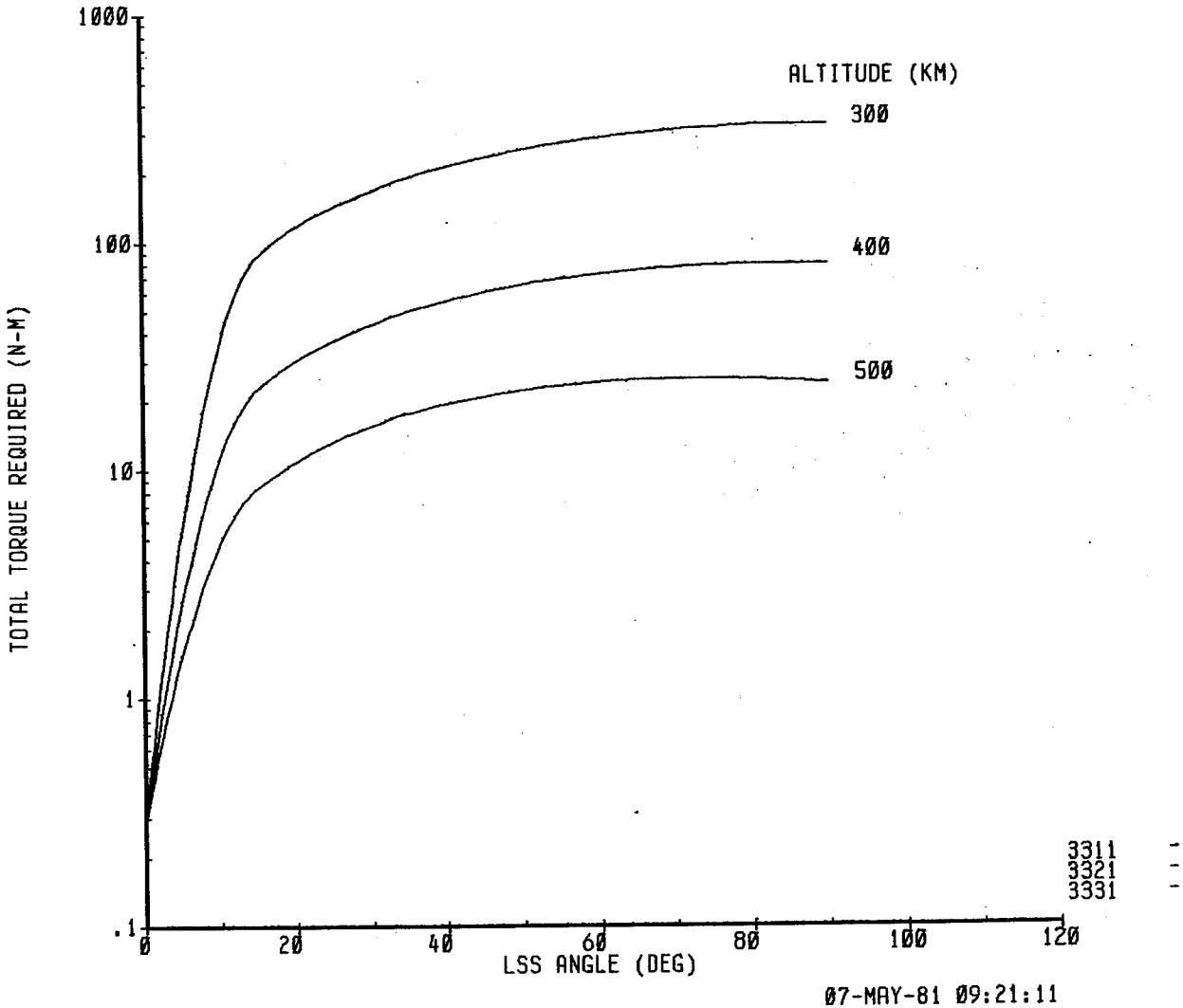

FIGURE D-47
TOTAL TORQUE REQUIREMENT
SERIES OF ANTENNAS - SMALL (2)
CP-CG = 5% MAX. DIM.

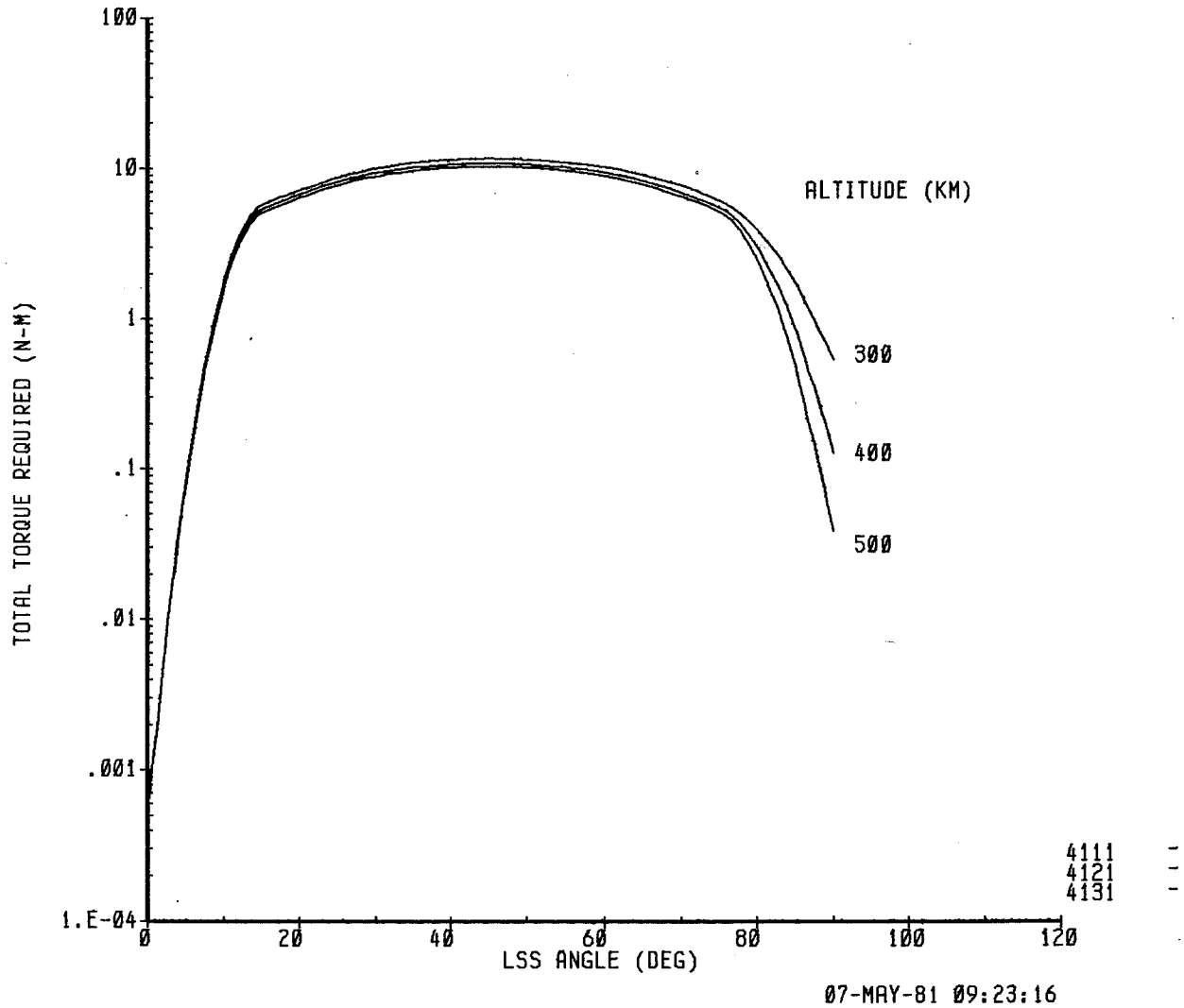

FIGURE D-48

TOTAL TORQUE REQUIREMENT
SERIES OF ANTENNAS - MEDIUM (3)
CP-CG = 5% MAX. DIM.

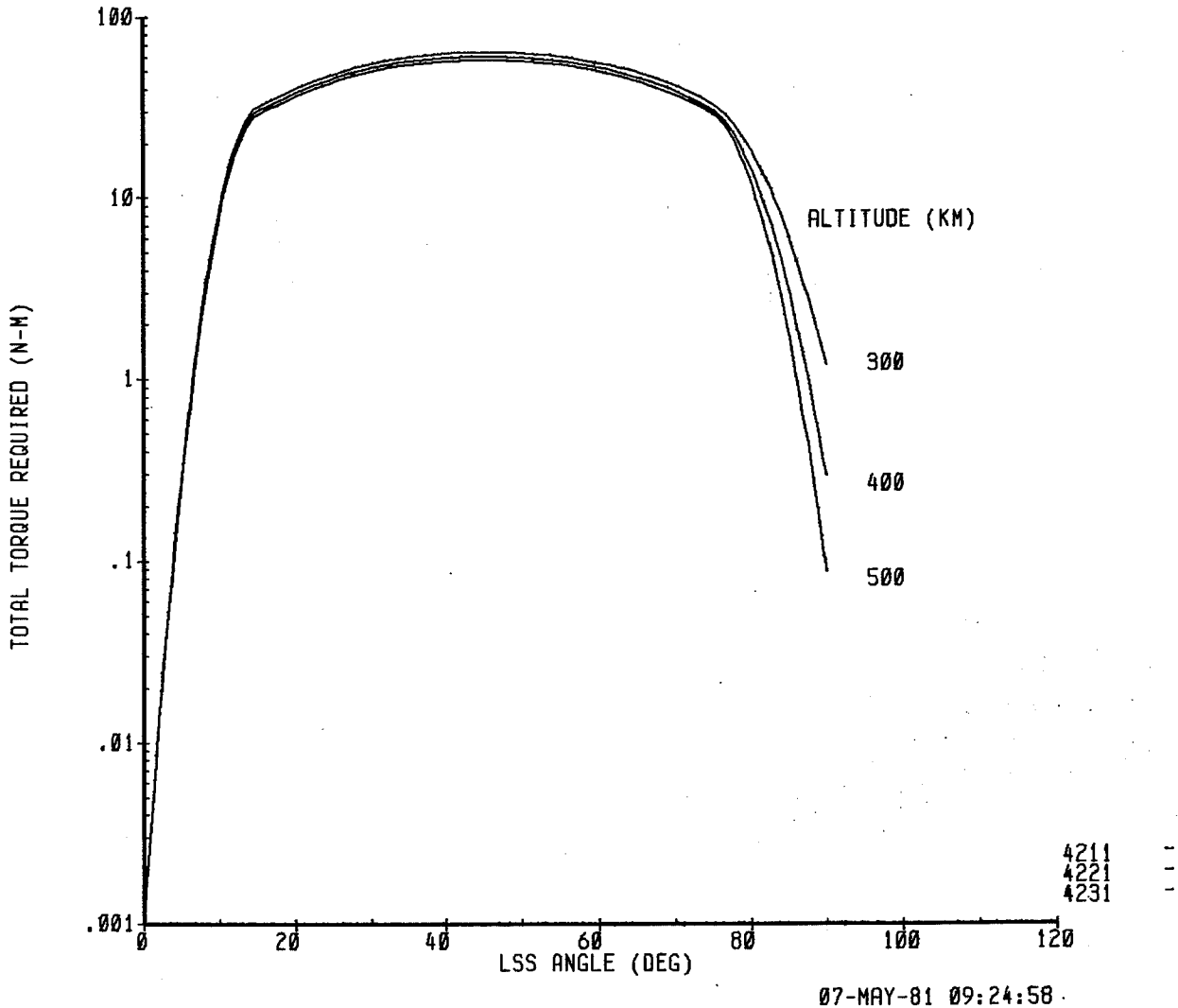

FIGURE D-49

TOTAL TORQUE REQUIREMENT
SERIES OF ANTENNAS - LARGE (4)
CP-CG = 5% MAX. DIM.

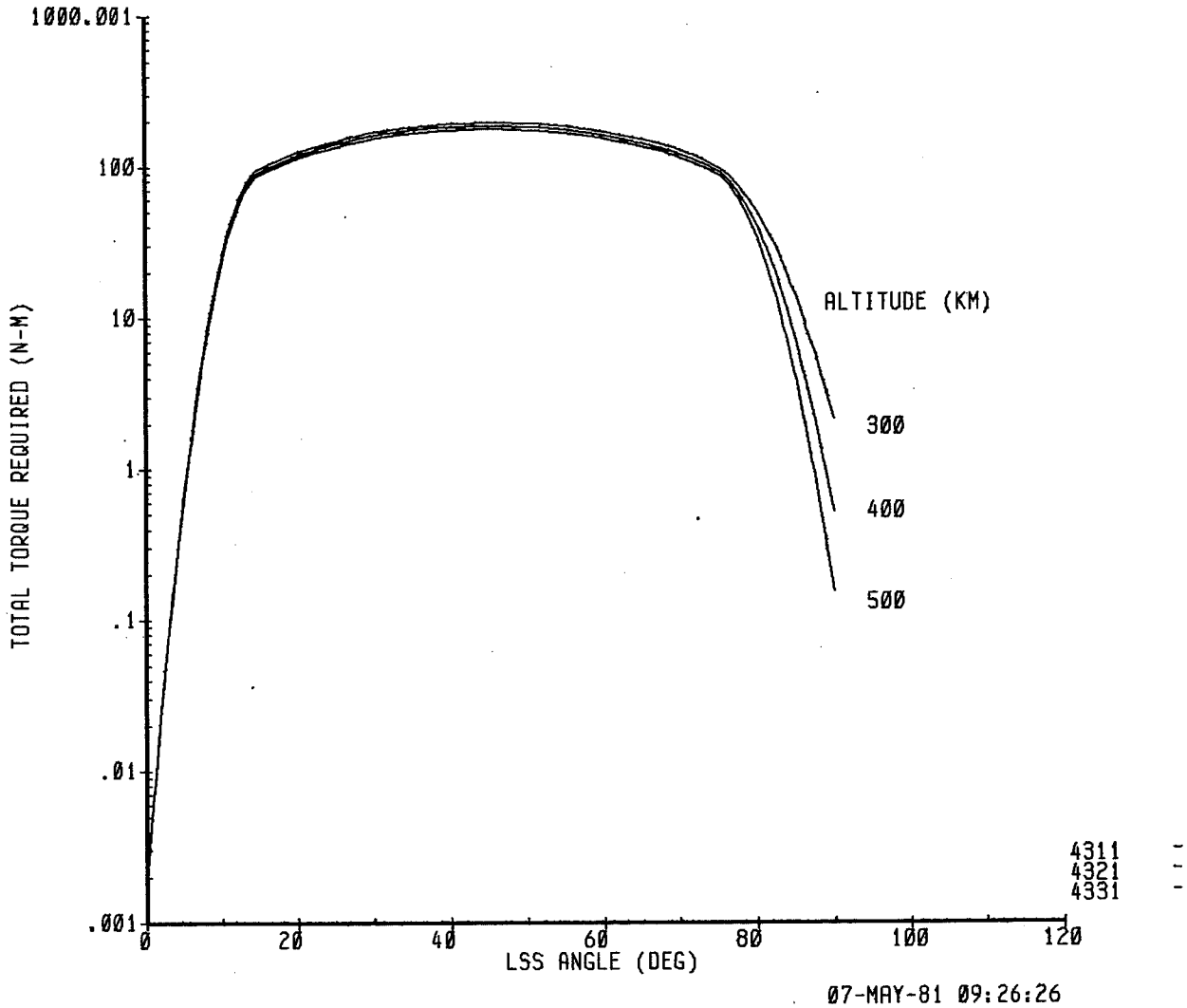

FIGURE D-50

TORQUE COMPOSITE BREAKDOWN - GEOSYNCHRONOUS ALTITUDE
PLATE STRUCTURE W/O BLANKET - SMALL (30 M)
CP-CG = 5% OF MAX. DIM.

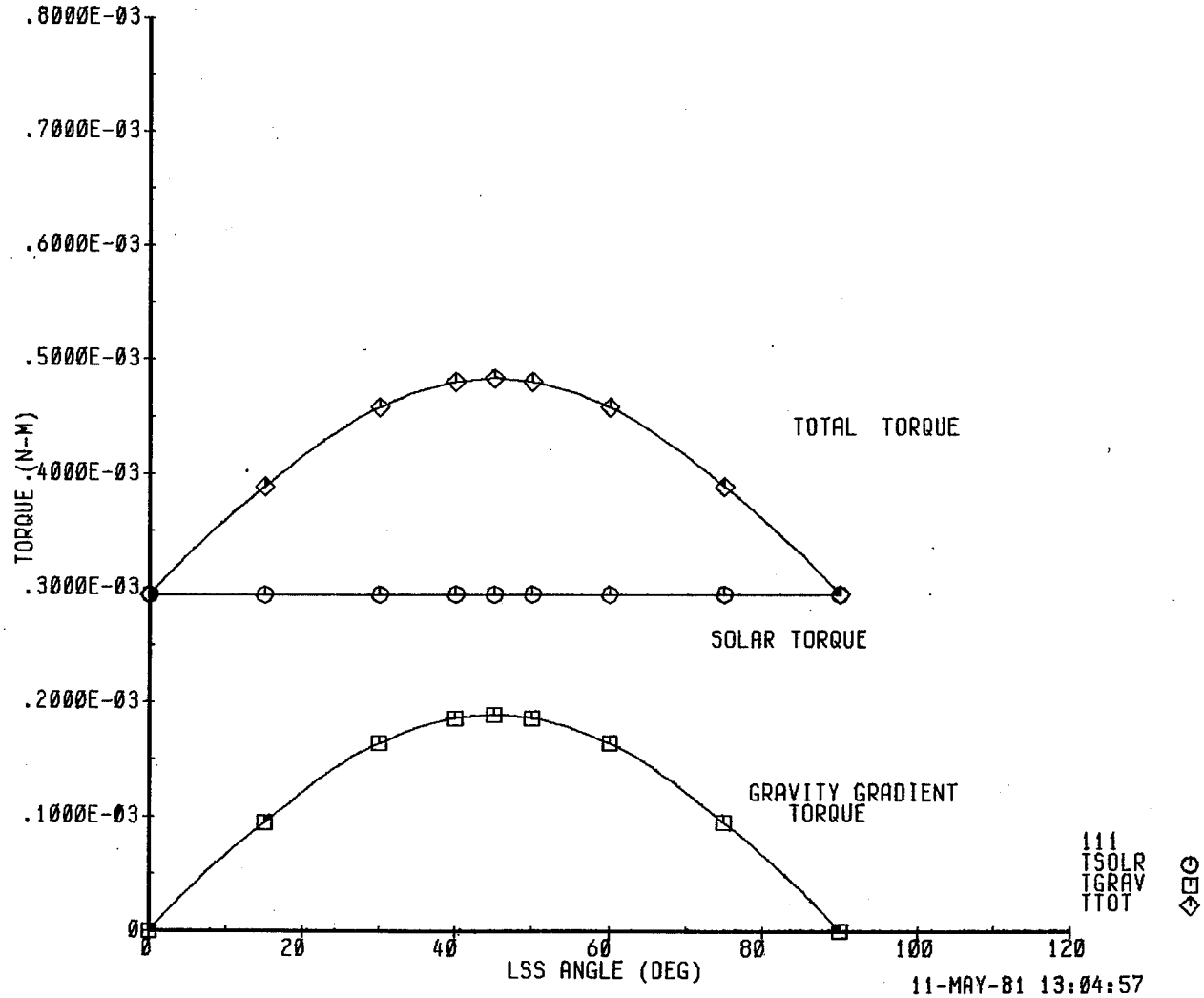

FIGURE D-51

TOTAL TORQUE REQUIREMENT - GEOSYNCHRONOUS ALTITUDE
PLATE STRUCTURE W/O BLANKET
CP-CG = 5% OF MAX. DIM.

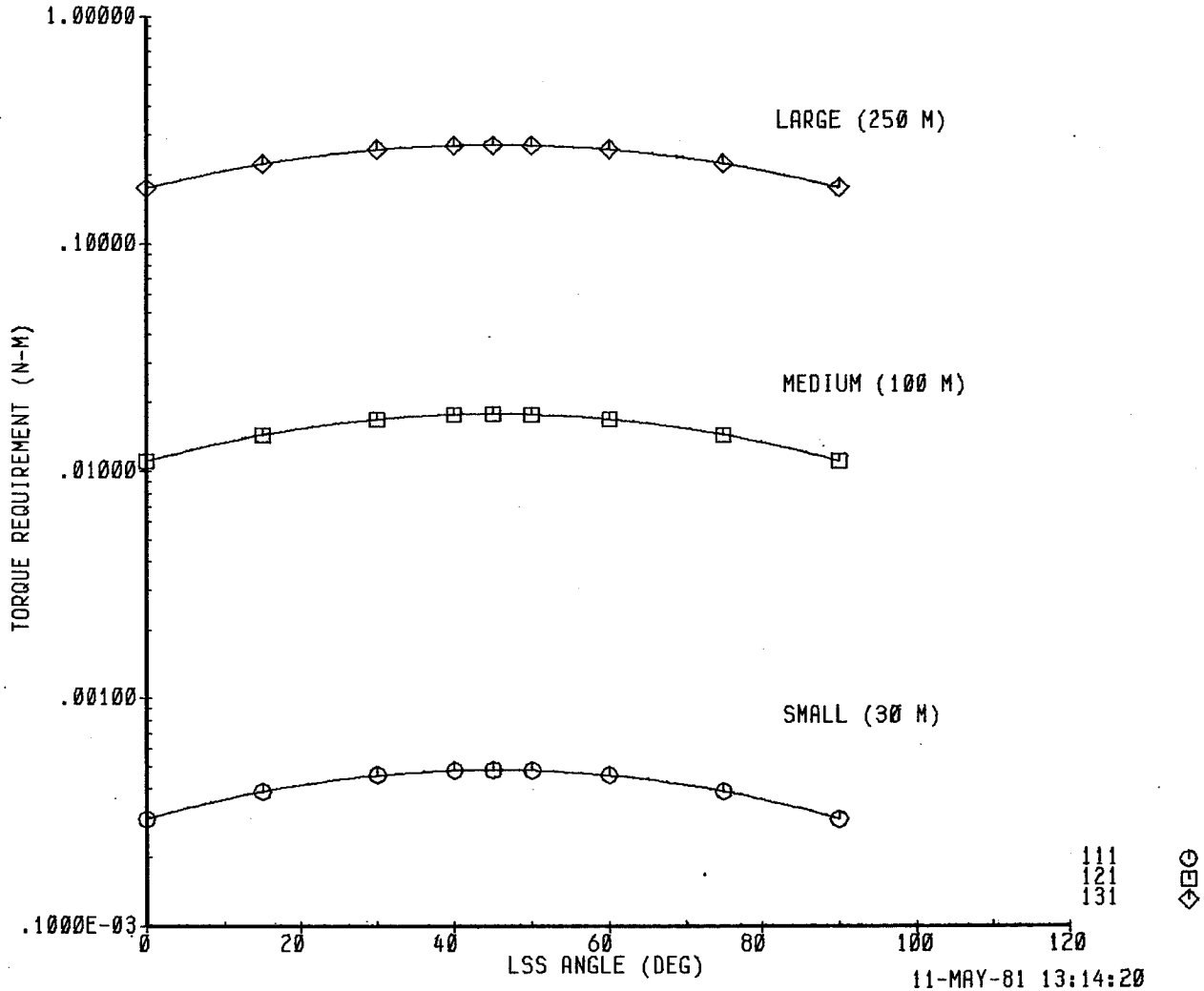

FIGURE D-52

TOTAL TORQUE REQUIREMENT - GEOSYNCHRONOUS ALTITUDE
PLATE STRUCTURE W/BLANKET
CP-CG = 5% OF MAX. DIM.

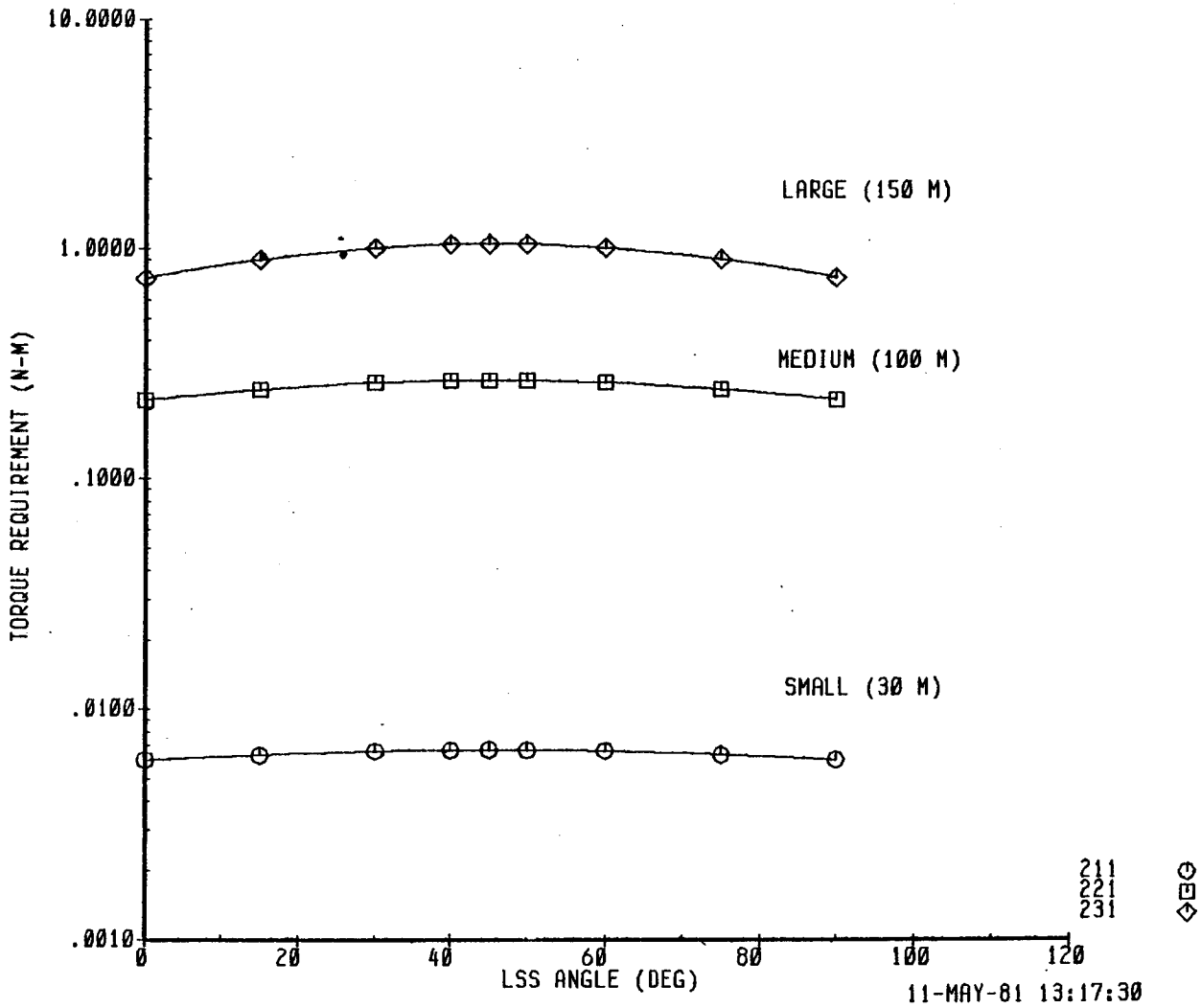

FIGURE D-53

TOTAL TORQUE REQUIREMENT - GEOSYNCHRONOUS ALTITUDE
MODULAR ANTENNA STRUCTURE
CP-CG = 5% OF MAX. DIM.

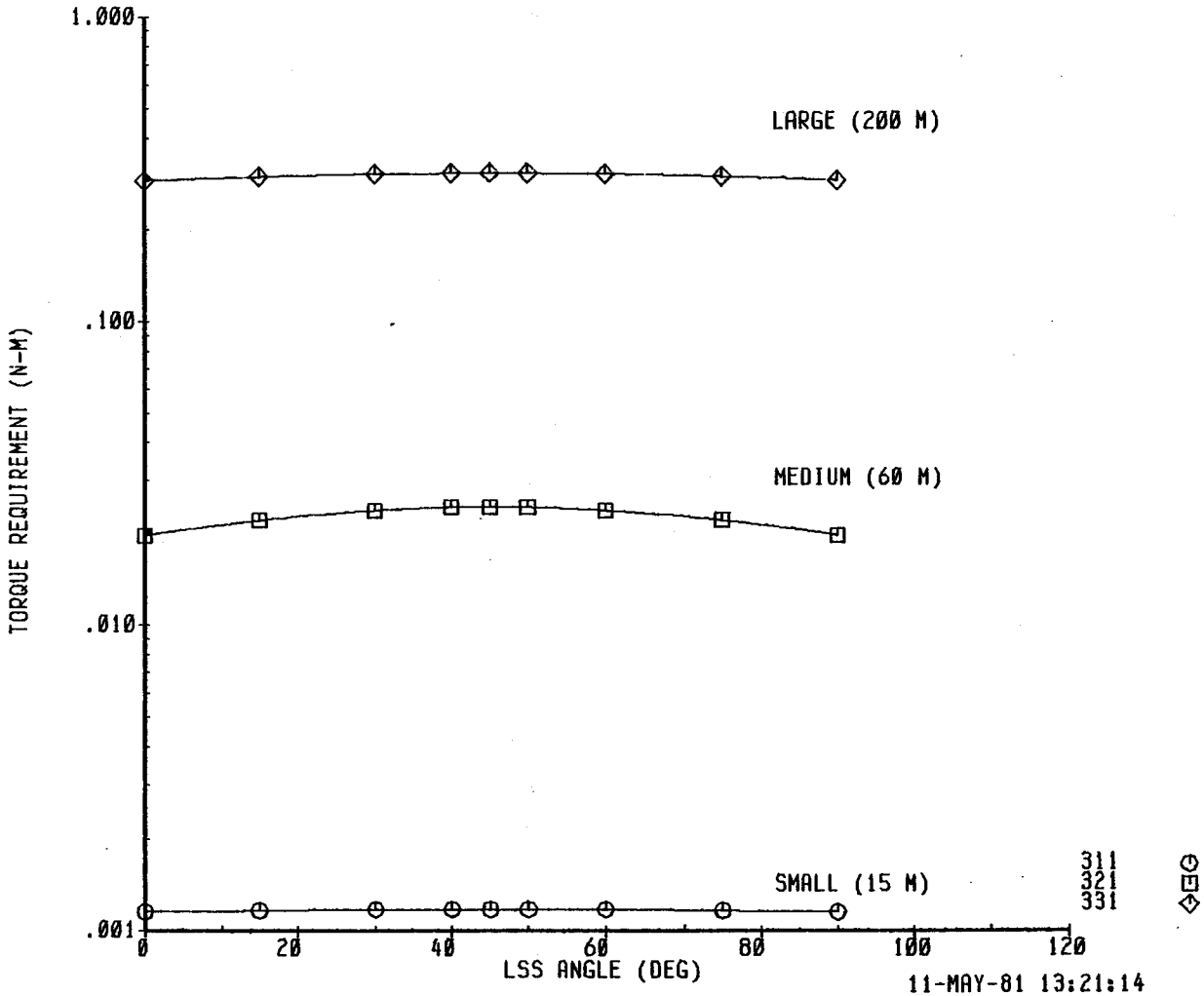

FIGURE D-54

TOTAL TORQUE REQUIREMENT - GEOSYNCHRONOUS ALTITUDE
SERIES OF ANTENNAS
CP-CG = 5% OF MAX. DIM.

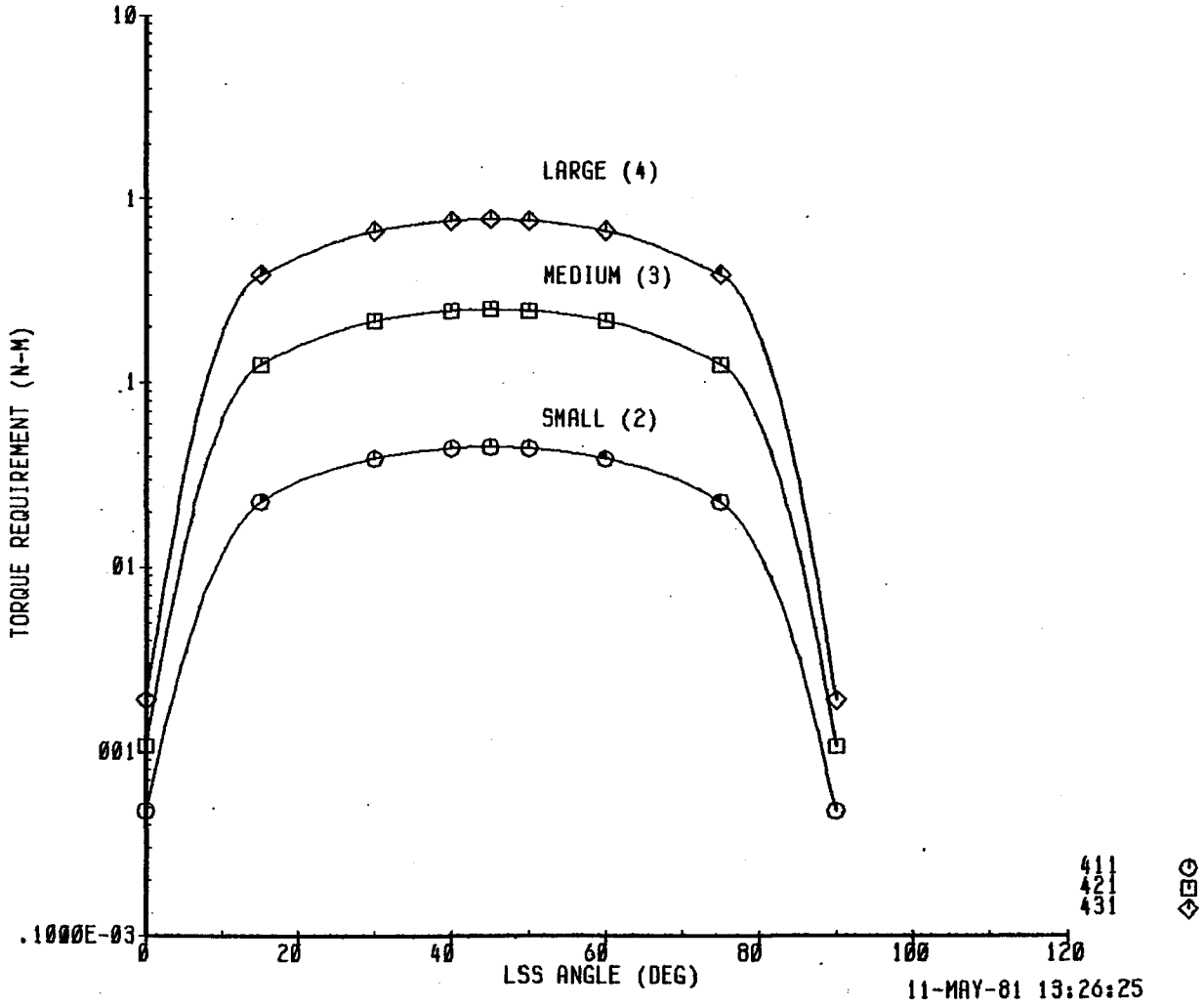

FIGURE D-55

STATIONKEEPING DELTA-V CALCULATIONS
PLATE STRUCTURE W/O BLANKET SMALL (30 M)
10 YEAR MISSION

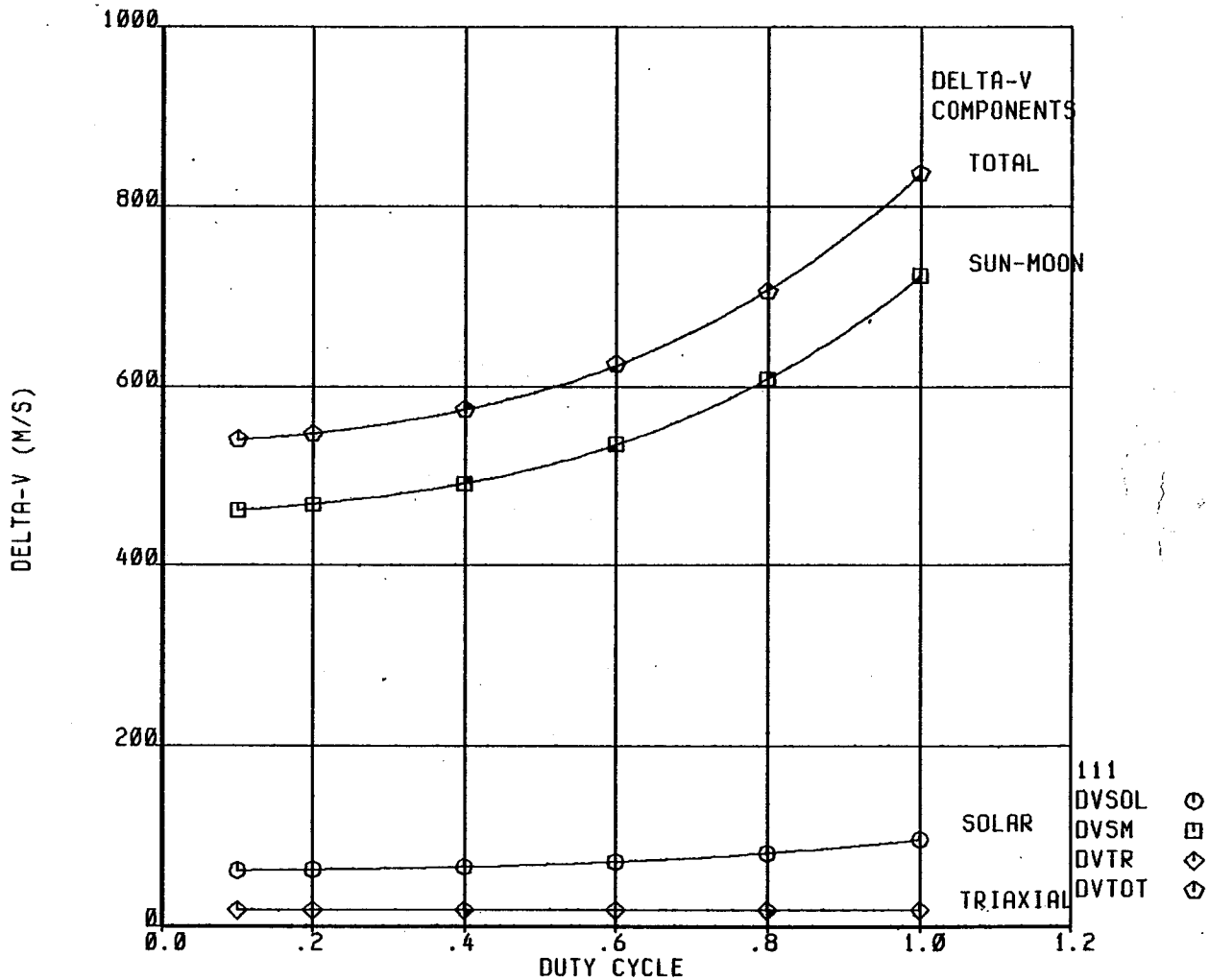

FIGURE D-56

STATIONKEEPING DELTA-V CALCULATIONS
PLATE STRUCTURE W/O BLANKET MEDIUM (100 M)
10 YEAR MISSION

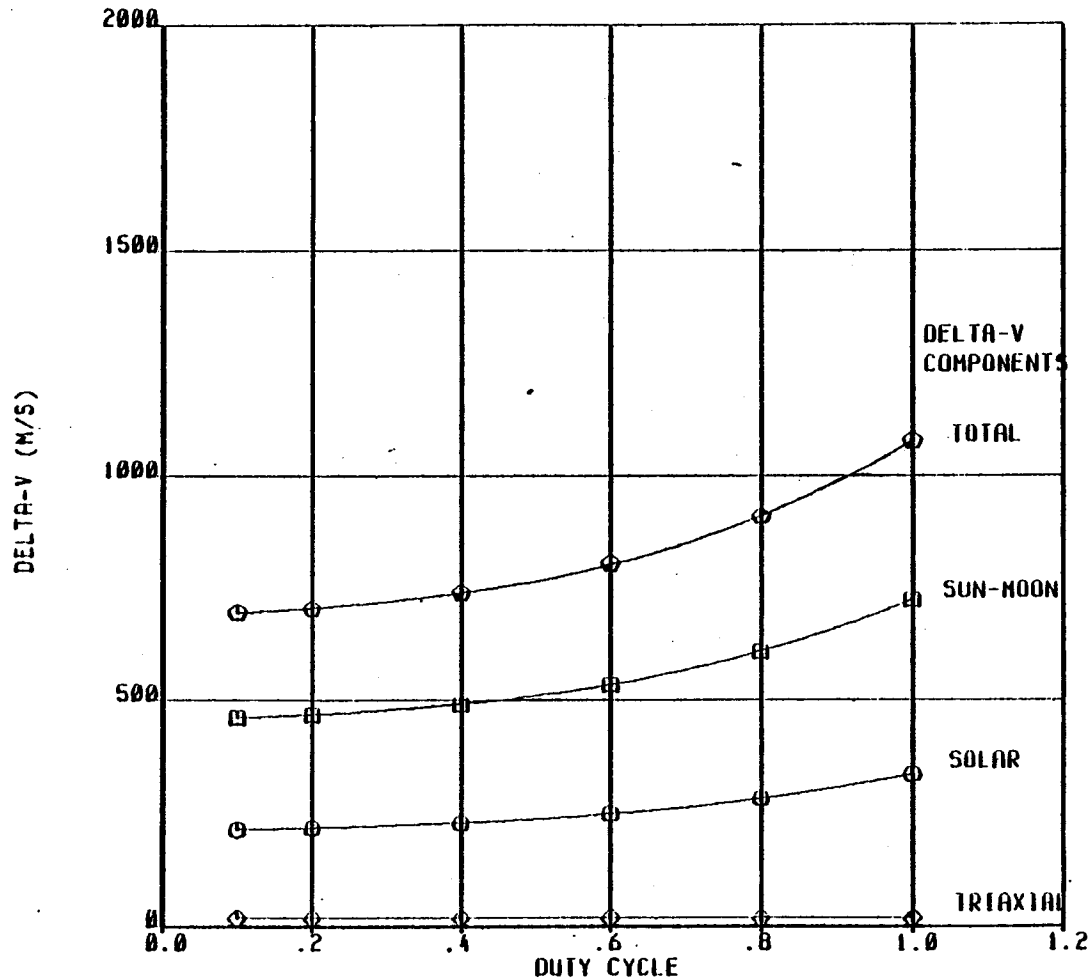

FIGURE D-57

STATIONKEEPING DELTA-V CALCULATIONS
PLATE STRUCTURE W/O BLANKET LARGE (250 M)
10 YEAR MISSION

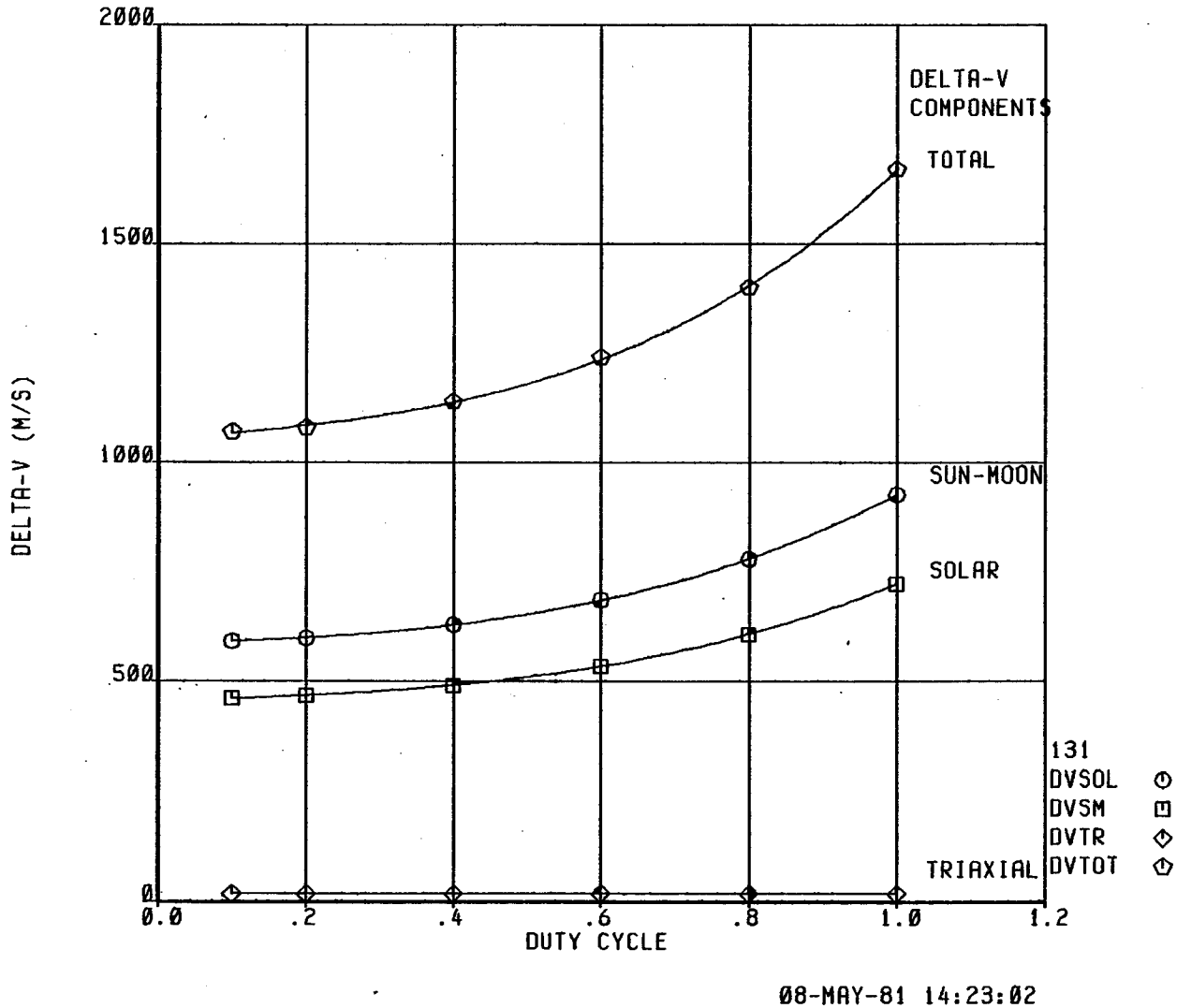

FIGURE D-58

STATIONKEEPING DELTA-V CALCULATIONS
PLATE STRUCTURE W/BLANKET SMALL (30 M)
10 YEAR MISSION

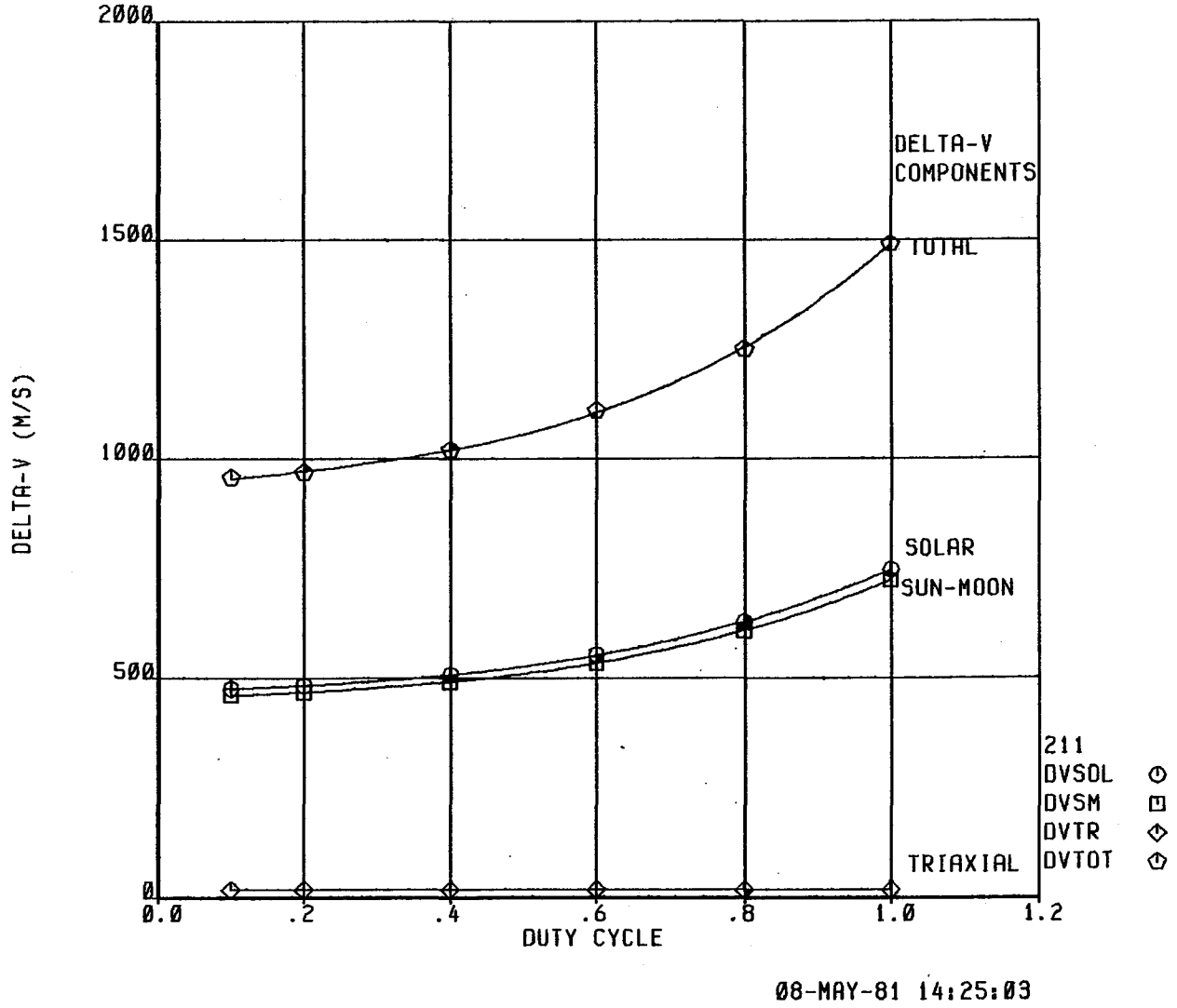

FIGURE D-59

STATIONKEEPING DELTA-V CALCULATIONS
PLATE STRUCTURE W/BLANKET MEDIUM (100 M)
10 YEAR MISSION

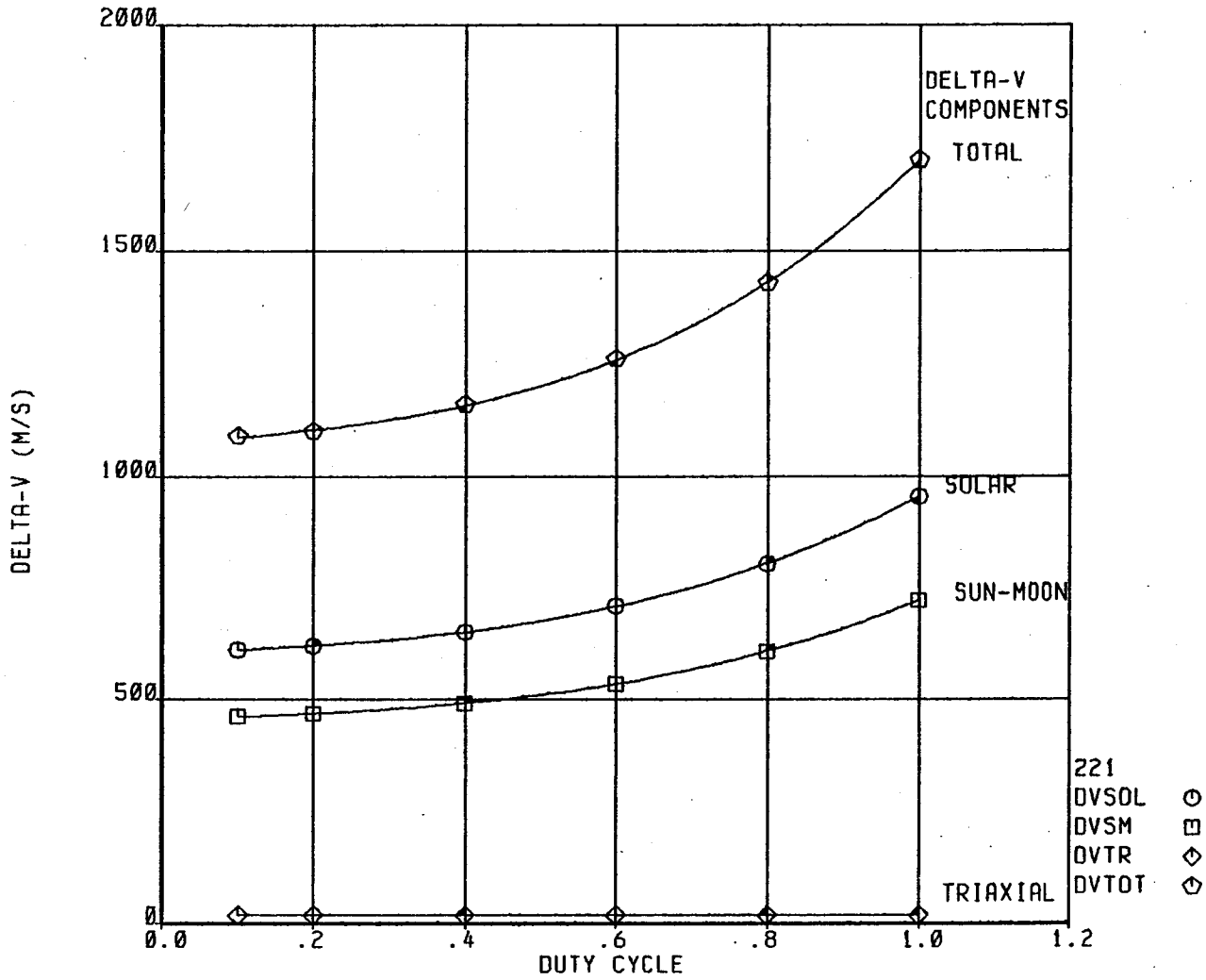

08-MAY-81 14:26:54

FIGURE D-60

STATIONKEEPING DELTA-V CALCULATIONS
PLATE STRUCTURE W/BLANKET LARGE (150 M)
10 YEAR MISSION

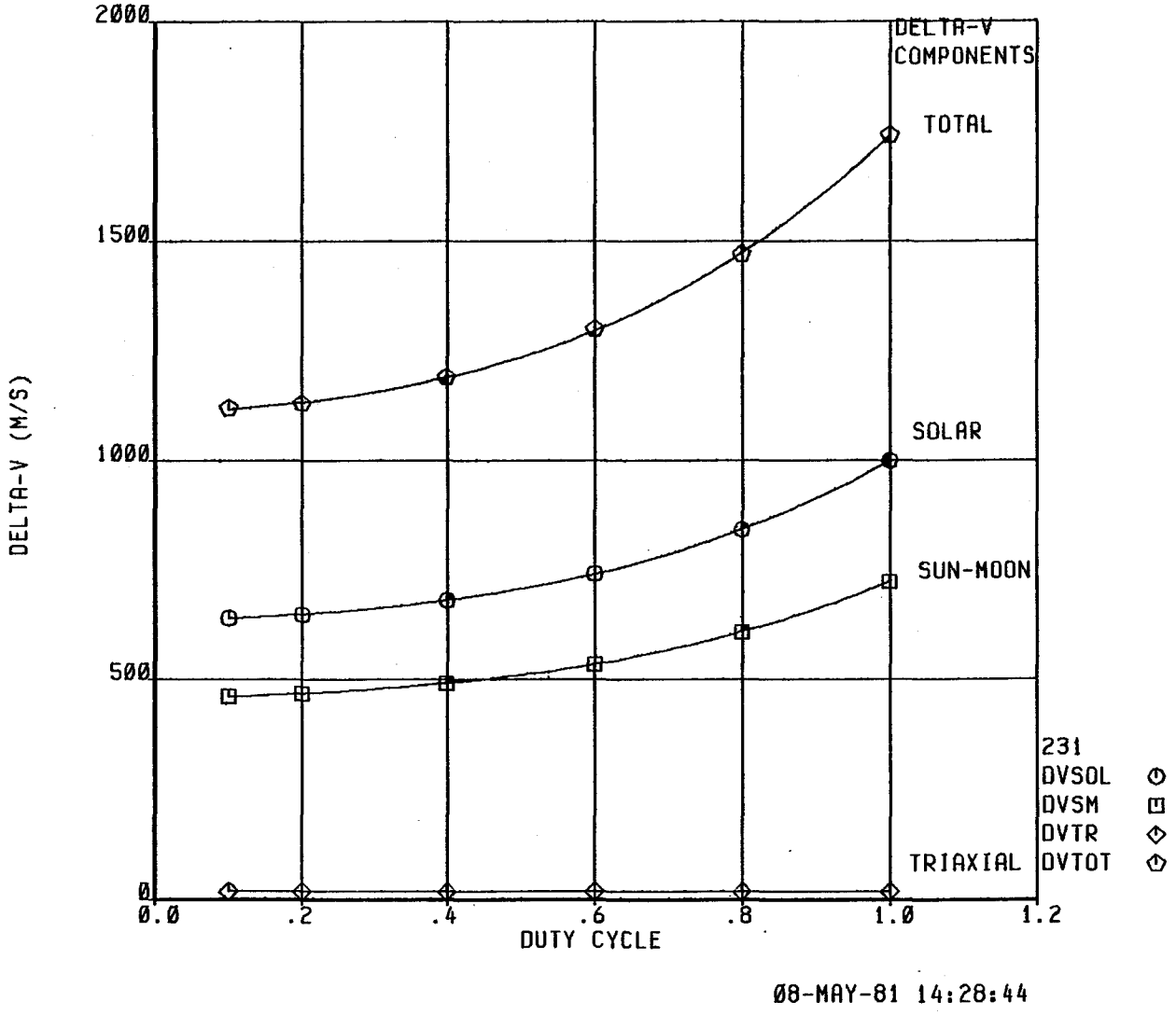

FIGURE D-61

STATIONKEEPING DELTA-V CALCULATIONS
MODULAR ANTENNA SMALL (15 M)
10 YEAR MISSION

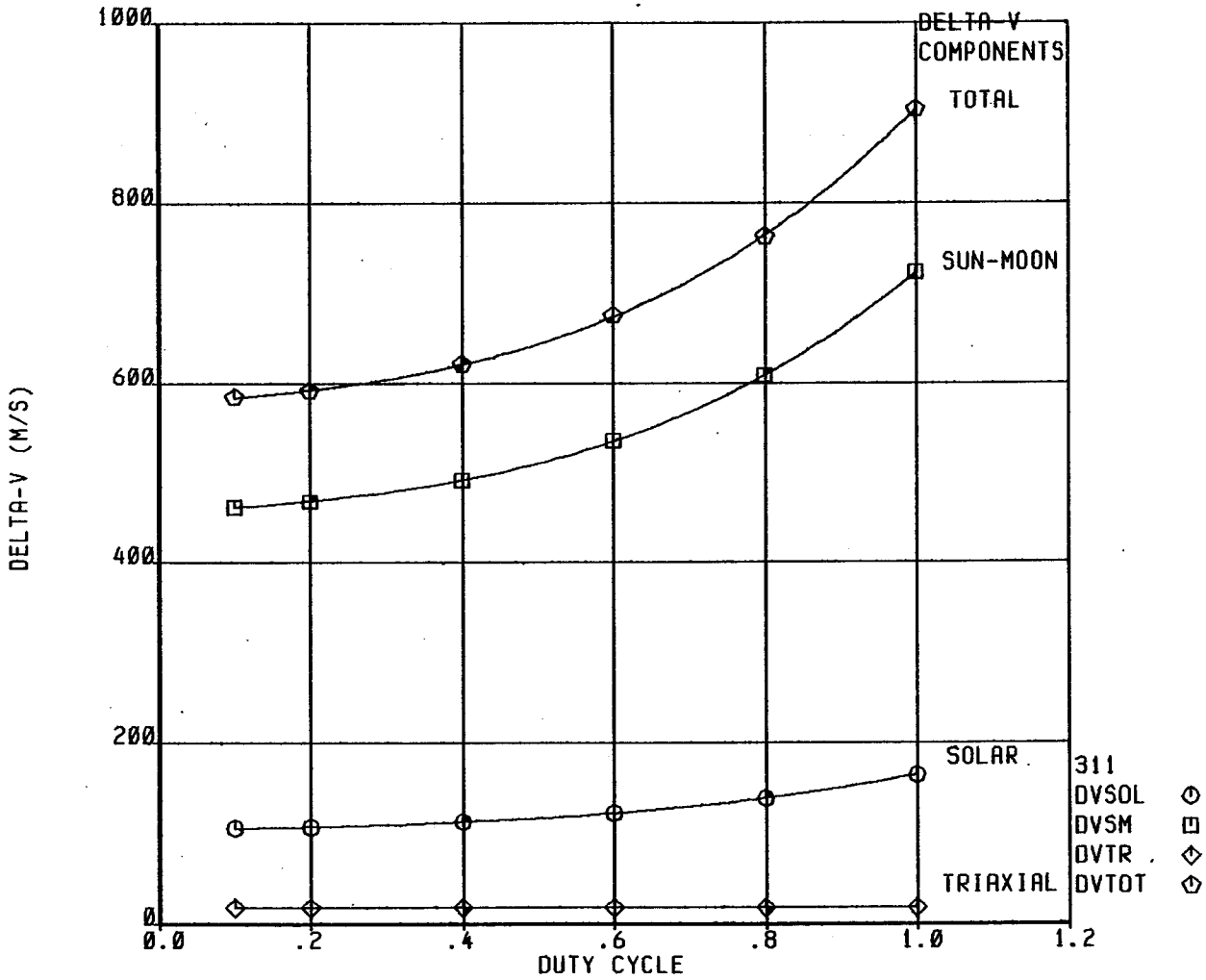

FIGURE D-62

STATIONKEEPING DELTA-V CALCULATIONS
MODULAR ANTENNA STRUCTURE MEDIUM(60 M)
10 YEAR MISSION

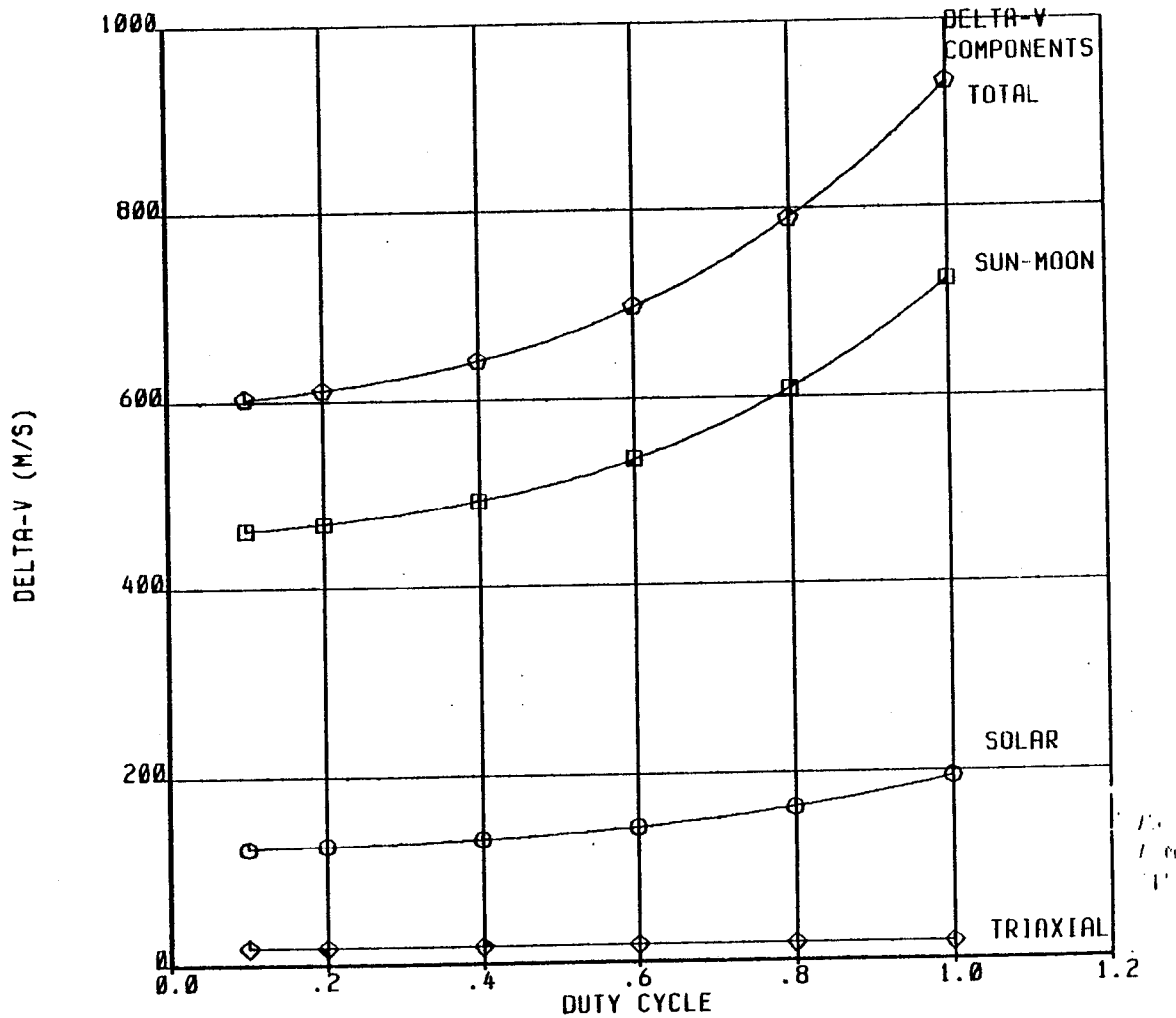

FIGURE D-63

STATIONKEEPING DELTA-V CALCULATIONS
MODULAR ANTENNA STRUCTURE LARGE (200 M)
10 YEAR MISSION

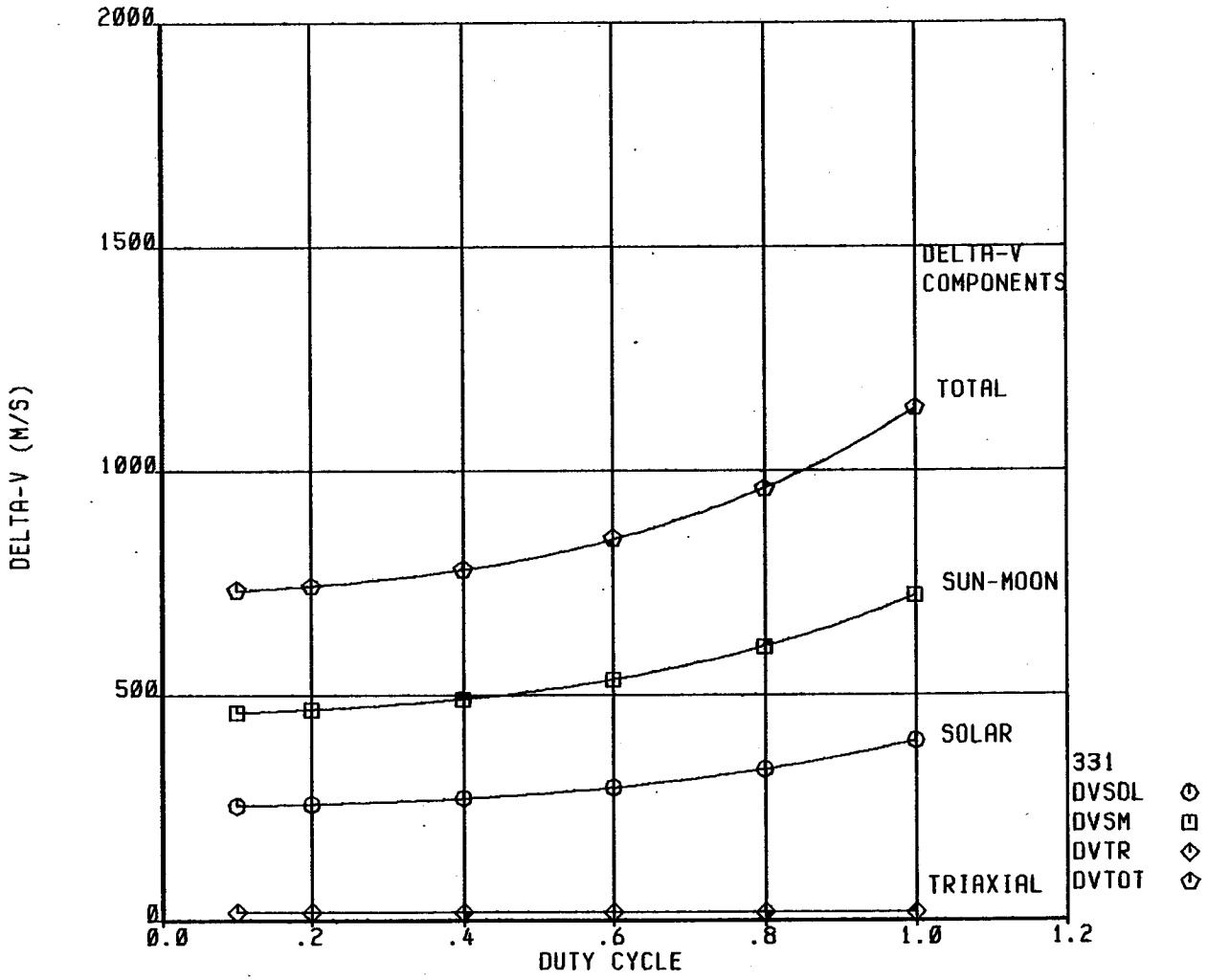

FIGURE D-64

STATIONKEEPING DELTA-V CALCULATIONS
SERIES OF ANTENNAS SMALL (2)
10 YEAR MISSION

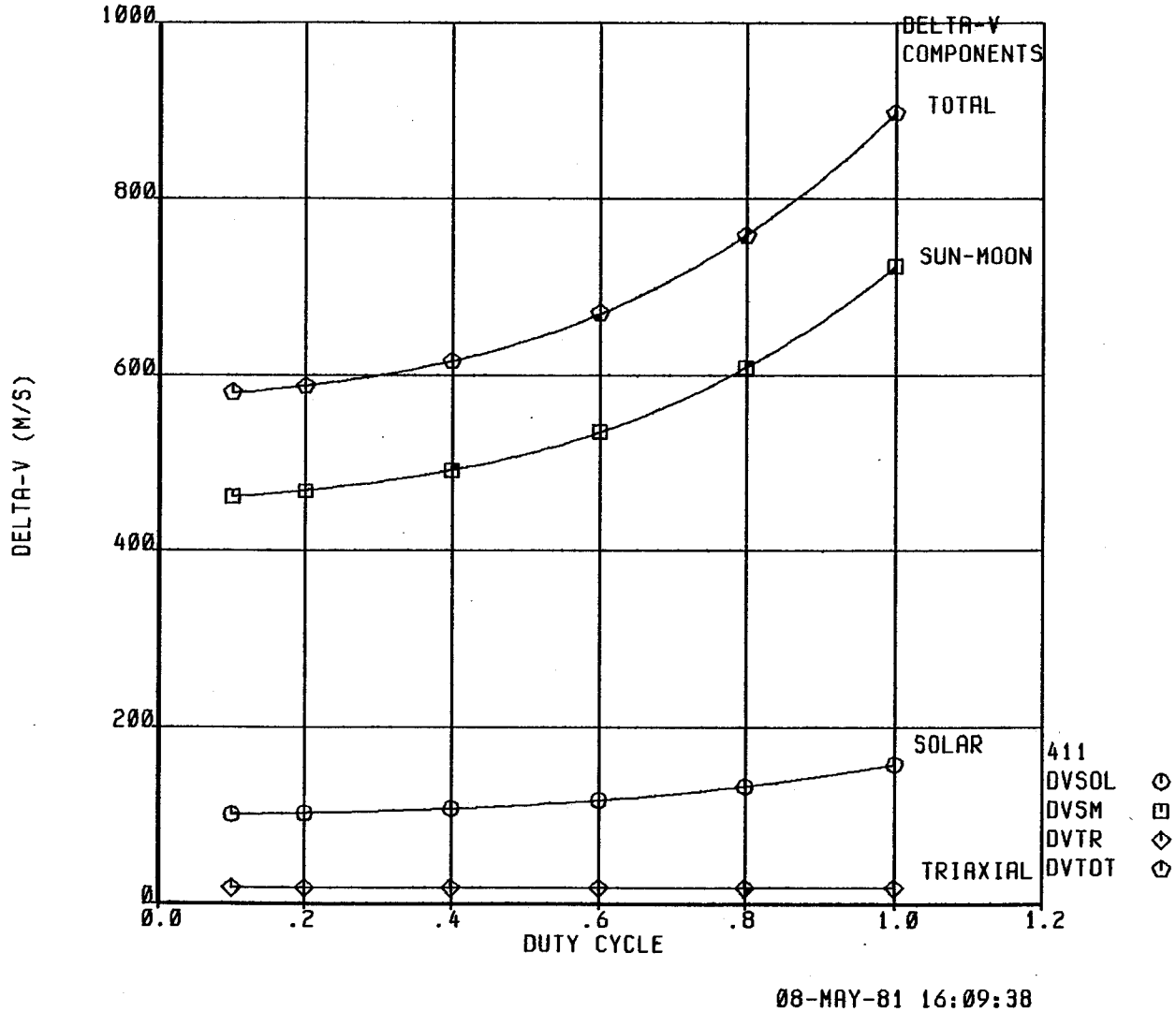

FIGURE D-65

STATIONKEEPING DELTA-V CALCULATIONS
SERIES OF ANTENNAS MEDIUM (3)
10 YEAR MISSION

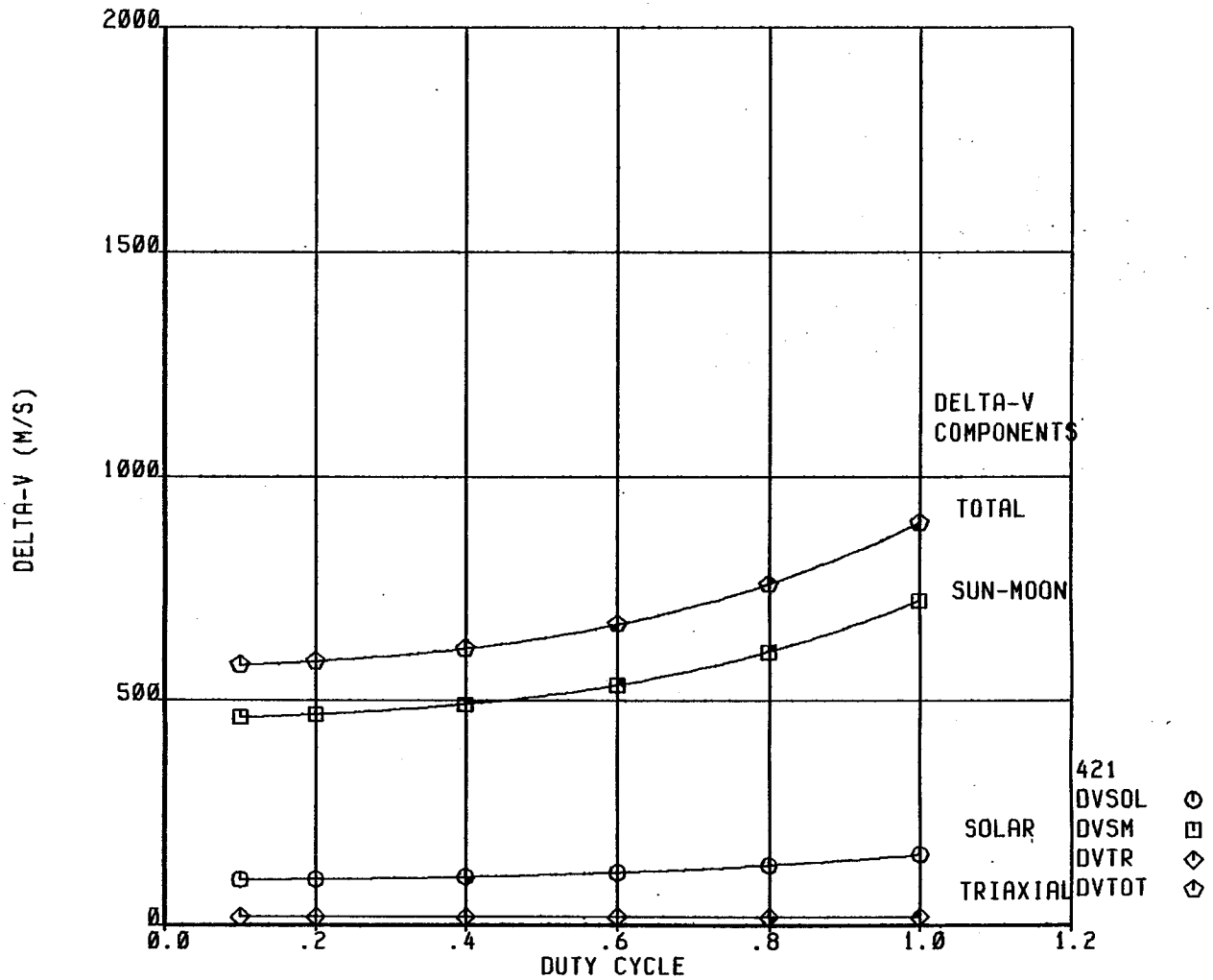

FIGURE D-66

STATIONKEEPING DELTA-V CALCULATIONS
SERIES OF ANTENNAS LARGE (4)
10 YEAR MISSION

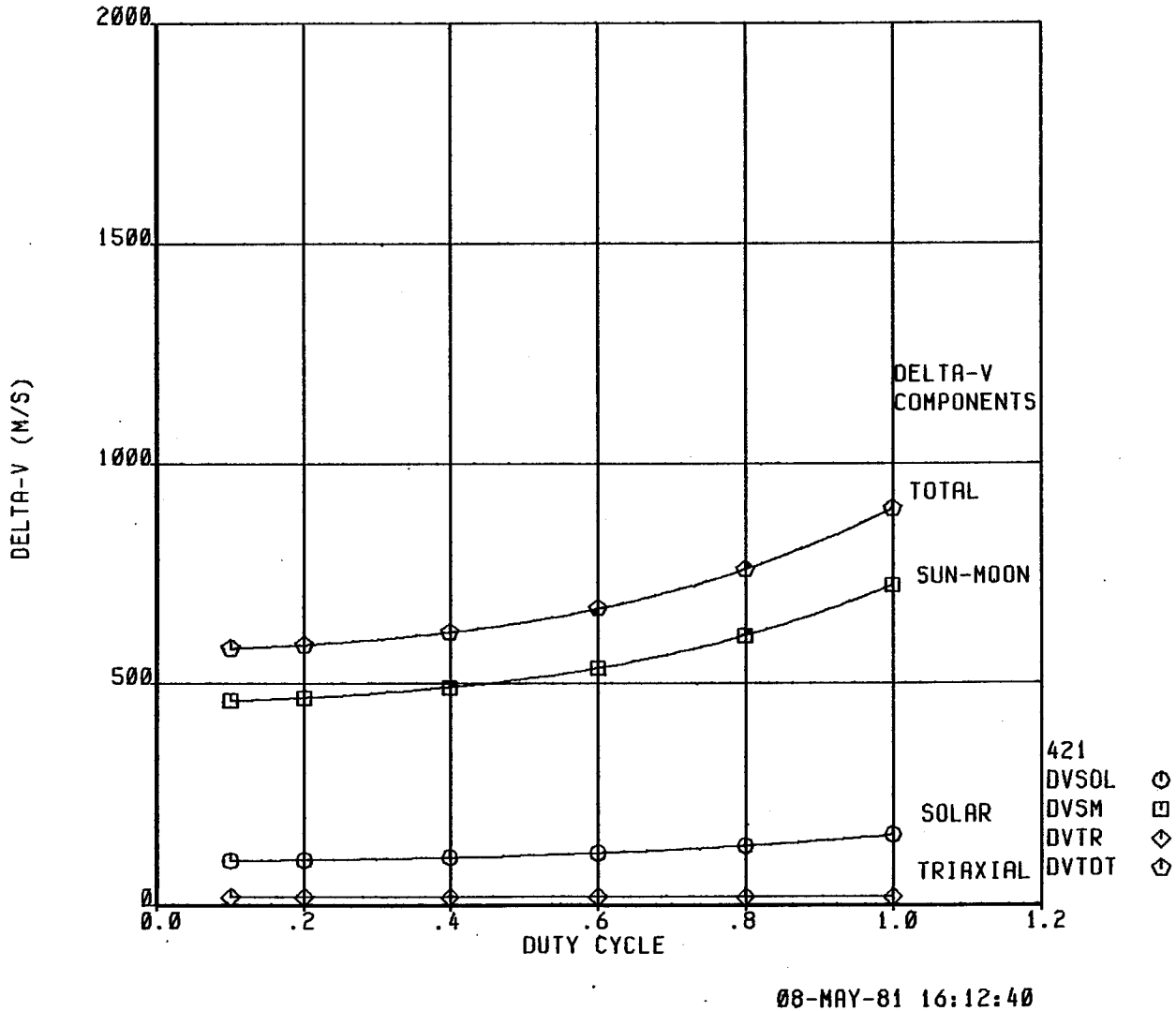

FIGURE D-67

STATIONKEEPING DELTA-V CALCULATIONS
PLATE STRUCTURE W/O BLANKET
10 YEAR MISSION

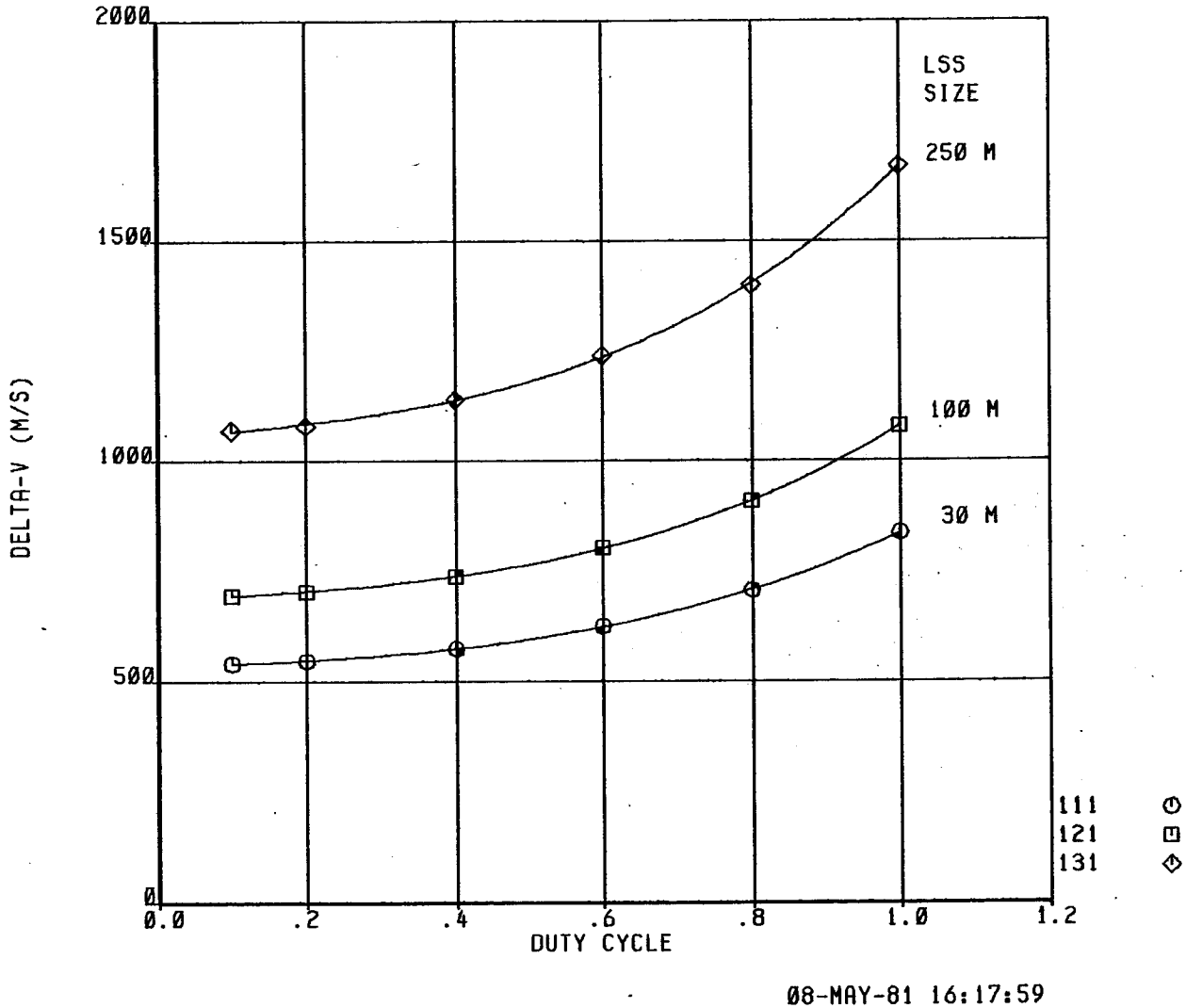

FIGURE D-68

STATIONKEEPING DELTA-V CALCULATIONS
PLATE STRUCTURE W/ BLANKET
10 YEAR MISSION

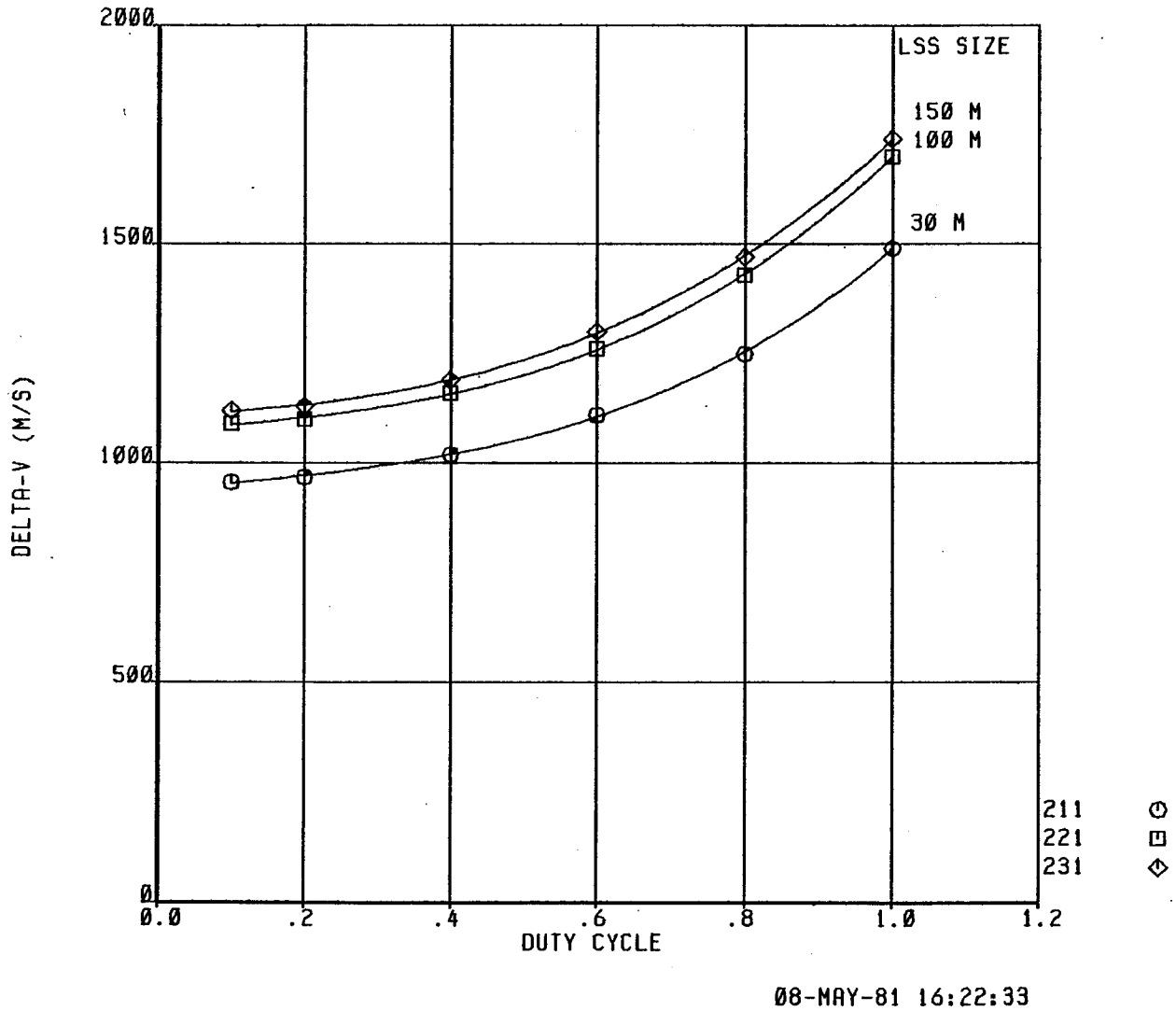

FIGURE D-69

STATIONKEEPING DELTA-V CALCULATIONS
MODULAR ANTENNA STRUCTURE
10 YEAR MISSION

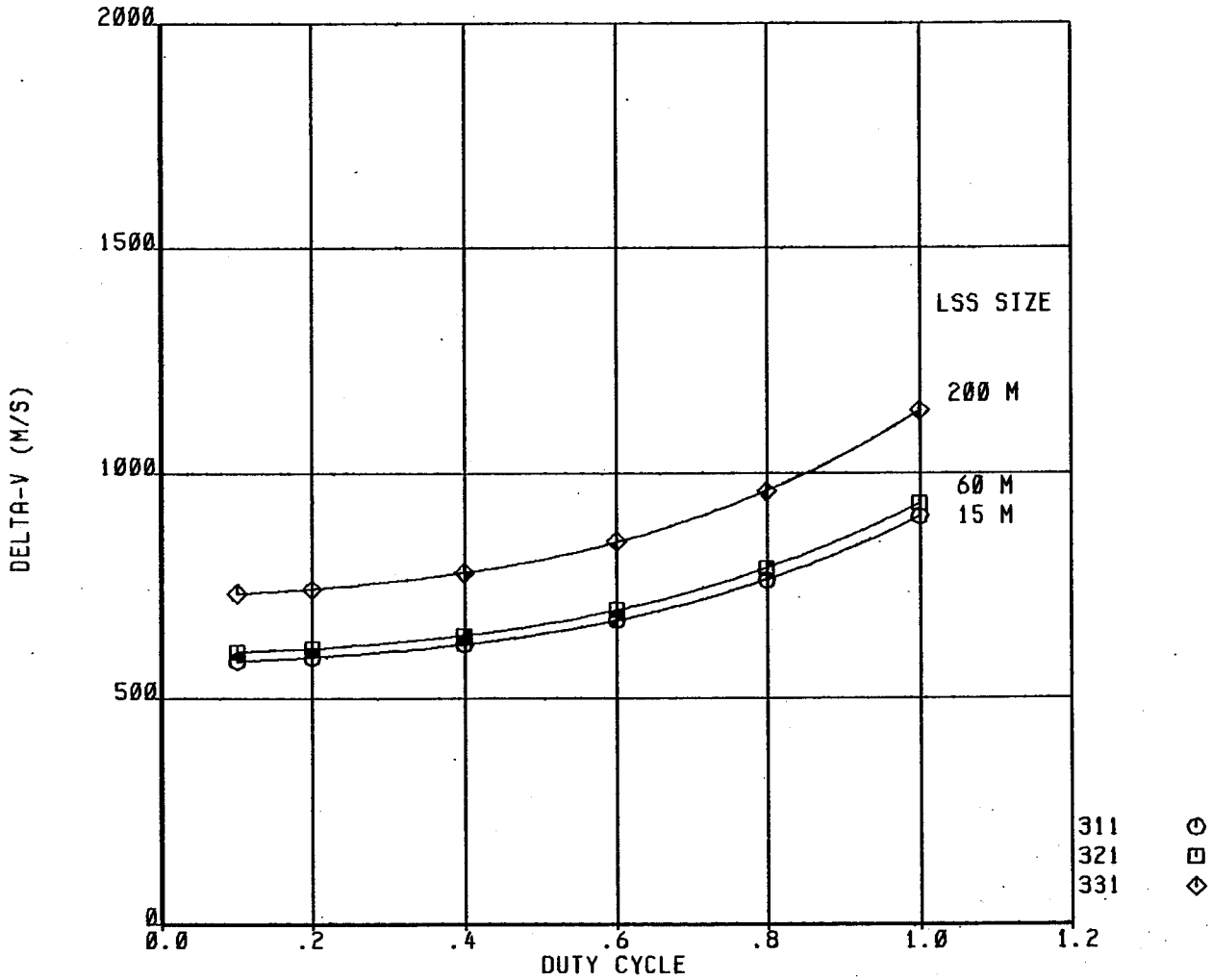

FIGURE D-70

STATIONKEEPING DELTA-V CALCULATIONS
SERIES OF ANTENNAS
10 YEAR MISSION

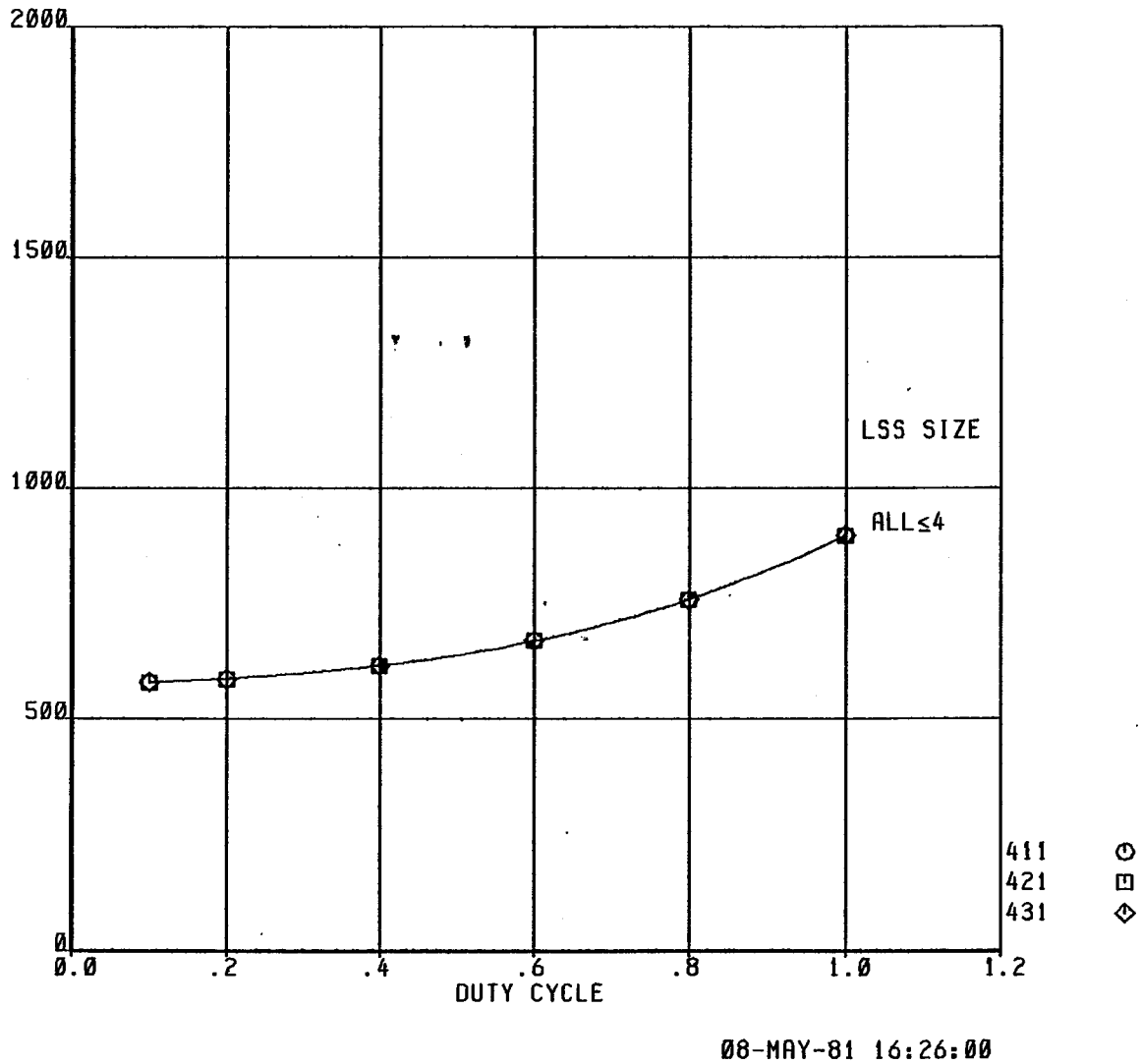

FIGURE D-71

STATIONKEEPING THRUST REQUIREMENTS
PLATE STRUCTURE W/O BLANKET

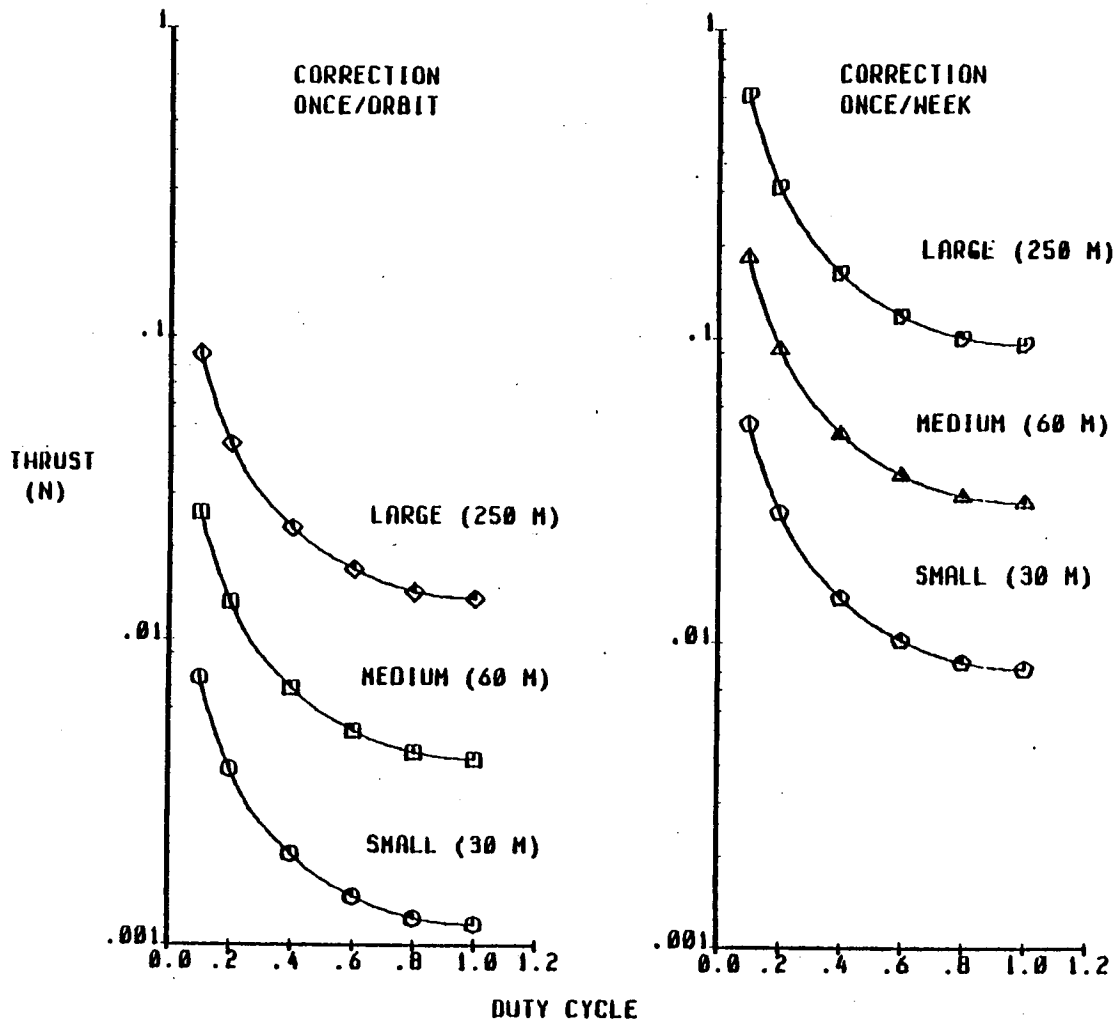

FIGURE D-72

STATIONKEEPING THRUST REQUIREMENTS
PLATE STRUCTURE W/BLANKET

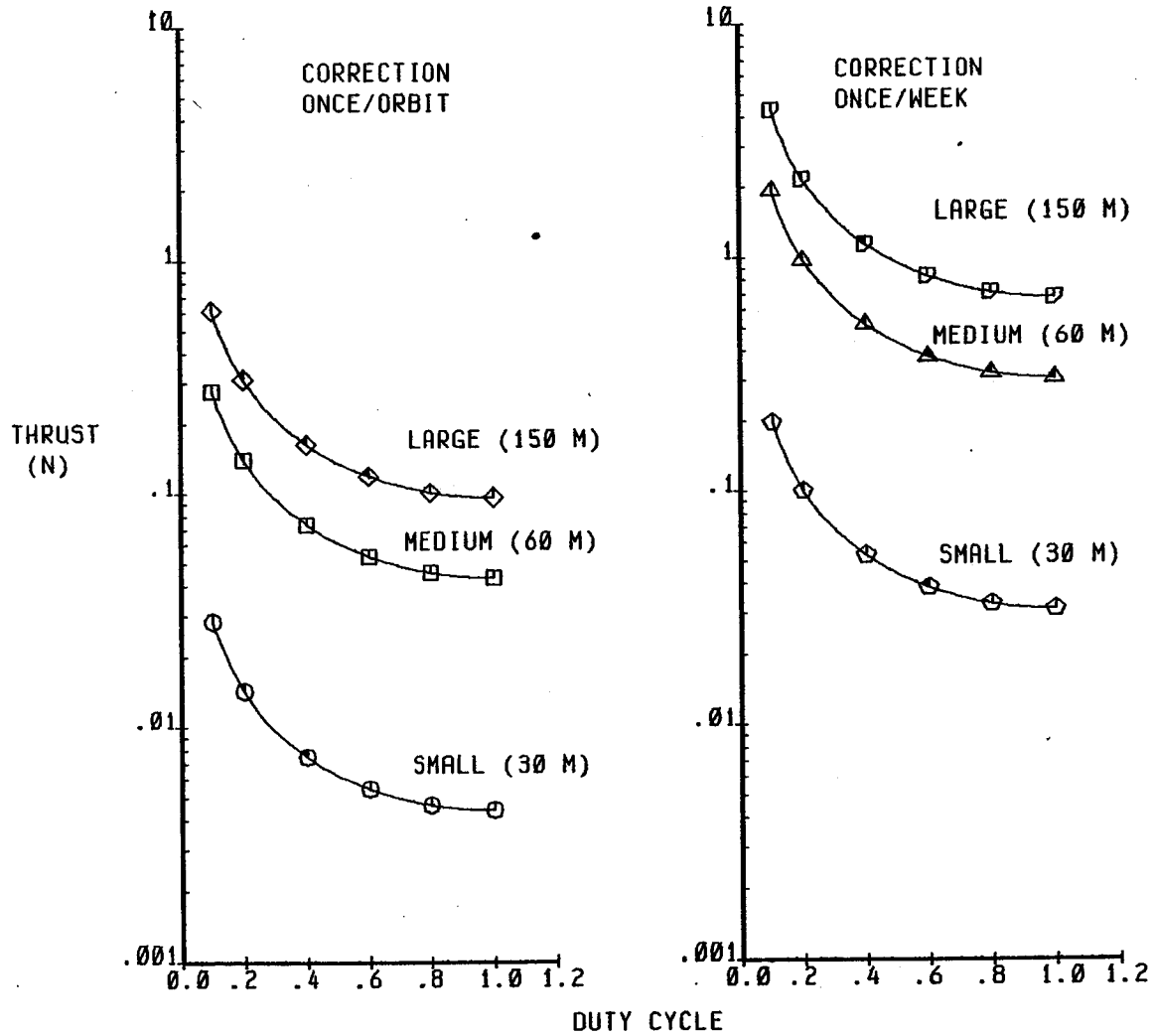

FIGURE D-73

STATIONKEEPING THRUST REQUIREMENTS
MODULAR ANTENNA STRUCTURE

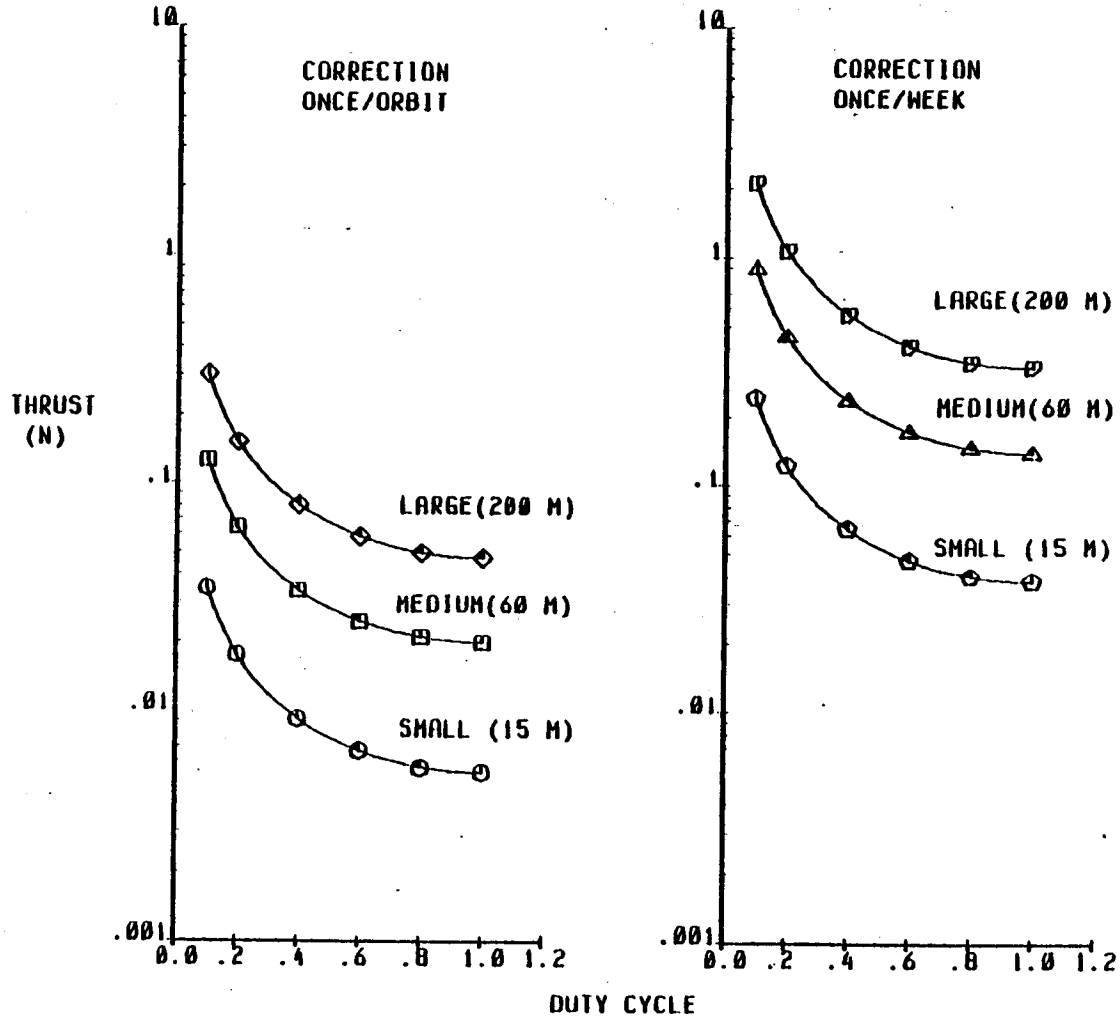

FIGURE D-74

STATIONKEEPING THRUST REQUIREMENTS
SERIES OF ANTENNAS

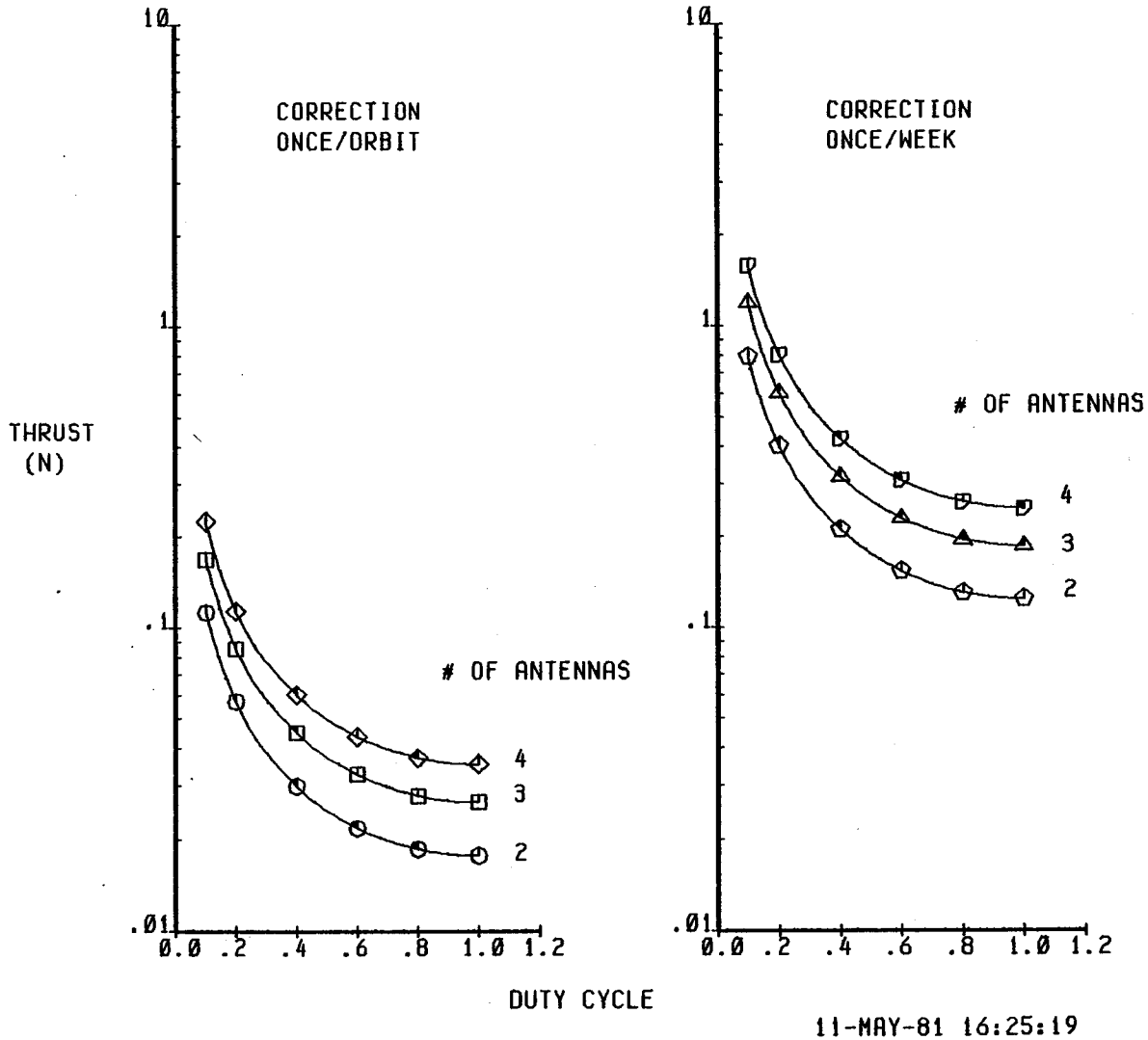

APPENDIX E

APS Mass, System Mass Component Breakdown

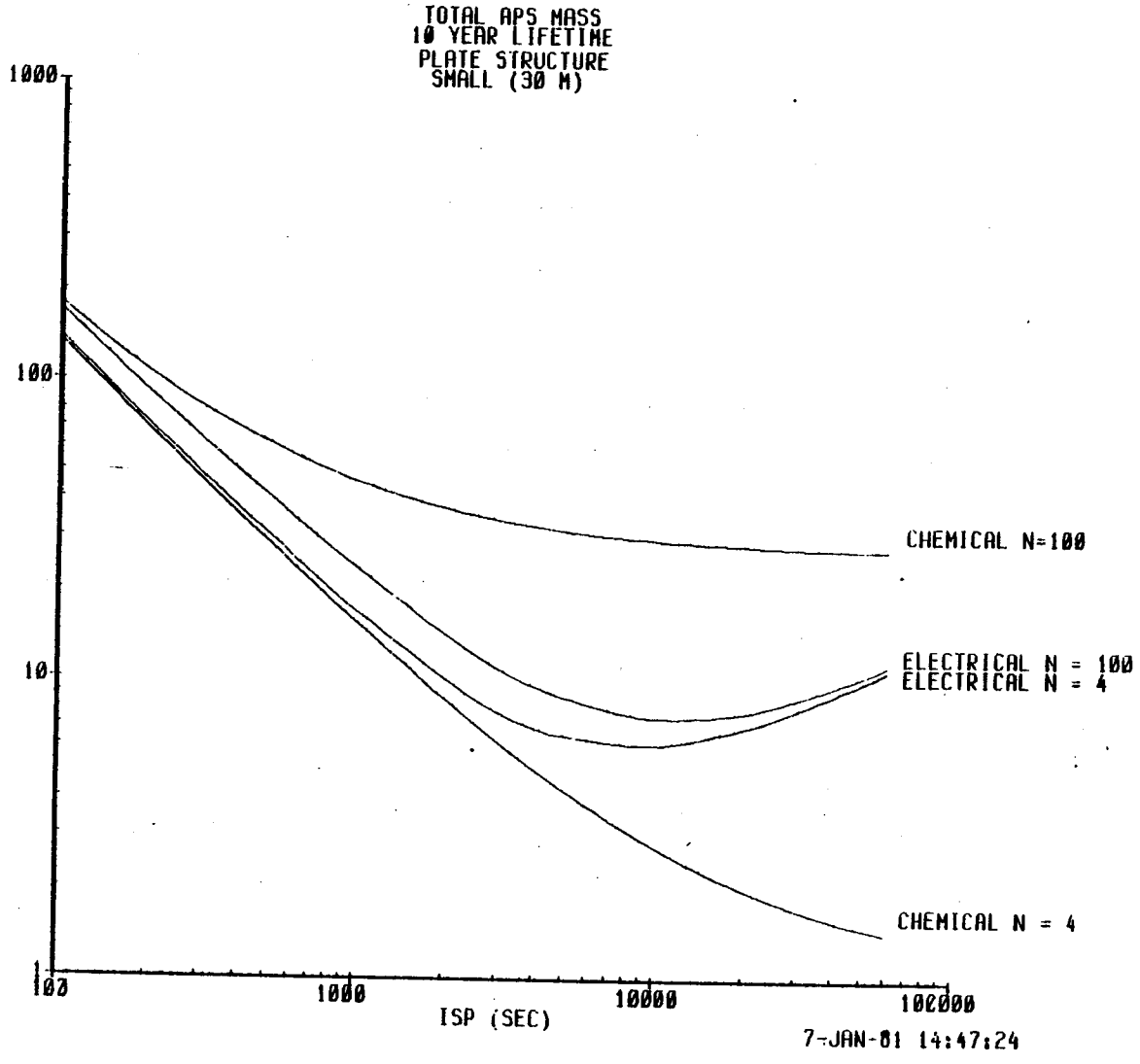

FIGURE E-1 TOTAL APS MASS, SMALL PLATE STRUCTURE

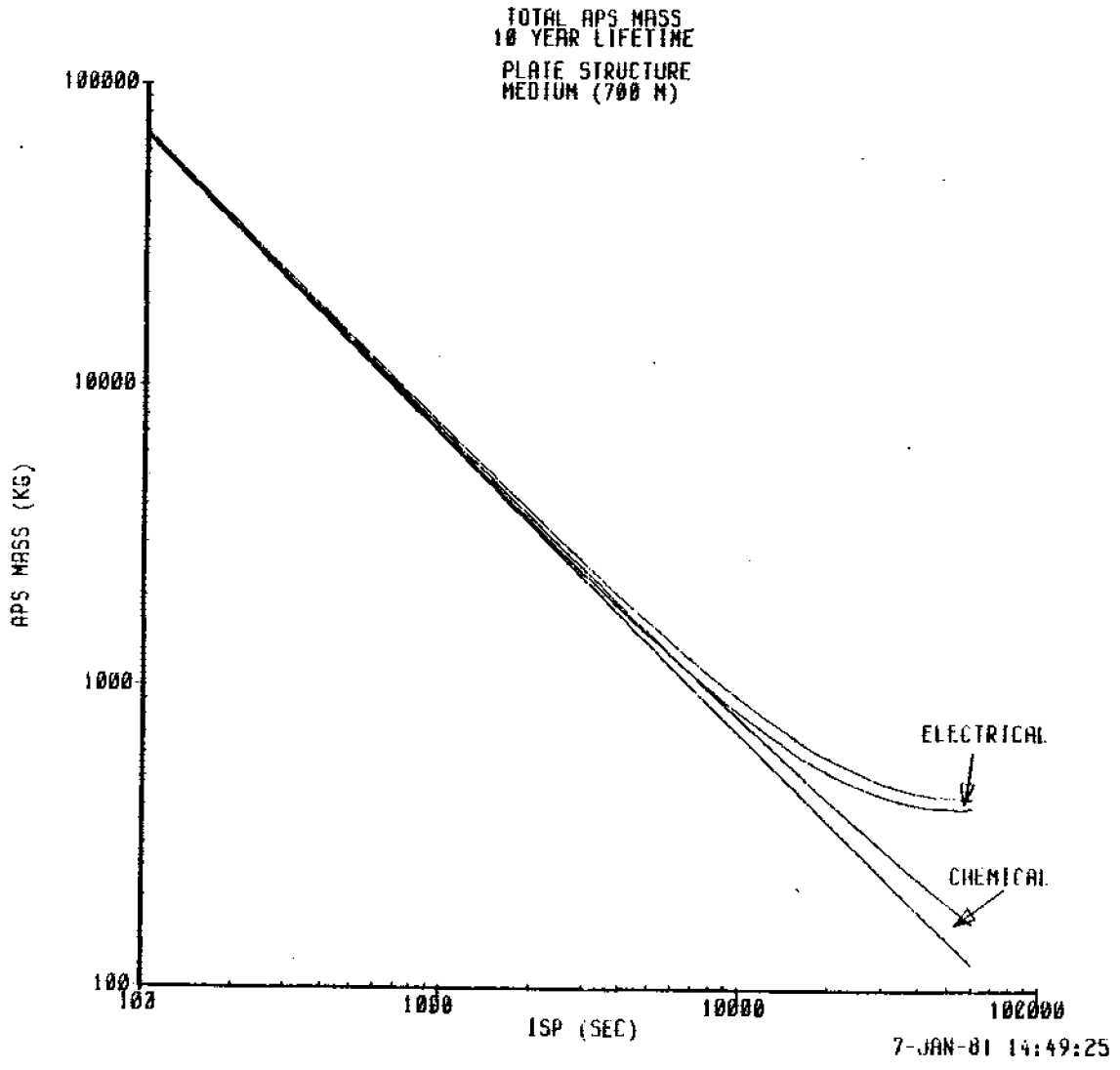

FIGURE E-2 TOTAL APS MASS, MEDIUM PLATE STRUCTURE

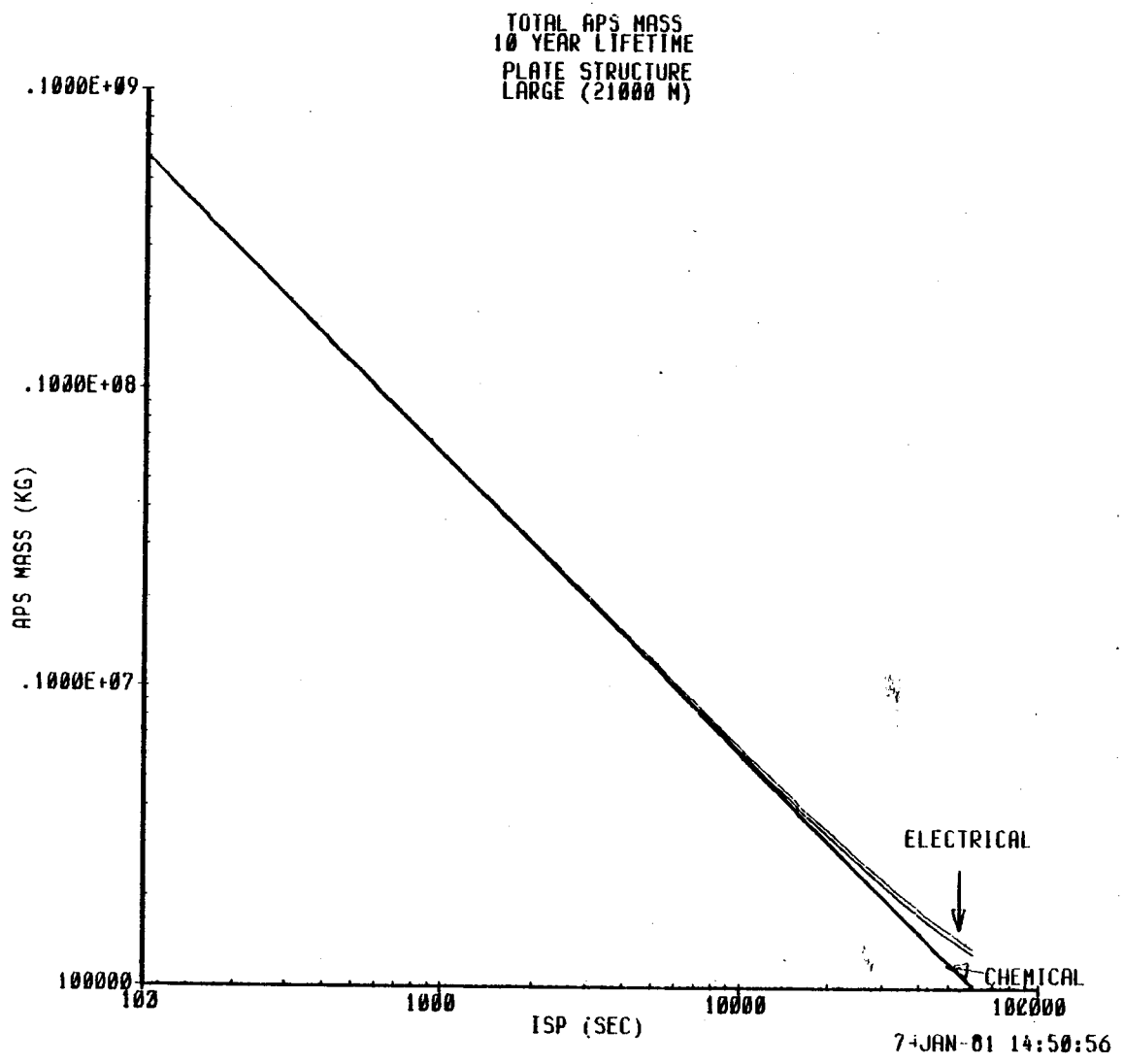

FIGURE E-3 TOTAL APS MASS, LARGE PLATE STRUCTURE

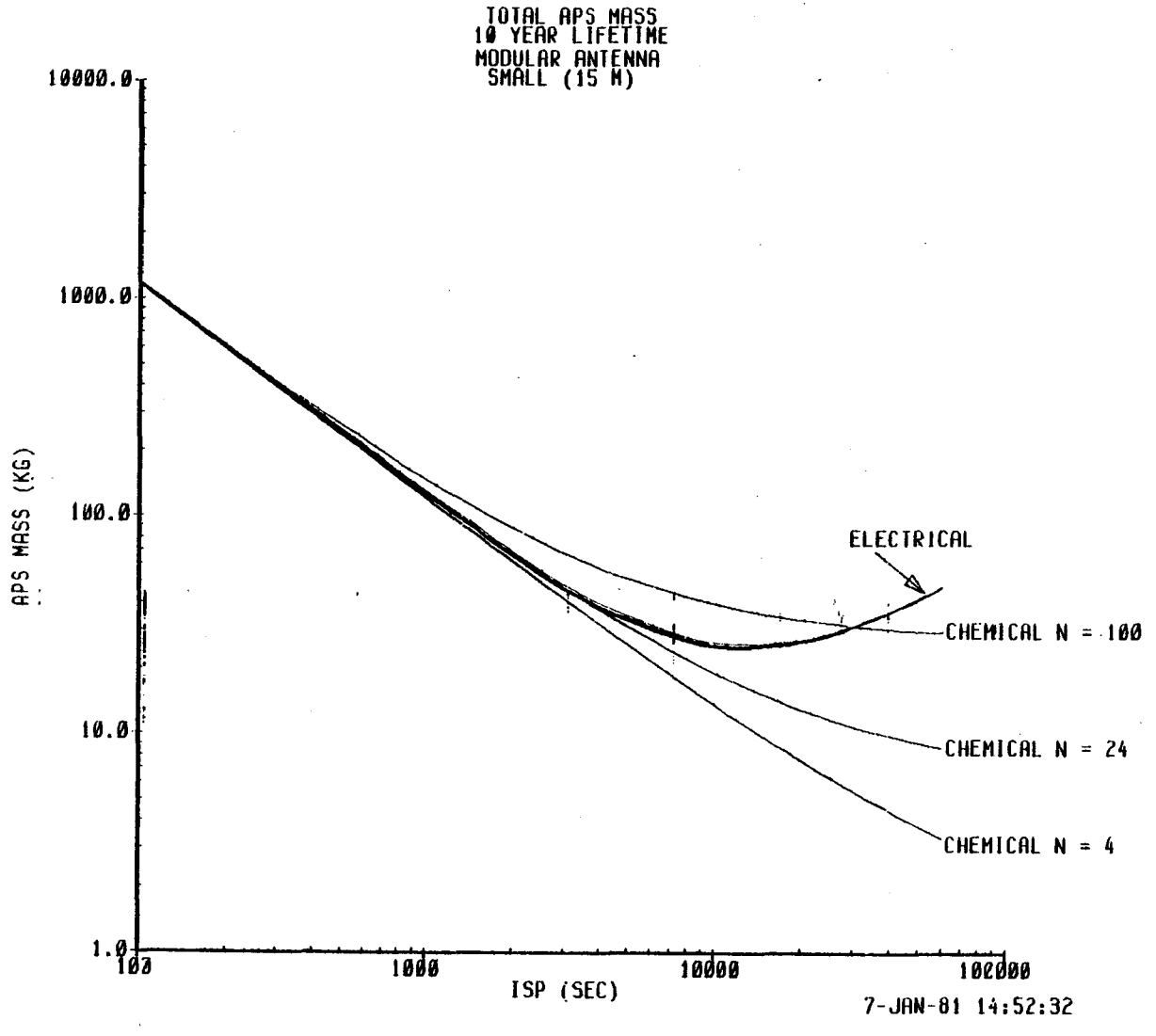

FIGURE E-4 TOTAL APS MASS, SMALL MODULAR ANTENNA

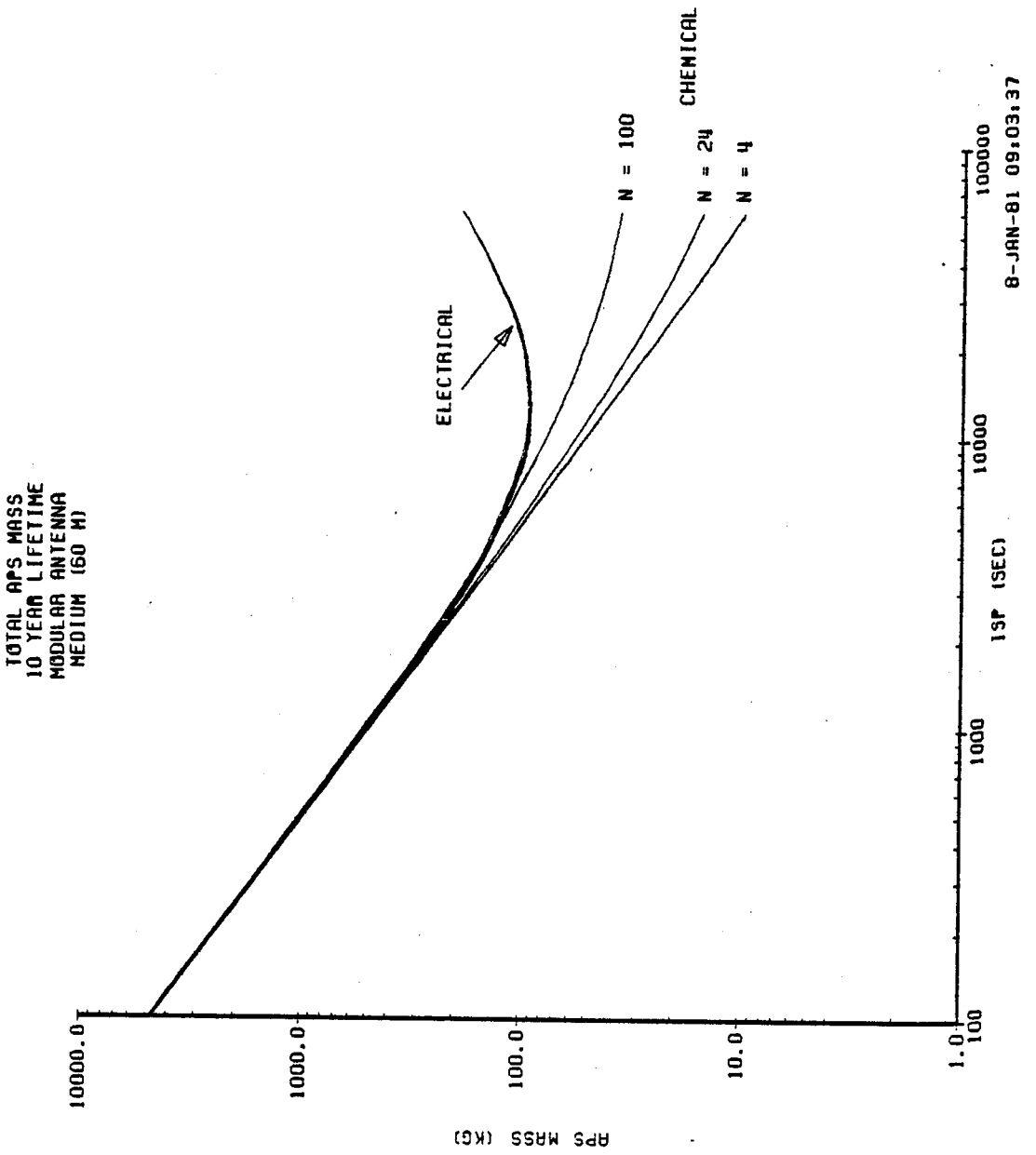

FIGURE E-5 TOTAL APS MASS, MEDIUM MODULAR ANTENNA

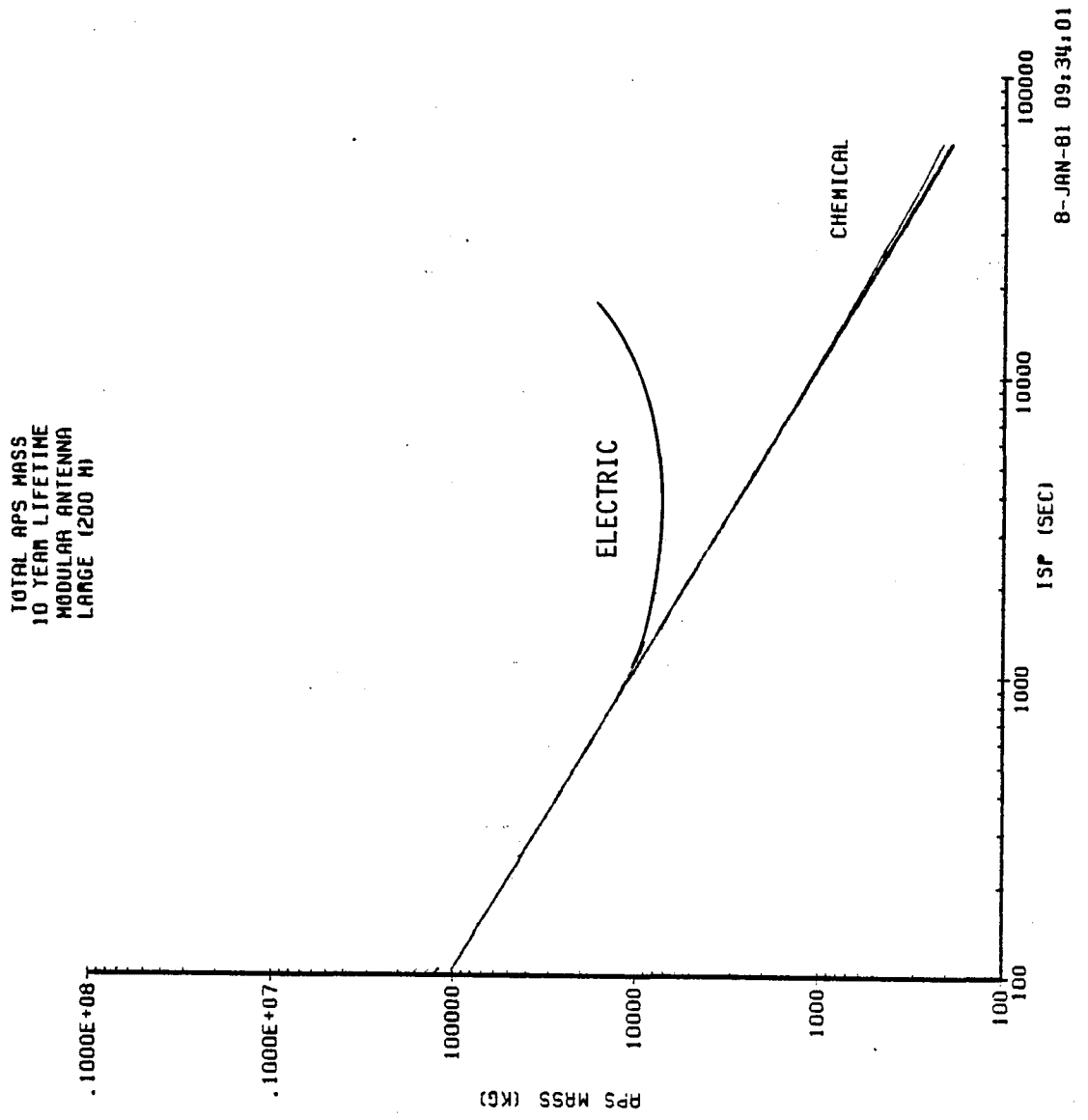

FIGURE E-6 TOTAL APS MASS, LARGE MODULAR ANTENNA

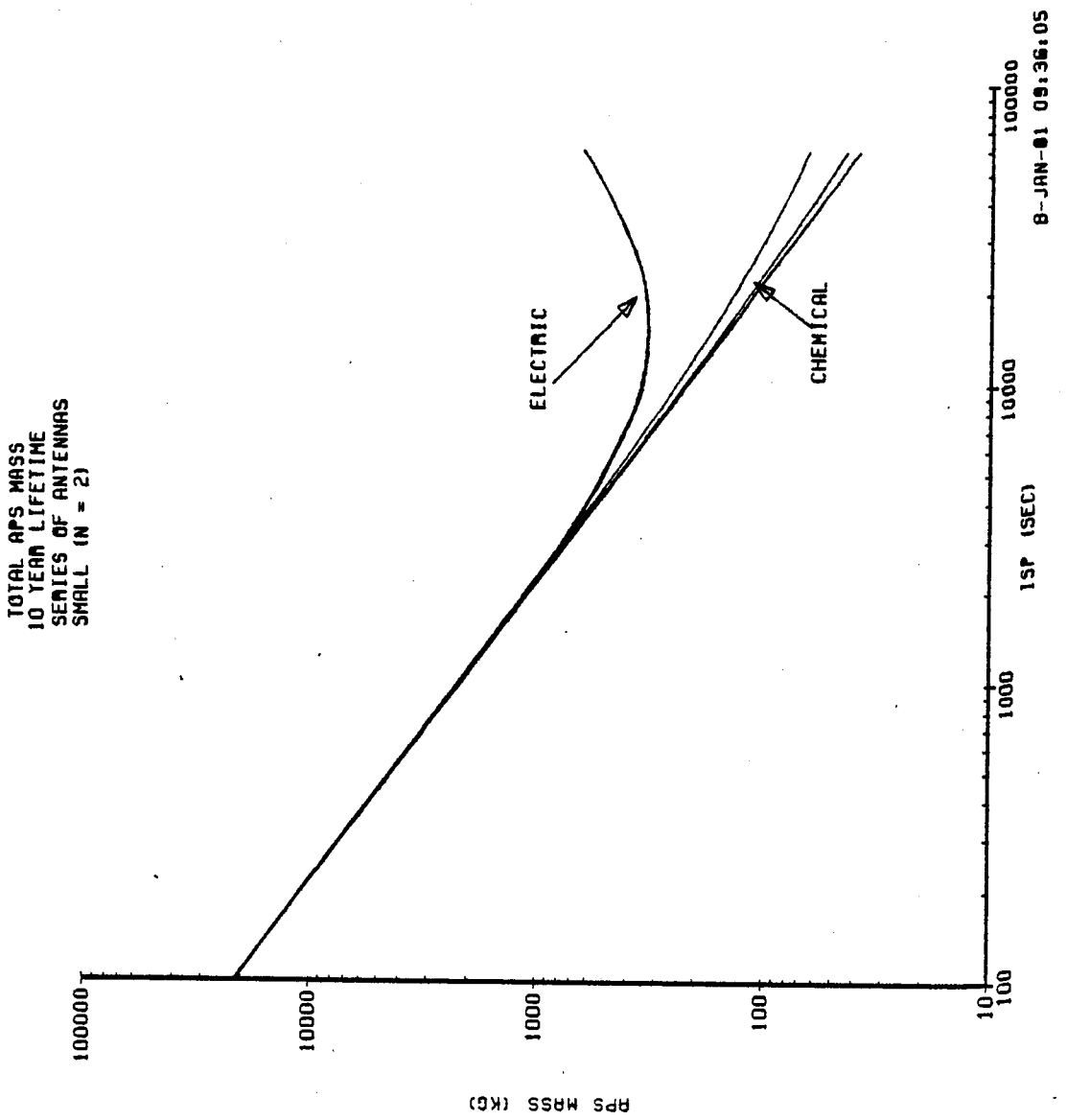

FIGURE E-7 TOTAL APS MASS, SMALL SERIES OF ANTENNAS

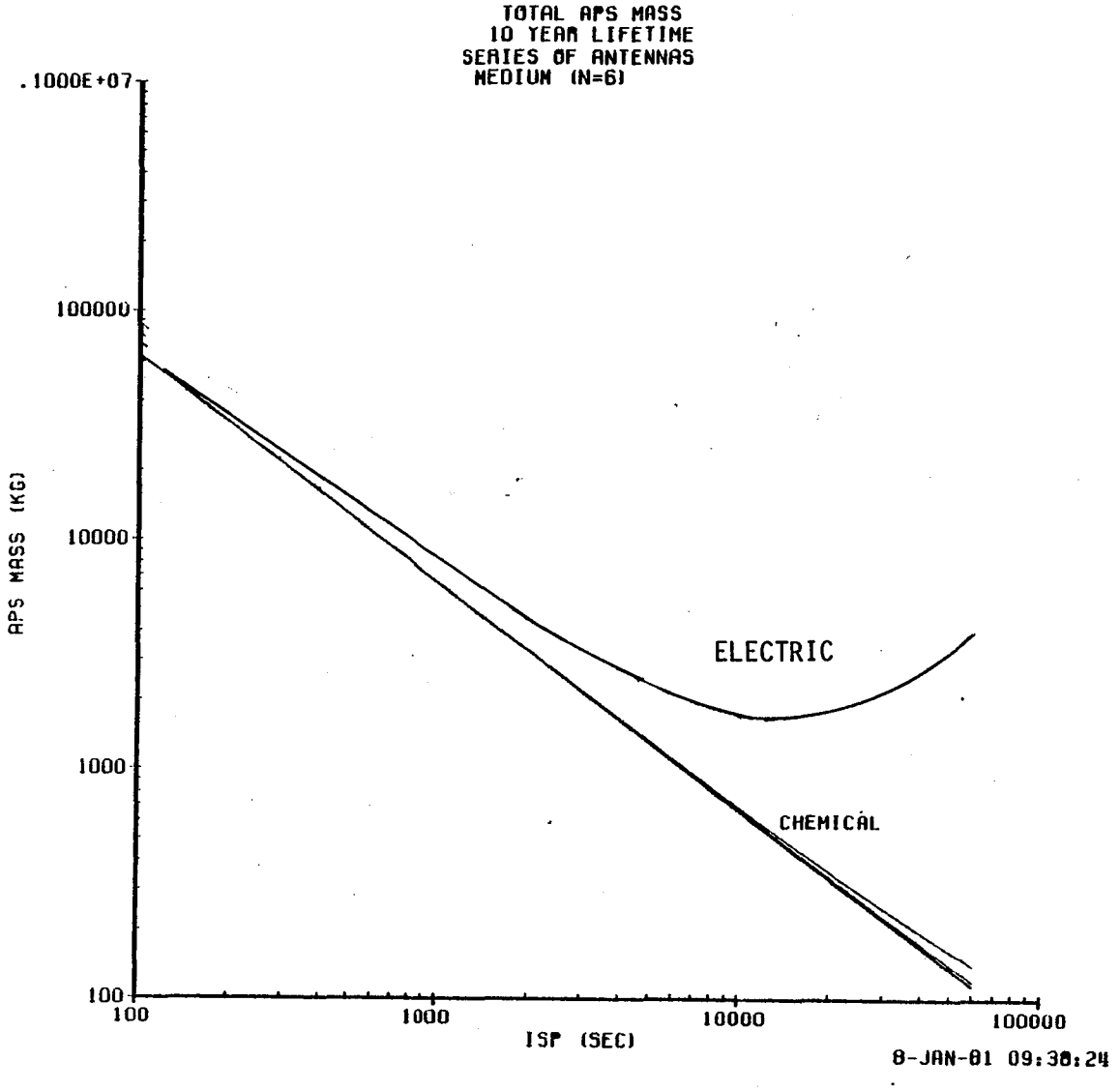

FIGURE E-8 TOTAL APS MASS, MEDIUM SERIES OF ANTENNAS

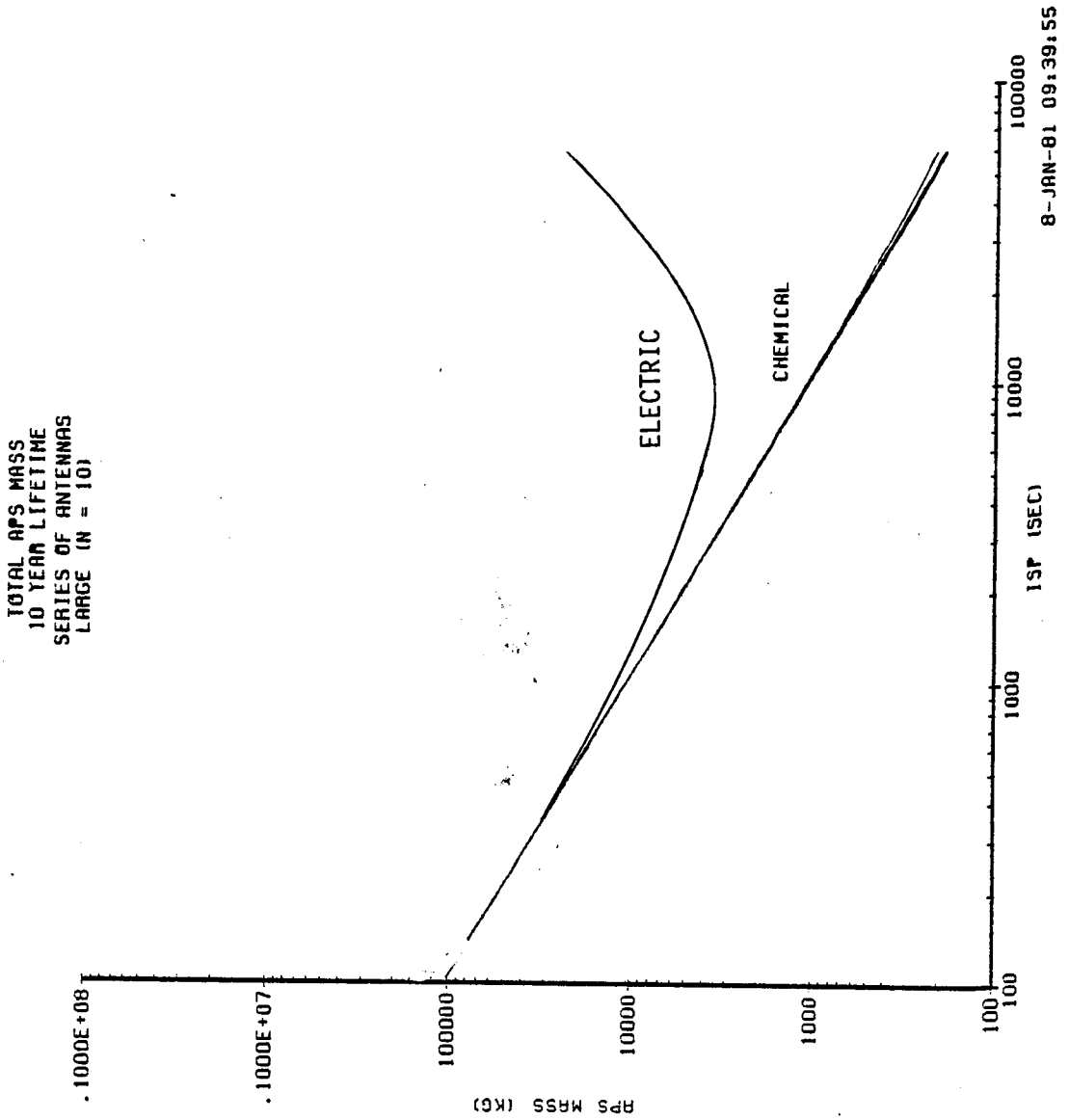

FIGURE E-9 TOTAL APS MASS, LARGE SERIES OF ANTENNAS

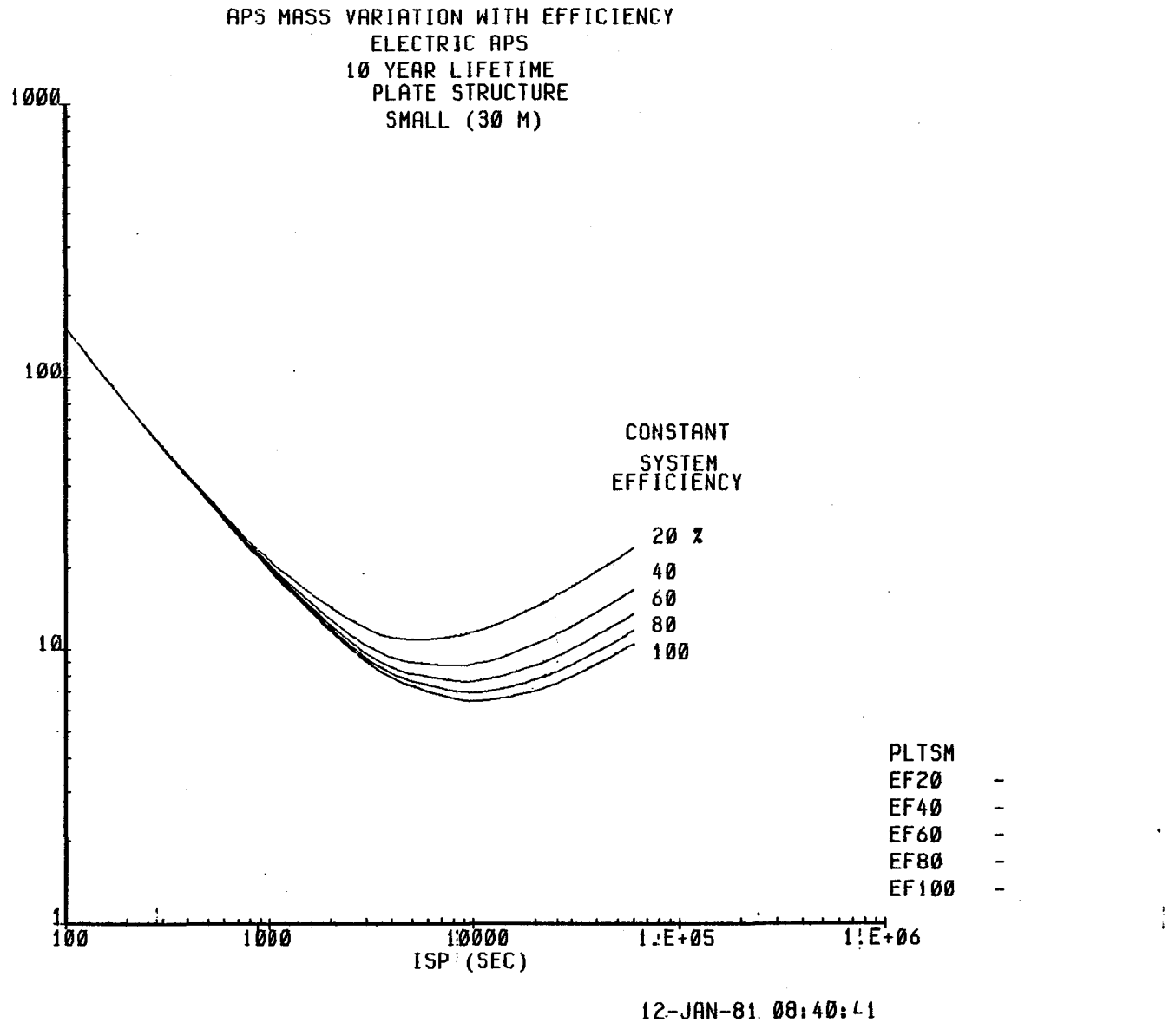

FIGURE E-10 APS MASS VARIATION WITH EFFICIENCY, SMALL PLATE STRUCTURE

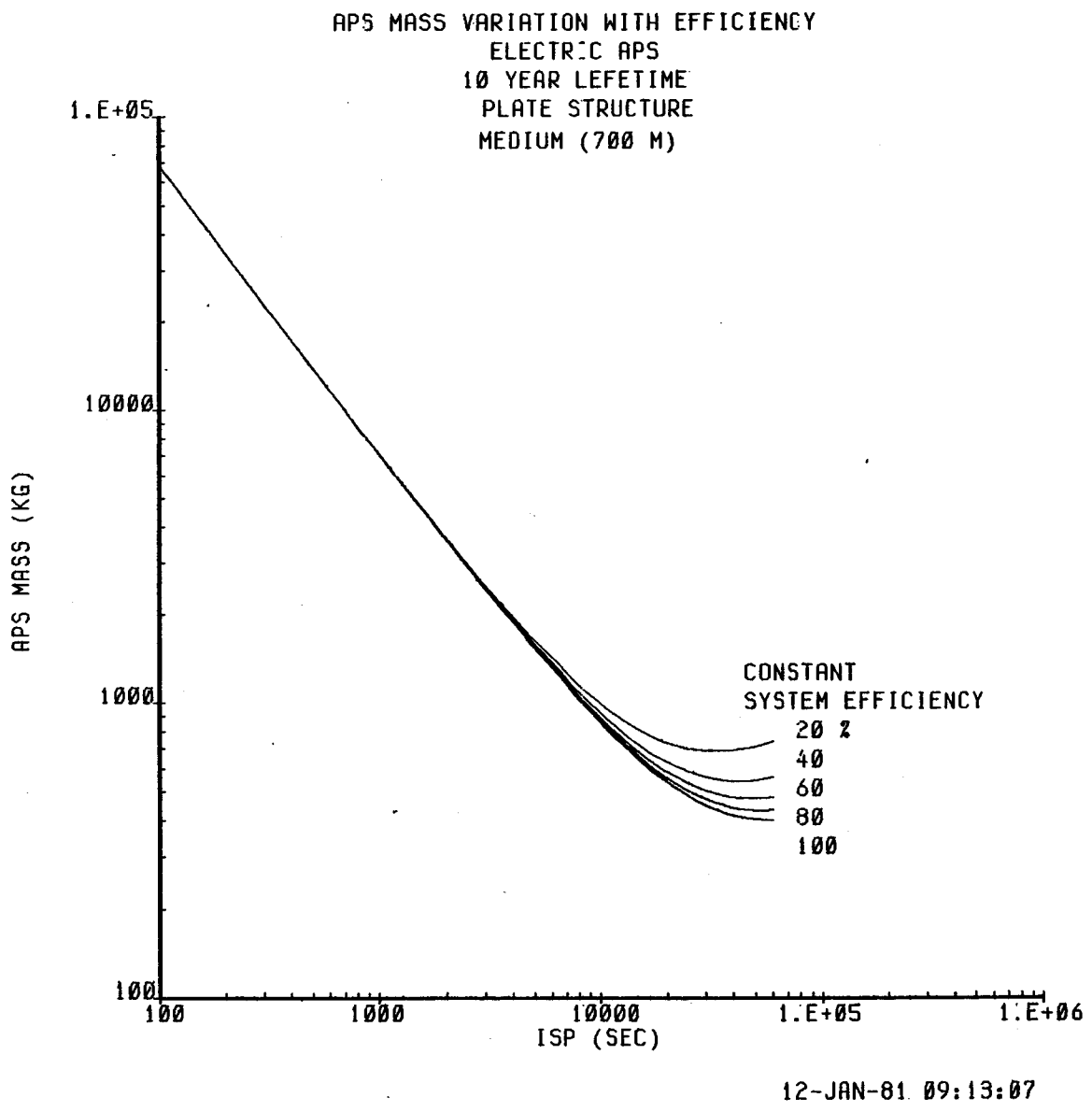

FIGURE E-11 APS MASS VARIATION WITH EFFICIENCY, MEDIUM PLATE STRUCTURE

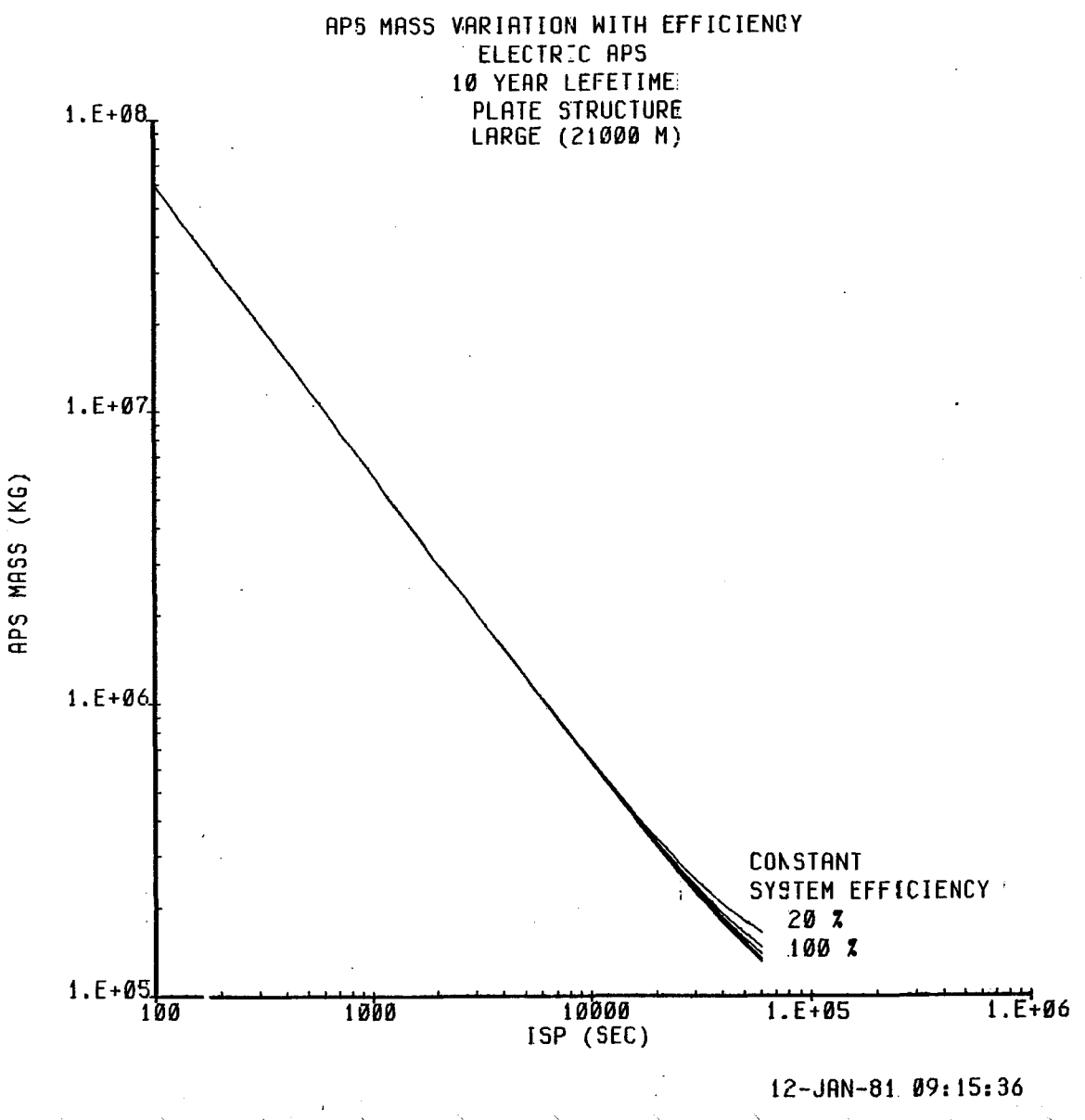

FIGURE E-12 APS MASS VARIATION WITH EFFICIENCY, LARGE PLATE STRUCTURE

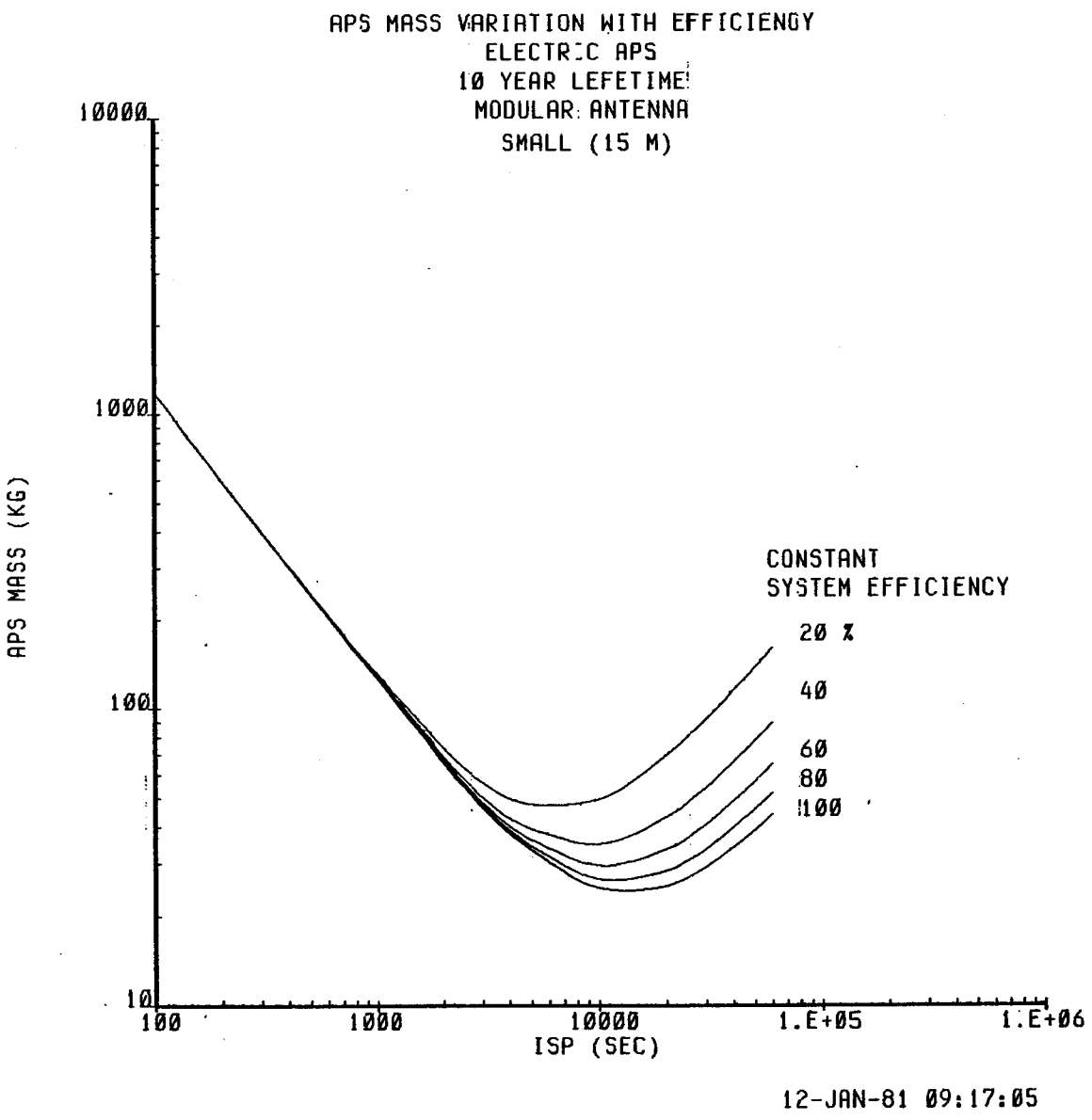

FIGURE E-13 APS MASS VARIATION WITH EFFICIENCY, SMALL MODULAR ANTENNA

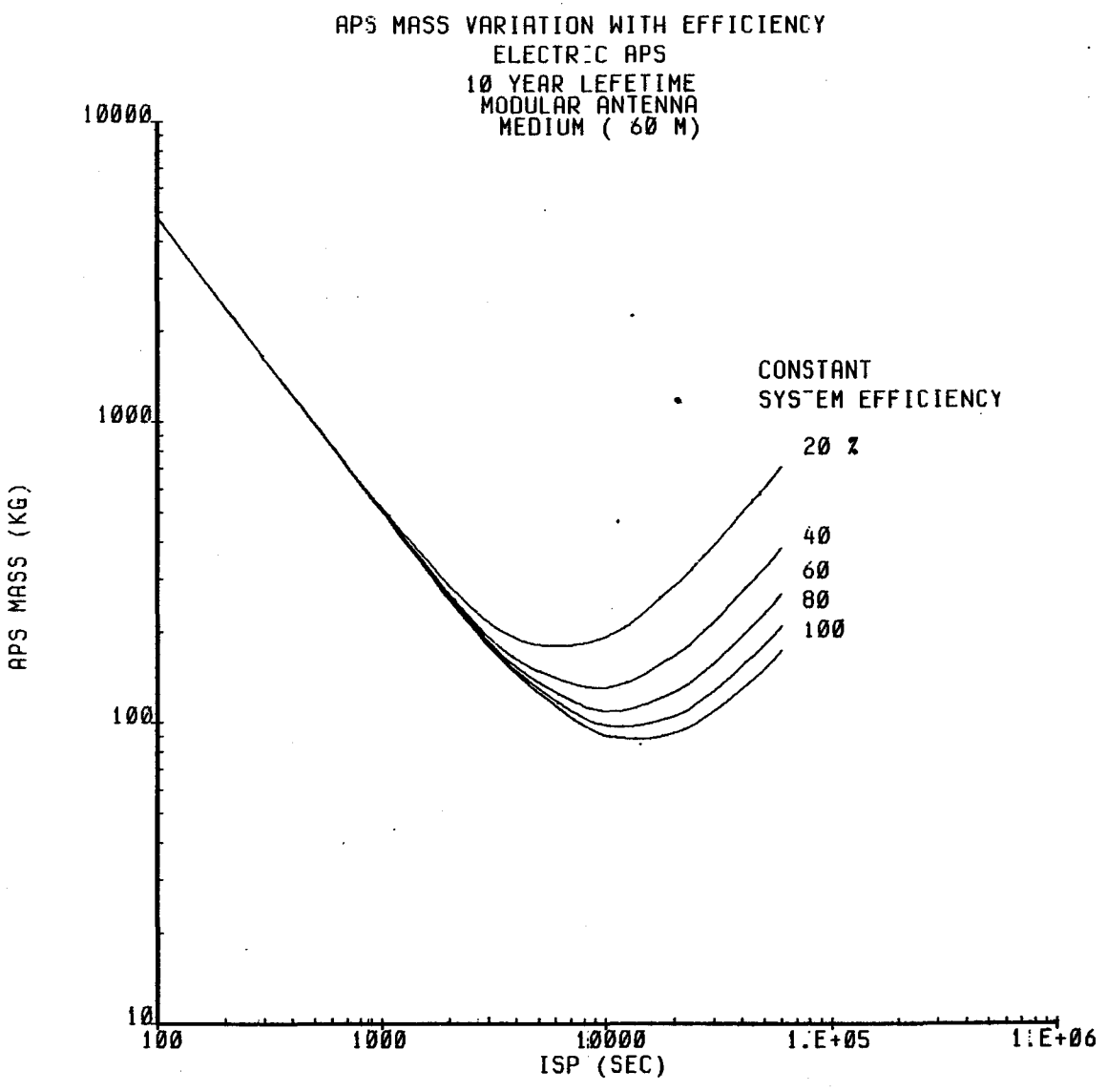

FIGURE E-14 APS MASS VARIATION WITH EFFICIENCY, MEDIUM MODULAR ANTENNA

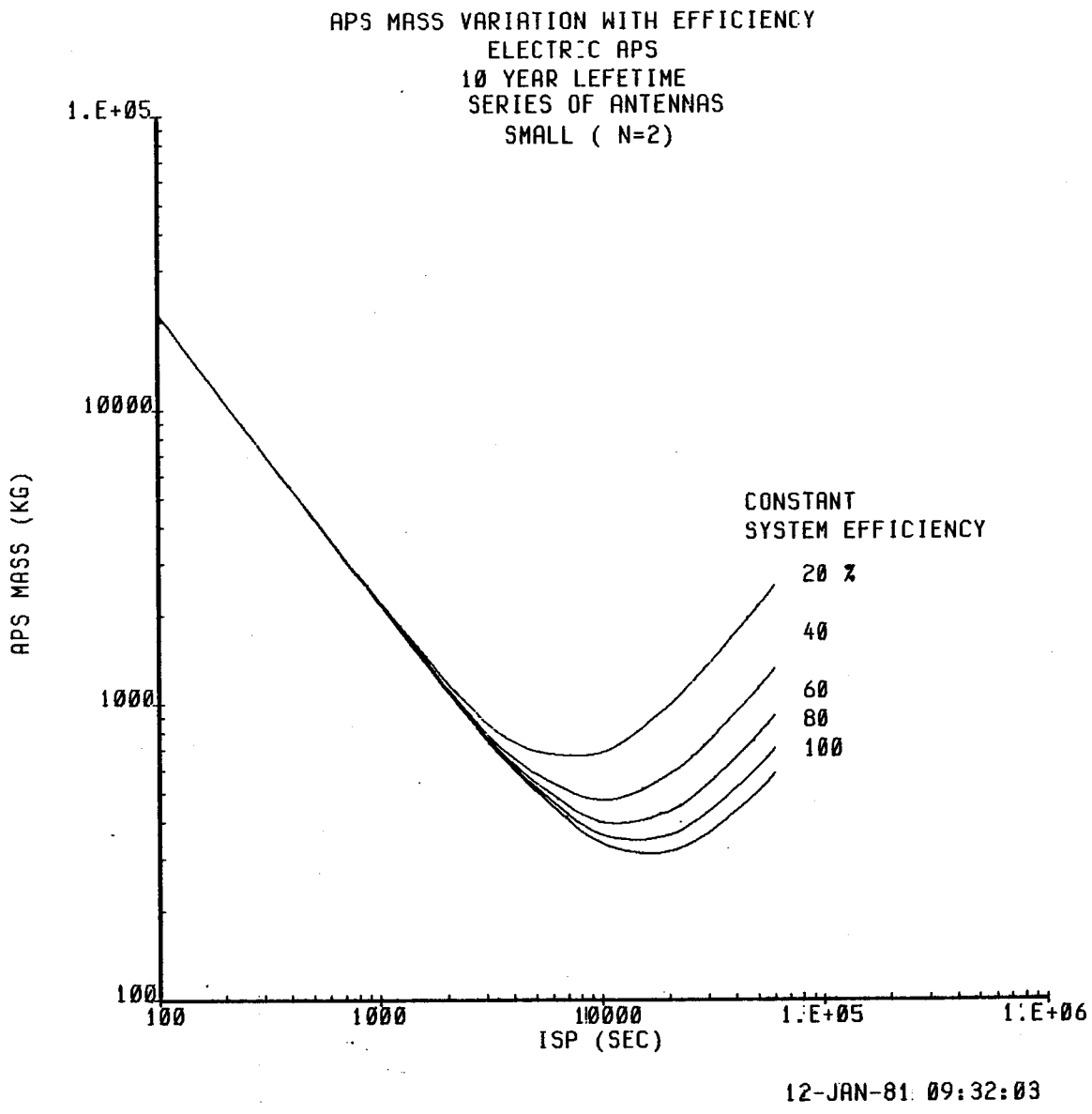

FIGURE E-15. APS MASS VARIATION WITH EFFICIENCY, SMALL SERIES OF ANTENNAS

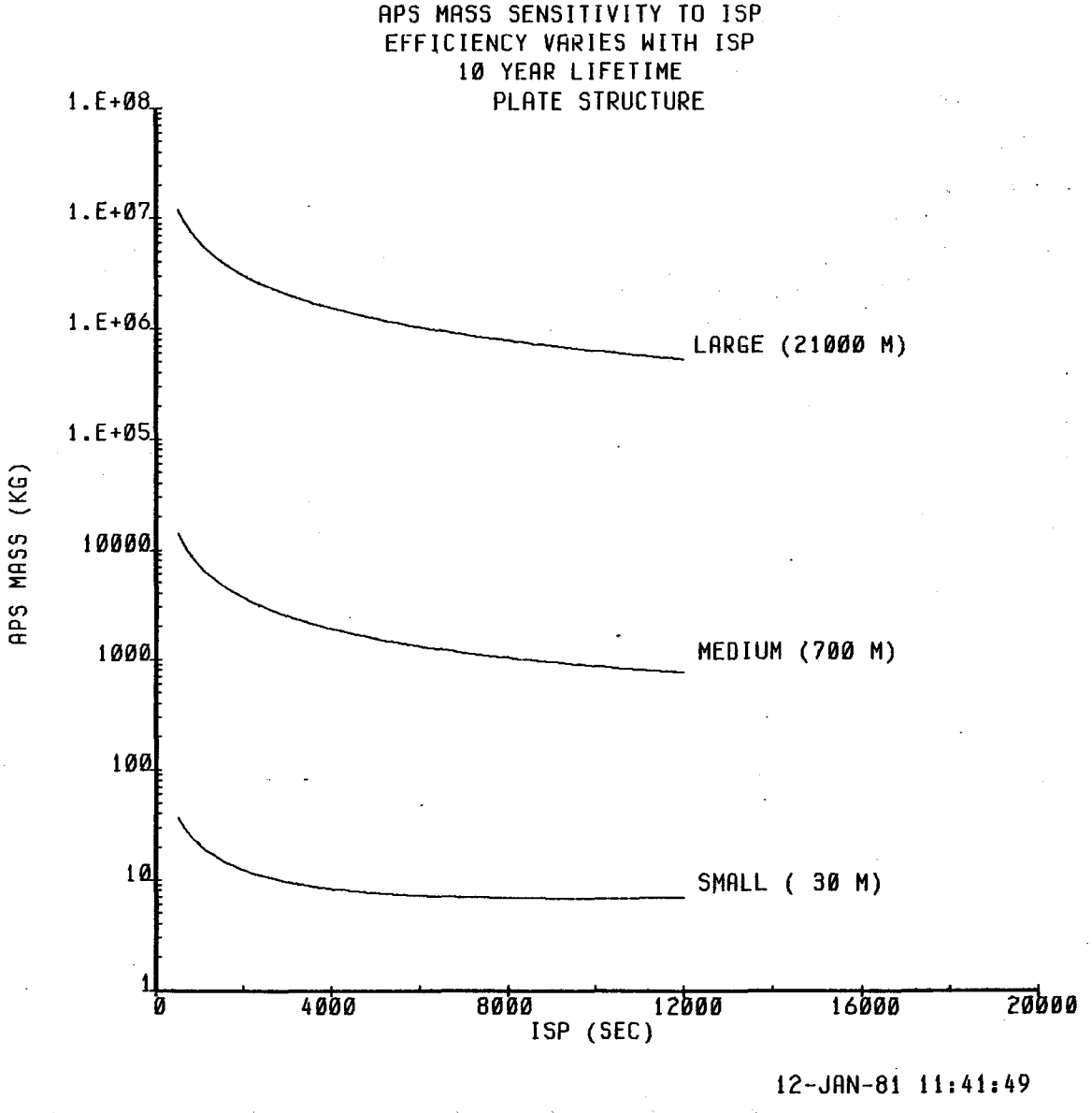

FIGURE E-16 APS MASS SENSITIVITY TO ISP, PLATE STRUCTURE

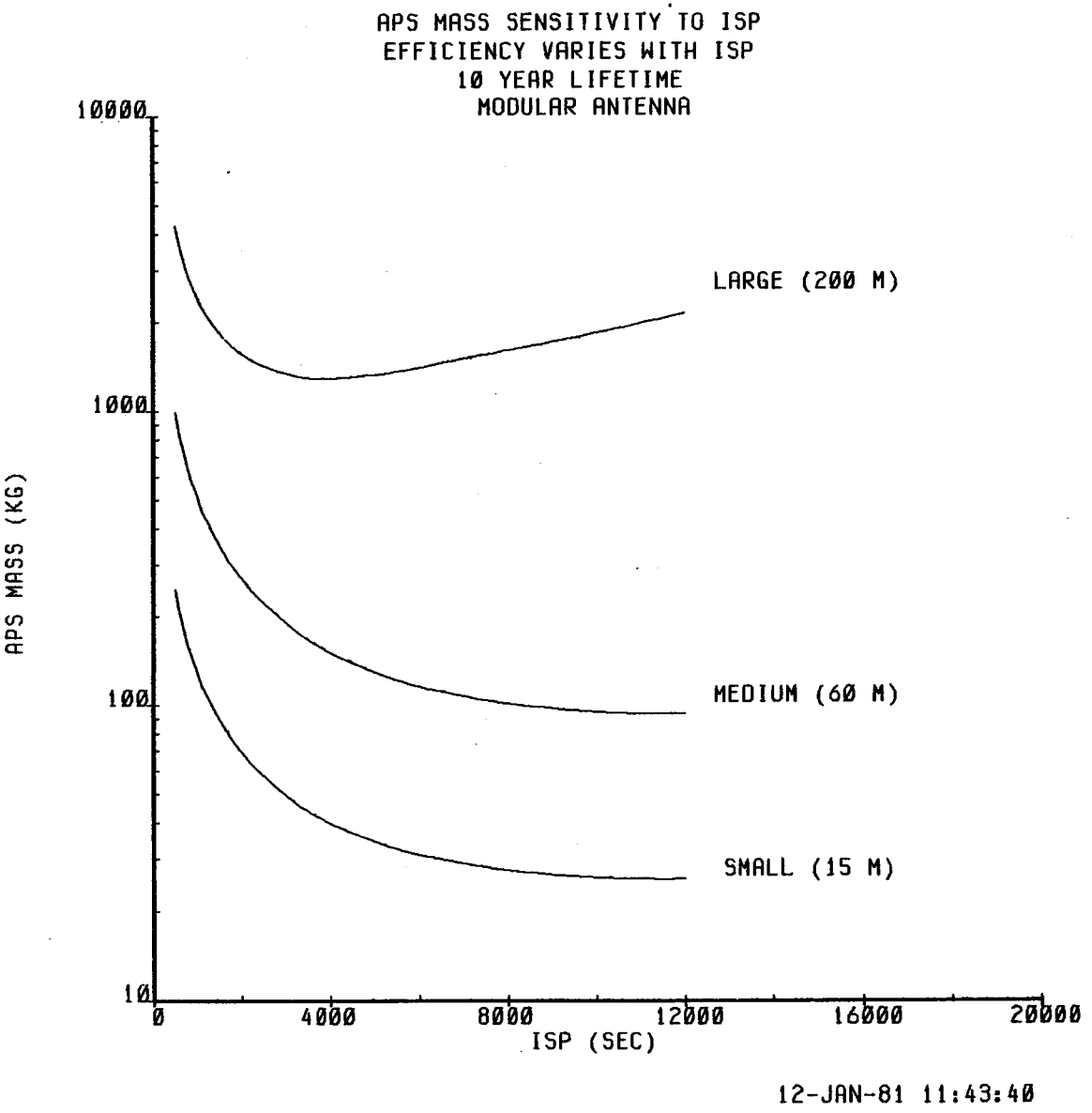

FIGURE E-17 APS MASS SENSITIVITY TO ISP, MODULAR ANTENNA

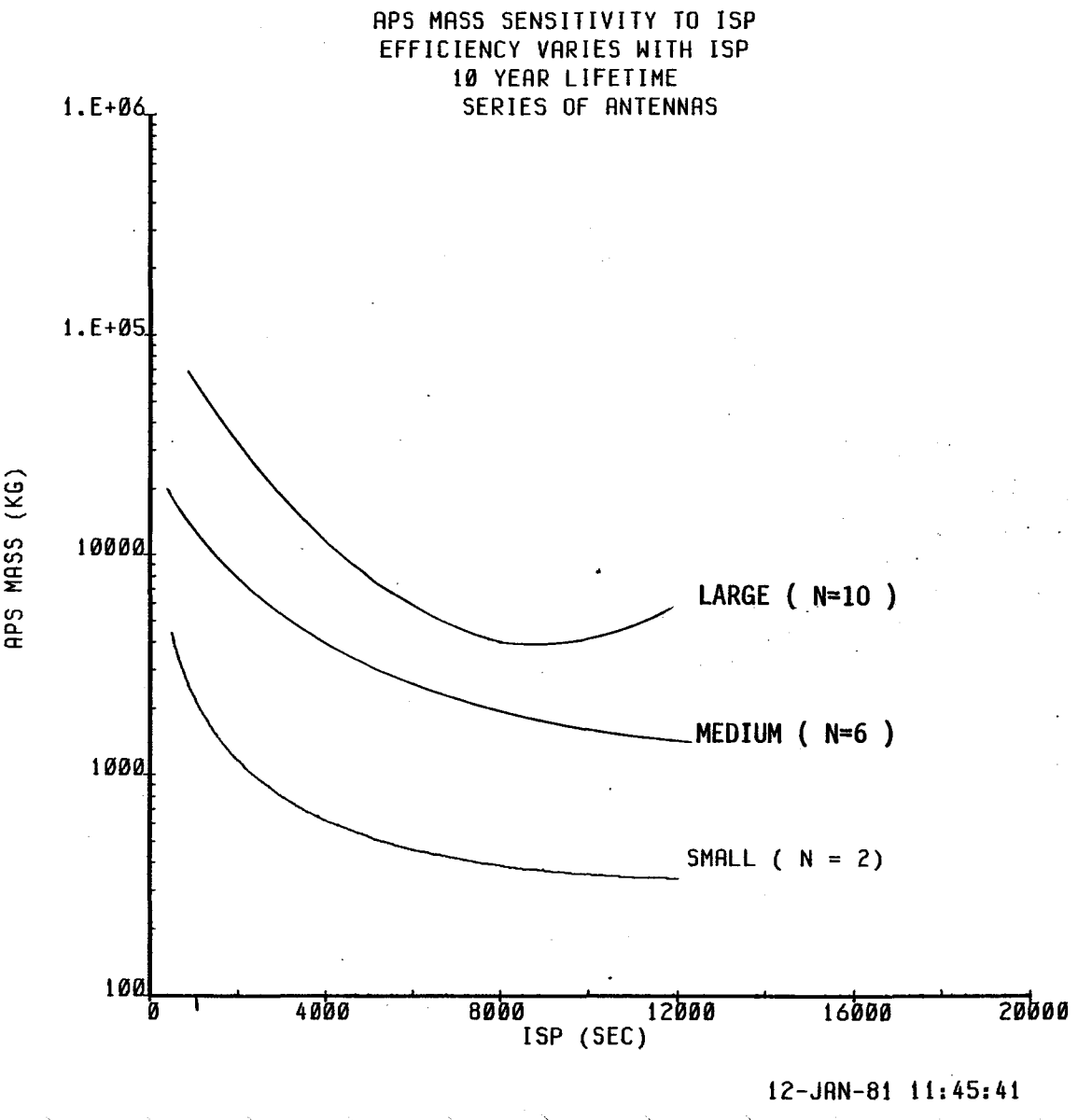

FIGURE E-18 APS MASS SENSITIVITY TO ISP, SERIES OF ANTENNAS

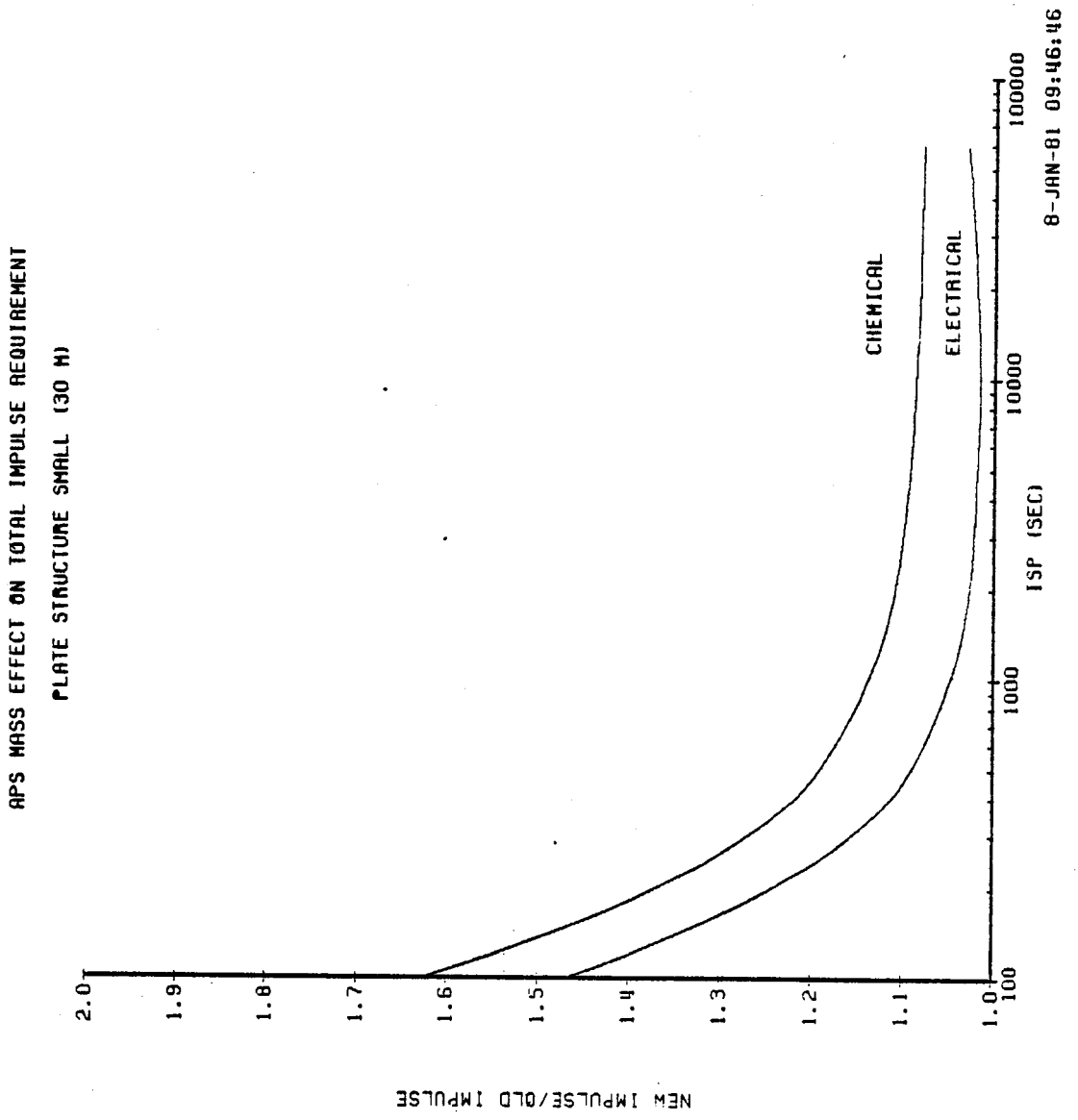

FIGURE E-19 APS MASS EFFECT ON TOTAL IMPULSE REQUIREMENT, SMALL PLATE STRUCTURE

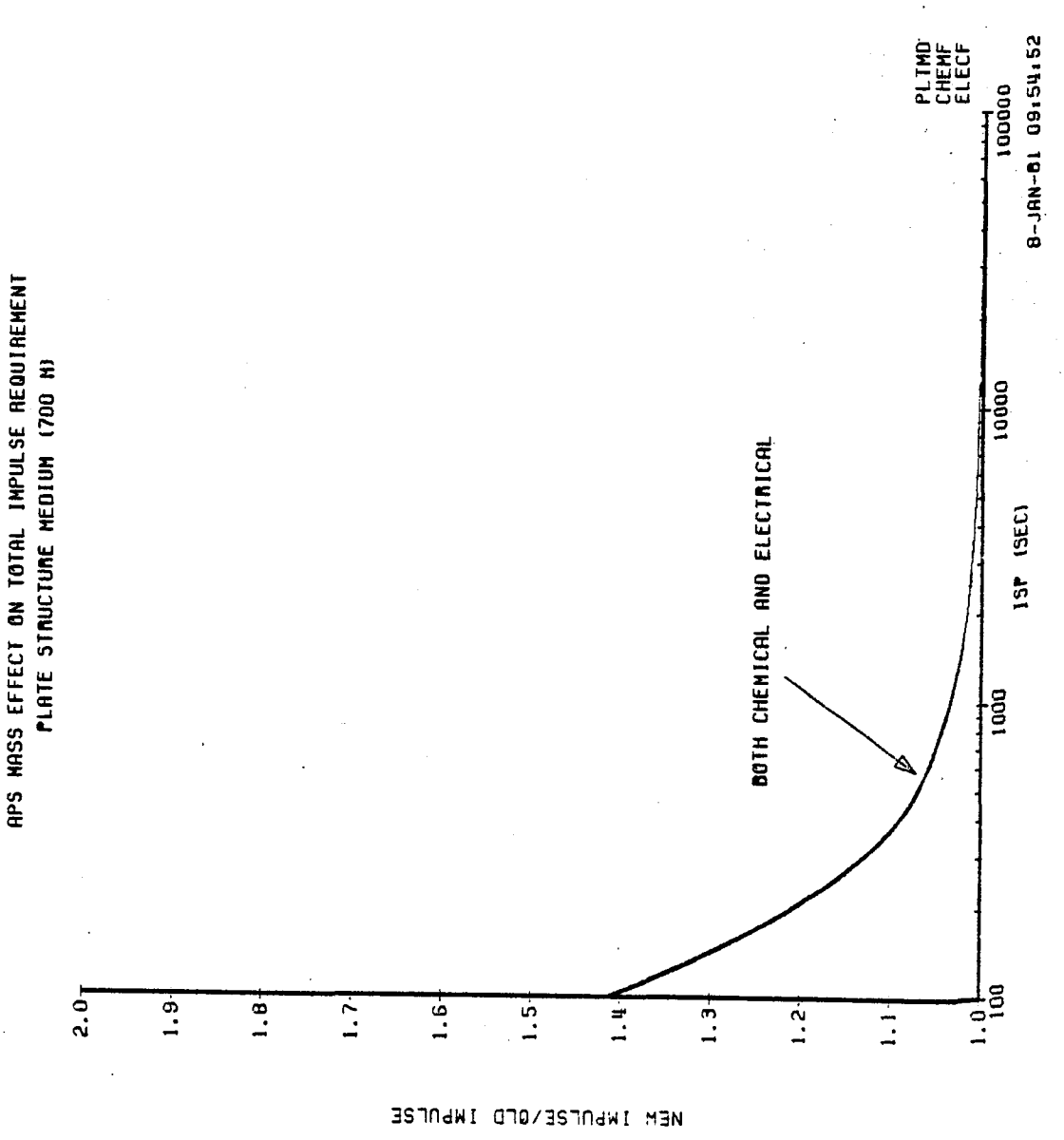

FIGURE E-20 APS MASS EFFECT ON TOTAL IMPULSE REQUIREMENT, MEDIUM PLATE STRUCTURE

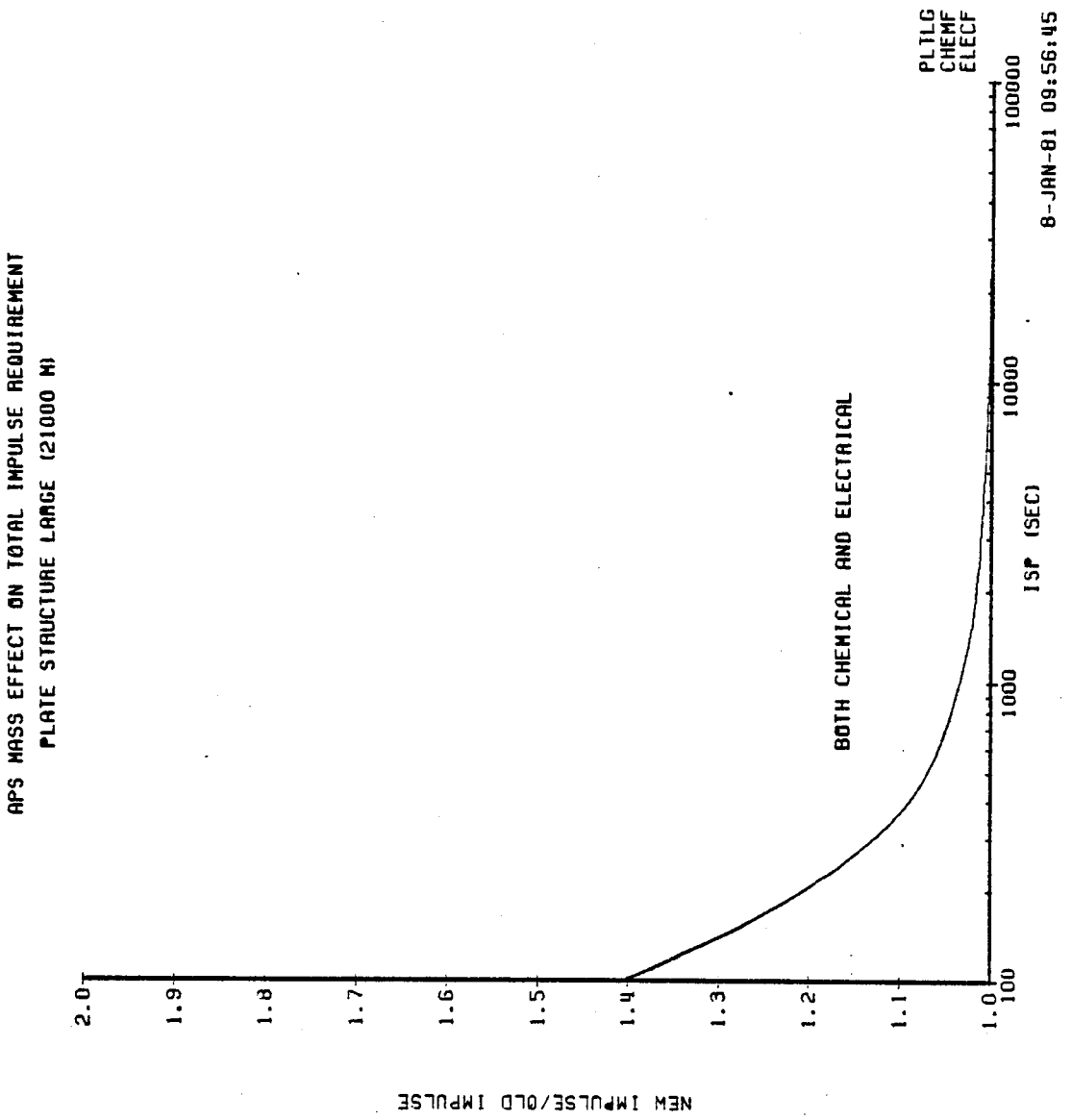

FIGURE E-21 APS MASS EFFECT ON TOTAL IMPULSE REQUIREMENT, LARGE PLATE STRUCTURE

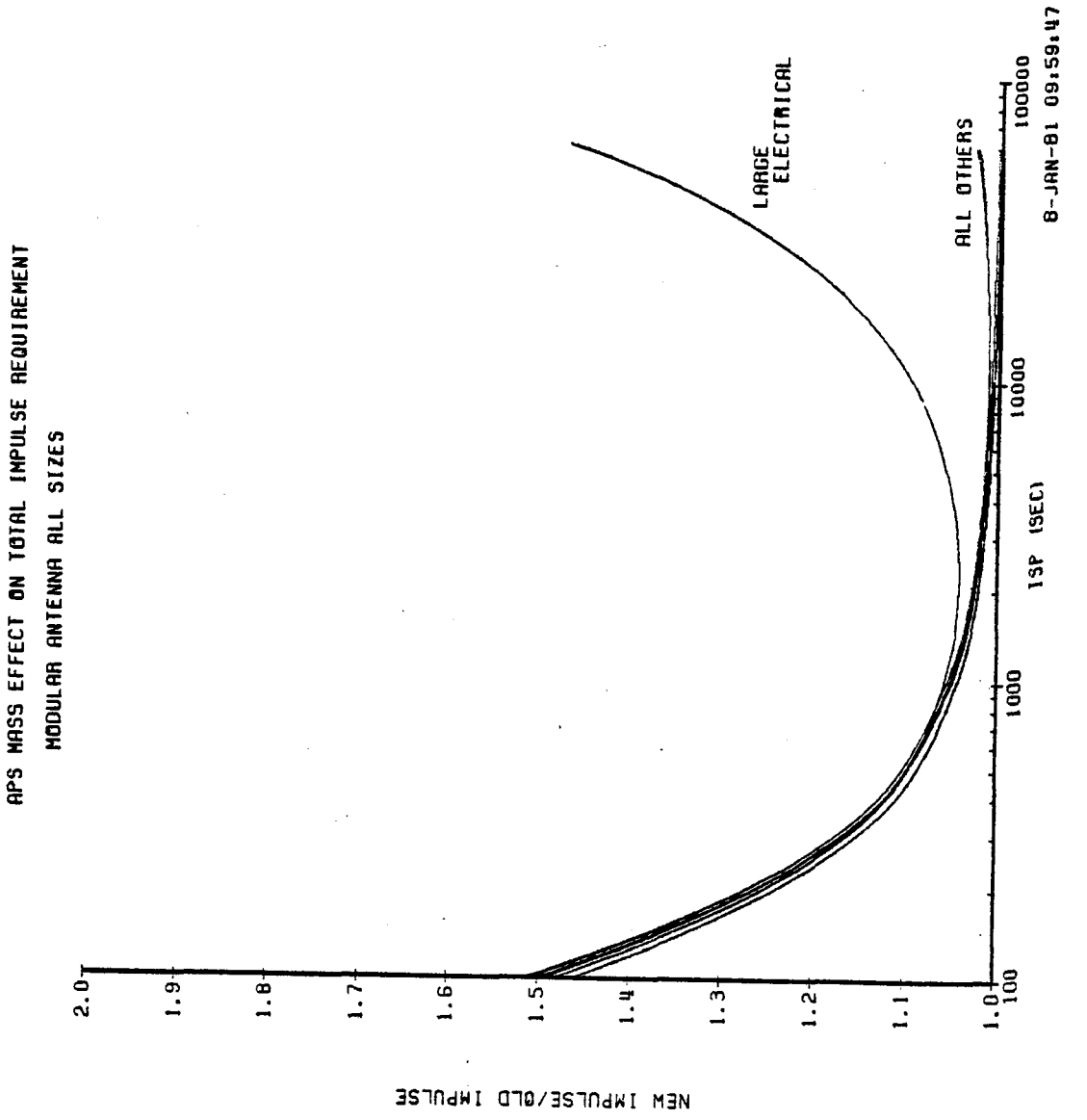

FIGURE E-22 APS MASS EFFECT ON TOTAL IMPULSE REQUIREMENT, MODULAR ANTENNA

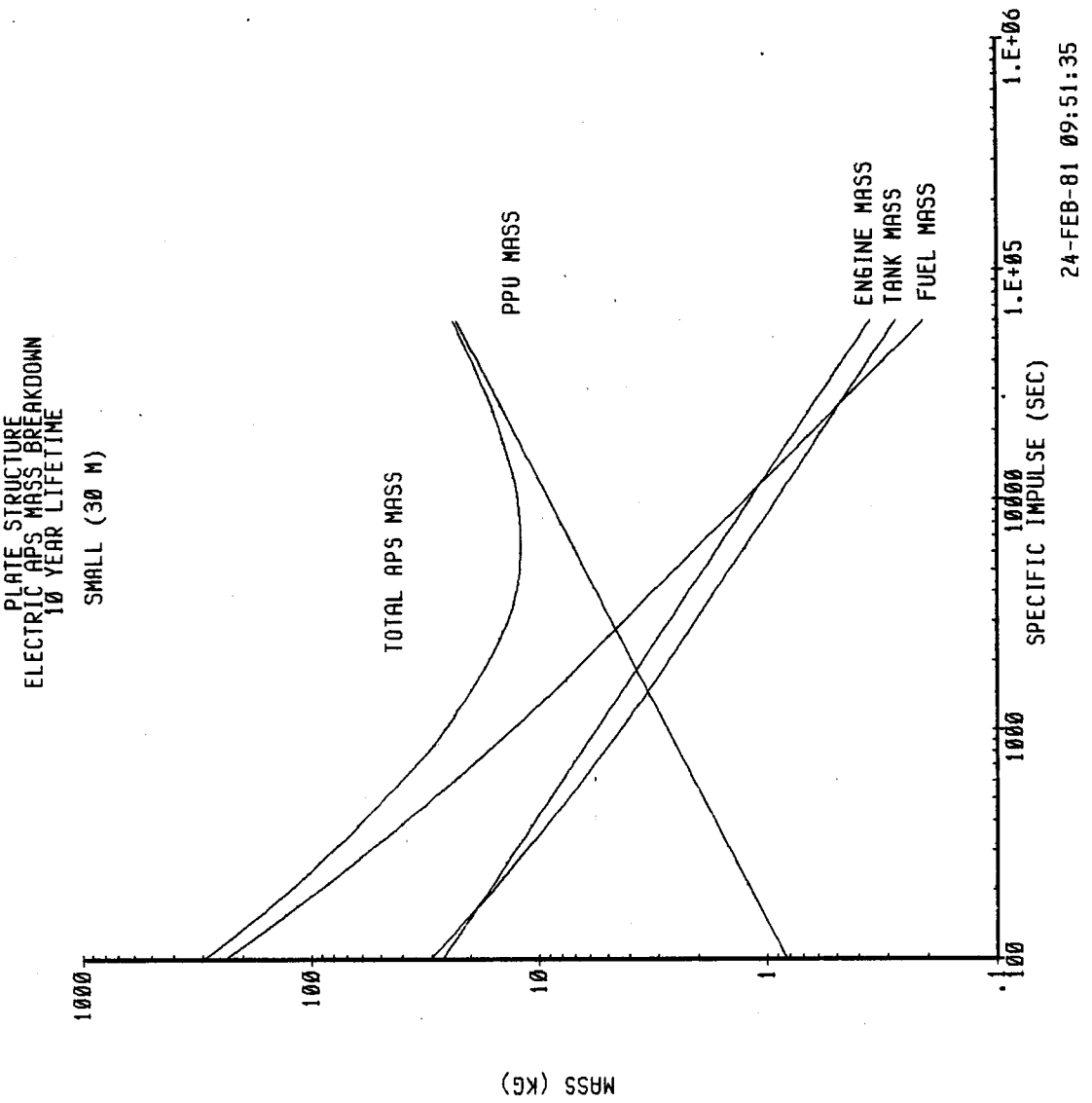

FIGURE E-23 MASS COMPONENTS - PLATE STRUCTURE (SMALL)

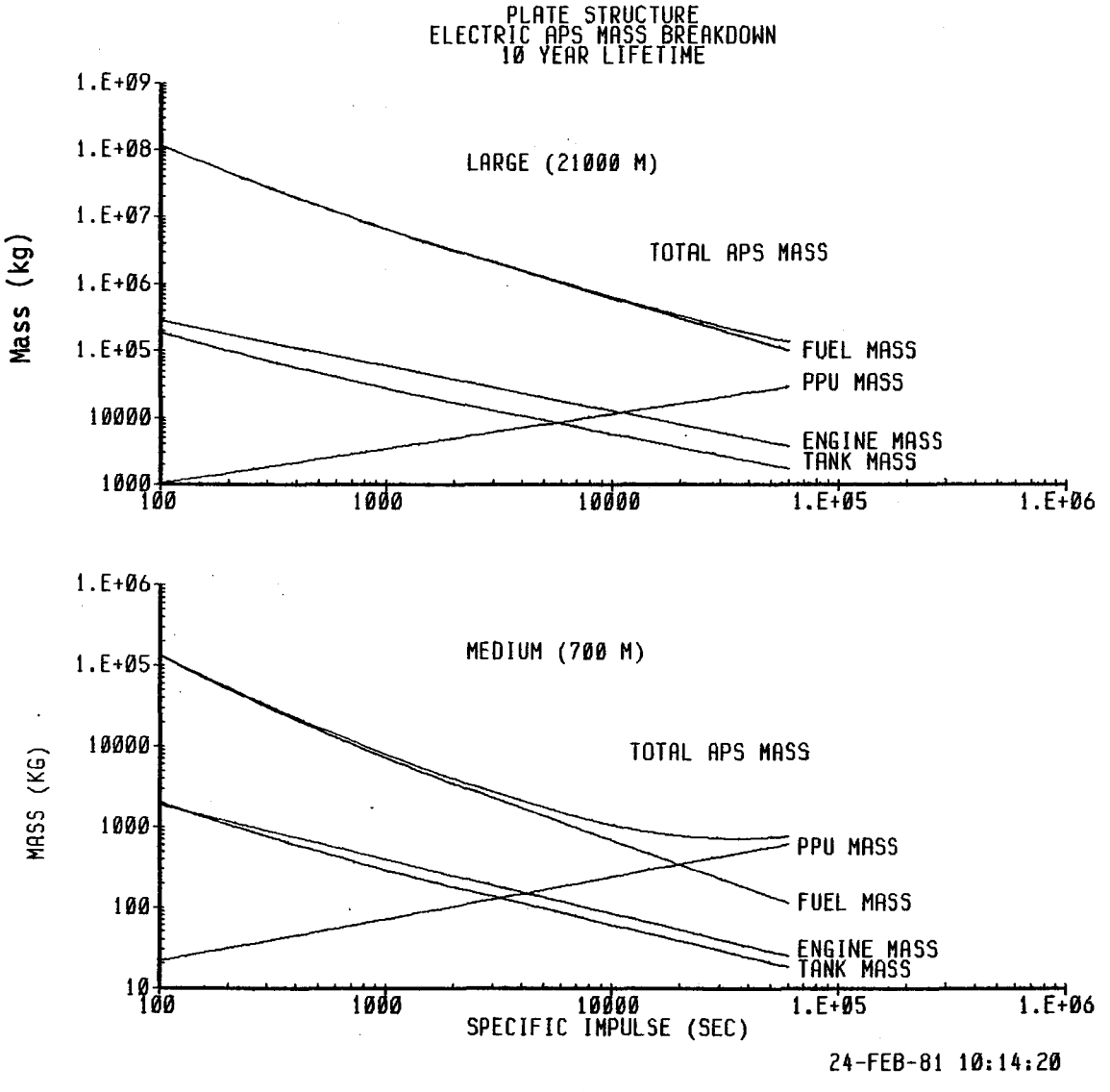

FIGURE E-24 MASS COMPONENTS - PLATE STRUCTURE (MEDIUM, LARGE)

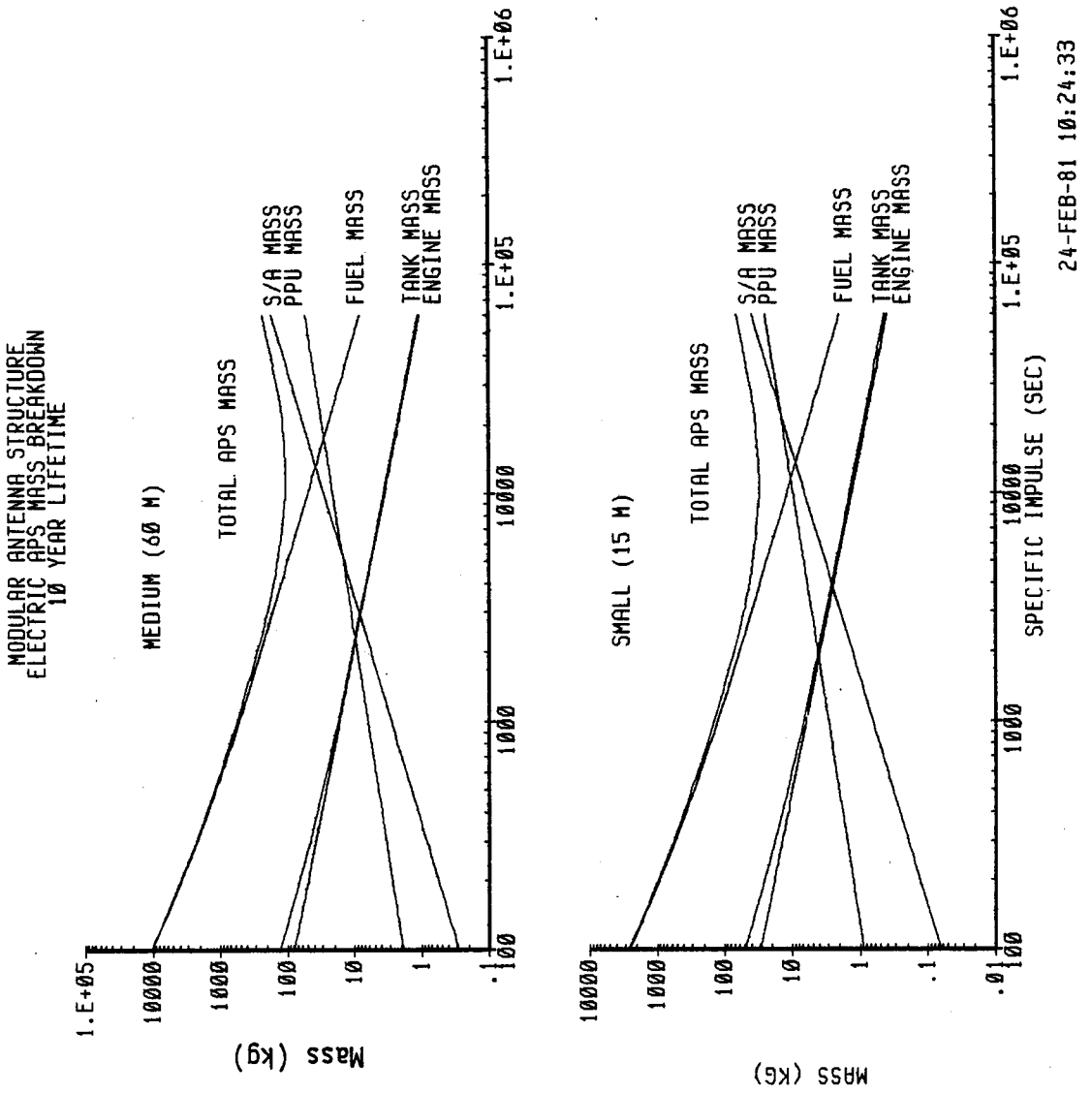

FIGURE E-25 MASS COMPONENTS - MODULAR ANTENNA (SMALL, MEDIUM)

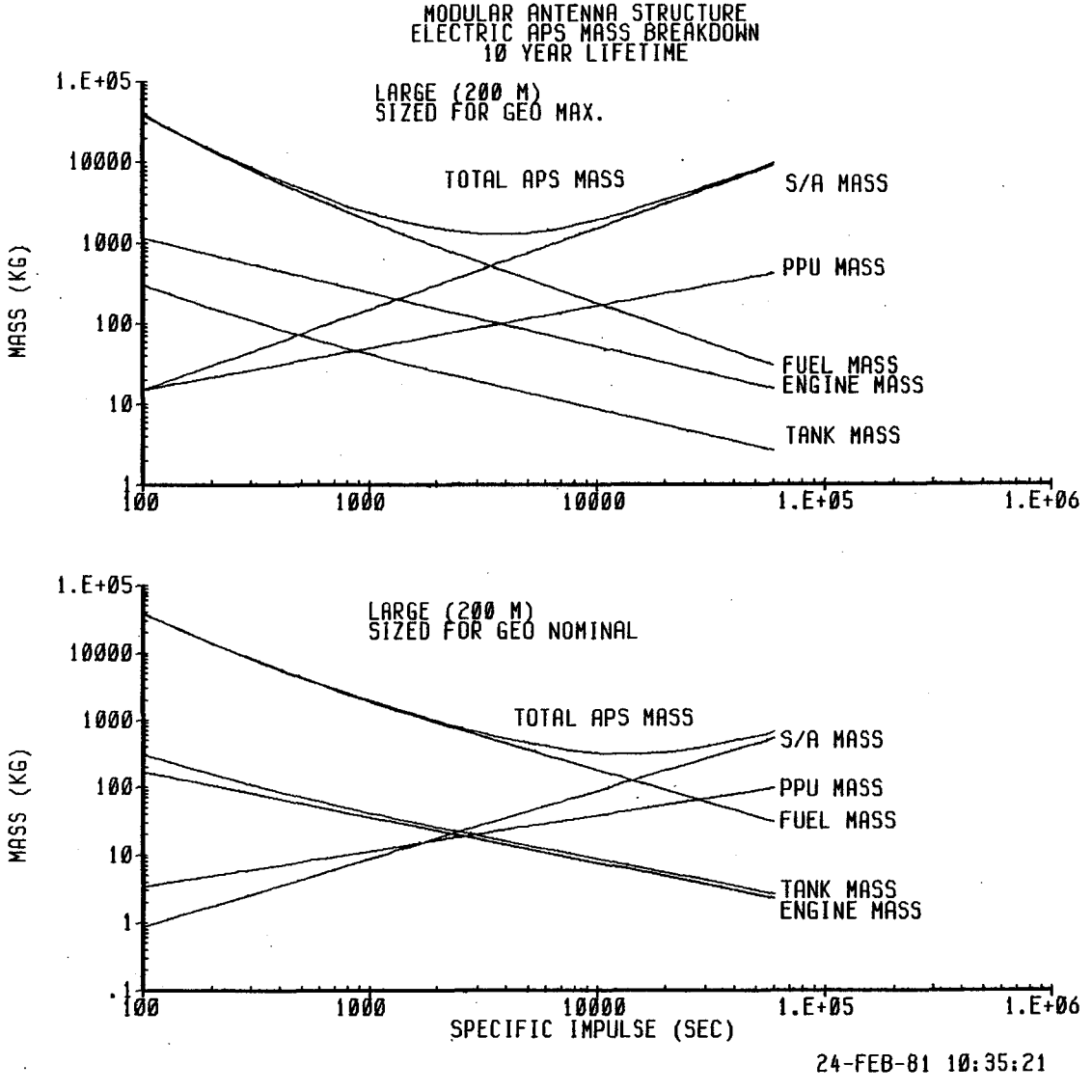

FIGURE E-26 MASS COMPONENTS - MODULAR ANTENNA (LARGE)

FIGURE E-27 MASS COMPONENTS - SERIES OF ANTENNAS (SMALL)

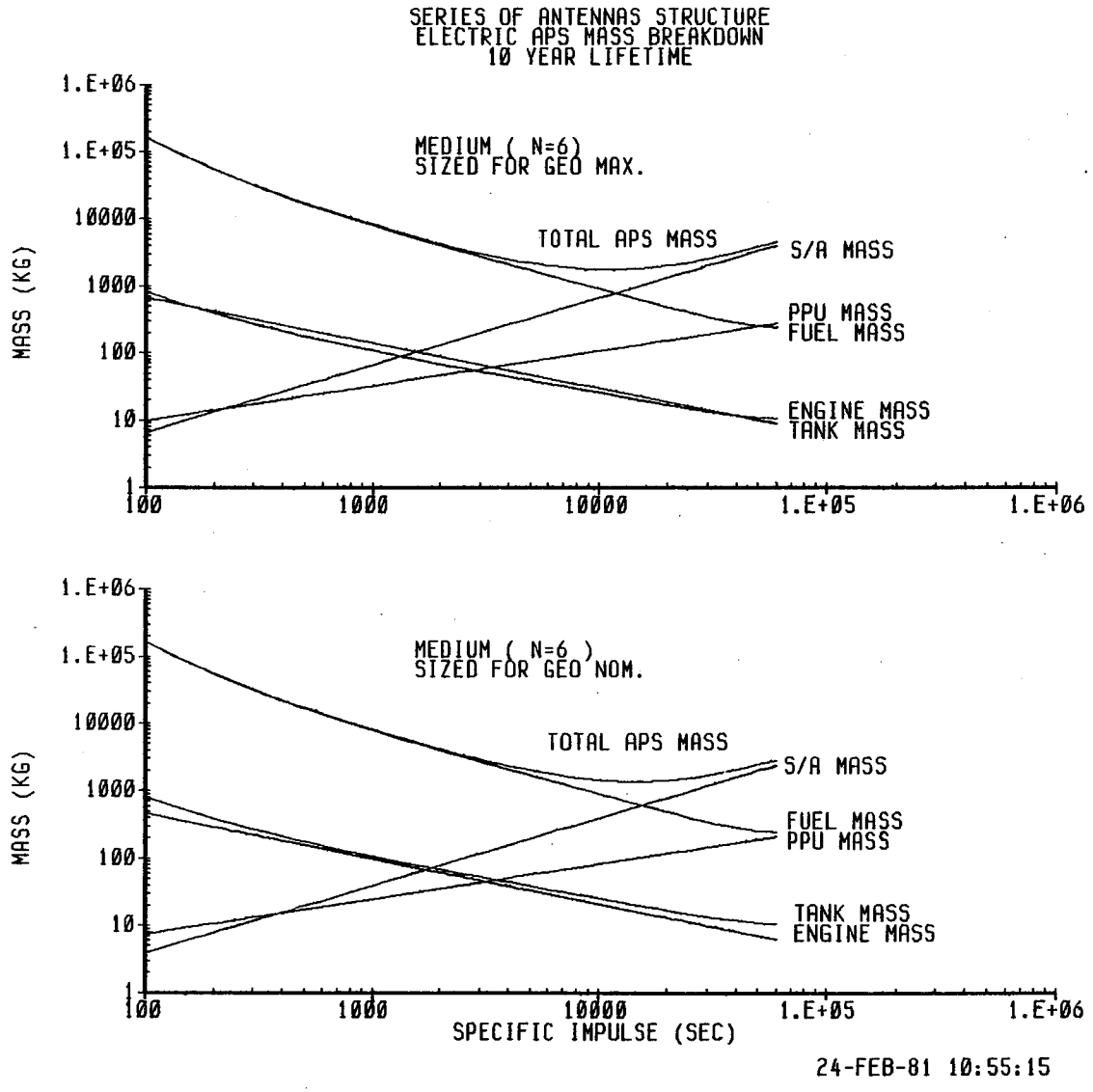

FIGURE E-28 MASS COMPONENTS - SERIES OF ANTENNAS (MEDIUM)

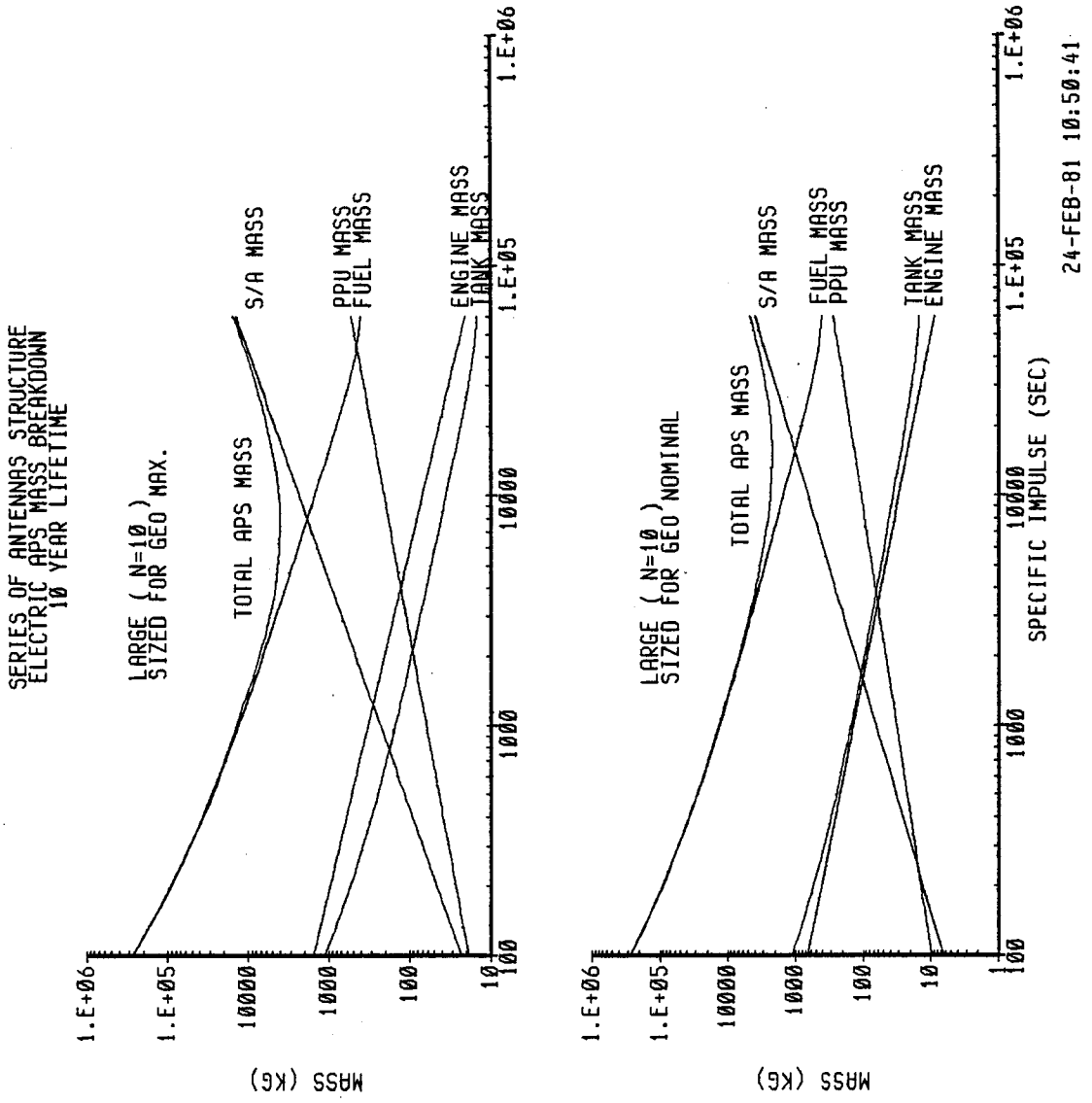

FIGURE E-29 MASS COMPONENTS - SERIES OF ANTENNAS (LARGE)

Figure E-30
PLATE STRUCTURE W/O BLANKET
SMALL (30 m)

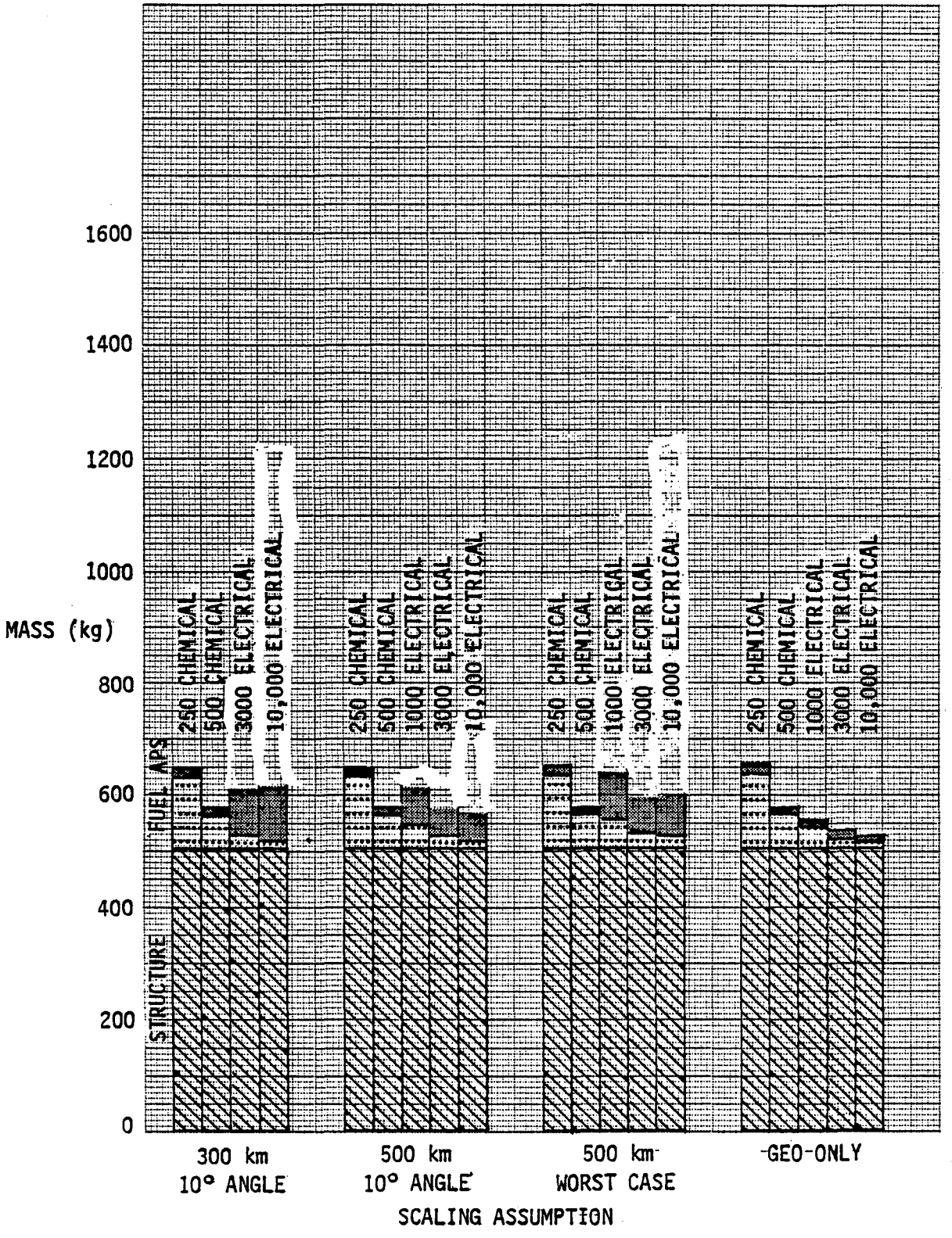

E30
D180-25956-2

Figure E-31

PLATE STRUCTURE W/O BLANKET

MEDIUM (100 m)

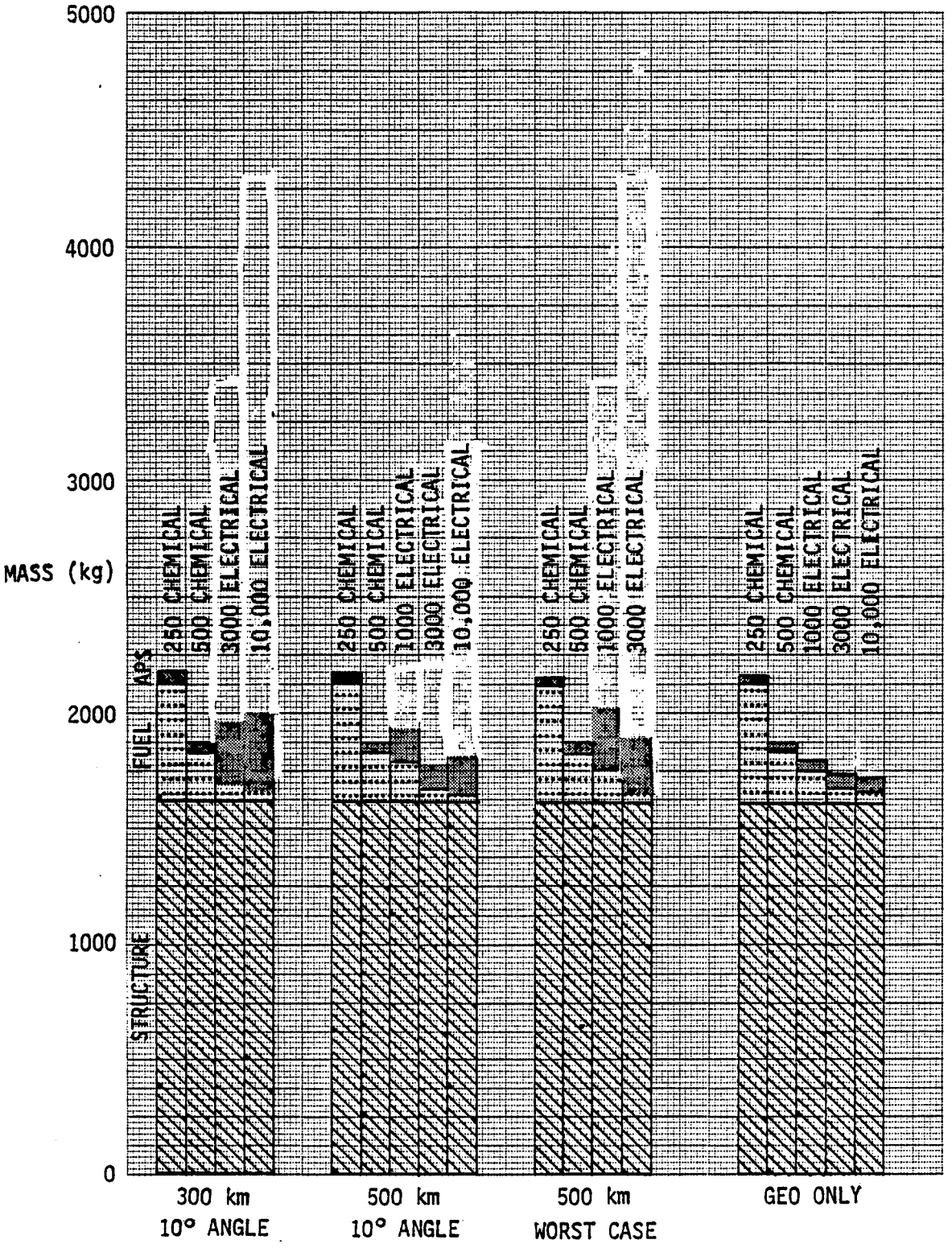

E31

D180-25956-2

Figure E-32
PLATE STRUCTURE W/O BLANKET
LARGE (250 M)

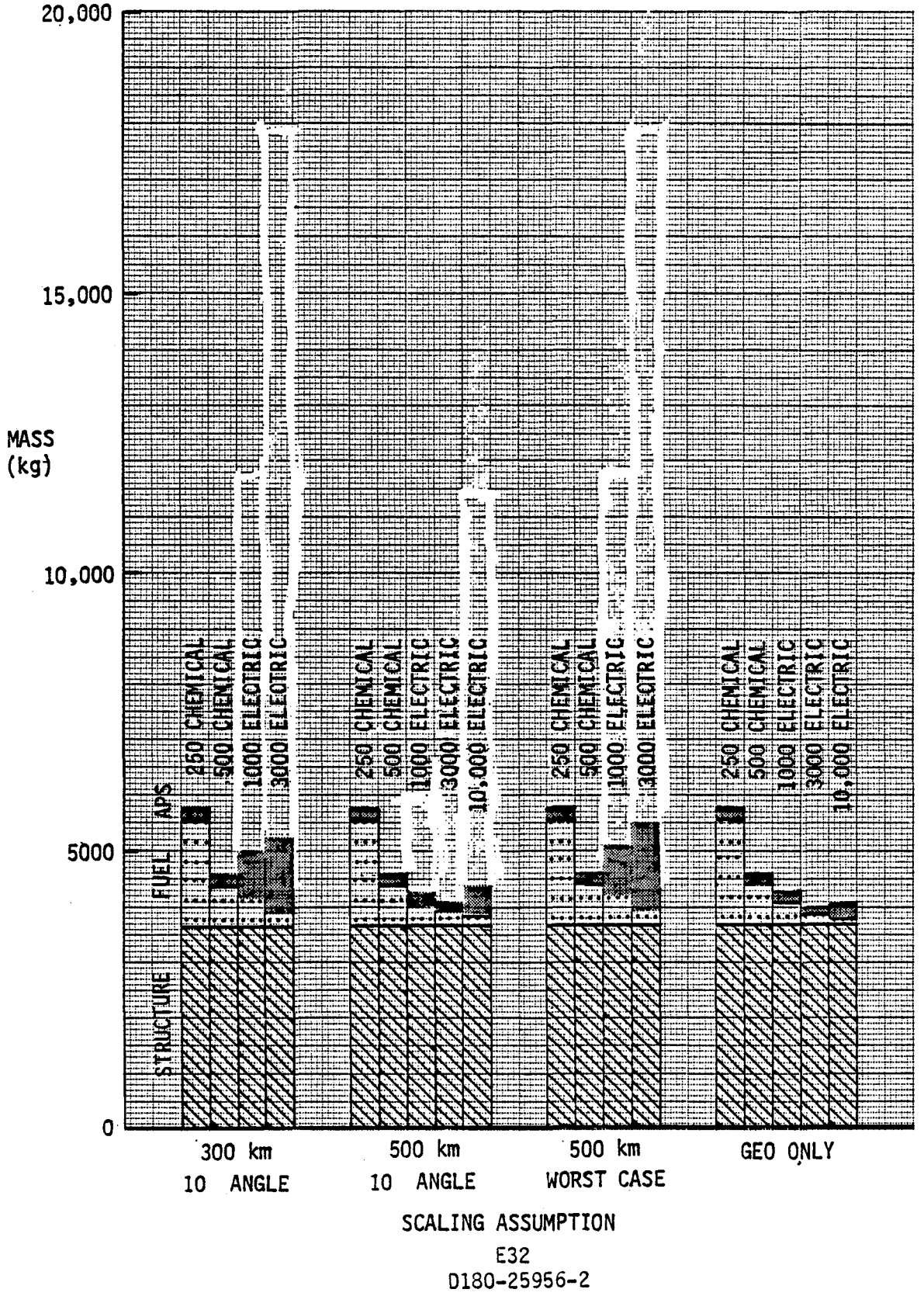

E32
D180-25956-2

Figure E-33
PLATE STRUCTURE W/BLANKET
SMALL (30 M)

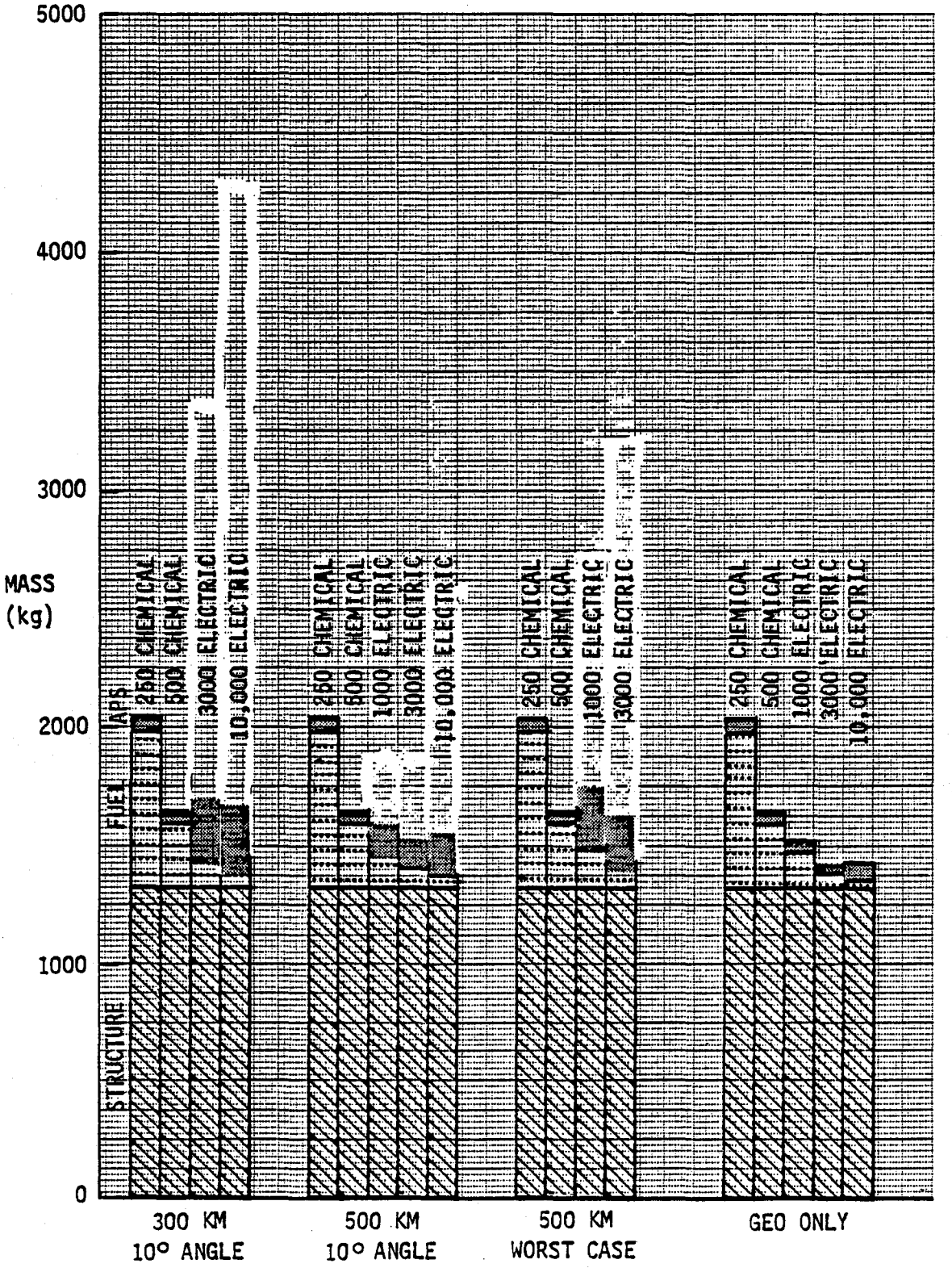

Figure E-34
PLATE STRUCTURE W/BLANKET
MEDIUM (100 M)

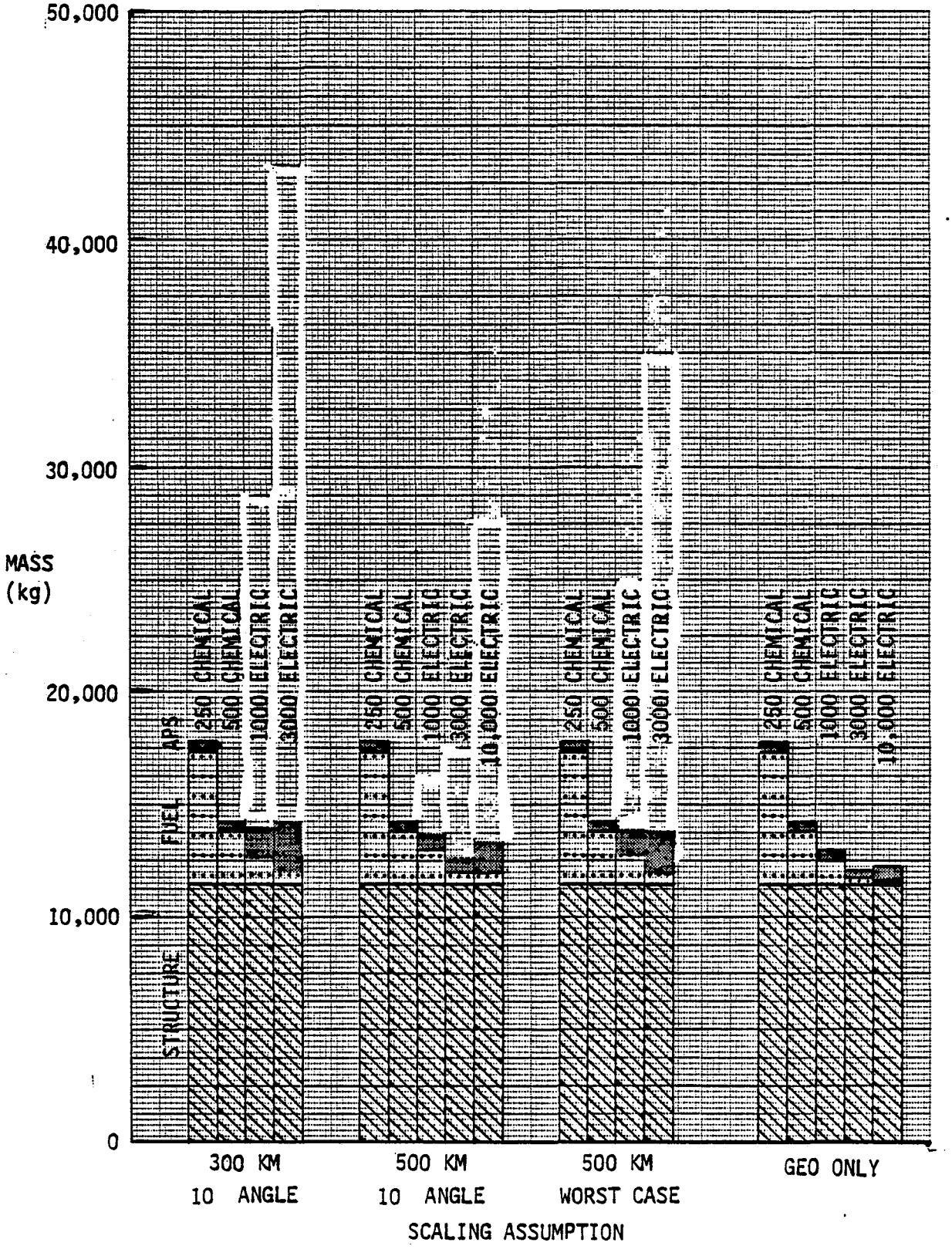

E34
D180-25956-2

Figure E-35
PLATE STRUCTURE W/BLANKET
LARGE (150 M)

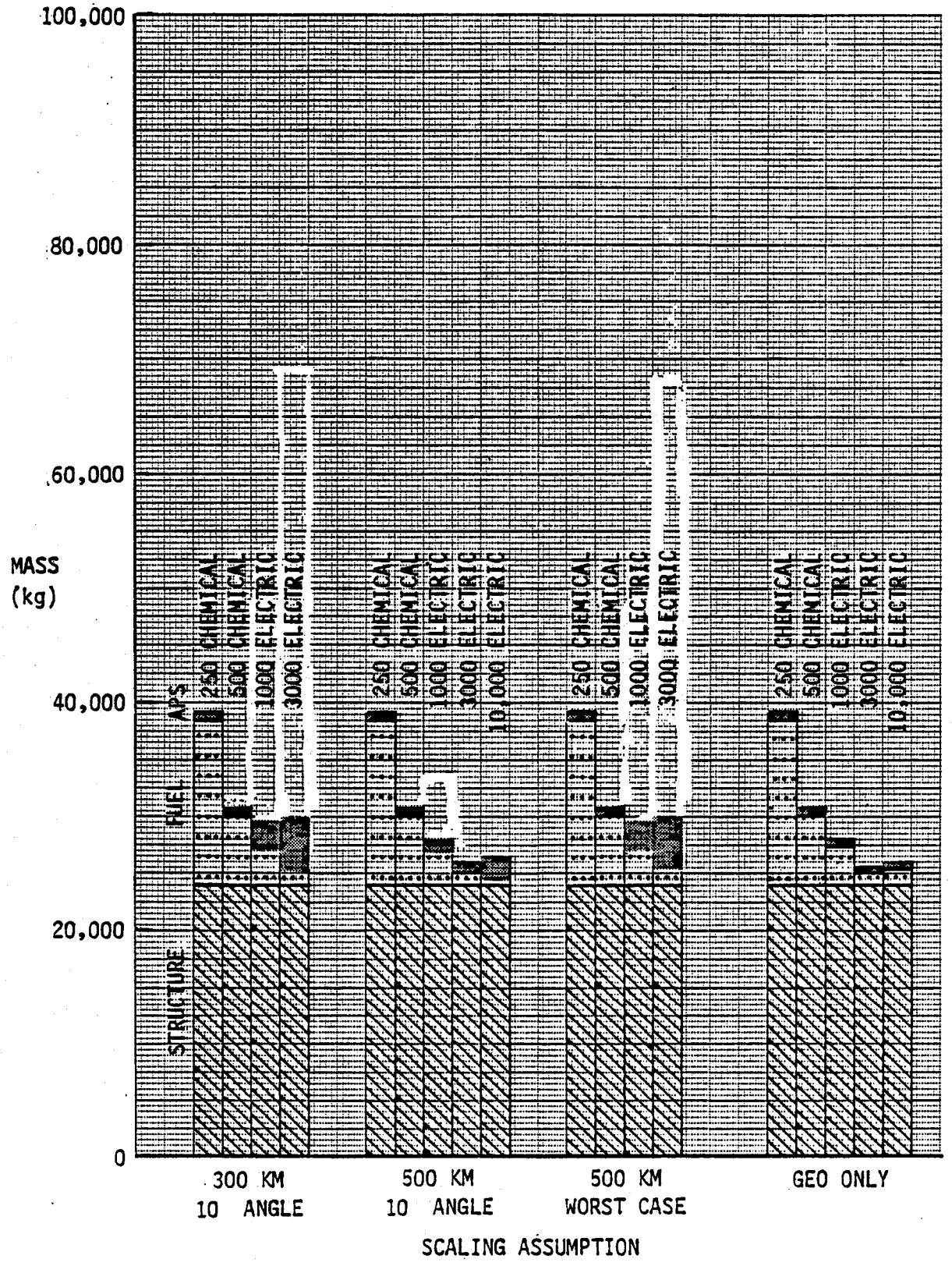

E35
D180-25956-2

Figure E-36
MODULAR ANTENNA
SMALL (15 M)

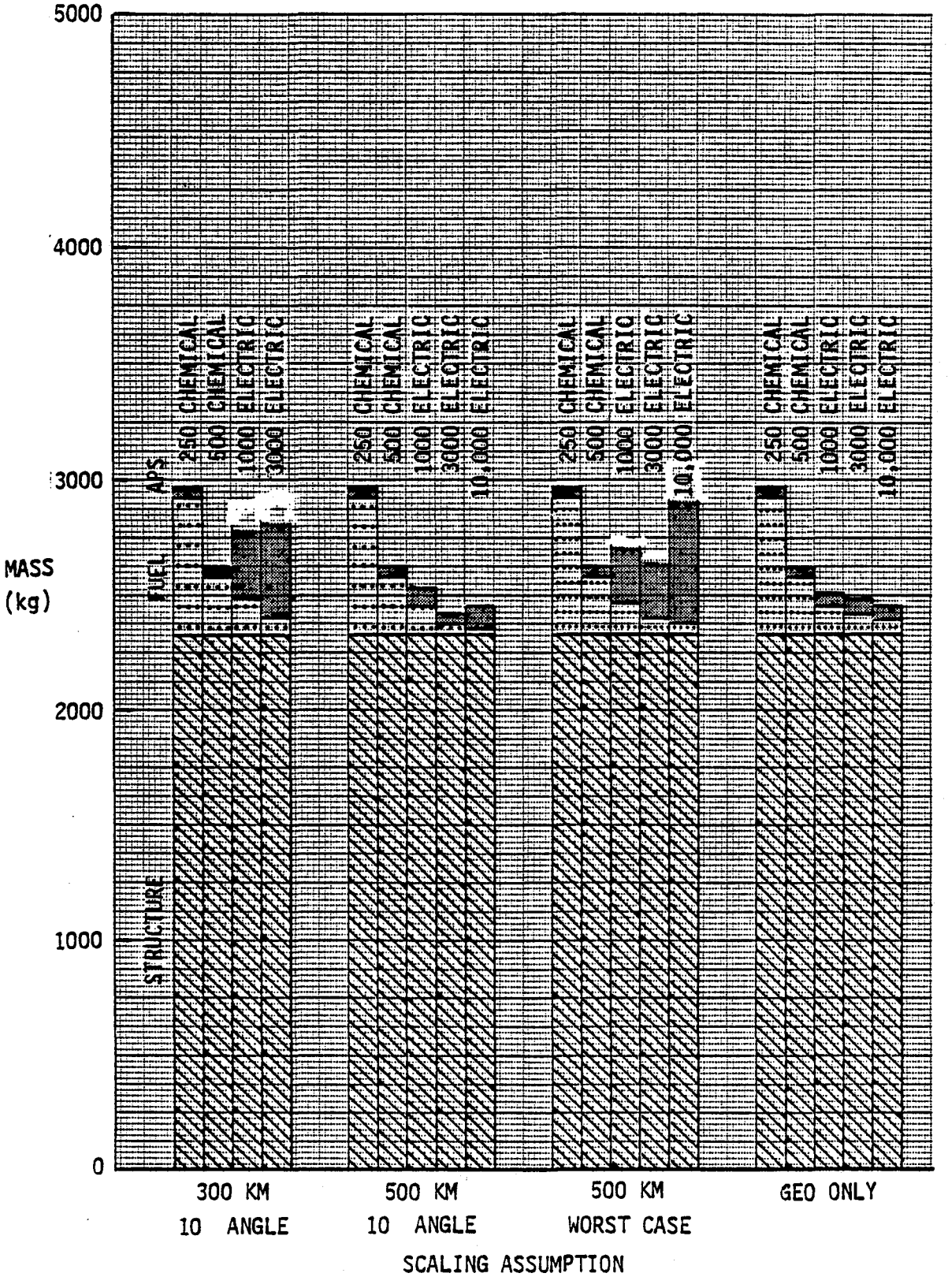

Figure E-37
MODULAR ANTENNA
MEDIUM (60 M)

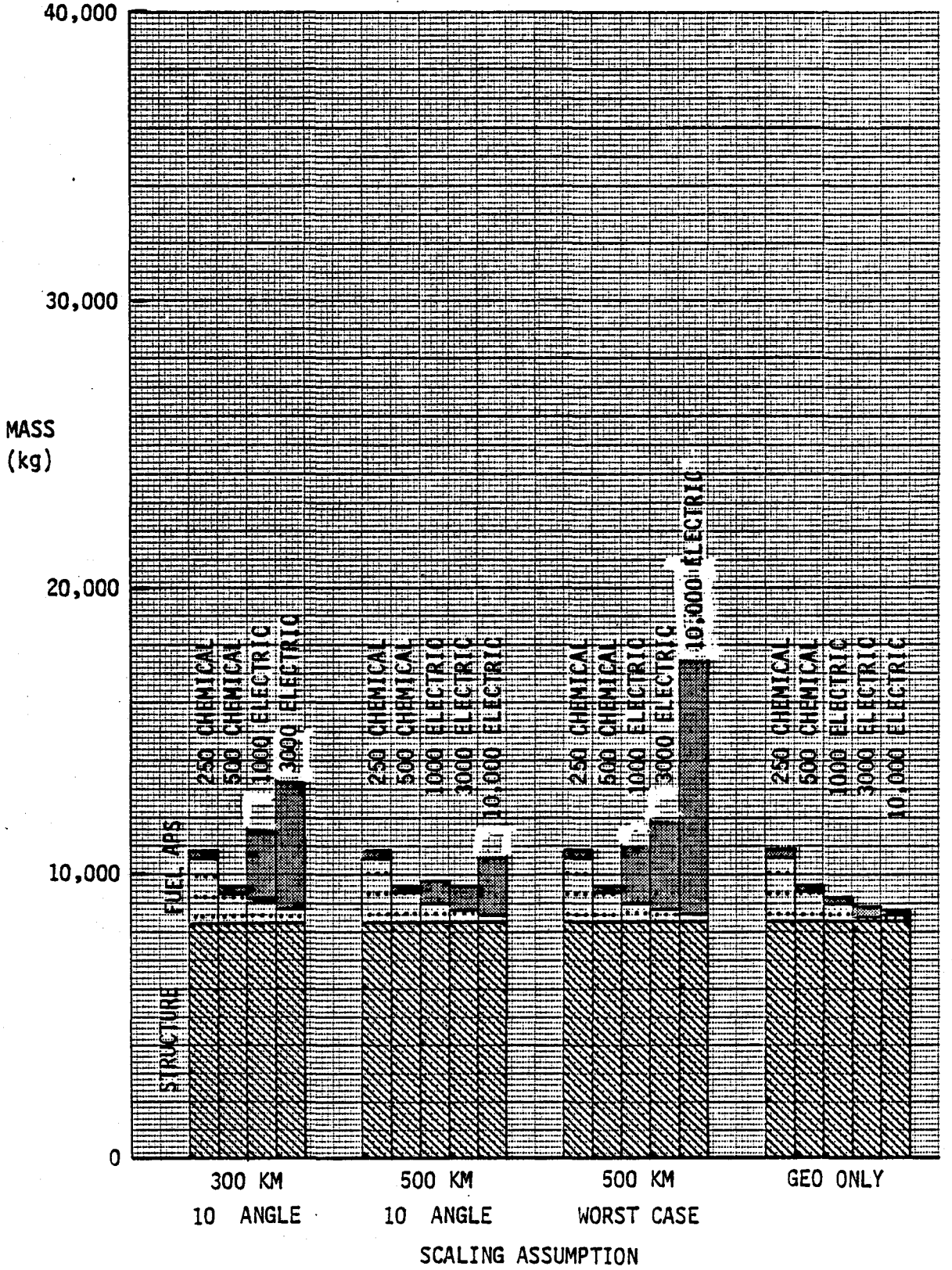

E37
D180-25956-2

Figure E-38
MODULAR ANTENNA
LARGE (200 M)

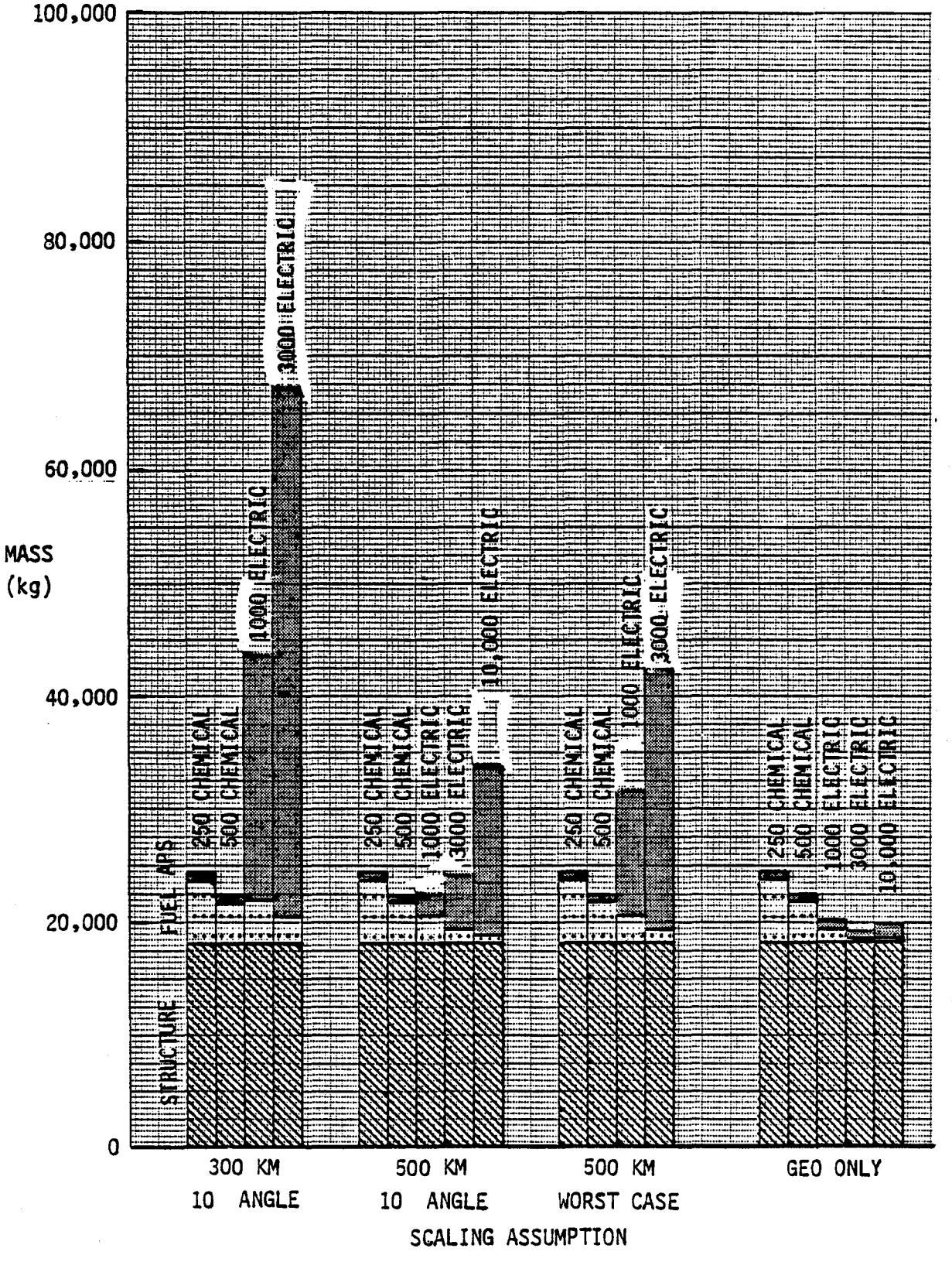

Figure E-39

SERIES OF ANTENNAS

SMALL (2)

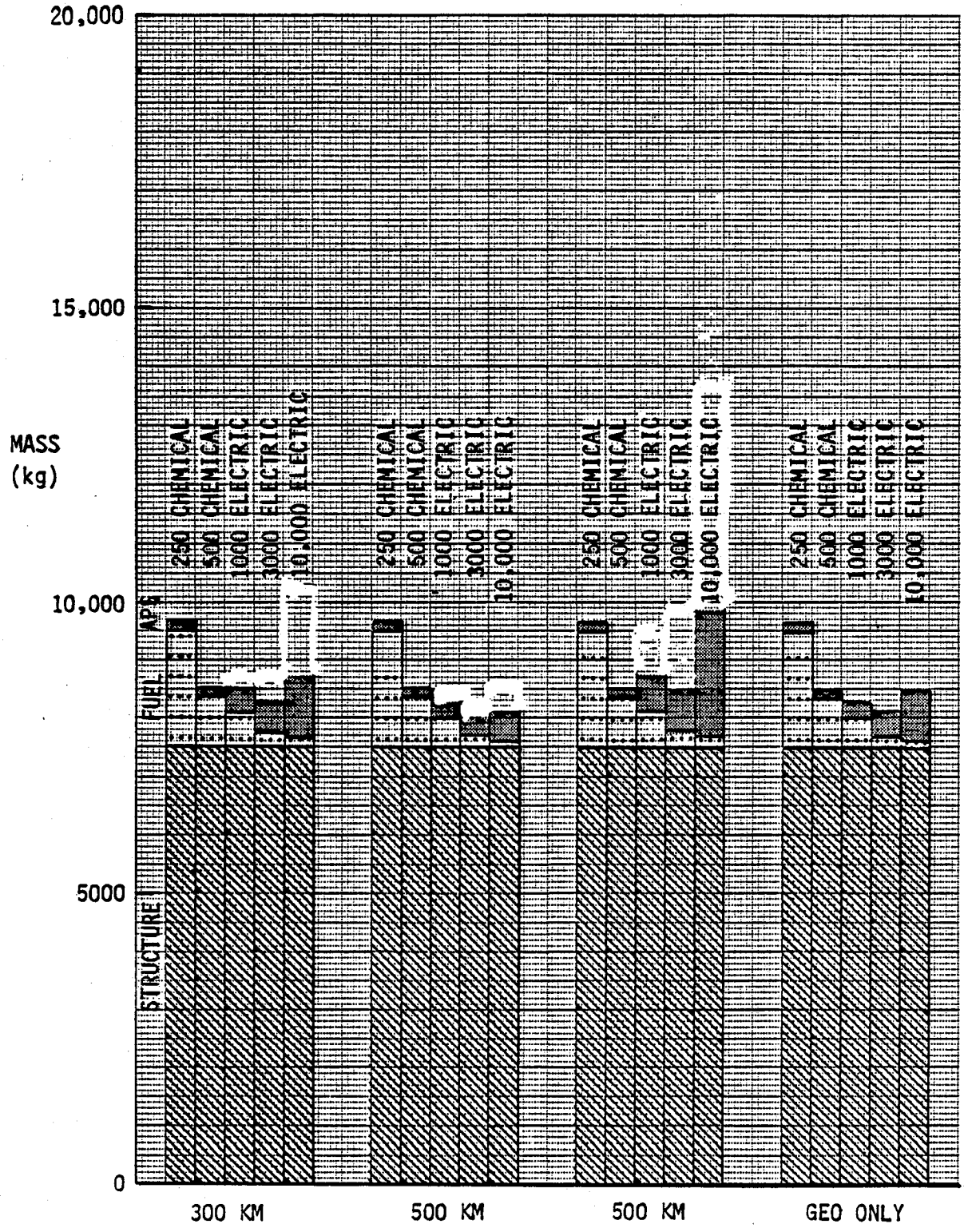

E39

D180-25956-2

Figure E-40
SERIES OF ANTENNAS
MEDIUM (3)

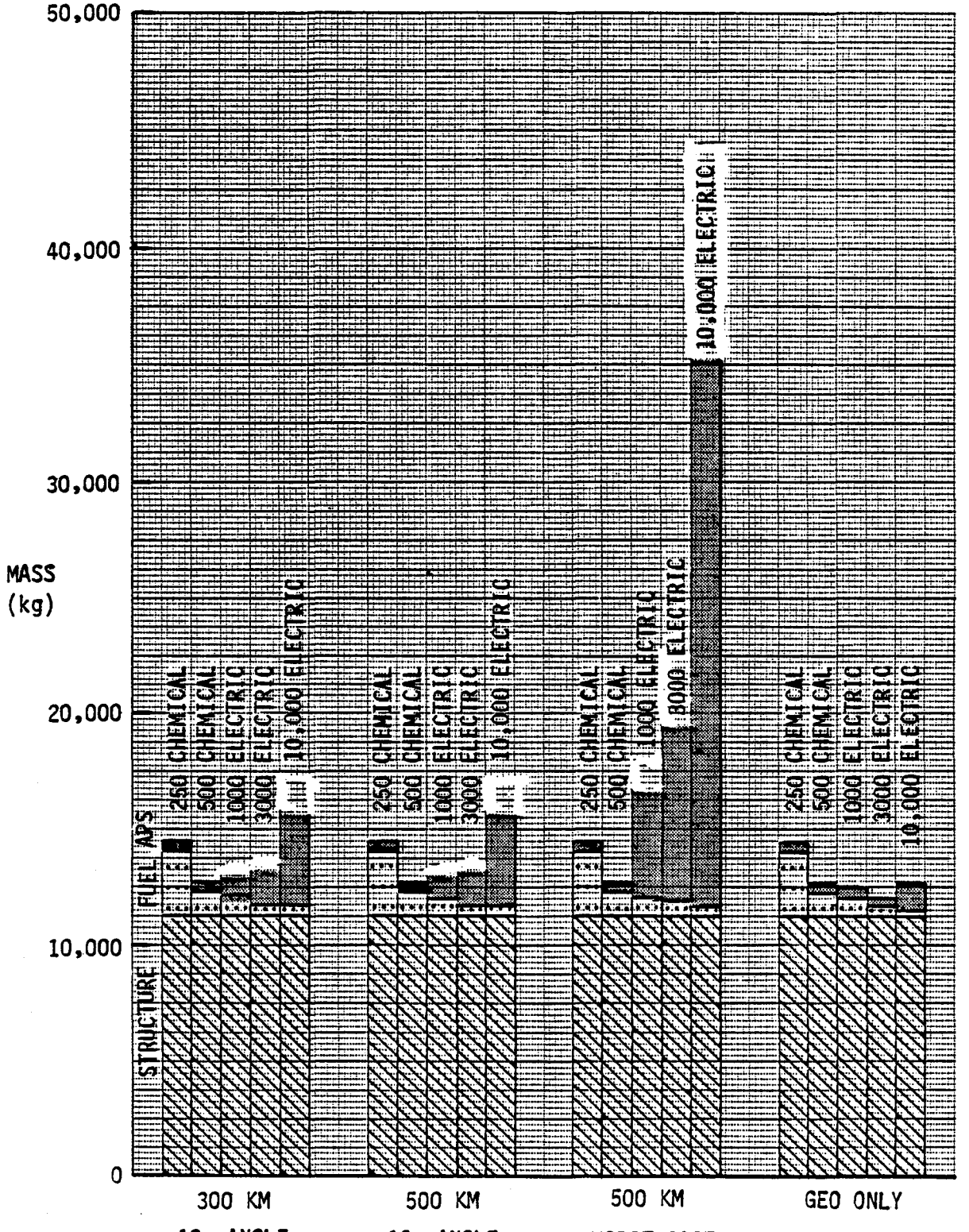

E40
D180-25956-2

Figure E-41

SERIES OF ANTENNAS

LARGE (4)

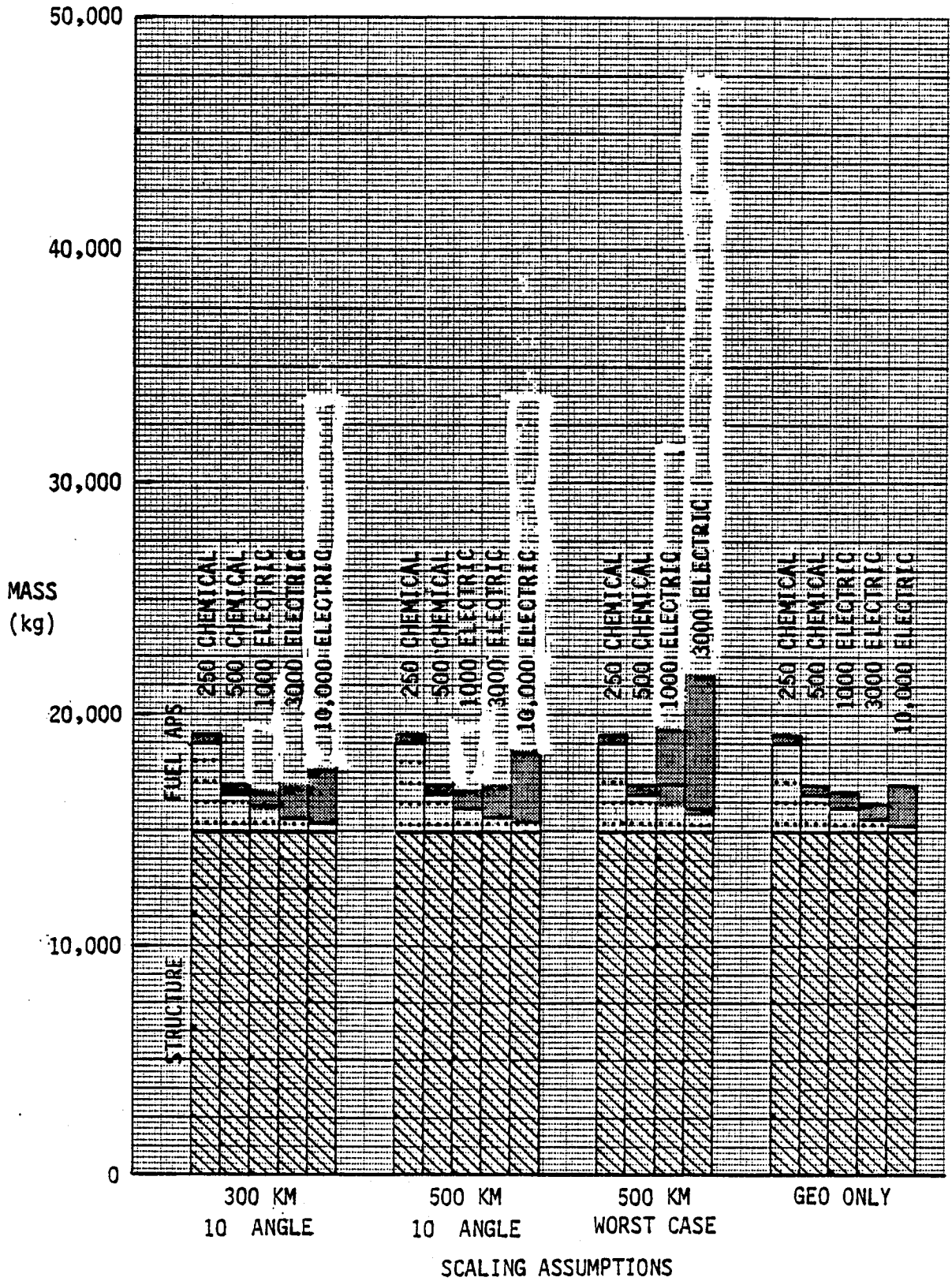

E41

D180-25956-2